STAR 2 0 AUG 13 1985

5101-258
Flat-Plate
Solar Array Project

DOE/JPL-1012-103
Distribution Category UC-63b

Proceedings of the Flat-Plate Solar Array Project Research Forum on High-Efficiency Crystalline Silicon Solar Cells

(NASA-CR-176047) PROCEEDINGS OF THE FLAT-PLATE SOLAR ARRAY PROJECT RESEARCH FORUM ON HIGH-EFFICIENCY CRYSTALLINE SILICON SOLAR CELLS (Jet Propulsion Lab.) 498 p HC A21/MF A01 CSCL 10A G3/44

N85-31615 THRU N85-31643 Unclas 21837

May 15, 1985

Prepared for
U.S. Department of Energy
Through an Agreement with
National Aeronautics and Space Administration
by
Jet Propulsion Laboratory
California Institute of Technology
Pasadena, California

JPL Publication 85-38

STAR
1428

5101-258
Flat-Plate
Solar Array Project

DOE/JPL-1012-103
Distribution Category UC-63b

Proceedings of the Flat-Plate Solar Array Project Research Forum on High-Efficiency Crystalline Silicon Solar Cells

May 15, 1985

Prepared for
U.S. Department of Energy
Through an Agreement with
National Aeronautics and Space Administration
by
Jet Propulsion Laboratory
California Institute of Technology
Pasadena, California

JPL Publication 85-38

Prepared by the Jet Propulsion Laboratory, California Institute of Technology, for the U.S. Department of Energy through an agreement with the National Aeronautics and Space Administration.

The JPL Flat-Plate Solar Array Project is sponsored by the U.S. Department of Energy and is part of the National Photovoltaics Program to initiate a major effort toward the development of cost-competitive solar arrays.

This report was prepared as an account of work sponsored by an agency of the United States Government. Neither the United States Government nor any agency thereof, nor any of their employees, makes any warranty, express or implied, or assumes any legal liability or responsibility for the accuracy, completeness, or usefulness of any information, apparatus, product, or process disclosed, or represents that its use would not infringe privately owned rights.

Reference herein to any specific commercial product, process, or service by trade name, trademark, manufacturer, or otherwise, does not necessarily constitute or imply its endorsement, recommendation, or favoring by the United States Government or any agency thereof. The views and opinions of authors expressed herein do not necessarily state or reflect those of the United States Government or any agency thereof.

This document reports on work done under NASA Task RE-152, Amendment 66, DOE/NASA IAA No. DE-AI01-76ET20356.

ABSTRACT

The High-Efficiency Crystalline Silicon Solar Cells Research Forum was held on July 9-11, 1984, in Phoenix, Arizona. The Research Forum addressed high-efficiency concepts, surface-interface effects, bulk effects, modeling and device processing. These topics were arranged into six interactive sessions, which focused on the state-of-the-art of device structures, identification of barriers to achieve high-efficiency cells and potential ways to overcome these barriers. The Forum arrangement was intended to enable and encourage interaction and discussion among participants. Promising technical areas of future research are presented in these Proceedings.

FOREWORD

The High-Efficiency Crystalline Silicon Solar Cells Research Forum was held at The Pointe Hotel in Phoenix, Arizona July 9 through 11, 1984. It is my pleasure to introduce to you the papers contained in these Proceedings. All of the papers were invited (not submitted) from the best of a wealth of suggestions put forward and discussed by experts in the field and the Organizing Committee.

The objectives of the Forum were to address theoretical solar cell conversion efficiency limitations, the state of the art of device structures, identification of barriers to achievement of high-efficiency cells, and potential ways to overcome the barriers, and to provide the opportunity for unrestricted technology exchange among those attending. The format used to achieve these objectives involved six intensive sessions.

The discussion sections have been edited with the intent of enchancing the clarity and continuity of each discussion. This procedure makes these Proceedings a most valuable reference document containing definitive work by some of the best solar-cell experts in the world.

This excellent collection of papers, and the success of the Research Forum it reports, result from the efforts of a large number of dedicated people. I wish to record my gratitude to the Organizing Committee, the authors, the session chairmen, and many other supporting people for their hard work and friendship.

Ram Kachare,
Chairman of the Forum
and Proceedings Editor

PRECEDING PAGE BLANK NOT FILMED

PARTICIPANTS

FLAT-PLATE SOLAR ARRAY PROJECT
HIGH-EFFICIENCY CRYSTALLINE
SILICON SOLAR CELL RESEARCH FORUM

ADDIS, F. William
Joint Center for Graduate Study
100 Sprout Road
Richland, WA 99352
(509) 375-3176

ANNAN, R. H. "Bud"
U. S. Department of Energy
Forrestal Building, CE 333
1000 Independence Ave., SW, 5E066
Washington, DC 20585

BACKUS, Charles E.
Arizona State University
Director, Engineering Research Center
Tempe, AZ 85287
(602) 965-1725

BELL, Richard O.
Mobil Solar Energy Corp.
16 Hickory Drive
Waltham, MA 02154
(617) 890-0909

BICKLER, Donald B.
Jet Propulsion Laboratory
4800 Oak Grove Drive, M.S. 512/103
Pasadena, CA 91109
(818) 577-9219

BURGER, Dale R.
Jet Propulsion Laboratory
4800 Oak Grove Drive, M.S. 512/103
Pasadena, CA 91109
(818) 577-9374

CALLAGHAN, William T.
Jet Propulsion Laboratory
4800 Oak Grove Drive, M.S. 502/422
Pasadena, CA 91109
(818) 577-9517

CAMPBELL, Robert
Westinghouse Electric Corp.
P.O. Box 10864
Pittsburgh, PA 15236
(412) 892-5600, X 5364

CHADI, D. James
Xerox Palo Alto Research
3333 Coyote Hills Road
Palo Alto, CA 94304
(415) 494-4136

CHENG, Li-Jen
Jet Propulsion Laboratory
4800 Oak Grove Drive, M.S. 238/343
Pasadena, CA 91109
(818) 354-3068

CISZEK, Ted
Solar Energy Research Institute
1617 Cole Blvd. M.S. 16/3
Golden, CO 80401
(303) 231-1769

COLEMAN, Michael G.
Solavolt International
P.O. Box 2934
Phoenix, AZ 95062
(602) 231-6455

CROTTY, Gerald
Jet Propulsion Laboratory
4800 Oak Grove Drive, M.S. 238/343
Pasadena, CA 91109
(818) 354-6294

CULIK, Jerry
Solarex Corp.
1335 Piccard Drive
Rockville, MD 20850
(301) 948-0202

DAUD, Taher
Jet Propulsion Laboratory
4800 Oak Grove Drive, M.S. 238/343
Pasadena, CA 91109
(818) 354-5782

DYER, Larry D.
Texas Instruments
P.O. Box 84
Sherman, TX 75090
(214) 892-5351

FLOOD, Dennis
NASA Lewis Research Center
21000 Brookpark Road
Cleveland, OH 44135
(216) 294-6303

FONASH, Stephen
Penn State Univerrsity
Engineering Sciences Programs
University Park, PA 16802
(814) 865-4931

GRUNTHANER, Frank
Jet Propulsion Laboratory
4800 Oak Grove Drive, 198/231
Pasadena, CA 91109
(818) 354-5564

HANOKA, Jack
Mobil Solar Energy Corp.
16 Hickory Drive
Waltham, MA 02254
(617) 890-0909

ILES, Peter
Applied Solar Energy Corp.
15251 E. Don Julian Road
City of Industry, CA 91749
(818) 963-6581

JOHNSON, Scott M.
Solarex Corp.
1335 Piccard Drive
Rockville, MD 20850
(301) 948-0202

KACHARE, Ram
Jet Propulsion Laboratory
4800 Oak Grove Drive, M.S. 238/343
Pasadena, CA 91109
(818) 354-4583

KARIUS, Siegfried
National Research Council
Montreal Road
Ottawa, Ontario, CANADA K1A 0R6
(613) 993-2730

KAZMERSKI, L. L.
Solar Energy Research Institute
1617 Cole Blvd.
Golden, CO 80401
(303) 231-1115

KEAVNEY, Chris
Spire Corp.
Patriots Park
Bedford, MA 01730
(617) 275-6000

KESLER, Matt
Solavolt International
P.O. Box 2934
Phoenix, AZ 85062
(602) 231-6434

KING, David L.
Sandia National Laboratories
Kirtland AFG Base - East
P.O. Box 5800, Div. 6224
Albuquerque, NM 87185
(505) 844-8220

KOLIWAD, Kris
Jet Propulsion Laboratory
4800 Oak Grove Drive, M.S. 238/343
Pasadena, CA 91109
(818) 354-5197

LAI, Stefan
Intel Corp.
3065 Bowers Ave., M.S. SC1-277
Santa Clara, CA 95051
(408) 987-5655

LAMBE, John
Jet Propulsion Laboratory
4800 Oak Grove Drive, M.S. 122-123
Pasadena, CA 91109
(818) 354-8238

LAMORTE, Michael F.
Research Triangle Institute
P.O. Box 12194
Research Triangle Park, NC 27709
(919)541-6477

LANDSBERG, Peter T.
University of Southampton
Southampton, England SOG 5N4
(011 44 703) 559122

LEIPOLD, Martin H.
Jet Propulsion Laborator
4800 Oak Grove Drive, M.S. 507/228
Pasadena, CA 91109
(818) 577-9267

LESK, Arnie
Solavolt International
P.O. Box 2934
Phoenix, AZ 85062
(602) 231-6458

LINDHOLM, Fredrik A.
University of Florida
4406 SW 17th Terrace
Gainesville, FL 32608
(904) 392-4929

LINDMAYER, Joseph
Solarex Corp.
1335 Piccard Drive
Rockville, MD 20850
(301) 948-0202

LOFERSKI, Joseph J.
Brown University
Prof. of Engineering
Box D
Providence, RI 02912
(401) 863-2870

MILSTEIN, Joseph
Solar Energy Research Institute
1617 Cole Blvd.
Golden, CO 80401
(303) 231-7299

MINAHAN, Joseph A.
Spectrolab, Inc.
12500 Gladstone Avenue
Sylmar, CA 91342
(818) 365-4611, X872

MOACANIN, Jovan
Jet Propulsion Laboratory
4800 Oak Grove Drive, M.S. 122-123
Pasadena, CA 91109

MOKASHI, Anant R.
Jet Propulsion Laboratory
4800 Oak Grove Drive, M.S. 238/343
Pasadena, CA 91109
(818) 354-6017

NATESH, Ram
Materials Research, Inc.
790 East 700 South
Centerville, UT 84014
(801) 298-4000

NEUGROSCHEL, Arnost
University of Florida
Electrical Engineering
Gainesville, FL 32611
(904) 392-4949

OLSEN, Larry C.
Joint Center for Graduate Study
100 Sprout Road
Richland, WA 99352
(509) 375-3176

PEARCE, Charles W.
AT&T Technology Systems
555 Union Blvd., 323800
Allentown, PA 18103
(215) 439-7711

PHILLIPS, Mary J.
Jet Propulsion Laboratory
4800 Oak Grove Drive, M.S. 502/422
Pasadena, CA 91109
(818) 577-9096

PRINCE, Dr. Morton
U. S. Department of Energy
Forrestal Building, CE 333
1000 Independence Ave., SW, 5E066
Washington, DC 20585
(202) 252-1725

PRYOR, Robert
Solavolt International
P.O. Box 2934
Phoenix, AZ 85062
(602) 231-6454

RAI-CHOUDHURY, P.
Westinghouse Electric Corp.
1310 Beulah Road
Pittsburgh, PA 15235
(412) 256-1891

RALPH, Eugene L.
Hughes Aircraft
6445 N. Willard Ave.
San Gabriel, CA 91775
(213) 647-8855

RAO, Hari
Mobil Solar Energy Corp.
4 Suburban Park Dr.
Billerica, MA 91821
(617) 893-8826

ROHATGI, Ajeet
Westinghouse Electric Corp.
1310 Beulah Road
Pittsburgh, PA 15235
(412) 256-1905

ROSE, Ben
Sandia National Laboratories
Kirtland AFG Base - East
P.O. Box 5800, Div. 6224
Albuquerque, NM 87185
(505) 846-4516

SAH, C. Tang
C. T. Sah Associates
403 Pond Ridge Lane
Urbana, IL 61801
(217) 384-5205

SAKIOTIS, Nick
Solavolt International
P.O. Box 2934
Phoenix, AZ 85062
(602) 231-6449

SALTZMAN, Dennis
Solavolt International
P.O. Box 2934
Phoenix, AZ 85062
(602) 231-6441

SCHMIDT, Wilfried
Telefunken Electronic GmbH
Theresienstr. 2
Heilbronn, West Germany 7100
(07131) 882-665

SCHMIT, Rusty
Solavolt International
P.O. Box 2934
Phoenix, AZ 80562
(602) 231- 6436

SCHRODER, Dieter K.
Arizona State University
Electrical Engineering Department
Tempe, AZ 85287
(602) 965-6621

SCHUMACHER, Joseph C.
J. C. Schumacher Co.
580 Airport Road
Oceanside, CA 92054
(619) 433-1663

SCHUYLER, Terry W.
Solar Energy Research Institute
1617 Cole Blvd.
Golden, C) 80404
(303) 231-1106

SCHWARTZ, Richard
Purdue University
Electrical Eng'g Department
West Lafayette, IN 47907

SCHWUTTKE, G.H.
GHS Research & Development
8162 East Del Pico Drive
Scottsdale, AZ 85258
(602) 951-0422

SCOLARO, Anthony
U. S. Department of Energy
Forrestal Building, CE 333
1000 Independence Ave., SW, 5E066
Washington, DC 20585
(202) 252-5548

SCOTT-MONCK, John A.
Jet Propulsion Laboratory
4800 Oak Grove Drive, M.S. 125/231
Pasadena, CA 91109
(818) 354-7625

SHIMADA, Katsunori
Jet Propulsion Laboratory
4800 Oak Grive Drive, M.S. 507/228
Pasadena, CA 91109
(818) 577-9626

SIRTL, Erhard
Heliotronic GMBH
Johannes-Hess-Strasse 24
8263 Burghausen, West Germany
08677-83-2580

SMOKLER, Melvin I.
Jet Propulsion Laboratory
4800 Oak Grove Drive, M.S. 507/201
Pasadena, CA 91109
(818) 577-9238

SOPORI, Bhushan
Solavolt International
P.O. Box 2934
Phoenix, SZ 85062
(602) 231- 6446

SPITZER, Mark
Spire Corp.
Patriots Park
Bedford, MA 01730
(617) 275-6000

SUREK, Thomas
Solar Energy Research Institute
Program Office Manager
1617 Cole Blvd.
Golden, CO 80401
(303) 231-1371

SWANSON, Richard M.
Associate Professor
Stanford University, Stanford Elec. Labs
McCullough 204
Stanford, CA 94305
(415) 497-0804

TAN, Teh Y.
IBM Corp. General Technology Division
Z-40E
Hopewell Heights, NY 12533
(914) 894-3140

TODOROF, William
Alternative Energy Systems, Inc.
20442 Sun Valley Drive
Laguna Beach, CA 92651
(714) 494-9433

TURNER, Gary B.
ARCO Solar, Inc.
P.O. Box 4400
Woodland Hills, CA 91365
(818) 700-7159

TUSTIN, David G.
Jet Propulsion Laboratory
4800 Oak Grove Drive, M.S. 502/422
Pasadena, CA 91109
(818) 577-9096

VANN, Hank VB
ARCO Solar, Inc.
P.O. Box 4400
Woodland Hills, CA 91365
(805) 489-7981

von ROOS, Oldwig
Jet Propulsion Laboratory
4800 Oak Grove Drive, M.S. 512/103
Pasadena, CA 91109
(818) 577-9994

WEINMEISTER, Roger
Solavolt International
P.O. Box 2934
Phoenix, AZ 85062
(602) 231- 6427

WOLF, Martin
University of Pennsylvania
304 Moore, D-2
Philadelphia, PA 19104
(215) 898-4822

YOO, Henry
ARCO Solar, Inc.
P.O. Box 4400
Woodland Hills, CA 91365
(805) 484-7981

CONTENTS

SESSION I

OVERVIEW
(M. Prince, U.S. Department of Energy, Chairman) 3

Historical Perspective of Barriers to Achieving High-Efficiency Silicon Solar Cells
(J. Lindmayer, Solarex Corp) 7

Some Aspects of the Minority Carriers Lifetime in Silicon
(P. Landsberg, University of Southampton) 13

Review of Recombination Phenomena in High-Efficiency Solar Cells
(C.T. Sah, C.T. Sah Associates) 37

SESSION II

HIGH-EFFICIENCY CONCEPTS
(M. Wolf, University of Pennsylvania, Chairman)

Silicon Solar Cell Efficiency Improvement: Status and Outlook
(M. Wolf, University of Pennsylvania) 53

Some Practical Considerations for Economical Back Contact Formation on High-Efficiency Solar Cells
(A. Lesk, Solavolt International) 77

High-Efficiency Cell Concepts on Low-Cost Silicon Sheet
(R. Bell, Mobil Solar Energy Corp.) 87

High Lifetime Silicon Processing
(R. Swanson, Stanford University) 107

Silicon MINP Solar Cells
(L. Olsen, University of Washington, Joint Center for Graduate Study) 123

DINNER SPEAKER
High-Efficiency Solar Cell Research for Space Applications
(D. Flood, NASA Lewis Research Center) 147

PRECEDING PAGE BLANK NOT FILMED

SESSION III

SURFACE-INTERFACE EFFECTS
(L. Kazmerski, Solar Energy Research Institute, Chairman)

Atomic Structure of the Annealed Si (111) Surface
(D. Chadi, Xerox Palo Alto Research Center) 163

Surface and Interface Characteristics
(L. Kazmerski, Solar Energy Research Institute) 189

Nitridation of SiO_2 for Surface Passivation
(S. Lai, Intel Corp.) 209

Surface Passivation and Junction Formation Using Low-Energy Hydrogen Implants
(S. Fonash, Pennsylvania State University) 221

Analysis of Interface Parameters
(C. Bates, Stanford University) 239

Chemical Structure of Interfaces
(F. Grunthaner, Jet Propulsion Laboratory) . . . . . .

SESSION IV

BULK EFFECTS
(E. Sirtl, Heliotronic GmbH, Chairman)

Structural Defects in Crystalline Silicon
(E. Sirtl, Heliotronic GmbH) 241

Oxygen and Carbon Impurities and Related Defects in Silicon
(C. Pearce, AT&T Technology) 243

Current Understanding of Point Defects and Diffusion Processes in Silicon
(T. Tan, IBM Corp.) 257

Defects in Web Dendrite Silicon Ribbon Crystals and Their Influence on Minority Carrier Lifetime
(G. Schwuttke, Arizona State University) 279

EBIC Characterization and Hydrogen Passivation in Silicon Sheet
(J. Hanoka, Mobil Solar Energy Corp.) 299

Measurement of Electrical Parameters and Current Components in the Bulk of Silicon Solar Cells
(A. Neugroschel, University of Florida) 311

SESSION V

MODELING
(R. Schwartz, Purdue University, Chairman)

Current Status of One and Two Dimensional Numerical Models: Successes and Limitations
(R. Schwartz, Purdue University) 331

Application of Closed-Form Solution Using Recursion Relationship in Silicon Solar Cells
(M. Lamorte, Research Triangle Institute) 351

Phenomena Simulation for Heavy Doping and Surface Recombination Velocity
(F. Lindholm, University of Florida) 371

SESSION VI

HIGH-EFFICIENCY DEVICE PROCESSING
(P. Rai-Choudhury, Westinghouse Electric Co., Chairman)

High-Efficiency Large-Area Polysilicon Solar Cells
(S. Johnson, Solarex Corp.) 403

High-Efficiency Solar Cell Processing
(F. Ho, Applied Solar Energy Corp.) 419

Process and Design Considerations for High-Efficiency Solar Cells
(A. Rohatgi, Westinghouse Electric Co.) 429

Processing Technology for High-Efficiency Silicon Solar Cells
(M. Spitzer, Spire Corp.) 447

Texture Etching of (100) Silicon for Solar Cells
(L. Dyer, Texas Instruments, Inc.) 471

SUMMARY AND DISCUSSION SESSION 485

INTRODUCTORY REMARKS

KOLIWAD: My name is Kris Koliwad. I am from the Flat-Plate Solar Array Project. It is my pleasure this morning to welcome you all to this Forum on High-Efficiency Crystalline Solar Cells on behalf of the FSA Project at the Jet Propulsion Laboratory, and of the Department of Energy. If you go through the agenda, you will notice that this is indeed an impressive gathering, and we are fortunate to have you at this meeting.

I will say a few words about the driving force for this Research Forum and the other Research Forums we have held covering different subjects relevant to our Project objectives.

The driving force for this workshop is, of course, the goals stated in the Five-Year Research Plan of the Department of Energy, which succinctly states that the five-year goal of flat-plate collector research is to establish technologies by 1988 that industry can apply to the production of 15%-efficient crystalline silicon modules. Among other things, this goal is coupled with $\$90/m^2$ silicon sheet.

SESSION I

OVERVIEW

M. Prince, Chairman

SESSION I

OVERVIEW

M.B. Prince
U.S. Department of Energy

PRINCE: I want to thank the organizers for inviting me to attend this meeting. It has given me an opportunity to get back and read some of the literature again, which I haven't done as thoroughly, perhaps, as I should have done during the last few years. In fact, I have here a whole stack of reports that indicate that high efficiency is extremely interesting to many of us here -- and I see that many of the authors of these reports are here today. There are a few who are not here, but I am sure that if we need them we can call upon them for some help.

Before getting into our program, I thought I should make a couple of comments to you about the 1985 budget, which many of you are concerned about. Two weeks ago, Congress finally got together and compromised on the recommendations from the Appropriations Committee. They compromised by going to the lower of the two numbers between the House and the Senate. So this puts us in a bind this coming year. The Administration asked for $47.5 million, and the House agreed to the $47.5 million with a provision that $2 million of that be spent on the Residential Experiment Stations. The Senate, on the other hand, took what we presented and upped it by $4 million, which would include $2 million on the Residential Experiment Stations. So the net result is that we have a Program operating budget of $46.5 million, a capital-equipment budget of $1 million, and a construction budget of $9.5 million for the SMUD project. So we are going to end up with about $2 million less than we had expected from the President's budget, and this is putting a squeeze on all three of the main laboratories, that is, SERI, Sandia, and JPL. We are working this out now trying to find out how we meet our budget, how we perhaps extend contracts into the next fiscal year so we don't have to reduce as much we might have to. You will hear more about that from the various laboratories over the next six months as we keep revising the budget and we will finally end up by the first of October or the first of November with a final budget.

This session will run until 11:55. We have three speakers, and this will give us plenty of time for discussions, questions, answers, and other comments that anyone wants to make.

I was originally going to start off the session with a historical review of the efficiency problem, where it started and where it is going, but on reading the abstracts, I see there are a couple of other papers on the subject, so I am just going to let those speakers cover it. Joe Lindmayer has a little bit in his and Martin Wolf has some in his abstract. So I thought what I would do today is give some general background so that those people who are not familiar with solar cells specifically, and there are several in the audience, would have a reference point as to what the terminology is that we use. Perhaps we can establish some terminology

that will allow us to talk consistently during the next three days.

On the first slide I show a general schematic of how the solar cell is composed; we have the material to start with, the diffused emitter or a p-n junction, and for this particular diagram I assumed n-on-p material. You put contacts on the back. We usually have some sort of an oxide on the top surface and an antireflective coating. We usually have some sort of a grid metal contact. I used the dimension w as the depth of the diffused or emitter region, and d is the thickness of the device.

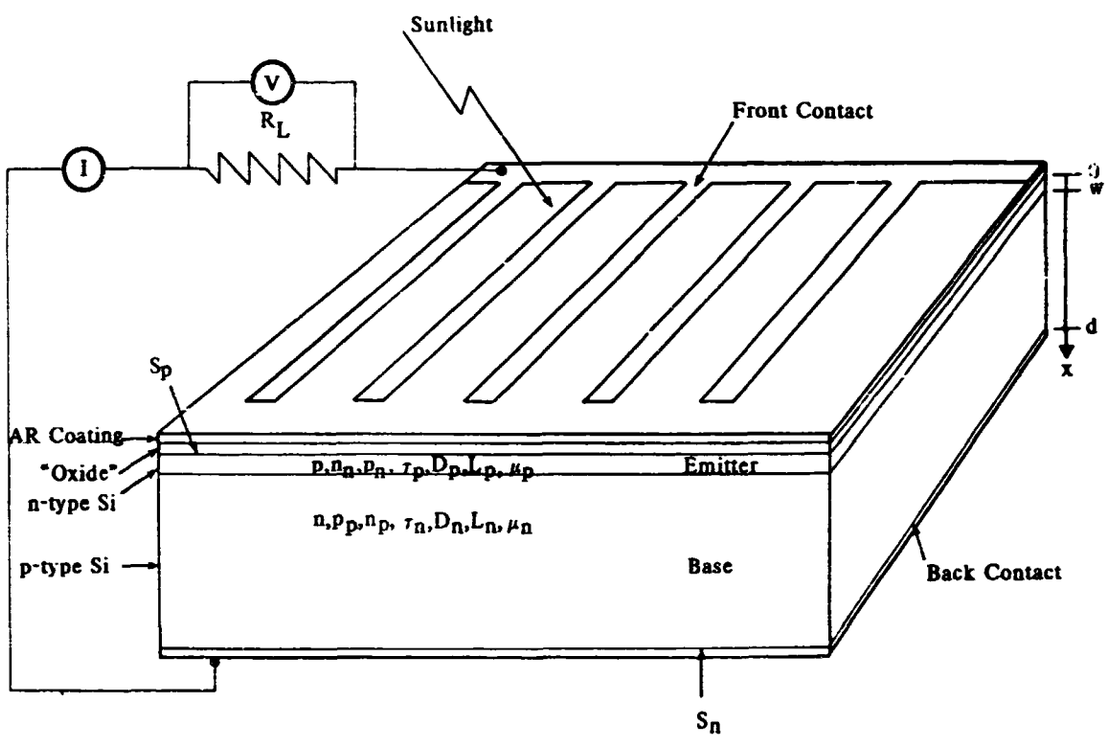

CONTINUITY EQUATIONS

$$\frac{\partial p}{\partial t} = -\frac{p}{\tau_p} + D_p \frac{\partial^2 p}{\partial x^2} - \mu_p \frac{\partial}{\partial x}[(p+p_n)E] + g(x)$$

$$\frac{\partial n}{\partial t} = -\frac{n}{\tau_n} + D_n \frac{\partial^2 n}{\partial x^2} - \mu_n \frac{\partial}{\partial x}[(n+n_p)E] + g(x)$$

BOUNDARY CONDITIONS

$$D_p \; (\partial p/\partial x)_{x=o} = S_p p$$

$$D_n \; (\partial n/\partial x)_{x=d} = S_n n$$

$$p\,(W) = 0$$
$$n\,(W) = 0$$

$$g(x) = \alpha N e^{-\alpha x}$$

CONTINUITY EQUATIONS

$$\frac{d^2p}{dx^2} - \frac{1}{L_p^2}\, p + \frac{\alpha N}{D_p}\, e^{-\alpha x} = 0$$

$$\frac{d^2n}{dx^2} - \frac{1}{L_n^2}\, n + \frac{\alpha N}{D_n}\, e^{-\alpha x} = 0$$

$$L_p = \sqrt{D_p \tau_p}$$

$$I = I_o \left[e^{\frac{q(V + IR_s)}{AkT}} - 1 \right] + \frac{V + IR_s}{R_{sh}} - I_L$$

$$R_{sh} \sim \infty$$

$$I_{sc} = -I_L$$

$$V_{oc} = \frac{AkT}{q} \ln \left(\frac{I_L}{I_o} + 1 \right) \simeq \frac{AkT}{q} \ln \frac{I_L}{I_o}$$

$$I_o = \frac{q\, p_n D_p}{L_p} + \frac{q\, n_p D_n}{L_n} = q \left(p_n \sqrt{\frac{D_p}{\tau_p}} + n_p \sqrt{\frac{D_n}{\tau_n}} \right)$$

$$P_{max} = I_{sc} * V_{oc} * FF$$

FACTORS AFFECTING EFFICIENCY

MECHANICAL FACTORS

- Depth of Junction (w)
- Thickness of Wafer (d)
- Series Resistance (contact geometry)
- Front Surface Roughness (light trapping)
- Contact Shadowing
- Operating Temperature

PHYSICAL FACTORS

- Base Resistivity
  (τ_n, D_n, μ_n, L_n, n_p)
- Emitter Impurity Distribution
  ($\tau_{p_{eff.}}$, $\mu_{p_{eff.}}$, $p_{n_{eff.}}$)
- Back Surface Impurity Distribution
- Recombination and Scattering Centers in Base and Emitter

DEVICE FACTORS

- Surface Recombination Velocity (front, back, under contacts)
- Reflecting Back Surface
- AR Coating
- High Eg Window (oxide, etc.)
- Series Resistance
- Shunt Resistance
- Reverse Saturation Current (I_o)

I hope this will give you some idea of the complexity of the problem. I can see that there are so many variations possible, and many of us have worked on a whole bunch of these, but to my knowledge very few of us have looked at the overall picture. In review of the abstracts, there are a couple of papers there that do cover a huge number of these parameters.

That gives you some background and I would like to get started with the three talks today that we have in this session. We have only one limitation, and that is that we want to break around 11:55 because we have a very narrow window for lunch. In this period we will be very flexible in the time that we use for presentations, and for questions and answers, and I hope we will have quite a few questions and answers from the floor.

We have asked Joe Lindmayer to give us the first paper this morning, because Joe made a major contribution in the space program back in the late 60's and he developed a purple cell that gave us a step-function increase in the efficiency we can get with space-type cells. He is going to talk to us on a historical perspective of barriers to achieving high-efficiency silicon solar cells. Joe founded and is still with the Solarex Corp. in Rockville, Maryland.

J. Lindmayer's abstract is presented here. His paper and visual material were not presented for publication.

HISTORICAL PERSPECTIVE OF BARRIERS TO ACHIEVING HIGH-EFFICIENCY SILICON SOLAR CELLS

J. Lindmayer

Solarex Corp.
Rockville, Maryland

N85-31616

Early silicon solar cells were made of metallurgical-grade silicon with very low efficiency; this was accomplished before the p-n junction theory was understood. The single-crystal silicon introduced in the mid-50's abruptly increased the efficiency to the 5% to 10% region. Throughout the 1960s significant research money was spent to establish the technology of the 2 x 2 cm or 2 x 4 cm space solar cell with 10% efficiency. At this point a certain plateau has developed.

In the early 1970s work related to the violet cell upset the status quo and space solar cells and cells in general became significantly more efficient. The rest of the decade became characterized by establishing a terrestrial photovoltaic technology to support the development of a new industry. Costs per watt became the dominant consideration and frequently the efficiency was compromised. This mentality is present even today as the terrestrial photovoltaic industry continues to develop. Attempts to introduce new materials and other forms of silicon dropped the efficiency and it is now a state of mind that accomplishing 10% efficiency with some alternative combination is regarded as success.

Silicon solar cells are clearly capable of delivering efficiencies much greater than 10%. As the photovoltaic industry will show signs of stabilization, the attention will once again focus on achieving the manufacturable higher efficiency solar cells.

DISCUSSION

PRINCE: As everyone here knows, you have been very forthright in pursuing semicrystalline silicon, and I am just wondering what your feelings are as to the ultimate potential efficiency that one can obtain from such materials? Have you given much thought to this?

LINDMAYER: I think that very frequently the efficiency is somewhat lower than normal single crystal Czochralski material. In getting into this kind of crystallization, anybody who works with it will know that it creates a whole set of new unanswered questions. But I think the efficiency is just a little bit, maybe just 5% or 10%, lower than normal single crystal at this time.

LESK: Joe, in Kris Koliwad's introductory remarks, he indicated that the objective was 15% efficiency in a module -- it wasn't on the slide -- but then he said the price has got to be a lot lower than it is now. His price projects to $90/m^2$ of substrate in the module, if you allow perhaps half of that for the cast polysilicon substrate. Do you feel it will ever get to that price, considering that we still lack 15% efficiency?

LINDMAYER: This is a difficult question. Right now I think we are running a gap to start with. I think if we had much better personnel, or much better-educated people in the production lines and among those running production lines -- there is a gap of maybe 12% to 13% already and that 15% would be possible to achieve. After all, many of us sit down in the lab and generate solar cells that are 15% or better. But somehow the production line never does it. So I think the 15% goal is achievable, definitely in the lab, anyway. But production is something else.

PRINCE: I think we should bring up one other point before we go on. In order to get this 15% module that Kris mentioned, we need to have cells that are about 18% efficient because you have losses in assembling these cells into the module, and covering the module with some protection, and lost area, and so forth. So when we talk about 15% modules, it means about an 18% cell in production, which may mean a 20% cell or a 21% cell in the laboratory. I do remember from an early experience that if you can do it in a laboratory, you can transfer to very good production people, then you can then produce exactly the same quality in the production line.

LINDMAYER: Yes. This is an important point. A 15% panel efficiency requires very much higher-efficiency cells.

LOFERSKI: I am surprised that you are saying that the problem is with the education level of people on the production line. It seems to me that if you have a good production line going, it has to be do-able with all the kinds of people that you have presently on production lines, basically. If you want to hold the price down, you can't have Ph.D.'s making solar cells, so I think it is not in the education of the people but rather in the industrial engineering that is involved or in manufacturing engineering, carrying things from the laboratory into production. We have to be

able to make that transition. After all, when Arnie asked you about the price at that 15% module efficiency, $90/m^2, it means $0.60 per peak watt and we can't even make the current 10% efficient cells at $0.60 per peak watt, so there is a lot to be done; there is a big gap between where we are now and what is required by 1988. But anyway, I would like your comment on this business of who is on the production line now. I am surprised at that comment that you need better people.

LINDMAYER: Well, I was merely referring to middle management. True Ph.D.'s cannot run a production line. They have never succeeded. I am not advocating that there should be more Ph.D.s on the production line. The workers themselves do routine work, so it is the middle management in technical capacities that is really missing. But with respect to the other goal, getting down to $90/m^2, I think it is going to be hard.

DYER: It is interesting that in the early 1950s, when Mark Shepard was head of Texas Instruments' production of semiconductor devices, he wrote an article, "Ph.D.'s on the Production Line," and the results are evident. I think what you are saying, Joe, is that in the early stages, that is what you need. Once it becomes a mature product, you can't afford it. But to get it going right, there is nothing wrong with it.

PRINCE: Are there any other questions? Yes, Gene.

RALPH: Joe, I think I see a conflict between what you practice and what you preach. Not just you but other companies as well. I think there is a definite feeling that making something cheaper means going to simpler and less sophisticated approaches, and I put the contacting systems, the use of the Semix type of materials, in that category. You give away efficiency in the hope of getting lower-cost processing, and of getting immediate gains that way. But you say now that you agree that the 15% module goal is really the right thing to go to. Now, it sounds to me as though your middle management or even your top management has to be educated then in the difference -- getting immediate cost gains by going to simple, cheap processing that gives you lower efficiency, versus very sophisticated processing that has to be automated or robotized or whatever it is to get the cost down. Are you saying that you are ready, or you would see management -- see that new approach to 15% being the right way, or are we going to go back to the old way?

LINDMAYER: Any technology change results in some efficiency drop but can be immediately observed as climbing up again in time as people begin to master that technology and understand its details. So sometimes it is very difficult to tell in advance that a technology change is automatically compromising efficiency. I think it is just a philosophical point.

MILSTEIN: I would like to comment that in the way our high-efficiency program has been conducted over the past year or two we have not, as we stated in the RFP that we issued in 1982, considered the matter of cost reduction. That is something that we feel is best left to industry. The point of doing that, though, is that it allows a researcher to investigate techniques that at the present time may be extremely expensive, but that

may lead to understanding or additional capability. They then may be re-engineered or reconfigured in some way to be done for less expense at the time you want to put them into production. In that sense, the conception of artificially holding down the cost, if you apply it to research, may simply prevent you from looking at techniques that you would otherwise be able to examine. You may miss something.

LINDMAYER: I don't think we have any real conflict here. Dr. Koliwad carefully put the emphasis on the cost because, as the industry is now, industry has put in more private money than the government has put into this program. And it is going to be doing more of this.

LANDSBERG: The discussion has prompted me to ask you a question, Mort, about the DOE program. You mentioned two figures, the $90/m^2$ and the 15% efficiency. Why not just give the $90/m^2$? Why is the efficiency constraint given as well? I mean, you have a very cheap amorphous cell that does better than $90/m^2$ but is less than 10% efficient. What do you say about that?

PRINCE: It is very straightforward, Peter. If you have a 5% cell versus a 15% cell or module, you need three times the area; the land cost, the wiring cost, and so forth. There are many other costs that go up, and that is why you need the combination of both parameters.

LINDMAYER: I also believe, if I could add to this, that maybe it is more appropriate for DOE to set up technology and scientific goals than R&D goals and economic goals at this point in time.

WOLF: Joe, you mentioned that it is often advantageous to introduce a somewhat cheaper process and take a loss in efficiency, and the efficiency may come back as we gain experience. This in some cases may happen. On the other hand, the opposite can also easily be the case: you move a step to higher efficiency, but at a higher cost, and then you are learning as your production teaches you how to do this more and more cheaply. In fact, it seems to me if you go the other way, you also have to be very careful in evaluating whether the cheaper process does not have a limit that doesn't permit you to get back more efficiency. You mentioned metallization screen printing. You use relatively expensive metals, but you never get low resistivity, you always end up with a higher resistivity in the center of materials, it seems. So you have a penalty. It seems you cannot get through narrower lines with the screen printing process than you can with some other processes. You may have to -- toward the beginning -- say yes, it would give me a cheaper process, but I don't see where it can get me back to the higher efficiencies. I think you have to evaluate it carefully before you make a decision of this sort.

LINDMAYER: I agree with you that there are two sides of this equation.

PRINCE: I think we have to be careful that we don't get off into the cost aspects of silicon cells and modules. This meeting is about efficiency, so unless you have a specific question relating to efficiency and not cost, please hold them for a discussion during the coffee break.

SCHWUTTKE: Joe, I would like to pick up on that comment you made, that we need better education in manufacturing. I look at it in a different way. I don't think we really need better education in manufacturing. We are confronted by a situation where you have relatively, and I say relatively, little or indifferent education on one side, and on the other side, the Ph.D. side, we have relatively too much education. You really are confronted with a problem; you are dealing with two different types of people, and this is the problem you have. It is a communication problem; the manufacturing guy does not respect the Ph.D. guy, the Ph.D. guy does not respect the manufacturing guy, so what you end up with is the following situation (I have seen this over the years over and over and over again): you have two efforts running parallel and these two characters never talk to each other, the manufacturing guys want to outdo the Ph.D.'s, and the Ph.D.'s want to outdo the manufacturing people. I think what we need is not better education; we need better communication, and that could save us an awful lot of money.

LINDMAYER: Very good point.

SIRTL: Mort, I come back to your comment about "let's not talk about economy, let's talk about high efficiency." I think it can be a dangerous attitude, at least in part, because an 18% solar cell, even in space technology, is not reality today on a 10 x 10 cm^2 substrate, and if we talk about the best we could do about making high-efficiency cells at present, we have to talk about float-zone material. It may be very nice to explore the best material available -- some mechanisms we don't understand -- but I think we should be careful not to emphasize too much that kind of investigation alone. After all we have learned to date, float-zone material would not be a good material as a basis for economical production, so we may be forced to switch too late to other systems that offer a much more economical background for making the solar cells. I just wanted to bring up that point because the float-zone defect situation, for instance, is much different from any kind of polycrystalline material or whatever else you may choose.

PRINCE: You have a very good point there. In fact, I talked with Ted Ciszek specifically about this problem: can we produce float-zone material at a similar cost to Czochralski material; he has given me some positive indication that it is possible. I don't know whether we should make comments about this at this time, or later.

SCHUMACHER: I would like to know if anyone has ever built a module that would give you 15% efficiency regardless of whether it was done by Ph.D.'s or who have you, and if not, why wouldn't that be a good objective -- just to assemble the best team you could and build the very best module you ever could -- and then you can begin as a second priority to go after reaching this cost objective. I happen to think that single-crystalline silicon would be a very nice thing to use in these solar cells. I would think you would try to get the very most out of it that you could, and I think that would be the ideal approach.

LINDMAYER: I think that at least small panels have been made that are good, but not 1 m^2. This was really just done in the lab.

ASPECTS OF SILICON BULK LIFETIMES

P.T. Landsberg
University of Southampton,
Southampton, SO9 5NH, England.

N85 31617

Abstract

Following some general remarks about (a) high efficiencies and (b) recombination lifetimes, two specific questions are considered. First, an analysis is made of the best lifetimes which have been attained for bulk crystalline silicon as a function of doping concentrations. This is done by adopting a separability assumption that the dopants which set the Fermi level do not contribute to the recombination traffic which is due to the unknown defect. This defect is assumed to have two charge states: neutral and negative, the neutral defect concentration being frozen-in at some temperature T_f. It is essential for the higher doping concentrations to include the band-band Auger effect by using a generalisation of the Shockley-Read-Hall (S.R.H.) mechanism. We infer single-electron band trap recombination coefficients of order 10^{-9} cm^3s^{-1} and an unknown defect level near mid-gap. Some speculations concerning its nature are also offered. Secondly, the above-mentioned generalisation of the SRH mechanism is discussed in detail by giving relevant formulae and quoting recent comparisons with experiment. This formulation gives a straightforward procedure for incorporating both band-band and band-trap Auger effects in the SRH procedure. There are two related questions which arise in this context: (a) It may sometimes be useful to write the steady-state occupation probability of the traps implied by SRH procedure in a form which approximates to the Fermi-Dirac distribution. It is shown how this can be done. (b) Some brief remarks about the effect on the SRH mechanism of spreading N_t levels at one energy uniformly over a range of energies will also be made.

PRECEDING PAGE BLANK NOT FILMED

1. Introduction

In this talk I want to discuss two topics of importance for the improvement of silicon solar cells. The first (§4), relates to the problem of the residual defect in silicon. Working backwards from the measured lifetime - doping relationship, we shall ask if there is some single level with some capture probabilities which can account for the best lifetimes. The answer turns out that there seems to be such a level, but to identify its precise nature requires more experiments. The second topic is the identification of Auger trap and/or Auger band coefficients by an analysis which closely resembles that familiar from the Shockley-Read-Hall (SRH) statistics. With the increasing importance of heavy doping in devices, this rarely used procedure is worth noting and it will be described in some detail. Although not new it has been used only once or twice, and it ought to be more widely known.

As this is an "overview" talk, the work indicated above is preceded by general remarks on high efficiencies (§2) and lifetimes (§3).

2. General remarks : efficiencies

The achievement of 18%+ efficient solar cells based on terrestrial conditions and single crystal silicon has recently been reported. A key element in the design is a thin (20-50 Å) SiO_2 layer to passivate those n^+ silicon surface regions which are without a contact [1]. A first question to be raised is if one knows that SiO_2 is the ideal layer. One knows that other layers can be used, for example in MIS structures[2] ; it would be interesting and important to know their effect on device performance. [There are of course other ways of attaining high efficiencies, for example by the use of ion implantation, high resistivity silicon and using surface passivation[3]]. This is the first problem to which I want to direct attention.

A second potential method of obtaining high efficiencies is to employ several cells of different energy gaps in one unit (or even in separate units so that there are four or more terminals). If one envisages black-body radiation at 6000K and a very idealised model, a two gap tandem cell might push the efficiency up from a theoretical one-gap value of 31% to a two-gap value of 42.9%[4,5]. Some idea of the fall-off of efficiencies for non-optimal band gaps is obtained from Figure 1[5]. More realistically, one can study tandem cells based on, for example, a combination of amorphous and crystalline silicon as has been done at M.I.T. Figure 2 shows the results of such a calculation assuming optimised gaps, silicon properties for all gaps, one sun and room temperature operation. A four-terminal arrangement is seen to be best, but in this calculation, one finds only a modest improvement of 30% efficiency over the ideal 27.5% for a single junction crystalline cell. This makes the additional complication arising from a second junction of doubtful benefit[6]. An additional problem with tandem cells is that an optimal adjustment of a tandem cell for one spectrum is upset if the incident spectrum is changed by cloudiness. The investigation of such matters represents a second problem to which I want to direct attention. Note that these high theoretical efficiencies for tandem cells have not even been

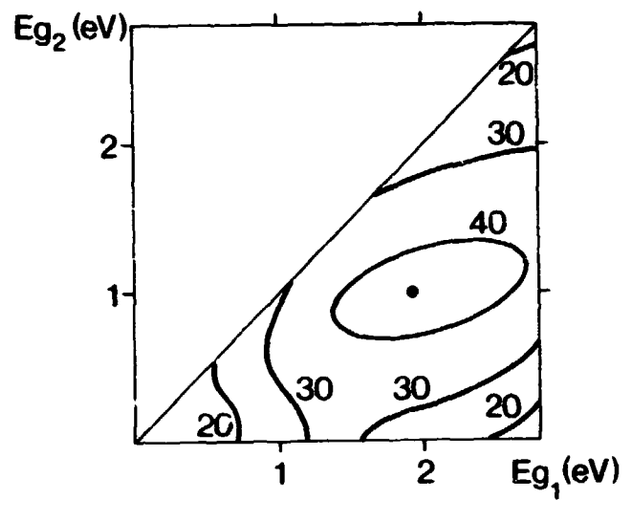

Figure 1. Maximum iso-efficiency curves for a two-band gap cell at 1 sun assuming a black-body spectrum at a black-body temperature twenty times the ambient temperature [5].

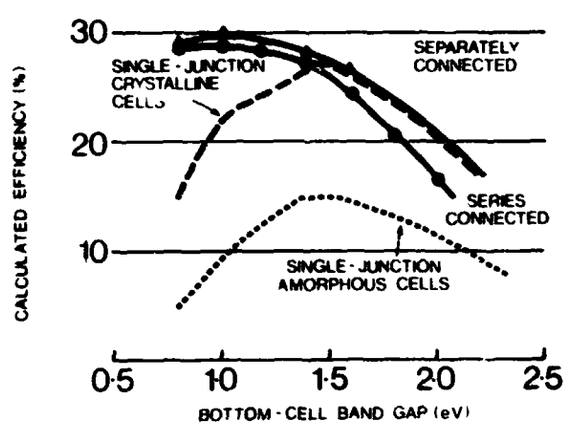

Figure 2. Maximum AMI, 1 sun conversion efficiencies of crystalline-on-amorphous silicon tandem structures at room temperature if separately connected (4-terminals) or in series (2-terminals) [6].

realised approximately in practice. Presumably surface problems and recombination at surfaces are among the difficulties which have impeded progress.

Multi-gap structures entirely based on amorphous silicon have also been considered. For a three-gap structure in series (E_g = 2.0, 1.7, 1.45 eV) a 7% efficiency was attained, compared with a theoretical 24% (7). Our main interest here is, however, in crystalline silicon.

There is an additional step which can be taken, namely to raise the mobility of the current carriers by confining them to a well in the conduction band produced by growing different materials on top of each other. In this kind of multi-hetero junction scheme the electrons travel in a two-dimensional well. They have dropped into it from a region containing the original dopants. These are thus left behind leaving to the electrons a region relatively free of ionised impurity scattering. The need to pursue these ideas, is my third problem. A start has been made with it at the Sandia National Laboratory(8).

3. General remarks : Lifetimes

Properties of a silicon wafer may be specified by giving details concerning:

- Electrical properties (resistivity, conductivity type, lifetime, etc.)
- Mechanical properties (thickness, vacancy and interstitial densites, etc.)
- Chemical properties (chemical impurity concentrations, stoichiometry, etc.)
- Surface properties (surface scratches and roughness, etc.).

Of all these many parameters I shall here been concerned only with the lifetime τ against recombination. Because it is normally larger than the dielectric relaxation time τ_D one keeps up a non-equilibrium steady state between electrons and holes and can have lifetimes and diffusion lengths which are greater than zero. [The opposite situation $\tau \ll \tau_D$ characterises the so-called relaxation semiconductor in which the Fermi levels are locally coincident.] In order to improve solar cells one has to increase τ further.

Lifetimes may be improved by gettering metallic impurities like Au, Fe, Cu which provide deep recombination centres, using a mixture of O_2 and HCl. Dislocations help to getter most impurities but unfortunately they provide recombination sites themselves, particularly in the presence of vacancies.

During processing the high temperatures induce the formation of thermal defects (vacancies, interstitials, etc.) some of which are quenched into the final material and cannot be annealed out altogether. Particularly when dislocation-free material is used, and dislocation gettering is therefore not available, these mechanical defects tend to agglomorate and to give rise to aggregates of defects (some are known as "swirls") which also shorten lifetimes. This problem presents a "point defect dilemma"(9).

It should be remembered that a good understanding of lifetimes is desirable not only because one wants long lifetimes in solar cells. One additional reason is that lifetime monitoring is important in device processing. It is used for example in neutron transmutation doping in which the uniformly distributed isotope ^{30}Si is converted into phosphorus dopant which is therefore also uniformly distributed:

$$^{30}Si \rightarrow {}^{31}P + \beta ray.$$

Lifetime measurements designed to assess the quality of the starting ingot is also in use[10,11]. A second additional reason for understanding lifetimes is that for some device applications lifetime reduction is required, notably for fast-switching bipolar transistors. This reduction may be achieved (after fabrication) by electron beam irradiation, or (during fabrication) by introducing "killer centres" such as Au and Pt.

4. The residual defect in silicon

If one looks at measured silicon lifetimes as a function of doping, one finds the jumble of points shown in Figure 3.

However, one may consider only the best lifetimes for given doping on the argument that these crystals have attained some ideal lifetime, limited only by a particular, but unknown, defect. This defect could be mechanical (interstitial), chemical, or an association of several of these. In this view the dopants help to set the Fermi level, but do not participate in the recombination traffic which limits the lifetime. The recombination defects, on the other hand, although of low concentration, are included in the Fermi level equation. This is a kind of "separability assumption" for Fermi level and lifetimes and it will be adopted here. What are the characteristics of this "residual" lifetime limiting defect?

To answer this question we have added to the separability assumption, secondly, the hypothesis that the defect has only one recombination level and that if it is occupied it is negatively charged; otherwise it is neutral. A third assumption is that the concentration of neutral defects is that which is "frozen in" at a temperature T_f with an activation energy E_a, so that[13]

$$N_d^x = (5 \times 10^{22}) \exp(-E_a/kT_f)\ cm^{-3}. \qquad (1)$$

The numerical factor is the atomic density of silicon.

The procedure now is to regard (1) as giving the maximum solubility of the neutral defect as T_f. This is independent of the location in the material and of Fermi level. The defect has a negative charge state linked to N_d^X by

$$N_d^- / N_d^X = \exp[(F - E_d)/kT_f].$$

Hence an increase in n-doping, by raising the Fermi level, raises N_d^- and so raises

$$N_d = N_d^X + N_d^-.$$

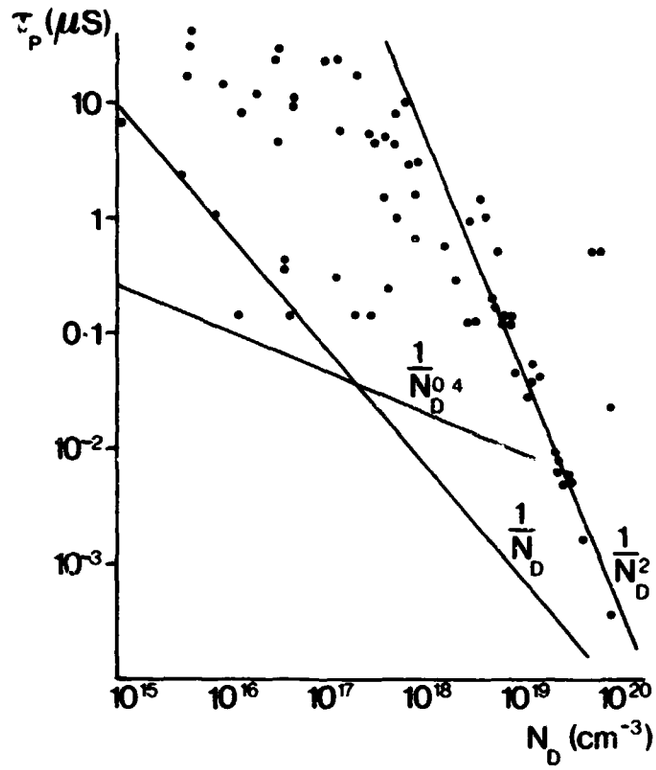

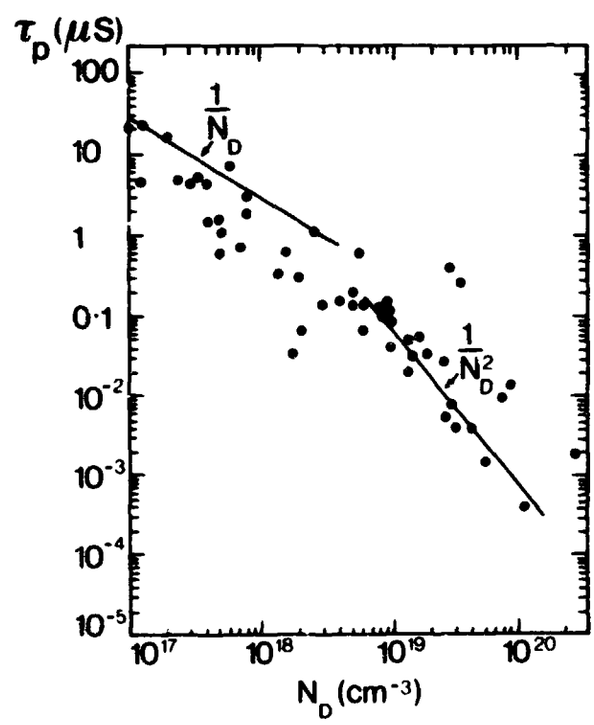

Figure 3 Some experimental minority hole lifetimes in n type silicon (a) from reference 12. (b) from reference 13.

This leads to a lowering of τ_p (N_D) with doping. However, increase in p-doping lowers the Fermi level and hence N_d. This leads to longer lifetimes $\tau_n(N_A)$ with doping until these lifetimes are pulled down again by the band-band Auger effect[14] as shown in Figure 4. Assumption 2 concerning the charge on the unknown defect enables therefore the model to reproduce the asymmetric behaviour observed experimentally as regards τ_n compared with τ_p.

The lifetime curves for the correct concentration N_d of defects, as calculated at T_f, are used at the lower measurement temperature T, assuming a generalised Shockley-Read mechanism[15]. They follow roughly $(N_d)^{-1}$ with doping, until they are both pulled down by band-band Auger effects.

The notation for the recombination constant is shown in Figure 5. We use B^S, B_1, B_2 for band-band recombination and T_1^S, T_2^S, T_1 ..... T_4 for recombination involving traps[14]. A superfix S indicates a single-electron (non-Auger) transition, the other symbols refer to Auger effects. Following Fossum et al[13,15] one can neglect T_1, T_2, T_3, T_4 and B^S and adopt

$$B_1 = 2B_2 = 2 \times 10^{-31}\ cm^6\ s^{-1}.$$

As to T_1^S, T_2^S, one may regard them as fitting parameters, along with T_f and E_a. The inferred values are then found to be :

$$\left.\begin{array}{l} 2T_1^S = T_2^S \sim 5 \times 10^{-9}\ cm^3\ s^{-1}, \\ E_a = 1.375\ eV, \quad T_f = 620\ K. \\ \text{Position of defect level : 45 meV above mid-gap.} \end{array}\right\} (2)$$

The resulting fit is shown in Figure 4.

We are left with two matters of controversy : (1) What is T_f in equn.(1)? (2) What is the nature of the defect specified in (2)?

As to the first question, recall the early quenching experiments on silicon which led to a relation of the type[17]

$$\frac{1}{\tau} = C \exp(-E_a/kT_q)$$

where the activation energy was found to be 0.6 eV, τ was the minority carrier lifetime and T_q was the temperature from which the sample was quenched. Data enabling one to find C was given later for these thermally generated recombination centres:

$$C \sim 2.13 \times 10^{13}\ s^{-1}, \qquad E_a = 0.9\ eV.$$

[18; note that the captions of Figures 8 and 10 should be interchanged]. More recently a thermally generated donor density

$$\nu = C' \exp(-E_a/kT_q)$$

was found with $C' \sim 8 \times 10^{23}\ cm^{-3}$, $E_a = 2.5$ eV in "pure" p-type silicon.

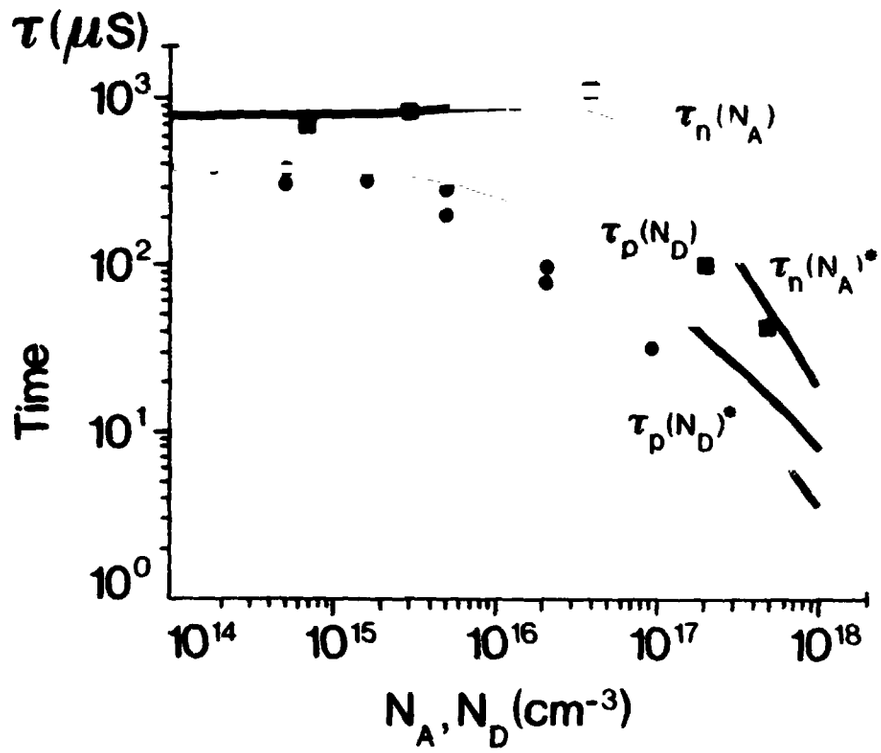

Figure 4. Doping dependence of the best room temperature minority carrier lifetime in silicon according to experiments (points). Asterisks indicate that the band Auger process is included along with the normal Shockley–Read process (unasterisked). Circles (for holes) and square (for electrons) represent experimental points (14).

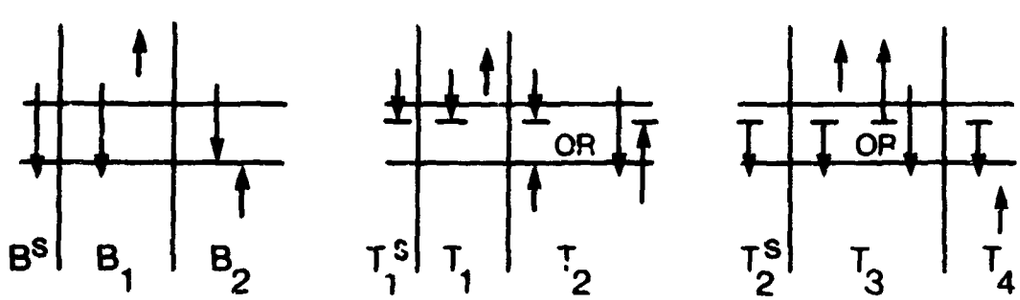

Figure 5. The notation for the recombination constants.

The appropriate level was located 0.37 eV above the valence band edge [19]. These results suggest that (1) is a reasonable assumption and that the freezing-in temperature T_f may be identified as the quenching temperature for infinitely rapid cooling at least for some heat treatment histories. This corresponds to the "perfect" quench. Departure from the perfect quench by slower cooling should lead to $T_f < T_q$. This relation between T_f and T_q needs further study.

The second question is made difficult by the variety of levels found by different methods in the forbidden gap of silicon. In particular we cite nine relevant pre-1980 papers on thermally generated and/or quenched-in centres in silicon [20-28]. Thus a donor level at $E_v + 0.4$ eV was found in p-type silicon in [19,20] and in boron-doped silicon in [21], but not in (22) where the boron concentration was heavier. It was again found in (24) as a complicated defect. The thermally generated defects were found to be hard to anneal out in (25) and in later work.

In a series of later papers fast ("s") and slow ("r", "r'", "r"") thermal recombination centres were found and characterised. They have formation energies of 1.0 eV, 1.2 eV and 2.5 eV (26), the slower centres being less soluble. The high binding energy and the consequent difficulty of annealing out thermal centres was confirmed (27,28). The slow centres were attributed to vacancy-Cu complexes and later to vacancy-oxygen complexes (29). The fast centres were attributed to native defects [(29), Figure 3].

As regards energy level structure, many inconsistencies remain. Some of the discrepancies between the various experiments have been attributed to electrically active defects connected with traces of iron in silicon which may have been present in varying amounts (30). They can be kept down to below 10^{14} cm^{-3} by special treatment. Iron-related deep levels have, in fact, been studied separately (31) as has the level at 0.45 eV above the valence band edge (32).

Swirl defects (due to point defect agglomerates, presumably interstitial) of formation energy 1.3 eV - 1.4 eV were also noted in p-type floating zone grown heat-treated silicon (33), and their annealing characteristics differ from those of divacancies of a similar formation energy (1.3 eV).

Two possible interpretations of the defect inferred here and characterised in (2) will now be proposed. The first suggestion is that it is a swirl. The A-type swirl, believed to consist of dislocation loops, loop clusters, etc., occurs in concentrations of typically 10^6 - 10^7 cm^{-3}, and is therefore not a serious candidate. B-type swirls are smaller and are found in concentrations up to 10^{11} cm^{-3} or so (34). This is of the order (10^{11} - 10^{13} cm^{-3}) of defect density implied by Figure 2 of (14). The formation activation energy of 1.3 - 1.4 eV (33) is also of the right order. If such swirls can supply an acceptor level near mid-gap (their energy level structure does not seem to be well known yet), the swirl B would be a serious candidate. This interpretation of the "residual" defect in silicon as used for semiconductor work, if correct, would be of importance for two reasons : In the first place swirl defects are known to have detrimental effects on silicon, and secondly the elimination of swirl defects is under active study. One can use slow or

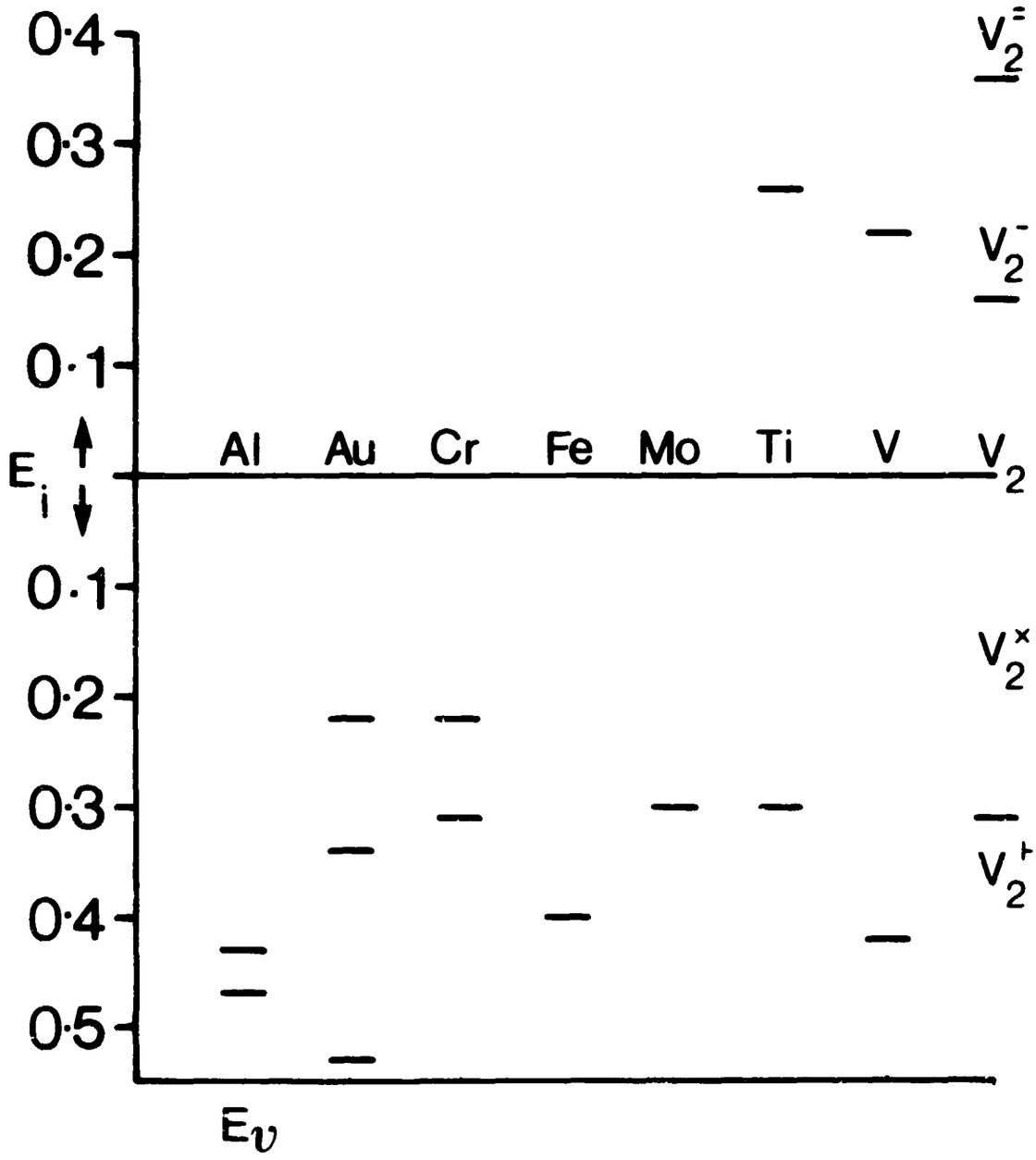

Figure 6. Some deep levels in silicon due to divacancies V_2 [36] and due to metallic ions [37].

fast crystal pulling rates, inert ambients during growth, or annealing after growth to reduce their occurrence.

A second candidate is the "s" (native, fast) recombination centre (29). The slow centres ("r, r', r" ") have levels which lie too close to the band edges, whereas the "s" centre has a level near mid-gap. A recombination coefficient for minority carriers of $\sim 10^{-7}$ cm^3 s^{-1} has been suggested (23) which is 100 times larger than our inferred values of $T_1^s \sim T_2^s \sim 10^{-9}$ cm^3 s^{-1}. This could, however, be understood in terms of different thermal histories. It is, of course, possible that the "s"-centre and the swirl B centre are the same defect. Even a very recent study (35) on the relation between recombination mechanisms and doping density leaves these matters unresolved. It is hoped that the above suggestions may, however, stimulate further work.

Deep level spectra are not well known, but some are shown in Figure 6 and it will be seen that they do <u>not</u> apply to the residual defect identified here.

5. Auger effects in trapping statistics

In the above discussion the Shockley-Read-Hall trapping mechanism has been invoked in order to arrive at a lifetime. However, the effect of additional Auger processes was not incorporated in the original version of 1952. This extension was made in 1963 (38) well before device engineers took an interest in heavy-doping phenomena. Because I believe this incorporation of Auger effects to yield an important new and useful concept, I have developed it and applied it from time to time(15,39,40). In the present context the motivation for such an extension of the Shockley-Read-Hall mechanism is particularly obvious: The reverse diode saturation current J_o should be kept small in a solar cell to reduce loss by recombination. The minority (electron) carrier recombination rate per unit volume is for the simplest picture of a p-type layer

$$\frac{n - n_{po}}{\tau_n} = \frac{n_{po}}{\tau_n} (\exp \delta\gamma_n - 1) = \frac{n_i^2}{N_A \tau_n} (\exp \delta\gamma_n - 1)$$

where $\delta\gamma_n$ is the electron Fermi level excess over its equilibrium value divided by kT. It has also been assumed that the p-type material is non-degenerate with all acceptors ionised :

$$n_{po} p_{po} = n_i^2 = n_{po} N_A$$

The bulk recombination can therefore be held down by heavy doping and this brings in Auger effects as their rate tends to dominate over single carrier transitions at high carrier densities. [The improvement of the basic material by identifying and, if possible, removing deep level recombination, also indicated by this argument, was dealt with in section 4].

The need for heavy doping can also be seen from the open-circuit voltage of solar cells which in a simple theory should increase with doping but i

fact declines after going through a maximum. An early curve of this kind was given by Iles and Soclof[41].

Turning to the incorporation of the Auger effects shown in Figure 6 into the SRH trapping statistics scheme, the simplest way of doing the algebra may be as follows.

Let N_0 and N_1 be the concentration of centres or defects without a trapped electron and with a trapped electron, and let $N_d = N_0 + N_1$ be the total defect concentration. Let n, p be electron and hole concentrations so that for non-degenerate material we have

Electron capture rate	$\propto nN_0$	(G)
Electron emission rate	$\propto N_1$	(Gn_1)
Hole capture rate	$\propto pN_1$	(H)
Hole emission rate	$\propto N_0$	(Hp_1)

The coefficients of proportionality, which we shall identify later, are also shown. All one needs is the steady state condition for the centres, by equating the nett electron and hole capture rates per unit volume:

$$G(nN_0 - n_1N_1) = H(pN_1 - p_1N_0) \qquad (3)$$

This gives steady-state occupation fractions

$$\frac{N_1}{N_d} = \frac{Gn + Hp_1}{G(n+n_1)+H(p+p_1)},$$

so that

$$\frac{N_0}{N_d} = 1 - \frac{N_1}{N_d} \qquad (4)$$

Substitution for N_0 and N_1 from (4) into the left-hand side of (3) gives the steady-state trap recombination rate per unit volume :

$$U_{st.st} = \frac{np - n_1p_1}{(N_dH)^{-1}(n+n_1)+(N_dG)^{-1}(p+p_1)} \qquad (5)$$

This has the general shape of the usual S.R.H. result, except that n_1, p_1, G, H need interpretation.

The factors n_1 and p_1 are not interesting ; they follow from (3) if detailed balance is assumed:

$$n_1 = \left(\frac{nN_0}{N_1}\right)_{eq} = N_c e^{\eta_d - \eta_c} \tag{6}$$

where η_t and η_c are the energies of trap level and conduction band edge, each divided by kT. Similarly

$$p_1 = \left(\frac{pN_1}{N_0}\right)_{eq} = e^{\eta_v - \eta_d} \tag{7}$$

where η_v refers to the valence band edge. It follows that

$$n_1 p_1 = (np)_{eq} = n_i^2 .$$

However, G and H are more interesting : we must include all the six trapping processes of Figure 5, making the electron capture rate per unit volume

$$GnN_0 = T_1^S nN_0 + T_1 n^2 N_0 + T_2 npN_0,$$

$$\text{i.e.} G = T_1^S + T_1 n + T_2 p. \tag{8}$$

Similarly

$$H = T_2^S + T_2 n + T_3 p \tag{9}$$

The picture is completed by adding the band-band recombination rate per unit volume

$$Fnp, \qquad F = B^S + B_1 n + B_2 p \tag{10}$$

Hence the total steady-state recombination rate per unit volume is [38]

$$U = \left[F + \frac{1}{(N_d H)^{-1}(n+n_1)+(N_d G)^{-1}(p+p_1)}\right](np-n_i^2) \tag{11}$$

We now proceed to some special cases of interest.

Consider now the minority carrier lifetimes. In p-type material one has $p \sim p_0$ (the equilibrium concentrations receive now a suffix zero) so that

$$\frac{1}{\tau_n} = \frac{U}{n-n_o} \simeq \frac{(n-n_o)p}{n-n_o}\left[F + \frac{N_d G}{p+p_1}\right] = pF + \frac{p}{p+p_1} N_d G. \tag{12}$$

$$\frac{1}{\tau_p} = \frac{U}{p-p_o} \simeq \frac{(p-p_o)n}{p-p_o}\left[F + \frac{N_d H}{n+n_1}\right] = nF + \frac{n}{n+n_1} N_d H. \qquad (13)$$

If $n_1 \ll n$, $p_1 \ll p$, one has, underlining terms liable to dominate,

$$\frac{1}{\tau_n} \simeq (B_1^S + B_1 n + \underline{B_2 p})p + (T_1^S + T_1 n + \underline{T_2 p})\, N_d \qquad (14)$$

$$\frac{1}{\tau_p} \simeq (B_1^S + \underline{B_1 n} + B_2 p)n + (T_2^S + \underline{T_3 n} + T_4 p)N_d \qquad (15)$$

These formulae were in reasonable agreement with earlier (1962) experiments on Germanium when these results were first tested shortly after they were proposed[42]. However, it took a surprising eighteen years before an explicit test was made [43]. Some of the results are shown in Figure 7 and Table 1. There is reasonable agreement between theory, equation (15) in this case, and experiment. [The classical S.R.H. results are found if one puts

$$B_1^S = B_1 = B_2 = T_1 = T_2 = T_3 = T_4 = 0]. \qquad (16)$$

Table 1

Some inferred values from a fit of equation (15) to the data of Figure 7 at 300K. Based on reference 43

	$(T_2^S N_d)^{-1}$	$T_3 N_d$	T_3/T_2^S
Au diffusion at 850°C	$15\ 10^{-8}$ s	5.3×10^{-12} cm^{3}s^{-1}	$7.95\ 10^{-19}$ cm^3
Au diffusion at 920°C	$1.3\ 10^{-8}$ s	82×10^{-12} cm^{3}s^{-1}	$10.7\ 10^{-19}$ cm^3

We thus have a method, capable of being applied to experiments, which is the natural extension of S.R.H. statistics. As Auger effects have often to be taken into account, this method should rival S.R.H. statistics in popularity. The only complication is the need to know the additional recombination coefficients. But as was seen in (16) some of these may be put equal to zero in specific cases.

There is a question of a more academic nature which the above results bring up: The steady-state occupation probability (4) of the recombination

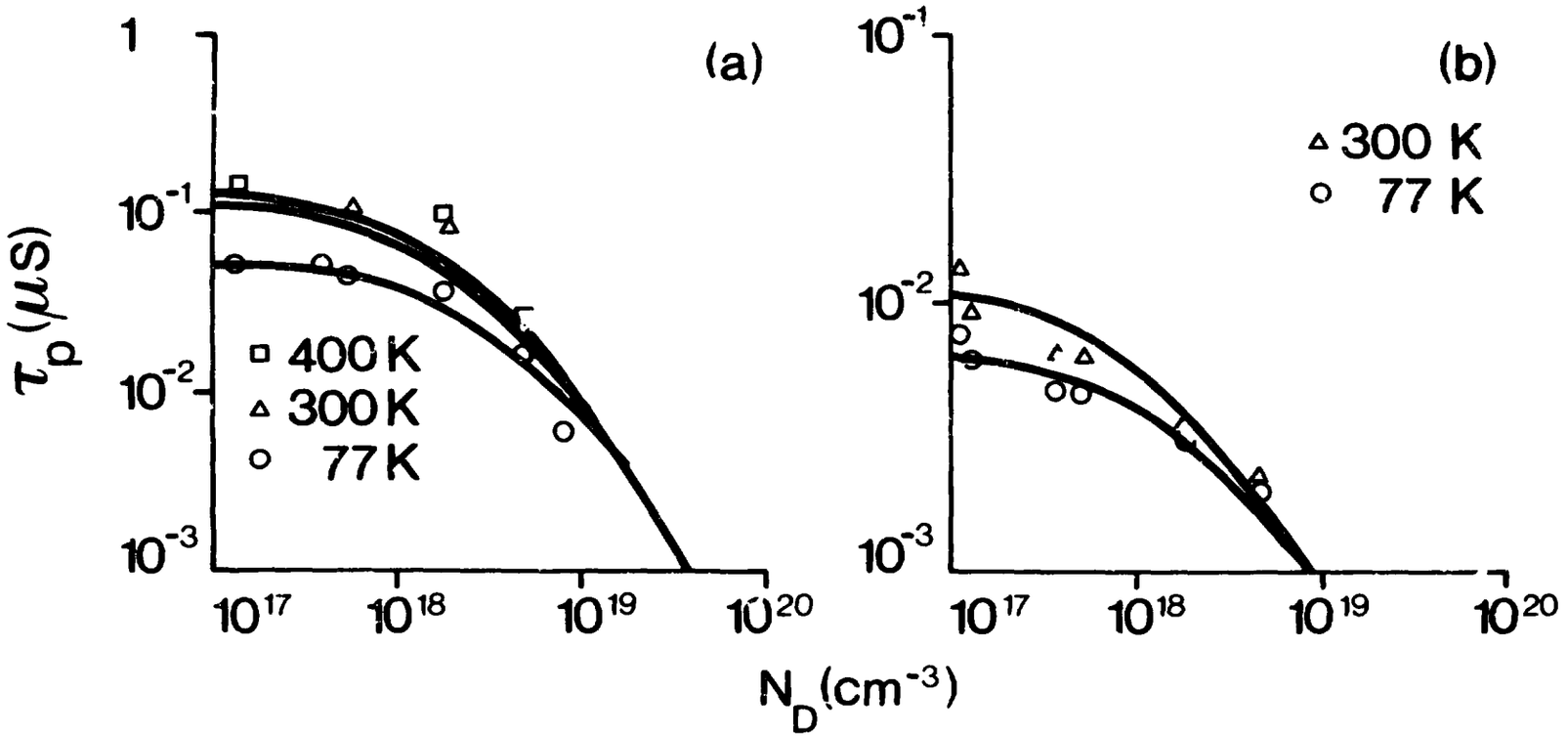

Figure 7. Hole lifetime in n-type Si as a function of electron concentration for different temperatures. The samples were diffused with Au : (a) at 850°C, (b) at 920°C. The curves are fits of equation (15) to the data with $B_1^S = B_2 = T_4 = 0$ [43].

centres should go over into the normal Fermi-Dirac function in equilibrium:

$$\left(\frac{N_1}{N_d}\right)_0 = \frac{1}{\exp(\eta_d - \gamma_o)+1} \tag{17}$$

where γ_o is the equilibrium Fermi level divided by kT and the degeneracy factor has been absorbed in η_d. At first sight it is not easy to see how this can come about. However, one can rewrite (4) as

$$\frac{N_1}{N_d} = \frac{1}{h\exp(\eta_d - \gamma_o)+1} \tag{18}$$

which solves the problem provided one can show that $h \to 1$ in thermal equilibrium. This is so. In fact one finds

$$h = \exp[\gamma_o - \frac{1}{2}(\gamma_e + \gamma_h)] \frac{\cosh[\alpha + \frac{1}{2}(\gamma_h - \gamma_o)]}{\cosh[\alpha + \frac{1}{2}(\gamma_e - \gamma_o)]} \tag{19}$$

where

$$\exp\alpha = Gn_1/Hp_o. \tag{20}$$

In thermal equilibrium $h \to 1$, as expected. The results (18) - (20) seem to be new. They were first found in reference 44.

A question not investigated much (but see [40]), though it could be of importance for lifetimes, is the following: How is the recombination lifetime changed if N_d levels at an energy E_d are spread out with constant density to extend from $E_d - \varepsilon$ to $E_d + \varepsilon$?. This doubt arises occasionally in modelling situations. To answer this question one can use the generalised S.R.H. process, assuming that defect-defect transitions are negligible. This matter is under investigation. Preliminary results suggest that, depending on the position of E_d and on the excess carrier concentration, the recombination rate can move in either direction. For a defect at midgap a decrease is more likely, while an increase is favoured if the defect is in the upper part of the gap provided the excess carrier concentration is not too large. More details will be reported in due course.

6. Additional comment after the work was completed.

A defect similar to the one inferred here (in section 4) appears to have been found in swirl-and dislocation-free float zone grown silicon by deep level transient spectroscopy and derivative surface photovoltage (45). This dominant recombination level was located at E_v + 0.56eV with a capture cross section for holes equal to twice the capture cross section for electrons:

$$\sigma_2{}^S = 2\sigma_1{}^S = 10^{-14}\ \mathrm{cm}^2 \qquad (21)$$

in fair agreement with the specification (2), above, of the defect identified here. If one puts

$$T_2{}^S = f\ v\ \sigma_2{}^S \quad (v \sim 10^7\ \mathrm{cm/s} \sim \text{thermal velocity})$$

and inserts our value for $T_2{}^S$ and relation (21) the factor f (giving a recombination efficiency) turns out to be

$$f = 0.05.$$

The same result is found if $T_1{}^S$ and $\sigma_1{}^S$ are used. These authors suggest that the defect may be a self-interstitial or a cluster of these - this is a third possibility in addition to the two noted in section 4.

REFERENCES

1. A. W. Blakers, M.A.Green, S. Jiqun, E. M. Kel[illegible], S.R. Wenham, R. B. Godfrey, T. Szpitalak and M.R.Willison, [illegible]-percent efficient terrestrial silicon solar cells", IEEE Electron Device Letters EDL 5, 12-13 (1984).

2. P. T. Landsberg and C. Klimpke, "Theory of the Schottky barrier solar cell", Proc. Roy. Soc. A 354, 101-118 (1977).
C. M. H. Klimpke and P. T. Landsberg, "An improved analysis of the Schottky barrier solar cell", Solid-State Electronics 24 401-406 (1981).

3. M. B. Spitzer, C. J. Keavney, S. P. Tobin and J. B. Milstein, "Ion implanted silicon solar cells with 18% conversion efficiency", 17th I.E.E.E. Photovoltaic Specialist Conference, Orlando, May 1984.

4. A. de Vos, "Detailed balance limit of the efficiency of tandem solar cells", J.Phys. D 13, 839-846 (1980). An exposition of these theories is given in P. T. Landsberg, "Non-equilibrium concepts in solar energy conversion", NATO Advanced Study Institute, Erice, 1983 Ed. B. di Bartolo (New York : Plenum Press), to be published.

5. A. de Vos and D. Vyncke. "Solar energy conversion : Photovoltaic versus photothermal conversion", 5th E.C. Photovoltaic Solar Energy Conference, Athens, October 1983.

6. J. C. C. Fan and B. J. Palm[illegible], "Optimal design of amorphous/crystalline tandem cells", Solar Cells 11 247-261 (1984).

7. Y. Kuwano, M. Ohnishi, H. Nishiwaki, S. Tsuda, T. Fukatsu, K. Enomoto, Y. Nakashima and H. Tarni, "Multi-gap amorphous Si solar cells prepared by the consecutive, separated reaction chamber method", 16th I.E.E.E. Photovoltaic Specialist Conference, San Diego, Sept. 1982.

8. R. J. Chaffin, G. C. Osbourn, L. K. Dawson and R. M. Biefeld, "Strained superlattice, quantum well, multijunction photovoltaic cell", 17th I.E.E.E. Photovoltaic Specialist Conference, Orlando, May 1984.

9. E. Sirtl, "Facts and trends in silicon material processing", in Semiconductor Silicon 1977, Ed. H. R. Huff and E. Sirtl, (Princeton: Electrochemical Society, 1977), p.4.

10. R. Westbrook (Ed.) Lifetime Factors in Silicon, Am. Soc. for the Testing of Materials, Spec. Tech. Publication No. 712 (1980).

11. D. C. Gupta (Ed.) Silicon Processing, Am. Soc for the Testing of Materials, Spec. Tech. Publication No. 804 (1983).

12. B. Ross, "Survey of literature on minority carrier lifetimes in silicon and related topics", in Lifetime Factors in Silicon reference as in 10, p.14-28.

13. J. G. Fossum and D. S. Lee, "A physical model for the dependence of carrier lifetime on doping density", Solid-State Electronics 25 741-747 (1982).

14. P. T. Landsberg and G. S. Kousik, "The connection between carrier lifetime and doping density in non-degenerate semiconductors", J. App. Phys. 55, (1984).

15. P. T. Landsberg, "Semiconductor Statistics", in Vol. 1 (Ed. W. Paul) of the Handbook of Semiconductors (Ed. T. S. Moss) (Amsterdam : North Holland, 1982), pp. 405-416.

16. J. G. Fossum, R. P. Mertens, D. S. Lee and J. F. Nijs, "Carrier recombination and lifetime in heavily doped silicon", Solid-State Electronics, 26 569-576 (1983).

17. G. Bemski, "Quenched-in recombination centres in silicon", Physical Review 103 567-569 (1956).

18. B. Ross and J. R. Madigan, "Thermal generation of recombination centres in silicon", Phys.Rev. 108 1428-1433 (1957).

19. L. Elstner and W. Kamprath, "Quenched-in levels in p-type silicon", Phys. Status Solidi 22 541-547 (1967).

20. G. Bemski and C. A. Dias, "Quenched-in defects in p-type silicon", J.App.Phys. 35 2983-2985 (1964).

21. M. L. Swanson, "Defects in quenched silicon", Phys.Status Solidi 33 721-730 (1969).

22. G. Swenson, "Impurity conduction in quenched p-type silicon", Phy.Status Solidi (a) 2 803-808 (1970).

23. V. D. Glinchuk, N. M. Litovchenko, L. F. Linnit and R. Merker, "Decay of excess carrier concentration in thermally treated silicon," Phys.Stat.Sol. (a) 18 749-756 (1973).

24. W. Leskochek, H. Feichtinger and G. Vidrich, "Thermally induced defects in n-type and p-type silicon", Phys. Status Solidi (a) 20 601-610 (1973).

25. L. D. Yau and C. T. Sah, "Quenched-in centres in silicon p^+n junctions", Solid-State Electronics, 17 193-201 (1974).

26. V. D. Glinchuk, N. M. Litovchenko and R. Merker, "Solubility and origin of thermally induced recombination centres in n-type and p-type silicon", Phys. Status Solidi (a) 30 K109-113 (1975).

27. K. D. Glinchuk, N. M. Litovchenko and R. Merker, "The role of impurities in the formation of quenched-in recombination centres in thermally treated silicon", Phys. Stat. Solidi (a) 33 K87-90 (1976).

28. K. D. Glinchuk, N. M. Litovchenko and R. Merker, "Effect of quenching rate and annealing on the concentration of quenched-in recombination centres in heat-treated silicon", Phys. Status Solidi (a) 35 K157-160 (1976).

29. K. D. Glinchuk and N. M. Litovchenko, "Decay of excess carriers in thermally treated oxygen-doped silicon", Phys.Stat.Solidi (a) 58 549-555 (1980).

30. G. Borchardt, E. Weber and N. Wiehl, "High-purity thermal treatment of silicon", J. App. Phys. 52 1603-1604 (1981).

31. K. Wünstel and P. Wagner, "Ion-related deep levels in silicon", Solid State Comm. 40 797-799 (1980).

32. D. W. Ioannou, "Comments on the E_v + 0.45 eV quenched-in level in silicon", Phys.Stat. Solidi (a) 72, K33-36 (1982).

33. A. Usami, Y. Fujii and K. Morioka, "The effect of swirl defects on the minority carrier lifetime in heat-treated silicon crystals", J.Phys. D10, 899-910 (1977).

34. A. J. R. de Kock, "Crystal growth of bulk crystals : purification, doping and defects", in Handbook of Semiconductors (Ed. T. S. Moss), Vol.3, Materials, Properties and Preparation (Ed. S. P. Keller), (Amsterdam : North Holland, 1980), p.272.

35. L. Passari and E. Susi, "Recombination mechanisms and doping density in silicon", J.App.Phys. 54, 3935-3937 (1983).

36. M. Jaros, Deep Levels in Semiconductors (Bristol:Adam Hilger, 1982), p.253.

37. A. Rohatgi and P. Rai-Choudhury, "Defects and carrier lifetime in silicon", in Silicon Processing (Ed. D. C. Gupta) American Society for the Testing of Materials, Special Technical Publication 804 (1983) pp 383-404.

38. D. A. Evans and P. T. Landsberg, "Recombination statistics for Auger effects with applications to p-n junctions", Solid-State Electronics, 6 169-181 (1963).

39. P. T. Landsberg, "Some general recombination statistics for semiconductor surfaces", I.E.E.E. Trans. Electron Devices ED 29, 1284-1286 (1982).

40. P. T. Landsberg and M. S. Abrahams, "Surface recombination statistics at traps", Solid-State Electronics 26 841-849 (1983).

41. P. A. Iles and S. I. Soclof "Effect of impurity doping concentration on solar cell output", 11th I.E.E.E. Photovoltaic Specialist Conference, Arizona, 1975 pp 19-24.

42. P. T. Landsberg, D. A. Evans and C. Rhys-Roberts, "Auger effect involving recombination centres", Proc.Phys.Soc. 83 325-326 (1964).

43. W. Schmid and J. Reiner , "Minority-carrier lifetime in gold-diffused silicon at high carrier concentration", J.App.Phys. 53 6250-6252 (1982).

44. P. T. Landsberg and M. S. Abrahams, "Effects of surface states and of excitation on barrier heights in a simple model of a grain boundary or a surface", J.App.Phys. 5 (1984).

45. L. Jastrzebski and P. Zanzucci "Electronic characteristics of float zone grown silicon", (Electrochemical Society, Ed. H. R. Huff), pp 138-156.

DISCUSSION

SCHUMACHER: Well, Peter, I guess I don't understand the whole story here, but after all, in the Shockley-Read-Hall treatment of lifetime, the shifting of the Fermi level is taken into account, and there is an occupancy factor that tells you how many electrons, how many majority carriers there are in the centers for recombination. Then, as a result of that, the lifetime in less heavily doped material is higher than the lifetime in more heavily doped material. Of course, if you change the total number of recombination centers, then you can change the lifetime. You are saying that the number of recombination centers is changing because of the position of the Fermi level, not just the occupancy number. In order for what you saying to be true, it would be necessary for the total number of recombination centers to change.

LANDSBERG: Right. And so it does. I think I might not have made it clear. It is entirely my fault. Perhaps what I didn't explain quite well enough is that these dopants don't act as recombination; a kind of separability assumption that the defect acts as a recombination center. The dopant is merely there to set the Fermi level. Now, what happens is, as you said, the lifetime increases because the total number of defects has decreased.

SCHUMACHER: Then the X is the total number of defects.

LANDSBERG: No. The X is the total number of neutrals. So the neutral defect density is given by the solubility of the defect in the silicon.

SCHUMACHER: Then N_d^X is not the total number of defects?

LANDSBERG: There is an old paper by Hall and Shockley many years ago that discussed solubility. There were other people after this. They were talking largely about the solubility of the neutral species. That is always uniform; it is not affected by the p-n junction, and so on, because it doesn't react in an electric field because it is neutral.

TAN: Peter, I have two simple comments, made in good faith, and I hope you will accept them in good faith too. The first one is that in one early slide you said that in order to specify the material, silicon, you have something called a mechanical property. Those of us who work in the material characterization field refer to that as a physical defect. This is simply a misnomer, not important. The important part is that to my knowledge, up to today, we do not know how to specify that property in the same sense as you would with your electrical property.

LANDSBERG: I think it is a very interesting point you are making, because it is just where I am rather ignorant.

TAN: That is why I mentioned I made these comments in good faith.

LINDHOLM: I will be very brief, but some of the people here might want to know where some of these things were published. Can you tell us what is the status of that manuscript?

LANDSBERG: We didn't pay any reprint charges because we couldn't afford to.

LINDHOLM: That is a good comment for the sponsors to listen to.

LANDSBERG: Therefore, it is delayed. It is in the Journal of Applied Physics. The proofs have been seen but as far as I know it has not appeared yet.

LINDHOLM: As a point of clarification in sort of following up Joe Loferski's question: I think that your T_f on the slide stands for temperature of formation. You have an activation energy of 1.3 eV, and roughly figuring that out, that must mean around 600K. Do you remember that?

LANDSBERG: Yes. It was around 620K, something of that order.

SCHWUTTKE: Just a comment in supporting the characterization people on the previous comment. Looking back to my early years as a student, there was one hot subject, and you will remember this as well as I do. People were totally concerned for what we called color centers, and they studied this from a to b to c. And every month, almost, they discovered a new symbol. Then later on, once I graduated, they discovered one particle of matter, another particle of matter and I don't know how many particles of matter they have discovered by now. And then we were very proud that we defined crystal perfection by zero dislocation density and so we got accustomed to zero dislocation density and crystal perfection -- to characterize crystal perfection by the number of dislocations. And then, I believe, a lot of nuclear physicists got into silicon, and from there on we have had this tremendous confusion about crystal perfection. Today crystal perfection does not mean that you have zero dislocation. You are really addressing the state, the point defect state, in the materials. Basically, you can only talk about crystal perfection if you know the condition of every atom and what else is floating around. You are faced with some very difficult problems if you want to calculate something, because we just cannot provide you with the necessary detailed information that you need to make the proper calculation. So it is basically our shortcoming, not yours, and I would like apologize for that.

RECOMBINATION PHENOMENA IN HIGH EFFICIENCY SILICON SOLAR CELLS

C. Tang Sah
University of Illinois
Urbana, Illinois 61801

N85-31618

ABSTRACT

The dominant recombination phenomena which limit the highest efficiency attainable in silicon solar cells under terrestrial sunlight are reviewed. The ultimate achievable efficiency is limited by the two intrinsic recombination mechanisms, the interband Auger recombination and interband Radiative recombination, both of which occur in the entire cell body but principally in the base layer. It is estimated that an upper efficiency of 25.4% at AM1 or AM1.5 solar illumination can be attained if either Radiative or high-injection-level Auger recombination in the base is the only recombination loss mechanism in a cell with 50 micron thick base and at an absorbed photocurrent of 0.36 A/W. Thicker base will increase the efficiency slightly via higher absorbed photocurrent less higher Auger and Radiative recombinations in the larger volume. At 500 micron, the photocurrent is raised by 10.6% and the open-circuit voltage is reduced by about 60 mV due to larger recombination volume, giving a net efficiency gain of only about 0.6% to 26% at AM1. The low-level Auger recombination in the base gives a smaller efficiency of 24% in 50-micron base cell. This suggests that an optimum (26%) cell design is one with lowly doped 50-100 micron thick base, a perfect BSF, and zero extrinsic recombination such as the thermal mechanism at recombination centers (the Shockley-Read-Hall process) in the bulk, on the surface and at the interfaces. The importance of recombination at the interfaces of a high-efficiency cell is demonstrated by the ohmic contact on the back surface whose interface recombination velocity is infinite. To attain the Auger-recombination-limited efficiency in the base without a minority-carrier-blocking back-surface-field layer, the total majority carrier density in the base must exceed $10^{17}cm^{-2}$, an impractically large value requiring a one-centimeter thick cell at a doping concentration of $10^{17}cm^{-3}$ which would increase Auger and Radiative recombination by 200 over a 50 micron cell and reduce the limiting efficiency by 5% to 20%. The importance of surface and interface recombination is further demonstrated by representing the Auger and Radiative recombination losses by effective recombination velocities which are about 0.33 and 3.1 cm/s respectively at 25.4%. Thus, to reach the ultimate efficiency limit of 25.4%, real interfaces must have recombination velocities less than about $10^{-17}N_s$ or 1 cm/s at a surface impurity concentration of $N_s=10^{17}cm^{-3}$. The paper is concluded by demonstrating that the three highest efficiency cells (17,18,19%) may all be limited by the SRH recombination losses at recombination centers in the base layer. To reach the Auger and Radiative recombination-limited efficiency of 25.4%, the SRH recombination loss in the base must be decreased to give a minority carrier lifetime greater than $2x10^{14}/N_B$ or 2 ms at $10^{17}cm^{-3}$ base doping density. This corresponds to a dark current of 0.2 fA/cm^2 in the ideal diode law.

PRECEDING PAGE BLANK NOT FILMED

I. INTRODUCTION

Energy loss by photogenerated electrons and holes through scattering and recombination limits the ultimate performance of solar cells. Scattering reduces the mobilities of electrons and holes, increases the series resistance and decreases the fill factor (FF). Recombination increases the shunt conductance and the dark leakage current and decreases both the open-circuit voltage (VOC) and the short-circuit current (JSC). Energy loss during these two collision processes (scattering and recombination) will reduce the maximum efficiency (EFF) which is given by EFF=FF*VOC*JSC/PIN at an absorbed areal solar power density of PIN.

The ultimate efficiency is limited by two intrinsic recombination mechanisms in an ideal cell structure in which the scattering or series resistance loss and the extrinsic recombination losses are reduced to negligible levels. These two intrinsic recombination mechanisms are the interband (conduction-band to valence-band) radiative process and the interband Auger process. The interband Radiative recombination mechanism poses the ultimate limit while the interband Auger recombination mechanism may be reduced by proper cell design via dopant impurity density and layer thickness control. In a silicon p+/n/n+ or n+/p/p+ back-surface-field (BSF) cell design with 50 micron base layer thickness, the ultimate AM1 (or AM1.5) efficiency is about 25% at room temperature and both the Radiative and Auger mechanisms contribute about equally to the recombination loss.

This paper presents an analysis of the effects of the intrinsic and extrinsic recombination mechanisms on the performance of silicon p/n junction solar cells. Section II provides a review of the recombination mechanisms and locations and their effects on the performance of solar cell devices. Section III provides an analysis of the ultimate performance of ideal cells with no scattering losses. Section IV illustrates the effect of surface recombination and its large degrading effect on performance. Section V gives an analysis of the three highest-efficiency single-crystalline silicon solar cells which have been reported. It delineates the material factors which may have reduced their measured performance below that predicted by ideal diode law. A short concluding summary is given in Section VI.

II. RECOMBINATION MECHANISMS AND SITES

The electron-hole recombination processes can be categorized according to their origin. They can be further divided by the energy exchange mechanisms which control the recombination rate. Recombination processes with the intrinsic origin are those which limit the ultimate performance of a solar cell. Recombination processes due to imperfections in the crystal lattice, grouped by their extrinsic origin, such as chemical impurities and physical defects, can be reduced so that their deleterious effects on cell performance can be nearly eliminated. A categorization of these recombination processes are given below [1].

INTRINSIC MECHANISMS (Interband Transitions)		ENERGY EXCHANGE PARTNER
I.1	Thermal Recombination	Phonons(Lattice Vibration)
I.2	Radiative Recombination	Photons
I.3	Auger Recombination	Third Electron or Hole

EXTRINSIC MECHANISMS (Band-Bound Transitions)		ENERGY EXCHANGE PARTNER
E.1	Thermal Recombination (SRH)	Phonons
E.2	Radiative Recombination	Photons
E.3	Auger Recombination	Third Electron or Hole

A main fundamental difference between the intrinsic and the extrinsic recombination mechanisms is that the initial and the final states of the electron are in different bands separated by a large energy gap for the intrinsic processes. The energy exchange during the transition is much larger than the largest phonon energy, about 60 meV in solids. While for the extrinsic processes, the initial or final states is a bound state localized at a lattice imperfection, either an impurity or defect site, while the other is an unlocalized band state. The energy exchange covers both the small energy range of the phonons as well as the large energies near the energy gap. Thus, the intrinsic processes cannot be eliminated completely, although the Auger process, I.3, can be reduced since it depends on the presence of a third electron or hole and hence will dominate only in regions of high electron or hole concentration. However, the extrinsic processes can be reduced to negligible level so that they no longer affect the solar cell performance. The reduction of the extrinsic recombination mechanisms requires crystal perfections and purities in starting silicon as well as stressless and clean solar cell fabrication processes which exceed the latest silicon very large scale integrated circuit (VLSI circuit) technology.

Among the recombination processes, the intrinsic Auger and Radiative mechanism pose the ultimate limit while the extrinsic thermal (SRH or Shockley-Read-Hall) mechanism is the current technology limit. The recombination rate of the SRH mechanism is proportional to the density of the impurities and defects. These imperfections can be unintentionally but readily introduced during the cell fabrication procedures and they may also be present in the starting crystal, having been incorporated during crystal growth. Thus, to reduce the SRH recombination rate will tax the latest silicon VLSI technology and beyond.

These recombination processes can occur preferentially at certain regions and locations of a solar cells which suggest device design and technology innovations to reduce and eliminate them. A schematic illustration is shown by a cross-sectional view of a p+/n/n+ cell in Fig.1. The recombination processes can occur in the quasi-neutral emitter p+/, base /n/, and back-surface-field /n+ layers. They can also occur in the junction space charge layer of the p+/n junction, as well as at the oxide/Si and metal/Si or metal/oxide/silicon interfaces on the front and the back surfaces of the cell.

However, they are not all important in all of these regions. For example, in the highly-doped p+/ emitter layer, only the interband Auger and the SRH recombination mechanisms may be important. The interband Auger recombination can be important if the majority carrier density in the quasi-neutral emitter exceeds about 1.0E17 hole/cm^2 or a sheet resistance of about 0.6 ohm per square

since Auger recombination rate for the injected or photogenerated electrons in the p+/ emitter layer is proportional to the square of the hole concentration, P^2. For another example, the SRH recombination mechanism could also be important in the quasi-neutral p+/ emitter if the density of the defect recombination centers is greatly increased due to the heavy doping of the p+/ layer by incorporating a high concentration of boron impurity. Heavy doping introduces localized band-tail states and broadens the boron impurity level into an impurity band, both of which give a narrowing of the energy gap for the minority carriers or an increase of the intrinsic carrier density, n_i, or the minority carrier density. This would increase the minority carrier or electron recombination rate in the quasi-neutral emitter layer and reduce the solar cell performance. There has been no concrete evidence showing the importance of the localized or band-bound Auger recombination process (E.3) in the heavily doped emitter, although it is anticipated due to both the large majority carrier density and high density of defect and dopant impurities.

In the quasi-neutral base layer, the interband Radiative, interband Auger, and the SRH processes may all be important. The Radiative process in the base layer is the ultimate performance limiting loss mechanism. It is not as important in the emitter since the emitter layer is rather thin and hence has a rather small recombination volume compared with the thicker quasi-neutral base layer. The interband Auger process in the base layer can be reduced by not-so-heavily doping the base. Lightly doped base would enhance the influence of recombination in the back-surface-field layer so base doping must be optimized or not so low, resulting in significant loss from the interband Auger recombination process.

Similar to the emitter, the dominant recombination processes in the heavily-doped quasi-neutral back-surface-field layer are the interband Auger and the SRH recombination processes, but their influences are not as large as they are in the emitter since the emitter is close to the solar source and the minority carrier collecting p+/n junction than the BSF layer.

Surface recombination can also seriously limit the efficiency of very-high-efficiency solar cells. Recombination of electrons and holes at exposed surfaces and interfaces can occur via the various mechanisms just described. However, the interfaces, such as the oxide/silicon, metal/silicon and metal/thin-oxide/silicon interfaces which can be present in a cell, are layers of high density of defects and impurities. The defects, commonly known as dangling bonds, and the impurities can form electron and hole bound states and serve as sites for electron-hole recombination. Generally, the SRH mechanism at these interface bound states is thought to be the most dominant. However, for heavily doped emitter and BSF layers, the surface concentration of the majority carrier is so high that one could also expect the Auger mechanisms to be important, especially the interband type although the bound-band type has not been eliminated as a candidate. In silicon solar cells of greater than 20% efficiency, the recombination loss in the cell must be so low that even a minute amount of recombination at the interfaces can be very detrimental to achieving higher efficiency. At the ultimate efficiency of about 25%, an effective interface recombination velocity of 1 cm/s or less must be required to render interface recombination unimportant. This places a severe constraint on the high temperature processing steps used during cell fabrication to obtain low recombination velocity interfaces. Each increase of ten of the interface recombination velocity will reduce the open circuit voltage by

2.3kT/q or 59 mV at 24C and the efficiency by 10%. Fortunately, low interface-recombination-velocity processing techniques are well advanced in silicon VLSI technology. However, areal uniformity over the extremely large areas required of solar cells and stability are still two key unknown factors.

The requirement of low interface recombination velocity for reaching very high efficiency has motivated innovative cell designs. For example, the very high (nearly infinite) interface recombination velocity at the metal/Si contact of the front contacts of a cell has prompted one design to use all back surface contacts [2,3] and another design in which a thin oxide layer is introduced between the metal and the silicon surface to take advantage of the very low interface recombination velocity of the oxide/silicon interface [4,5]. Some of the latest high efficiency silicon solar cells, recently reported, seem to have the interface recombination loss reduced to a negligible level compared with the recombination loss in the quasi-neutral base layer [4,5,6]. Some quantitative analyses on these cells are given in section V.

Another important recombination loss originates from impurity-defect clusters in the bulk of the cell [7] and damaged and at the exposed perimeter surface of the p+/n and n/n+ high/low junctions of the cell [8]. In principle, these recombination sites can be eliminated by revising processing procedures and cell structure designs.

III. ULTIMATE PERFORMANCE OF IDEAL CELLS

The ideal cell is one that has only the lowest intrinsic recombination losses, the interband Radiative and interband Auger recombination losses. Operating in the low injection level is also desired to further minimize any SRH recombination losses and in particular, to take advantage of the more box-like current voltage characteristics given by the ideal diode law, J=J1*[exp(qV/kT)-1] compared with the high level law. J=J2*[exp(qV/2kT)-1] which has a more rounded or soft shoulder.

In the following subsections of this section, the ideal diode cell will be analyzed to illustrate the numerical range of the solar cell parameters, JSC, VOC, FF and a diode parameter, the dark current J1, in very high efficiency cells. This is followed by an analysis to give projected ultimate performance limit if the only losses left are the intrinsic Radiative and Auger processes. In the next section, section IV, the importance of surface recombination is illustrated by two design examples. In the last section, section V, analyses of the three highest efficiency cells recently reported are analyzed based on the ideal diode cell model given here.

3.1 IDEAL DIODE CELL

The d.c. current-voltage equation of a diode solar cell is given by

$$J = JL - J1*[\exp(qV/kT) - 1]$$

$$- Jm*[\exp(qV/mkT) - 1]$$

where JL is the photocurrent density (areal), J1 is the dark leakage current of the ideal Shockley p/n junction diode, m and Jm are the reciprocal slope

and dark current of the nonideal junction diode. m=1 to 2 for recombination in the space charger layer of the p/n junction [9]. m=2 for recombination in the quasi-neutral base layer at high injection level, i.e. when N=P>>Dopant Density. m=4 if a surface channel exists across the p/n junction perimeter such as the inversion channel of a MOSFET [9]. If a shunt resistive path exists across the bulk or the surface of the junction, m can be greater than 4 [9]. For the interband Auger recombination mechanism, m=1 at low injection level but drops to m=2/3 at high injection level. This occurs because the interband Auger recombination rate is proportional to N P + P N while quasi-neutrality at high injection levels requires that N=P=n *exp(qV/2kT), resulting in a current law proportional to N^3 or P^3 or [exp(3qV/2kT)] .

For high efficiency cells, all the nonideal recombination losses are eliminated except the interband Auger mechanism at high injection levels. Thus, the Jm term can be dropped except for the interband Auger process. The ideal diode solar cell equation is t given by

J = JL - J1*[exp(qV/kT) - 1].

The photocurrent, JL, is a weak function of recombination loss for very-high-efficiency cells. It can be taken as a constant and set to the maximum available photocurrent for a given cell thickness. In the numerical analyses to be presented in this paper, JL=36mA/cm^2 will be assumed for a AM1.5 spectra at a photon power PIN=100mW/cm^2. This closely approximates the photocurre of the measured AM spectra which gives 31.49mA/cm^2 at 88.92mW/cm^2 photon power in a cell of 50 micron thick under one pass with no front surface reflection, presented earlier [10] based on the spectra of Thekaekara. For other conditions and cell thicknesses, only the ratio, JL/PIN=36/100=0.36 A/W needs to be modified. This photoresponse increases to 0.4594 A/W when the cell becomes infinitely thick or all the photons are absorbed, a 27.6% increase. To reach higher efficiency, the cell thickness may be increased to increase the short-circuit current, but this will increase the recombination volume so that a optimum thickness will be reached beyond which the efficiency will drop. Multiple passes using back-surface optical reflector in a thin cell can avoid the high recombination loss in the base of a thick cell.

The relationship between the short-circuit current, JSC, and the open-circuit voltage. VOC, is then given by

JSC = JL = J1*[exp(qVOC/kT) - 1].

The maximum power point can be computed, without any approximation by setting d(J*V)/dV=0. The efficiency, EFF, at the maximum power point is then given by

EFF = PMAX/PIN = JMAX*VMAX/PIN

which is also used to define the fill factor, FF, given by

FF = JMAX*VMAX/JSC*VOC.

Thus, the maximum efficiency is given by

EFF = FF*JSC*VOC/PIN = (JSC/PIN)*FF*VOC = 0.36*FF*VOC.

This is a familiar result which has been used to analyze high efficiency cell designs. To illustrate the numerical range of the parameters in the very-high efficiency cells, a set of values are computed and tabulated in Table I. It shows that the dark current, J1, must be less than 2E-13 A/cm^2 or 0.2 pA/cm^2 for a 20% cell. It decreases one decade for each efficiency rise of 2%, reducing to 0.2 fA/cm^2 at 26%, which is about the ultimate limit for a 50 micron thick cell. The table also shows that for each 2% rise of efficiency, the open-circuit voltage is increased by 60 mV, consistent with the simple estimate we made earlier, 58.96 mV.

TABLE I
PERFORMANCE PARAMETERS OF VERY-HIGH-EFFICIENCY
IDEAL DIODE SILICON SOLAR CELLS
(AM1 or AM1.5, 24.0C)

SOURCE	J_1 (A)	J_{SC} (mA)	V_{OC} (mV)	FF	EFF (%)
Theory	2.0×10^{-16}	36.0	840	0.8664	26.0
Theory	2.0×10^{-15}	36.0	780	0.8588	24.0
Theory	2.0×10^{-14}	36.0	720	0.8501	22.0
Theory	2.0×10^{-13}	36.0	660	0.8402	20.0

3.2 ULTIMATE PERFORMANCE

The ultimate performance is limited by the interband Radiative and Auger recombination mechanisms. The ultimate efficiency is reached when all the extrinsic recombination losses are eliminated. The numerical results are obtained by assuming also that all the emitter recombination losses are negligible, especially the low-level interband Auger recombination loss in the highly doped quasi-neutral emitter layer. This is achievable by proper design of the emitter concentration profile so that the total majority carrier density in the emitter is not much higher than about 1E14 and there is a good p++/p+ front surface field layer to maintain the high sheet conductance and low series resistance. Thus, in this limit where only base recombination dominates, the dark current, J1 can be readily obtained by multiplying the position independent base recombination rate to the base thickness. The results for both the two intrinsic loss mechanisms and the SRH extrinsic mechanisms are listed next.

Radiative Recombination (Interband)

$$J1 = qC^{o}*XB*n_i^2$$

Auger Recombination (Interband)

$$J_{0.6} = qC^{a}*XB*n_i^3 \quad \text{(High Level)}$$

$$J1 = qC^{a}*XB*n_i^2*NB \quad \text{(Low Level)}$$

Thermal Recombination (Bound-Band) SRH

$$J1 = q\tau_B^{-1}*XB*n_i^2/NB \quad \text{(Low Level)}$$

$$J2 = q\tau_B^{-1}*XB*n_i \quad \text{(High Level)}$$

Numerical calculations are performed for silicon cells with base layer thickness of XB=50 microns at 24.0C where n_i=1.0E10 cm^{-3}. The Radiative recombination rate of $C^{o}n_i^2$=0.62E6 is employed while the interband Auger rates are: C^{o}=2.8E-31 and C_p=0.99E31 cm^6/s. To illustrate the condition at which the SRH recombination loss will reduce the ultimate efficiency, a base lifetime of 100 us and diffusivity of 20 cm^2/s are assumed.

The results are tabulated in Table II. This table also shows the results of two ohmic-contact cells to illustrate the effect of surface and interface recombination. They are discussed in the next section.

Table II shows that the ultimate efficiency limited by Radiative recombination alone is about 25%. The Auger limits are computed for the extremes of the injection levels and both are close to the 25% Radiative limit. The high injection limit of the Auger case is reached if the majority carrier or doping impurity concentration in the base layer is less than about 5E16cm^{-3} for the 50 um base thickness which gives a total carrier density in the base of 2.5E14 cm^{-3}. Designing and operating the cell in the high level Auger range by reducing the base doping may help in maintaining the high SRH recombination lifetime which is necessary to achieve the high efficiency, but the sensitivity to surface recombination becomes more severe at this high level as indicated in the table and discussed in the next section.

Table II also gives the results of SRH recombination loss at both low and high injection levels. Two design ideas may be drawn. (i) High level injection should be avoided. This was arrived at previously by a simple observation that the high level recombination current law, exp(qV/2kT), gives a softer illuminated I-V curve and hence lower fill factor and efficiency. (ii) Table II also shows the condition at which SRH recombination loss will become important to lower the ultimate efficiency. The example assumes a SRH recombination lifetime of 100 us to give a 23% efficiency. To reach 25%, the SRH base lifetime must be greater than about 1000 us or 1 ms which is at the limit of the state-of-the-art for VLSI grade silicon crystals.

TABLE II

ULTIMATE PERFORMANCE OF SILICON SOLAR CELLS
(Including the Effect of Surface Recombination)

SOURCE	J_1 (A)	J_{SC} (mA)	V_{OC} (mV)	FF	EFF (%)	m	J_1/q	S_{EFF} (cm/s)
Radiat. Recomb.	5.0×10^{-16}	36.0	817	0.8637	25.4	1	$C^o x_B n_i^2$	3.1
Auger H	3.0×10^{-22}	36.0	786	0.8968	25.4	2/3	$C^a x_B n_i^3$	0.33
Auger L	2.3×10^{-15}	36.0	776	0.8582	24.0	1	$C^a x_B n_i^2 N_B$	14
SRH L	8.0×10^{-15}	36.0	746	0.8540	23.0	1	$\tau_B^{-1} x_B n_i^2 N_B^{-1}$	50
Ohmic L	6.4×10^{-13}	36.0	634	0.8354	19.1	1	$D x_B^{-1} n_i^2 N_B^{1}$	4000
SRH H	8.0×10^{-8}	36.0	666	0.7415	17.8	2	$\tau_B^{-1} x_B n_i$	50
Ohmic H	6.4×10^{-6}	36.0	442	0.6645	10.6	2	$D x_B^{-1} n_i$	4000

$T=24°C$; $n_i=10^{10}cm^{-3}$; Area=1 cm^2; $x_B=50\ \mu m$; $N_B=10^{17}cm^{-3}$; $D=20\ cm^2/s$;
$\tau_B=100\ \mu s$; $P_{IN}=100$ mW(AM1.5); L=Low Level; H=High Level;
$C^o n_i^2=0.62\times10^6$; $C_L^a=C^n=2.8\times10^{-31}cm^6/s$; $C_H^a=C^n+C^p=3.8\times10^{-31}cm^6/s$.

IV. EFFECTS OF SURFACE AND INTERFACE RECOMBINATION

The influence of surface and interface recombination on the efficiency of high efficiency cells is quite large, which has been both demonstrated in the laboratory [4,5,6] and recognized from simple device modeling. The latter will be presented in this section.

To provide a quantitative idea of the importance of recombination at the surfaces and interfaces of a solar cell, the bulk recombination losses may be written in terms of an effective recombination velocity so that its magnitude can be compared with the surface and interface recombination velocity at the real surfaces and interfaces of a solar cell. This effective recombination velocity can be defined both at the low and high injection levels. In the following two subsections, 4.1 and 4.2, the effect of surface recombination will be considered for two cases.

4.1 THE EQUIVALENT RECOMBINATION VELOCITY OF A BULK RECOMBINATION PROCESS

The equivalent recombination velocity of a bulk recombination process which occurs in a volume element, such as the base region, can be defined as that velocity at the minority carrier entrance surface which would produce the same recombination current. These are illustrated in Fig.2 for several recombination locations, some of which are the true interface recombination velocities and others are the equivalent recombination velocities. For example, SE and SB are the equivalent recombination velocities of the quasi-neutral emitter and base layers at the minority carrier entrance or injection interfaces. The true interface recombination velocity illustrated in Fig.2 is SFI, the recombination velocity at the front oxide/silicon interface. Another equivalent recombination velocity in Fig.2 is SBI which is the effective recombination velocity of minority carriers flowing into the n+ BSF layer at the n/n+ entrance surface.

These equivalent recombination velocities may be explicitly defined to give accurate numerical estimates on the importance of true interface recombination loss. They are defined through the dark current density,

$$J1 = q*PB*SB + q*NE*SE$$

which, when combined with the dark current expression listed in Table II and section 3.2, gives

$$SB = (XB/\tau_B) + SBI + SBA + SBO$$

and

$$SE = (XE/\tau_B) + SFI + SEA + SEO$$

Here, XB and XE are the base and emitter layer thickness; SBI and SFI are the effective and real recombination velocity at the back and front interfaces; SBA and SEA are the effective recombination velocities from volume interband Auger recombination in the quasi-neutral base and emitter layers; and SBO and SEO are those from volume interband Radiative recombinations. These especially simple expressions are applicable for base and emitter layers which are thin compared with the minority carrier diffusion length, a condition that holds well in a high efficiency cell. They are given by

$SBT = XB/\tau_B$	(All Level SRH)
$SBA = C^a*XB*NB^2$	(Low Level Auger)
$SBA = C^a*XB*n_i^2\exp(qV/kT)$	(High Level Auger)
$SBO = C^o*XB*NB$	(All Level Radiative)

for the base layer, and a similar set for the emitter layer.

The numerical values are computed and listed in Table II. It is evident that the effective recombination velocities of the limiting loss mechanisms are extremely low at the ultimate 25% efficiency. The value of 3.1 cm/s for the Radiative recombination loss to give the 25.4% efficiency illustrates the importance to have low surface recombination interfaces. Unless the interface recombination velocity is reduced substantially below 3.1 cm/s, recombination losses at the interfaces will seriously reduce the efficiency.

The rather small value of 0.33 cm/s for the high-level Auger limit shown in Table 2 illustrates the large carrier density and the very high Auger recombination rate in the base. This makes the dependence on the surface recombination even more sensitive.

4.2 EFFECT OF OHMIC CONTACT AND THE BACK-SURFACE-FIELD

Table II gives another example which illustrates the importance of having a back surface field layer to reduce the effect of back surface recombination loss. This example arises from the question: Can the back surface field layer be replaced by a thick base and still have a very high efficiency? This is a practical question since the BSF layer requires extra cell fabrication processing at high temperatures which usually reduces the bulk lifetime in the quasi-neutral base.

Since a thick base means more Auger and Radiative recombination loss, an ideal device model can be set up to answer the above question. In this mode, the only recombination in the base is the minute Auger and Radiative recombination and there is no BSF so that the injected minority carriers face the full recombination at the Si/metalcontact on the back surface. The interface recombination velocity at the back Si/Metal interface is assumed to be infinite or a perfect ohmic. Then, the dark current due to this component is given by

$$J1 = q*DB*XB^{-1}*(n_i^2/NB); \qquad SB=DB/XB \text{ (Low Level)}$$

and

$$J1 = q*DB*XB^{-1}*(n_i); \qquad SB=DB/XB \text{ (High Level)}$$

To determine the thickness required to reduce the efect of interface recombination at the back surface below that of Auger recombination in the [uasi-neutral emitter, we set the two recombination velocities or J1 equal. Consider the low level case, we have

$$XB*C^a*NB*n_i^2 = DB*n_i^2/(NB*XB)$$

or

$$NB*XB = SQRT(DB/C^a) = SQRT(20/2.8E-31) = 1.0E16cm^{-2}$$

Thus, for a base doping of NB=1.0E17, we need to have a base thickness of XB=1000um=1mm, an impractical result. This shows the importance of having a good high-low potential barrier on the back surface to reduce the back surface recombination loss.

IV. EVALUATION OF THREE RECENT HIGH-EFFICIENCY CELLS

Silicon solar cells with efficiency approaching 20% (AM1) have been fabricated in the laboratory. Innovative cell designs have been developed to reduce interface and emitter recombination losses. In this section, the experimental data of the best cells of three industrial laboratories are compared with that predicted by the ideal diode cell theory which was used to produce Table I. From a comparison of the theory and experiments, it appears that bulk recombination in the quasi-neutral base via the SRH mechanism is the limiting loss on all three cells.

The experimental and computed cell performance parameters are tabulated in Table III. The first three rows are for the highest performance cell from Green [ted and listed in the first row. The computed results are all higher than the measured values, suggesting effects from several sources.

TABLE III

PERFORMANCE OF THREE HIGHEST EFFICIENCY SILICON SOLAR CELLS AND COMPARISON WITH IDEAL DIODE CELL THEORY

SOURCE	J_1 (A)	J_{SC} (mA)	V_{OC} (mV)	FF	EFF (%)
Theory	3.2×10^{-13}	35.6	660	0.8402	19.7
Theory	6.6×10^{-13}	35.6	641	0.8350	19.0
GREEN	3.2×10^{-13}	35.6	641	0.822	18.7
Theory	1.2×10^{-12}	35.9	627	0.8340	18.8
SPITZER	---	35.9	627	0.800	18.0
Theory	2.0×10^{-12}	36.2	605	0.8296	18.2
Theory	2.4×10^{-12}	36.2	600	0.8286	18.0
ROHATGI	2.0×10^{-12}	36.2	600	0.793	17.2

The second two rows are for the best cell from Spitzer [5]. The theory is computed using the measured JSC=35.9 and VOC=627mV. The larger computed fill factor, 0.8340 compared with measured 0.800 suggests possible series resistance loss in the actual cell which is not accounted for in the ideal diode cell model.

The third three rows are for the best cell from Rohatgi [6] which is a higher resistivity cell (4 ohm-cm versus the 0.1 to 0.3 ohm-cm of Green and Spitzer). The first theory row is based on the measured J1=2E-12 and JSC=36.2 which gives VOC=605mV, FF=0.8296 and EFF=18.2%. The measured VOC and the theory are quite close, only 5 mV different, and the lower observed efficiency is mainly due to the lower experimental fill factor which again suggests possible series resistance losses in the real cell.

In all three cases, the computed and the measured cell performance data are quite close, indicating that low level recombination in the quasi-neutral base layer via the thermal or Shockley-Read-Hall mechanism at defect and impurity recombination sites is the dominant loss mechanism. Further

improvement to achieve efficiency greater than 20% must depend first on identifying the base recombination center species and then reducing their density further. Although emitter bulk and surface recombination are substantially reduced in these three cells so that they are not important at less than 20%, these losses may be important again and must be further reduced at higher efficiencies.

VI. CONCLUSION

Interband Auger and Radiative recombination losses in the base layer limit the AM1 efficiency to about 25% in silicon solar cells with a base thickness of about 50 microns. Increasing the thickness will increase the efficiency only slightly, via higher short-circuit current. In order to eliminate the influence of recombination losses in the base due to the SRH thermal recombination mechanism at impurity and defect centers, the base lifetime must be greater than about 1 ms or an equivalent recombination trap density of less than $1E11 cm^{-2}$. In addition, all interface and surface recombination losses must also be reduced to give a effective recombination velocity of less than about 1 cm/s. These very stringent requirements indicate that the latest state-of-the-art silicon VLSI technology is needed to provide the nearly perfect silicon crystal and the very clean and low-stress fabrication techniques which are necessary to produce very-high-efficiency solar cells that will approach the ultimate theoretical limiting efficiency.

REFERENCES

1. C. T. Sah, "Fquivalent circuit models in semiconductor transport for thermal optical. Auger-impact, and tunneling recombination-generation-trapping processes," physica status solidi (a)7, 541-559, 16 October 1971.
2. Michael D. Lammert and Richard J. Schwartz, "The interdigitated back contact solar cell: A silicon solar cell for use in concentrated sunlight," IEEE Transaction on Electron Devices, ED-24(4),337-342, April 1977.
3. Richard M. Swanson, S.K.Beckwith, R.A.Crane, W.D.Eades, Y.H.Kwark, D.A.Sinton and S.E.Swirhun, "Point-contact silicon solar cells," IEEE Trans. ED-31(5), 661-664, May 1984.
4. Martin A. Green, A.W.Blakers, J.Shi, E.M.Keller and S.R.Wenham, "High-efficiency silicon solar cells," IEEE Trans. ED-31(5), 679-683, May 1984.
5. Mark B. Spitzer, S.P.Tobin, C.J.Keavney, "High-efficiency ion-implanted silicon solar cells," IEEE Trans. ED-31(5), 546-550, May 1984.
6. Ajeet Rohatgi and P. Rai-Choudhury, "Design, fabrication and analysis of 17-18 percent efficient surfac-passivated silicon solar cells," IEEE Trans. ED-31(5), 596-601, May 1984.
7. C. T. Sah, K.A.Yamakawa and R.Lutwack, "Reduction of solar cell efficiency by bulk defects across the back-surface-field junction," Journal of Applied Physics, 53(4), 3278-3290, April 1982.
8. C. T. Sah, K.A.Yamakawa and R.Lutwack, "Reduction of solar cell efficiency by edge defects across the back-surface-field junction:- a developed perimeter model," Solid-State Electronics, 25(9), 851-858, Sept. 1982.
9. C. T. Sah, "Effects of surface recombination and channel on p-n junction and transistor characteristics," IRE Trans. ED-9(1), 94-108, Jan. 1962.
10. C. T. Sah, P.C.Chan, C-K Wang, R.L-Y Sah, K.A.Yamakawa and R.Lutwack, "Effect of zinc impurity on silicon solar-cell efficiency," IEEE Trans. ED-28(3), 304-313, March 1981.

ORIGINAL PAGE IS
OF POOR QUALITY

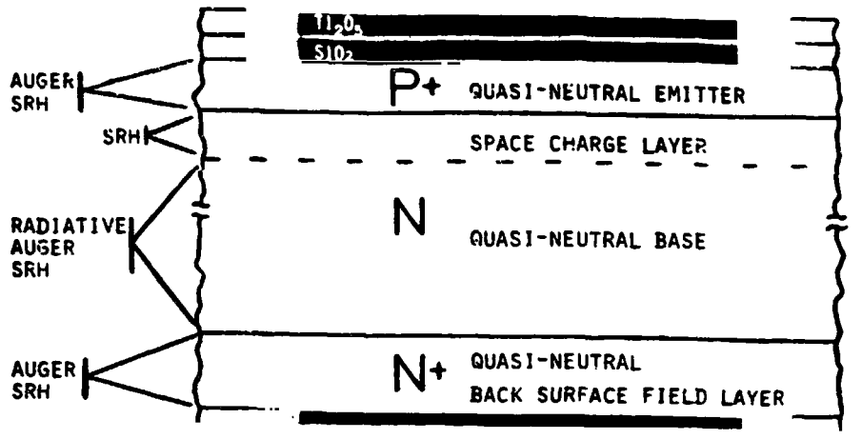

Figure 1 A cross-section view of solar cell showing the dominant recombination processes and locations. RADIATIVE and AUGER are the interband radiative and Auger recombination mechanisms. SRH is the Shockley-Read-Hall thermal recombination at defect and impurity recombination centers. Recombination occurs both in the bulk layers and at the interfaces between oxide, silicon and metal(dark).

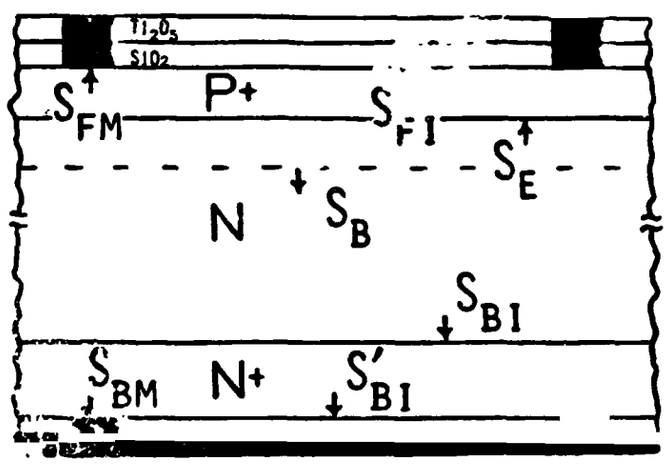

Figure 2 A cross-section view of solar cell showing the recombination velocity representation of the recombination rates. S_E, S_B and S_{BI} are the effective recombiantion velocities of volume recombination processes. S_{FI}, S_{FM}, S'_{BI} and S_{BM} are the real interface recombination velocities at the front oxide/silicon, front metal/silicon, back oxide/silicon and back metal/silicon interfaces.

DISCUSSION

PRINCE: While we have this slide on here, if you remove the very heavy doping on the surface, how would that affect the efficiency?

SAH: We can do a quick calculation. Let me just illustrate this with a viewgraph so you can see how to go about doing that.

TAN: Can I make a comment? I have done a similar calculation by taking the tail off and I see a V_{oc} goes up by about 20 millivolts. If you start with 10^{19} and come all the way down, your V_{oc} goes up by 20 millivolts.

SAH: My model here is based on all of these being from the emitter; then I can get a good agreement. If the base is not a limiting factor -- suppose it is not at all, it is just an emitter -- then it is going to make quite a substantial difference.

QUESTION: Where did the profile come from? Is that an experimental profile. Did that come from spreading resistance?

SAH: No. That is from SIMS.

LANDSBERG: I have a quick question about the possibility of radiative-limited lifetime. If that was ever achieved, or if that ever occurred, one would obviously have practically 100% radiative converter and although, in one way of looking at it, it is bad to have some limit on the efficiency by this recombination mechanism; I could perhaps take advantage of it. Do you think there is any example where the efficiency is really radiative-limited? It would be quite interesting, it is just a hypothesis.

SAH: I don't know of any example. The highest one that is recorded so far is still only 19%.

SCHRODER: If you drop the surface concentration more and more, what do you think happens to the contact resistance? Have you looked at that?

SAH: No. I have not taken any contact resistance.

LOFERSKI: Just what is the difference between the high and the low level Auger recombination?

SAH: The low-level Auger follows the ideal Shockley diode because the minority carrier density increases very little compared with base doping.

SESSION II

HIGH-EFFICIENCY CONCEPTS

M. Wolf, Chairman

SILICON SOLAR CELL EFFICIENCY IMPROVEMENT: STATUS AND OUTLOOK

M. Wolf
Dept. of Electrical Engineering, University of Pennsylvania
Philadelphia, PA 19104

N85-31619

INTRODUCTION

The struggle to improve the efficiency of silicon solar cells has been going on as long as these devices have been a commercial product. The reason is simply that efficiency, as well as operating life, is an economic attribute in their application as part of a system. Fig. 1 illustrates the efficiency improvements made during the thirty year existence of the silicon solar cells, from about 6% efficiency at the beginning to 19% in the most recent experimental cells. Clearly the progress has not been a steady one. In the more stationary periods, the effort was more oriented towards improving radiation resistance and yields or the production lines, while, in other periods, the emphasis was more directed to reaching new levels of efficiency through better cell design and improved material processing. The last few years were again in such an "efficiency push" period, and encouraging first results have been forthcoming from the recent efforts. Nevertheless, considerably more efficiency advancement in silicon solar cells is expected, and anticipated attainment of efficiencies significantly above 20% (AM 1.5) is being more and more discussed. Whether this goal will be achieved is an open question, as major advances in material processing and in the resulting material perfection will be required.

The achievements along the road to efficiency improvement are best gauged by an analysis of the contributions of the individual principal loss mechanisms to the overall performance of a given device. Such analyses are presented in Table I, which lists the individual performance attributes of the milestone solar cells of the last fifteen years. Between 1959 and 1978, all solar cell development represented in the table was oriented towards application in space. Therefore, the available performance data are all based on AMO solar radiation, while the data for the more recent cells are based on AM 1.5 sunlight. To permit comparison in Table I, the space cell data were converted to AM 1.5 sunlight, using the spectral responses of the cells.

Table I indicates that the improvements achieved in the 1970s on the space cells included primarily an advancement of the collection efficiency, and a reduction of the "secondary" loss factors, such as residual reflectance, or series resistance losses. In the more recent efforts, directed at efficiency improvement for terrestrial applications, further advances have been made in the reduction of the impact of these secondary losses, but the main emphasis has been placed on the improvement of the voltages.

A study of the data in Table I leads to an evaluation of the status of silicon solar cell technology: the technology is available to decrease all the secondary loss mechanisms to the level where efforts for their further reduction will be fairly unproductive; the basic collection efficiency has been improved

to the point where the beginning of its "saturation" with further reductions of minority carrier recombination has been reached; and further improvements are primarily to be achieved in the area of voltage increases through reduced minority carrier recombination.

MINORITY CARRIER RECOMBINATION AND SOLAR CELL EFFICIENCY

A study of the loss mechanisms and of their impacts, as displayed in Table I, reveals that recombination of minority carriers is the major basic effect which presently limits the efficiency of solar cells. Thus, a maximum efficiency value is associated with each level of the recombination rate in the device. The ultimate efficiency is reached when the only effective recombination mechanisms are radiative and direct band-to-band recombination.

An investigation of the relationship between recombination rates and maximum achievable efficiency is most transparent when it is carried out on the "basic" solar cell (Fig. 2). This device contains only those parts which are absolutely necessary for its functioning as a solar cell. These parts are: a volume for the absorption of photons and generation of free charge carriers: a potential barrier for the device to perform as a generator; and contacts for the extraction of a current. The basic analysis even considers the contacts as ideal, and omits a direct consideration of their functioning. The idealized analysis also chooses those impurity concentrations which, in consideration of minority carrier recombination, provide the highest efficiency. It then uses the same impurity density on both sides of the junction.

Recombination takes place both in the volume and at the surfaces of the device. It is practical to start the investigation with the assumption that all surface recombination velocities can be made equal to zero, and that the volume minority carrier lifetimes are equal in all parts of the device. This eliminates most influences of the device structure. Also, other device performance influencing effects are, at first, assumed to contribute zero losses. These considerations lead to curve 1 of Fig. 3, which represents efficiency as function of the minority carrier lifetime in such an idealized device, essentially as an upper limit for the achievable conversion efficiencies. The curve is basically composed of two straight lines in this semilogarithmic plot. Below about 1 ms lifetime, where the curve is represented by the straight line with the greater slope, the recombination is strictly determined by a varying density of recombination centers as described by the Shockley-Read-Hall theory. The resulting variation of the lifetime at constant resistivity is indicated by the vertical part of the dashed line in Fig. 4. Above the value of approximately 1 ms, the lifetime is dominated by Auger recombination, that is direct band-to-band recombination rather than recombination via centers. From this point on, to achieve a higher minority carrier lifetime, the impurity concentration has to be reduced. As maximum solar cell performance is obtained when the contributions of Shockley-Read-Hall type recombination and Auger recombination are equal, the dashed line in Fig. 4 approximately represents this condition above the 1 ms lifetime value. In this case, Shockley-Read-Hall recombination is assumed to be dominated by deep trap levels, which result in the independence of the lifetime from the impurity concentration (saturation lifetime) up to the transition to Auger recombination. Thus, for the 10 and 100 ms lifetimes, the impurity concentration has to be reduced to 1.5×10^{16} and 5×10^{15} cm^{-3},

respectively. Also, because of the difference in Auger coefficients, a small difference in the minority carrier lifetime values for the n and the p region is obtained in these cases.

As Fig. 4 shows, the lifetime values in recently obtained FZ ingots fall well below the Auger line, and are thus dominated by recombination via centers. For the efficiency improvements expected in the future, it will become necessary to reduce the recombination center density so far that Auger recombination will, in effect, become the lifetime limiter.

The data discussed so far are those typically obtained by use of fully analytical modeling. Such modeling is restricted to low level injection. Estimation of the excess minority carrier densities injected across the junction at open circuit voltage shows that the low level injection condition (e.g., $n_p << p_{p,o}$) starts to be violated between the 1 ms and 10 ms bulk lifetime values. This would not be of much consequence were it not for the fact that the minority carrier lifetime values have been chosen to be at the edge of domination by Auger recombination. In consequence, the impurity densities had to decrease for increasing lifetime values, while the excess minority carrier concentrations increase. Thus, the effective lifetimes are determined by the excess carrier concentrations, because of Auger recombination, rather than by the recombination center density. This leads to an efficiency saturation which is indicated in Fig. 3 by the wavy lines. Such an efficiency limitation has recently also been discussed by Green [1] and by Tiedje et al [2], who both found this limitation to be less severe for very thin cells, where it actually can approach the radiative recombination limit near 30%.

It has been seen repeatedly that the influence of the surface recombination velocity on the efficiency has the shape of an S-curve (Fig. 5), with practically no performance impact below a certain value of surface recombination velocity. Above this value, the solar cell performance falls off rather rapidly, until it reaches a lower saturation level. It is thus of interest to determine this threshold value for the surface recombination velocity. Using a range of surface recombination velocity values for each value of minority carrier lifetime, surface recombination threshold values have been determined, defined as that value at which the power output of the device has been reduced by 2.5%, from its s = 0 value. This process has been carried out first for the back surface, and then for the front surface, leading to a total reduction in power output of 5%. Surface recombination on the generally narrow edges of the device has been neglected in this process. The result is curve 2 in Fig. 3. The surface recombination velocity threshold values themselves are given in Fig. 6. Two curves are presented, as the threshold values differ for the front and the base surface recombination velocities for the given device structure, which has a nominal junction depth of 2 μm. It is noteworthy that the surface recombination velocity thresholds lie above 100 cm/s, and in the 30-60 cm/s range for bulk lifetimes of 100 μs and 1 ms, respectively. Such velocity values are attainable with current technology. However, to achieve the highest efficiency values, the surface recombination velocities have to be reduced below the 1 cm/s level.

In the device geometry chosen, the minority carrier lifetime in the front region can be less than assumed for Fig. 3. A sensitivity analysis similar to that carried out for the surface recombination velocities provides the

"threshold" value for the front region minority carrier lifetime. It is defined as that value at which the power output is degraded by 1%. The resulting lifetime is shown in Fig. 7 for the various efficiency levels. As Fig. 7 shows, the threshold front region minority carrier lifetimes are approximately two orders of magnitude lower than those required for the base region. These lower front region values are more readily achievable in device fabrication than the original higher ones.

Finally, there is an optimum device thickness connected with every minority carrier lifetime value. This thickness constitutes the peak value of a rather flat maximum. Figure 8 presents the optimum base thickness as function of the minority carrier lifetime for the efficiency values of Fig. 3. It is seen in Fig. 8 that a 500 μm thick device is best for lifetime values above 1 ms, with the optimum thickness dropping off rapidly for lower lifetime values. The application of texturing was found to permit the use of a reduced thickness, as would be expected from it as well as from other light trapping measures. But it is also seen that the texturing provides only a small efficiency improvement at the highest efficiency values, as indicated by the cross in Fig. 3.

To obtain a conception of realistically achievable efficiencies, the values of curve 2 in Fig. 3 have been reduced by another 10%, in order to account for the effects of the secondary losses. It is known that these losses, in combination, are reduceable to this level by application of the best current technologies. This 10% reduction leads to curve 3 in Fig. 3. It shows that with a base minority carrier lifetime of 100 μs, an efficiency of 19.8% should be achievable, which is a value not much above the one achieved so far in the best devices with somewhat lower lifetimes. It also shows that a lifetime value near a millisecond will be needed to achieve 22% efficiency. While millisecond lifetimes should be achievable by a combination of today's best technologies in semiconductor material processing, the achievement of efficiencies above 22% will require a considerable advancement of the material science of silicon.

CONCEPTS FOR HIGH EFFICIENCY SOLAR CELL DESIGN

Evaluating the current status of silicon solar cell technology (summarized in Table II) makes it evident that the technology is available to reduce all the contributions from secondary loss mechanisms to the level of maximally 2 to 3% each. This will be close to the practically achievable limits. Secondary loss mechanisms are those which are determined by technology factors, and which have a fundamental limit of zero, with the exception of the collection efficiency. These secondary losses include the reflectance, shading due to front surface metal coverage, Joule losses due to series resistance, excess junction current, etc.

The evaluation also shows that the (internal) collection efficiency is, in all modern cells, significantly above 90%. It has also been found that the collection efficiency increases only slowly with further reductions of minority carrier recombination, giving the effect of an apparent "saturation."

In contrast to the collection efficiency, the open circuit voltage continues to increase significantly with continued reduction of minority carrier recombination. This is the performance attribute which has the largest margin

for improvement at the current status of solar cell technolo-gy. The curve factor, finally, increases together with the open circuit voltage, although its increase proceeds at a smaller rate.

A review of the progression towards the current high level of silicon solar cell performance indicates that this level has been accomplished only by taking a global view of the device. The expression "global view" means simultaneously considering the influence of all loss mechanisms, and reducing each of them to the lowest possible level (Table III). In fact, where there are several performance determining mechanisms, which act on the same attribute and which cannot be reduced to zero, then the optimum performance is generally obtained when the different contributions are brought to equal, low levels. This rule, for instance, applies to the contributions to the saturation current from the base and from the front region. A device where the saturation current is clearly dominated by one or the other region is not optimized until the higher contribution is brought down to the level of that from the other region.

The efforts towards efficiency improvement have so far led to a number of "add-ons" to the basic cell. They include: (1) a grid metallization structure to reduce the front layer sheet resistance; (2) a single or dual layer anti-reflection coating; (3) texturing of the front surface to enhance the anti-reflection effect and to increase the effective internal optical path length; (4) an optical reflector at the back surface to increase the optical path length ("light trapping"); (5) passivating layers at the front and back surfaces to lower the effective surface recombination velocities; (6) potential steps or drift field regions; (7) isolating layers; and (8) reduced area metallization (dot contacts)--the last three also primarily for the reduction of the effective surface recombination velocity. This could lead to a complicated device structure (Fig. 9). At least part of the purpose of applying the measures (3) to (8) is to reduce the recombination rates of minority carriers, and their effects and limitations will be considered in the following.

The discussions up to this point have shown that the reduction of minority carrier recombination is the key element in achieving significant further improvements in silicon solar cell performance. Contemplation of the subject reveals that there are essentially three principal paths available to the reduction of recombination (Table IV). The first is the normally considered avenue of decreasing the density of recombination centers. This has to be accomplished in the volume of the device and on its surfaces. The second avenue is the reduction of the volume of the material, or of its surface area, both of which contain the recombination centers. For the volume, the concept is to utilize "thin layers" which means that their thickness is smaller than the diffusion length, while, for surfaces, it is principally to reduce the total surface area which contains recombination centers For solar cells this would be possible only by using optical concentration. A secondary approach is to reduce areas of unavoidably high surface recombination velocity in favor of surfaces with a lower surface recombination velocity. The typical example of this approach is the reduction of the ohmic contact area ("dot contacts"). The third avenue, finally, is that of reducing the density of the excess minority carriers, as the recombination currents both for the volume and for the surfaces are proportional to the excess minority carrier concentration. The density of the excess minority carriers can be reduced, e.g., if their flow towards the outside of the volume in which recombination occurs, can be accelerated. This

particular approach is available for minority carriers generated by the absorption of light, which means for the improvement of the collection efficiency. A second method is to "shield" the areas with higher excess minority carrier density from the areas with higher recombination rates by steps of the electrostatic potential in the appropriate direction. This leads to a lower density of the excess minority carriers within the region of higher recombination rates. The third approach is to isolate regions or surfaces with high recombination rates, such as the metal/semiconductor boundaries at the contacts, from the regions with higher minority carrier density by an intervening "thick layer." The effect of this "isolating layer" is that the region with the higher excess minority carrier density "sees" the bulk recombination rate of the intervening layer rather than the higher surface recombination rate at the other boundary of the thick layer. The final approach utilizes an increased dopant concentration. This is particularly effective in the case of injection of minority carriers across a forward biased potential barrier.

Having recognized the principal concept for the reduction of minority carrier recombination, the question turns to the implementation of these concepts. A number of device structures and of design concepts are available, each of which addresses one or two of the principal paths to recombination reduction.

Reducing the volume of the semiconductor in which excess minority carriers are present, as a means for reducing recombination, is elucidated by considering the relationship for the diode current (Table V). This current is proportional to the transport velocity which, for infinitely thick layers, equals the ratio of diffusion length to minority carrier lifetime. For layers which are thin compared to the diffusion length, however, the transport velocity approaches the ratio of the layer thickness to the minority carrier lifetime. Thus, continued reduction of the thickness further reduces the recombination current. In a solar cell in the open circuit condition, where the diode current has to equal the light generated current, the injected excess minority carrier density is proportional to the inverse transport velocity, that is proportional to the minority carrier lifetime and inversely proportional to the layer thickness. When the lifetimes become very large or the layer thicknesses very small, the injected excess minority carrier density can exceed the magnitudes required for the low-level injection condition to hold, as discussed before, and a transition to Auger dominated recombination can occur. Thus, a reduction of volume recombination may not be achieved beyond the point of transition to Auger recombination.

For the principle of the reduction of the recombination volume, only reduction of the layer thickness has been discussed. An area reduction appears to be potentially effective only if the device cross section for the light generated current could be made different from that for the diode current.

A second item for the reduction of recombination is the reduction of surface area which contains a substantial number of recombination centers Table VI). While in principle devices can be made smaller, the reduction of the "open" surfaces is difficult for solar cells, as the area is needed for the absorption of photons from the incident solar radiation flux. Optical concentration also may not be a remedy to this situation, as it leads to an increased light generated current density, which again can more easily drive the device into the Auger recombination regime.

Surface area reduction can be very effective, however, where the contact areas are concerned, as these represent surfaces of high recombination rates. While means seem to be available to reduce the surface recombination velocities at the open surfaces, particularly if they do not have to effectively pass incident photons, the contact recombination velocities do not seem to be substantially reducible in practical devices. Thus the approach is being pursued to reduce the weighted average surface recombination velocity, by reducing the area of high s and replacing it with an increased area of low s. Limits to the method are approached when the spacing between the areas of high surface recombination velocity reaches the magnitude of the diffusion length. Also, when the individual contact areas become very small, their spreading resistance becomes substantial, so that they start to make a significant contribution to the series resistance.

The next possibility for decreasing recombination rates involves a reduction of the number of excess minority carriers available in regions of higher recombination center density. The first approach to this is "shielding" these areas by interspersing a suitable step in the electrostatic potential, often called a "high/low junction," or a drift field (Table VII). The effect of reduced recombination expresses itself in the transport velocity for minority carriers across a real or imagined boundary within a given region of the device. The reduction of the transport velocity by the addition of a potential step is equal to the negative exponential of the height of the potential step or, expressed differently, to the ratio of the majority carrier concentrations at the two sides of the potential step.

Such potential steps can be incorporated in a semiconductor device in many different forms. They may be layers containing a drift field resulting from a doping gradient. When such layers are relatively thin, they are often called high/low junctions. Such potential steps may be "accumulation layers" near the surface of a device, and are present particularly in the cases where an insulator covers the surface of the semiconductor, particularly when it is interposed between a metal and the semiconductor. Depletion layers increase the transport velocity and should, therefore, be avoided. Going beyond depletion leads to inversion layers which act more like floating pn junctions which also have been proposed for shielding purposes in solar cells. The floating junctions seem to be most effective when they act as true "emitters," which means injection only from the emitter, no recombination current into the emitter. This may be the only beneficial application of an "emitter" in a solar cell. The final form of a potential step is achieved in the transition to a material with a different bandgap, i.e., a wider bandgap. The transition to the wider bandgap layer is generally arranged so that it results in a high/low junction of the proper direction. These wide bandgap layers, when applied to the open part of the front surface, are generally designed so as not to collect a significant amount of current, but to transmit the photons to the active semiconductor volume. They are then called "window layers."

The use of potential steps has several limitations. Firstly, the use of moderately high doping at the low side of high/low junctions, in order to achieve a high open circuit voltage (V_{OC}), reduces the available step height. This condition is further accentuated by the need to avoid the heavy doping effects on the high side, which can seriously influence the device performance. Similar considerations apply to accumulation layers, where it is in some cases

also difficult to provide enough charge to adequately "accumulate" in a more heavily doped semiconductor. An item to also watch is the capability for avoiding "absorption without collection" in window layers. In addition, at the transition between the active semiconductor and the window layer, a high concentration of interface states can substantially increase recombination.

A third approach is to isolate the active volume of the device from a region with a high recombination center density by interspersing an "isolating layer." If such an interspersed layer is thicker than the difussion length within it, then the transport velocity at the interface between the active volume and the isolating layer is determined only by the ratio of diffusion length to minority carrier lifetime, and is practically independent of the transport velocity at the other boundary of the isolating layer, which, e.g., may be the high effective surface recombination velocity of a metal/semiconductor interface (Table VIII). The limit to the effectiveness of such an isolating layer is that the L/τ ratio has to be adequately high, certainly higher than the transport velocity at the outside boundary of the isolating layer. Also, if such an isolating layer is placed in the optical path, it can severely degrade the collection efficiency.

More and more use is being made of such isolating layers. They appeared first in connection with the high/low junctions applied in the base of solar cells, which frequently go under the name "BSF structures." The use of such isolating layers has also been proposed for the front region of the device, where they are limited to the area shaded by the ohmic contacts (Fig. 10), while another recent high efficiency design uses an isolating layer in the base without application of the high/low junction (Fig. 11).

A commonly used approach to reducing the density of injected excess minority carriers, e.g., n_p, and to consequently achieving higher open circuit voltages, is to decrease the thermal equilibrium minority carrier concentration $n_{p,o}$ (Table IX). $n_{p,o}$ is inversely proportional to the majority carrier concentration and consequently the dopant concentration. This reduces the saturation current, and yields a higher V_{oc}. At the open circuit condition, however, the excess minority carrier concentration is returned to the same value as present in the case of lower dopant concentration. The limits of achieving improvements through higher dopant concentrations are reached by the onset of Auger recombination, and deleterious effects are experienced through bandgap narrowing.

After all these avenues available through device structuring possibilities are exhausted, then the only recourse left for the reduction of recombination becomes the decrease of the recombination center density itself (Table X). For those of these centers which are located in the volume of the material (bulk centers), the interest focuses on the original material processing (crystal growth), and on the further role of these previously introduced centers during device processing. In the original material processing, attention needs to be directed to the reduced incorporation of impurities which cause recombination centers; to the avoidance of crystal defect introduction, particularly through control of the thermal environment during crystal growth; to the roles of oxygen and carbon which are present in the silicon in relatively high concentrations; and to the formation of defect complexes, and particularly to their roles in forming or neutralizing recombination centers.

The second area, device processing, is equally important for the reduction of the recombination center density in the final device. The first and most obvious point of attention is the prevention of the introduction of new lifetime killing impurities. A second approach is to remove existing defects in the material at various stages during the device process, using treatments which are generally connected with the name "gettering." One of the major problems in device processing, particularly during the application of high temperature processes, is the transformation of existing inactive defects into recombination centers. On the other hand, it is desirable to foster the transformation of recombination centers to electrically inactive defects. These transformations may involve changes in existing complexes, or the formation of new ones. The transformations are often connected with the name "passivation," and one of the major open questions in this area is the role which hydrogen can play.

Somewhat related to the question of reducing the bulk recombination center density is that of dealing with the surface recombination centers. What is meant here is the actual reduction of the density of recombination centers at the surface, rather than the effect of a reduced surface recombination velocity which often is connected with the introduction of a potential step just below the surface (Table XI). The usual recombination center density of untreated silicon surfaces is in the 10^{15} cm^{-2} range. This number happens to be near the density of dangling bonds which would be expected to exist at a perfect silicon surface. If these dangling bonds should actually be responsible for the recombination centers, then the question arises of how these dangling bonds interact with other chemical species, and particularly which of these interactions result in a substantial decrease in the recombination center concentration. In addition, there is the question of which other defects form surface traps which act as recombination centers. Definitive answers to these questions may lead to the methods for effectively avoiding the introduction of these defects, or for their elimination, once they are in existence.

The whole question complex on the reduction of the recombination center density leads to the conclusion that considerable progress in the silicon material science is needed, as well as in the technology of crystal preparation and of device processing.

The preceding discussions lead to the conclusion that a high efficiency solar cell design will by necessity combine at least several of the methods known for the reduction of recombination (Table XII). It will further have to strike the right compromise between the conflicting design requirements, as a particular method may improve certain attributes of the device, but have a negative impact on others. And finally, all the second order effects need to be included in the design considerations, and the best available technologies for their reduction be applied in order to achieve the highest efficiency extractable from the silicon solar cell. The general high efficiency design concept, thus, will pursue the two-pronged approach of decreasing the recombination loss of minority carriers, and particularly that of the carriers injected under forward bias, and of simultaneously reducing all the secondary effects to near negligible values. Several cell design approaches seem to exist for each of these performance attributes, and the designer will have to select those which will yield the highest overall device performance, when applied in combination. And, of course, this device will have to be fabricated at a competitive price.

CONCLUSION

It has been seen that the achievement of higher efficiencies in silicon solar cells depends on the reduction of all secondary losses to negligible values, which is about possible with current technology, and then on the reduction of minority carrier recombination (summarized in Table XIII). For the latter, four principal approaches are available, three of which are essentially remedial, handled through device design, and one is fundamental, namely the reduction of the recombination center density.

All the reduction of recombination via recombination centers will only lead to the dominance of Auger recombination, which appears to impose the ultimate practical limitation on solar cell efficiency. As there exist still some doubts on the magnitude of the Auger coefficients, this ultimately achievable efficiency can also not be certain at this time. Some rather fundamental research will be needed to gain the complete understanding of the band-to-band recombination effects which carry Auger's name.

Several of the "remedial" methods for reduction of recombination involve high majority carrier concentrations. The onset of Auger recombination tends to force the efficiency versus carrier concentration curves towards zero slope, and the onset of bandgap narrowing then to a negative slope. Again, the bandgap narrowing effect does not seem fully explained, with the result that the various bandgap models in existence now lead not only to different solar cell performance expectations, but also to different cell designs for optimum performance. Again, fundamental research is needed.

Outside of these fundamental research needs, substantial silicon material research, both bulk and surface, will be needed to reach substantially higher efficiency levels. And then we should not forget the inventiveness which could bring forward new, more effective remedial design concepts.

REFERENCES

1] Green, M. A., "Limits on the Open-Circuit Voltage and Efficiency of Silicon Solar Cells Imposed by Intrinsic Auger Processes," IEEE Trans. El. Devices, ED-31, pp. 671-678, May 1984.

2] Tiedje, T., Yablonovitch, E., Cody, G. D., and Brook, B. G., "Limiting Efficiency of Silicon Solar Cells," ibid., pp. 711-716.

PRIMARY CAUSES OF LOSSES	SYMBOL	DESIGN PARAM	1970 COM'L CELL	"VIOLET CELL"	"BLACK CELL"	1978 SPACE CELL	1984 EXPER'L CELLS SPIRE	WESTINGH	M.A.GREEN	GOALS 20%	22.6%
		BASE: WIDTH	?	300μm	300 μm	300μm(A)	380 μm	375 μm	280 μm	200μm	200μm
		$\tau_{n,p}$	3μs	?	?	?	~40 μm	~23 μm	~25 μm	95μs	950μs
		τ_{n,p^+}	—	—	—	?		(0.1 μs)	(0.1 μs)	0.26μs	2.6μs
		FRONT: WIDTH	0.4 μm	~0.15 μm	~ 0.2μm	~0.2 μm	~0.2μm	~0.3 μm	~0.3 μm	2 μm	2 μm
		$\tau_{p,n}$	?	?	?	?			1ns -15μs	0.1μs	10μs
		S	?	?	?	?	~10^4 cm s^{-1}	~10^4 cm s^{-1}	10^3 cm s^{-1}	10^3 cm s^{-1}	10^2 cm s^{-1}
		TREATM.	SiO	Ta_2O_5+ GLASS	TEXT'D + Ta_2O_5 + GLASS	TEX T'D + Ta_2O_5	TEXT'D + SiO_2 + TiO_2	TiO_2/SiO_2	ZnS/ MgF_2	DUAL AR	DUAL AR
1. LIGHT GENERATED CURRENT:											
FUNDAMENTAL LIMIT (AM1)	$j_{L,id}$		44mA cm^{-2}								
A. OPTICAL SURFACE PROPERTIES (REFLECTION)	(1-R)		0.905	0.90	0.9[illegible]	0.96	0.975	0.966	0.954	0.97	0.97
B. CONTACT COVERAGE	S		0.96	0.95	0.95	0.96	0.965	0.97(A)	0.948	0.966	0.966
C. INCOMPLETE ABSORPTION (THICKNESS)	η_{coll}		0.72	0.95	0.96	0.96(A)	0.956	0.956	0.973	0.92	0.95
D. RECOMBINATION OUTSIDE DEPLETION REGION (BULK AND SURFACE, INCLUDING CONTACTS)	η_{coll}			0.95 =0.90	0.94	0.94	0.91	0.915	0.93		
E. ("DEAD LAYERS")	(1-A)			1.0	1.0	1.0	1.0	1.0	1.0	1.0	1.0
OVERALL COLLECTION EFFICIENCY:	γ		0.63	0.77	0.84	0.84	0.82	0.82	0.82	0.86	0.89
LIGHT GENERATED CURRENT (AM1)	$j_L = \gamma \cdot j_{L,id}$ (mA cm^{-2})		28.1	34.0	37.1	37.0	36.2	36.0	36.0	37.9	39.2
2. OPEN CIRCUIT VOLTAGE:											
FUNDAMENTAL LIMIT:	$(VF)_{fund}$ = 0.76		0.836 V (j_0 = 4.2 · 10^{-16} A cm^{-2})								
A. RECOMBINATION OUTSIDE DEPLETION REGION (BULK AND SURFACE, INCLUDING CONTACTS)	$(VF) = (VF)_{techn} \cdot (VF)_{fund}$		0.522	0.528	0.533	0.555	0.565	0.57	0.59	0.60	0.65
B. BANDGAP NARROWING											
C. "CURRENT LEAKAGE"	(R_{sh})		1.0	1.0	1.0	1.0	1.0	1.0	1.0	1.0	1.0
OPEN CIRCUIT VOLTAGE:	$V_{oc} = (VF) \cdot E_g$ (V)		0.574	0.581	0.586	0.610	0.622	0.627	0.653	0.661	0.715
3. FILL FACTOR:											
FUNDAMENTAL LIMIT:	$(CF)_{fund}$		0.865								
A. SAME AS OPEN CIRCUIT VOLTAGE	$(CF) = (CF)_{techn} \cdot (CF)_{fund}$		0.82	0.823	0.823	0.824	0.83	0.833	0.839	0.84	0.85
B.											
C.	(R_{sh})		1.0 (A)	1.0	1.0	1.0	1.0	1.0	1.0	1.0	1.0
D. RECOMBINATION IN DEPLETION REGION	$(CF)_{add'l}$		0.91	0.97	0.97	0.97	0.985	0.98	0.982	0.97	0.97
E. SERIES RESISTANCE	(R_s)		0.96	0.985	0.984	0.98 (A)	0.98	0.98	0.984	0.98	0.98
FILL FACTOR	(FF)		0.716	0.78	0.78	0.78	0.801	0.800	0.811	0.80	0.81
RESULTING CONVERSION EFFICIENCY	η		11.6	15.4	17.0	17.6	18.1	18.1	19.1	0.200	0.226

(A) = ASSUMED

Table I

ORIGINAL PAGE IS OF POOR QUALITY

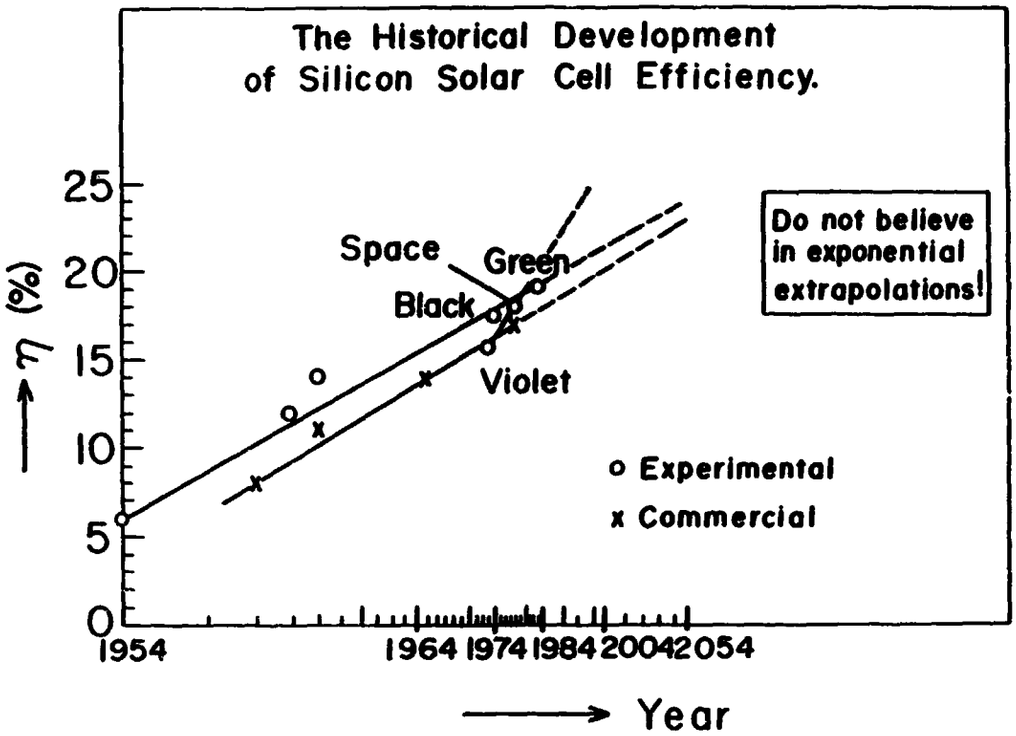

Figure 1

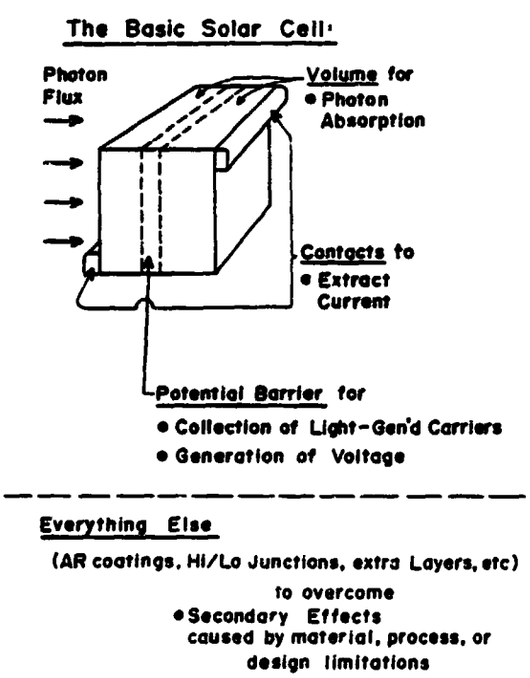

Figure 2

ORIGINAL PAGE IS
OF POOR QUALITY

STATUS OF Si SOLAR CELL TECHNOLOGY

- TECHNOLOGY IS AVAILABLE TO REDUCE THE CONTRIBUTION OF EACH SECONDARY LOSS MECHANISM (REFLECTION, CONTACT SHADING, SERIES RESISTANCE, ETC.) TO THE MAXIMALLY 2-3% LEVEL.
- INTERNAL COLLECTION EFFICIENCY IS GENERALLY >90%; "SATURATES" WITH FURTHER REDUCED RECOMBINATION.
- OPEN CIRCUIT VOLTAGE CONTINUES TO SUBSTANTIALLY INCREASE WITH DECREASING MINORITY CARRIER RECOMBINATION, UP TO BASIC RECOMBINATION LIMIT (RADIATIVE AND AUGER).
- CURVE FACTOR (FUNDAMENTAL PART OF FILL FACTOR) CAN INCREASE (WITH V_{oc}) BY A FEW PERCENT.

Table II

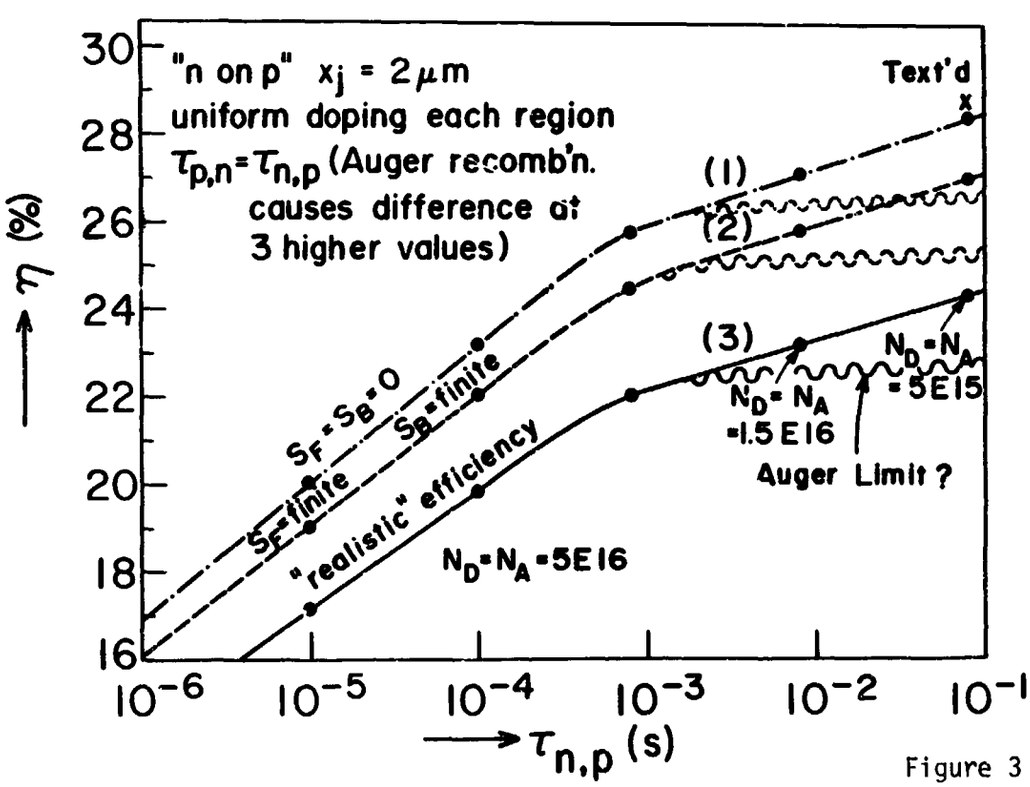

Figure 3

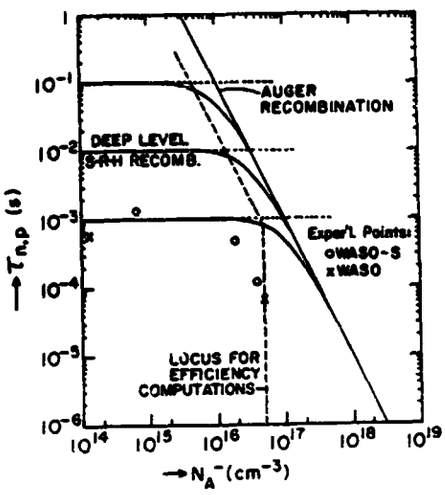

Figure 4

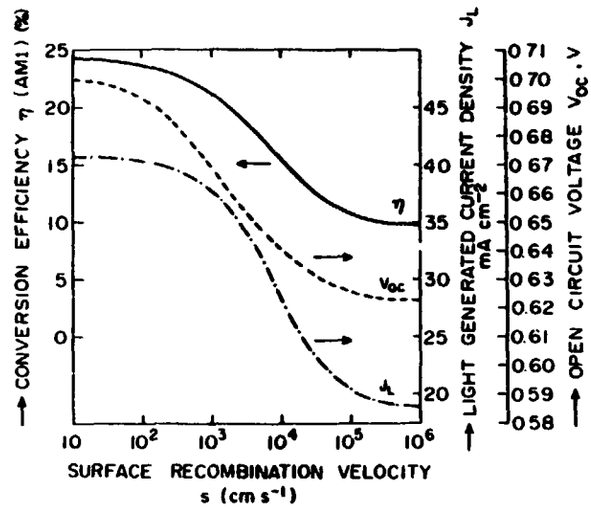

Figure 5

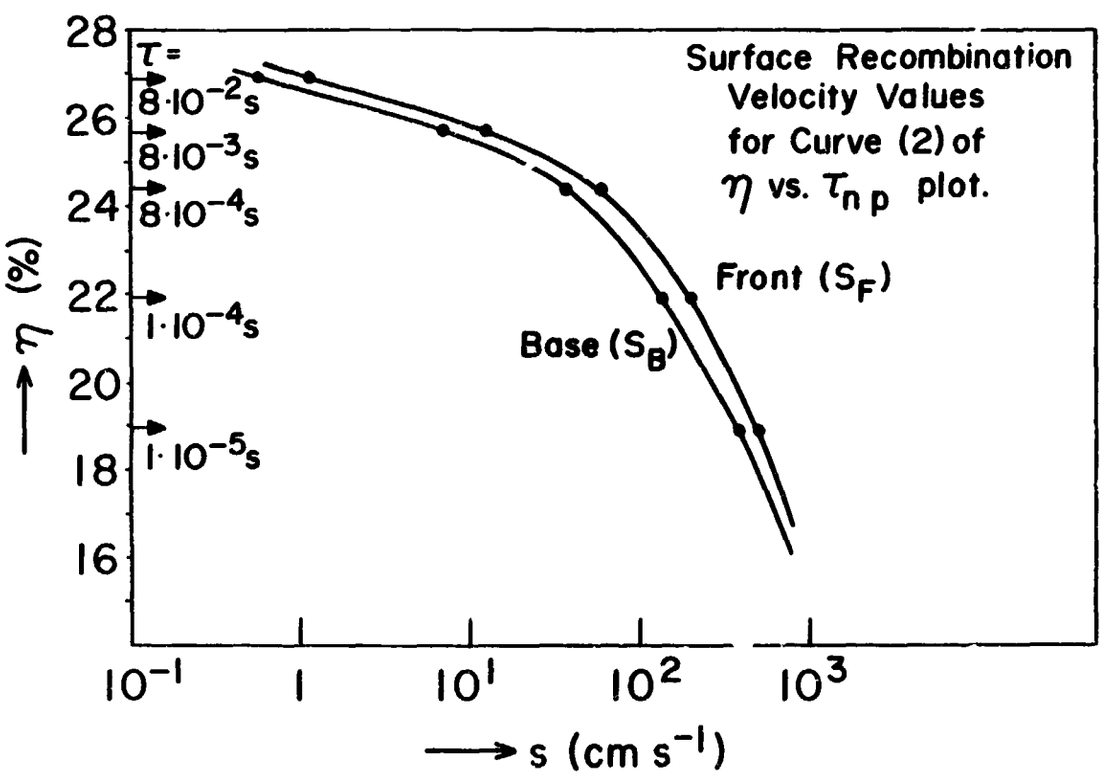

Figure 6

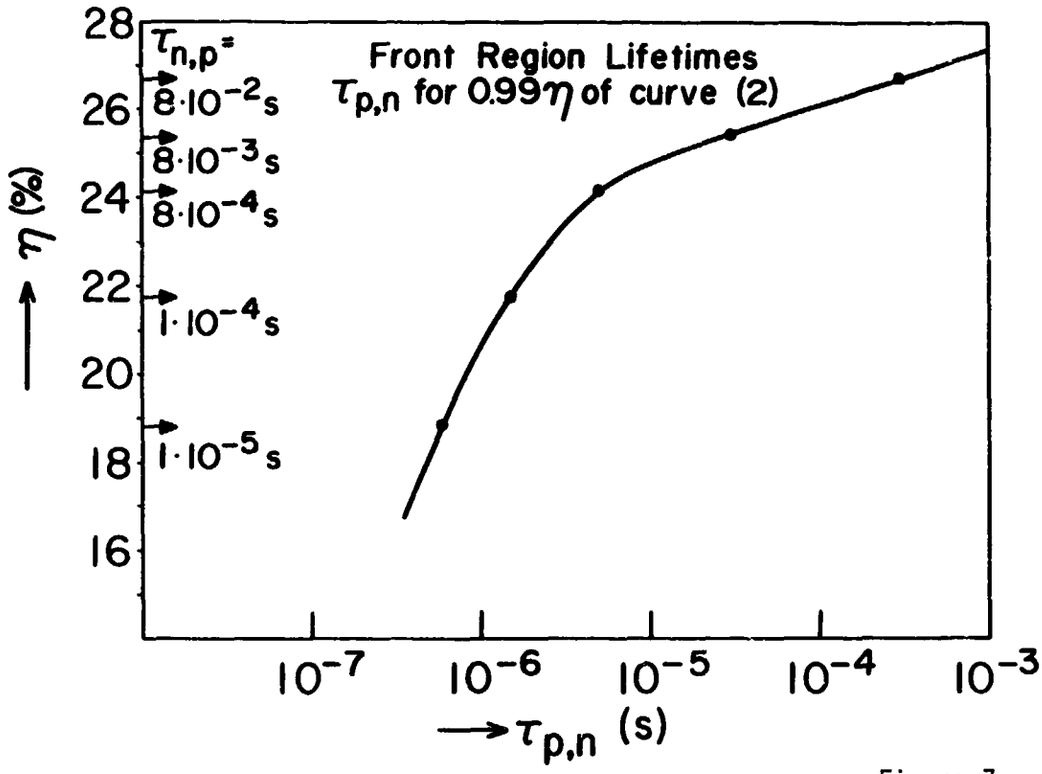

Figure 7

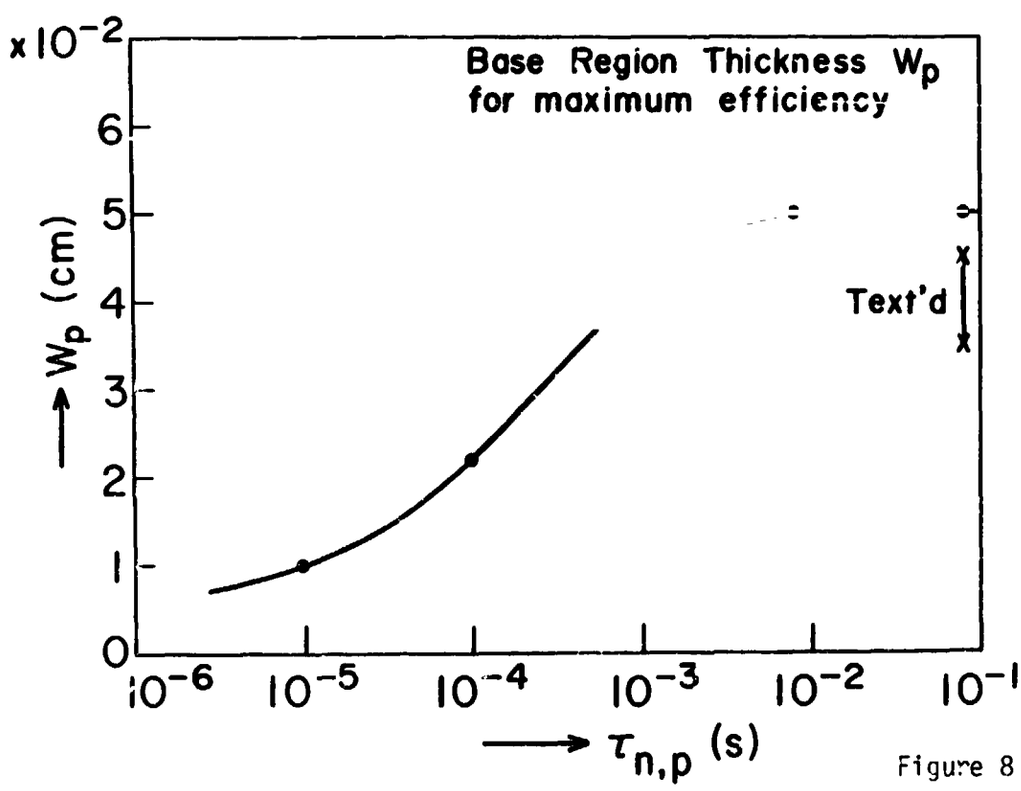

Figure 8

HIGH EFFICIENCY REQUIRES

A GLOBAL VIEW OF THE DEVICE, SO THAT
ALL TECHNOLOGY-DETERMINED LOSSES
WILL BECOME LOW.

IF ONE LOSS MECHANISM DOMINATES —> NOT OPTIMIZED
—> REDUCE IT

[OLD OPTIMIZATION RULE:
CONTRIBUTIONS FROM DIFFERENT COMPONENTS
ARE EQUAL AT MAXIMUM OR MINIMUM.]

Table III

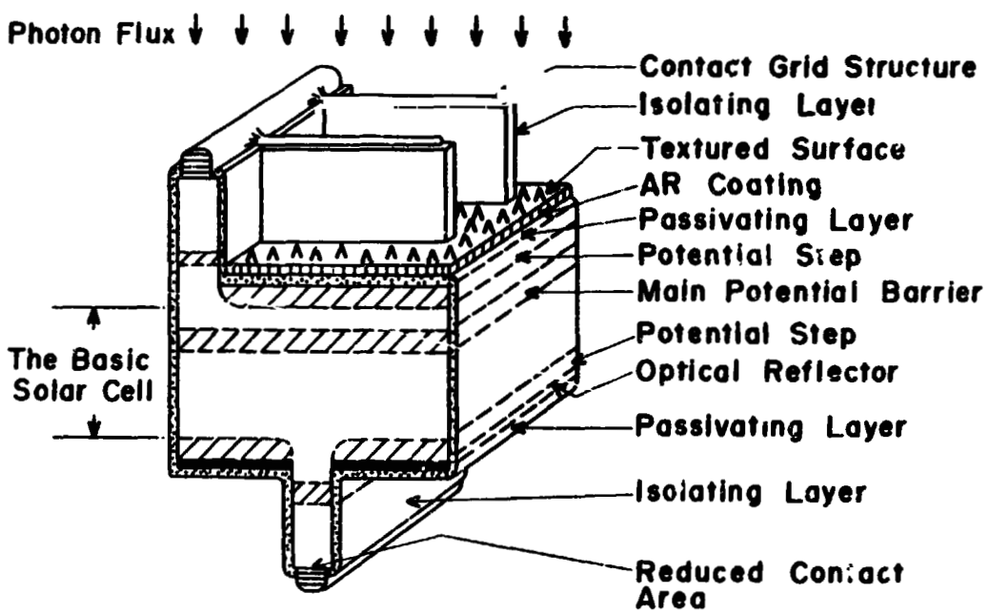

Schematic View of the Solar Cell "That Has Everything"

Figure 9

THE THREE PRINCIPAL PATHS TO REDUCED RECOMBINATION

DECREASE

1. DENSITY OF RECOMBINATION CENTERS

- IN BULK N_t $[cm^{-3}]$ $\longrightarrow$ HIGHER τ
- AT SURFACES $N_{s,t}$ $[cm^{-2}]$ $\longrightarrow$ LOWER s

2. VOLUME OR AREA CONTAINING RECOMBINATION CENTERS.

- "THIN" LAYERS
- "DOT CONTACTS"

3. DENSITY OF EXCESS MINORITY CARRIERS

- FAST REMOVAL TO OUTSIDE (FOR η_{coll})
- "SHIELDING" WITH POTENTIAL STEPS
- "ISOLATING" FROM HIGHER RECOMBINATION RATE

} FOR η_{coll}

- HIGH DOPANT CONCENTRATION

} FOR V_{oc}

Table IV

REDUCE VOLUME:

(I.E., THICKNESS OF LAYERS)

PRINCIPLE: $j_d = qn_p \frac{L}{\tau} \Big|_{d>>L} \longrightarrow j_d = qn_p \frac{d}{\tau} \Big|_{d<<L}$

("THICK" LAYER) ("THIN" LAYER)

LIMIT: $I_d = I_L$ for V_{oc}: VARIABLE

$$n_p = \frac{j_L}{q} \cdot \frac{\tau}{d} \not\ll p_{p,o}$$

NO LONGER LOW LEVEL INJECTION

$$\tau_{Auger} = \frac{1}{C_{Auger}(p_{p,o}+n_p)^2} < \tau_{S-R-H}$$

$(Aj_d = Aj_L)$

(AREA REDUCTION COULD BE EFFECTIVE ONLY, IF j_d/j_L RATIO COULD BE CHANGED, WITH I_d/I_L CONSTANT.)

Table V

REDUCE SURFACE AREA:

OPEN SURFACES:

LIMIT: ● NEEDED FOR PHOTON ABSORPTION

(CONCENTRATION: INCREASED j_L:

$$n_p = \frac{j_L \tau}{q\,d} \overset{?}{<<} p_p)$$

CONTACT AREAS: "DOT" CONTACTS

UTILIZE AVERAGE EFFECTIVE s:

$$j_{r,s} = q n_p(x_s) \frac{A_1 s_1 + A_2 s_2}{A_1 + A_2}$$

LIMITS: ● LESS EFFECTIVE WHEN SPACING < L

● SPREADING RESISTANCE INCREASES R_s

Table VI

SHIELDING WITH POTENTIAL STEPS:

GENERALLY REDUCES TRANSPORT VELOCITIES (FOR RECOMBINATION CURRENTS)

BY: $\frac{u_1}{u_2} = e^{-\frac{q\Delta(E_F - E_V)}{kT}} = \frac{p_p(x_1)}{p_p(x_2)}$; (FOR p-TYPE,

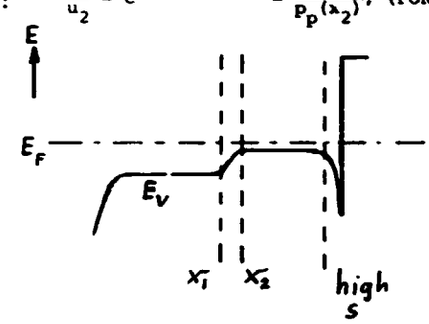

$$j_r(x_1) = q n_p(x_1) u_1(x_1)$$
$$= q n_p(x_1) \frac{p_p(x_1)}{p_p(x_2)} u_2(x_2)$$

FORMS OF POTENTIAL "STEPS":

- DRIFT FIELD REGIONS
- HIGH/LOW JUNCTIONS
- ACCUMULATION LAYERS (USUALLY UNDER INSULATORS, INCLUDING "TUNNEL CONTACTS").
- "FLOATING" pn JUNCTIONS (OR INVERSION LAYERS).
- BANDGAP CHANGES (USUALLY ΔE_G WITH HIGH/LOW JUNCTION, "WINDOW LAYER").

LIMITS:

- INCREASED DOPING AT "LOW" SIDE REDUCES AVAILABLE STEP HEIGHT.
- "HEAVY DOPING" EFFECTS ON "HIGH SIDE" LIMIT USEFUL STEP HEIGHT.
- ABSORPTION W/O COLLECTION IN "WINDOW LAYERS."
- INTERFACE STATES AT TRANSITION TO "WINDOW LAYER."

Table VII

ISOLATING WITH "THICK LAYERS"

PRINCIPLE:

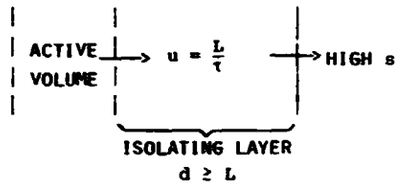

LIMITS:

- ADEQUATELY HIGH L/τ.
- AFFECTS COLLECTION EFFICIENCY, IF IN IPTICAL PATH.

Table VIII

HIGH DOPANT CONCENTRATION

PRINCIPLE:

$$j_d = q\, n_p \cdot \frac{L}{\tau} = q\, n_{p,o}\, e^{\frac{qV}{kT}} \cdot \frac{L}{\tau}\ ;$$

$$V = \text{HIGH IF } n_{p,o} = \text{SMALL:}\quad n_{p,o} = \frac{n_i^2}{p_{p,o}}$$

LIMITS:

- HEAVY DOPING EFFECTS.

Table IX

REDUCE VOLUME RECOMBINATION CENTER DENSITY:

- ORIGINAL MATERIAL PROCESSING:
  - FEWER IMPURITIES
  - ROLES OF OXYGEN, CARBON?
  - FEWER CRYSTAL DEFECTS (THERMAL ENVIRONMENT IN X-TAL GROWTH?)
  - ROLES OF DEFECT COMPLEXES
- DEVICE PROCESSING:
  - NO NEW IMPURITY INTRODUCTION
  - REMOVE EXISTING DEFECTS (GETTERING)
  - AVOID TRANSFORMATION OF DEFECTS TO RECOMBINATION CENTERS (EFFECTS OF THERMAL PROCESSES?)
  - FOSTER TRANSFORMATION OF RECOMBINATION CENTERS TO HARMLESS DEFECTS (PASSIVATION; CHANGES OF COMPLEXES?; ROLE OF HYDROGEN?)

Table X

ORIGINAL PAGE IS
OF POOR QUALITY

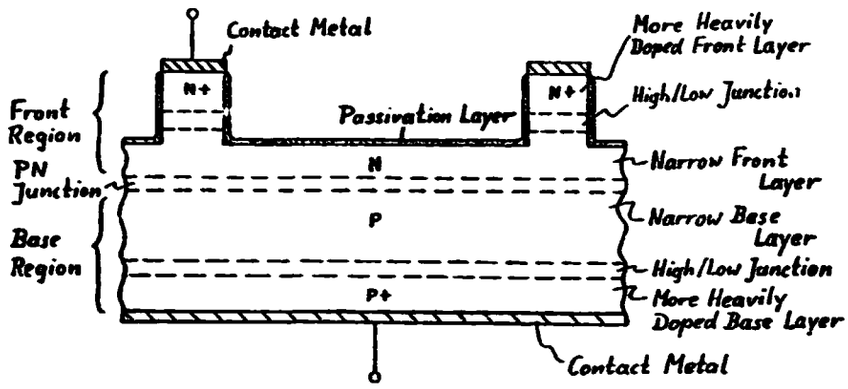

Figure 10

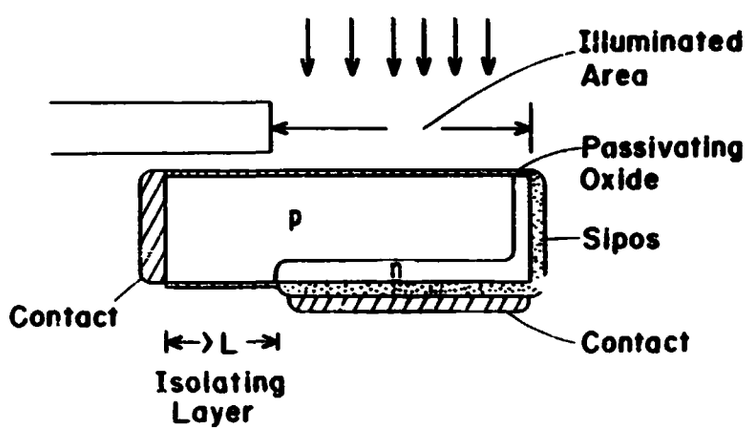

THE EXXON HIGH EFFICIENCY DESIGN

Figure 11

REDUCE SURFACE RECOMBINATION CENTER DENSITY:

- PASSIVATION OF DANGLING BONDS.

  (WHICH LAYERS ARE MORE EFFECTIVE IN REDUCING S_0, WHICH IN SUPPORTING ACCUMULATION LAYERS?)

- WHAT OTHER DEFECTS FORM SURFACE TRAPS

  (HOW CAN THEY BE AVOIDED OR ELIMINATED?)

Table XI

A HIGH EFFICIENCY CELL DESIGN

- COMBINES SEVERAL OF THE METHODS FOR REDUCTION OF RECOMBINATION.
- STRIKES THE RIGHT COMPROMISE BETWEEN CONFLICTING DESIGN REQUIREMENTS.
- REDUCES ALL SECOND ORDER EFFECTS.

Table XII

THE GENERAL HIGH EFFICIENCY DESIGN CONCEPT

EFFECT	LOCATION	AVAILABLE MEASURES PRINCIPLE	METHOD
● REDUCE RECOMBINATION LOSS OF MINORITY CARRIERS, PARTICULARLY INJECTED CARRIERS (HIGH V_{oc}):			
BULK RECOMBINATION	BASE, FRONT	REDUCE N_t	PROCESSING
		REDUCE VOLUME	APPLY LIGHT TRAPPING
SURFACE RECOMBINATION	OPEN SURFACE	REDUCE $N_{t,s}$	PASSIVATION LAYER
		SHIELDING	DRIFT FIELD
		ISOLATION	WINDOW LAYER
	CONTACT	REDUCE AREA	"DOT CONTACT"
		SHIELDING	TUNNEL CONTACT WITH ACCUMULATION LAYER
			HIGH/LOW JUNCTION, BSF
			HIGH/LOW JUNCTION, WITH THICK p^+ OR n^+ LAYER, OR WIDE BANDGAP LAYER
		ISOLATION	THICK LAYER ALONE
● SECONDARY EFFECTS			
REFLECTION	FRONT	AR	MULTI-LAYER AR
		TEXTURE	TEXTURE + SINGLE AR
CONTACT	FRONT	REDUCE METAL COVERAGE	WRAP-AROUND DESIGN
			FINE LINE GRID
R_S	FRONT, BACK	KEEP LOW	DEGENERATE SURFACE
			LOW METAL SHEET-RESISTANCE
			GOOD INTERCONNECT DESIGN
EXCESS CURRENT	JUNCTION	KEEP LOW	GOOD PROCESSING

Table XIII

DISCUSSION
(WOLF)

SPITZER: Given all the tradeoffs on grid design, passivation, and the other things that are necessary to make a 20% efficient cell, the question is, can screen-printed contacts be used for the 15% module, or will they not offer enough for high-efficiency features?

WOLF: I have been talking against screen printers at a number of meetings. The biggest problem I see in them is that in screen printing and sintering you don't get better resistivity or better conductivity. Even with silver it seems you get conductivity only about one-third, in general, of what you get if you electroplate or deposit silver. You are limited by how thick you can make the layer in one pass. The sheet resistance becomes limited by the bulk conductivity you can get. The second problem is, you cannot make them very narrow. It seems that 5 mils might be achievable with today's technology. These are the two things I see against screen-printed contacts.

SPITZER: Then, probably no.

WOLF: I would think if you go for high efficiency, at least consider a secondary later. I always find the first thing is to show we can really make high efficiency, so let's use the best technology we know we can apply to get to high efficiency, then later let's think of how can we make them cheaper.

Now I want to introduce the next speaker. Here is a little contradiction. I have been saying that all the secondary problems are minor, our current technology is solved; just worry about recombination. Arnie Lesk from Solavolt is going to tell us about all the problems that still exist in trying to make low-resistance contacts. So, basically, I guess it is not easy, and there are still a lot of problems connected with it.

SOME PRACTICAL CONSIDERATIONS FOR ECONOMICAL BACK CONTACT FORMATION ON HIGH EFFICIENCY SOLAR CELLS

I. A. Lesk
Solavolt International
Phoenix, Arizona

N85-31620

Abstract

The back contact can detract from solar cell performance by a number of means: high recombination, barrier, photovoltage, minority carrier collection, resistance. These effects may act in a non-uniform fashion over the cell area, and complicate the analysis of photovoltaic performance aimed at a better understanding of the effects of device geometry and material and/or processing parameters.

The back contact can be tested by reproducing it on both sides of a substrate. The dark current-voltage characteristic should obey Ohm's law calculated using the resistivity of the substrate. Sintered aluminum on p-type silicon substrates of moderate and low resistivity behaves in this way, and so may be used as a reference against which other back contact technologies are measured.

The objective is to find a back contact which performs well as a back contact, can be applied cheaply to large area solar cells, fits well into a practical process sequence, does not introduce structural damage or undesirable impurities into the silicon substrate, is compatible with an effective front contact technology, permits low temperature solder contacting, adheres well to silicon, and is reliable.

1. HIGH RECOMBINATION
2. MINORITY CARRIER COLLECTION
3. RESISTANCE
   - LINEAR
   - NON-LINEAR
4. BARRIER
5. PHOTOVOLTAGE

BACK CONTACT PROBLEMS

TABLE 1

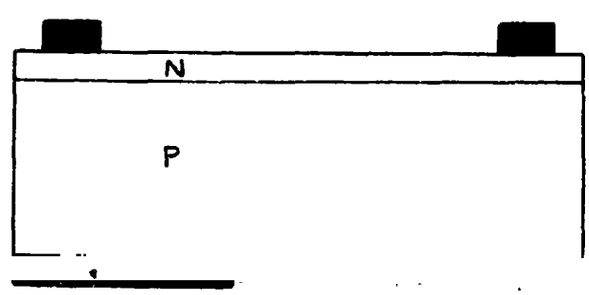

FIGURE 1. Simple solar cell section.

PRECEDING PAGE BLANK NOT FILMED

Introduction

Reduction of the cost of solar cell metallization is necessary if the projected low prices for modules are to be realized. Towards this goal, various new technologies are under investigation.[1,2,3] Back contact problems have been seen with some material systems, as - fabricated[3] or after stress ageing.[4] Back contact problems that can occur are listed in Table 1.

A Model for Back Contact Studies

Figure 1 shows a simple solar cell cross section. The back contact can degrade performance of the structure in two ways:

1. by removing carriers (through recombination or collection) which would otherwise contribute to photocurrent at the P-N junction, or by generating carriers that increase the diffusion component of dark current, and
2. by introducing resistances or barriers that reduce terminal voltage.

Barrier effects on overall solar cell performance may be modified by photovoltage generation due to light reaching the back contact region.

If we ascribe back-surface minority carrier effects on the P-N junction to photocurrent losses in the photogenerator and dark diffusion current increases in the n=1 diode, the rest of the back surface problems (3,4 and 5 in Table 1) may be removed into a separate 2-port network section, as shown in Figure 2. The top 2-port section is the active one, with J_{ph} reduced by minority carrier recombination and collection at the back contact, and the n=1 diode having its dark current influenced by minority carrier generation or injection at the back contact. The n diode contains all the n>1 components. The shunt conductance Z_{sh} may be non-linear.

In the 2-port section at the bottom of Figure 2, barriers of either polarity, with photocurrents J_{ph_B} and $J_{ph_B}^{I}$ are indicated as possible parasitics. The V-I characteristics of these barriers are generally much more conductive than those of a p-n junction because they are often low grade Schottky barriers and, particularly for large area devices, shunted in a non-uniform fashion. The shunt impedance Z_{SB} may be nonlinear if the ohmic solar cell current traverses grain regions; this can be particularly prominent if the back contact region is segmented so lateral ohmic current in the base is appreciable.

Experimental observations of the parasitic dark characteristics of the back contact are instructive in determining their cause and helping with their elimination. Figure 3(a) shows a section of a solar cell. Leaving off the p-n junction and making ohmic contact to top and bottom, Figure 3(b), would place two of the lower (parasitic) 2-ports in series. If the top-to-bottom V-I characteristic of the structure in Figure 3(b) obeys Ohm's Law for the substrate material, there are no prominent back contact parasitics. Otherwise, it will be necessary to use a known ohmic structure. Figure 3(c), with p^+ contacts, can be entirely ohmic, e.g. for a 0.25 Ω - cm substrate 250 μM thick, top-to-bottom conductance is 160 mhos/cm^2 (resistance = 6.25 mΩ - cm^2). At 36

ma/cm^2, the parasitic bulk drop is less than ½ mV. For a 100 cm^2 cell, conductance = 16000 mhos (series resistance = .06 mΩ). This p^+ contact then becomes a standard against which other technologies are measured. The structure in Figure 3(d) can be used to measure the ohmic character of the experimental contact formed on the top side.

Solar cells are sometimes made with segmented back contacts, Figure 4. In this type of geometry, there is a considerable amount of lateral current flow. By omitting the P-N junction, back contact parasitics can be tested for photogeneration. However, the bulk series resistance will be larger, and more susceptible to grain boundary effects. Quantitatively, consider a solar cell 250μM thick with 5 equispaced contact lines/cm top and bottom, and a substrate resistivity of 0.25 Ω-cm. Conductance between top and bottom contact sets will be approximately 20 mhos, assuming the average photocurrent induced majority carrier path length is 0.05cm., half the contact spacing, and no grain boundary impedance. For a 100 cm^2 cell, g=2000 mhos, or series resistance is 0.5 mΩ. This resistance is about an order of magnitude larger than that of a similar cell with full back-surface metallization, but still small enough to serve as an effective shunt for an otherwise severe back surface barrier (e.g. an npn structure with a network of p^+ back contacts penetrating to the p-type substrate).

Some Examples

Examples of how parasitic back-surface elements can degrade the V-I characteristic of an otherwise good cell are constructed by adding voltages of the 2-port sections at common currents. The upper 2-port V-I characteristic for a theoretical resistance-free base-dominated thick diode is shown in Figure 5. Parameters chosen are n=1, p=1.5x10^{17}/cm^3, L_n=100μM, μ_n=624 cm^2/V sec ($J_o \sim 10^{-10}$ mA/cm^2). Under 1-sun illumination, assuming 36 mA/cm^2, the V-I characteristic is shifted downward as shown in Figure 6.

Figure 7 shows the effect on a 1 cm^2 cell of a series resistance of 1 Ω; this would be obtained on a structure as given in the example illustrated in Figure 4 if the base resistivity were 5 Ω-cm.

Figure 8 shows the effect of a diode with a polarity opposing the P-N junction. The diode V-I characteristic is sketched on the left side of the current axis; when added to the theoretical diode curve the resultant form is S-shaped. This diode is on the left side of the bottom 2-port in Figure 2. If this diode has a photocurrent J_{ph_B} of 2 ma/cm^2, the resultant solar cell V-I characteristic is as sketched in Figure 9.

If the back-surface barrier is directed in the same sense as the P-N junction, the main photocurrent will drive it in the reverse-bias direction. Figure 10 indicates the effect of a very leaky "reverse" barrier, and Figure 11 shows that for a J_{ph_B} of 10 mA/cm^2, Voc is increased although the peak power region is degraded. For this polarity of barrier to provide a net increase in cell power, its photocurrent must be very nearly as large as that of the main P-N junction; a thin cell made on high resistivity, high lifetime material

(i.e. a BSF cell) would be of this type.

Total Back Contact Requirements

The back contact must be relatively free from the problems listed in Table 1, i.e., it must be capable of good optoelectronic performance. In addition, it must have the rest of the characteristics listed in Table 2 if it is to contribute to meeting the DOE long range cost/performance goals.

References

1. MOD Silver Metallization for Photovoltaics, G. M. Vest and R. W. Vest, Quarterly Technical Report, December 1, 1983-February 29, 1984, DOE Contract No. NAS-7-100-956679.

2. Development of Metallization Process, Alexander Garcia III, Quarterly Technical Progress Report, December 31, 1983, JPL Contract 956205.

3. Development of an All-Metal Thick Film Cost Effective Metallization System for Solar Cells, Bernd Ross and Joseph Parker, Final Report, December 1983, DOE Contract No. NAS-7-100-955688.

4. Accelerated Degradation of Silicon Metallization Systems, Jay W. Lathrop, Proceedings of the Flat-Plate Solar Array Project Research Forum on Photovoltaic Metallization Systems, DOE/JPL-1012-92, November 15, 1983.

CAPABLE OF GOOD OPTOELECTRONIC PERFORMANCE
ECONOMICALLY APPLICABLE TO LARGE AREA CELLS
CONSISTENT WITH A PRACTICAL PROCESS SEQUENCE
NON-DETERIORATING OF BULK SILICON PROPERTIES
- STRUCTURAL
- IMPURITIES

COMPATIBLE WITH EFFECTIVE FRONT CONTACT TECHNOLOGY
ADHERENT
RELIABLE
SOLDERABLE

BACK CONTACT REQUIREMENTS

TABLE 2

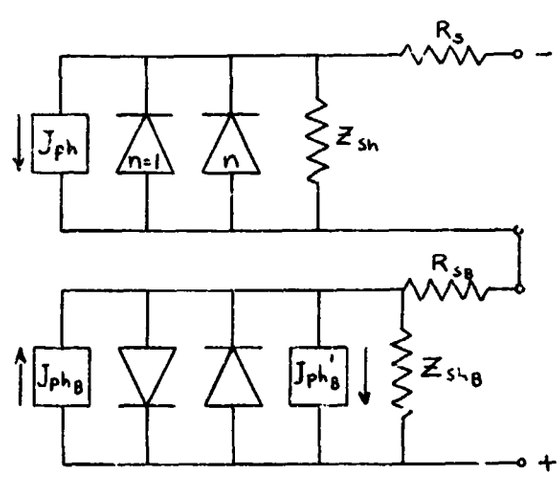

FIGURE 2. Active (top) and passive (bottom) 2-port network sections.

ORIGINAL PAGE IS
OF POOR QUALITY

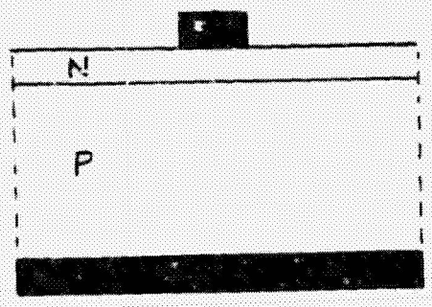

FIGURE 3(a). Simple solar cell section.

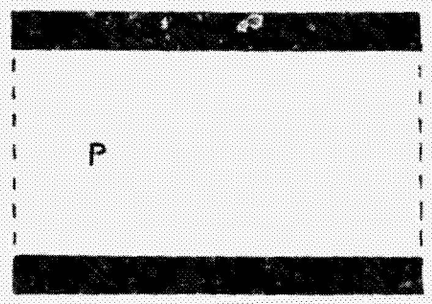

FIGURE 3(b). Bottom contact structure produced on both sides of a substrate.

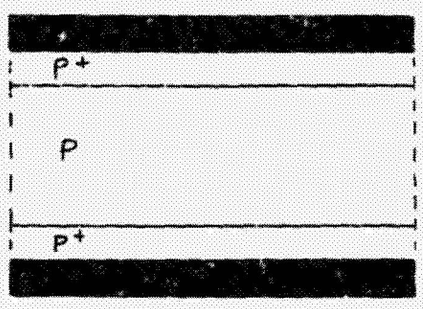

FIGURE 3(c). Ohmic contact produced on both sides of a substrate.

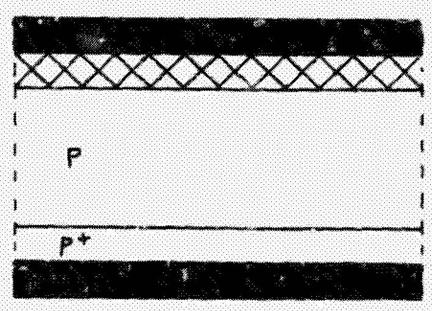

FIGURE 3(d). Geometry for measuring ohmic characteristics of experimental contact (top).

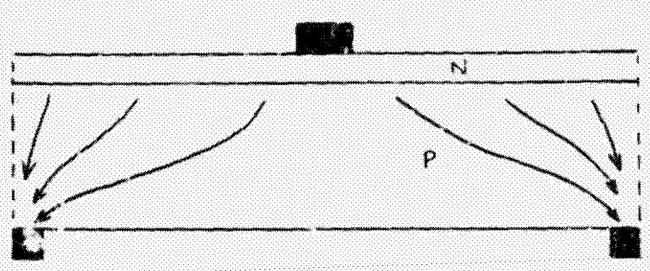

FIGURE 4. Segmented back contact structure.

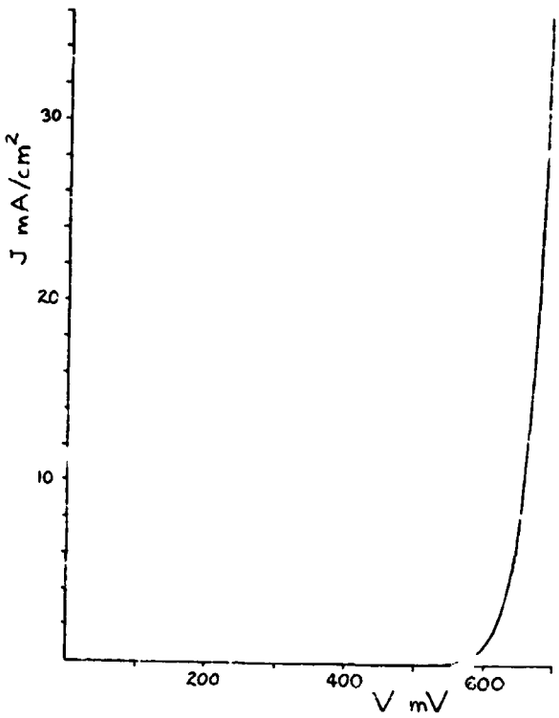

FIGURE 5. Dark V-I characteristic calculated for selected diode.

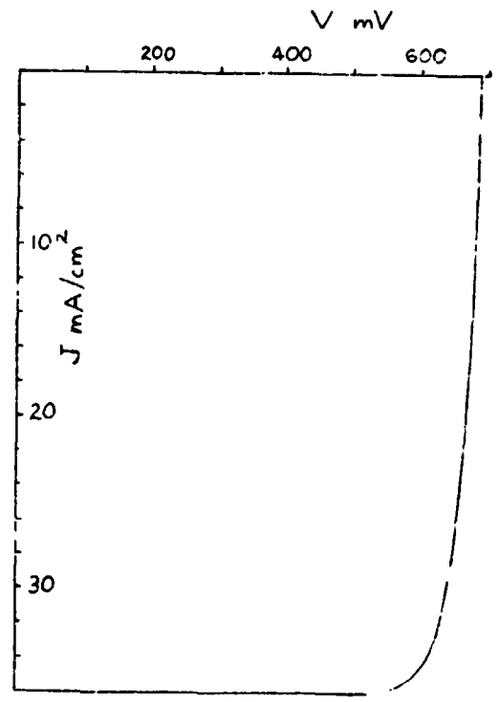

FIGURE 6. Illuminated V-I characteristic calculated with J_{sc} = 36 mA/cm^2.

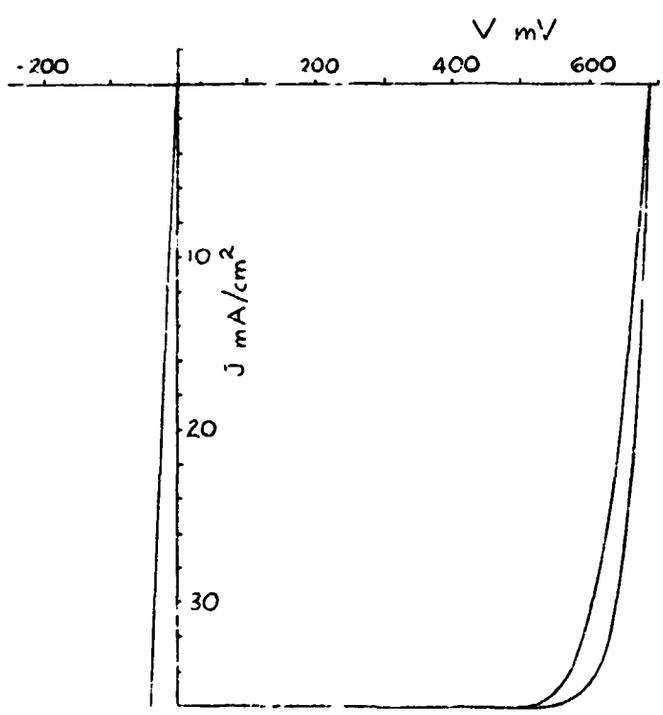

FIGURE 7. Series resistance = 1 Ω for 1 cm^2.

ORIGINAL PAGE IS
OF POOR QUALITY

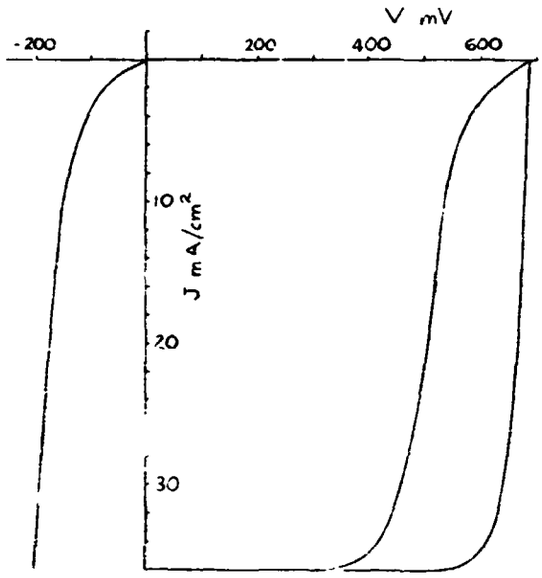

FIGURE 8. Series "forward" diode.

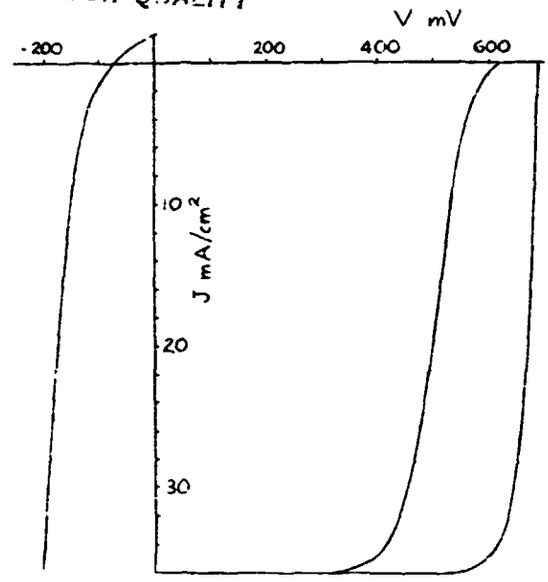

FIGURE 9. Series "forward" diode with photocurrent.

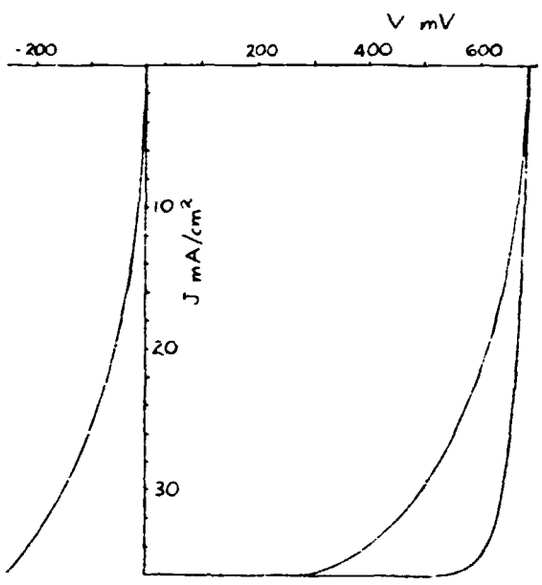

FIGURE 10. Effect of a "reverse" barrier.

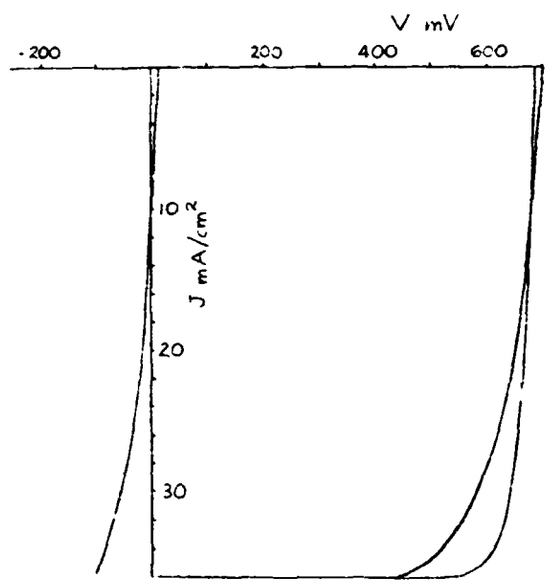

FIGURE 11. Effect of a "reverse" barrier with 10 mA/cm² photocurrent.

C-2

DISCUSSION

CAMPBELL: Your discussion of the gridded back contacts: as I understand it, the requirement for a gridded back-contact system is more stringent than for the front contact in terms of coverage and so forth?

LESK: I didn't mean to imply that it was tighter coverage problem. If you want to measure a system that looks good, you can put full coverage metal in the front or the back, the same metal or the same contact system, and it looks ohmic and you've got no resistance problems. You could still be doing some other things wrong; you could be putting impurities in the silicon, changing the structure, and so on, so you want to look also any photoeffects you might have in the back contact.

CAMPBELL: I have a specific reference. You mentioned 10 lines per centimeter as being optimum for the back grid.

LESK: No, I didn't say optimum. I did the calculation for that; in fact, that was five of each, five on the front and five on the back, and if you do that, and if you have a quarter of a centimeter of material, by going to that geometry where your current is flowing laterally over most of its path, its resistance is still very small.

ILES: Here is a quick one. Do you have any views about the doubling the efficiency by using bifacial cells, talking about back contacts?

LESK: Bifacial cells? Well, there is a lot written on that. I really don't know. If you want to make n-p-n-like structure and pick up the base contact in the middle and pick up two junctions -- is that what you are talking about?

ILES: It seems a pity to spend a lot of time on the back contact and then not use it for generating additional current, in a sense, but it may be rather complicated, perhaps.

LESK: All the schemes I've seen are much more complex because you've got to get the current out somehow, so you are faced perhaps with a double grid structure and a back, one ohmic and one p-n junction, and you've got to match your currents coming out of the top and the bottom, and that isn't the simplest. I have seen some results printed that are pretty good, but to my knowledge nobody has this in production.

BICKLER: Arnie, I want to ask a question about this back surface you described, which would have a diode in the same direction as the main junction. I guess it relates to what Peter just said: where do you get the second cathode?

LESK: Like an n-p-n structure?

BICKLER: Well, if you have the end top cathode and bulk is the anode p what do you do beneath that? You could put another p as a p^+ but what do you do for a cathode for that back layer?

LESK: Well, no, that's it, if you had -- let's say -- high resistivity and put a metal on there, you could form a Schottky barrier between the metal and the bulk. That would be the barrier on the back surface facing in the same direction as the p-n junction. The back-surface field junction tends to be in that direction.

QUESTION: Could you tell us a little more about that good cell you've shown, having V_{oc} of 690 volts?

LESK: A very good cell that's calculated from a lot of the numbers I've seen in the literature; n = 1. It wasn't made; it's calculated, just to show if you had that in terms of the front, how you can ruin it by what you do in the back. These numbers are not far from the numbers you were talking about as state-of-the-art.

High-Efficiency Cell Concepts on Low-Cost Silicon Sheets

R.O. Bell and K.V. Ravi
Mobil Solar Energy Corporation
Waltham, Massachusetts 02254

N85-31621

INTRODUCTION

The strongest leverage for reducing the cost of power generated from solar energy is the efficiency of the solar cell. It is easy to see that given a target cost for electrical energy there is a minimum solar efficiency that must be exceeded even if the module cost becomes negligible. This arises because of the balance of systems cost (land, support structures, power conditioning, wiring, etc.). For example, for competition with an intermediate load coal-fired plant, a module efficiency of above 10% must be maintained [1]. As this minimum efficiency is exceeded, the power costs fall rapidly.

Thus, the drive to produce high efficiency solar cells is very strong. If the technology does not have the potential for realizing this minimum value, then it will be non-competitive for the particular scenario projected.

In this paper we will discuss the limitations on sheet growth material (primarily with reference to EFG) in terms of the defect structure and minority carrier lifetime. Using simple models for material parameters and behavior of solar cells, we will estimate what effect these various defects will have on performance. Given these limitations we can then propose designs for a sheet growth cell that will make the best of the material characteristics.

When discussing solar cells, the material is often characterized in terms of a diffusion length, L_D, whose square is directly proportional to the lifetime, τ, i.e., $L_D^2 = D\tau$, where the constant D is the diffusion coefficient. For a homogeneous material the diffusion length is also a measure of the distance over which minority carriers are collected. For inhomogeneous material where the scale of the lifetime variations may be less than the local diffusion length, the meaning of the diffusion length as a collection distance breaks down.

When techniques such as SPV or spectral response measurements are applied to measure diffusion lengths in inhomogeneous material, it must be kept in mind that the derived quantity, while often referred to as a diffusion length, is really a charge collection distance. It is a complex average depending on how the minority carrier lifetime varies with position. Generally it is clear from the context if we are using diffusion length as a measure of local lifetime or as a charge collection distance.

PRECEDING PAGE BLANK NOT FILMED

I. DEFECTS

The primary defects in silicon that show electrical activity, i.e., contribute to the majority carrier concentration or act as recombination centers, are dislocations, grain boundaries, twins, inclusions including SiC and silicates, point defects of either a substitutional or interstitial character and impurities such as transition metals and oxygen and carbon [2]. There are other closely related defects such as swirls, stacking faults, partial dislocations, etc., but in this paper we will concentrate our remarks on the more general types listed above.

F. Wald has recently presented a comprehensive review of defects in EFG silicon with a discussion of the type and number of defects [2]. Rather than including figures illustrating the defects, we will simply reference his paper.

A. Dislocations

The classic edge dislocation, which can be visualized as being formed by removing an atomic half plane, should exhibit a single line of silicon atoms whose bonding requirements are not satisfied. In a simple minded picture, a dislocation would exhibit a series of dangling bonds, one of which is associated with each plane. If each of these atoms behaved as a recombination center, then for a dislocation density of 10^5 cm^{-2} with a typical cross-section of 10^{-15} cm^{-2}, the lifetime would be of the order of 30 μsec which corresponds to a 300 μm diffusion length in p-type material.

In actual fact most of the broken bonds will be reconstructed [2] so the number of "dangling bonds" will be substantially less, thus giving a much lower potential for recombination.

Another possibility might be that recombination occurs not at dangling bonds but rather at an impurity cloud attracted to the dislocations. If more than one electrically active atom were associated with each atomic lane, then the potential diffusion length could be reduced. We should note, though, that as will be discussed in Section IIB, having the electrically active recombination centers concentrated around the dislocations may actually result in a higher efficiency cell than if the same total number of impurities were uniformly distributed throughout the solid.

B. Grain Boundaries

When two grains with different orientations intersect, they form a grain boundary. First order and higher order twins can be considered a sub-class of grain boundaries. In the general case, grain boundaries can be constructed from a series of edge and screw dislocations. In twins a specific orientation between the grains exists, but for general grain boundaries this is not necessary.

A convenient way to observe the electrical/recombination activity of dislocations and grain boundaries is by the use of EBIC. By making line scans perpendicular to the grain boundaries their recombination properties can be characterized typically in terms of a recombination velocity, v_s, and diffusion length, L_D [3,4]. Optical techniques, LBIC, have also been used in a similar

fashion to obtain the same material characteristics [4]. Velocities up to 10^5 cm/sec have been observed with typical velocities for "strong boundaries" being the order of 10^4 cm/sec. For such a velocity, the effective grain boundary width (L_n = 100 μm, α = 1000 cm^{-1}) is about 5 μm. The concept of an effective grain boundary width is due to Zook, and is defined as the equivalent width of a region from which no charge is collected. If we have a high density of strong boundaries (10^2/cm), the loss in short circuit current can become significant (5%). By no means do all grain boundaries have high recombination, and in fact many are electrically very weak or invisible.

Also of importance is the contribution that grain boundary recombination can make to the reverse saturation current. A reduction of 5% in the current collected corresponds to a decrease in the diffusion length by 35% for a homogeneous distribution of recombination centers. This would reduce the reverse saturation current also by 35% and produce a decrease in open circuit voltage of about 10 mV.

Grain boundary recombination can be important if the density of electrically active boundaries is high. Only in the case of small grain size such as produced by CVD or in silicon with a very high intragranular diffusion length will they dominate performance.

C. Inclusions

The principal effect of inclusions is either to physically block the light or to shunt the junction. Typically, inclusions are found to be SiC or silicates. The contribution an ideal shunting particle makes to reverse leakage depends on its diameter and the sheet resistivity of the surface layer to which the shunting occurs. It is easy to show that for a circular shunt of radius, a, and sheet resistivity, $\rho_\square$, the voltage drop, ΔV, for a distance, d, away from the particle is

$$\Delta V = \frac{\rho_\square I_{sc}}{2} [d^2(\ln(d/a) + 1/2) - a^2/2] \quad (1)$$

For a typical I_{sc} of 30 mA/cm^2, ΔV of 0.25V, $\rho_\square$ of 50 Ω/□, the current not collected (which is equal to $\pi d^2 I_{sc}$) is about 5 mA/particle. In most cases the finite resistivity of the SiC limits the current to less than that predicted by Eq. (1). The SiC density is generally less than one per cm^2, and experimentally it is observed that such shunting is rarely a problem.

In the unfortunate case, though, that the metallization covers the inclusion, the cell will be almost completely shunted since in this case $\rho_\square$ is very small (the order of 5 mΩ/□). Since only about 5% of the solar cell is metallized, this is a rare occurrence.

The fractional volume of a silicate particle is so small and the resistivity is so high that any contribution to losses by light blockage or shunting can probably be safely ignored.

Measurements of the junction characteristics of EFG solar cells often show a contribution to the reverse saturation current that has a temperature

dependence characteristic of tunneling rather than space charge recombination [5]. It has been suggested that this phenomenon could be due to very small precipitates that introduce charge centers into the space charge region. The loss in efficiency shows up as a soft knee and is easily measured using the dark I-V characteristic.

D. Point Defects and Impurities

So far the discussion has dealt with defects that are visible, at least under moderate magnification with an optical microscope or in an SEM. Point defects and impurities in sheet silicon are those that occupy either a single or a few lattice sites and cannot generally be directly imaged. The defects may be native, such as self interstitials or vacancies, metallic, such as Fe, Ti, Mn, etc., or non-metallic, such as carbon and oxygen. Dopants such as B and P are in a sense substitutional defects.

In order for a point defect or impurity to significantly affect the minority carrier lifetime (for the sake of definiteness we will talk about electrons in p-type material), its energy level must be located above the quasi-Fermi level for electrons, but not so near the conduction band edge that any trapped carriers can easily be excited [6]. Shockley-Read-Hall (SRH) theory predicts that the most efficient recombination centers are located at the center of the energy gap.

A large number of elements have been found to produce centers in the band gap of silicon. Their characteristics have been the subject of a number of publications, including those by Weber [7], Sze [8] and Schibli and Milnes [9]. The density of the centers must be high enough such that the probability of trapping a charge is significant. For a 1 μsec lifetime with a reasonable cross-section (10^{-15} cm^{-3}), the trapping center density should be 10^{14} cm^{-3}, which is a very small number in terms of chemical concentration.

Thus, it is natural to expect that inadvertent contamination can drastically reduce the lifetime in silicon. In fact, it is surprising how tolerant EFG is to the level of metallic impurities. Typically impurity levels range from one to 10 ppm and have little correlation with cell performance. There is apparently a major difference between the total impurity content and those that contribute to recombination. Experiments [2,10] show that the introduction of Fe and Mo at concentrations up to 5 x 10^{18} cm^{-3} can be tolerated.

Besides the metallic impurities, other species such as carbon and oxygen are present in large quantities. The carbon comes from the crucible (if graphite) and die material, and the oxygen from the crucible (if fused quartz) and gaseous ambient. Individual carbon atoms in a silicon lattice are not electrically active but probably express their activity because of interactions with other defects. Oxygen when interstitial is not electrically active, but under various heat treatments forms complexes that act as donors or recombination centers.

Oxygen has been shown to play an important role in producing EFG silicon with the longest diffusion length [11]. The oxygen can be introduced either from the ambient or from the crucible. The diffusion length for oxygenated EFG

silicon is not only higher than in EFG without additional oxygen at low light levels, but also it shows a stronger dependence on illumination level.

In non-degenerate silicon, including CZ, float zone, EFG, etc., the lifetime is dominated by an SRH recombination process. This lifetime is generally found to decrease rapidly with doping density. Fuller [12] and Fossum et al. [13,14] have modeled the defect density as if it were a chemical reaction driven by the doping density. The lifetime, τ, can be approximated to depend on the doping level, N_D, as

$$\tau = \tau_o/(1 + N_D/N_o) \qquad (2)$$

where τ_o is a constant that is a function of material quality. This is the expression used by Rohatgi and Rai-Choudhury [15] when modeling high efficiency solar cells. For N_o they use 7×10^{15} cm^{-3}.

In one EFG experiment in which the boron concentration was varied to give resistivities between 0.2 and 10 Ω·cm, the data can be approximately fit with τ_o having a value of 0.7 μsec [2,16]. By contrast the Auger recombination, even in high quality material, does not dominate until the resistivity is below 0.1 Ω·cm. Other EFG material has been grown with a diffusion length of over 150 μm at 4 Ω·cm which would imply a value of τ_o of 10 μsec.

II. SOLAR CELL PERFORMANCE

A good deal of work has been devoted to modeling the behavior of solar cells but mostly on homogeneous material (both with respect to depth and areal distribution). With ribbon material this is not necessarily a good assumption and at times the effect of inhomogeneous distributions of minority recombination centers, crystalline defects and majority carrier doping cannot be neglected.

In this section we model the behavior of an EFG solar cell to determine how to get the most out of it. An outline of the technique is given in the Appendix. It is similar to the approach suggested by Wolf [17] and can include surface recombination, doping dependent lifetimes including Auger and SRH, and band gap narrowing. Calculations based on the solution of the diffusion equation, including electric fields produced by doping gradients, give similar results when applied to the same cases modeled here.

In the first part of this section we calculate the charge generation and collection distributions produced by the solar spectrum. Next we discuss some aspects of inhomogeneous distributions of lifetime and effect on solar cells. Finally, the effect of resistivity and surface passivation is considered.

Of course, as when attempting to extract the highest possible efficiency from any cell, it is important that the metal coverage be as little as possible consistent with a low series resistance and that any anti-reflection coating be optimized whether one or two layers. Because sheet growth materials, except for web, generally do not have a predetermined orientation, surface etching to produce faceting is not an option, although growth using a corrugated die to produce an equivalent effect may be possible.

A. Charge Generation Rate

Figure 1 shows a plot of the charge generation rate for an AM1.5 [18] spectrum in silicon [19]. By far the highest generation rate is close to the surface. If we integrate this curve and normalize it relative to the total possible hole electron pairs produced (Fig. 2), we see that 50% of the possible charge is generated within 5 μm of the surface and 90% within 150 μm.

There is quite a long tail on the optical absorption so even though most charge is generated relatively near the surface, if we want to collect almost all minority carriers (95 to 99%) a very long diffusion length (the order of 1000 μm) would be required.

B. Areal Inhomogeneities

Calculations have been made of the effect of areal lifetime inhomogeneities on solar cells. In general the regions with a low lifetime dominate the performance, both by the effect on short circuit current and open circuit voltage [20]. Although this result might, at first reading, seem to indicate that a homogeneous material is best, it can be shown through simple arguments that when the total number of recombination centers is held fixed, an inhomogeneous distribution can produce a cell with a higher efficiency than one in which the centers are uniformly distributed [21]. Thus, what at first glance might be considered a disadvantage of sheet grown silicon can really be an advantage. Assuming that the behavior of recombination centers is independent of concentration, if the recombination centers are concentrated in a few small regions, then the performance may be improved.

Figure 3 shows a plot of the relative efficiency as a function of the amount of poor area. Depending upon the ratio of the number of recombination centers in the poor area to the good area, the maximum efficiency occurs when the poor area occupies between 10 and 30% of the total cell area. Obviously it is better if the total number of impurities or recombination centers can be minimized, but if they are present it is desirable that they be segregated rather than uniformly distributed.

C. Optimum Resistivity

High efficiency solar cells have been made using either moderate resistivity silicon with a long lifetime or low resistivity with a moderate lifetime material. Recently, Green [22] has analyzed the effect of Auger recombination on the open circuit voltage and efficiency and concludes that for heavily and lightly doped material, Auger recombination places the most stringent limitation on solar cell performance. He estimates a maximum open circuit voltage of about 720 mV for "thick" cells. As we have seen in Section IID, the observed practical lifetime limit of the base is not Auger but is probably related to a defect/dopant interaction.

Figure 4 shows a plot of the calculated efficiency assuming that the lifetime is given by Eq. (2) with τ_o of 1 and 10 μsec. The parameters of the n^+ region have been adjusted so that they do not contribute to losses of the solar cell. Clearly a 15% efficient solar cell can be made for the larger value of τ_o but not for the lower value.

D. Surface Passivation

In the analysis made above, it was assumed that the the surface was well passivated, i.e., recombination was negligible. Much recent work demonstrates the importance of the correct treatment of the n^+ region if the maximum is to be obtained from solar cells [15,23,24]. With a base lifetime of 10 μsec, the effective recombination velocity, $v_s = D/L$, must be less than about 2×10^3 cm/sec. To be base limited requires that the contribution from the emitter, including surface and material recombination, must be less than this.

Techniques have been developed for passivating both float zone and CZ [15,24]. There is no reason to believe that they cannot be applied to sheet grown materials. At the doping levels used in the n^+ layer, Auger limitations on the lifetime should be dominant even in relatively low quality material. Auger recombination varies like the square of the doping density, whereas defect/doping recombination varies directly with doping density. This means that at high enough doping the ultimate limitation will be Auger. The inherent built-in electric fields produced during any diffusion process, especially for shallow junctions, will minimize emitter recombination.

III. SUMMARY

The optimum EFG cell will have the highest doping consistent with the defect/doping limit on lifetime. It probably will be below 1 Ω·cm. The junction depth will be shallow with a sheet resistivity of at least 100 Ω/□. Green et al. [23] have shown that the sheet resistivity needs to be above 100 Ω/□ if the recombination is to be dominated by the surface rather than the bulk properties of the n^+ region.

The thickness of the base will probably be determined by the ability to handle thin sheets rather than the requirement for any back surface field. With modest diffusion lengths, the gain in efficiency with back surface fields is not important until the substrates are so thin that practical handling problems rule out their use. For example, the peak efficiency for a 100 μm diffusion length BSF cell, peaks at a sample thickness of about 60 μm, but it is only about 8% better than a thick (> 300 μm) solar cell.

Another critical aspect is to control the lifetime of the finished cell. Post fabrication techniques have been developed, such as hydrogen passivation, to improve material quality after fabrication [25]. This works well even though only a relatively thin region is affected because the open circuit voltage and fill factor are controlled to a large extent by the material properties very close to the surface.

IV. CONCLUSION

The achievement of high cell efficiencies in sheet silicon, grown at high rates and prone to contain significant densities of imperfections and impurities, requires developments in both crystal growth technology and cell processing approaches. Variations in crystal growth of importance include control over defect structure and impurity content. Key developments include the following:

(a) Control over impurity content in crystal growth from the melt is needed to decrease the number of lifetime reducing impurities. In the case of EFG, this includes appropriate purification of elements of the crystal growth machine.

(b) Control over defect structure and density is needed to minimize defect-impurity interactions. Areas of interest here include reduction in plastic deformation as a consequence of post-growth heat treatment and the minimization of residual stress. In this context, it is preferable to increase the area rate of production by the growth of wide crystals grown at moderate linear growth rates than by increasing linear growth rates, since defect generation by plastic deformation in response to thermo-elastic and thermo-plastic stresses appears to be a stronger function of linear growth rates than of the crystal width.

(c) The influence and role of carbon in silicon continues to be an unknown quantity. A better understanding of the influence of carbon (and oxygen) on electrical phenomena in silicon is needed.

Device processing implications are many. The key ones have been touched upon in this paper. The fundamental issue is one of achieving the optimum synergy between base material quality and device processing variables. At the current stage of development of low-cost silicon sheet technologies, a strong coupling between material quality, and thus the variables during crystal growth, and device processing variables exists. The challenges are twofold: (1) the optimization of this coupling for maximum performance at minimal cost, and (2) a decoupling of materials from processing by continual improvement in base material quality to make it less sensitive to processing variables.

Appendix - Solar Cell Efficiency Calculation

A number of different schemes to model solar cells have been developed over the years since Prince [26] showed how cell efficiency varied with band gap. Probably the most accurate and mathematically rigorous is that by Hauser and co-workers [27,28]. They solve the fundamental device equations but the procedure is complicated and requires large amounts of computer time. Other first order models such as the use of a shifted diode curve, a typical example being Wysocki and Rappaport [29], do not generally allow for inclusion of effects such as electric fields, heavy doping and back surface fields.

Recently though, Wolf [17,30] has suggested a technique which relies on the simplicity of the diode model but allows inclusion of heavy doping effects by the concept of a so-called transport velocity. This idea was introduced by Gunn [31] for the study of carrier accumulation associated with semiconductor junctions. Bowler and Wolf [17] have used the technique to make estimates of the ultimate efficiency of solar cells and how they depend on various geometrical and material parameters.

We have adapted their procedure to examine what might be expected for EFG material. The transport velocity concept was combined with models of charge generation and collection to look at the solar cell output parameters.

Theory

As shown by Gunn [31], for p-type material the diode current at any position, j(x), can be expressed by

$$j(x) = qn(x)u(x) \tag{A1}$$

where n(x) is the minority carrier density, u(x) is the transport velocity, and q is the electronic charge.

If the diffusion coefficient, D, and minority carrier diffusion length, L, are constant over a region between x and x', u(x) transforms such that

$$u(x) = \frac{D}{L}\left[\frac{\frac{u(x')L}{D} + \tanh\frac{x - x'}{L}}{1 + \frac{u(x')L}{D}\tanh\frac{x - x'}{L}}\right] \tag{A2}$$

Thus, if we know the value of u at some position x', then with Eq. (A2) we can calculate it at x. If the various parameters are not constant, then the region can be divided up into steps such that the variation is small over any given region and repeated applications of Eq. (A2) can be use. Note that as (x - x') becomes large compared to L, u(x) goes to D/L.

The transformation for a high/low junction (a change in carrier concentration such as at a p/p^+ or n/n^+ junction) is

$$u(x^+) = \frac{p^+}{p^-} u(x^-) \tag{A3}$$

At the junction, $n(x_j)$ is determined by the barrier height, V, such that

$$n(x_j) = \frac{n_i^2}{p} [\exp(qV/kT) - 1] \tag{A4}$$

where n_i is the intrinsic carrier concentration.

Combining Eqs. (A1) and (A4) at the junction and using the light generated current, j_{sc}, to offset the diode equation, we obtain

$$j = j_o [\exp(qV/kT) - 1] + j_{sc} \tag{A5a}$$

$$j_o = q \frac{n_i^2}{p} u(x_j) \tag{A5b}$$

A similar treatment will give the contribution from the n region. Also, to account for recombination in the space charge region, a term of the form $j_o'[\exp(qV/2kT) - 1]$, where $j_o' = qn_iW/\tau$ is added to Eq. (A5a). W is the width of the space charge region and $\tau = L^2/D$ is the lifetime.

Thus, to model a solar cell, we divide it up into regions where the properties are uniform. Starting with a value for the surface recombination velocity, S, where $u(x) = S$, we apply either Eq. (A2) or (A3) repeatedly until we have arrived at the junction with a value of $u(x_j)$. We next calculate j_{sc} with an expression of the form

$$j_{sc} = q \int_0^{\lambda_{min}} (1 - R(\lambda))\, \phi(\lambda)\, Q(\lambda)\, d\lambda \tag{A6}$$

where $\phi(\lambda)$ is the flux for the desired spectrum (here we have used AM1.5 [11] normalized to 100 mW/cm²), $Q(\lambda)$ is the charge collection discussed below and $R(\lambda)$ is the reflectivity at the front surface. The contributions from the space charge region and the surface n^+ layer also are added to j_{sc}.

The solar cell is now characterized by Eq. (A5) where j_o, j_o' and j_{sc} depend on material and geometrical parameters. Because of surface coverage by the metal grid and optical losses in the AR coating, $R(\lambda)$ is not zero. For simplicity, in the calculation $R(\lambda) = 0.15$ was used for all wavelengths. The peak power, P_m, is given by $d(jV)dV = 0$ and the open circuit voltage by $j(V_{oc}) = 0$, both of which expressions were evaluated numerically. The fill factor, FF, is

$$FF = P_m/V_{oc}\, j_{sc} \tag{A7}$$

A couple of other items must also be included. At high carrier concentrations, Auger and defect/doping recombination becomes important and their effect on lifetime is included. D also depends on carrier concentration. Through band gap narrowing, n_i varies at high doping levels. Appropriate models for these dependencies were used.

Calculation of $Q(\lambda)$

The basic equations governing the flow of minority carriers in a semiconductor are the current equation and charge continuity equation [19], which in one dimension are

$$j_n = q\,\mu n E + q\,D\,\frac{\partial n}{\partial x} \tag{A8}$$

$$\frac{\partial n}{\partial t} = U + G + \frac{1}{q}\frac{\partial j_n}{\partial x} \tag{A9}$$

U is the net recombination rate and normally is set equal to n/τ. At equilibrium where $\partial n/\partial t = 0$ and with no electric field, i.e., $E = 0$. by substituting Eq. (A8) into (A9) we obtain the diffusion equation

$$qD\,\frac{d^2n}{dx^2} - \frac{n}{\tau} + G = 0 \tag{A10}$$

G is the optical generation term. For the geometry shown in Fig A1. where light can reflect off the back surface, G will be

$$G = \alpha[\exp(-\alpha x) + R\,\exp(\alpha(x - 2d))] \tag{A11}$$

where R is the reflectivity of the back surface.

We use the general boundary conditions that the carrier concentration is zero at the front junction and that the current, including surface recombination, is continuous at $x = d$

$$n = 0 \quad \text{at} \quad x = 0 \tag{A12a}$$

$$q\,D\,\frac{dn}{dx} = Snq - J_o \qquad x = d \tag{A12b}$$

J_o is the current produced in the region outside d. The current, J_p, is determined by

$$J_p = q\,D\,\frac{dn}{dx} \quad \text{at} \quad x = 0 \tag{A13}$$

The solution requires some algebraic manipulation and is as follows.

$$J_p = \frac{qaL}{1 - (aL)^2} [K_- + K_+ R\, e^{-2ad}]$$

$$+ J_o/[\cosh(t/L) + \frac{SL}{D} \sinh(t/L)] \tag{A14}$$

where $K_\pm = [(D/L \pm aLS) + (S \pm aD)\mathrm{ctnh}(t/L)$

$$- \exp(\pm at)\ (S \pm aD)/\sinh(t/L)] \tag{A15}$$

$$/[D/L\ \mathrm{ctnh}(t/L) + S]$$

For the n^+ layer, a similar expression, J_n, is obtained. It is essentially Eqs. (A14) and (A15) with t replaced by $-t'$ where t' is the thickness of the n^+ region.

After multiplying by a factor that accounts for the optical absorption in the n^+ layer, the charge collection, $Q(\lambda)$ used in Eq. (A6) is just

$$Q(\lambda) = (J_p + J_n)/q \tag{A16}$$

Typical results are shown in Fig A2 where the efficiency is plotted as a function of thickness of the base thickness for various resistivities, diffusion lengths and back surface conditions.

REFERENCES

1. Five Year Research Plan, 1984-1988, Photovoltaics: Electricity from Sunlight, DOE/CE-0072, U.S. Department of Energy, May 1983.

2. F. Wald, Presented at the European Materials Research Society and to be published in J. Phys. Applique.

3. J.D. Zook, Appl. Phys. Letters, 37, 223 (1980).

4. C. Donolato, J. Appl. Phys., 54, 1314 (1983).

5. G.F.J. Garlick and A.H. Kachare, Appl. Phys. Letters, 36, 911 (1980).

6. J.I. Hanoka, R.O. Bell and B.R. Bathey, Proc. of Sym. on Electronic and Optical Properties of Polycrystalline or Impure Semiconductors and Novel Growth Methods, (Ed. by K.V. Ravi and B. O'Mara) p. 76, (The Electrochem. Soc. Pennington, N.J., 1980).

7. E.R. Weber, Appl. Phys. A20, 1 (1983).

8. S.M. Sze, "Physics of Semiconductor Devices", (Wiley-Interscience, New York, 1969), p. 30.

9. E. Schibli and A.G. Milnes, Mater. Science Engr., 2, 173 (1967).

10. Private communication, M.C. Cretella and B. Bathey.

11. B. Mackintosh, J.P. Kalejs, C.T. Ho and F. V. Wald, Proceedings of the Third CEC Photovoltaic Solar Energy Conf., Ed. W. Palz (Dordrecht, D. Reidel, 1980).

12. C.S. Fuller, "Defect Interactions in Semiconductors", Semiconductors, (Edited by N.B. Hannay), Academic Press, New York (1975).

13. J.G. Fossum and D.S. Lee, Solid State Electron., 25, 741 (1982).

14. J.G. Fossum, R.P. Mertens, D.S. Lee and J.F. Nijs, Solid State Electron. 26, 569 (1983).

15. A. Rhohatgi and P. Rai-Choudhury, IEEE Trans. Electron Dev., ED-31, 596 (1984).

16. Private communication M.C. Cretella.

17. D.L. Bowler and M. Wolf, IEEE Trans. Components, Hybrids and Manufacturing Tech., CHMT-3, 464 (1980).

18. ASTM Standard E-891, "Terrestrial Direct Normal Solar Spectral Irradiance for Air Mass 1.5".

19. D.E. Aspnes and A.A. Stunda, Phys. Rev. B, 27, 985 (1983).

20. F.A. Lindholm, J.A. Mazer, J.E. Dacis and J.I. Arreola, Solid State Electron., 23, 967 (1980).

21. R.O. Bell, Solid State Electron., 25, 175 (1982).

22. M.A. Green, IEEE Trans Electron. Dev., ED-31, 671 (1984).

23. M.A. Green, A.W. Blakers, J. Shi, E.M. Keller and S.R. Wenham, IEEE Trans. Electron. Dev., ED-31, 679 (1984).

24. M.B. Spitzer, S.P. Tobin and C.J. Keavney, IEEE Trans. Electron. Dev., ED-31, 546 (1984)

25. J.I. Hanoka, C.H. Seager, D.J. Sharp and J.K.G. Panitz, Appl. Phys. Letters, 42, 618 (1983).

26. M. Prince, J. Appl. Phys., 26, 534 (1955).

27. P.M. Dunbar and J.R. Hauser, A Theoretical Analysis of the Current-Voltage Characteristic of Solar Cells, Semiconductor Device Laboratory, North Carolina State University, Raleigh, NC, NASA Grant NGR 34-002-195, August 1975 and August 1976.

28. R.C. Y. Fang and J.R. Hauser, ibid., September 1977 and January 1979.

29. J.J. Wysocki and P. Rappaport, J. Appl. Phys., 31, 571 (1960).

30. M. Wolf, IEEE Trans. Electron Devices, ED-27, 751 (1980).

31. J.B. Gunn, J. Electron. Contr., 4, 17 (1958).

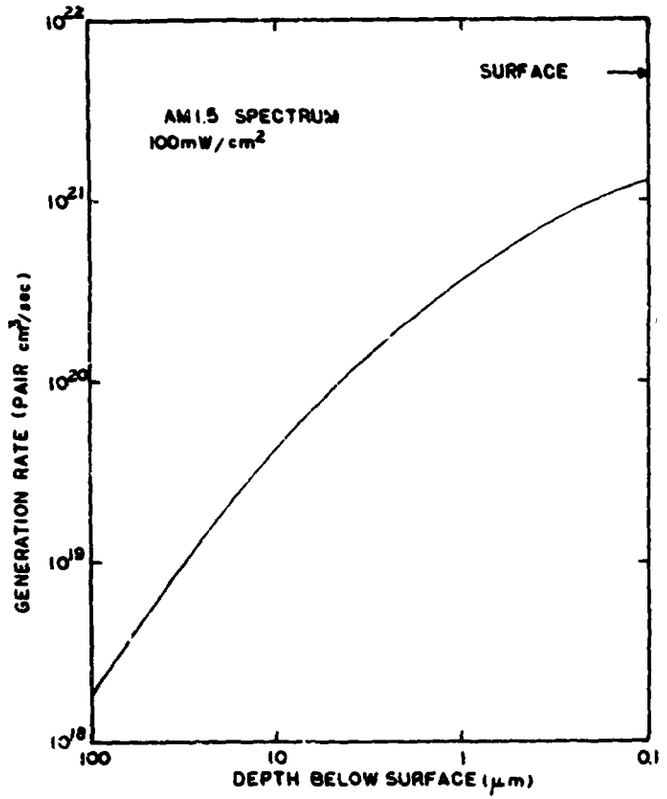

Fig. 1. Charge generation rate as a function of depth below the surface of the standard AM1.5 spectrum.

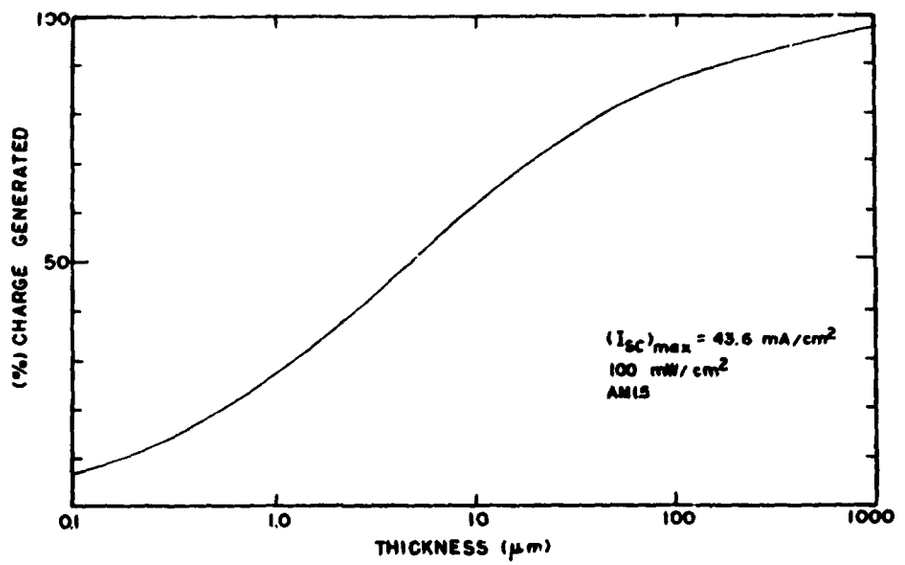

Fig. 2. Relative number of hole-electron pairs generated between the surface and depth t. The curve is normalized with respect to the number of photons being absorbed in a thick piece of silicon.

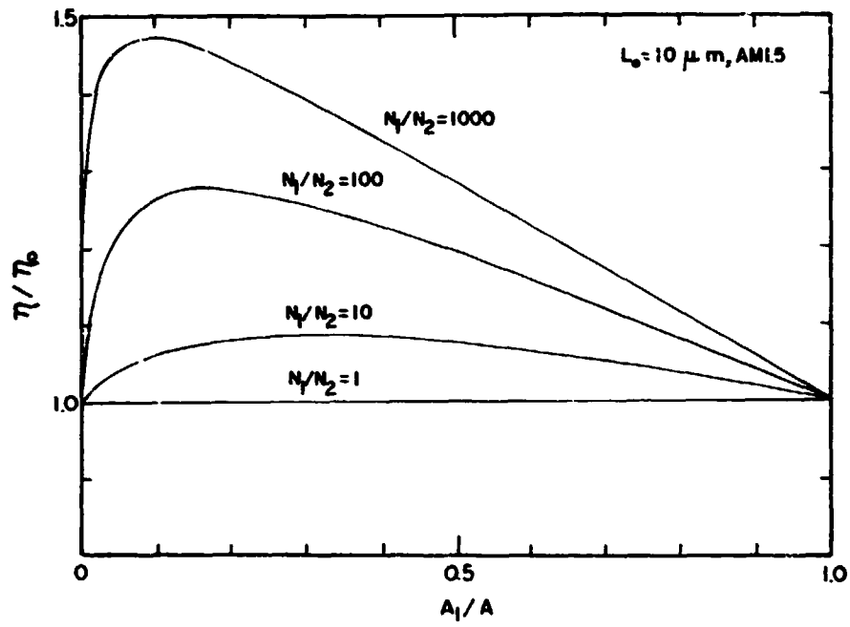

Fig. 3. Normalized solar cell efficiency as a function of poor area for different relative numbers of recombination centers.

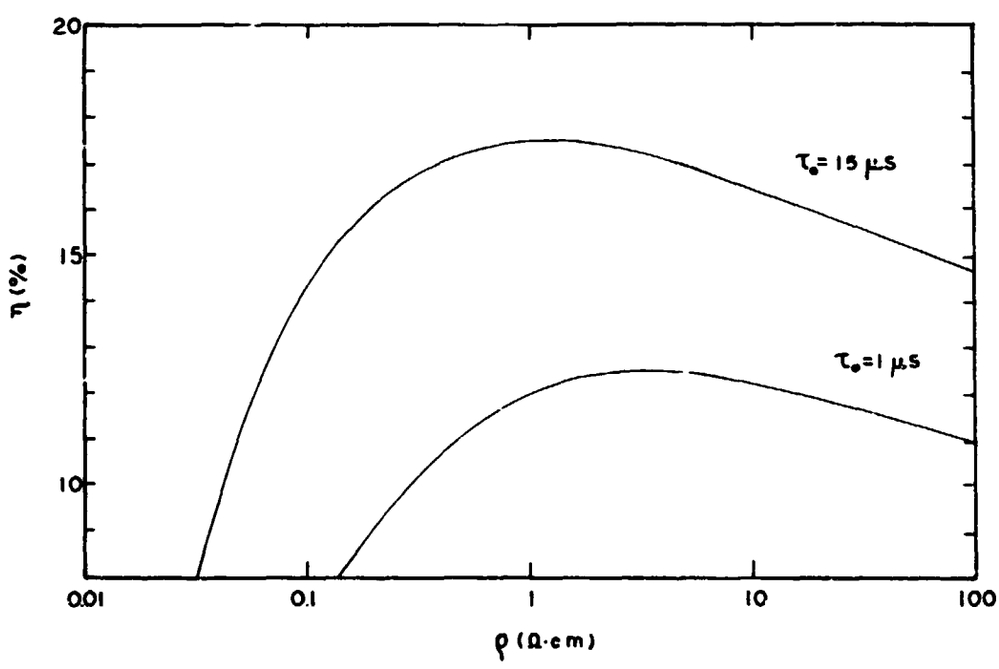

Fig. 4. Efficiency of a solar cell as a function of resistivity whose minority carrier lifetime varies as given by Eq. (2) in the text.

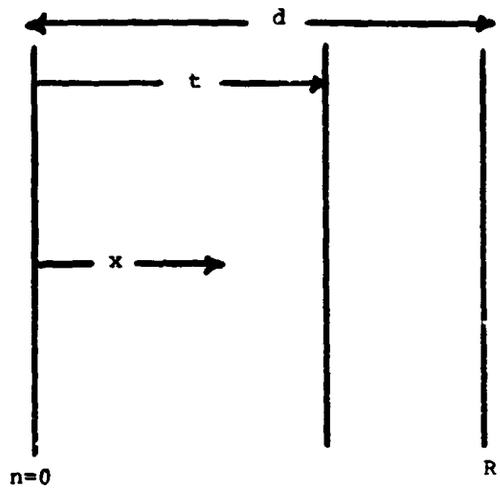

Fig. A1. Geometry used to calculate solar cell performance. The photons are incident on the left-hand side.

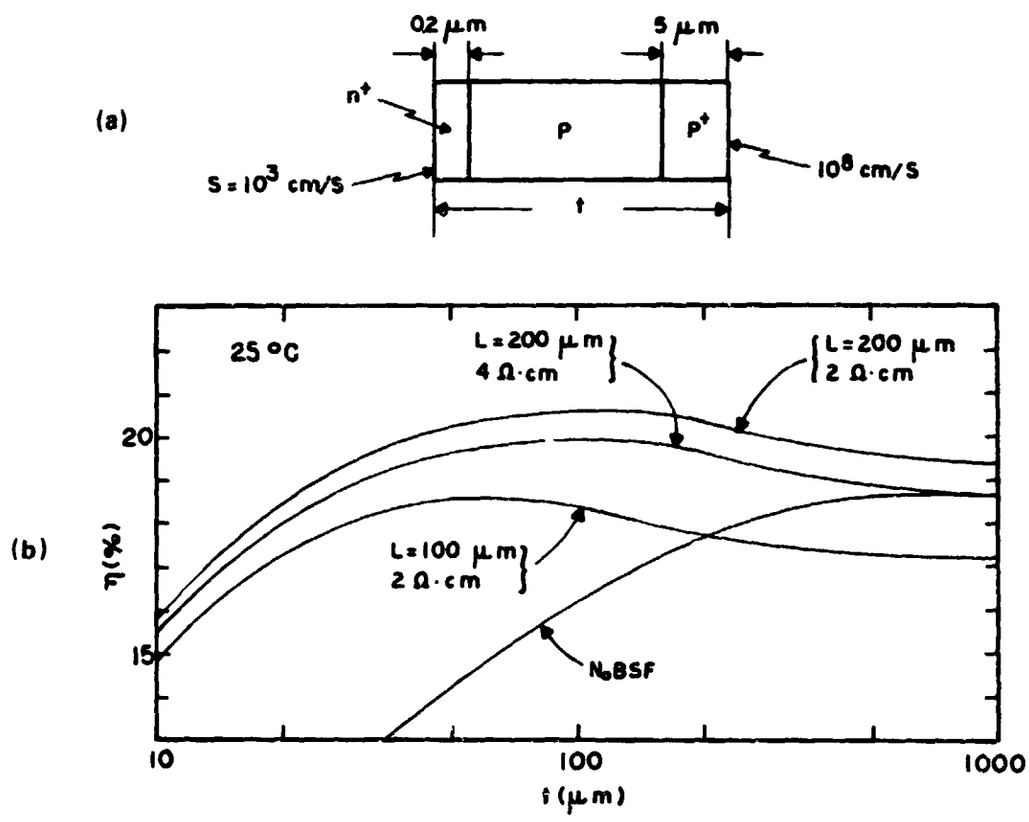

Fig. A2. (a) Physical dimensions and electrical parameters used in calculating solar cell performance. (b) Calculated efficiency of solar cell as a function of total sample thickness for various diffusion lengths and resistivities. The curve labeled N_0 BSF is the result with no back surface field being present.

DISCUSSION

DYER: Is there still a preferred orientation of the grain structure in these sheet structures, and is that [110], the surface of it?

BELL: The surface tends to be OK, the orientation is a {211}. Correction: it tends to be.

DYER: What about the surface?

BELL: I believe it is close to [110], we call it an equilibrium structure. As you grow, no matter what orientation you start with, you are growing to a certain distance. It essentially tends to become {211}.

DYER: How close is that to <110>? Is it plus or minus 10 degrees, five degrees---?

BELL: Ten or 20 degrees is the type of thing that one sees.

QUESTION: You mentioned the possibility of silicon carbide particles shunting the junction. Have you run into a situation where a grid line hits a particle?

BELL: Yes, I should mention that in the unfortunate event that a grid line hits a particle, the cell is shorted. Luckily, if you only have 5% good coverage and something less than 1 per cube per cm^2, the probability is fairly low.

QUESTION: As you go to larger cells the probability of that will increase.

BELL: That's right, but even when we are talking about 50 cm^2 cells it is well under 0.1%, I really don't know what the statistics are but it is quite low.

LESK: Ast has written several reports in which he uses a 1200°C anneal on EFG materials, passivates the grain boundaries at this location. The results in his reports are quite striking. You haven't mentioned that hydrogen passivation. I wonder if you might comment on which one works best.

BELL: We find, certainly, that the heat treatments that one gives to the material can have fairly dramatic effects on its behavior. We have found that if one goes to a high temperature, like to 1200°, for a fairly short period of time - 10 minutes to a half an hour, something like that -- often one finds an improved performance. The problem is, we are deslingwith a fairly complicated situation; material grown from a quartz crucible and material grown from a carbon crucible often have somewhat different behavior. Although people from Mobil and others have had a lot of theories and ideas on what is going on, in my mind there is no clear picture. There is a lot of interaction going on.

QUESTION: I would like to ask a question about hydrogen passivation. Are

these passivating the grain boundaries, mainly, or also impurities and defects? How do you apply it in the high-temperature form, atomic form or cosmic form?

BELL: I really wish I had another slide to show the grain. Jack Hanoka is going to discuss the work that we have done with hydrogen passivation; I'll just say that it does passivate the grain boundaries and other parameters, but we will let Jack talk about the details.

HIGH LIFETIME SOLAR CELL PROCESSING AND DESIGN

R. M. Swanson
Stanford University
Stanford, California

N85-31622

Introduction

In order to maximize efficiency a solar cell must, a) absorb as much light as possible in electron-hole production, b) transport as large a fraction as possible of the electrons to the n-type terminal and holes to the p-type terminal without their first recombining, and c) produce as high as possible terminal voltage. Step a) is largely fixed by the spectrum of sunlight and the fundamental absorption characteristics of silicon, although some improvements are possible through texturizing induced light trapping and back-surface reflectors. Steps b) and c) are, however, dependent on the recombination mechanisms of the cell. The recombination, on the contrary, is strongly influenced by cell processing and design. This paper presents some of the lessons learned during the development of the EPRI point-contact-cell (1).

Cell Dependence on Recombination

A useful way to visualize solar cell operation is through the following pair of equations:

$$I = I_{ph} - I_{rec} \tag{1}$$

$$V = (kT/q)\ln(pn/n_i^2) - V_{res} \tag{2}$$

The first equation is easily derived by integrating the continuity equation (1, p. A-1) and says that the terminal current, I, equals the photo-current of electron-hole pairs, I_{ph}, minus the recombination current, I_{rec}. In this case the recombination current must be defined as follows

$$I_{rec} = I_{bulk} + I_{surface} + I_{p,n\ cont} + I_{n,p\ cont} \tag{3}$$

The nature of each term in (3) will be described briefly here and then in more detail in the next section.

I_{bulk} is the bulk recombination throughout the entire volume of silicon. In otherwords, if the steady-state electron-hole volume recombination rate is R, then I_{bulk} is the volume integral of R throughout the entire device.

$I_{surface}$ is the recombination occuring at the surface in regions with no metal contact.

$I_{p,\ n\ cont}$ is the current of holes flowing into the n-type metal contact (ie. the minority carrier recombination current) and $I_{n,\ p\ cont}$ that of electrons flowing into the p-type metal contact.

To a first approximation the terminal voltage is simply related to the pn product through equation (2) which, in effect, assumes constant quasi-Fermi levels throughout the device. Even though the actual pn product varies with position in a real device, this equation reveals the essential element in device design because, along with voltage, all the recombination mechanisms increase with pn product. Thus the maximum power point occurs at that pn product which balances recombination loss with voltage gain. Improving efficiency comes down to reducing recombination as much as possible.

The last term in equation (2) is the resistive loss in the cell. In devices which rely on conductivity modulation to obtain low base region resisitive loss it is additionally important to maintain a high pn

PRECEDING PAGE BLANK NOT FILMED

product to provide as much conductivity modulation as possible. Thus these devices are particularly sensitve to recombinataion.

Reducing Recombination

bulk recombination

Typically bulk recombination is a combination of devect related recombination (which is usually modeled by a Shockley-Read-Hall (SRH) type formula, without any real experimental justification), Auger recombination, and radiative recombination. In this case one has

$$R = v_{th} N_T \frac{pn - n_i^2}{\frac{1}{\sigma_p}\left[n + n_i exp\left(\frac{E_T - E_i}{kT}\right)\right] + \frac{1}{\sigma_n}\left[p + n_i exp\left(-\frac{E_T - E_i}{kT}\right)\right]}$$

$$+ B(pn - n_i^2) + C_n(n^2p - n_o^2p_o) + C_p(p^2n - p_o^2n_o) \quad (4)$$

where

$B = 2 \times 10^{-15}$ cm^3/sec	(radiative recombination)
$C_n = 3 \times 10^{-31}$ cm^6/sec	(eeh Auger coefficient)
$C_p = 1 \times 10^{-31}$ cm^6/sec	(ehh Auger coefficient)

The radiative term is usually negligible, except when discussing fundamental limits where the remaining recombination terms have arbitrarily been set to zero. The magnitudes of C_n and C_p are somewhat in dispute but are undoubtedly within an orger of magnitude of those shown in equation (4) which are from (2). The designer can control Auger recombination only by varying the doping density as a function of position in the device.

The defect related (SRH) term is strongly dependent on the nature and concemtration of process induced defects and contaminants. Typically a material will have both donor and acceptor type deep level defects. Under low level injection acceptors will usually dominate the recombination process in n-type material and vise-versa in p-type material. This is because hole capture in n-type material would be the rate limiting process and hole capture is an attractive process for acceptors. Under high level injection the SRH recombination lifetime becomes $\tau = 1/N_t v_{th}(1/\sigma_n + 1/\sigma_p)$. Since one of the capture processes (electron or hole) must be attractive and the other neutral one would expect that under high level injetion the lifetime would be considerably greater as the neutral capture becomes rate limiting for both acceptors and donors. We have found that high level bulk lifetimes over 1000 μs can be obtained in completed devices when high resisitivity float-zone silicon is used as the starting material. The low-level lifetime is typically a factor of 3 to 10 less. Careful processing is required to routinely obtain high lifetime. We have found the following procedures sufficient (but not necessarily necessary) to this end

a) Never use metal tweezers to handle wafers.

b) Always perform a RCA (3) clean prior to high temperature steps.

c) Process in a class 100 clean area.

d) Perodically clean furnace tubes with HCl.

surface recombination

Surface recombination appears to be more a function of the preparation procedure for forming the passivating oxide layer, rather than being highly sensitive to contamination as is bulk recombination. Those procedures that have been found to produce high quality $Si\text{-}SiO_2$ interfaces for MOS transistors appear to minimize the surface recombination velocity.

Dry thermal oxidation followed by a low temperature hydrogenation produces surfaces with a mid-gap interface state density of around 1×10^{10} /cm^{2}eV. Figures 1 and 2 show the measured interface state density for such an oxide in the upper and lower portions of the bandgap, respectively. These measurements, done using DLTS, show no evidence of the so called U shaped continuum but rather a monotonic decrease from conduction to valence band.

By performing an inert atmosphere anneal after oxidation the density of interface states can be reduced to about 1×10^{9} /cm^{2}eV. Such a surface has a measured high level interface recombination velocity of 2 to 5 cm/sec. This rather low value can be understood by referring to figures 3 and 4 which show the measured electron and hole capture cross-sections (4). One finds that the electron capture cross section is generally orders of magnitude larger than that for holes. Under high level conditions most of the recombination will occur for those states where σ_n and σ_p are approximately equal. This occurs at about 0.2 eV below mid-gap where they are in the mid 10^{-16}/cm^{2}eV range. At higher energies σ_p becomes smaller and limits the recombination rate, and similarly for σ_n. Using the data of figures 1 through 4 to calculate the recombination velocity using SRH theory yields 2 cm/sec, in agreement with mesurements. (This calculation assumes that the interface charge is small enough to produce negligible band bending.)

The data of figures 3 and 4 indicate the surprising result that p-type surfaces should have a much larger recombination velocity than n-type because of the large differences in cross sections. We are currently investigating whether this is proves to be the case.

Further work is needed to develop methods which produce MOS quality interfaces on very thin oxides suitable for use under anti-reflection layers.

contact recombination

Keeping carriers from the contact metal proves to be a most challanging problem of the cell design. The traditional approach is to create potential barriers by doping which are sufficiently wide to support a significant diffusion potential (ie., the gradient in pn product across the barrier does not cause too much minority carrier current).

Because of the well known confluence of heavy doping effects such as reduced bandgap and lifetime such barriers are not as effective as one might want. Never-the-less, it can be shown (1, p. A8) the recombination current in the barrier and contact can always be writen, so long as the doped barrier is not high level injected,

$$I_{rec} = I_0(pn/n_i^2 - 1) \qquad (5)$$

where the pn product is evaluated in the space charge region at the edge of the barrier. I_0 will be called the barrier saturation current in analogy with the terminology of ideal diode theory. Indeed, if the separation of quasi Fermi levels at the space charge region equals the applied terminal voltage then equation (5) gives the typical

$$I_{rec} = I_0(\exp(qV/kT) - 1) \tag{6}$$

Calculated saturation currents appear in figures 5 and 6 for Gaussian n-type doping profiles (6). Notice that in regions which have a high recombination velocity such as under metal contacts, deep diffusions with surface concentration around 10^{20} cm_{-3} produce the best results. If such diffusions are used to keep carriers away from surfaces Our experwith low recombination velocity, then shallow diffusions with surface concentration around 10^{19} cm^{-3} give the best results. Our experience, however, is that in this case no diffusion at all is the best choice, provided the surface is well passivated. Of course, in a conventional cell the surface diffusion has the additional role of transporting majority carriers to the contacts and cannot be simply eliminated. In cells with high lifetime and hence long diffusion length, it is possible to rely on diffusion of carriers to the contact regions and dispense with the surface diffusion except under the contacts. This is the approach of the point-contact-cell (1).

It is interesting to compare the relative magnitudes of the various sources of recombination. Assuming that, a), we have a 100 μm thick undoped base with a high level lifetime of 1000 μs, b) the surface recombination velocity is 2 cm/sec, and c) the n and p barrier saturation currents are both 3 X 10^{-13} A/cm^2 the methods of the preceeding sections can be used to calculate the recombination currents.

When the pn product is $(10^{17}$ $cm_3)^2$, as might occur in a concentrator cell, one calculates the following:

	J_{rec} A/cm^2
bulk, SRH	0.160
bulk, radiative	0.032
bulk, Auger	0.160
surface	0.064
diffused regions	28.5

These results show the overwhelming influence of contact recombination on the operation of the cell when the other sources of recombination are reduced by careful processing. At a pn product of (3 X 10^{15} $cm^{-3})^2$, as might occur at one sun, these results become

	I_{rec} mA/cm^2
bulk, SRH	4.8
bulk radiative	2.9 X 10^{-2}
bulk, Auger	4.3 X 10^{-3}
surface	1.9
diffused regions	25.7

At one sun the contact recombination dominates the other sources of recombination , though not so completely as in the concentrator case.

references

1. R. M. Swanson, "Point Contact Silicon Solar Cells," EPRI report AP-2859, May 1983.
2. J. Dziewiour and W. Schmid, Appl. Phys. Lett. 31, p. 346 (1977).
3. W. Kerm and D. A. Poutinen, RCA Review, June 1970, pp. 187-207.
4. R. M. Swanson and W. D. Eades, being prepared for publication.

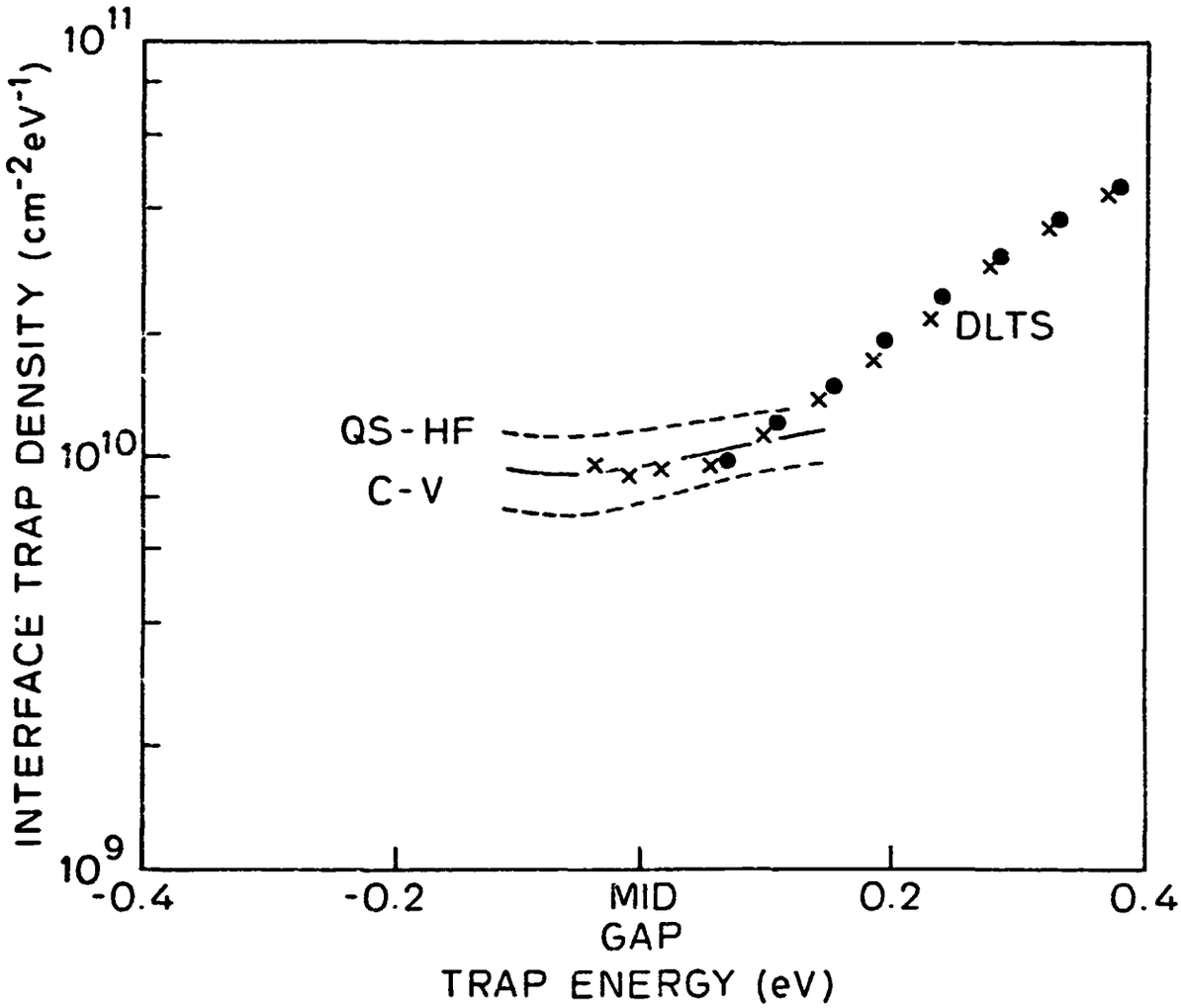

Figure 1. Density of interface states in the upper portion of the bandgap.

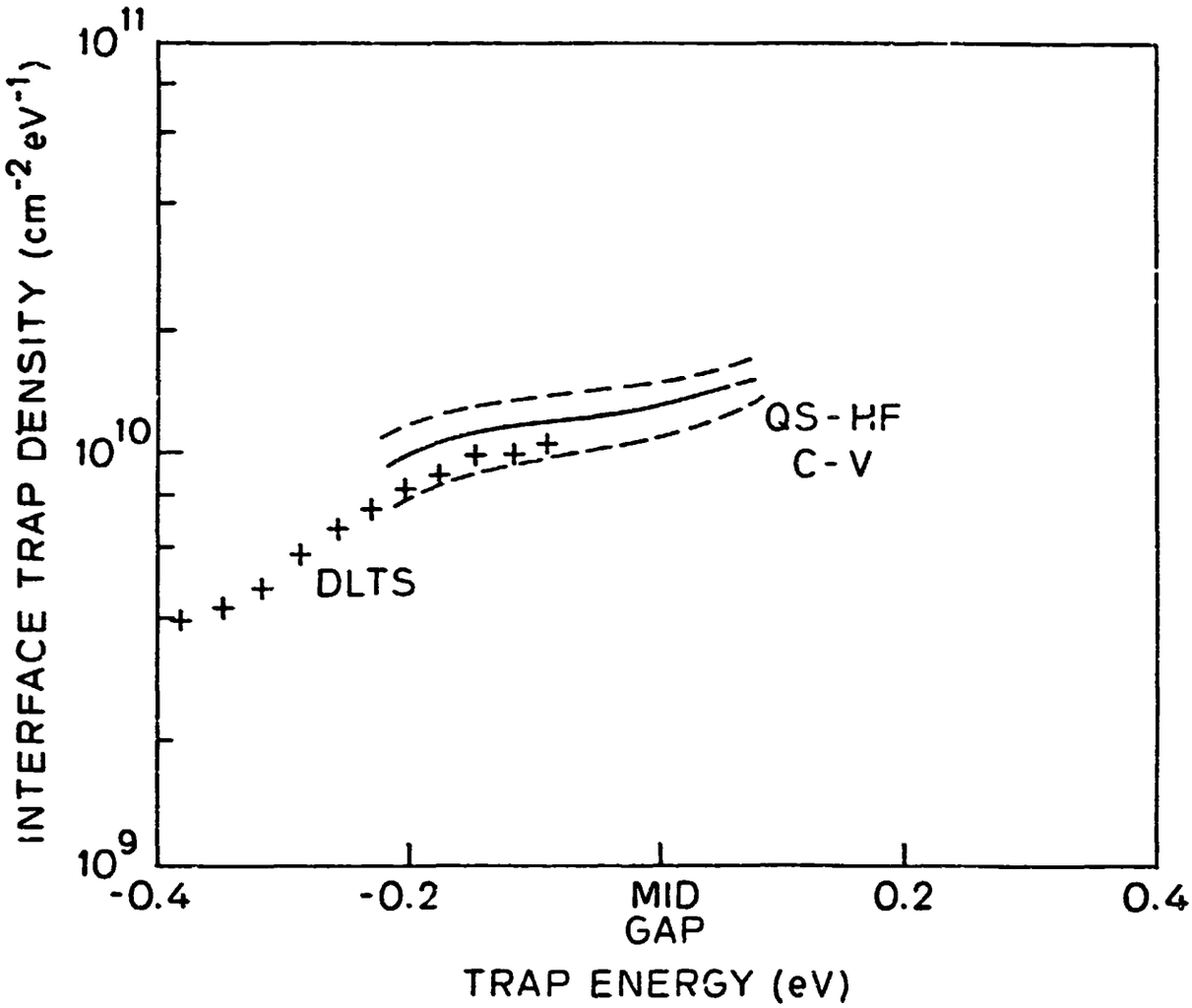

Figure 2. Density of interface states in the lower portion of the bandgap.

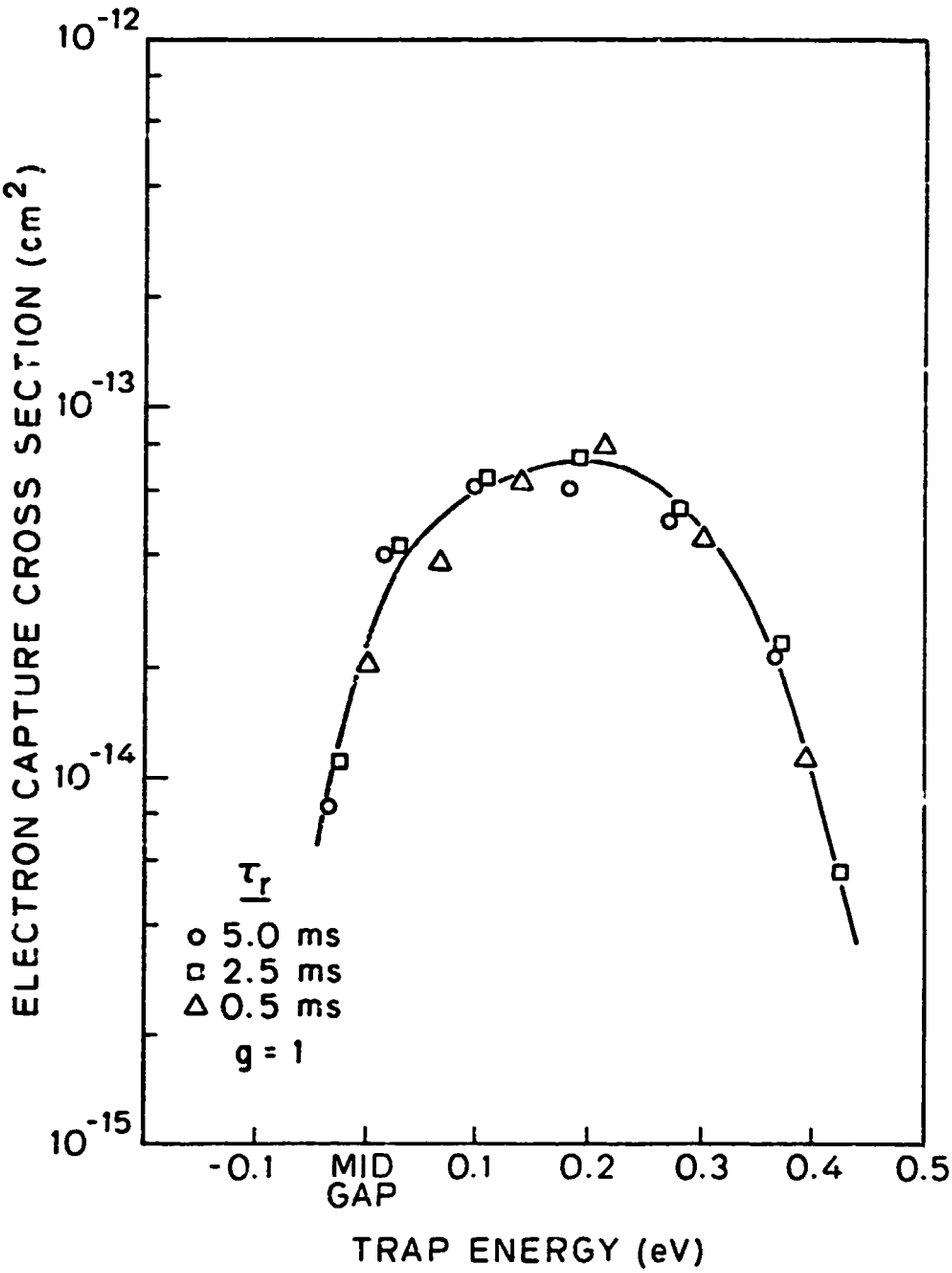

Figure 3. Electron capture cross section of Si-SiO_2 interface states.

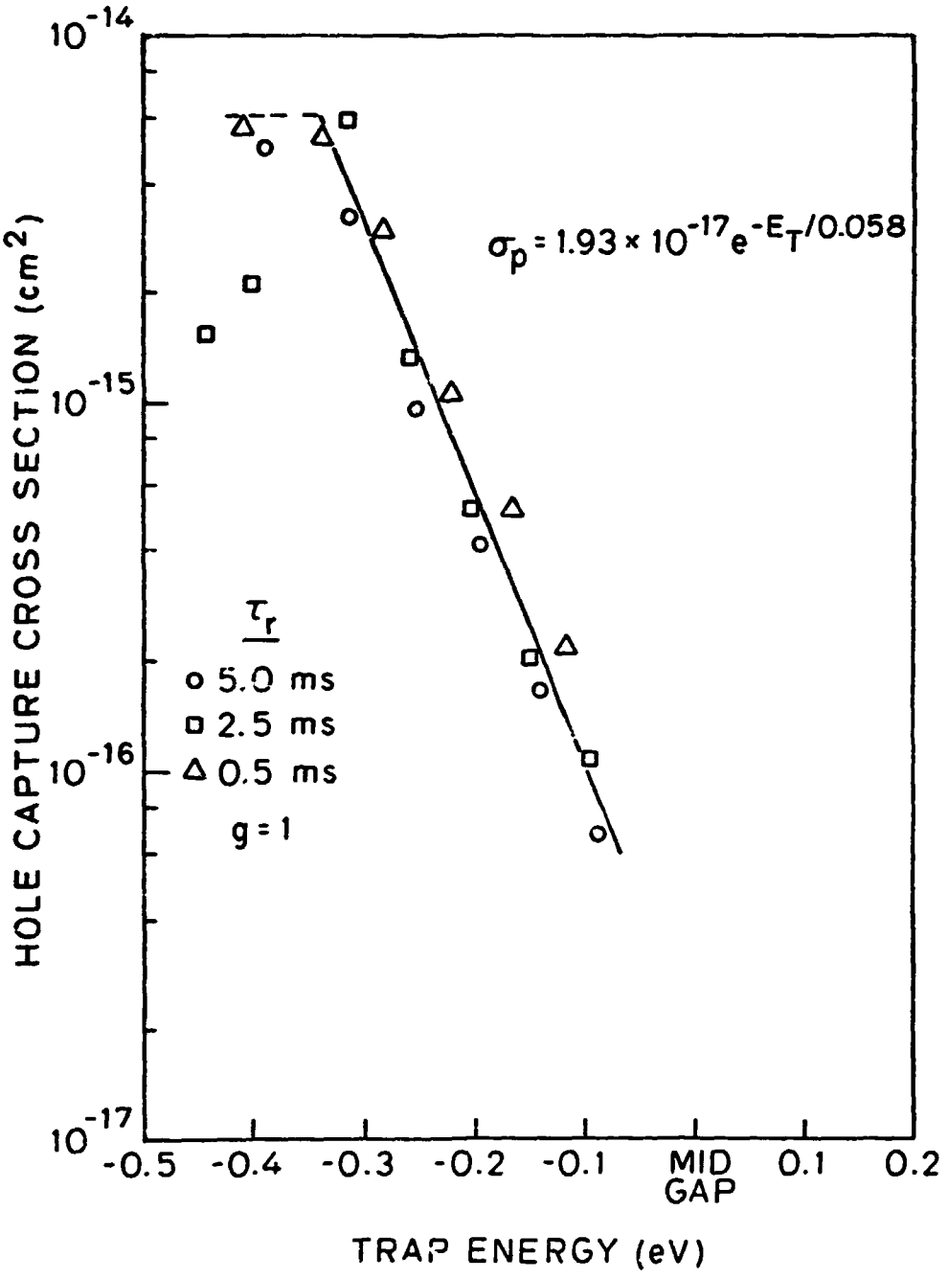

Figure 4. Hole capture cross section of Si-SiO_2 interface states.

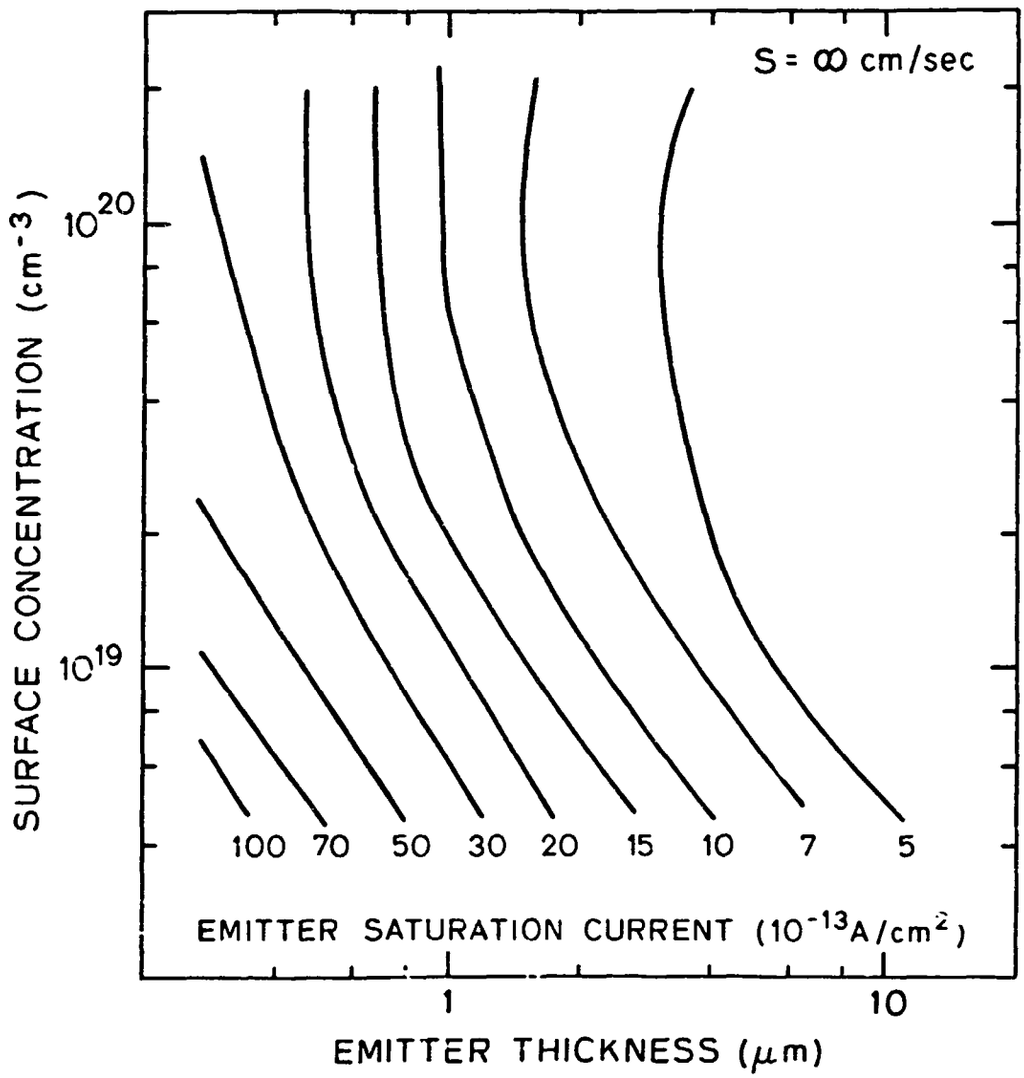

Figure 5. Calculated saturation current density for Gaussian profile emitters with infinite surface recombination velocity

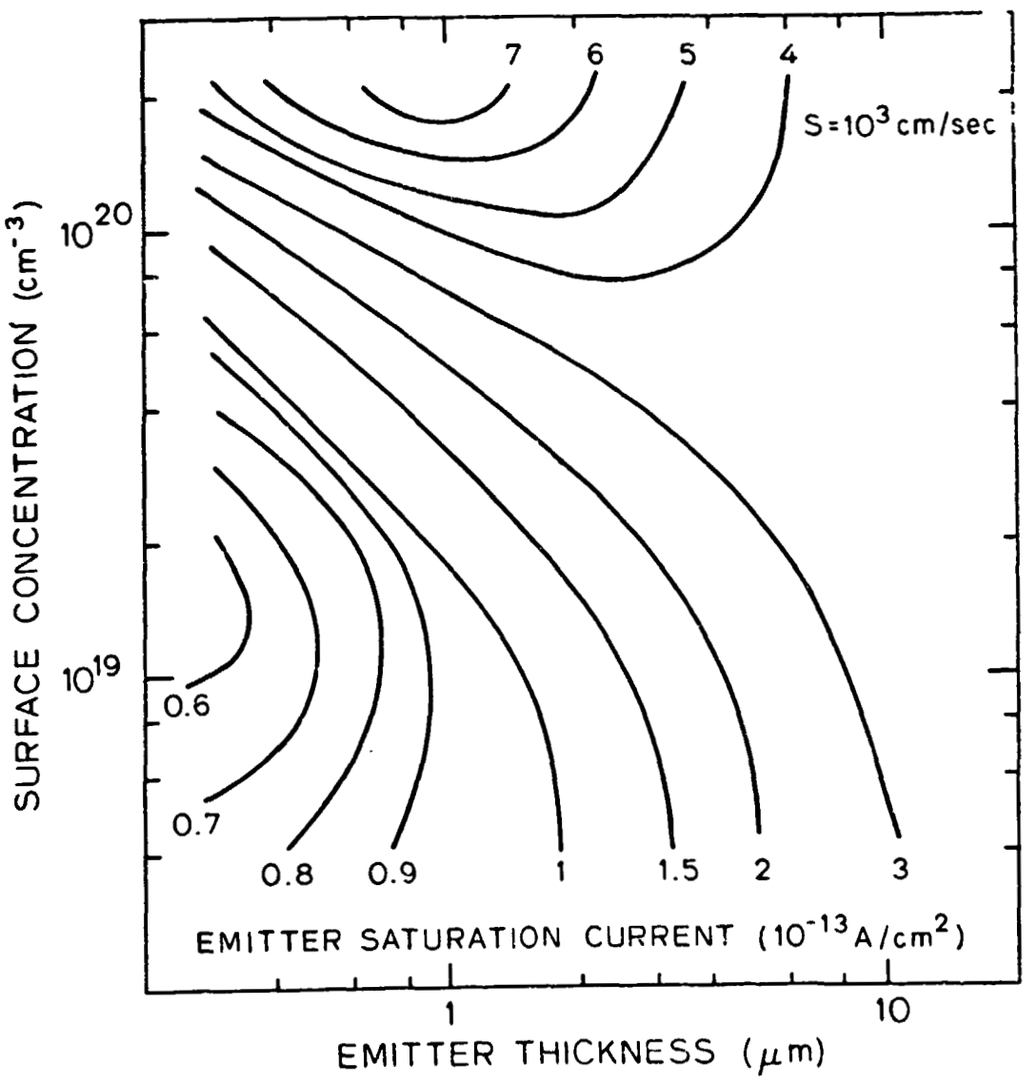

Figure 6. Calculated saturation current density for Gaussian emitters with $s = 10^3$ cm/sec.

DISCUSSION

LINDHOLM: Dick, I have a couple of questions. The first is in connection with your last remark. Do you think you need a two-dimensional code or a three-dimensional code?

SWANSON: For the point contact cell I think you need a three-dimensional code. If you made the lines as stripes, a two-dimensional code would be adequate.

LINDHOLM: Would you comment on your preference for the open voltage over the conductivity method for determining high injection lifetime? Why you use it at the end, and also say a little more on the photoconductive decay method for in-process lifetime?

SWANSON: The open-circuit voltage decay: I like it because it is very easy to do, and once you understand what it is doing it is easy to extract data from it. In the type of cell we are talking about, where the diffusion length is much greater than the thickness of the device: after interrupting the current, a very short period of time later the carriers are more or less uniformly distributed from the front to the back of the device, and this makes the analysis of the transient very simple. Basically you have one recombination term that is going as n^2, that is the diffused areas, and that gives you a steeper slope in the beginning. It allows you to extract the J_0's and then it goes into a linear region where the recombination going is n, and there is a straight line on the decay, and you pick the lifetime off that.

LINDHOLM: Have you written something on that? Published?

SWANSON: No. There is, but I am just using things from the literature on it.

LINDHOLM: How about the photoconductivity decay in process lifetime monitoring?

SWANSON: That is essentially a similar circuit to the one in High Lifetime Factors in Silicon Processing, which is a book from ASGF. Our particular implementation of it is simply a three-turn coil with 10 megahertz of RF flowing through it that is laid near the sample, and then we use a General Radio strobe attached to it to excite the carriers. We look at, essentially, the back EMF across the coil as a function of time, which -- in effect the silicon looks like a single-turn secondary, coupled to this, whose resistance is a function of time, and that gets reflected into the impedance looking into the coil, so that the real part of the impedance of the coil is a function of the conductivity, etc. I will send you a writeup we have on that. I wrote it up because the people from Westinghouse wanted to see it, so I made a bunch of copies. We had no intention of publishing because it really is the same --

SPITZER: I am interested in hearing some more about your tips for high-lifetime processing. That is something we are working hard on. The first question is: did you find it necessary to use double-wall furnaces,

or do you use those?

SWANSON: Well, Mark, you will have to understand: being in the University environment, I have no secrets at all. However, we have tried silicon tubes, silicon carbide tubes, double-wall quartz tubes, double-wall quartz tubes inside of silicon carbide tubes, and plain silicon tubes with and without alumina liners.

SPITZER: We can't afford that in industry.

SWANSON: We couldn't afford that either. They were all given to us by interested parties. What I can say in retrospect is, though, that the system we are using now, which has given us the best results, is a plain quartz tube inside an alumina liner.

SPITZER: What about processing gases? Did you spend a lot of time judging various suppliers and things like that?

SWANSON: We did. We just used boil-off nitrogen and oxygen but we have had about five major lifetime crashes in the history of the program. At one time we thought it was gas. We hooked up a residual gas analyzer to our gas system and saw sulphur dioxide in the nitrogen and thought it was sulphur but then it turned out that was an artifact of the residual gas analyzer, and it turned out not, in that particular case, to be from the gas but to be from bacteria in the water. So we have never seen any evidence in boil-off that there was any need for more purity than we are obtaining routinely in the boil-off.

SPITZER: Do you use boil-off hydrogen?

SWANSON: We don't use hydrogen.

SPITZER: No hydrogen.

SCHRODER: How do you measure S of 2 cm/second?

SWANSON: We measured that by the photoconductivity decay method.

SCHRODER: These are surface recombinations velocities, right?

SWANSON: These are high-level surface recombinations velocities, which were measured by taking samples of different thicknesses, ranging from around 20 micrometers to 300 micrometers, and their high-resistivity float-zone material, oxidizing both sides and measuring the recombination lifetime, with our standard, as a function of thickness.

WOLF: Do these lifetimes then include the effect of the accumulation layer?

SWANSON: We measure effective recombination lifetime. However, the oxides we have produced, which are standard MOS-type oxides, have fixed charge densities under 10^9, I think, and when they are injected at 10^{17}, any kind of potential band due to that is very, very small. One of the challenges that faces one in this, one we have not fully resolved, is how

to get similar performance on very thin oxides suitable for putting under an antireflection coating. These are all state-of-the-art MOS-type oxides, high-temperature dry oxidation followed by nitrogen atmosphere anneal and low-temperature hydrogenation.

WOLF: Now, what you mentioned about the DI water and the bacteria sounds extremely interesting and it seems to me that you said if you have really pure water then there are no bacteria. So the bacteria comes with the indication whether your water is basically purified well or not. Is that right?

SWANSON: No. The problem is that most people monitor -- at least, in our laboratory until we discovered this -- we routinely monitor resistivity but not bacteria count. The resistivity can be in real good shape and have a very high bacteria count.

WOLF: DI water generally does not contain ions, and still bacteria can thrive on that?

SWANSON: I really don't know how they live in there but they do. They metabolize the plastic pipe, or that is what I have been told. They are anaerobic and whatever.

TAN: Allow me to make a comment on your last. Except for the first item, which is the float-zone silicon, the rest is standard practice of the integrated circuit industry. Off the record, I can also support him about the bacteria business. It is all true.

SWANSON: I don't know how you can go about getting these kinds of lifetimes in Czochralski or other materials. We were misled because, being a poor university, we were in one of those periods where silicon was hard to get. Wacker gave us silicon in boxes that said it was Czochralski material. But it turned out that it was mislabeled. It was actually float-zone material. We worked on that for a year, and we then ordered new material from them thinking they have got the hot stuff. It came back that we were getting 20 to 50 microseconds, and that is when we had the material analyzed and found that it was indeed float-zone material. Then we worked with the Czochralski material for over a year and were unable to get the lifetime.

SCHWARTZ: How did you measure the capture cross sections in surface states? To me it is a very surprising result.

SWANSON: It was to us too, and these data are being prepared for publication. It was done using DLTS in a capture mode. Just like you would use DLTS for bulk levels by shortening and filling the pulse width. We used essentially small-signal DLTS, where we wiggled the interface a little bit, so we filled emptying traps in a ΔE about a known point, and then varied the filling pulse time and watched the decay signals.

SCHWARTZ: It appears to me that your fall-off in capture cross section is so rapid that one would not see it, so that experiment doesn't seem to fit.

SWANSON: Right now we are making measurements of recombination velocity versus doping levels to see if we get the results predicted by integrating the SRH equation over those.

SILICON MINP SOLAR CELLS

N85-31623

Larry C. Olsen, F.W. Addis and W.A. Miller
Joint Center for Graduate Study
Richland, Washington 99352

ABSTRACT

The MINP solar cell concept refers to a cell structure designed to be a base region dominated device. Thus, it is desirable that recombination losses are reduced to the point that they occur only in the base region. The most unique feature of the MINP cell design is that a tunneling contact is utilized for the metallic contact on the front surface. The areas under the collector grid and bus bar are passivated by a thin oxide of tunneling thickness. Efforts must also be taken to minimize recombination at the surface between grid lines, at the junction periphery and within the emitter. This paper includes results of both theoretical and experimental studies of silicon MINP cells. Performance calculations are described which give expected efficiencies as a function of base resistivity and junction depth. Fabrication and Characterization of cells are discussed which are based on 0.2 ohm-cm substrates, diffused emitters on the order of 0.15 to 0.20 μm deep, and with Mg MIS collector grids. A total area, AM1 efficiency of 16.8% has been achieved. Detailed analyses of photocurrent and current loss mechanisms are presented and utilized to discuss future directions of research. Finally, results reported by other workers are discussed.

1. INTRODUCTION

This paper concerns approaches to high efficiency silicon solar cells based on the MINP concept. This term is used to denote shallow junction N^+/P cells which utilize a MIS contact for the front collector grid. The MINP structure was first discussed by Green, et al.[1] Recently Green and coworkers have fabricated cells exhibiting efficiencies on the order of 19%. As a result, the MINP concept has become one of the most promising approaches to fabricating high efficiency silicon cells.

Key features of MINP cells are described in Figure 1. A shallow emitter is used in an effort to minimize current losses in the emitter region. The front surface is passivated to reduce surface recombination. If the base region losses can be reduced as a result of a back-surface-field, then a P^+ region is established at the back surface. In order that the emitter current losses are further reduced, an MIS contact is used for the front collector grid. A metal must be chosen which will accumulate the N^+ surface. Thus, the area under the front contact is also passivated. Ti and Mg have work functions below 4.0 eV. As a result, these two metals are appropriate for the front tunneling contact. In summary the MINP cell has features similar to other shallow emitter, high efficiency silicon cells. Clearly, the most unique feature is the MIS (tunneling) contact used for the collector grid.

In the next section the theoretical performance of MINP cells will be discussed. Detailed discussions are then given regarding cell fabrication, photocurrent, current loss mechanisms, the Mg/nSi tunnelling contact, and solar cell efficiency.

 PRECEDING PAGE BLANK NOT FILMED

2. LIMITING THEORETICAL PERFORMANCE

Modeling calculations have been conducted to appraise the potential of the MINP concept and to provide guidance for device design. These studies are based on two sources of minority carrier lifetime data, namely, the LSA advisory board[2], and that of Fischer and Pschunder[3].

In order to determine an upper limit to cell performance, it was assumed that the device properties were completely determined by the base region. Thus, the junction depth was considered to be vanishingly small and the front surface recombination velocity was set equal to zero. Modeling calculations discussed in this paper are based on an assumed cell thickness of 380 μm (15 mils), since experimental studies have primarily been based on cells with that thickness.

Calculated values of the maximum, active area photocurrent are plotted versus base region resistivity in Figure 2. The modeling calculations were carried out for the two sets of lifetime data and for two conditions at the back contact. An AM1 irradiance spectrum appropriate for Phoenix, Arizona was used in calculating photocurrent.

Theoretical values of the reverse saturation current (J_{BO}) are plotted versus base resistivity and N_A in Figure 3. Auger recombination and bandgap narrowing are taken into account as done in Reference 1. Calculated values of V_{OC} are also given assuming J_{SC} = 36 mA/cm^2. With LSA lifetimes, the V_{OC} for a base region dominated cell can approach 690 mV. Due to Auger recombination, there is no reason to use base resistivities below 0.1 ohm-cm.

Calculated active area AM1 efficiencies are described by Figure 4. If one assumes that lifetimes are given by LSA values, then a base resistivity in the range of 0.1 to 0.2 ohm-cm is optimum for cells with ohmic contacts, while the resistivity can be any value greater than 0.1 ohm-cm for cells with a BSF. If FP values are assumed, then it is best to use base region resistivities between 0.1 and 1.0 ohm-cm.

3. CELL FABRICATION

The basic approaches to cell fabrication involve steps listed in Table 1. To date emitter diffusions have been obtained from ASEC and Spectrolab. The junction depths are on the order of 0.15 to 0.20 μm. Phosphorus concentration profiles obtained by SIMS and spreading resistance analysis (SPA) are shown in Figure 5. The error limits are estimated to be ± 50% for both profiles. Thus, the error limits overlap. Although very limited data has been acquired, it appears that the surface donor concentration is on the order of 0.5 to 1.0x10^{20} cm^{-3}.

In the case of approach A (Table 1), the wafers are scribed and cleaned, an Al layer is deposited onto the back surface. Heat treatment at 500°C establishes an ohmic contact on the back and a 15 to 20 A, tunnelable oxide forms on the front surface. This oxide layer provides some passivation on the front surface. Of course, it also serves as an interfacial layer for the MIS, collector grid or 'tunneling' contacts on the front surface. The MIS collector grid is formed with a low work function metal. Mg has been used in this work. Using Approach A, the cell is completed by depositing an AR coating(s).

The key difference with Approach B is that a 100 to 150 A layer of SiO2 is grown onto the front surface to achieve a lower surface state density.

4. PHOTOCURRENT

In order to maximize the photocurrent, and to interpret experimental results, detailed analyses of photon and carrier economy have been carried out. In particular, optimum AR structures have been determined for both polished and textured cells. Essential information for such analysis is the internal photoresponse for the cell.

Figure 6 shows a typical result for the internal photoresponse of a polished cell structure. Calculated curves are based on cell parameters as indicated. The wave length region between 750 nm and 1050 nm is the most important one for determining the minority carrier diffusion length. A value of L = 150 m appears to fit the data fairly well.

Figure 7 describes the approach taken in determining the optimum AR layer structure for polished and textured cells. Optical cconstants must be known for each layer in the multilayer stack. Photon transmittance into silicon is calculated with a computer code, and used in an integration over the chosen irradiance spectrum. The optimum AR layer structure is determined by maximizing J_{PH}.

Figure 8 summarizes calculation of J_{PH} for polished and textured cells. Most of the plots are for L = 150 μm. The active area J_{PH} is plotted versus N_1, the index of the antireflecting layer adjacent to silicon. For a single AR case (1L-AR), N_1 is of course the index of the single AR coating. For each value of N_1 in single AR structures, there is an optimum value of the layer thickness. In the case of a two layer structure, there are, of course, optimum value of thickness at which the plotted value of J_{PH} occurs.

Calculations show that it is desirable to use a textured surface. A single AR coating on top of a textured cell leads to a possible 38.3 mA/cm^2 compared to the possible 37 mA/cm^2 achievable with a double AR on a polished surface. Furthermore, with a double AR on a textured surface, a value of nearly 39 mA/cm^2 becomes possible. Thus results are based on assuming L = 150 m. If one assumes a Fischer-Pschunder value for L (500 μm), a value of 42.5 mA/cm^2 becomes a possibility.

Table 2 indicates some of the best active area values of J_{PH} measured by SERI. Those values are fairly compatible with results given in Figure 8. It would appear that the diffusion length of the material used by Green and coworkers is slightly larger than 150 μm. The JCGS result of 37.8 mA/cm^2 for a textured/1L-AR case is slightly less than the possible 38.2 mA/cm^2, probably due to absorption. The Spire reesult may be due to a smaller diffusion length or absorption in the AR coating.

5. CURRENT LOSS MECHANISMS

Current-voltage characteristics are being studied in detail in order that limiting current mechanisms can be identified and understood. Figure 9 summarizes the theory for the current loss mechanisms under consideration. Temperature dependent current-voltage characteristics are particularly useful for determining I-V mechanisms. The activation energy coupled with the n-value and magnitude of J_0 can often suggest the operative current loss mechanism. Table 3 lists the range of values for key I-V parameters.

The emitter recombination current likely to be a dominant loss mechanism in low resistivity devices. Calculated lues of J_{OE} are plotted vs the surface donor concentration (N_s) in Figure 10. The work of Fossum and Shibib[4] was used to calculate J_{OE}. The effects of bandgap narrowing and of the low lifetime in the emitter are taken into account. Values of J_{OB} are indicated assuming LSA and FP lifetimes, as well as ohmic and BSF conditions for the back contact. In addition. values of V_{OC} calculated assuming J_{SC} = 36 mA/cm^2 are given. The estimated value of J_0 for the 19% cell of Green, et al is based on the assumption that n = 1.

I-V data are taken with a computer based data acquisition system over a range of temperatures and under both dark and illuminated conditions. The approach to data analysis is summarized in Figure 11. The approach used for analyzing illuminated data is similar. In general, we observe two current mechanisms, one dominant at low voltages and one dominant at higher voltages. These current mechanisms are referred to as the lower and upper mechanisms, respectively.

Transformed I-V characteristics for an MINP cell are shown in Figure 12. The two mechanisms are clearly evident. Values for the J_0 and n of the upper mechanism, and J_0 and B of the lower mechanism were determined for each temperature. Results are typically obtained for ten temperatures. The value of the upper mechanism is plotted versus 1000/T in Figure 12. From this plot, one obtains a value for ϕ = 1.08 eV. In analyzing the temperature dependent data, $J_{00}(T)$ is assumed to vary with temperature as $\Gamma(T-T_o)$, with T_o = 100°K.

Some results of I-V analyses carried out for MINP cells are given in Table 4. In particular, the results for the upper mechanism are given. The lower mechanism is discussed below. Results for analysis of both illuminated and dark data are given. Only results of I-V analyses were included, for which temperature studies were made, except for cells 84-21 and 84-22. These devices were made just recently. Consider cell 83-25. Since n = 1, and ϕ = 1.08 eV, it appears that the current-voltage characteristics are limited by the emitter current with bandgap narrowing of ΔE = 0.12 eV. In all of the other cases, n is in the range of 1.04 to 1.09, and ϕ lies in the range of 0.7 to 0.8 eV, except for cell 84-5. These parameters suggest either depletion region recombination or field emission. Further study is required to allow one to choose between these possibilities, and to relate the results to processing. It is not clear at this time what is the proper model for 84-5.

The upper mechansim is usually described by n ≃ 1.0 to 1.07 and J_0 ≃ 2 x 10^{-12} A/cm^2. At this point it would appear that recombination in the depletion region or field emission by holes near the metallurgical junction explain the upper mechanism. A possible reduction of the magnitude of this mechanism may be accomplished by reducing N_S.

The lower mechanism is not presently limiting cell performance. It could do so in the future, as the upper mechanism is improved. Thus, we must eventually understand the lower mechanism.

6. THE Mg/n-Si TUNNELING CONTACT

The MIS collector grid is a key feature of the MINP cell. The term 'tunneling contact' is often applied to this contact and will be used in this paper. Figure 13A illustrates the expected electron band diagram at the Mg-nSi interface. Since the work function of Mg is less than 4.0 eV, the silicon surface is accumulated as shown. Majority carriers can readily tunnel through the 20 A interfacial layer, thus providing a good ohmic contact.

The primary purpose for using a tunneling contact is to minimize the recombination under the contact. Thus, it is of interest to estimate the surface recombination velocity for this interface. We will examine this question in two ways. First, it is informative to investigate MIS diodes on p-type silicon. Figure 10B indicates possible comman current loss mechanisms. Mg/pSi MIS cells have been fabricated and found to have excellent properties. Figure 14 shows I-V characteristics for two devices. Device 82 MgSi-14 shows a rather weak lower voltage mechanism, while the more recently fabricated device 84 MgSi-1 exhibits essentially no lower mechanism. More significantly, the upper mechanism for 84 MgSi-1 corresponds to an ideal diode. The I-V parameters are n = 1.00 and $J_0 = 4.8 \times 10^{-13}$ A/cm^2. This value of J_{02} can be interpreted in terms of a barrier height of ϕ_{Br} = Eg and A = 32 a/cm^2. Thus, one can conclude that in the case of an Mg/pSi contact, there is no significant surface recombination (c), or tunneling/recombination (d).

The I-V analyses of MINP cells can provide information about surface recombination under the Mg contact on N^+/P structures more directly. The Mg contact area is not the same for the cells listed in Table 4. Referring to cells 84-21 and 84-22, the Mg contact area differs by a factor of 20. Yet the J_0 is very similar for the two devices. In fact, J_0 for 84-21 is larger than for 84-22. If recombination under the Mg contact were the dominant loss mechanism for 84-22, the J_0 should be smaller for a device with the contact covering less area.

More effort will be devoted to characterize recombination under the MIS contact. However, recombination losses appear to be low enough to allow J_0 to decrease below 10^{-12} A/cm^2.

7. CELL EFFICIENCIES

Two types of cell structure are being pursued, namely: an MINP configuration with a polished front surface; and MINP cells with textured front surfaces. These structures will be referred to as 'polished' and 'textured'.

The best result obtained with a polished cell is described by Figure 11. The current-voltage characteristics were measured by SERI. As noted, the efficiency was 15.6%, and V_{OC} = 636 mV. This cell utilized a single AR layer of SiO. The SiO is deposited rapidly so that the index of refraction is near 1.9. Analysis indicates that a silicon homojunction with a single AR layer can provide an active area AM1 photocurrent of 35.5 mA/cm^2. The total area current in such a case for our cells would be 33.4 mA/cm^2 (6% shadowing). The best total area value of J_{SC} obtained for a cell with a single SiO layer is 31.8 mA/cm^2. Thus, it appears that approximately 1.6 mA/cm^2 are lost due to photon absorption in the SiO film. Future efforts will concentrate on the use of a double AR coating on a polished cell structure.

SERI measured current-voltage characteristics for the best textured cell are given in Figure 16. Although J_{SC} has been increased to 35.5 mA/cm^2, FF and V_{OC} are slightly lower than that achieved with a polished cell. Part of this decrease is due to the fact that the junction area of the textured cell is larger than the standard cell by a factor of 1.7, but most of the effect is primarily because the junction has not been optimized for the textured cells.

8. CONCLUSIONS

The MINP cell structure is a shallow emmitter cell structure. The unique feature of the MINP cell is the tunneling contact used for the collector grid. Like any shallow emitter cell, the front surface must be well passivated and emitter losses minimized before base limited performance can be achieved. Efficiencies of 25% should eventually be possible. Figure 17 indicates the kind of property improvements needed to achieve 20%, and then 25%.

ACKNOWLEDGEMENTS

The authors wish to acknowledge the financial support of the Solar Energy Research Institute(Contract XBB-2-02090-5).

REFERENCES

1. M. A. Green, et al, "The MINP Solar Cell - A New High Voltage, High Efficiency Silicon Solar Cell," Conf. Record, 15th IEEE Photovoltaics Specialists Conf., Orlando, p. 1405, 1981.

2. M. Wolf, "High Efficiency Silicon Solar Cells," Conf. Rec., 14th IEEE Photovoltaics Specialists Conf., San Diego, p. 674, 1980.

3. H. Fischer and W. Pschunder, "Impact of Material and Junction Properties on Silicon Solar Cell Efficiency," Conf. Rec., 11th IEEE Photovoltaics Specialists Conf., Scottsdale, p. 15, 1975.

4. Jerry G. Fossum and M. Ayman Shibib, IEEE TRANS ON ELEC. DEV ED-28, 1018(1981).

TABLE 1

MINP CELL FABRICATION

A. WITH THIN PASSIVATING OXIDE

1. Diffuse Emitter into Wafer.
2. Scribe into 2 cm x 2 cm Substrates.
3. Clean Substrate (Basically RCA Process).
4. Deposit Aluminum Back Contact.
5. Sinter Back Contact at 500 C and Grow 15 to 20 A Tunnelable Oxide on Front Surface
6. Deposit Collector Grid Based on a Tunneling Contact.
7. Deposit an AR layer(s).

B. WITH THICK PASSIVATING OXIDE

1,2 and 3 Same as Above.
4. Grow 100 to 150 A SiO_2 Layer for Passivation of Front Surface.
5. Define Contact Openings and Remove Oxide on Back Surface.
6. Complete cell by Using Steps 4 Through 7 Given Above.

TABLE 2

EXPERIMENTAL RESULTS FOR AM1 PHOTOCURRENT

0.2 Ohm-cm P-TYPE BASE
CELL THICKNESS = 15 mils

CELL	AR STRUCTURE	GRID SHADOWING	TOTAL AREA AM1 J_{PH}	ACTIVE AREA AM1 J_{PH}
GREEN, ET AL	2L-AR ZnS/MgF_2	4.2%	36.0	37.6
SPIRE	TEXTURED 1L-AR(Ta_2O_5)	3-4%	36.1	37.2-37.6
JCGS 84-6	TEXTURED 1L-AR(SiO_x)	6%	35.5	37.8

TABLE 3

KEY PARAMETERS FOR CURRENT MECHANISMS

CURRENT MECHANISM	J-V RELATIONSHIP FOR $V >> kT$	ACTIVATION ENERGY ϕ (eV)
EMITTER RECOMBINATION	J_{OE} exp(V/nkT) $n = 1$	$1.2 - (\Delta E)_{\substack{EMITTER \\ BGN}}$
BASE REGION RECOMBINATION	J_{OB}exp (V/nkT) $n = 1$	$1.2 \quad (\Delta E)_{\substack{BASE \\ BGN}}$
DEPLETION LAYER RECOMBINATION	J_{OR} exp(V/nkT) $n \cong 1$ TO 2	$E_c - E_t$ OR $E_t - E_v$
FIELD EMISSION	J_{OF} exp(CV) $C = \frac{1}{nkT} + B$	0.8 TO 1.0
TUNNELING	J_{OT} exp(BV)	TYPICALLY 0.1 TO 0.2

ASSUMED FORM OF J_{oi}:
$J_{oi} = J_{oo}(T) \exp(-\phi/kT)$

TABLE 4

I-V PARAMETERS FOR HIGH-VOLTAGE CURRENT-LOSS MECHANISM

CELL	FRONT Mg CONTACT AREA (%)	DARK OR ILLUM	AVERAGE ERROR FOR UPPER RANGE (%)	UPPER MECHANISM		
				ACTIVATION ENERGY, ϕ (eV)	n	J_o (A/cm²)
83-22	6	ILLUM	0.19	0.73	1.04	2.1 E-12
83-23	6	DARK	0.19	0.77	1.09	1.5 E-11
83-25	6	DARK	0.63	1.08	1.00	2.2 E-12
83-26	6	DARK	0.28	0.81	1.04	4.4 E-12
84-5	0.6	DARK	0.19	1.15	1.04	2.4 E-12
84-6	6	DARK	0.33	0.80	1.07	2.4 E-11
84-21	0.3	ILLUM	0.40	–	1.09	5.3 E-12
84-22	6	ILLUM	0.40	–	1.05	2.6 E-12

TABLE 5

EXPERIMENTAL RESULTS FOR MINP CELL AM1 EFFICIENCIES

0.2 Ohm-cm P-TYPE BASE
CELL THICKNESS = 15 mils

CELL	METAL USED FOR MIS CONTACT	AR STRUCTURE	GRID SHADOWING	J_{SC} (mA/cm²)	V_{OC} (mV)	FF	AM1 EFFICIENCY (%)
GREEN, Et al	Ti	2L-AR ZnS/MgF_2	4%	36.0	650	0.812	19.0
JCGS 84-4	Mg	2L-AR SiN/SiO_x	6%	31.1	636	0.787	15.6
JCGS 84-6	Mg	TEXTURED 1L-AR(SiO_x)	6%	35.5	617	0.768	16.84

Results for Green, et al, were reported at the IEEE 16 th Photovoltaic Specialists Conference.

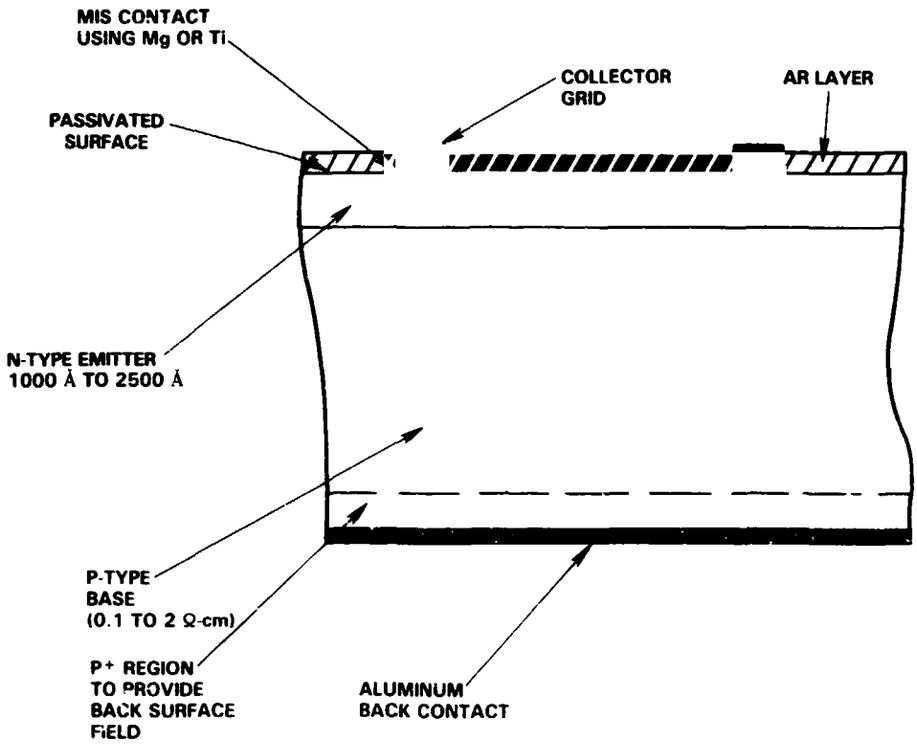

Figure 1. MINP Solar Cell Concept.

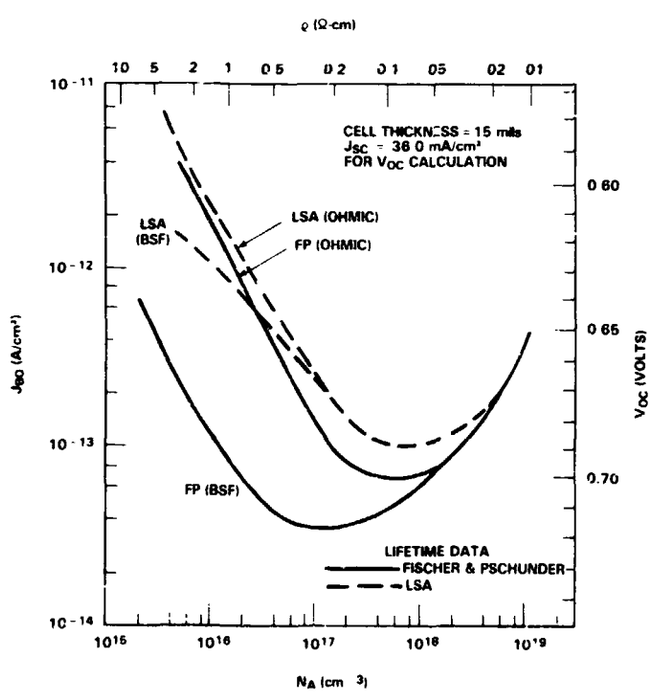

Figure 2. Base Region Contribution to J_0 vs Acceptor Concentration for 15 mil Cell Thickness.

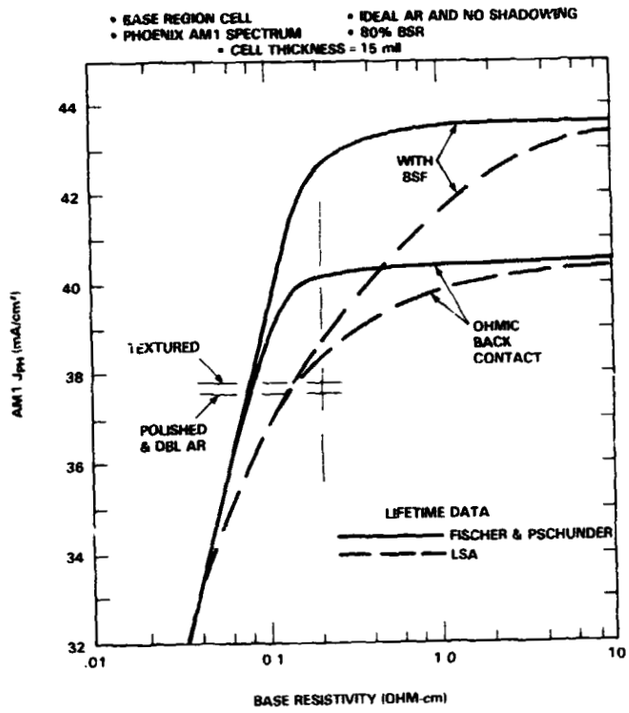

Figure 3. Calculated AM1 J_{PH} vs Base Resistivity for 15 mil Cell Thickness, Assuming 100% Photon Transmittance And No Grid Shadowing.

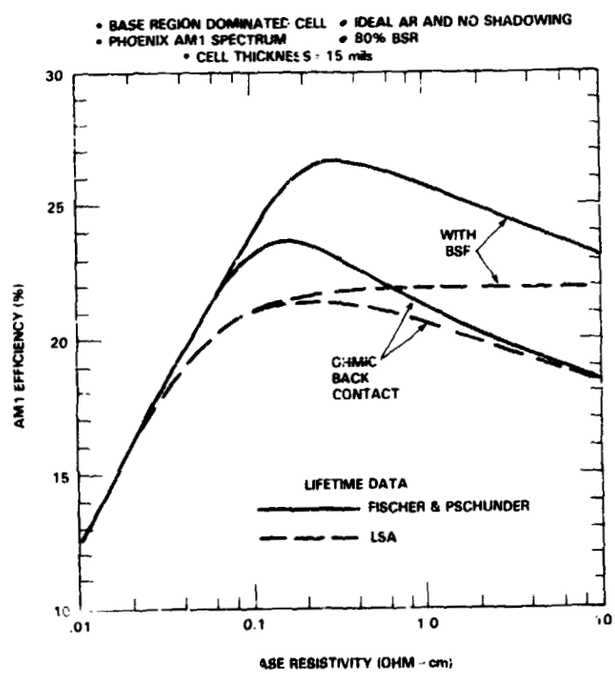

Figure 4. Calculated AM1 Cell Efficiency For 15 mil Cell Thickness, Assuming 100% Photon Transmittance And No Grid Shadowing.

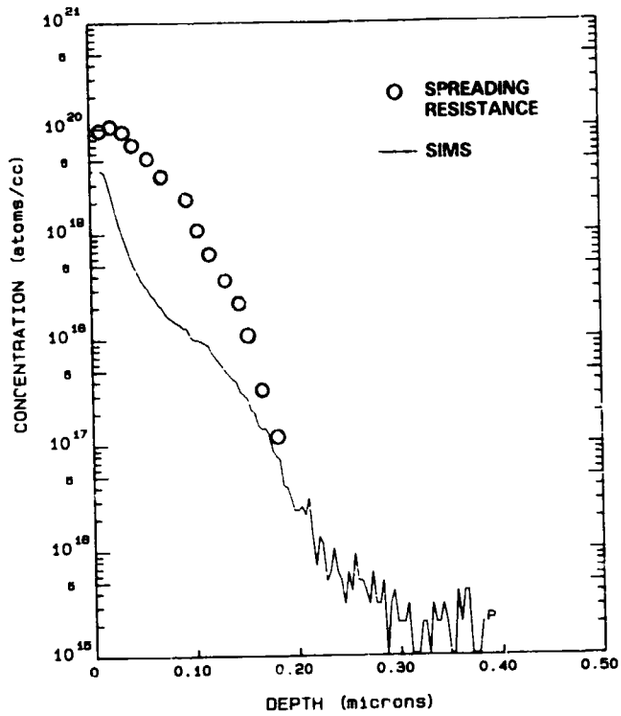

Figure 5. Phosphorus Concentration vs Depth For MINP Cell.

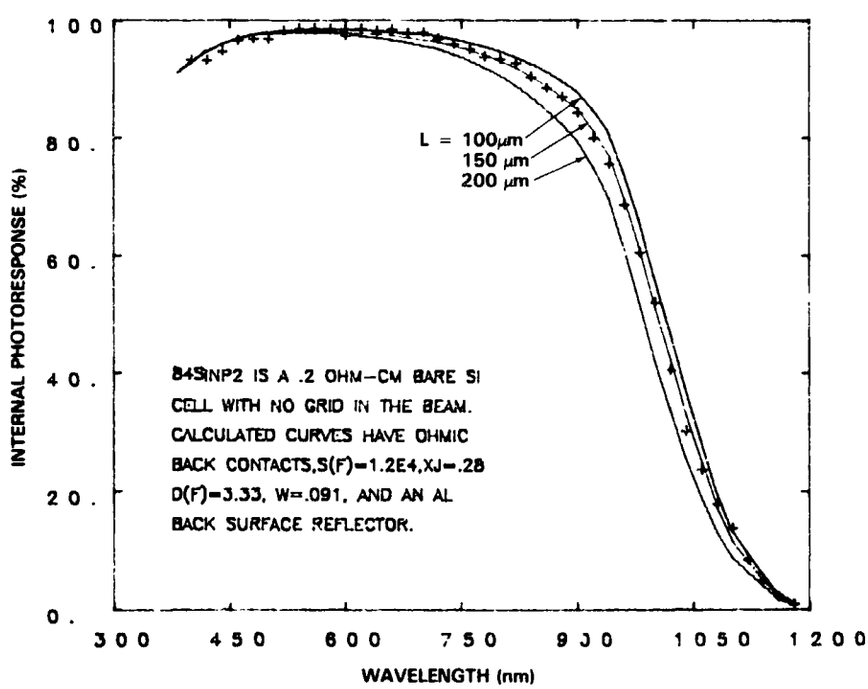

Figure 6. Internal Photoresponse For MINP Cell.

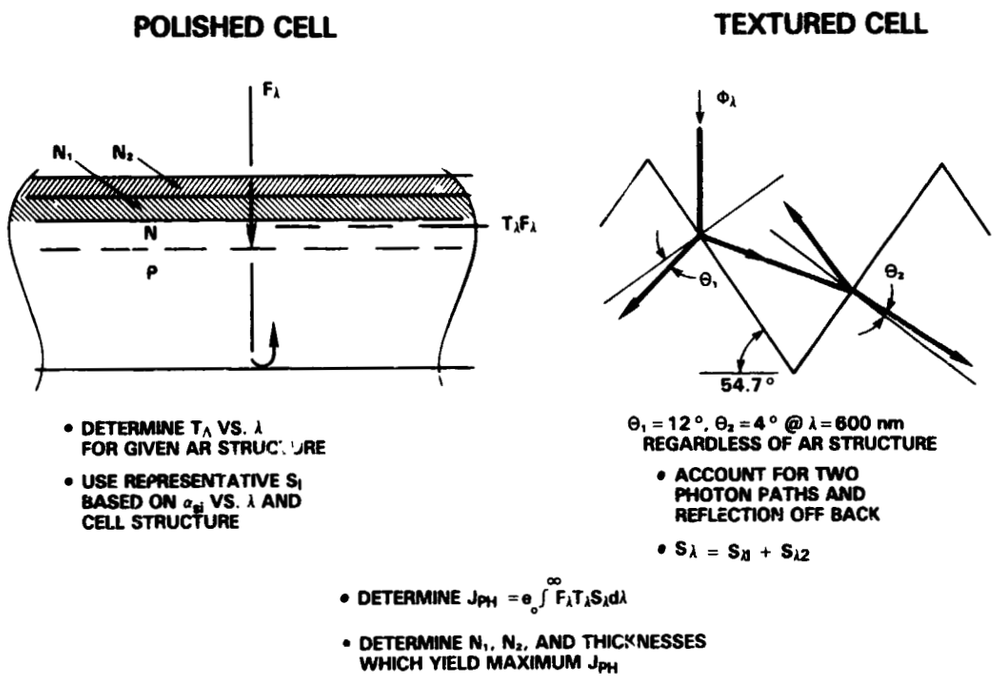

Figure 7. Description of Approach to Optimum AR Layer Analysis.

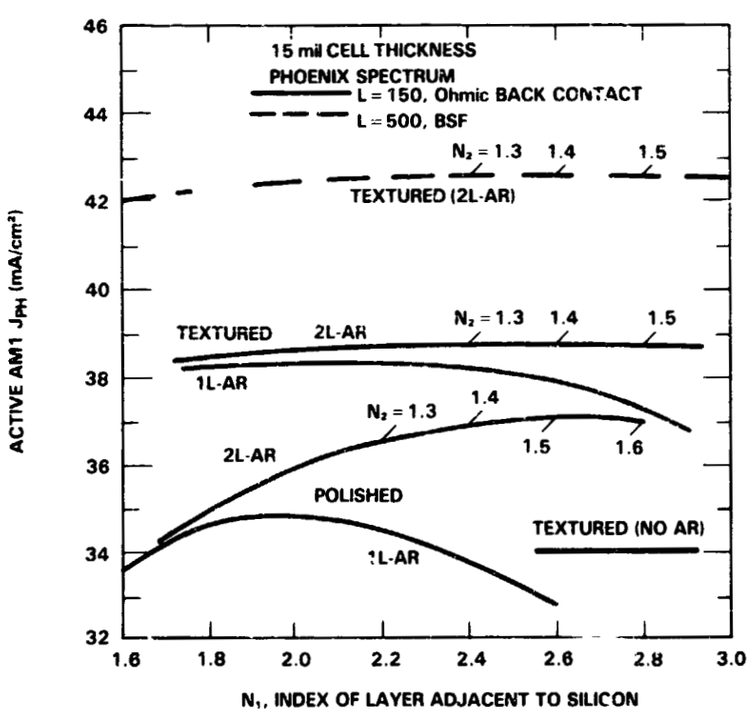

Figure 3. Calculated J_{PH} vs N_1, The Index Of The AR Layer Adjacent To Silicon, For Polished And Textured Cells.

1. **EMITTER RECOMBINATION CURRENT**

$J = J_{OE}\,[\exp(\frac{V}{nkT}) - 1]$

$n = 1$

FOR RM TEMP ANALYSIS:

$J_{OE} = \frac{en_i^2}{N_D^{(EH)}} \cdot GF$

GF IS A FCT OF W_H, S_P, D_{PO} & τ_P

FOR INTERPRETATION OF TEMPERATURE DEPENDENT DATA:

$J_{OE} = J_{OO}(T)\exp(\frac{-\phi}{kT})$

$\phi = 1.20 - (\Delta E)_{\text{EMITTER BGN}}$

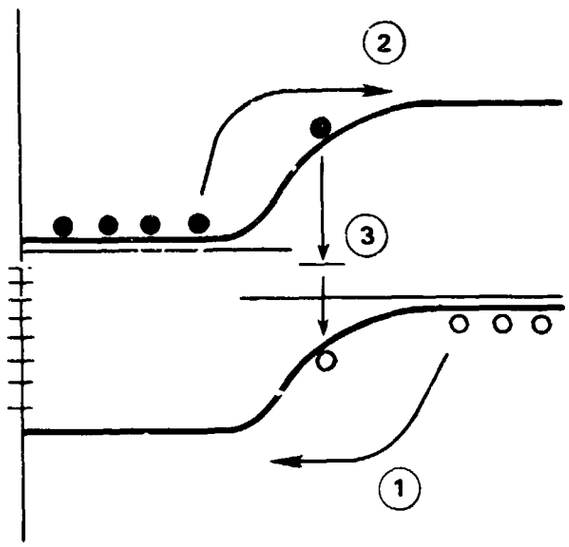

2. **BASE REGION RECOMBINATION CURRENT**

$J = J_{OB}\,[\exp(\frac{V}{nkT}) - 1]$

$n = 1$

$J_{OB} = \frac{en_i^2}{N_A}\frac{L_n}{\tau_n} \cdot G_F$

$= J_{OO}(T)\exp(\frac{-\phi}{kT})$

$\phi = 1.20 - (\Delta E)_{\text{BASE RGN}}$

3. **DEPLETION LAYER RECOMBINATION CURRENT**

$J = J_{OR}\exp(\frac{V}{nkT})\ V >> kT$

$J_{OR} = J_{OO}\exp(\frac{-\phi}{kT})$

$\phi = (E_t - E_v)$ OR $(E_c - E_t)$ $\quad n = 1$ TO 2

FOR $n \simeq 2, \phi \simeq E_g/2$ $\quad$ FOR $n \simeq 1, \phi \simeq 0.8$ eV

4. **TUNNELING/RECOMBINATION**

$J = J_{OT}\exp(BV) \quad V >> kT$

B TEMPERATURE INDEPENDENT

$J_{OT} = J_{OO}\exp(\frac{-\phi}{kT})$

ϕ TYPICALLY 0 TO 0.5 eV

5. **FIELD EMISSION**

$J = J_{OF}\exp(CV)$

$C = \frac{1}{nkT} + B$

$J_{OF} = J_{OO}\exp(-\phi/kT)$

$\phi = fV_{bi} \quad f = n^{-1}$

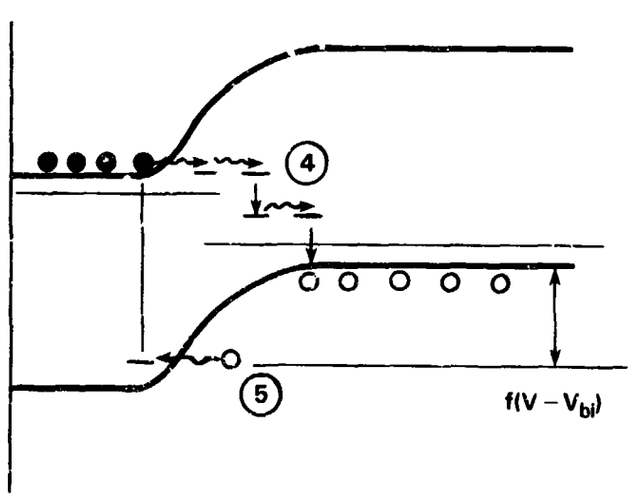

Figure 9. Summary Of Theory For Current Loss Mechanisms.

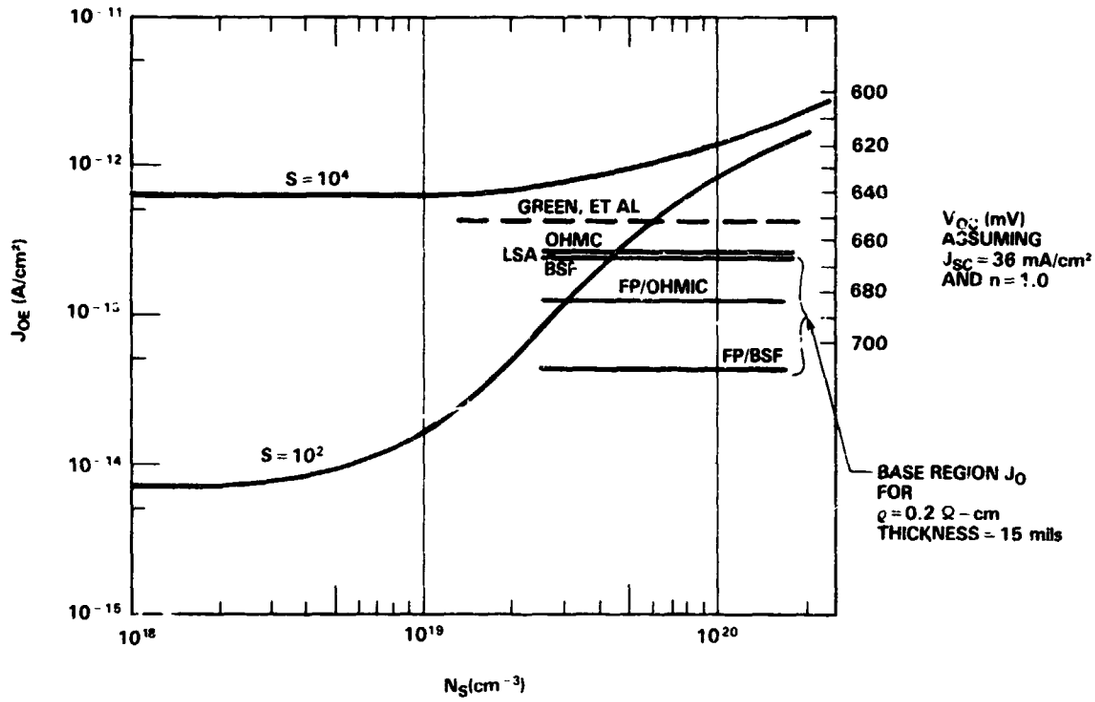

Figure 10. J_{OE} vs Surface Donor Concentration (N_S) For Range Of Values of Surface Recombination Velocity.

I-V RELATIONSHIP (V_j >> kT)

$I_{MEAS} = I_j + V_j/nkT$

$V_j = V_{MEAS} - R_S \; I_{MEAS}$

$I_j = I_{o1} \exp(BV_j) + I_{o2} \exp(V_j/nkT)$

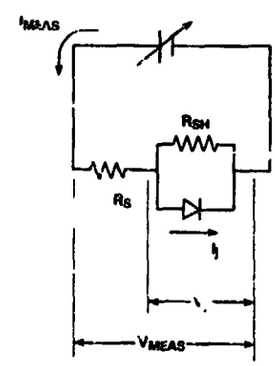

FITTING PROCEDURE

1. SELECT R_S AND R_{SH}
2. GENERATE (I_j, V_j)
3. CONSIDER (I_j, V_j) FOR REGION 1

   $I_j \approx I_{o1} \exp(BV_j)$

   $\text{Log}_e(I_j) = \text{Log}_e(I_{o1}) + BV_j$

   LEAST SQUARES FIT ⇒ I_{o1}, B
4. CONSIDER (I_j, V_j) FOR REGION 2

   $I_{j2} = I_j - I_{o1} \exp(BV_j)$

   $= I_{o2} \exp(V_j/nkT)$

   LEAST SQUARES FIT ⇒ I_{o2}, B
5. ITERATE BETWEEN REGIONS 1 AND 2 UNTIL ACHIEVE CONVERGENCE.
6. CARRY OUT STEPS 1 THROUGH 5 FOR ARRAY OF R_S AND R_{SH} VALUES. SELECT VALUES OF PARAMETERS WHICH PROVIDE BEST FIT TO DATA.

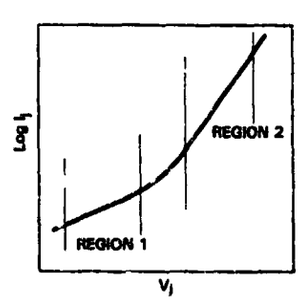

Figure 11. Approach To Dark I-V Analysis.

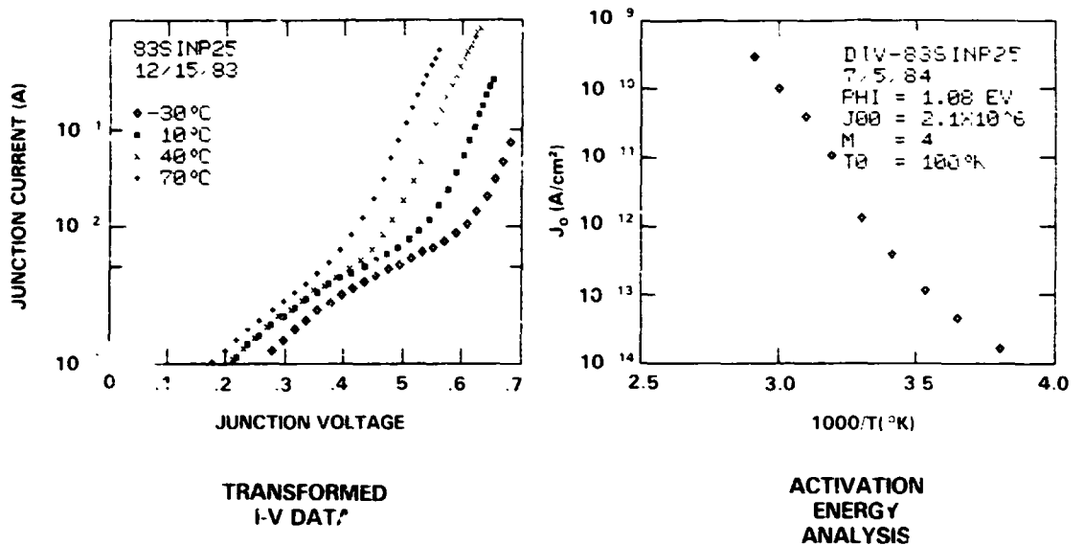

Figure 12. Current-Voltage Characteristics Of An MINP Cell Based On A Polished Substrate.

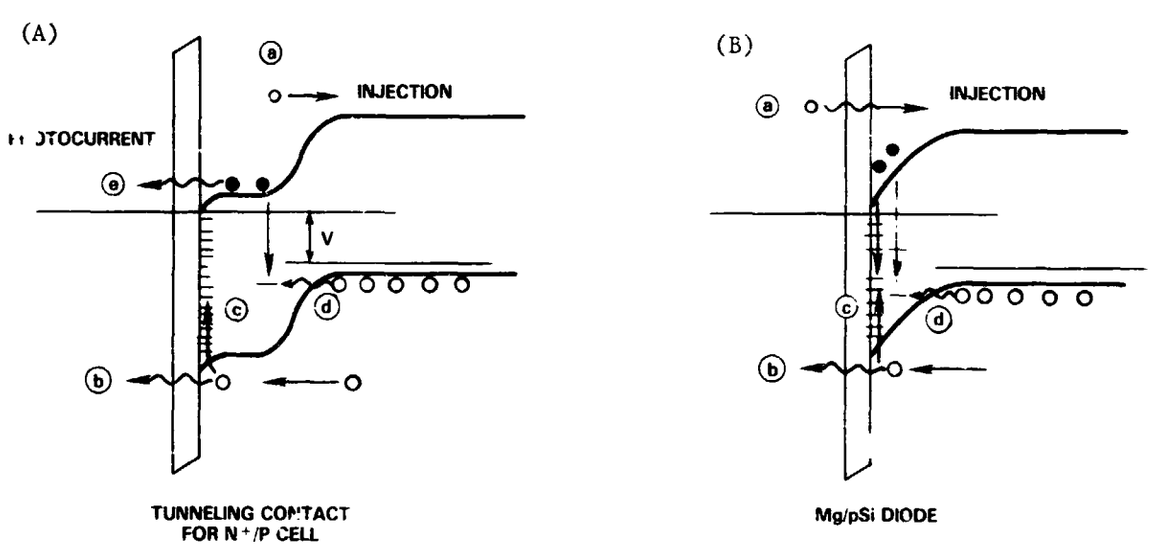

Figure 13. Electron Band Diagrams For Tunneling Contact On N^+ Surface, And MIS Device On A P-type Substrate.

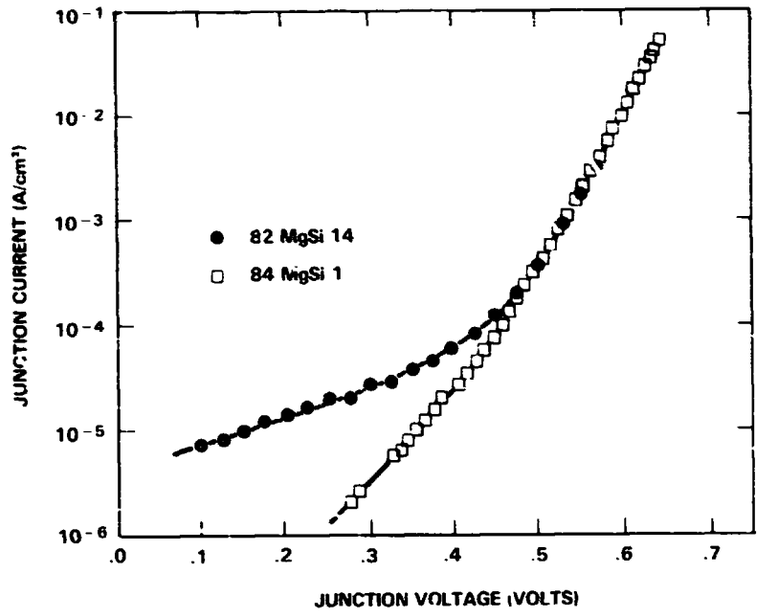

Figure 14. Current-Voltage Characteristics Of Mg/pSi MIS Devices Based On 0.2 Ω-cm Silicon.

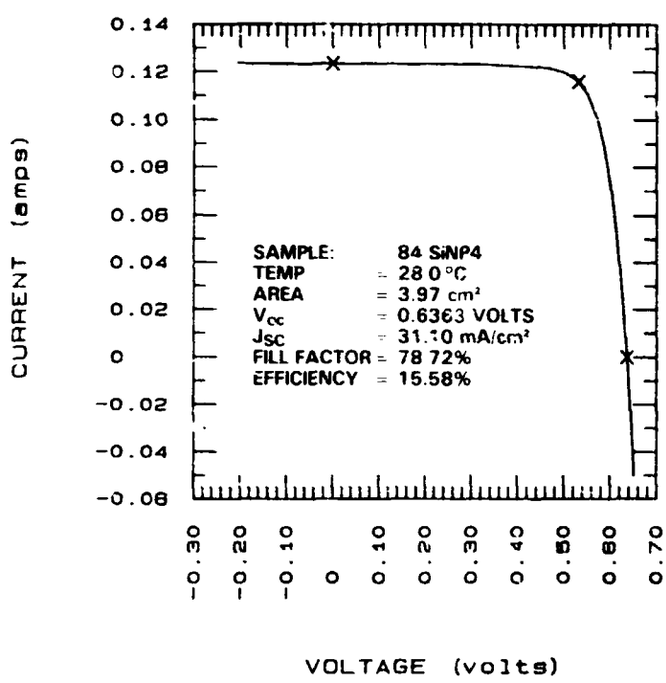

Figure 15. Illuminated Current-Voltage Characteristics Measured By SERI For MINP Cell With Polished Surface And SiO AR Layer.

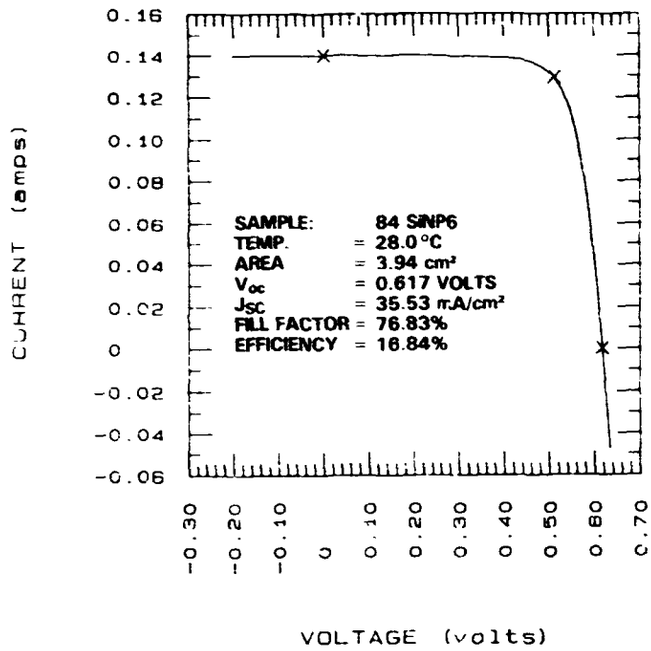

Figure 16 Illuminated Current-Voltage Characteristics Measured By SERI For MINP CELL With Textured Surface.

PROJECTED PERFORMANCE

TO ACHIEVE 20%

- MUST REDUCE J_{OE} BY DECREASING N_S AND S_p
- NEED SLIGHT IMPROVEMENT IN L

TO ACHIEVE 25%

- NEED F&P DIFFUSION LENGTH
- MUST REDUCE S_p TO 10^2
- WITH THESE VALUES OF L AND S_p, J_o WILL BE DECREASED TO $\geq 3 \times 10^{-14}$ A/cm²
- MUST USE DOUBLE AR WITH TEXTURED SURFACE OR WITH COMPLETE OPTICAL CONFINEMENT

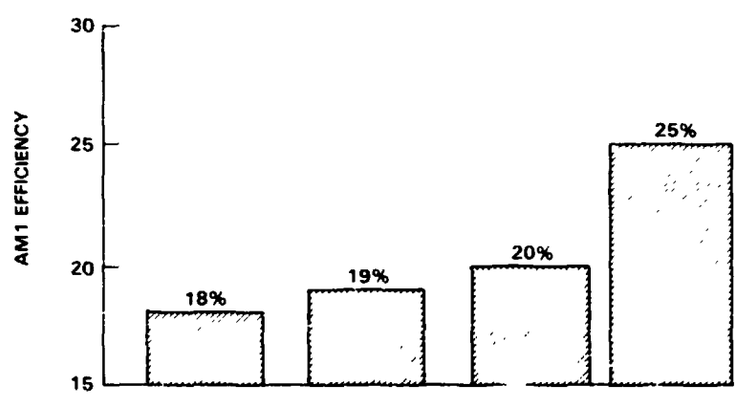

J_{SC}(mA/cm²)	36.0	36.0	36.7	40.9
V_{OC}(mV)	630	650	670	720
FF	.794	.812	820	.850
J_o(A/cm²)	1×10^{-12}	4.5×10^{13}	2×10^{13}	3×10^{14}
n-VALUE	1.0	1.0	1.0	1.0
N_S(cm^{-3})	6×10^{19}	4×10^{19}	2×10^{19}	2×10^{19}
SURF REC VEL	10^4	10^3	10^3	10^2
DIFF LENGTH	150	150	200	500 (F&P)
GRID SHADOW	4%	4%	3%	2%
CELL THICKNESS	15 mils	15 mils	15 mils	10 mils
BACK SURF	Ohmic	Ohmic	BSF	BSF

Figure 17. Estimated Property Improvements For High Efficiency MINP Cells.

DISCUSSION

SWANSON: How did you grow the thin oxides?

OLSEN: After we deposit aluminum to establish the back contact, a heat treatment at 500°C is carried out, and that process will grow a 20Å oxide.

SWANSON: Just from residual water, from the air?

OLSEN: Bill (Addis), why don't you comment on that?

ADDIS: The oxidation is carried out in a tube furnace.

SWANSON: Dry oxygen?

OLSEN: Yes.

SWANSON: Have you investigated different ways of forming the oxide and found whether any are better than others?

OLSEN: Not yet. We would like to try nitriding, and I have some thoughts on pursuing that further, but right now we have been going with the standard 20Å oxide.

SWANSON: Have you measured the contact resistance?

OLSEN: I think so. On the 0.3% area coverage, on a 2 x 2 solar cell, R_S is still below 0.1 ohm.

SWANSON: Doesn't seem good for concentrators.

OLSEN: Something seems to happen. It's strange; when the area goes down you get higher current density. The contact resistance goes down.

SWANSON: Did I read you correctly that you got a better J_0 without the n layer under there than you did with the n layer? You said 3×10^{-13} (A/cm^2).

OLSEN: No. That was for an MIS structure. Magnesium on p-type.

SWANSON: That is what I meant.

OLSEN: I think that is pertinent, mainly because it tells you something of the quality of the magnesium deposition and what it does to the p-type material. But it is a different situation, it appears, when you deposit onto an n-type surface. For a Mg/p-Si MIS diode, the value of 3×10^{-13} is approximately the theoretical value for J_0.

SWANSON: One would think you would want to take the n-layer out then, if it is--

OLSEN: Well, the problem with an MIS structure is the magnitude of photocurrent, which is too low. You just can't get adequate optical coupling, that is, transmission of the photons through the metal. Maybe something worth considering along the same lines is an inversion-layer cell. That is one without any doping done at all. That is something we have worked on in the past.

SWANSON: I sort of had the feeling that the phosphorus diffusion is not giving you the performance it could.

OLSEN: That's true. I think it is really hard to pin all this down. But I think it is clear that Green and his group have tailored their emitter to some degree and they have reduced the emitter recombination.

KEAVNEY: When you said you had 20 Å of oxide underneath the metal, I assume you measured that by ellipsometry.

OLSEN: That is right.

KEAVNEY: Do you have any ideas as to whether that is really 20 Å of oxide or whether there is an organic contamination throwing off the measurement?

OLSEN: The ellipsometry gives you 15 to 20 Å and it is not really clear what that means. You really have to couple that information with other information such as MIS current-voltage characterization. The MIS devices we have looked at are really high-quality ones. So that tells us that the interfacial layer is of high quality. Then, also, surface recombination effects in the solar cells themselves seem to be reasonable.

WOLF: It seems to me that Marty Green told us at the Photovoltaic Specialists Conference that his 19% cell was not an MINP structure but a dot contact structure. He had a new acronym for it too, PEST or something like that.

OLSEN: A dot contact cell, that is just what we made too. That simply means that you put slots in the thermal oxide on the surface, and the collector grid only contacts a small area. But the question is: what is the nature of his contact at the interface?

WOLF: That is right. That is what I thinking.

OLSEN: He didn't think it was MIS anymore?

WOLF: That was my impression.

OLSEN: I wouldn't argue about it. They do sinter, like the standard procedure. I think, in theory, titanium can be used as an MIS contact. It just may be very difficult to keep the oxygen out of it and get a decent contact. Maybe that is why you have to sinter. We have stuck with magnesium because it is not limiting us at this point and we haven't been motivated to change. But we are considering changing, because the use of magnesium impacts other processes. So we will move to try titanium as well, eventually.

WOLF: Another thing. I was a little surprised that you took the band gap as 1.2 eV. That is the zero Kelvin number. Really it is, at room temperature, more like 1.1.

OLSEN: I know that. But if you look at the band gap expression versus temperature, it is 1.2, minus some constant, times temperature. The constant times temperature divided by kT gives you an $e^{-constant}$ so that goes out into the pre-exponential number.

WOLF: So that is where you put it?

OLSEN: Yes. I hope that was clear to others. The band gap, I agree is 1.12, but it is the temperature dependence that I wanted to account for. An activation analysis gets 1.2 minus the bandgap narrowing.

QUESTION: (Inaudible; concerning the use of magnesium.)

OLSEN: No. We can't heat treat it. We haven't used titanium, but Green, for example, does heat treat at something like 450°C.

WOLF: I thought we might have some questions with respect to all the papers together, and overall comments on the afternoon session -- even the morning session -- before we break up. One comment I would like to make: I feel that what we really all sat and listened to this afternoon was perhaps more how do we model, what do we learn out of the modeling, and how does what we are doing actually relate to what we calculate? Rather than, really, concepts on how to get higher efficiency. So it seems to me it was more really modeling results and what did we learn from the modeling. I don't know whether that is challenging enough for more discussion or not. We certainly, some of us, use low-level modeling and get up to some point with that, and then comes high-level modeling beyond that. We will hear more about modeling tomorrow in any case.

LESK: I am still confused. In the back contact you had only BSF. Specifically, what is the difference between ohmic and a BSF back-surface contact?

OLSEN: Well, BSF refers to back-surface field. An adequate BSF yields a surface recombination velocity of zero.

LESK: I am not sure I got that right. In BSF -- in your equation you put S = 0 -- that means BSF?

OLSEN: That's right.

LESK: For ohmic, S is infinity but if you are maintaining the equilibrium in order to carry concentration to the back contact, that means ohmic. Is that the way it is used?

OLSEN: Yes. The point is with low-cost silicon sheet material, the use of a BSF makes little difference to current. But, if you increase the lifetime, then a BSF can have a significant impact on photocurrent.

WOLF: Are these things we are looking at here really all the approaches we can pursue to get to a higher efficiency? Are there things we should be looking at in addition? Does what we have been talking about really exhaust the methods available at this time?

SPITZER: I wanted to mention a few things. On the idea of how to improve efficiency, I think some people referred to this. We are neglecting lots of current. The theoretical limit is 44 and if you tune up the base diffusion length, that current could easily be raised from 36, which most people are achieving, to about 38 with a back-surface reflector and diffusion length of 300 micrometers, which doesn't seem that hard to do. And, say, with 38 milliamps/m^2 and a voltage of 660, with a fill factor of 0.8, that would be 20%. So I think some attention should be addressed to improving J_{sc}.

WOLF: It seems essentially that everybody who is working on high-efficiency cells sees how he can make the next step to get 20%. It seems that this is just about imminent. I think the big question after that becomes, how do we get to 22 or 23, and do we really have to get the trap densities down, or are there other remedial steps we can be doing to get the efficiencies up? Have we really exhausted all the cell-design approaches to a large enough degree for this next step?

SWANSON: I think the goal of 15% modules is rather modest in view of the 19% cells that are already being made.

WOLF: No.

SWANSON: We are talking efficiency, not getting cost down. But I think if you want to go to the 15% range, you should very seriously consider the Yablonovich design, which in my opinion has the potential of 25%.

WOLF: He combines again a number of the things we have been discussing, and also Dick Swanson. How to get high lifetime is one of his key aspects. How to get the lifetime up, how to get the surface recombination velocity down, use a wider band-gap material on one side, etc.

DYER: I have been out of this field for a number of years, but what are the difficulties with that overlap approach that someone mentioned earlier?

WOLF: It is called the shingling of cells.

DYER: What is the difficulty with that? You mentioned it, but I don't see any --

WOLF: Well, I don't think I mentioned that by saying there was a difficulty with it. It has been used for a long time in making submodules for space arrays. I guess it has given a certain amount of inflexibility within the array. One other approach was to make flexible interconnects, but still overlapping as far as individual soldering together is concerned.

DYER: Does it come out so it is not worth it, is what I am after.

WOLF: No.

DYER: Is it such that it is very successful and you can say, Well, we can gain back all that we devote to metallization, or is it not worth it?

WOLF: Well, you have no contact shading at all on the front, so you have all active surface that way. I see a little bit of a problem if the whole cell length is only 2 millimeters and then you overlap. You get quite a bit out of the horizontal with the whole thing, but I don't think that is too much of a problem area. You can somehow adjust for it again. No. I don't see a major problem with it. I guess from a manufacturing viewpoint it might be tough to make so many very small little devices and then assemble them into a bigger thing. It might give extra cost. But that's not fundamental. Somehow you can imagine some nice assembly machine that handles all these tiny little parts and makes a bigger thing out of it.

DINNER PRESENTATION

HIGH-EFFICIENCY SOLAR-CELL RESEARCH FOR SPACE APPLICATIONS

D. Flood, NASA Lewis
Research Center

HIGH EFFICIENCY SOLAR CELL RESEARCH FOR SPACE APPLICATIONS

Dennis J. Flood
NASA Lewis Research Center
Cleveland, Ohio

N85-31624

ABSTRACT

NASA involvement in photovoltaic energy conversion research, development, and applications spans over two decades of continuous progress. Led by the Lewis Research Center's Photovoltaic Branch, Agency programs in solar cell research and development have produced a sound technology base for a broad range of space applications. Although space power requirements are mission dependent, there are fundamental objectives which guide the NASA photovoltaic program. They are to improve efficiency, increase life, reduce mass, and reduce the cost of photovoltaic energy converters and arrays. Consequently, the programs in place at Lewis Research Center range from fundamental research on advanced concepts to technology advances for improving the space-worthiness of solar arrays. This paper will describe several key activities in the Lewis program.

INTRODUCTION

The cell research activities at Lewis divide roughly into the following categories: advanced devices, gallium arsenide and other III-V compound solar cells, and high efficiency silicon cells. Work in all of these categories will be described. Particular attention will be given to a new strategy for efficient solar energy conversion which seeks to overcome the fundamental limitations inherent with all semiconductor photovoltaic converters. The approach exploits a well-known mechanism for absorption of light in thin metallic films of common metals, such as aluminum or silver: the coupling of light to surface plasmons. Surface plasmons can have suitable ranges for energy transport, (up to centimeters in the IR), and can absorb from the ultraviolet to the infrared. Energy conversion then occurs by transfering the surface plasmon energy to an array of inelastic tunnel diodes, where a current of tunneling electrons can be created. Key technical barriers have been identified and will be discussed, along with recent results aimed at eliminating them.

The magnitude of NASA's photovoltaic space power activities can be seen in Figure 1. With the exception of the Skylab launch in 1973, most NASA missions have been at the 2 or 3 kilowatt level or below. Future NASA missions may be an entirely different story, however. The desire for more sophisticated, longer-lived missions will push power requirements up an order of magnitude and more. A low-earth orbiting manned space station, for example, might require up to 125 kilowatts of power in the station itself. This would, in turn, require a solar array output capacity in excess of 300 kilowatts, and would represent over two and one-half times the power generating capacity that NASA has launched in the past 20 years. Such an

array will be the dominant physical feature of the Space Station, and will place a premium on reducing the area, weight, and cost of large space arrays.

Future power requirements for geosynchronous applications are also expected to rise in the coming decades, although few such missions will be soley NASA's. The primary uses of GEO spacecraft will be for commercial and military communications networks. In these applications in particular, a premium is placed on higher efficiency, lighter weight, and longer life. Cost is important, but is not as important a driver as it is for large LEO arrays. A key figure of merit for GEO arrays is the ratio of power out to total array mass in W/kg. NASA's most recent GEO satellite, TDRSS, had an approximate beginning-of-life specific power of 35 W/kg, with a BOL power of about 3 kilowatts. Future communications satellite power requirements are expected to be from 3 to 5 times that level. Moreover, volume and weight constraints of current and proposed GEO launch vehicles make it desirable to increase both efficiency and specific power significantly beyond present levels. End-of-life specific powers approaching 250 W/kg may well be required to meet such constraints. The payoff will be measured directly in terms of increases in the active payload of the satellite.

The foregoing discussion is by no means exhaustive of all future space photovoltaic applications. It is intended only to put into context the rationale behind the current major thrusts of NASA's solar cell research and development program.

HIGH EFFICIENCY SILICON SOLAR CELL RESEARCH

Figure 2 summarizes the situation with regard to space solar cells since approximately 1960. Essentially, all space cells flown at that time were made from 10 ohm-cm starting material, and had AMO efficiencies on the order of 10 percent. Work in the early 1970's resulted in the COMSAT violet cell (Reference 1) with an efficiency approaching 15 percent, but it quickly became clear that higher efficiencies could not be achieved without improving the open-circuit voltage, and that could not be done without lowering the resistivity of the starting material. Current densities in the high efficiency 10 ohm-cm cells approached 50 ma/cm^2, and could not reasonably be expected to go much higher in that material. In the mid 1970's, therefore, Lewis Research Center initiated a concerted effort to develop an 18 percent AMO cell, which had been estimated by Brandhorst (Reference 2) to be the maximum practical efficiency for silicon. The effort concentrated on raising the open-circuit voltage to the 700 millivolt range. The initial work resulted in open circuit voltages of nearly 650 mV, but efficiencies were lower than desired because of the lower current-generating capabilities of the low resistivity cells.

Several techniques have been advanced for raising the voltage in low resistivity cells. Among them is the multi-step diffusion process developed at Lewis Research Center, which produced a Voc approaching 650 mV (Reference 3). The process was later used by COMSAT to produce a 14.5 percent AMO cell (Reference 4). This achievement was quickly followed by the development of cell designs at the University of New South Wales, under a NASA grant, which achieved 16 percent AMO, and Voc's approaching 680 mV. These cells, developed by Martin Green and co-workers (References 5, 6), have been

subjected to an intensive analysis at Lewis Research Center in an attempt to elucidate the mechanism(s) responsible for their improved performance. That work, reported by Weizer (Reference 7) at the last Photovoltaic Specialists Conference, has produced some surprising results. In brief, it was shown that:

1. It is not the perfection of the emitter, but a previously unrecognized improvement in the base that is responsible for the high Voc's obtained in the MINMIS cell.

2. The high voltage in the MINP cell is the result of the same improvement in the base as in the MINMIS cell, coupled with a reduction in the emitter Io.

3. The enhanced base characteristics of both cell designs are the result of a reduced minority carrier mobility in the starting silicon material used for these cells.

Based on these results, it now appears that voltages approaching 800 mV are achievable in 0.1 ohm-cm silicon cells with full utilization of the MINP surface passivation techniques. AMO efficiencies approaching 20 percent may yet be possible in silicon. Work toward that goal will be continued in the Lewis Research Center program.

III-V CELL RESEARCH

Emphasis in the NASA solar cell research program has shifted from silicon during the past few years to the wide variety of semiconducting compounds formed from elements in columns three and five in the periodic table. The program ranges from basic materials science to pre-pilot cell design optimization studies. The activities fall roughly into three categories: (1) GaAs concentrator cells; (2) thin film cells; and (3) multi-junction cells. Resistance to the damage caused by charged particle radiation in the natural space environment is a major consideration in the III-V cell area, and along with efficiency, forms an important part of the justification for it.

NASA's interest in III-V concentrator cells arises in part because of their potential for lowering the cost of very large solar arrays, such as are anticipated for a future Space Station. Figure 3 summarizes the results of a study of multi-hundred kilowatt array designs (Reference 8). The plot of combined cell and component costs versus concentration ratio shows the existance of a broad minimum between approximately 20x and 200x. Figure 4 illustrates a concentrator design currently under development at TRW, under contract to Marshall Space Flight Center. Specifications for this miniature cassegrainian system call for a 4 mm diameter cell capable of 20 percent at 125x and 85°C. Lewis Research Center has two contracts in place, one with Varian and one with Hughes Research, to design and produce such cells. With 19 percent already demonstrated, there appear to be no apparent technical "show-stoppers" which will prevent realization of the program goal of 22 percent at operating conditions. This application dramatically illustrates the higher efficiency and higher temperature capabilities of GaAs compared to silicon. GaAs concentrator cells will have over twice the efficiency of

silicon at the operating temperatures projected for this array design. The physical dimensions of the cell are illustrated in Figure 5. The diameter of the illuminated area is 4 mm, while the length of one edge is 5 mm. The approximately 60 to 1 reduction in processed semiconductor area compared to a planar of equal output is the primary reason for the projected lower cost of this array design. An additional assumption, of course, is that the cost per unit area of the concentrator optics will be significantly lower than the equivalent area of processed semiconductor material. The anticipated cell output at operating conditions is approximately 0.4 watts. Based on informal estimates, the projected cost of such cells could be on the order of 30 to 50 $/watt.

Cost is not the only reason for interest in concentrator arrays for space application. A second very important reason, again depending on mission requirements, is the inherent shielding provided by the concentrator element against the natural radiation environment encountered in many orbits. Although not important for LEO applications, the design may make possible the use of photovoltaic power generators in some of the mid-altitude orbits that have previously been dismissed because of their high density radiation environment. Beyond that, if high efficiency can be coupled with lightweight concentrator optics, such arrays could eventually be flown in GEO.

Research on thin film solar cells is directed toward improving their performance, not only in terms of their efficiency, but also in terms of their radiation resistance. An important thrust for the NASA space power program is the development of technology for the next generation of GEO communications spacecraft. At present, about 23 percent of the satellite mass launched to orbit must be dedicated to the power system, which is approximately the same fraction that is available for the payload itself. The benefits derivable from reducing the power system mass are directly translatable into revenue for commercial satellites, and into increased capability for non-commercial satellites. One approach under investigation at the present time for producing ultralightweight solar cells is the CLEFT process developed at the Lincoln Laboratory by John Fan and co-workers (References 9, 10, 11, 12). Progress in this area is well-known, and a detailed discussion need not be included here. The NASA goal is to demonstrate a 4 micron thick GaAs cell with at least 20 percent AMO efficiency, which suffers no more than a 10 percent loss of power after 10 years of exposure to the GEO radiation environment. The goal is ambitious, but achieving it could result in significant reductions in the mass of the solar array for GEO systems. The cell development work at Lincoln Laboratory is supported at Lewis Research Center by in-house cell evaluation measurements and radiation damage studies. The best cell specific power demonstrated to-date is 5400 watts/kg, achieved with a 5.5 micron thick cell with gridded back contacts with an AMO efficiency slightly greater than 14 percent. A cross-section of the cell is shown in Figure 6. The illuminated area is 0.51 cm^2. There are many technological challenges to overcome before the CLEFT cell can be considered a viable candidate for use in space. Chief among them are the following: development of a UV-resistant adhesive to use in the film transfer process; improving the open-circuit voltage and fill-factor; establishing the radiation tolerance of the cell; and perhaps the most formidible among them, developing a suitable interconnect technology for joining 5 micron thick cells together in an array!

As is well-known, the efficiency of a typical single junction solar cell is limited fundamentally by the location of its bandgap within the solar spectrum, in this case the air mass zero (AMO) spectrum. Early calculations of multi-bandgap cell efficiencies at AMO (Reference 13) indicated that a total conversion efficiency of approximately 30 percent could be achieved in a three-cell stack under 100x illumination. The cell structure initially selected by NASA is shown in the first column of the table below, and was driven by the assumed requirement that the structure had to be lattice-matched throughout. The second column shows the current distribution of bandgaps for the structure, and is a result of the successful demonstration of composition grading between the various active layers of the cell. The latter technique allows for greater flexibility in the choice of bandgaps to achieve short-circuit current matching from each constituent cell in the stack. The lower bandgaps should produce a slightly higher efficiency than those of column one, and should make fabrication of the tunnel junction between the bottom and middle cells somewhat easier. (The high doping densities required for a tunnel junction interconnect are easier to achieve in a lower bandgap material.) The interconnect between the middle and top cells can be some sort of metal interconnect, such as the Varian-developed MIC (Reference 14).

TABLE 1

Multi-Junction Cell Bandgaps

Cell	L-M	C-G
Lower	1.15	1.15
Middle	1.55	1.43
Upper	2.05	1.95

An interesting simplification of the above structure is to use just two junctions, and to mechanically stack them. As has been pointed out by Fan (Reference 15), such a structure can be either a two, three, or four terminal device, without introducing much complexity into its fabrication. The monolithic stack, on the other hand, is most easily made into a two terminal device. There is some loss of efficiency in the AMO spectrum for a two junction cell, but there may also be a trade-off in the radiation hardness of the two structures which favors a two-junction, four terminal device. If the end-of-life performance of a series-connected multi-junction cell is to be maintained at reasonable levels, it becomes necessary to develop constituent cells which degrade by in a matched fashion in a radiation environment. Although possible in principle, it presents a formidable challenge to realize in practice. A four terminal device avoids the requirement for current-matching altogethers and does not, therefore, suffer any additional degradation beyond that of each of the constituent cells.

ADVANCED CONCEPT SOLAR CELLS

The calculated efficiency of an ideal cascade solar cell reaches a maximum when more than six bandgaps have been included in the stack, and can approach 60 percent in the AMO spectrum (Reference 16). Taking the real system losses into account, however, shows that the maximum has been passed

after three bandgaps have been included (Reference 17). As mentioned above, the practical maximum AMO efficiency of a three cell stack is expected to be 30 percent, even under 100x illumination. The question that naturally arises is whether that efficiency limit, which appears to be inherent with semiconductor p-n junctions, can be transcended by some means. The problem is that the ordinary p-n junction solar cell in effect converts the incoming broadband solar radiation into a flow of monoenergetic electrons (and holes), the energy of which is determined by the semiconductor bandgap. While the coupling mechanism, i.e. the creation of electron-hole pairs, is broadband in nature, the excess kinetic energy imparted to the electron-hole pairs by photons with energies greater than the bandgap is essentially not transportable. It is lost in collisions with lattice phonons in a matter of picoseconds, resulting in very short ranges for the excited carriers. An initial requirement, then, for any major increase in efficiency, is to identify a mechanism for broadband absorption of the solar spectrum which creates a corresponding spectrum of electronic excitations in the absorber with ranges long enough that energy can be extracted from them. Thin films of common metals such as silver, aluminum, and gold can support a quantized, oscillatory excitation of their two-dimensional quasi-free electron gas known as a surface plasmon. The surface plasmons are produced by exterior electric fields incident on the boundary between the metal film and a dielectric medium. For large wave vectors the plasma waves behave like real surface waves: their electromagnetic field is concentrated around the boundary within a distance of approximately 10 angstroms. For small wave vectors the fields extend far into space, and resemble more and more those of a photon propagating along the boundary. The surface plasma wave behaves very much like a guided electromagnetic wave in a dielectric waveguide, except that the waveguide in this case is a metal film, and therefore very lossy. The latter fact limits the range of the surface plasmons at the high energy end of the spectrum to distances on the order of 70 to 100 microns. Propagation lengths for surface plasmons in the infrared, however, can approach several centimeters (Reference 18). A large body of literature exists which describes the properties of surface plasmons, and discusses several experiments in which they can either be observed or utilized. (See e.g., the monograph by Raether, Reference 19). The coupling between surface plasmons and photons can be very strong under the proper conditions, and is well understood theoretically. It can be shown that only the p-polarized component of the incident radiation can be coupled to a smooth film for example, and in such a way that the width of the acceptance angle is very small. In addition, the acceptance angle itself varies with wavelength. Such properties have all been verified experimentally.

Conceptually, the direct conversion of solar energy to electricity requires the following processes: photon absorption, which either creates "free" charges (electron-hole pairs, photoelectrons, etc.) or imparts kinetic energy to a charge carrier (the surface plasmon, e.g.); and charge separation. The latter occurs by creating a potential barrier for some of the charge carriers while others are allowed to pass (the p-n junction for electron-hole pairs, e.g., and a tunnel diode for energetic electrons). If photon absorption does not occur in the region where the charges are separated, then energy transport must occur from the absorption region to the barrier region. Charge collection and flow in an external circuit complete the picture. Since the surface plasmon is a quantized, collective oscillation of a two dimensional electron gas, the momentum imparted to the

surface plasmon by the incoming photon must be transferred to a mobile, free electron below the surface before any charge separation can occur. The latter requires, therefore, some sort of interaction mechanism between the surface plasmon and a free electron.

It is clear from the preceeding discussions that any attempt to create a solar energy conversion device based on surface plasmon absorption of the solar spectrum must address for key technical barriers: (1) broadband coupling of sunlight to surface plasmons at a single acceptance angle; (2) low-loss energy transfer from the absorption to the barrier region; (3) coupling between the surface plasmons and mobile charge carriers in the region of the potential barrier; and (4) efficient charge transfer from the low to the high energy side of the potential barrier. A possible approach for dealing with the fourth problem involves inelastic electron tunneling through a thin film metal-insulator-metal structure. If the film thicknesses have been properly chosen, such a structure supports a coupled mode between surface plasmons in both metal films. This coupled mode, or junction plasmon, is able to propagate along the length of the structure, and by virtue of the strong electric field it creates in the oxide, can provide an inelastic tunneling channel for an electron impinging on the barrier at that instant. Preliminary calculations conducted at Lewis Research Center indicate such a mechanism, while possible in principle, is beset with difficulties. Not the least among them are the need to limit the reverse tunneling current to acceptably low levels, and the very limited range of the junction plasmon in general (typically a few tenths of a micron). A suitably chosen semiconductor thin film can be incorporated on the low energy side of the junction in such a way that its bandgap eliminates the final states for the reverse tunneling process, but the impact of doing so on the ability of the structure to support a junction plasmon is unknown at present. In order for the process to go at all, it is first necessary to transfer energy from the surface to the junction plasmons. Here the problem is that the junction plasmon has a much lower velocity than a surface plasmon of the same frequency, so some sort of momentum-matching transfer mechanism is required. Figure 7 shows schematically one possibility. Calculations show that a grating can promote energy transfer between monoenergetic surface and junction plasmons with better than 90 percent efficiency (Reference 20). The feasibility of doing the same with a broad spectrum of plasmons has yet to be firmly established. The proposed approach in effect uses a junction plasmon as an intermediary between the surface plasmons and tunneling electrons. What is still required, however, is experimental verification of the approaches that have been outlined here.

Mechanisms which affect surface plasmon coupling and range (barriers 1 and 2) are relatively well-known and understood. Recent results for the latter obtained in the NASA program are summarized in Figure 8 (Reference 21), which contains a plot of surface plasmon range as a function of wavelength with film thickness as a parameter. The structure for which the propagation distances have been calculated is shown in the inset. An important result is that the calculated damping matches experimental results on dirty films, and seems to indicate that ohmic losses have been overestimated in previous calculations. A series of experiments aimed at exploring surface plasmon propagation in such structures has been started. The initial work will investigate the so-called end-fire coupling technique for injecting surface plasmons into the structure shown in Figure 8. The

technique is well-known in integrated optics. Instead of matching the incident field to a surface plasmon wave vector along the direction of propagation, the field distributions are matched across the end face of the sample. That is, the incident field is focussed onto the end face of the structure with a field distribution which matches as closely as possible that of a surface plasmon. In addition to investigating the generation of long-range surface plasmons, the same experiments will investigate the coupling efficiency of the technique. The results of a first order perturbation theory calculation are shown in Figure 9 (Reference 22). The salient point is that an optimized incident field distribution yields a greater than 80 percent coupling efficiency for a silver film for wavelengths from 0 4 microns to more than 1.2 microns, and as the figure shows, the efficiency is relatively independent of the incident spot size. This approach has several important features. For example, all of the modes originate at the same point, and therefore the propagation distance can be used to discriminate wavelength regions for absorption. In addition, the beam shaping and focussing can be done by external, miniature optics. Both of these have impact not only on the experimental efforts just described, but also on the actual configuration of such a device should it become a reality. Is is conceivable, for example, that such a device could be used in the miniature cassegrainian concentrator system described earlier in this paper.

A second approach for investigating the coupling of sunlight to surface plasmons is shown schematically in Figure 10. In this approach, the film on which surface plasmon generation is desired is evaporated onto a glass prism, and is covered with a dielectric layer onto which a metal-island film is then evaporated. The effect of the island film is to broaden the acceptance angle from a few tenths of a degree to as much a five degrees at half-maximum in the absorption (Reference 23). The measurements also show that as much as 90 percent of the p-polarized component of the top quarter of the solar spectrum can be absorbed by a silver island-film, with similar results for the mid-quarter with a gold island film. The results can be explained in terms of an incident radiation field interacting with dipole located near a conducting thin film, with suitable modifications which take the macroscopic size of the metal-island into account. By combining measurements of the surface plasmon dispersion curve for a silver film and measurements of the dipole frequency shifts (isolated dipole vs. a dipole near a conducting film) with theory, the coupling efficiency between the radiation field and surface plasmons can be estimated. (The dipole absorbs energy from the normally-incident, unpolarized light beam and loses it by one of three processes: reradiation; surface plasmon generation in the thin film; and ohmic heating.) The earlier reflectivity data indicated that as much as 97 percent of the indicent radiation was absorbed by a silver island film. However, the detailed calculations indicate that a maximum of about 40 percent of the total incoming energy is transfered to surface plasmons in the underlying silver film (Reference 24). Moreover, the maximum is a function of both the wavelength of the incident light, and of the spacer-layer thickness. An important feature of this approach, however, is that both the s and p polarizations can couple to the structure. Additional work is required to assess the importance of the shape of the metal-islands on the absorption, and to determine the optimum structure for maximum efficiency.

As the preceeding discussion demonstrates, there are several key barriers that must be addressed just to determine the feasibility of a surface plasmon solar converter. Although we have made strides in our basic understanding of many of them, the final outcome is far from clear. Work will continue on the key questions that have thus far been identified. If and when any technical "show-stoppers" are identified, the progran will be brought to an end. Until such time, however, the effort presumes success.

CONCLUSION

The NASA space photovoltaic research and technology program has its roots in the days of the first real solar cell. In the three decades since then (1954-1984), the Agency's program has not only developed technology for the current generation of photovoltaic power systems in space, it continues to lay foundations for the future. A key element in the success of the NASA program is its overriding philosophy that the most important driver is high efficiency. Without exception, program objectives are to achieve high cell efficiency first, and to address balance-of-system considerations second. The success of this approach is attested to by the many applications of space photovoltaics, from NASA to military to commercial missions. Once the path to high efficiency has been demonstrated, additional developments follow which reduce it to practice in a cost-effective manner. In many instances those developments are encouraged with government funding. In many other instances such developments have occurred at the initiative of the commercial sector. The net result has been steady progress for nearly three decades.

References

1. J. Lindmayer and J.F. Allison, Ninth IEEE Photovoltaic Specialists Conference, 1973

2. Henry W. Brandhorst, Jr., "Silicon Solar Cell Efficiency - Practice and Promise," Ninth IEEE Photovoltaic Specialists Conference, 1973

3. M.P. Godlewski, T.M. Klucher, G.A. Mazaris, and V.G. Weizer, "Open Circuit Voltage Improvements in Low Resistivity Solar Cells," Fourteenth IEEE Photovoltaic Specialists Conf., 1980

4. R.A.Arndt, A Meulenberg, J.F. Allison, and V.G. Weizer, "Advances in High Output Voltage Silicon Solar Cells," Fifteenth Photovoltaic Specialists Conf., 1981

5. R.B. Godfrey and M.A. Green, "High Efficiency Silicon MinMis Solar Cell Design and Experimental Results," IEEE Trans. Electron Devices, vol. ED-27, pp. 737-745, April, 1980

6. A.W. Bakers and M.A. Green, "678-mv Open-Circuit Voltage Silicon Solar Cells," App. Phys. Lett., vol. 39, pp. 483-485, 15 Sept., 1981

7. V.G. Weizer, C.K. Swartz, R.E. Hart, and M.P. Godlewski, "Voltage Controlling Mechanisms in Low Resistivity Silicon Solar Cells - A Unified Approach," Seventeenth Photovoltaic Specialists Conf., 1984

8. "Study of Multi-Hundred Kilowatt Solar Arrays for Earth-Orbital Applications," NASA Contract #NAS8-32986, Final Report

9. John C.C. Fan, C.O. Bozler, and R.L. Chapman, Appl. Phys. Lett. 32, 390, 1978

10. John C.C. Fan, "GaAs Shallow Homojunction Solar Cells" NASA CR-165167, 1980

11. R.W. McClelland, C.O. Bozler, and J.C.C. Fan, Appl. Phys. Lett. 37,560, 1980

12. J.C.C. Fan "High Efficiency, Low Cost Thin GaAs Solar Cells," NASA CR-168265, 1982

13. T.J. Maloney, Solar Energy Mater. 4, 359, 1981

14. P.G. Borden, et al, "Progress Toward Cascade Cells Made by OM-VPE," Proceedings of a Conference on Space Photovoltaic Research and Technology, Lewis Research Center, Cleveland, Ohio, 1982

15. J.C.C. Fan, "Optimal Design of High Efficiency Single-Junction and Tandem Concentrator Space Cells at 80C and 100 Suns," Proceedings of a Conference on Space Photovoltaic Research and Technology, Lewis Research Center, Cleveland Ohio, 1983

16. N.A. Gokcen and J.J. Loferski, "Efficiency of Tandem Solar Cell Systems as a Function of Temperature and Concentration Ratio," Proceedings of a Conference on Solar Cell High Efficiency and Radiation Damage, Lewis Research Center, Cleveland, Ohio, 1979

17. A. Bennett and L.C. Olsen, "Analysis of Multiple Cell Concentrator Photovoltaic Systems," Thirteenth IEEE Photovoltaic Specialists Conference, 868, 1978

18. A.S. Barker, Jr., Phys. Rev. B8, 5418, 1973

19. H. Raether, "Surface Polaritons," edited by V.M. Agranovich and D.L. Mills, North Holland Press,New York, 1982

20. Lynn Anderson, private communication

21. G. Stegeman, NASA Grant NAG3-250, private communication

22. G. Stegeman, NASA Grant NAG3-250, private communication

23. W.R. Holland and D.G. Hall, Phys Rev. Lett. 52 #12, 1041, 1984

24. D.G. Hall, private communication

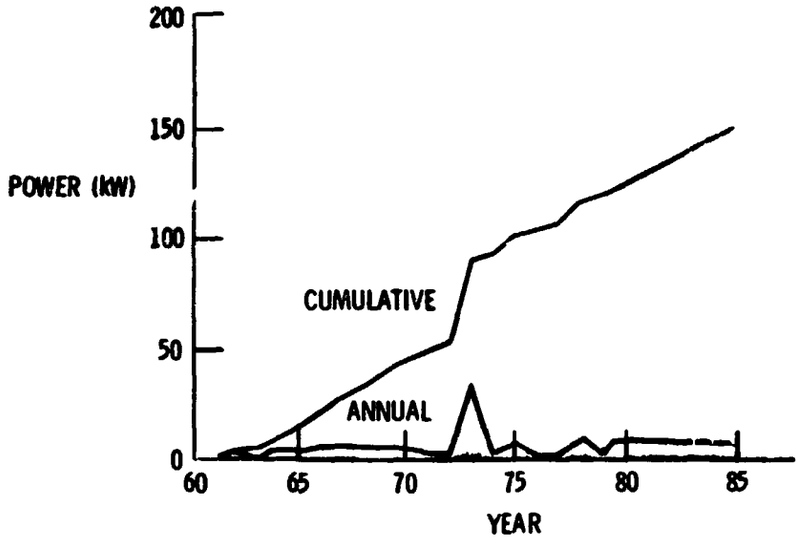

Figure 1. Total Space Power Launched for NASA Missions.

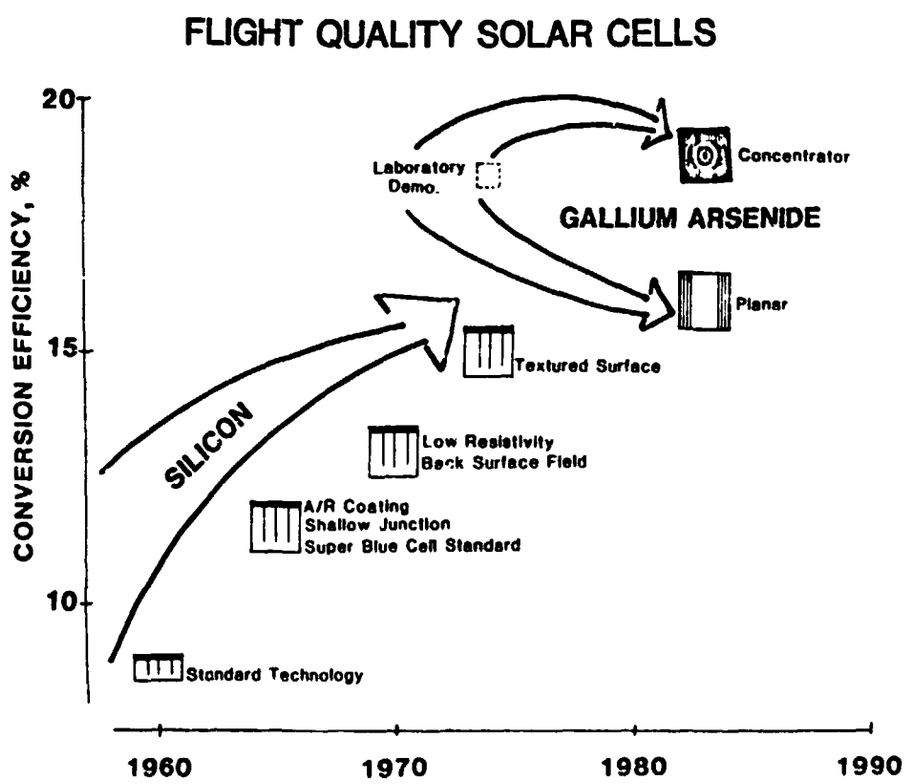

Figure 2. Space Quality Solar Cell Technology.

ORIGINAL PAGE IS
OF POOR QUALITY

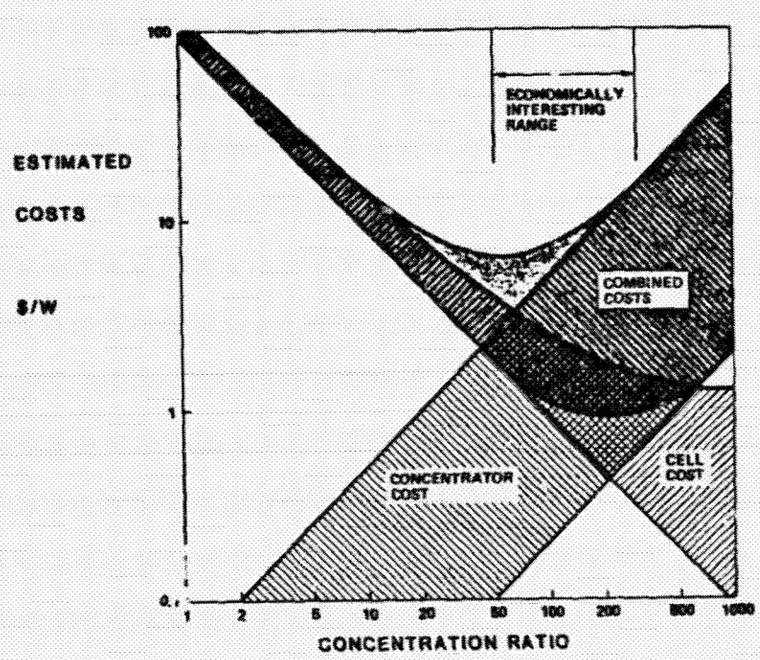

Figure 3. Array Component Costs Versus Concentration Ratio.

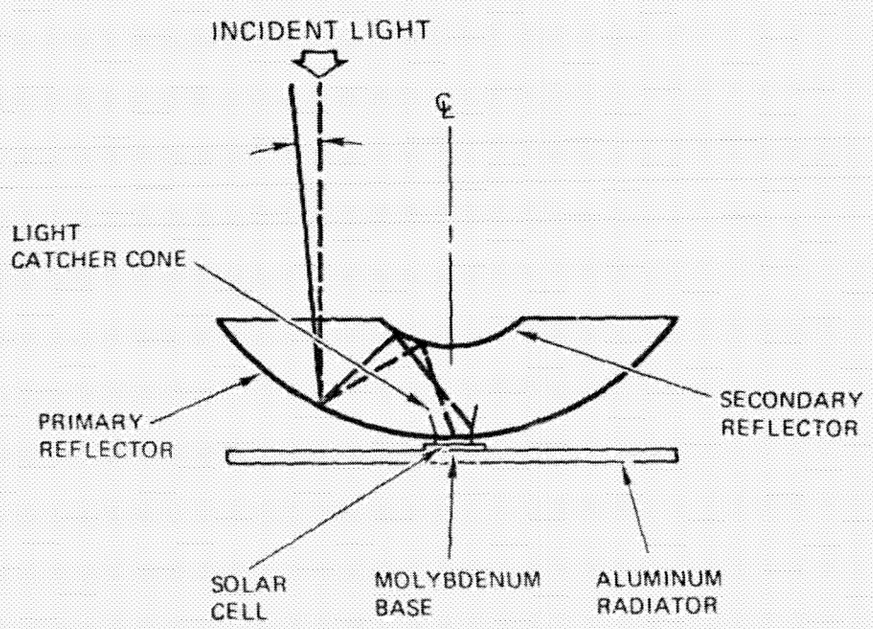

Figure 4. Miniature Cassegrainian Concentrator Concept.

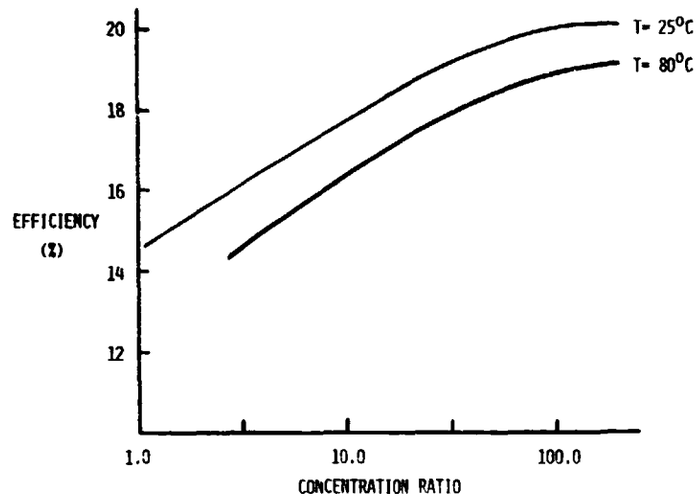

Figure 5. Miniature Concentrator Cell Efficiency vs. Concentration Ratio (AMO).

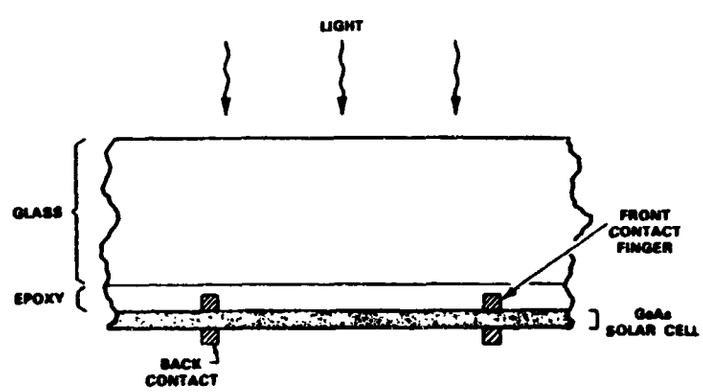

Figure 6. CLEFT Cell Cross Section.

ORIGINAL PAGE IS
OF POOR QUALITY

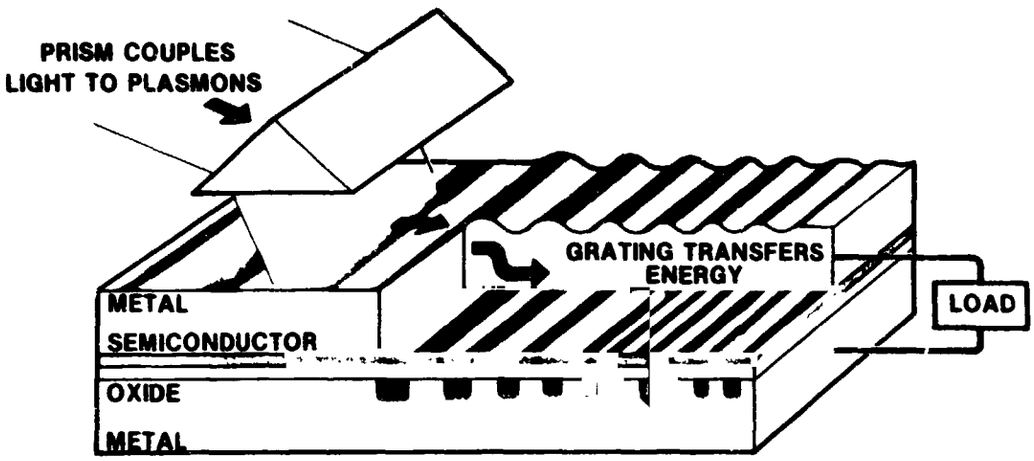

Figure 7. Surface to Junction Plasmon Grating Coupler Concept.

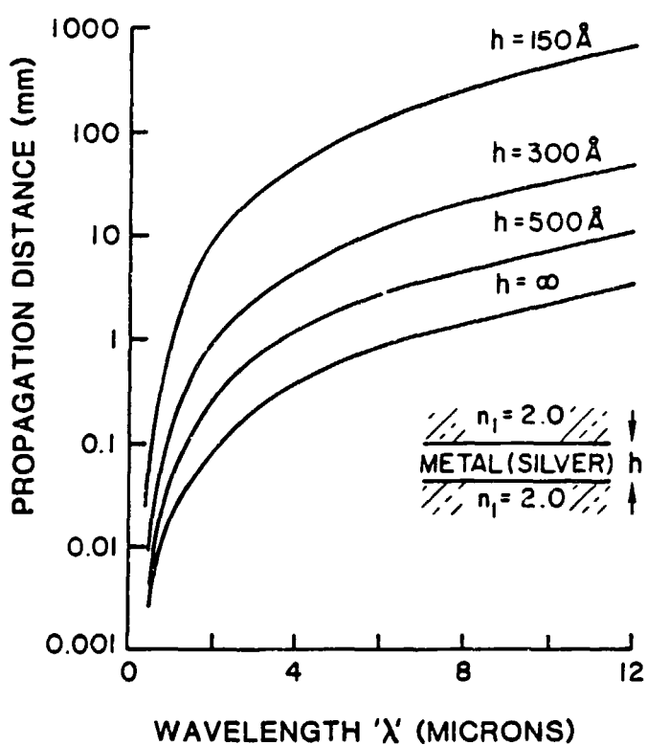

Figure 8. Surface Plasmon Range.

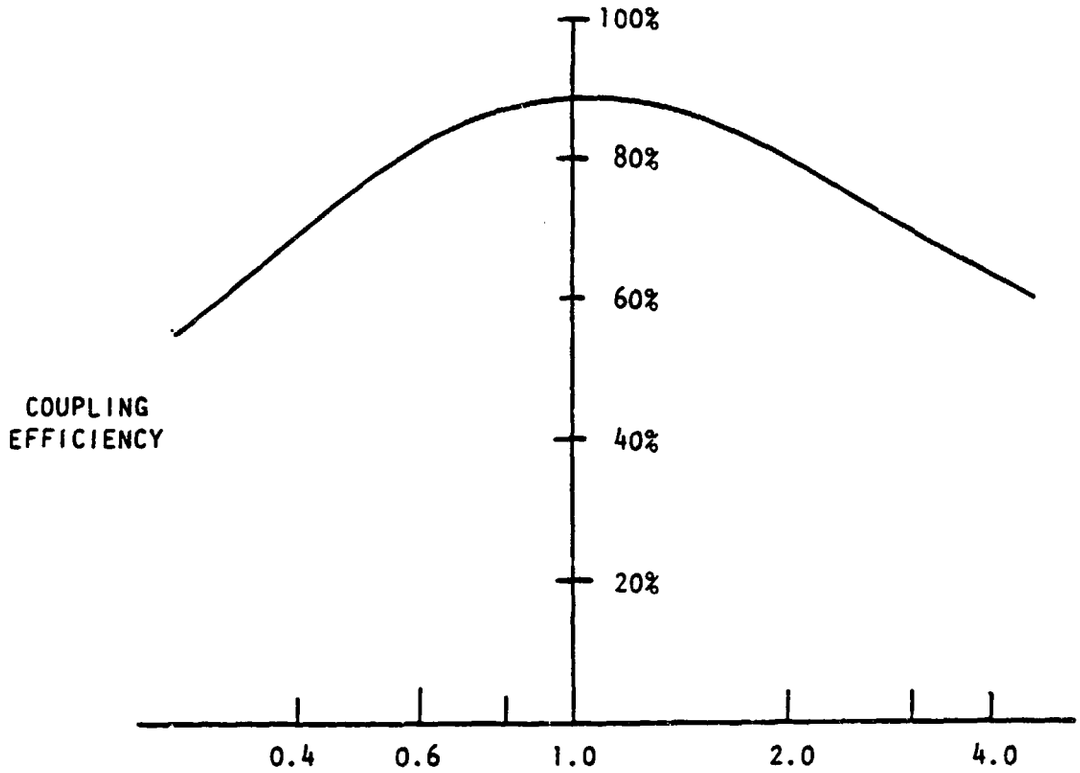

Figure 9. Endfire Coupling Efficiency as a Function of the Ratio R of the Beam Width Plasmon Field Penetration Depth.

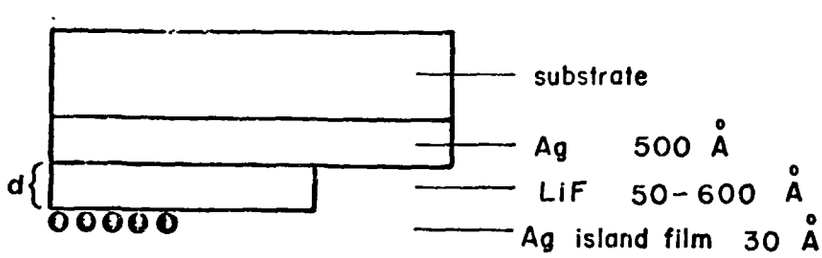

Figure 10. Light Coupling by Metal-Island Films. Sample Cross-section at Top. Measurement Schematic at Side.

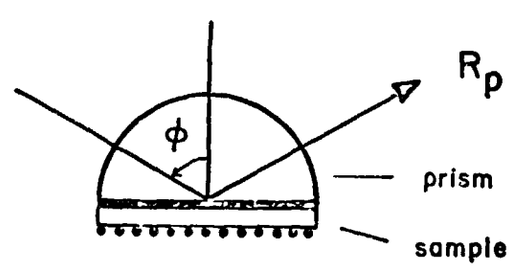

SESSION III

SURFACE-INTERFACE EFFECTS

L. Kazmerski, Chairman

N85-31625

NEW ADATOM MODEL FOR Si(111) 7X7 AND Si(111)Ge 5X5 RECONSTRUCTED SURFACES

(Initially published in Phys. Review B, Vol. 30, No. 8, 15 October 1984)

D.J. Chadi

Palo Alto Research Center
Xerox Corp.
Palo Alto, California 94304

A new adatom structure with significantly less angular strain than the simple adatom geometry is proposed. The model involves a rebonding of ≈1/8 of surface atoms to the substrate in a manner similar to that occurring in the π-bonded-chain structure for the Si(111) 2X1 surface. The interference between adatom and substrate reconstructions forces the smallest threefold-symmetric unit cells to be 5X5 and 7X7 in size. The proposed reconstructed-adatom model gives rise to structural features in good agreement with experiment. In particular, the inhomogeneous corrugation of the two halves of the 7X7 unit cell seen in vacuum-tunneling microscopy and the apparent need for stacking fault sequences in tunneling experiments are accounted for. The results of surface energy and structure calculations on 2X2, 3X3, 5X5, and 7X7 adatom models are presented.

I. INTRODUCTION

The first real space imaging of the 7X7 reconstructed Si(111) surface by Binnig et al.[1] has generated new interest in the precise nature of the atomic bonding at this surface. Vacuum-tunneling microscopy[1] reveals 12 maxima in the unit cell and deep holes at the corners and sides of the unit cell with a corrugation as large as 2.8 Å. Except for a corner site, the lateral positions of the maxima coincide with the adatoms of Harrison's model[2] and the vacancies of the Lander model.[3] Binnig et al [1] suggested that the deep and inhomogeneous corrugations of the surface should be explainable by a simple relaxation or modification of the Harrison adatom model. The nature of the modifications to be made has remained unclear, however, because tunneling microscopy does not provide direct information on the surface bonding geometry even though it yields valuable information on the surface corrugation.

Despite the fact that the adatom model gives the best agreement of any simple structure with the vacuum-tunneling results, it has not received universal acceptance as the correct structure for the 7X7 surface. This is primarily because it is presently unclear whether this model is consistent with other experimental data or with theoretical considerations. For example, complementary information on the surface atomic structure from a recent analysis[4] of Rutherford backscattering experiments[5,6] indicates that the . . . ABCABC . . . stacking sequence, characteristic of face-centered-cubic crystals, may be broken at the surface. Additional evidence for stacking faults or surface dislocations has been deduced from low-energy-electron diffraction (LEED) data,[4] and from transmission electron microscopy.[7]

Several models[8-10] which incorporate stacking fault sequences in the unit cell and have structural features consistent with the observations of Binnig et al.[1] have been proposed recently and will be examined in this paper.

The acceptance of the adatom model for the 7X7 surface appears difficult also from theoretical considerations. The surface energy of the thermodynamically stable 7X7 surface should be lower than that of the metastable cleaved 2X1 surface. In particular, the 7X7 surface should have a lower surface energy than the π-bonded-chain structure.[11,12] In going from a chain to an adatom structure, the favorable energy lowering from π bonding is presumably lost and, in addition, a significantly larger lattice strain is introduced. The recent calculations of Northrup and Cohen[13] for a 2X2 adatom model indicate, however, that the lowering of the dangling-bond density by a factor of 2 is sufficient to compensate for most of this energy loss. The 2X2 adatom model is found to be 0.12 eV (per 1X1 unit area) higher in energy than the π-bonded structure. This energy, although comparable in size to the magnitude of typical surface reconstruction energies, is sufficiently small that it makes further investigations of the adatom model necessary.[13]

In addition to constraints from vacuum-tunneling microscopy,[1] ion-channeling[4] and surface-energy considerations the model for the annealed (111) surfaces of Si and Ge has to account for a large body of other experimental data. These include nucleation of the 7X7 structure at steps;[14] the appearance of stable 5X5 and 7X7 periodicities[15] for Sn on Ge(111) and[16] for Ge on Si(111) surfaces; the similarities and differences in the photoemission[17-19] and optical-absorption[20,21] spectra of 2X1 and 7X7 surfaces; evidence for unique surface and subsurface hydrogen chemisorption sites on the 7X7 surface;[22] the possibility of magnetic ordering at low temperatures;[23] and a unique physisorption site geometry[24] for Xe and Kr.

In this paper the structural and energetic aspects of the 7X7 and 5X5 reconstructions are examined via total-energy calculations on a variety of models and on unit cells ranging from 2X2 to 7X7 in size. Large unit cells were used to eliminate uncertainties regarding the influence of unit-cell dimensions on the magnitude of the relaxation energy for any particular model, and because for the adatom geometry proposed in this paper, the minimum unit cell size is 5X5.

The paper is organized as follows. The results of energy-minimization calculations for the conventional type of adatom model are discussed in Sec. II. For the particular case of a 2X2 rectangular lattice, the results are compared with those from ab initio self-consistent pseudopotential calculations of Northrup and Cohen.[13] The surface energy for this structure is taken as a reference for comparing the differences between various structures discussed in this and subsequent sections.

The possibility of substrate reconstruction involving a rebonding of atoms (as opposed to simple atomic relaxation) is discussed in Sec. III. The motivation for this is the reduction of the large angular strains present in the conventional adatom model. The smallest structure for which this is possible is a rectangular 2X2 lattice. For this lattice, the results are found to be only marginally better than the old rectangular adatom model.

Surprisingly, as shown in this section, it is found that as a result of the interference between the adatom and substrate reconstructions, hexagonal 2X2, 4X4, and 6X6 periodic structures are not possible for the new geometry. If the structure is required to have threefold symmetry, then the smallest hexagonal nXn unit cells are 5X5 and 7X7. A 3X3 structure lacking the threefold symmetry is calculated to have a much higher surface energy than the conventional adatom model. The reduced surface energy of larger unit cells is not primarily a result of the rotational symmetry but arises from a removal of constraints inherent in smaller lattices.

The results of calculations on the new 5X5 adatom geometry and a discussion of experimental results on the 5X5 and 7X7 structures are presented in Sec. IV where it is shown that the model gives the following.

(i) A surface corrugation consistent with that observed in vacuum-tunneling experiments.[1] It provides an explanation for the inhomogeneous corrugation of the surface by having different relaxations and reconstructions in the two halves of the unit cell.

(ii) Structural elements resembling those arising from stacking faults at the surface.[4] These come about directly as a consequence of the rebonding occurring in the substrate layer and are in good agreement with structural features deduced from ion channeling.

(iii) A lowering of the surface energy making the new structure energetically competitive with the π-bonded chain model[11,12] for the 2X1 surface.

(iv) An explanation for the striking similarity in polarization and angular dependence of normal photoemission spectra for the surface states at $\approx$0.8 eV below the Fermi energy E_F in both the 2X1 and 7X7 surfaces.[17,18] Measured relative to the valence-band maximum[19] instead of E_F, this state is $\approx$0.3 eV more bound in the 2X1 surface than in the 7X7 surface. The new adatom model provides a simple explanation for this energy difference.

(v) Specific surface sites where hydrogen chemisorption is most likely to occur. It is proposed that hydrogen chemisorption at these sites leads to a large decrease of the surface energy.

(vi) A greatly enhanced interaction among distant dangling bonds as compared to the simple adatom model. This suggests that a magnetic ordering of spins should make a small but non-negligible contribution to the stability of 5X5 and 7X5 structures.

The results of calculations for Himpsel's trimer model[8] are discussed in Sec. V. The tight-binding-based method of calculation[25] is reviewed briefly in Sec. VI.

II. SIMPLE ADATOM MODELS

A. Angular strains

Two adatom models with rectangular and hexagonal 2X2 unit cells are shown in Fig. 1. In the "-1" configuration where all bond lengths are equal to

those in the bulk, the adatom is one interlayer spacing (≈0.78 Å in Si) above the substrate. The large angular strains in this simple adatom configuration can be appreciated by considering the distributions of angles θ at the fourfold-coordinated surface atoms capped by the adatom. At each one of these second-layer atoms, there are three angles with the values of

$$\theta = 180^{\circ} \text{ and } \theta_2 = \theta_3 = 70.53^{\circ} \tag{1}$$

which deviate sharply from the ideal tetrahedral angle of 109.47°.

The adatom models shown in Fig. 1 are for the situation where the adatom is on a "hollow" site. If the adatom is placed on a site above a second-layer atom, then larger angular strains in addition to large bond-length strains develop.

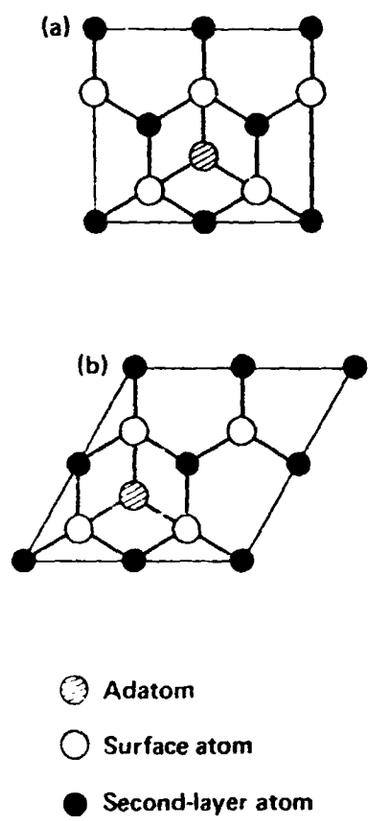

Fig. 1. Top views of simple adatom models with rectangular and hexagonal 2X2 periodicities are shown in (a) and (b). In the unrelaxed geometry, the adatom falls the intersection of the three straight lines joining surface atoms to second-layer atoms. The resulting 180° angles go to 160°-165° after relaxation.

The surface energy of the top-site geometry is sufficiently higher than the hollow-site configuration[13] that it will not be considered in this paper. The top-site geometry is also inconsistent with the results of vacuum-tunneling microscopy.[1]

It may be argued that relaxation of surface atoms will result in a large decrease of the angular strain energy. However, the present calculations for lattices from 2X2 to 7X7 in size show that the angles in Eq. (1) relax at best to values of 160° and 81°, respectively. The angular relaxation is achieved at the cost of increasing the adatom-substrate bond length by ≈4.5% over the bulk bond length. For a 2X2 hexagonal lattice, the reduction in total energy resulting from relaxation is about 1.4 eV per adatom.

Considerations based on the angular strain energy of the adatom model suggest that this energy can be decreased appreciably if the equilibrium adatom-substrate bond length is larger than the underlying bulk bond length. A larger bond length prevents the adatom from falling on a straight line with surface and second-layer atoms, thus decreasing θ_1 from 180°. For the Ge(111)-Sn and Si(111)-Ge systems where the Ge-Sn and Si-Ge bond lengths are both larger than substrate bond lengths, other possibilities for the optimization of the angular distributions exist if an intermixing of the different atomic species takes place. The Ge(111)-Sn adatom model is discussed below in Sec. C. The role of misfit strain energies in the reconstruction of annealed surfaces has been discussed by Phillips.[26]

B. Surface energy of the rectangular 2X2 adatom model from tight-binding and pseudopotential calculations

Northrup and Cohen[13] have recently calculated the total-energy and atomic structure of a rectangular 2X2 adatom model [see Fig. 1(a)] using the self-consistent pseudopotential method. They find that the relaxed adatom geometry has a surface energy lower by 0.17 eV/(1X1 unit cell) relative to the unrelaxed ideal 2X2 surface and higher by 0.19 eV/(1X2 unit cell) as compared to Pandey's π-bonded chain geometry.[11,12] The removal of the lateral strains and frustrations inherent in the rectangular 2X2 lattice, which can be achieved, for example, by going to a hexagonal lattice, was proposed to lead to an even more stable adatom geometry. The present calculations, as described in more detail below, confirm this picture and show that a reduction of 0.05 eV/(1X1 unit cell) occurs in going from the rectangular to the hexagonal adatom geometry.

The atomic and electronic structure of the adatom geometry obtained from the two calculations are in generally very good agreement. However, the tight-binding calculations presented here for various adatom geometries predict the relative surface-energy differences between various adatom geometries more accurately than the differences between dissimilar geometries such as the ideal surface and the adatom geometry. This is because the limited sp^3 basis set used in the calculations is too small to adequately account for the large angular strains present in adatom models. Compared to pseudopotential calculations,[13] the energy of the optimized rectangular adatom model is calculated to be 0.03 eV/(1x1 cell) higher than that of the unrelaxed ideal surface instead of 0.17 eV/(1X1 cell) lower. Despite this problem of the tight-binding method in underestimating the binding energy of an adatom, it is expected to be more useful and accurate in comparing the relative energy differences between similar types of adatom structures considered in this paper. Defining γ as

$$\gamma = \text{surface energy (in eV/1X1 unit cell)} \qquad (2)$$

and taking the rectangular 2X2 lattice as reference, in the following sections the changes $\Delta\gamma$ in surface energy relative to the value for this lattice are given. On the basis of Northrup and Cohen's calculation,[13] a decrease in γ of greater than 0.19 eV/(1X1 cell) should make the adatom geometry more favorable than the π-bonded-chain model.

C. Results of calculations on Si(111) adatom models

1. Rectangular 2X2 cell

The adatom and three substrate layers were allowed to relax. The optimum atomic geometry was calculated from a minimization of Hellmann-Feynman forces.[25] In the unrelaxed geometry the adatom is approximately 0.78 Å above the surface layer. After relaxation, the adatom moves away from the surface by an extra 0.39 Å. This is in good agreement with the 0.33 Å calculated by Northrup and Cohen.[13] The present tight-binding calculations give a bond-length stretching of 4.9% at the surface as compared to 3.4% obtained previously.[13] Some angular distributions, with the pseudopotential values given in parentheses, are

$$\theta = 94.7^{\circ},\ 94.7^{\circ},\ 97.5^{\circ}\ (98^{\circ}) \tag{3}$$

about the adatom, and

$$\theta = 163^{\circ},\ 165^{\circ},\ 81^{\circ},\ 78^{\circ}\ (165^{\circ},\ 169^{\circ},\ 79^{\circ},\ 79^{\circ} \tag{4}$$

around the surface atoms capped by the adatom. Much smaller maximal angular deviations of $+12^{\circ}$ and -5° from the ideal tetrahedral value occur about atoms on the second and third layers at the surface, respectively. The rectangular lattices lead to lateral strains and frustrations which are expected to be less severe in the hexagonal 2X2 cell discussed below.

2. Hexagonal 2X2 cell

The use of a hexagonal instead of a rectangular cell is calculated to lead to an energy lowering of 0.2 eV/adatom or equivalently to a change in surface energy of

$$\Delta\gamma = -0.05\ \text{eV/(1X1 unit cell)}. \tag{5}$$

This can be attributed to a slight decrease of the angular and bond-length strains on this surface. The adatom-surface bond length is stretched by $\simeq$4.4% (as compared to $\simeq$4.9% before) and the angular distributions are

$$\theta = 95^{\circ} \tag{6}$$

about the adatom, and

$$\theta = 160.4^{\circ},\ 81.4^{\circ} \tag{7}$$

around the surface atoms capped by the adatom. Smaller deviations of $+10^{\circ}$ and -4° from the ideal tetrahedral value are also found in the second and third layers below the surface.

The 0.05-eV drop per 1X1 unit cell in the energy of the 2X2 hexagonal cell relative to the rectangular geometry brings the energy of this structure to within 0.14 eV/atom of the π-bonded-chain structure. The question, therefore, arises as to whether the use of larger unit cells will lead to a further reduction of this energy.

3. Ge(111)-Sn: 2X2 adatom model

The addition of a fraction of a monolayer of Sn to the Ge(111) surface is known[27] to result in a metastable 2X2 structure before the formation of stable 5X5 and 7X7 patterns.[15,27] The larger covalent radius of Sn compared to Ge reduces the angular strains. For the optimum hexagonal 2X2 geometry, the Sn adatoms are calculated to be 1.6 Å above the Ge surface. The optimization of structure leads to a Sn-Ge bond length of 2.73 Å which is 4% larger than the sum of the respective covalent radii. The angular distributions are

$$\theta = 88.6^{\circ} \tag{8}$$

on the adatoms, and

$$\theta - 157.3^{\circ},\ 83.2^{\circ} \tag{9}$$

on the substrate atoms capped by Sn. As shown in Sec. IV, a reconstruction of the subsurface leads to a lowering of the energy and results in a larger unit cell This is consistent with the observed [27] metastability of the 2X2 reconstructed Ge(111)-Sn structure.

4. 5X5 and 7X7 adatom models

Simple adatom models with 5X5 and 7X7 unit cells, with, respectively, 6 and 12 adatoms per cell, were examined to test whether the greater degrees of freedom for atomic relaxation would lead to a lower surface energy. No restrictions on the atomic displacements were imposed. Each surface atom was moved in the direction of the Hellmann-Feynman forces[25] acting on it by an amount proportional to the force. New forces were then calculated and the process was repeated. The most extensive tests were made on 5X5 lattices. The adatoms as well as the first three atomic layers at the surface (i.e., a total of 81 atoms per cell) were allowed to relax. After many iterations, the surface energy of the 5X5 adatom structure was calculated to be ≈0.04 eV/atom lower than that of the hexagonal 2X2 structure. About 10 iterations were also made for the 7X7 structure. Because of the large size of the unit cell, only the 12 adatoms and the first surface layer were allowed to relax. From the magnitude of the Hellmann-Feynman forces acting on the atoms, it can be estimated that the structure and surface energy of the 7X7 lattice will be nearly the same as that of the 5X5 lattice. It appears that an increase in unit-cell size will not result in a sufficiently large decrease in the surface energy of the adatom model to explain the occurrence of such superstructures on annealed surfaces. For the simple adatom model, a 4X4 unit cell should be nearly as likely to occur as a 5X5, 6X6, or a 7X7 cell.

III. NEW ADATOM MODEL

A. Rectangular 2X2 cell

The simple adatom model leads to three highly strained 180° angles per adatom in the ideal structure where all bond lengths are equal to the bulk value. As shown in Sec. II, atomic relaxations lead to somewhat reduced angular strains and to values of around 160° for these angles. A reconstruction mechanism that leads to a further reduction in the strain energy resulting in angles of ≃135° is demonstrated in Fig. 2 for the case of a rectangular 2X2 lattice. The reconstruction involves a rebonding of the "rest" atom (i.e., the surface atom not capped by the adatom) to the substrate in a manner similar to that occurring for the π-bonded chain model.[11,12] The reconstruction results in a reversal of the coordinations of the rest atom and a second-layer atom: The rest atoms become fourfold coordinated by becoming, in essence, a second-layer atom bonded to a third-layer atom, and the second-layer atoms becomes like a threefold-coordinated first-layer atom. The top views of the ideal and reconstructed surface are depicted schematically in Figs. 2(a) and 2(b); the corresponding side views are shown in Figs. 2(c) and 2(d). It can be seen that the reconstruction improves the values of two out of three ≃180° angles at the surface. There does not appear to be any simple way of reducing all the strains via reconstruction. The reconstruction shown in Fig. 2(b) improves the bonding of the adatom to the substrate by forcing two of the dangling bonds to become better aligned with the adatom. An optimization of the structure also shows reduced bond-length strains. The adatom substrate bond length is calculated to be ≃3.5% longer than the bulk value (instead of ≃4.9% before the reconstruction). The model has mirror reflection symmetry through a plane passing through the adatom.

The constraints on atomic relaxations inherent in a rectangular 2X2 rectangular lattice are found to limit the energy reduction from rebonding to ≃0.06 eV/adatom. The energy of the new structure is, therefore, still ≃0.14 eV/adatom higher than that of the simple hexagonal 2X2 adatom structure discussed in Sec. II. One reason for the relatively high energy of the new structure is that the release of the strains at the surface creates additional stress at subsurface layers. The 2X2 lattice does not allow a satisfactory relaxation of these layers that will lead to a significant reduction of the surface energy. The new adatom geometry leads to an enhanced interaction between the dangling bonds on adatoms and rest atoms. For the particular case of the rectangular 2X2 geometry, this does not lead to a lowering of the electronic energy because the term involving this interaction has a zero sum over the two-dimensional Brillouin zone. The predicted higher surface energy of rectangular versus relaxed or reconstructed hexagonal 2X2 cells is consistent with the experimental observation[27] of only the latter periodicity for the Ge(111)-Sn 2X2 system.

B. Hexagonal 2X2, 4X4, and 6X6 cells

The new reconstructed type of adatom model, surprisingly, rules out hexagonal 2X2, 4X4, or even 6X6 unit cells. This results from the requirement that the adatom should always be kept threefold coordinated. As shown in Fig. 3 for the hexagonal 2X2 case, this condition is incompatible with the

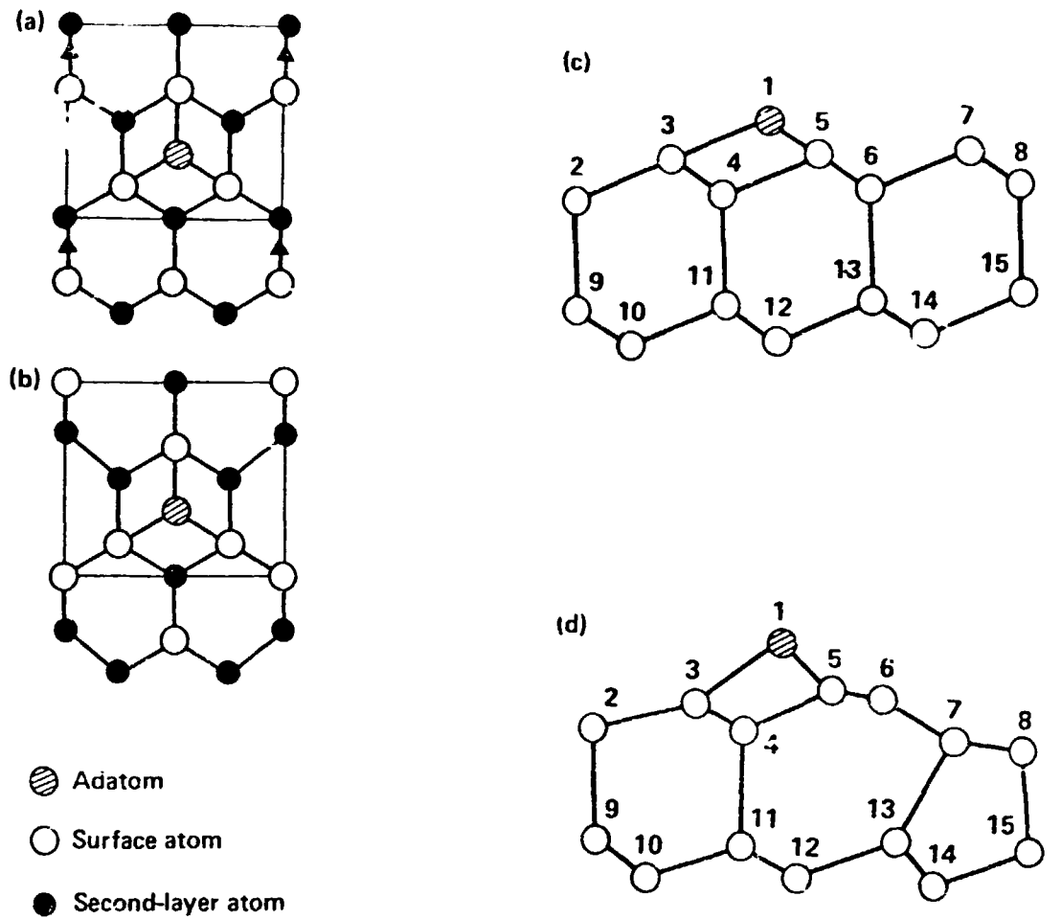

FIG. 2. Arrows in (a) show the top view of the directions of surface atomic displacements leading to a reconstruction of the simple 2X2 rectangular adatom model. The resulting structure is shown in (b). The rebonding is similar to that occurring in the π-bonded-chain reconstruction of the Si(111) 2X1 surface. It transforms 2/3 of the $\simeq 165^{\circ}$ angles to $\simeq 135^{\circ}$. The corresponding side views of the ideal and reconstructed surfaces are shown in (c) and (d).

periodicity of the unit cell. The rebonding of the rest atom (i.e., atom 3 in Fig. 3) to the substrate does not lead to relaxation of any of the $\simeq 180^{\circ}$ angles created by the adatom. To reduce these angles, it is necessary to rebond type-1 atom to the substrate. This, however, would result in the adatom becoming twofold coordinated, raising the surface energy considerably. It is simply not possible to keep the adatom threefold coordinated and, simultaneously, relax the angular strains in a hexagonal 2X2 lattice. Exactly the same type of problem persists for the larger 4X4, 6X6, and possibly other 2nX2n hexagonal cells. This aspect of the new adatom model is in sharp contract to the conventional adatom geometry where 2nX2n periodicities can be easily achieved.

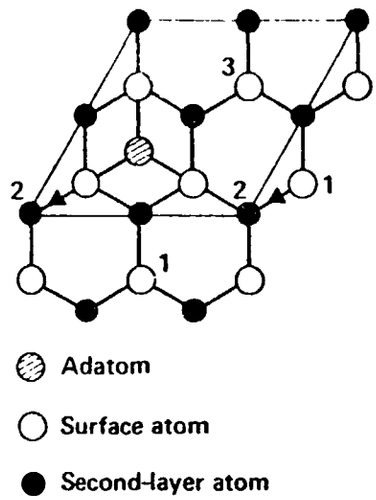

FIG. 3. This top-view figure illustrates that a rebonding of atoms, of the type shown in Fig. 2 for the rectangular 2X2 cell, is not possible for the hexagonal 2X2 cell. In order to get a reduction in the angular strain energy, it would be necessary to move atom 1 in the direction shown and make it a second-layer atom while making atom 2 a first-layer atom. This would result in the adatom becoming twofold coordinated, leading to an increase in the surface energy. It can be seen that the rebonding of "rest" atom 3 does not lead to any lowering of the strain energy.

C. Hexagonal 3X3 lattice

The smallest hexagonal nXn lattice for the reconstructed adatom model is 3X3 in size, as shown in Fig. 4. The directions of surface atomic displacements leading to the reconstruction of the substrate are indicated by arrows in Fig. 4(a) and the resulting structure is shown in Fig. 4(b). The optimized structure is calculated to have a surface energy 0.5 eV/(3X3 unit cell) higher than for the relaxed but unreconstructed adatom geometry. One reason for this is the extremely large bond-length strains (≈6.4% and 5.7%) at the surface resulting from reconstruction. These are the largest strains for any of the adatom models examined. Another reason for the high surface energy is that reconstructions transform only 2/9 of the 160°-180° angles to $\approx 135^{\circ}$ as opposed to 2/3 of such angles in the rectangular 2X2 case. In addition, the reconstructed 3X3 adatom model cannot be made to have the threefold symmetry of the underlying substrate.

IV. 5X5 AND 7X7 RECONSTRUCTED (111) SURFACES

A. Reconstructed adatom model

The smallest unit cells for which the reconstruction of the adatom model can be made to have threefold rotational symmetry are 5X5 and 7X7 in size. The presence of this symmetry is accompanied by the removal of frustrations encountered in smaller unit cells. The directions of motion of surface-layer

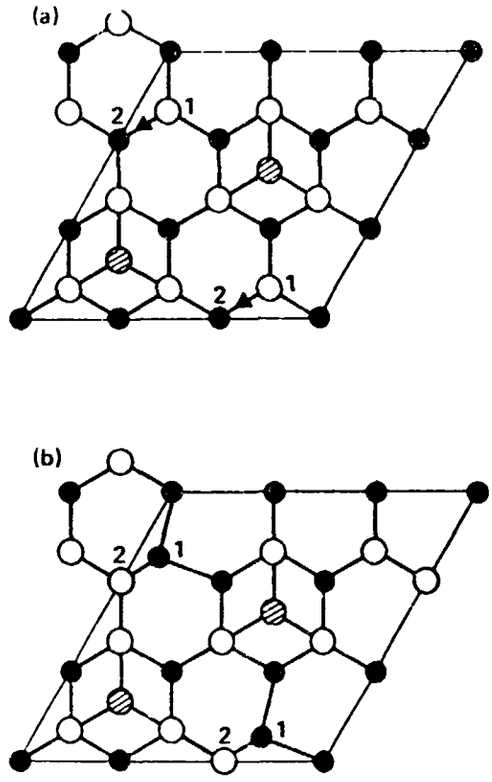

FIG. 4. Top views of the Si(111) 3X3 surface are shown. The reconstructed 3X3 adatom model has a mirror plane going through the long diagonal but it lacks threefold rotational symmetry. The directions of atomic motions leading to a reconstruction of the substrate is shown in (a) and the resulting structure is shown in (b). Only one $\simeq 165^{\circ}$ angle is transformed to a $\simeq 135^{\circ}$ angle for each rebonding, as opposed to twice as many in 5X5 and 7X7 lattices. The atomic designations are the same as in Figs. 1-3.

atoms (i.e., rest atoms) which bond to the substrate to form the modified adatom model are shown by arrows in Figs. 5(a) and 6(a). The fraction of surface atoms participating in the reconstruction of the adatom model is nearly 1/8 in both the 5X5 and 7X7 structures. The rebonding of each atom transforms two 160°-180° angles into $\simeq 134^{\circ}$ angles. The lateral positions of the adatoms on the left triangular region of the 5X5 structure are calculated to be modified by $\simeq 0.05$ Å relative to their ideal values as a result of this rebonding. No such change occurs on the right triangular section.

The requirement that every adatom should be close to a boundary of the unit cell (such that a reconstruction of the underlying surface similar to those for the 5X5 and 7X7 surfaces can occur) rules out adatom models with marginally larger (e.g., 9X9) unit cells. For the 5X5 and 7X7 structures, the short diagonal of the unit cell is equivalent to a boundary line of the cell as a result of threefold rotational symmetry. All the adatoms within the

structures are, therefore, adjacent to a boundary. For larger cells, a number of adatoms would be forced to the interior of the unit cell and away from the boundaries. This would raise the surface energy since comparable reconstruction of the substrate could not occur for these atoms.

The release of strain energy associated with the reconstruction of the substrate is calculated to be large locally. Each rebonding is calculated to release ≈0.7 eV in energy. This value is obtained by comparing the total energy for the optimized conventional 5X5 adatom model with that obtained for the new 5X5 structure. The latter has a surface energy which is lower than the reference rectangular 2X2 lattice (see Sec. II) by

$$\Delta\gamma \simeq -0.14 \text{ eV/(1X1 unit cell)}. \tag{10}$$

The simple reconstruction of just the left half of the 5X5 lattice goes a long way towards the ≈-0.19 eV/atom needed to make the adatom model competitive with the chain model for the 2X1 cleaved surface. Because of the depth of the reconstruction, it is not presently feasible to do any meaningful calculations on the new 7X7 structure. It is assumed here that the results of the calculations on the 5X5 surface are applicable for the most part to the 7X7 surface.

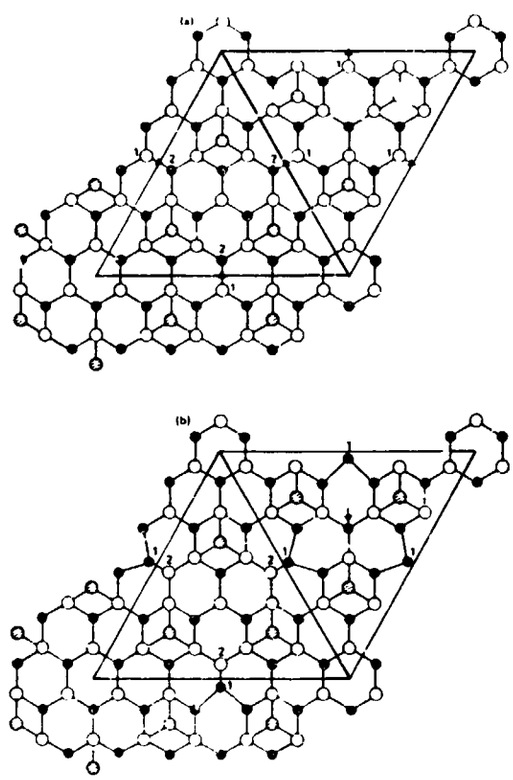

FIG. 5. A top view of the ideal 5X5 adatom model is shown in (a). The directions of atomic motions leading to a reconstruction of the substrate are indicated by arrows. The resulting reconstructed structure is shown in (b), and the point of large stress in the right triangular region is indicated by an arrow. The atomic designations are the same as in Figs. 1-3.

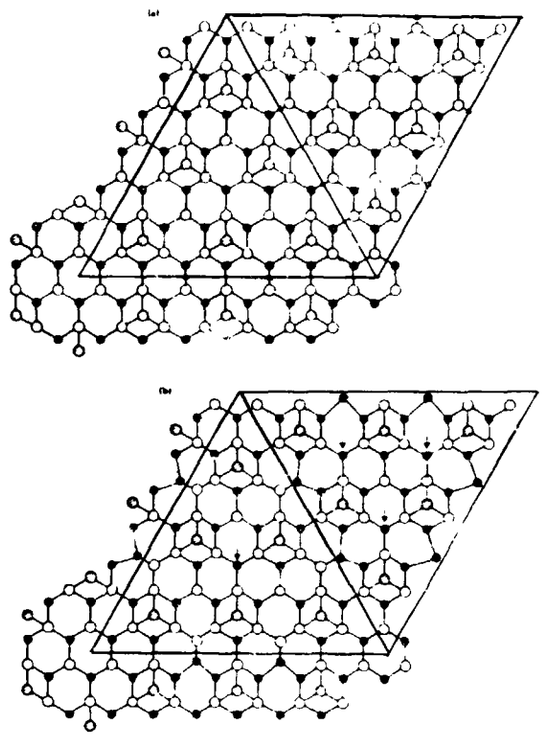

FIG. 6. Ideal and reconstructed adatom models for the 7X7 surface are shown in (a) and (b), respectively. The arrows in (a) give the directions of atomic displacements leading to the rebonding. The points of high stress in the left and right triangular regions are indicated by arrows in (b). As discussed in the text, hydrogen chemisorption at these sites would enhance the stability of the structure. The atomic designations are the same as in Figs. 1-3.

The 5X5 and 7X7 structures shown in Figs. 5(b) and 6(b) have a reconstructed adatom geometry on the left half of the cell and a conventional type of adatom structure on the right half. The presence of an adatom at the corner of the unit cell is energetically unfavorable since it leads to a locally $\sqrt{3}X\sqrt{3}$ structure. Adatom structures with this periodicity have a higher surface energy than those with a 2X2 lattice. From Figs. 5(b) and 6(b) it can be seen that the relation of equivalent sets of adatoms in the 5X5 and 7X7 lattices [e.g., the adatoms in the left half of the unit cells in Figs. 5(b) and 6(b)] with respect to the centers of their respective triangular regions is reversed in the two cell structures.

Several possibilities for the reconstruction of the right triangular section of the unit cell, as well as for the corner, were considered. Three of the reconstructions for the corner are shown in Fig. 7. The last two reconstructions preserve the threefold symmetry of the unit cell, whereas the first one breaks this symmetry. For the 5X5 lattice, none of these reconstructions is found to lower the energy; in fact, they all result in an increase of the total energy. Other types of atomic rearrangements at the corner cannot be ruled out. A comparison of the calculated structural and electronic properties of the 5X5 structure with the available experimental data is given in the following sections.

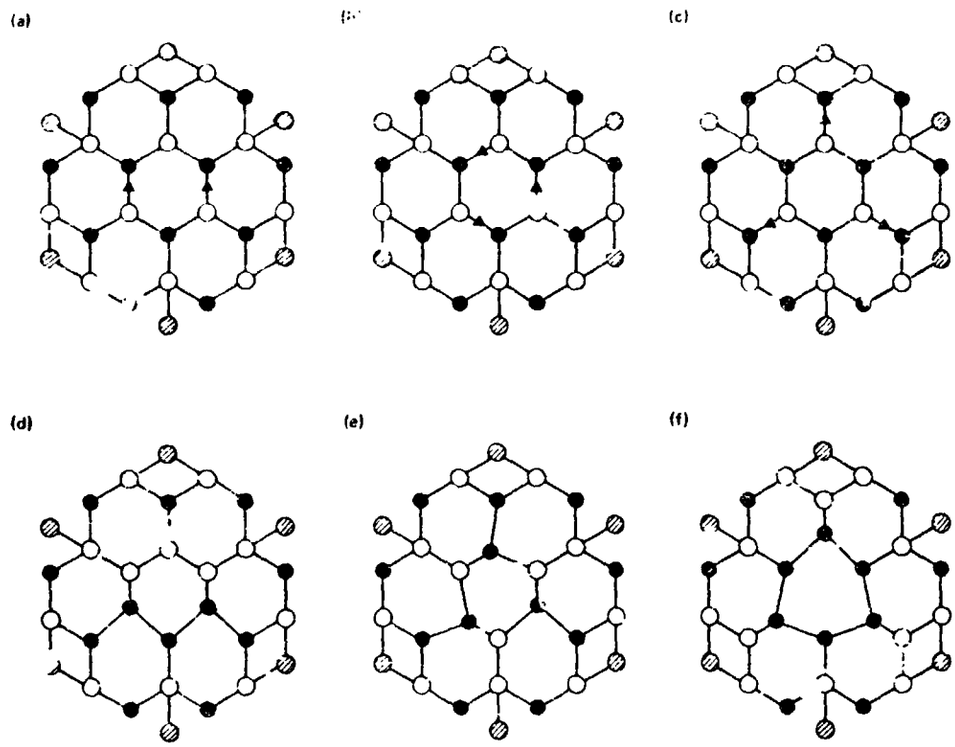

FIG. 7. Three possible modes of atomic displacements at the corner of a 5X5 or 7X7 unit cell are shown in (a), (b), and (c). The corresponding structures resulting from reconstruction are shown in (d), (e), and (f), respectively. Structures (b) and (c) preserve the threefold symmetry of the unit cell whereas (a) breaks this symmetry but maintains mirror reflection symmetry. All three types of reconstruction are found to result in an increase in energy. The atomic designations are the same as in Figs. 1-3.

B. Vacuum-tunneling microscopy

The presence of two different adatom structures on each triangular half of the cell is consistent with results from vacuum-tunneling measurements[1,28] on the Si(111)-7X7 surface. The present calculations on a 5X5 surface show that the adatoms on the two halves of the unit cell differ in their heights relative to a reference (111) plane by $\Delta z \approx 0.19 \pm 0.03$ Å, with the adatoms on the left half being higher. This is reversed for the conventional adatom model where the difference is calculated to be -0.05 Å for the 5X5 surface and -0.02 Å for the 7X7 surface. Recent tunneling measurements[28] indicate a difference of ≈0.3 Å. The sign of the difference is in

agreement with that calculated for the new adatom geometry. The atomic rebonding occurring along the boundaries of the unit cell leads to depressions along the edges and the short diagonal of the unit cell which are consistent with those observed in tunneling microscopy.

The maximum difference between the height of an adatom to a second-layer atom at the corner is calculated to be ≈1.9±0.3 Å. The experimental[1] value of the corrugation is ≈2.8±0.3 Å. The rest atoms at the corner would have to relax more deeply towards the bulk for the measured corrugation to be this large. For the particular case of the rectangular 2X2 lattice, the tight-binding method (as compared to the pseudopotential method[13]) may underestimate this inward relaxation. Applying the results of the calculations for the 5X5 lattice to the 7X7 structure, the height difference between adatoms on the left (right) and the central atom of the left (right) triangular region is 1.55±0.2 Å (0.94±0.2 Å) as compared to the values of 1.2±0.3 Å (0.7±0.2 Å) from vacuum tunneling.[1] With the possible exception of the corner where further atomic relaxations may occur, the modified adatom provides a satisfactory overall description of the experimental results on the 7X7 surface corrugation.

C. Rutherford backscattering

The proposed 5X5 and 7X7 structures have structural features, arising from reconstruction, resembling those from stacking faults at the surface. On the ideal (111) surface, the projection of the three bonds made by a surface atom with its three nearest-neighbor second-layer atoms onto a (111) plane forms either a Y pattern or an "inverted" Y pattern which is rotated by 180° from it. If stacking fault sequences occur at the surface,[4] then both patterns are simultaneously present. The modified adatom model demonstrates that such a feature can also arise as a result of reconstruction even in the absence of stacking faults. The rebonding of a surface atom to the substrate causes a reversal of the Y pattern next to it. An examination of the calculated atomic structure and lattice spacings of the modified adatom model shows it to be in good agreement with the structural features deduced by Bennett et al.[4] from recent Rutherford backscattering experiments.[5,6] The new adatom model is expected to be consistent with the results of impact-collision ion spectroscopy of Aono et al.[29] which give evidence for an adatom geometry but, at the same time, rule out the conventional, unreconstructed adatom model.

D. Magnetic ordering

The reconstruction of the simple adatom model greatly enhances the interactions between neighboring dangling bonds by bringing them much closer together. The interaction between the dangling bonds on the 5X5 surface is estimated to make a small [≈0.5 eV/(1X1 unit cell)] but non-negligible contribution to the lowering of the total energy. This is in contrast to the situation for the 2X1 π-bonded chain structure where second-nearest-neighbor interactions make no contribution to the stabilization of the structure because the phase constraint on the wave function resulting from the Bloch condition leads to a cos(ka) term in the electronic energy with a zero integral over the Brillouin zone. For the proposed 5X5 and 7X7 structures spin-polarization effects similar to those considered previously[30-32] for

smaller lattices are also expected to make a further (≈0.04 eV/interacting dangling bond) contribution to the stability of the structure. Possible evidence for a magnetic ordering on the 7X7 surface resulting in a very small gap in the electronic excitation spectrum has been obtained recently from low-temperature measurements.[23]

E. Photoemission

Strong indirect evidence for the adatom reconstruction proposed in this paper is provided by normal photoemission spectra[17-19] on Si(111) 2X1 and 7X7 reconstructed surfaces. These measurements show a surface state at 0.8 eV below the Fermi energy E_F on both surfaces with nearly identical polarization and angular dependence of photoemission intensity at normal emission.[17,18] Measured relative to the bulk valence-band maximum instead of E_F, the two states lie at -0.7 eV and -0.4 eV for the 2X1 and 7X7 surfaces, respectively.[19] The present calculations of the electronic structure for the 5X5 structure shown in Fig. 5(b) and for the 2X1 reconstructed π-bonded-chain model[11,12] predict a binding-energy difference of 0.24 eV and show the common origin of the two states. The sharply localized and multiply degenerate state at -0.4 eV for the 5X5 surface is calculated to arise primarily from the dangling bonds of the threefold-coordinated surface atoms that were initially second-layer atoms before the (2X2)-like reconstruction. The lower binding energy of this state relative to the one on the 2X1 surface is a consequence of the absence of nearest-neighbor π bonding on the 7X7 surface. The reduced emission intensity for the 7X7 surface is consistent with the smaller density of these type of atoms on this surface. The similarity between the 2X1 and 7X7 surfaces is expected to hold only near normal emission where the phase of the wave function is invariant over all equivalent dangling bonds on the 2X1 surface.

F LEED

Additional strong evidence in favor of some 2X1-type reconstruction on the 7X7 surface is provided by LEED. Defining the effective "1/2-order" spectra of the 7X7 surface to be the average of the 3/7 and 4/7 fractional-order spectra, Yang and Jona[33] have found remarkable similarities in the 1/2 spectra of the 2X1 and 7X7 surfaces. They have also shown that the 7X7 surface possesses at least one mirror plane along the doubling direction of the 2X1 surface. These results of LEED are in agreement with the modified adatom model proposed in this paper. The question of whether the 7X7 surface possesses only one mirror plane or three such planes leading to threefold rotational symmetry was also raised by the LEED measurements. Surface reconstruction leading to a reduced symmetry can lead, in principle, to a reduction in the total energy. The present calculations show that the removal of threefold symmetry on the 5X5 surface, by additional 2X1-like reconstructions at the corner atoms, Figs. 7(a) and 7(b), which still maintain mirror symmetry along the $[2\bar{1}\bar{1}]$ direction, results in an increase in the surface energy. The present calculations indicate that the threefold symmetry of the 7X7 LEED Pattern is intrinsic and not the result of an averaging over three single domain patterns.

G. Hydrogen chemisorption

The 5X5 and 7X7 unit cell contain points of high stress at the positions of second-layer atoms marked by arrows in Figs. 5(b) and 6(b). The stress is caused by the passage of three $\simeq 180^{\circ}$ angles through these sites. The surface minimizes its energy by exerting a large outward force on these second-layer atoms which moves them up by $\simeq 0.35$ Å, reducing the 180° angles to $\simeq 163^{\circ}$. The large stress at these points increases the probability of bond rupture upon exposure to hydrogen. The breaking of the second- to third-layer bonds at these points, together with the chemisorption of one hydrogen atom at each of the resulting dangling bonds, should lead to a very large decrease in energy. The recent high-resolution infrared spectroscopy of Chabal et al.[22] on Si(111) 7X7 surfaces covered by a few percent of a monolayer of hydrogen has provided evidence for unique chemisorption sites at the surface and the subsurface. For the 7X7 model proposed here [Fib. 6(b)] this would suggest a greater probability for hydrogen chemisorption on the left half of the unit cell (at the position of the arrow) than on the right triangular region.

Evidence for the formation of SiH_2 and SiH_3 complexes in the early stages of hydrogen chemisorption on the Si(111) 7X7 surface has been obtained by Wagner et al.[34] from electron-energy-loss studies. The most probable atomic sites to form such complexes are the adatoms where the strained adatom-surface bonds are most likely to break upon exposure to atomic hydrogen. Hydrogen chemisorption leads to a lowering of the surface energies of 5X5 and 7X7 adatom structures. Experimentally, it is known[35] that hydrogen chemisorption does not remove the seventh-order periodicity of the Si(111) surface.

H. Optical absorption

In the energy range of $\simeq 0.4$-1.0 eV, the strength of optical absorption between surface states on the Si(111) 7X7 surface is at least an order of magnitude smaller than on the 2X1 surface. For the latter case, two recent optical studies[36,37] have provided strong evidence for the π-bonded-chain model.[11] For this structure, the magnitude of the optical transition matrix element can be shown to be proportional to the nearest-neighbor π-bonding interaction between dangling bonds. The weakness of the optical-absorption intensity on the 7X7 surface is related to the more distant and much weaker hopping matrix element between dangling bonds. The calculations for the 5X5 structure show narrow empty sp_z-symmetry surface-state bands at 0.13-0.28 eV and at 0.39-0.45 eV at above the valence-band maximum (VBM) which are strongly localized on the adatoms. The highest filled surface states are calculated to be $\simeq 0.4$ eV below the VBM. These states are also sp_z in character and are localized on the fourfold atoms which become threefold coordinated as a result of reconstruction. Transitions between these states are expected to be very weak as a result of the small hybridization between the orbitals. At higher excitation energies (1-3 eV), differential external reflectivity measurements[38] show a surface-state transition at 1.76 eV.

I. Nucleation at steps

A study of the phase transition between the Si(111) 7X7 and 1X1

structures at $T_c \simeq 830^oC$ via reflection electron microscopy[14] reveals that the 7X7 structure nucleates preferentially at steps. From the observation that the shapes of the steps change spontaneously and continuously above T_c, it was concluded that the 7X7 reconstruction involved an ordering of either adatoms or vacancies.[14] In the context of the new adatom model for the 7X7 surface, the role of steps in the nucleation process is to force initially a linear ordering of adatoms along the step. If the binding energy of adatoms near the step is larger than that of adatoms on the terrace so that they remain effectively pinned at the step while the other adatoms can move, then a two-dimensional ordering of atoms should eventually result. A greater binding energy near a step is reasonable because of the greater freedom for atomic relaxation at such a site. The 7X7 to 1X1 order-disorder transition[39] probably results when all adatoms become mobile. At lower temperatures ($T \lesssim 425^oC$), where surface atomic mobilities are smaller, steps tend to increase the 2X1 to 7X7 transition temperature.[40]

J. Adsorption of closed-shell atoms

Recent studies[24,41] of Ar, Kr, and Xe adsorption on the Si(111) 7X7 surface have provided useful information on the atomic structure of this surface. The measurements provide evidence for a unique chemisorption site at the surface which is most probably associated with the deep hole at the corner of the unit cell seen in tunneling microscopy. By measuring the amount of adsorbed Kr and Xe as a function of temperature at fixed pressure, Conrad and Webb[24] were able to demonstrate inadequacies in nearly all the structural models that have been proposed for this surface. More recently Demuth and Schell-Sorokin[41] have reported ultraviolet photoemission measurements of the coverage-dependent electron binding energies of adsorbed Ar and Xe on Si(111) surfaces. Their results favor the Harrison-Binnig[1,2] type of adatom model for the 7X7 surface to the exclusion of most other structural models. The three types of adsorption sites inferred from the measurements are indicative, however, of a structure more complex than the simple adatom geometry. This is consistent with vacuum-tunneling results[1] and with the reconstructed adatom model presented in this paper.

V. TRIMER MODEL

In addition to adatom models, Himpsel's trimer model[8] for the 7X7 reconstruction was examined in detail. The model is similar to the π-bonded-chain model for the Si(111) 2X1 surface except that only one-half as much rebonding of atoms is required to create it. Furthermore, in common with the models proposed by McRae[9] and Bennett,[10] stacking-fault sequences are explicitly included in the structure. This leads to bonding between second-layer atoms along the boundaries of the unit cell leading to a $\simeq 16\%$ reduction in dangling-bond density from the 1X1 surface. It was suggested[8] that the reduction in the number of broken bonds together with π bonding would stabilize the timer model against the 2X1 chain model.

Using a 5X5 lattice, the atomic structure of the trimer model was fully optimized. The calculations show that the model has a higher surface energy than either the ideal 1X1 surface or the simple adatom model. The surface energy is calculated to be $\simeq 0.3$ eV/1X1 unit cell higher than the reconstructed adatom model. The π bonding in the trimer model is found to

be not as effective as in the 2X1 chain model. Calculations for an optimized 2X2 trimer model (which replaces the large strains associated with the stacking-fault sequences of the 5X5 structure with other unavoidable strains) give an identical surface energy when corrections for a 16% lower dangling-bond density are made. For 5X5 and 7X7 lattices, the results of the calculations indicate that the bonding between second-layer atoms which is required in stacking-fault models of the surface reconstruction leads to large strains which are energetically unfavorable.

VI. METHOD OF CALCULATION

The use of the empirical tight-binding method in force and energy-minimization calculations is discussed in detail in Ref. 25. In this section, the approach employed in calculating the surface energies for the large unit cells discussed above is examined.

As in previous calculations, a slab geometry infinitely periodic in two dimensions was used. The criterion for choosing the thickness of the slab is that the relaxations or reconstructions on the two ends of the slab should remain independent of each other. To reduce the need for a large number of layers in the present calculations, the dangling bonds on one end of the slab were eliminated by the addition of hydrogen for all the surfaces studies. To account for the effects of hydrogenation on the total energy, an additional calculation in which hydrogen was added to both ends of an ideal slab had to be made. One-half of the total energy of the latter geometry was subtracted from the energy of the structure with hydrogen on only one side of it, to determine the total energy $\underline{E}_{tot}$ of the remaining $\underline{N}$ atoms. The surface energy γ was then calculated by dividing the energy

$$\Delta\underline{E} = \underline{E}_{tot}(N) - \underline{N}\underline{E}_0 \qquad (11)$$

by the area of the surface unit cell. In Eq. (11), $\underline{E}_0$ is the binding energy per atom in the crystalline, diamond-structure environment.

The calculations on 5X5 adatom geometries were done with a 131-atom unit cell consisting of six adatoms, four complete (111) layers (100 atoms), and 25 hydrogen atoms. The hydrogen layer and the Si layer adjacent to it were held fixed in nearly all the calculations. The remaining 81 atoms were allowed to relax. The relaxed atomic geometries were determined by moving each atom along the direction of the Hellmann-Feynman force acting on it. The calculation of this force within the tight-binding method is straightforward and has been previously discussed.[25] The modified adatom model proposed in this paper leads to a relaxation extending deeper into the bulk than is the case for the simple adatom model. For this reason, it was not possible to test the new adatom model for the 7X7 surface. For the conventional adatom model, however, a calculation of the atomic structure was made. In these calculations, a 159-atom unit cell consisting of 12 adatoms, two full (111) layers (98 atoms), and 49 hydrogen atoms was used.

VII. CONCLUSIONS

A new adatom model differing from the conventional model by a reconstruction of the substrate is proposed. The new adatom structure

provides an explanation for the 7X7 and 5X5 size of the unit cells seen on annealed Si(111) and Si(111)-Ge surfaces, respectively. The model is consistent with structural information from vacuum-tunneling microscopy. It also provides simple explanations for stacking-fault-type features expected from Rutherford backscattering experiments and for similarities in the LEED and photoemission spectra of 2X1 and 7X7 surfaces.

ACKNOWLEDGMENTS

I am grateful to Dr. John Northrup for many stimulating discussions. This work is supported in part by the U.S. Office of Naval Research through Contract No. N00014-82-C-0244.

REFERENCES

1 G. Binnig, H. Rohrer, Ch. Gerber, and E. Weibel, Phys. Rev. Lett. 50, 120 (1983).

2 W.A. Harrison, Surf. Sci. 55, 1 (1976).

3 J.J. Lander, G.W. Gobeli, and J. Morrison, J. Appl. Phys. 34, 2298 (1963); J.J. Lander, in Progress in Solid State Chemistry, edited by H. Reiss (Pergamon, Oxford, 1965), Vol. II, p. 26.

4 P.A. Bennett, L.C. Feldman, Y. Kuk, E.G. McRae, and J.E. Rowe, Phys. Rev. B 28, 3656 (1983).

5 R.J. Culbertson, L.C. Feldman, and P.J. Silverman, Phys. Rev. Lett. 45, 2043 (1980).

6 R.M. Tromp, E.J. van Loenen, M. Iwami, and F.W. Saris, Solid State Commun. 44, 971 (1982).

7 P.M. Petroff and R.J. Wilson, Phys. Rev. Lett. 51, 199 (1983).

8 F.J. Himpsel, Phys. Rev. B 27, 7782 (1983).

9 E.G. McRae, Phys. Rev. B 28, 2305 (1983).

10 P.A. Bennett (unpublished). This model involves adatoms, stacking-fault sequences, and dimers at the surface.

11 K.C. Pandey, Phys. Rev. Lett. 47, 1913 (1981); 49, 223 (1982).

12 J.E. Northrup and M.L. Cohen, Phys. Rev. Lett. 49, 1349 (1982); J. Vac. Sci. Technol. 21, 333 (1982).

13 J.E. Northrup and M.L. Cohen, Phys. Rev. B 29, 1966 (1984).

14 N. Osakabe, Y. Tanishiro, K. Yagi, and G. Honjo, Surf. Sci. 109, 353 (1981); N. Osakabe, K. Yagi, and G. Honjo, Jpn. J. Apl. Phys. 19, L309 (1980).

15 T. Ichikawa and S. Ino, Solid State Commun. 27, 483 (1978).

16 H.J. Gossmann, J.C. Bean, L.C. Feldman, and W.M. Gibson, Surf. Sci. 138, L175 (1984).

17 D.J. Chadi, R.S. Bauer, R.H. Williams, G.V. Hansson, R.Z. Bachrach, J.C. Middelsen, F. Houzay, G.M. Guichar, R. Pinchaux, and Y. Petroff, Phys. Rev. Lett. 44, 799 (1980).

18 F. Houzay, G.M. Guichar, R. Pinchaux, and Y. Petroff, J. Vac. Sci. Technol. 18, 860 (1981).

19 F.J. Himpsel, P. Heimann, and D.E. Eastman, Phys. Rev. B 24, 2003 (1981); F.J. Himpsel, D.E. Eastman, P. Heimann, and B. Reihl, Phys. Rev. B 24, 1120 (1981).

20 G. Chiarotti, P. Chiaradia, and S. Nannarone, Surf. Sci. 49, 315 (1975).

21 G. Chiarotti, S. Nannarone, R. Pastore, and P. Chiaradia, Phys. Rev. B 4, 3398 (1971).

22 Y.J. Chabal, G.S. Higashi, and S.B. Christman, Phys. Rev. B 28, 4472 (1983); Y.J. Chabal, Phys. Rev. Lett. 50, 1850 (1983).

23 J.E. Demuth, B.N.J. Persson, and A.J. Schell-Sorokin, Phys. Rev. Lett. 51, 2214 (1983).

24 E. Conrad and M.B. Webb, Surf. Sci. 129, 37 (1980).

25 D.J. Chadi, Phys. Rev. B 29, 785 (1984).

26 J.C. Phillips, Phys. Rev. Lett. 45, 905 (1980).

27 S.B. DiCenzo, P.A. Bennett, D. Tribula, P. Thiry, C.K. Wertheim, and J.E. Rowe (unpublished).

28 G. Binnig and H. Rohrer, J. Vac. Sci. Technol. (to be published).

29 M. Aono, R. Souda, C. Oshima, and Y. Ishizawa, Phys. Rev. Lett. 51, 801 (1983).

30 R. Del Sole and D.J. Chadi, Phys. Rev. B 24, 7431 (1981); D.J. Chadi and R. Del Sole, J. Vac. Sci. Technol. 21, 319 (1982).

31 J.E. Northrup and M.L. Cohen, Phys. Rev. Lett. 47, 1910 (1981).

32 M. Lannoo and G. Allan, Surf. Sci. 115, L138 (1982); G. Allan and M. Lannoo, ibid., 73, 11 (1977).

33 W.S. Yang and F. Jona, Solid State Commun. 48, 377 (1983).

34 H. Wagner, R. Butz, U. Backes, and D. Bruchmann, Solid State Commun. 38, 1155 (1981).

35 T. Sakurai and H.D. Hagstrum, Phys. Rev. B 12 5349 (1975).

36 P. Chiaradia, A. Cricenti, S. Selci, and G. Chiarotti, Phys. Rev. Lett. 52, 1145 (1984).

37 M.A. Olmstead and N.M. Amer, Phys. Rev. Lett. 52, 1148 (1984).

38 P.E. Wierenga, A. Van Silfhout, and M.J. Sparnaay, Surf. Sci. 87, 43 (1979).

39 M.B. Webb and P.A. Bennett, Surf. Sci. 31, 104 (1981); J. Vac. Sci. Technol. 18, 847 (1981).

40 P.O. Auer and W. Monch, Jpn. J. Appl. Phys. Suppl. 2, Pt. 2, p. 397 (1974).

41 J.E. Demuth and A.J. Schell-Sorokin, J. Vac. Sci. Technol. A 2, 808 (1984).

DISCUSSION

RAO: I believe you said as part of your talk that these bonds have residual ionic charges. What is the effect of ionic charges? Can you get compensation in these charges by other atoms moving in? What is the physical manifestation of this?

KAZMERSKI: The physical manifestation is an increase in the work function at the surface. You can actually predict that there should be about 0.5 eV increase in the work function. Measured, the work function increases about 0.35 eV. You can get rid of most of these things by hydrogen ion. You get an increase in the work function because of the way the atoms are oriented. You can tell which end is negative and which one is positive, and then calculate the work function increase.

DYER: This work has very far-reaching, important considerations for many uses of silicon, and I compliment you and your workers on this. I have a question that arises in my mind right away. Supposing you were dissolving away silicon or melting away silicon, do you visualize that these structures would occur instantaneously or would they take some time to come up?

CHADI: The reason is, for the activation barrier to go to the annealed silicon 7 x 7 structure you can measure the activation energy by going to the following experiment: You take the [100] surface, which is 2 x 1, and you keep it at, let's say, 200°C. When this has been done, then you wait, and measure the time that you have to wait to get the 7 x 7, and you do that at 300°C, 400°C, and so on. From the time that is required to transform the 2 x 1 to the 7 x 7 surface, you get an activation energy of about one-half eV per atom, to go from the 2 x 1 to the 7 x 7 structure. But if the temperature is high, if you are close to 800°C, then the structure appears spontaneously. The atomic mobilities are very large at 800°C. The Japanese have shown by beautiful microscopy measurements that the 7 x 7 structure nucleates at steps. I believe the reason it nucleates at steps is that you get a one-dimensional ordering of the atoms along the steps, which eventually lead to a three-dimensional ordering over the entire surface.

SAH: I would like to ask you if you could give us the implication of the results you find on oxidized silicon? How does that affect the interface states recombination velocity? On oxidized silicon at high temperature?

CHADI: I have done some work on silicon oxide interfaces that I did not mention here. This work has been done mostly on clean surfaces with no oxide. I have done some work on hydrogenated silicon [111] and [100] surfaces. If you add hydrogen to these surfaces, then all the reconstruction goes away. You end up with a much lower surface energy if you have essentially an ideal surface with every dangling bond saturated by hydrogen. The 7 x 7 surface, however, is known to to be an extremely stable surface. A Japanese group reported that they exposed it to hydrogen and oxygen and to air for several days and they were still seeing 7th-order spots in their leads. It is a very stable structure.

GRUNTHANER: I have two questions. One is: are you familiar with a recent paper that Linus Pauling put out, looking at your asymmetric dimer situation on <100>?

CHADI: I forgot to mention that there was some controversy with the silicon <100>. The chemists, particularly Goddard at Caltech, suggested that asymmetry was not reasonable, that it should remain symmetric. I heard that in a conference where Pauling was present; Pauling took issue with Goddard. I later wrote this paper in the Physical Review suggesting giving chemical arguments why silicon <100> should have asymmetric dimer structure. In fact, they found the structure very close to mine, using very simple chemical arguments. His idea was that, essentially, there were two configurations, covalent configuration and ionic configuration, and these two configurations had roughly similar energies -- that they would mix in two different configurations that gave asymmetry.

GRUNTHANER: The thought that was quite fascinating that came out of that was these incredibly simple arguments that he has developed out of atomic orbital theory. He comes up with disgustingly close numbers in terms of what you were able to get out.

CHADI: I had the same ideas after I did the calculations. In fact, I had the angles on the viewgraph. If you look at what happens when you go from the symmetric to the asymmetric dimer: in the symmetric dimer you still have all 190° angles. Very close to tetrahedral. Whereas when you go to the asymmetric dimer, one of the bonds becomes SP^2-bonded, essentially. The angles can relax to close to 120°. The SP^2 bond is very strong; much stronger than the SP^3 bond. The other one becomes P-bonded and the P bonding is close to the SP^3 bond. So you gain energy that way, and that is essentially Pauling's argument.

GRUNTHANER: That is what brings up the second question. When you did this calculation of the effective grain boundary in silicon material, I assume that out of the calculation you get the chemical implication of bonding and antibonding states, and of the energy distances between those. For the grain boundary in silicon, buried down in the silicon in your slab, you essentially get something like a bonding-antibonding splitting in there that I assume you can compare with what you can get for the normal SP^3 bonding in silicon. So the question is, was there any difference in gap implied in that rehybridization in the 5- and 7-membered rings? And then the second part of that: was there any indication of the change in hybridization? Namely, is the S contribution to bonding really following the kind of orbital electro-negativity ideas that are being developed now?

CHADI: As I am sure that you are aware, the grain boundary I considered was a continuous grain boundary. There were no dangling bonds. It was a perfect bonding at every site.

GRUNTHANER: But the geometry is quite different around the silicon site. I am wondering whether there is an application for that in the gap.

CHADI: I looked at the static charge distribution at the grain boundary and I found, amazingly, that most of the atoms were neutral to within 200ths of an electron. However, there were a few atoms at the boundary that had deviations from neutrality of $\pm$ 0.1 electrons. As far as the electronic states -- I looked at those; whenever you have five or seven full rings, there is a very characteristic state that is forbidden essentially for even numbers of rings of atoms, and these states occur at two well-defined positions where you have pseudo-gaps. If you look at the four bands of density state then there is one of these pseudo-gaps at about 0.08 eV below the valence band. This is a very sharp state. There is also sharp state in the conduction band, I don't know at what energy, but there is nothing in the band gap. The band gap is free of any defect state associated with the grain boundary.

MILSTEIN: After Grunthaner's comment about Linus Pauling discussing this, I am not sure that I have anything further to say. The issue I was looking at was the matter where you described the thermodynamic transformation, and the argument that crossed my mind is that in the carbon system, diamond is not thermodynamically stable, although we have all seen such objects, and they stand around for quite some time. I think the issue I would raise is that this should be viewed from the point of view of the bonding of Period 4 elements. In that sense, I think, when you go from carbon to silicon the transformations occur more readily, clearly, but when you talk about a pi-bonded system, it's a straight organic system. That is where it comes from.

CHADI: That's right. However, this might be easy for you to say, but the chemist, I know Goddard for example, believes that the pi-bonding of silicon is very weak and I think it is weak, it is much, much -- by a factor of three -- weaker in magnitude than the pi-bonding in carbon. However, it does occur. Some would argue that pi-bonding should not exist in silicon, whereas there is strong evidence now, at least on the silicon surface, that pi-bonding does exist, and it is very, very weak. As I mentioned, absorption between surface states, with the polarization dependence of the absorption. The only structure that agrees with that measurement and also photon emission is the chain structure. So you have to convince the chemists. I believe, at the surface at least, there is pi-bonding, and it makes a contribution to the stability of the surface. The question is: how strong is it? The chemists say it is very weak.

MILSTEIN: Obviously, it has to be very weak. I don't think there is any argument about that.

CHADI: It is much stronger than carbon.

MILSTEIN: That probably also explains why diamond exists, because thermodynamically it ought not to. You have a big enough activation energy to get over it to change it to graphite.

CHADI: Yes. The activation energy is very big there.

HANOKA: I would like to pursue this thing about the hydrogen on the surface again. That was for a [111] surface, is that right?

CHADI: For the [111] surface it goes to an ideal, yes, the reconstruction goes away and also for the [100], if you add hydrogen; it first saturates the dangling bonds, and it stays 2 x 1, but then if you add more hydrogen then it breaks the silicon-silicon dimer bond and you get a dihydride on the [100] surface.

HANOKA: That is interesting, because there is IR spectroscopic evidence of an SiH_2 being formed at the surface. Of course, there you have much higher concentrations. That is what I was going to ask you about.

CHADI: In fact, if you put water on the silicon [100] you get both silicon hydrogen and silicon OH modes, you get the association. There is a lot of work in IR with oxygen, hydrogen and water on the silicon surfaces.

KAZMERSKI: We want to thank you very much, D.J. I will point out that this is an ideal case for the experimentalists, where D.J. won the Peter Mark Award and got $500 for his work, and I just saw that Benig and Rohr got the King Faisal Award at considerably more money, almost like a Nobel Prize.

N85-31626

COMPOSITIONAL ANALYSIS OF SILICON

L.L. Kazmerski
Solar Energy Research Institute
Golden, Colorado 80401

ABSTRACT

The use of surface analysis methods in the detection and evaluation of elemental and impurity species in Si is presented. Examples are provided from polycrystalline Si and high-efficiency MINP cells. Auger electron spectroscopy and secondary ion mass spectrometry are used to complement microelectrical data obtained by electron-beam induced-current measurements. A new method is discussed which utilizes the volume indexing of digital SIMS signals, providing compositional information and impurity maps on internal materials/device interfaces.

I. INTRODUCTION

Impurities control the electro-optical properties of semiconductors and the operating lifetime and performance of solid-state devices. For such devices (including solar cells), it is important to know not only the levels of such impurities, but also their location and chemical state within the host lattice. A number of compositional characterization techniques are available to perform these analyses, mostly based on a bulk or volume scale. Surface analysis methods (1) - those that provide chemical and compositional information on the topmost atomic layers of a surface - have enhanced research and problem-solving in the semiconductor device area due to their complementary abilities to detect impurity (elemental, ionic, molecular) species, provide depth-compositional information (with ion-etching), determine chemical bonding states, map impurity localizations on surfaces or interfaces, and, evaluate integrity of interfaces. The common surface analysis techniques are summarized in Table 1. From this information, some of the strengths and limitations of the techniques can be deduced. For example, Auger electron spectroscopy (AES) can provide excellent spatial resolution due to the ability to focus the electron input probe. It lacks, however, the sensitivity to trace impurities which secondary ion mass spectrometry (SIMS) provides. X-ray photoelectron spectroscopy (XPS) complements these techniques in that it is the most developed and most reliable for providing chemical state information, with minimum inherent beam damage.

This paper focuses on the investigation of impurities in silicon solar cells, examining both single-crystal and polycrystalline types. The applications of AES and SIMS to elemental analysis in these devices are emphasized. Specifically, the interrelationships among the chemistry and composition of grains and grain boundaries, the electro-optical properties of the intergrain regions, and photovoltaic cell performance will be covered. The microelec-

Table 1. Summary of Selected Surface Analysis Techniques

	AES	EELS	SIMS	XPS	UPS
Probe	electron	electron	ion (+, -)	x-ray	ultraviolet
Detected Species	electron	electron	ion (+, -)	electron	electron
Spatial Resolution	~300 Å	~300 Å	<1 μm	10^2 - 10^3 μm	~10^3 μm
Depth Resolution	5 - 50 Å	5 - 50 Å	≥3 Å	5 - 50 Å	5 - 50 Å
Detection Sensitivity	0.1 at-%	0.1 at-%	<0.001 at-%	0.1 at-%	0.1 at-%

trical characterization of specific cell regions is accomplished by electron-beam-induced-current (EBIC) measurements, which provide information on the spatial distribution of current losses. Two impurity mechanisms are covered: (i) the segregation of oxygen (and other impurities) to the grain boundaries during heat treatments or high temperature processing of the devices. And, (ii) the passivation of the grain boundaries by incorporation of hydrogen in these regions. This hydrogen localization is determined directly and correlated with the microelectrical properties of these same regions, as well as cell performance. Of special interest is the introduction of a new method to detect and spatially-resolve impurities and elemental distributions within solid-state devices using digitally-acquired and indexed SIMS (2). This method permits the determination of impurity localization or distributions on internal device interfaces, with fracturing or otherwise exposing such areas. The utilization of this method in profiling higher efficiency Si cells is exampled.

II. OXYGEN SEGREGATION IN POLYCRYSTALLINE SILICON

At the grain boundary, dislocations and bonding alterations make the material structurally and possibly chemically different than the bulk material in the grains. Thus the electrochemical potential in the grain boundary is generally different than in the grains. This potential difference provides a depletion region that can be the site of minority carrier recombination. The disruption can also provide a region for the localization of impurities, either from segregation of inherent species or of purposely-placed ones. The segregation of impurities to the intergrain regions has been demonstrated in cast and directionally-solidified Si (3). AES and SIMS has been utilized in conjunction with fracturing techniques to identify impurity species on the grain boundary planes. The fracturing process provides a method for the side-by-side analysis of a region - as indicated by the AES data of Fig. 1. However, inherent to this process is the loss of a large portion of the grain boundary plane. Because the electron probe can be scanned very effectively, impurity maps can be produced in the course of such AES (or SIMS) investigations. Such a mapping sequence is presented in Fig. 2. The benefit of this segregation process is that the grain regions themselves have significantly higher purity - with associated improvement of their electronic properties and device suitability. The grain boundary regions which act as sinks for such impurities are potential regions for enhanced minority carrier loss or impurity diffusion (shunting), but do not significantly degrade the cell performance unless impurity content is exceedingly high or the grain size is very small.

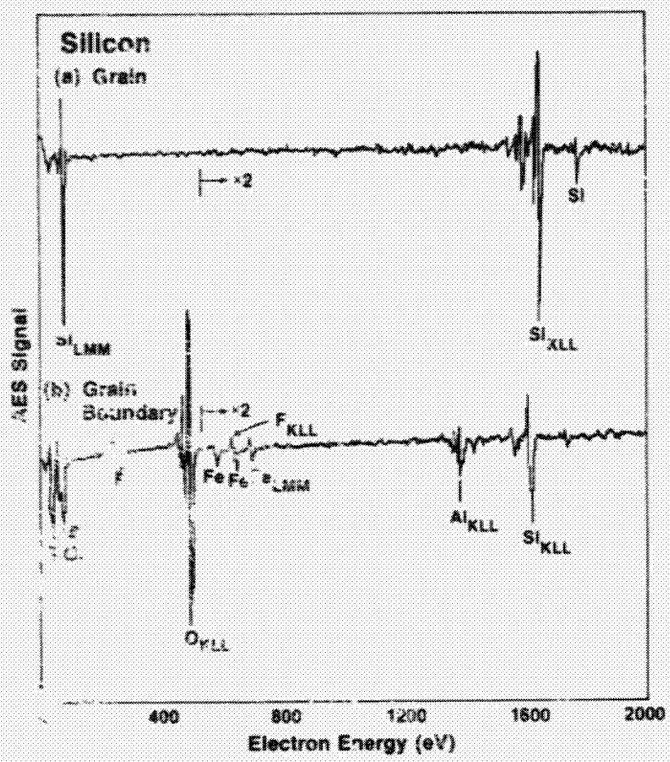

Fig. 1. AES surveys of fractured Si grain boundary: (a) grain region; (b) grain boundary.

ORIGINAL PAGE IS
OF POOR QUALITY

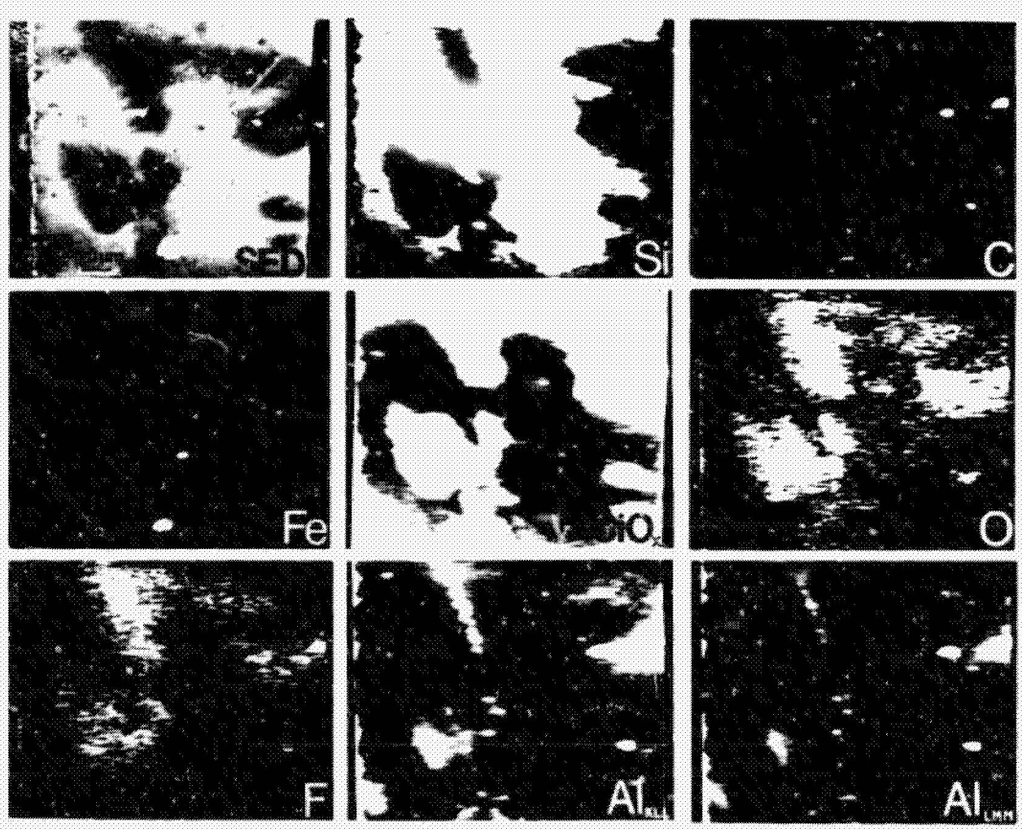

Fig. 2. AES mapping sequence of impurities on fractured grain boundary.

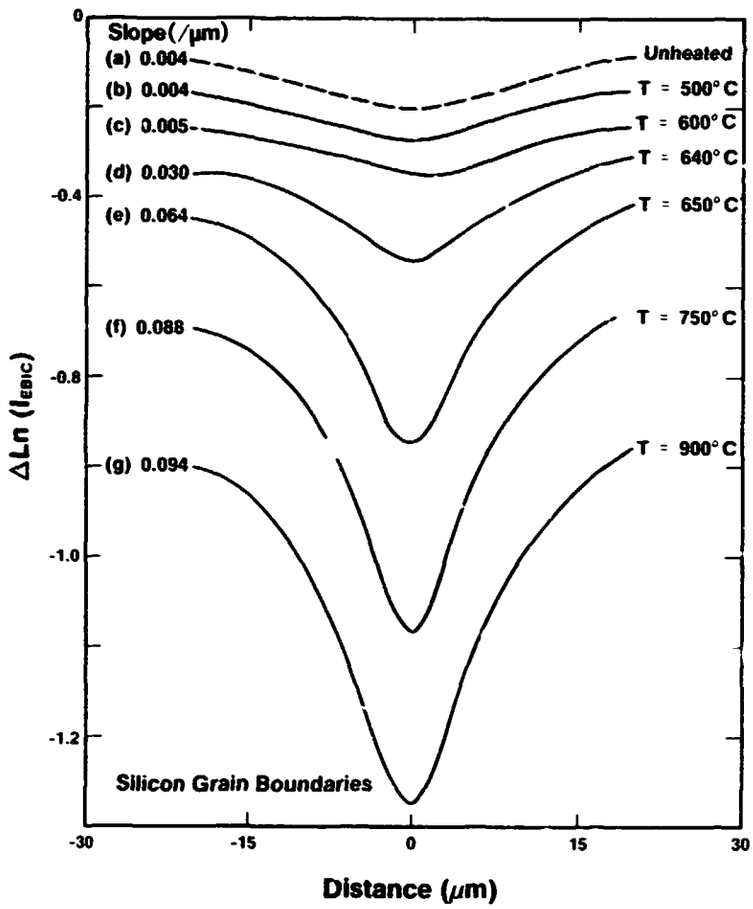

Fig. 3. EBIC linescans across Si grain boundaries as a function of thermal processing. Heat treatments are for 30 min in argon atmosphere.

The electrical activity of some grain boundaries in polycrystalline Si has been reported to be strongly affected by heat treatment (3,4). EBIC and compositional data from surface analysis measurements have been used to correlate the presences of oxygen at the grain boundaries with the electrical activation of these regions. The origin of the oxygen and resulting activity of the grain boundary is linked to the thermal history of the sample of devices (5). This is illustrated in the EBIC data of Fig. 3. The junction in this case is formed by an MIS structure fabricated on the individual grain boundary and adjacent grains at temperatures below 100°C in order to minimize additional thermal effects. The EBIC responses for unheated, T = 500°C, and T = 600°C cases are very similar, indicating that this mild thermal processing has little effect on the boundary region. If the temperature is increased, the EBIC responses increase correspondingly, indicating the electrical activation of these regions. The critical range for this activation is between 600°C and 650°C. Heating beyond 900°C does not seem to further affect the EBIC response, unless recrystallization occurs near the melting temperature. The slope of the $Ln(I_{EBIC})$ vs. distance curves relates to the values of grain boundary recombination velocity (S_{gb}) and effective diffusion length (L_{eff}) (6). The existance of oxygen at the grain boundaries of annealed Si has been demonstrated using fracturing with SIMS. Figure 4 shows such data for an unanealled sample and one heated to 750°C. Increases in the oxide-signals (e.g., the SiO^{44} peak) are apparent. However, the fracturing process is difficult, and has less-than-desired repeatability and control.

Fig. 4. SIMS survey of unannealed and annealed grain boundaries.

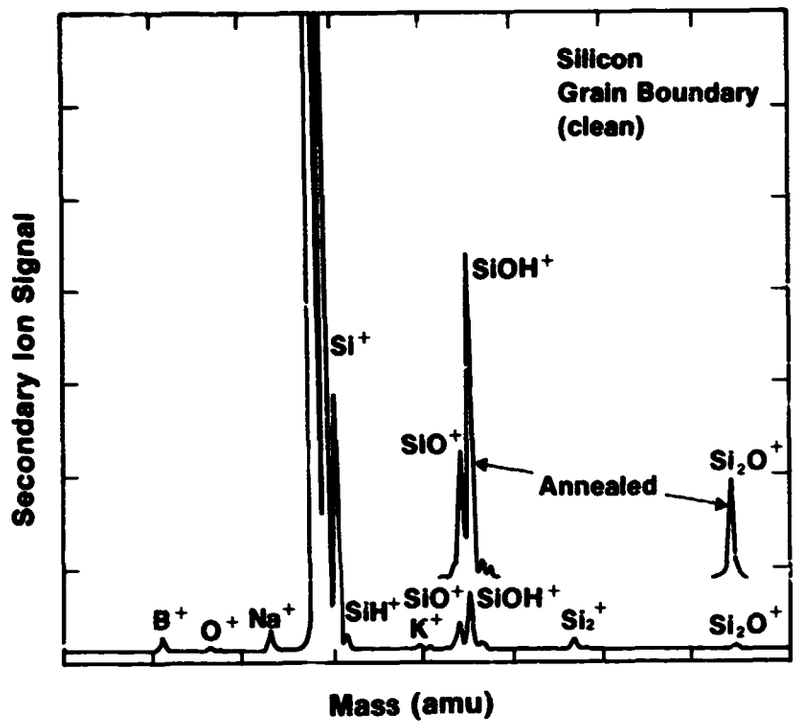

III. VOLUME INDEXING OF IMPURITIES AND ELEMENTS

The ability to reliably defect, map and quantify elemental or compositional information at regions within a solid-state device has been accomplished by the method illustrated in Fig. 5. In this, selected ion signals corresponding to elements or molecules of interest, are measured and stored (indexed for intensity, spatial location) digitally for an incremental volume encompassing the region or interface under analysis. A computer can be used to track the region of interest (e.g., grain boundary plane) by maximizing the presence of impurities which are known to exist in such regions. Thus, the internal interface can be exposed by spatially transforming the detected signals - even though the sputter profiling/SIMS operation is carried out at some angle to this plane. This avoids the loss of information experienced in the fracturing technique. The data can be coded for ion type, spatial origin (X, Y, Z) and concentration level. Additionally, the results can be color coded for more effective presentation.

A simple example, which utilizes the depth profiling capabilities of the technique, is presented in Fig. 6. These data show the cross-sectional distribution of impurities in a high-efficiency Si MINP solar cell. The device structure has a double layer (ZnS/MgF) anti-reflection coating. A thin Si-oxide layer (~ 30 Å) covers the phosphorous-diffused, boron-doped substrate. The relevant secondary ion species utilized in the profiling sequence designated in Fig. 6. The expanded view of the oxide-semiconductor region illustrate the uniformity of the oxide itself. Because only a black/white

ORIGINAL PAGE IS
OF POOR QUALITY

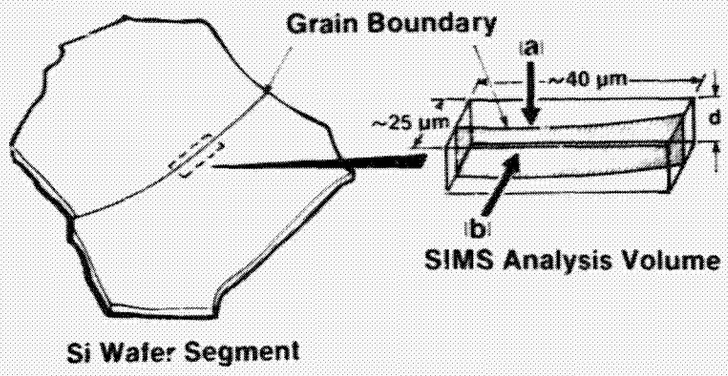

Fig. 5. Representation of SIMS volume indexing scheme.

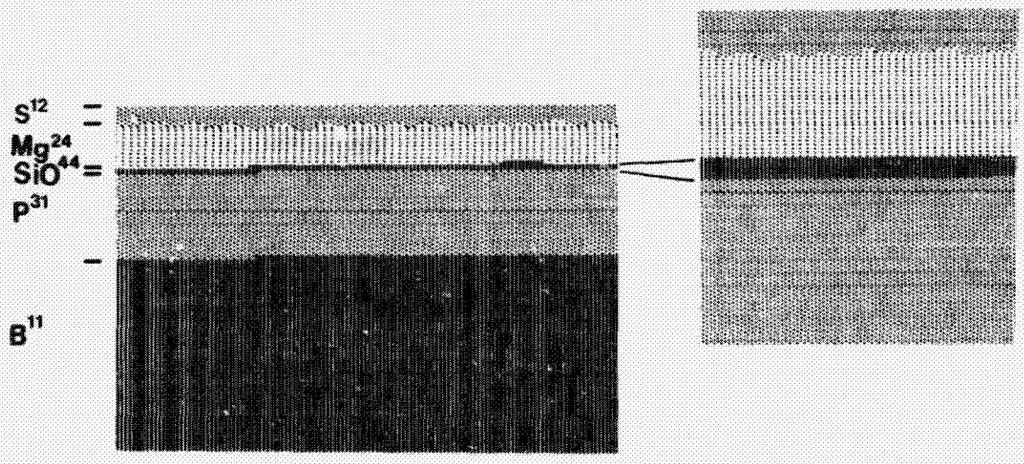

Fig. 6. Cross-section SIMS profile of Si MINP structure.

illustration is permitted in this publication, the relative concentrations are not indexed to ensure clarity. However, the phosphorous distribution is shown to peak at about $10^{20}/cm^3$, with a minimum of $10^{17}/cm^3$ detected in Fig. 6. Same interdiffusion of the ARC is also observable.

This method has also been effective for investigation the segregation of oxygen in polycrystalline Si with heat treatment. The data presented in Fig. 7 are obtained by translating the volume-indexed SIMS data in order to view the boundary from "b" in Fig. 5. Again, the black and white format required for this paper has prevented the unambiguous coding for concentration level, and the data presented in Fig. 7 represent a threshold of $1 \times 10^{17}/cm^2$ for SiO^{44} and $1 \times 10^{18}/cm^3$ for C. Figure 7a represents the grain boundary plane for a boundary heated to 600°C. The solid black regions are carbon, and are decorated by oxygen--as indicated by the intense dot pattern from the SiO^{44} SIMS signal. The presence of any Si-O content for grain boundaries processed

ORIGINAL PAGE IS
OF POOR QUALITY

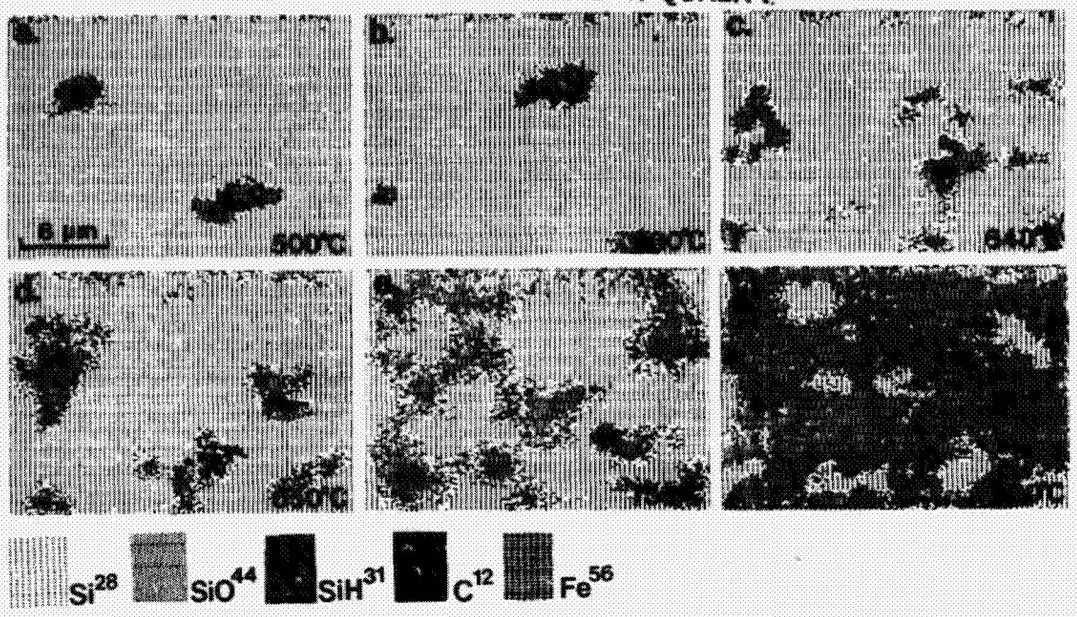

Fig. 7. SIMS mapping sequence of Si grain boundary showing oxygen segregation as a function of heat treatment. Impurity species key is included.

below 500°C is usually at some segregated impurity species (e.g., C, Fe, Ni, Al). As the annealing temperature is increased, the amount of oxygen at the boundary is observed to increase. Such data are shown in Figs. 7b-f, and correlate directly with the electrical activation of these regions determined by EBIC (Fig. 3). Spatially-resolved-minority carrier lifetime measurements, and the determination of the grain boundary barrier height have been reported (4,5) and directly complement these results. Thus, the segregation of oxygen to the grain boundaries results from high-temperature material/cell processing, and appears to be the origin of the electrical activation of these regions.

IV. HYDROGEN PASSIVATION

The effectiveness of hydrogen treatment on altering the electrical properties of polycrystalline Si and in improving the operational characteristics of cells has been demonstrated. The effect of such hydrogen processing is shown in the J-V characteristics of Fig. 8. The cell undergoes a change in efficiency from 5.8% to 7.7% (no antireflection coating) upon hydrogen treatment. Although the phenomenological effects of the hydrogen processing on cell improvement have been observed, little is known about the incorporation of this impurity species into the grain boundary or its possible interaction with the segregated oxygen that might be present in that region. Dube, et al. (7) have shown that hydrogen does alter the EBIC response of representative devices. They have deduced a diffusion coefficient for H in the Si grain boundary by examining the boundary from the side and along its length.

This analysis does not detect hydrogen directly, and assumes that the hydrogen is indeed localized there and responsible for the response. Figure 9 shows the effect of hydrogen treatment on a specific grain boundary. The EBIC response of Fig. 9a is for a decrease significantly with hydrogen treatment (Fig. 9b). Reheating this same boundary to 900°C "restores" the active response, but the magnitude is decreased somewhat. A second hydrogen treatment passivates the region again, with the response slightly less than after the initial hydrogen processing. These data are complemented by the grain boundary barrier height vs. light irradiation data of Fig. 10. The sequence is (a) unannealed grain boundary; (b) hydrogen-treated; (c) annealed, 900°C; (d) second hydrogen treatment; (e) annealed, 900°C; and, (f) third hydrogen treatment. The barrier height is improved, and becomes less sensitive to light intensity after the hydrogen passivation. In addition, the barrier height is observed to decrease with each successive hydrogen processing.

The incorporation of the hydrogen in the grain boundary and the relationship between the hydrogen and oxygen concentrations in that region are illustrated in Figs. 11-15. Figure 11 presents conventional SIMS depth-compositional profiles of hydrogen, measured by the magnitude of the SiH^{31} peak (with a threshold of $10^{18}/cm^2$ in these figures). The Si^{28} peak is provided for reference. Figure 11a, b and c represent data on similar grain boundaries hydrogen-processed for 1, 2 and 4 minutes. Figure 12 provides similar data taken on a grain boundary (a) before and (b) after hydrogen passivation. A generally constant SiO^{44} signal is measured before the hydrogen processing. Since previous data have shown that the heat treatment and correlated oxygen segregation is primarily responsible for the activation of grain boundary electrical response, it is proposed that the hydrogen passivation is a result of the chemical interaction of the species at the grain boundary plane.

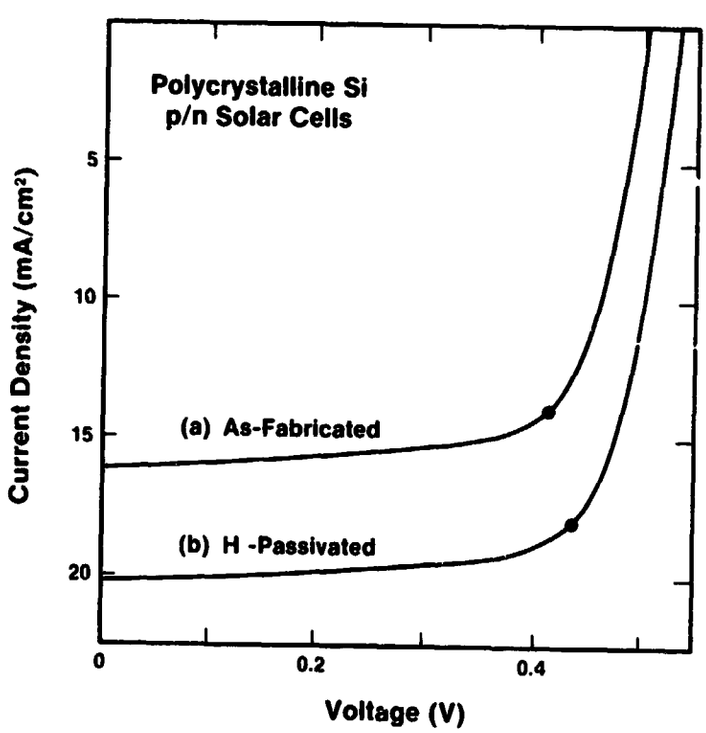

Fig. 8. Light current-voltage characterization for polycrystalline Si solar cells: (a) as fabricated; (b) H_2-passivated.

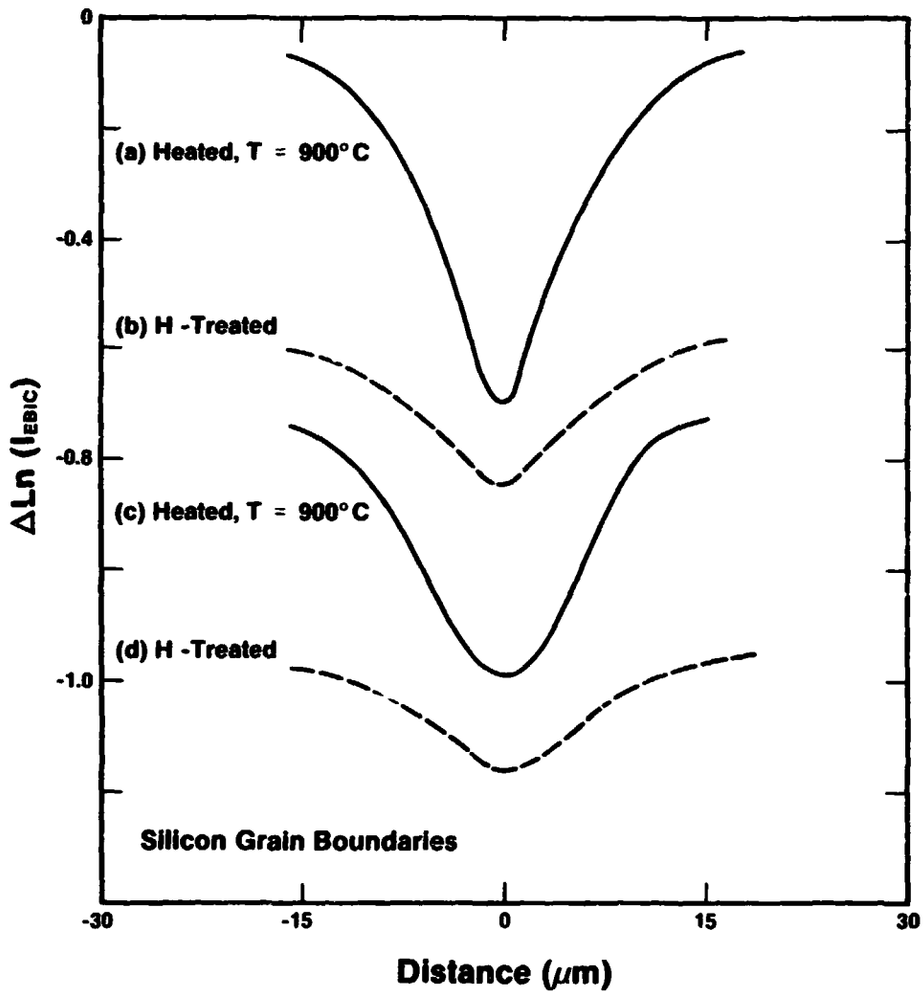

Fig. 9. EBIC linescans for Si grain boundary: (a) annealed at 900°C, for 30 min. in Ar: (b) H_2-passivated, 4 min. 275°C; (c) reheated, T = 900°C, 30 min. in Ar; and, (d) H_2-passivated again.

This interaction is illustrated in the SIMS area maps of Figs. (13-15). A computer-processed SIMS map sequence of the intersection of the grain boundary with the wafer surface is presented in Fig. 13. The sample was initially annealed to 900°C, and the boundary contains a high oxygen content. Hydrogen decoration of the region is noted after 1 min of the passivation processing. Figure 13c shows almost complete hydrogen decoration after 2 min of processing. Using the technique to examine the grain boundary composition within plane described earlier in this paper, the penetration of the hydrogen down the boundary plane as a function of processing time is evidenced in Fig. 14 for passivation treatments of 0.5, 1, 3, 4 and 6 minutes. The grain boundary was annealed initially to 900°C. The relatively high initial heat treatment pro-

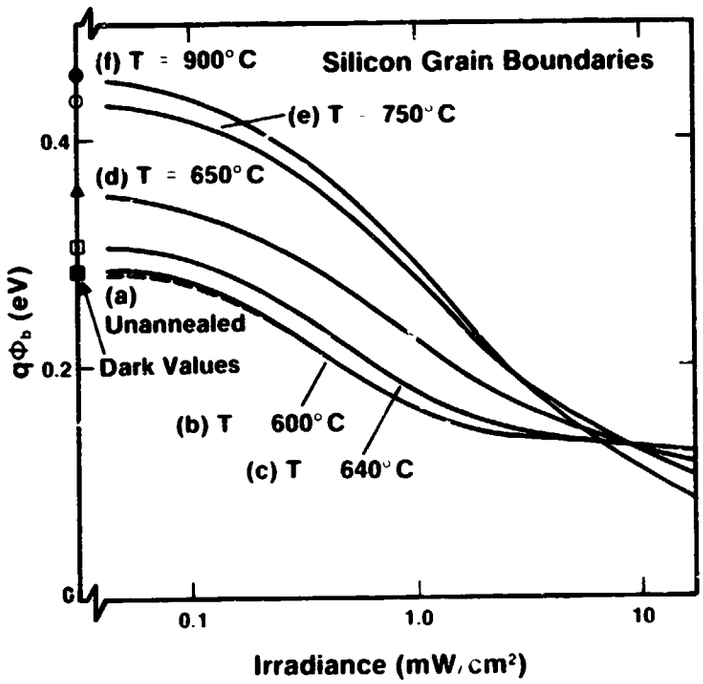

Fig. 10. Dependence of grain boundary barrier potential on light irradiation level for unannealed grain boundary in sequence of alternate treatments similar to Fig. 9.

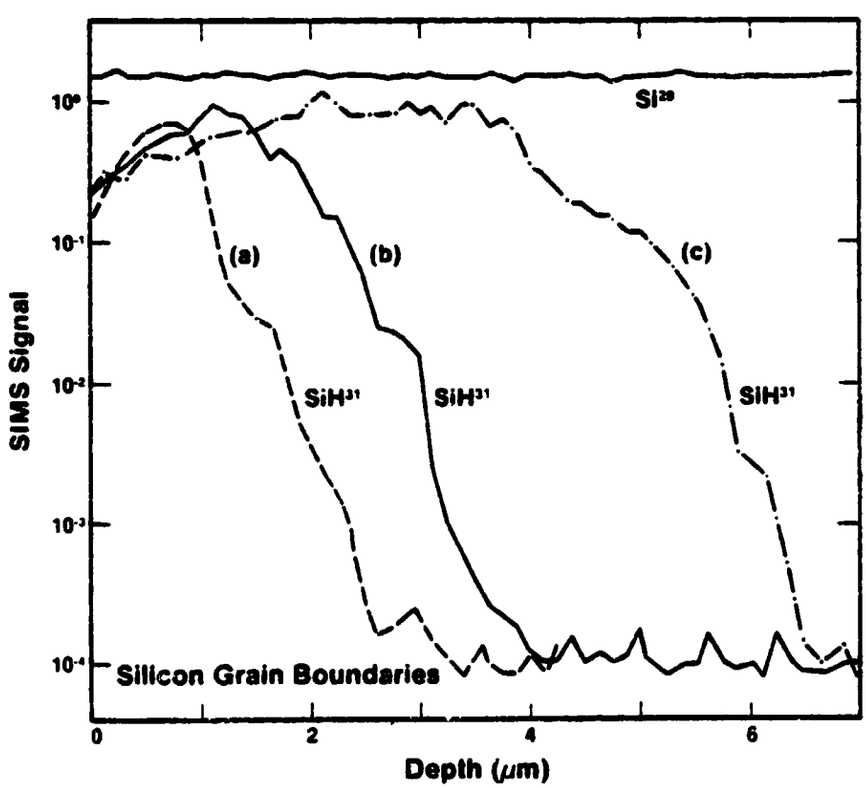

Fig. 11. SIMS depth compositional profile down grain boundary for: (a) 1 min; (b) 2 min.; and (c) 4 min. H_2-passivation processed Si.

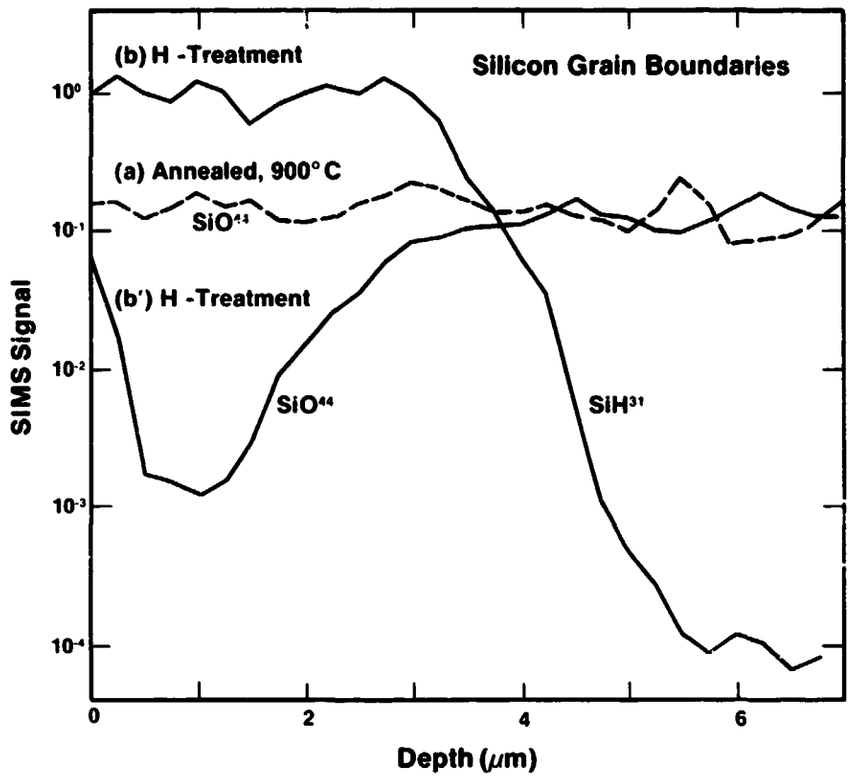

Fig. 12. SIMS depth compositional profile data for: (a) annealed, 900°C, 30 min. in Ar; and, (b) H_2-passivated processed Si grain boundary. (b') shows oxide level as function of depth after H_2-treatment.

vides for a high oxygen content of the boundary. The interaction of the hydrogen with the oxygen present at the boundary is better illustrated in the grain boundary of Fig. 15. This sample had been annealed to 750°C before the passivation process, and the oxygen at the boundary is somewhat less than the previous case. The hydrogen incorporation is observed to be enhanced in those regions that initially are oxidized. The exact chemistry of this process is not known. Methods similar to the specialized SIMS technique are currently being developed (e.g., digitally-resolved EELS) in order to investigate the chemical interaction of the species in-situ, during the treatments.

ORIGINAL PAGE IS
OF POOR QUALITY

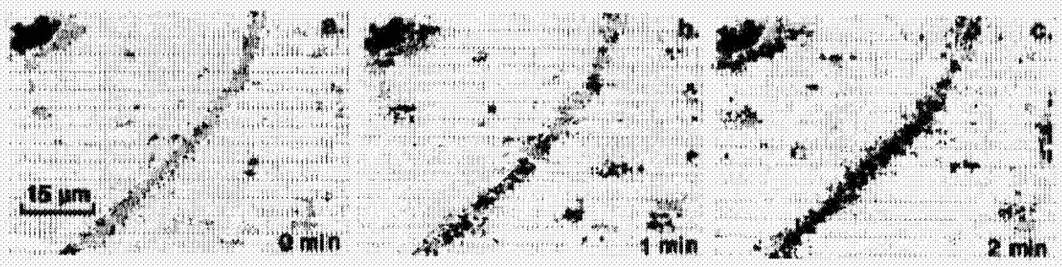

Fig. 13. SIMS mapping sequence of grain boundary intersection with wafer surface as function of passivation time showing decoration of boundary with hydrogen.

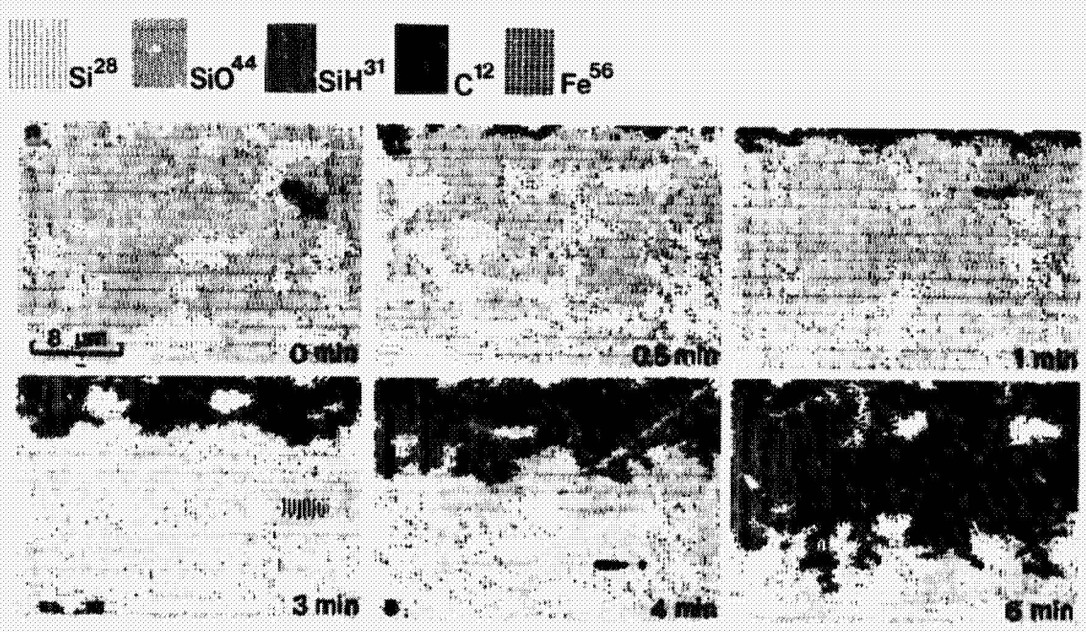

Fig. 14. SIMS mapping sequence showing hydrogen penetration of grain boundary plane as a function of passivation processing time. Grain boundary heated to 900°C before passivation.

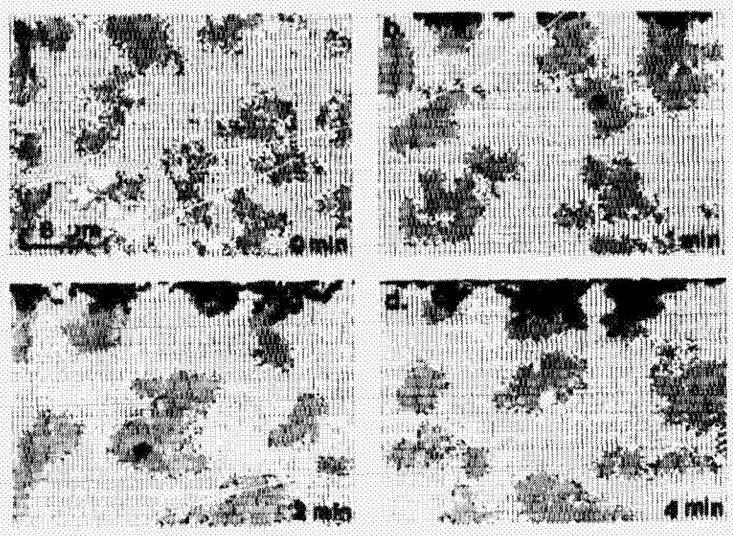

ORIGINAL PAGE IS
OF POOR QUALITY

Fig. 15. SIMS mapping sequence showing hydrogen - oxygen interaction at grain boundary heated to 750°C before passivation.

V. SUMMARY

The detection of impurities in silicon using AES and SIMS has been demonstrated, and the correlation of impurities with microelectrical characteristics has been exampled. The interrelationships among grain boundary impurity species, grain boundary electrical properties and solar cell performance in polycrystalline Si have been demonstrated. Specifically, two impurity mechanisms have been evaluated: (i) the segregation of oxygen to the intergrain regions during heat treatments; and, (ii) the incorporation of hydrogen in these regions during the passivation process. Finally, a specially-developed SIMS impurity mapping technique has been introduced which, for the first time, allows the investigation of the composition of a grain boundary surface utilizing volume indexing during the SIMS profiling.

Acknowledgement

The author gratefully acknowledges the inputs, assistance and work of J.R. Dick, R.J. Matson, T.P. Massopust, P.J. Ireland and A. Swartzlander of SERI, all of whom contributed greatly to the work of this paper. The author is also greateful to D.W. Ritchie of SERI for his encouragement of this work. This work was supported by the U.S. Department of Energy under Contract Number EG-77-C-01-4042.

REFERENCES

1. See, for example, A.W. Czanderna, ed., Methods of Surface Analysis (Elsevier Scientific, New York; 1975).
2. L.L. Kazmerski, Proc. 17th IEEE Photovoltaic Spec. Conf., Orlando (IEEE, New York; 1984) (in-press).
3. D. Redfield, Appl. Phys. Lett. 38, 174 (1981).
4. L.L. Kazmerski and J.R. Dick, J. Vac. Sci. Technol. A2, 1120 (1984).
5. L.L. Kazmerski, Proc. 5th EC Solar Photovoltaic Conf. (Reidel, 1984) (in-press).
6. J.I. Hanoka, C.H. Seager, D.J. Sharp and J.K.G. Panitz, J. Appl. Phys. 42, 618 (1983).
7. C. Dube, J.I. Hanoka and D.B. Sandstrom, Appl. Phys. Lett. 44, 425 (1983).

DISCUSSION

LOFERSKI: Toward the surface part of the Green cell, it's certainly a little bit astonishing, isn't it, that the phosphorus concentration is decreasing as you go toward the surface? Is that what you really meant or did you say it backwards?

KAZMERSKI: I think that in most SIMS data you will see a slight decrease in the signal right toward the surface. The whole thickness of the phosphorus region we showed there is only about 2000 Å.

LOFERSKI: And how about the thickness of the oxide region? What did you say it was, greater than 20 Å?

KAZMERSKI: Well it should be about 20 Å but if you look there, it looks like the data is spread out and it looks more like 50 or 60 Å.

LOFERSKI: So it is 50 or 60 Å, is what you would estimate?

KAZMERSKI: Yes, I am sure it is about 50 or 60 Å.

LOFERSKI: But you are saying that as you go toward the surface, even in an ordinary cell, if you did it with this volume indexing, you would find a decrease in the phosphorus concentration?

KAZMERSKI: Yes. I think so. You are seeing about 500 Å, that region that it decreases from 20^{20} down to 10^{18} cm^{-3}.

LOFERSKI: Yesterday Larry Olsen was showing some comparisons of a spreading resistance measurement profile and a SIMS profile, and there is a significant difference in the way they look. You mentioned being careful about using SIMS profiling because of the damage it does. If you compare a spreading resistance with a SIMS profile, which you would recommend as the more likely one to be correct?

KAZMERSKI: It depends on what you are looking for. Certainly one wouldn't want to measure resistance using SIMS, but for a pure representation of the profile, if the SIMS is done correctly, I'd would go with the SIMS.

LOFERSKI: I guess that actually his profile did show a drop-off at the surface too, as I recall.

MILSTEIN: The RCA SIMS profile showed it going up all the way to the surface.

To change the subject on you, you mentioned in terms of your SIMS resolution that you could resolve mass peaks for different species which had the same mass-to-charge ratio, for example, 31, phosphorus, and three silicon species, and quite frankly I am quite curious as to how that is done and whether you care to comment on it.

KAZMERSKI: You mean how to resolve it?

MILSTEIN: Well, if you had the same charge-to-mass ratio, and going through something like a quadripole mass analyzer.

KAZMERSKI: It's not a quadripole. This is a magnetic sector. You would never be able to do it in a quadripole. You just have the mass separation. It is done with a magnetic sector and this is all done on the Cemaca system. So you have your mass resolution as something like 50,000. It is not a quadripole. You would never be able to get that mass resolution with a quadripole. On a quadripole it would look just like one peak. In fact, on some quadripoles that we have seen, the mass resolution even drops off as a function of the time to mass, and sometimes you get an overlapping of two masses.

CAMPBELL: Have you looked at the hydrogen distribution as a function of depth in any single-crystal silicon?

KAZMERSKI: We looked at -- not really in single-crystal -- we looked at the grain regions in the silicon material here too, you know in the adjacent grain, and did not see any penetration. As a matter of fact, what we saw was some interaction with the oxide that might have been present right on the surface, but not a penetration into the grains.

CAMPBELL: There was some indication at the last PVSC that there was a bulk effect with hydrogen passivation.

KAZMERSKI: Yes. I heard that too, and we talked to the people and I think the penetration on the grains was not significant.

KEAVNEY: I wanted to ask about the low-temperature-annealed samples that have unactivated grain boundaries. What was their thermal history before they were annealed?

KAZMERSKI: I should go back. What we are doing is looking at one grain boundary of an unannealed sample. It doesn't mean that there weren't active grain boundaries also in that sample. We selected one that was not active to begin with. Its thermal history was that this was a directionally solidified sample with a grain size of about one-half to three-quarters of a centimeter that had not seen any processing beforehand, forming the junction for EBIC was done by a low-temperature oxidation at about 100°C. So that is the highest temperature the device had seen before any electrical measurements were taken.

KEAVNEY: Do you know how quickly it was cooled from the melt?

KAZMERSKI: No.

KEAVNEY: How quickly was the temperature cooled from the samples that were annealed at 900°C?

KAZMERSKI: The annealing procedure was to remove them from the annealing furnace and they were probably cooled over one-half hour or so.

RAI-CHOUDHURY: You mentioned hydrogen passivating defects; apparently oxygen

is active in it. I have two questions: Did you look at this defect by DLTS as to what kind of defect level it is? The other question is: Do you feel that oxygen was present in a precipitated form, rather than a single point defect, for it to be activated or deactivated? Can you make any comments on those?

KAZMERSKI: The first one: We did not do any DLTS on those things so I have no idea. I think that the people at SERI who had been doing DLTS on this polycrystalline material -- it is not a very satisfying measurement. You really have to spend a lot of time, so when the people attempted to do some DLTS, it looked like it was very difficult to identify any levels. I am sorry, I missed your second question.

RAI-CHOUDHURY: I have a lot of concern about oxygen, what it is doing to silicon, Czochralski silicon, and so forth. Does the oxygen, for it to be passivated by hydrogen -- it seemed like it should be present as it precipitated -- or can it react with hydrogen if it is present in the point defect without a cluster, without a precipitation?

KAZMERSKI: I really can't answer that, but I see no reason why not, if you look at the hydrogen and see there are also some point defects and other defects in there which are decorated by oxygen. The hydrogen seems to passivate those too, so I guess that would be true.

By the way, something in here, even though we see the hydrogen going down the grain boundary, there is still oxygen in the background. It is not like the oxygen is coming off, when the hydrogen goes the oxygen is leaving. There still is oxygen present.

TAN: If I may make a comment. Normally oxygen in silicon is not electrically active. Very difficult to pick up any level by the DLTS. So I believe, really, that we simply don't know what we are passivating. Where is this hydrogen? And the final thing is to say some form of dangling bond -- whether they are related to oxygen or not -- I don't think that question can be settled at this moment.

KAZMERSKI: I think that all we can do is say, there is the existence of oxygen and hydrogen, and there is some interaction between the two species.

WOLF: You answered only one part of my question, namely, the oxygen is still there until the hydrogen comes, but as you showed, as you increase the annealing temperature, more and more oxygen appears. Now where does it come from? Is it just activated so it becomes visible, or does it diffuse there from the outside, from the atmosphere, like the hydrogen comes in from the outside, or does it come out of the crystal?

KAZMERSKI: Well, presumably, it comes from the crystal. The annealing has been done in vacuum and it has been done in argon, it has been done in nitrogen, in a controlled atmosphere, so it is doubtful that it is coming from outside, and we presume that it is coming from the inside. Once again, the level here is about 10^{17} cm^{-3} of oxygen.

WOLF: Which is probably an order of magnitude less than what you would expect to be present in Czochralski, if it is a Cz type crystal.

KAZMERSKI: Or an order of magnitude more.

WOLF: You expect around 10^{18} cm^{-3} usually, don't you?

KAZMERSKI: I guess, at least in these data, the bulk data shows about 10^{16} cm^{-3}.

WOLF: Another comment I want to make is with respect to the Green cell. It seems your cross section was done not under the metal contact, but in between the contacts, and there should be about 100 to 200 Å of oxide, not 20 Å. There is a thicker oxide between the contacts normally. The 20 Å are only under the contacts.

KAZMERSKI: These data might be correct but the surface was thicker than 20 Å. I said more like 60 Å.

WOLF: Yes. That is what you said.

OLSEN: I think it is between 50 and 100 Å, is where he is using now. Between the contacts. That is what I was going to say.

KAZMERSKI: Well, then the data might be OK.

OLSEN: I have another question. Was that a zinc sulfide and magnesium fluoride? Is that the correct order? Is zinc sulfide on top? It is usually the other way around.

HANOKA: What is your sensitivity for oxygen? Isn't it around the low 10^{17} cm^{-3}? At least that is what I hear from Evans who does SIMS, out on the West Coast.

KAZMERSKI: It is 10^{16} cm^{-3}.

HANOKA: So yours is better than that, then. Second question: When you do this volume imaging, you showed a picture of your sputtering, basically a perfect parallel pipe, and in fact when you sputter your volume isn't it a thing where your sides slope? And isn't that sputter in that shape also a function of material when you are sputtering?

KAZMERSKI: What I am doing is only collecting the data from that rectangle. The sputtering may be more than that but the data are only being recorded from that rectangle.

HANOKA: So you are picking your rectangle within the sputter volume.

KAZMERSKI: That is correct.

QUESTION: I wanted to go back to Joe Loferski's question on the profile. You indicated that the concentration of the phosphorus fell off near the surface, but I didn't understand whether that was an artifact of the

measurement or whether you think that that is, in fact, what is happening to the profile.

KAZMERSKI: I think that is what is happening to the profile. Right near, within 500 Å of the surface, it drops off a little and then comes up and then goes down.

RAO: It seems to me that when the hydrogen passivates, not all grain boundaries are passivated equally. Now, do you have a characterization of these grain boundaries? Which kind of grain boundaries get deactivated with the hydrogen and which don't?

KAZMERSKI: We have seen that same thing. The only data I have showed you here is to be able to represent the volume indexing and attrition, but I think that is true that the grain boundaries are being affected differently. In fact, the only grain boundaries we are working with here are medium-angle grain boundaries, and I should point that out too. There is about a 28 or 30 degree mismatch between the <111> angles and the two grains. So that it could very well be that the structure of those grain boundaries is different, if you go to low-angle grain boundaries or even to higher-angle grain boundaries which will have different electrical properties.

RAO: Another question, which has to do with Martin Wolf's question. As you go away from the grain boundary do you find a concentration gradient of the oxygen, can we see it?

KAZMERSKI: Yes. You can do the same sort of thing. As you go away from the boundary itself you can see the decrease in oxygen concentration.

RAO: So can you calculate the diffusion coefficient and see if it matches up with the bulk diffusion coefficient of oxygen in silicon?

KAZMERSKI: You could do that. I never thought of that but you could do that.

GRUNTHANER: When I have looked at silicon oxide structures that have seen ion beams, whether those ion beams be argon systems or they be cesium systems, there is substantial generation of intermediate oxidation states from silicon sputtering mixing. Now, in the data you are showing here, in these grain boundaries in the oxygen and hydrogen passivation, they are quite clearly being taken on the same sample in the same general area where you are then exposing the system subsequently to the hydrogen. Now my question is, to what extent do you expect there is a degree of activation of the ion beam interactions with the oxygen going on to the subsequent decoration that you are seeing with the hydrogen, since presumably you are doing this in a static mode?

KAZMERSKI: First of all, each one of those hydrogen cases is for a separate sample of a grain boundary that has been cut and divided so the hydrogen passivation was done separately on each one. So it is not the same grain boundary in that case. You can see if you look at it that there are different structures. As a matter of fact, when the carbon that is present at some of the regions are not the same grain boundary itself, it is a

sequence of six grain boundaries that are cut in sequence going across. They are in the same grain boundary length but the grain boundary is cut into six adjacent pieces. It is not the same region each time. So it is not passivated. And then measure, because as soon as you measure it you are done with that sample.

N85-31627

Nitridation of SiO_2 for Surface Passivation

Stefan K-C Lai
Intel Corp., 3065 Bowers Ave.,
Santa Clara, CA 95051

I. INTRODUCTION

Thermal silicon dioxide has been one of the most important insulator for the present microelectronic technology. Not only is it an almost perfect insulator, its interface with silicon is very close to ideal, giving the lowest density of electrically active interface traps. Active transistors can only be fabricated successfully because of the low density of electronic traps. Furthermore, the low density of interface traps also provides an ideal passivation for the silicon surface electrically.

Silicon dioxide, however, is not perfect. The oxide network is actually a very porous network, allowing the diffusion of gaseous species through it, especially at elevated temperatures. This can change the electrical and thus the passivation properties of the oxide. Also, the oxide network can be very easily damaged by energetic particles and high energy radiation. This damage gives rise to an increased density of electronic states, both in the bulk of the oxide and at the silicon-silicon dioxide interface. The sum of the above effects is a long term degradation of the oxide and its interface with silicon, especially in the space environment.

Besides the above factors, there is a third factor that provides the driving force in the search for a better insulator: the defect density of silicon dioxide increases with decreasing oxide thicknesses. With the scaling of device dimensions in the quest for the highest packing density in integrated circuits, the vertical dimensions are also scaled. It is expected that 10nm oxides will be used extensively in half micron devices by the end of this decade. The yield and reliability of the present oxide system may not be able to satisfy the requirement.

It was under these conditions that Ito et al set out to develop a better insulator for silicon. They first reported the direct nitridation process to form a thermal nitride (1). However, such processes require very high temperatures and long process times. The nitrides formed were only of limited thicknesses (up to 5nm) and rich in oxygen (1,2). The films obtained are believed to be basically oxynitride layers. Next, they reported on the nitridation of silicon dioxide, which is the subject of this paper (3,4).

II. NITRIDATION OF SILICON DIOXIDE

Experiments on the nitridation of silicon dioxide has been reported many times in the literature (5). Ito et al first reported the thermal nitridation of silicon dioxide in ammonia (3). They reported that nitridation retarded the

destructive breakdown of silicon dioxide films (4). They explained the effect by the fact that the current through the oxide was much more uniform. They had also reported in detail the MOS characteristics of silicon dioxide nitrided under different conditions (6). Since then, it has been reported that nitrided oxide was effective in reducing the diffusion of boron through the dielectric, compared to the case of pure oxide (7). Terry et al reported on the radiation effects in nitrided oxide (8). They observed that there was very little generation of interface traps after radiation damage.

There have also been many papers published on the material characterization of the nitrided oxide (5). The common observation was that after nitridation, the dielectric was a very effective barrier to the diffusion of oxygen and water: it demonstrated very high oxidation resistance. This is consistent with the observation that it is an effective boron diffusion barrier. Auger experiments showed that there was a build up of nitrogen close to the silicon-silicon dioxide interface, resulting in a layer that was difficult to etch chemically and was probably the major barrier layer (9). Recently, more detail XPS (X-ray Photoelectron Spectroscopy) experiments showed that the nitrogen layer was located at a small distance (2.5nm) away from the interface (10). In general, the results were not completely consistent, which was probably due to the fact the process control was very difficult. Trace amount of oxygen or other impurities can change the reaction kinetics. The process history of the film may also affect the material characteristics.

In the present paper, an attempt will be made to relate the electrical properties of the film to the process history. A model is proposed to explain some of the observed results. It will be shown that with our present knowledge of the dielectric, it shows a lot of promise for its use in surface passivation, both for its resistance to impurity diffusion and for its resistance to radiation damage effects.

III. ELECTRON TRAPPING

Electron trapping can be used as a sensitive probe to the impurities and defects in silicon dioxide or related insulators and their interfaces with silicon. Generally, electron traps can be divided into two categories: intrinsic traps and high field generated traps (11). Intrinsic traps are traps that are present in the oxide after processing, either as impurities such as arsenic (12) or water related centers (13), or due to high energy processing such as plasma etching (14). The plasma or other high energy radiation give rise to hole trapping close to the interface and neutral electron traps in the bulk of the oxide. The electron traps can be filled by low field electron trapping experiments, most conveniently the injection of electrons by RF avalanche processes in silicon (13). Each kind of electron traps have their characteristic capture cross section which can act as a signature to their origin (11). The trapping process also follows classical trapping kinetics: the traps are filled over time, and the flatband voltage shift due to electron trapping will saturate.

When an oxide is subjected t high current and high electric field under the Fowler Nordheim tunneling condition, additional electron traps are actually generated by the process (15). In this case, the flatband voltage

does not saturate but will continue to increase with increasing electron fluence, until final breakdown due to the build up of a very high internal electric field due to the high density of trapped electron (16). The high field trap generation process is very similar to radiation damage. They both give rise to positive charge at the interface and the interface traps in both cases show a characteristic peak above midgap close to the conduction band (17). An increase in electron traps is observed in the bulk of the oxide, similar to the generation of neutral traps (11).

The change in the density of low field electron traps after the nitridation process was studied (18). In the experiment, oxides were annealed in ammonia at different temperatures for different times, wit' the results for one temperature shown in Figure 1. It can be seen after the nitridation process, there was a large increase in electron trapping at low electron fluence. When the trapping curves were analyzed, it was concluded that the increase in trapping was due to an electron trap with capture cross section of 10^{-17} cm^2. Nitridation at higher temperatures and longer times gave the same electron trap with the same capture cross section. However, the saturation density was slightly different, with slight increases for higher temperatures and longer times. This electron trap has been identified as due to OH centers in the oxide. This was confirmed when it was shown that from infrared absorption spectroscopy, an increase in density of OH bonds similar in density to the electron traps was observed. It was postulated that in the nitridation reaction, oxygen might be released from the oxide and reacted with the hydrogen in ammonia to give rise to the OH bonds.

The trapping process under high electric field for Fowler Nordheim tunneling in thin dielectric was then studied. The experiment involved the passing of constant current through the dielectric. Any electron trapping would increase the voltage required for the same current. Thus, the change in gate voltage is a measure of electron trapping. The trapping curve for the oxide in Figure 2 is characteristic of high field trapping process: there was an initial decrease in gate voltage due to the generation of holes, which actually enhanced the injection of electron. After about ten seconds, the curve changed in direction and there was a continuous increase in voltage shift due to the generation of additional electron traps. This is to be contrasted with the classical picture where the curve would saturate when all the traps are filled. For the nitrided oxide (NO), there was little or no hole trapping and the increase in electron trapping was faster compared to an oxide. The dielectric actually broke down in a short time because of the high internal field. The third sample called ONO (oxidized nitrided oxide) showed little hole trapping as well as little electron trapping. Electrically, this seems to be the most stable dielectric for the three studied. The lack of electron trapping in ONO was confirmed when it was shown that there was no window closing after extended cycles in E^2PROMs (19). Other experiments in E^2PROM had shown that there was hardly any hole trapping for ONO.

The properties of the dielectrics were studied further by subjecting the samples to high temperature anneal in an inert atmosphere (Nitrogen). The results were shown in Figure 3. For the oxide, the trapping process was increased slightly, but with the same characteristic features. The most dramatic change was observed in the nitrided oxide (NO). The density of electron traps was reduced to very low levels, similar to ONO before anneal. For ONO, there was actually a slight increase in trapping.

The above results is for a given nitridation condition. When the nitridation time is reduced by half, different results were obtained. For NO, the initial electron trapping was reduced. On the other hand, after the high temperature anneal, the electron trapping was only partially reduced. The results seemed to indicate that the dielectric is a mix between oxide and nitrided oxide. It is very important to realize that different process conditions affect the trapping properties significantly. The degree of nitridation initially and the post nitridation thermal cycle both change the dielectric characteristic. Furthermore, the nitridation conditions used in the present experiments are typically much more gentle compared to those reported in literature because the films were intended to be used in state of the art VLSI processes. Different results may be obtained for those heavily nitrided films.

To understand the experiments better, quasi-static capacitance curves (QCV) were obtained for the samples before and after different amount of electron fluence. Any interface trap generation will give distortion in the QCV curves while bulk trapping will give horizontal shift in the curves. The interface trap generation process was very similar to the bulk electron trapping process. The results are shown in Figure 4. For an oxide, after the high electron fluence, there was increasing distortion in the QCV curve. There was also a characteristic structure in the curve which was due to an interface trap peak. Similar peaks were observed in oxides damaged by radiation. This strongly links the present high field damage process to the radiation damage process. For the unannealed NO, little or no distortion in the QCV curve was observed. Instead, an almost parallel shift in the curve was observed. It can then be concluded that there was no generation of interface traps, and there was high density of electron traps in the bulk of the dielectric. Finally, for ONO and also annealed NO, there was little of no change in the CV curves after up to two coulombs/cm^2.

IV. MODEL

The above results can be explained by a very simple model. For an oxide, the electron trapping was due to high field generated traps. For the nitrided oxide with no anneal, there was more electron trapping which can be explained by the increase in OH centers shown in Figure 1. The only question is: what happened in the case of ONO? The effect can be explained by assuming that after nitridation, the density of high field generated traps were reduced to very low levels. This is supported by the results of the QCV experiment: there was no generation of interface traps, which are related to high field generated traps in the bulk of the oxide. Then, for ONO, the extra anneal reduces the density of OH to very low levels. This reduction after anneal has been reported before (20). With no OH sites and no high field generated traps, there is very little electron trapping. Oxygen is not required to reduce the density of electron traps. When the nitrided oxide was annealed in nitrogen, the lowest density of electron traps were obtained.

For a pure oxide, the high temperature anneal actually has an opposite effect on trap generation. Such an anneal has been shown to increase positive charge trapping and interface trap generation after radiation damage (21). In Figure 3, the high field trap generation in oxide was increased after the high temperature anneal. For ONO, the oxidation could have increased the oxide

properties such that after anneal, the rate of electron trapping was also increased.

The same model can be used to explain the observation at the silicon-dielectric interface. The nitridation process changes the interface such that it is no longer susceptible to high field damage. Recently, the detail of the interface damage process at the interface was studied (22). It was shown that the characteristic interface peak was not generated when holes were first trapped at the interface. Only when an electron was captured by the hole that the interface trap peak was observed. A model based on strained bonds at the interface was used satisfactorily to explain the observation. It was also proposed that the model can be used to explain radiation damage and neutral trap generation in the bulk of the oxide. From the present experimental results, the high field trap generation process can also be explained by the same model. In the simplest term, the damage process under high electric field and high energy radiation have similar origin.

The present results thus show that nitridation modifies the oxide network in a major way. It can be postulated that the nitrogen may go in and replace the strained bonds selectively, forming a silicon-nitrogen structure which may be much more stable. Possibly, the bonds are no longer "strained" and when holes are captured at the sites, the bonds do not go through a relaxation process. On capture of electrons, the bonds will return to their original state and no permanent damage states are generated.

For samples which were not nitrided for as long a time, there will be a lower density of OH traps. Also, the reduction of strained bonds by nitridation will also be limited. After the OH sites are reduced by an anneal process, the remaining strained bonds can give rise to significant electron trapping under high field conditions.

The reduction of OH bonds through anneal is basically a diffusion process. The thickness of oxide and the annealed temperature thus play a very important part in determining the final density of OH sites in the dielectric. The above experiments were carried out in oxides in the 10nm range because the dielectric was intended to be used in E^2PROMs. In this thickness range, it was shown above that it is possible to reduce the OH sites to very low levels. However, it is also important to remember that after the nitridation process, the dielectric is a very effective diffusion barrier. It would not be surprising that for thicker nitrided oxide, it would be much more difficult to reduce the OH sites, giving rise to a high density of bulk electron traps. This may explain some of the inconsistency that may have been observed.

V. DISCUSSION

There are two properties of the nitrided oxide discussed above that make it promising as a new dielectric for surface passivation. Firstly, the dielectric is a very good diffusion barrier. It gives the surface much better protection to the possibility of degradation from impurity elements. Secondly, from the results presented above, it appears that the dielectric is also very stable electrically. Specifically, the silicon-dielectric interface may not be degraded in a radiation environment. The use of the dielectric thus provides potentially a very stable passivation for silicon.

The present work has been only limited in scope, even though it shed a lot of light on the electrical properties as related to the chemistry of the system. No attempt had been made to study the detail of all the process conditions and correlate to radiation damage experiments. It is important to study the whole system in a comprehensive and detail manner in order to realize the full potential of the system.

VI. ACKNOWLEDGEMENT

The work reported in this paper was started while the author was with IBM Thomas J. Watson Research Center and continued when he joined Intel Corporation. He would like to thank the many people at both places who have contributed to the work and that the names are too many to be listed here.

VII. REFERENCES

(1) T. Ito, S. Hijiya, T. Nozaki, H. Arakawa, M. Shinoda and Y. Fukukawa, J. Electrochem. Soc., **125**, 448-452, (1978).
(2) S.P. Murarka, C.C. Chang and A.C. Adams, J. Electrochem. Soc., **126**, 996-1003, (1979).
(3) T. Ito, T. Nozaki and H. Ishikawa, J. Electrochem. Soc., **127**, 2053-2057, (1980).
(4) T. Ito, H. Arakawa, T. Nozaki and H. Ishikawa, J. Electrochem. Soc., **127**, 2248-2251, (1980).
(5) For a general review: I.A. Nemetz and R.E. Tressler, Solid State Tech., **26(2)**, 79-85 and **26(9)**, 209-216, (1983).
(6) T. Ito, T. Nakamura and H. Ishikawa, J. Electrochem. Soc., **129**, 184-188, (1982).
(7) S.S. Wong, C.G. Sodini, T.W. Ekstedt, H.R. Grinolds, K.H. Jackson and S.H. Kwan, J. Electrochem. Soc., **130**, 1139-1143, (1983).
(8) F.L. Terry, Jr., R.J. Aucoin, M.L. Naiman and S.D. Senturia, IEEE Elect. Dev. Lett., **EDL-4**, 191-193, (1983).
(9) F.H.P.M. Habraken, A.E.T. Kuiper, Y. Tamminga and J.B. Theeten, J. Appl. Phys., **53**, 6996-7002, (1982).
(10) R.P. Vasquez, M.H. Hecht, F.J. Grunthaner and M.L. Naiman, Appl. Phys. Lett., **44**, 969-971, (1984).
(11) D.J. DiMaria, The Physics of SiO_2 and Its Interface, Proceedings of the International Topical Conference, Pergamon Press, N.Y., 160-178, (1978).
(12) R.F. DeKeersmaecker and D.J. DiMaria, J. Appl. Phys., **51**, 1085-1101, (1980).
(13) D.R. Young, E.A. Irene, D.J. DiMaria, R.F. Dekeersmaecker and H.Z. Massoud, J. Appl. Phys., **50**, 6366-6372, (1979).
(14) L.M. Ephrath and D.J. DiMaria, Solid State Tech., **24(4)**, 182-188, (1981).
(15) C. Jenq, T. Rananath, C. Huang, S. Jones and T. Chang IEDM Tech. Digest, **IEDM81**, 388-391, (1981).
(16) E. Harari, J. Appl. Phys., **49**, 2478-2489, (1978).
(17) T.P. Ma, G. Scoggan and R. Leone, Appl. Phys. Lett., **27**, 61-63, (1975).
(18) S.K. Lai, D.W. Dong and A. Hartstein, J. Electrochem. Soc., **129**, 2042-2044, (1982).
(19) C.S. Jenq, T.L. Chiu, B. Joshi and J. Hu, IEDM Tech. Digest, **IEDM82**, 811-812, (1982).
(20) S.K. Lai, D.R. Young, J.A. Calise and F.J. Feigl, J. Appl. Phys., **52**, 5691-5695, (1981).

(21) E.P. EerNisse and G.F. Derbenwick, IEEE Trans. on Nucl. Sci., **NS-23**, 1534-1539, (1976).
(22) S.K. Lai, J. Appl. Phys., **54**, 2540-2546, (1983).

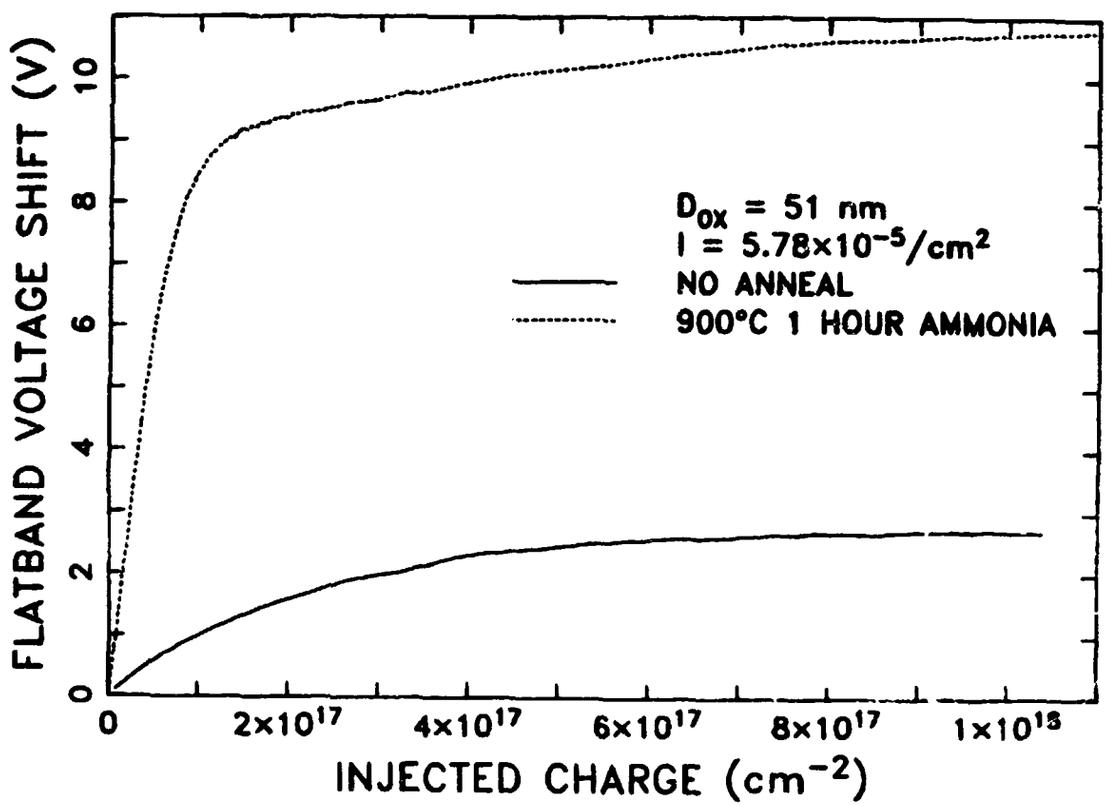

Figure 1: Flatband voltage shift as a function of injected electrons for a 51nm oxide with and without the ammonia anneal. The large increase initially for the annealed sample was due to a new electron trap with capture cross section of 10^{-17}/cm^2.

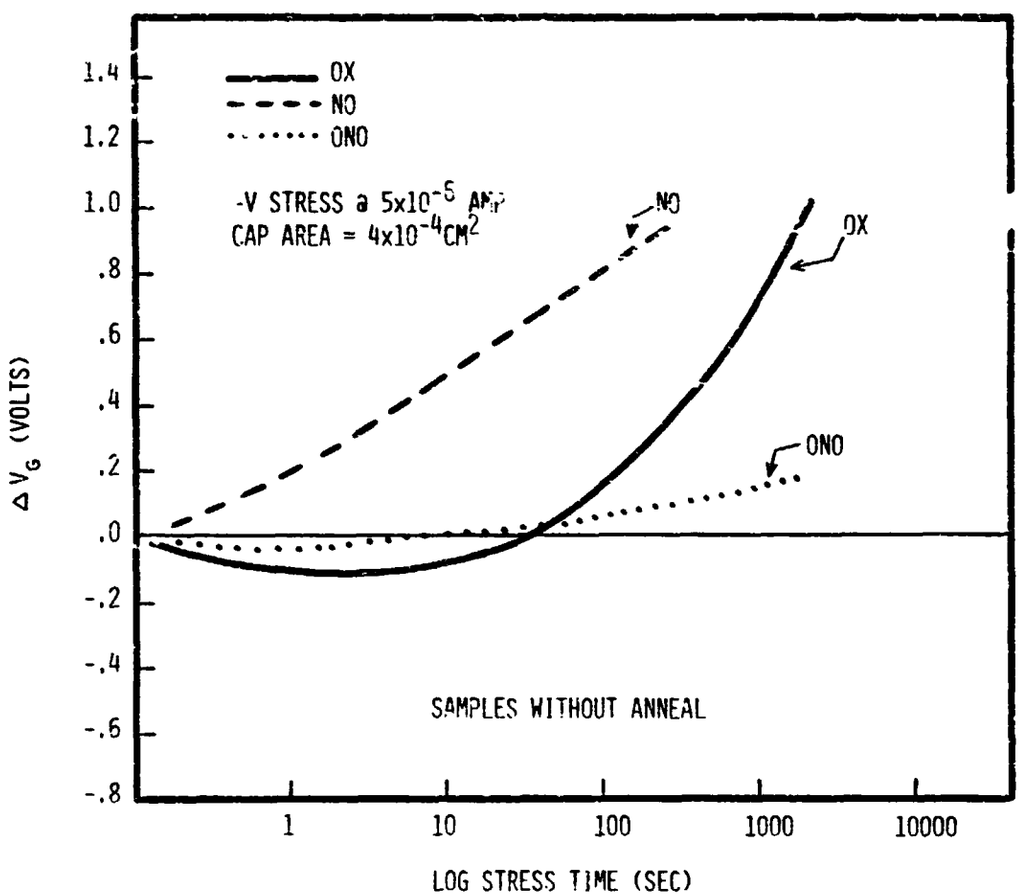

Figure 2: The changes in voltages across oxide, NO and ONO capacitors under constant current as a function of Log time. This is a measure of electron trapping which results in the shifts of IV curves under Fowler Nordheim injection.

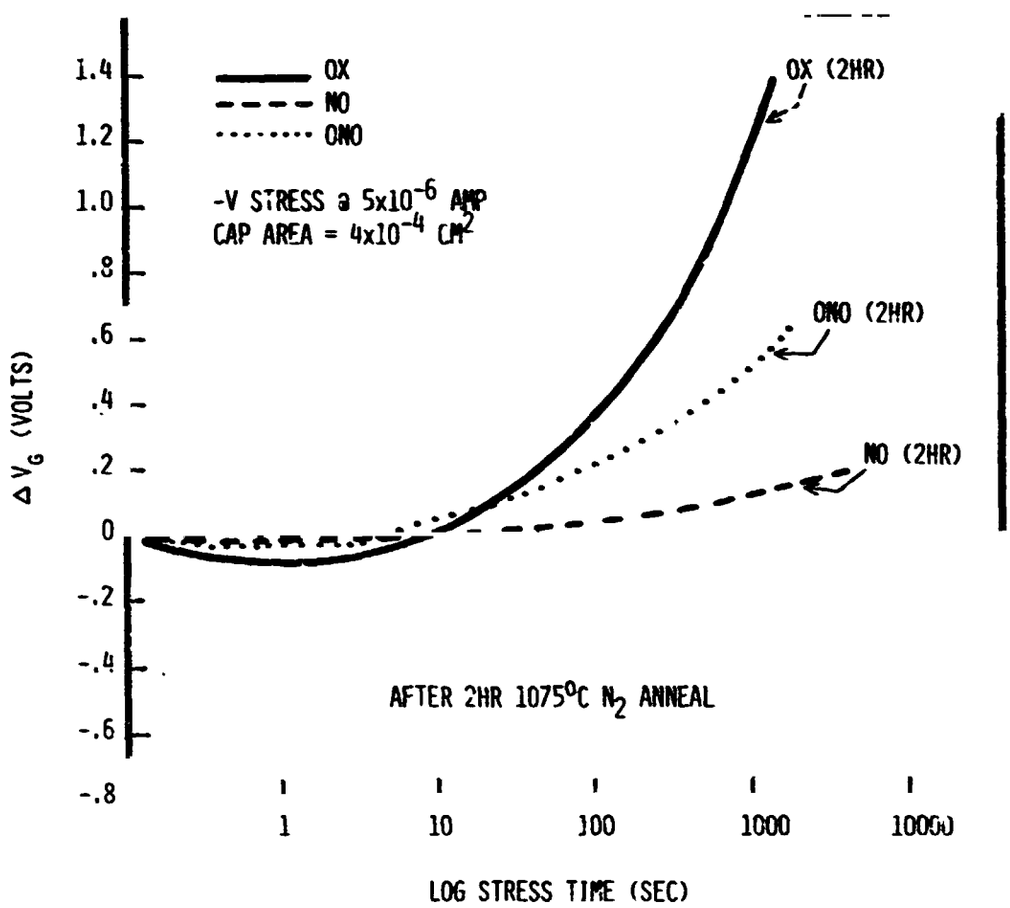

Figure 3: The changes in voltages across oxide, NO and ONO capacitors under constant current as a function of Log time. The samples were annealed for 2 hours at 1075°C in nitrogen.

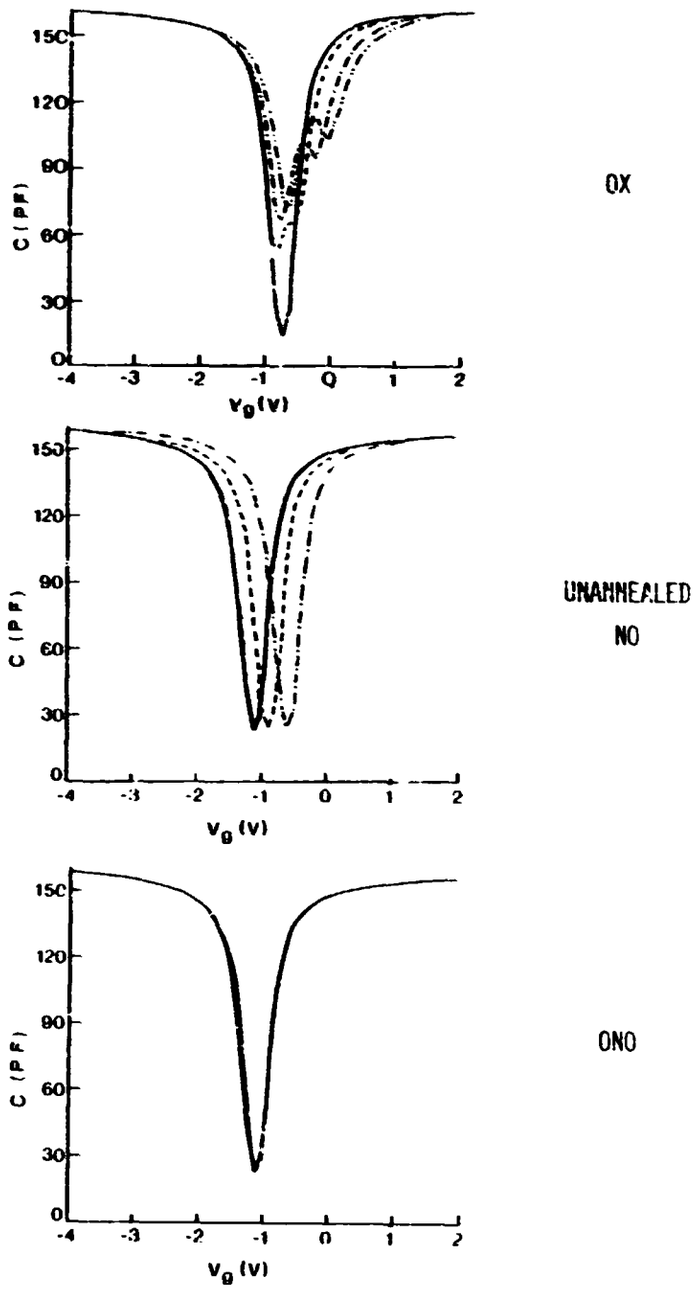

Figure 4: Quasi-static capacitance curves for an oxide, NO and ONO. The family of capacitance curves in each plot was due to increasing stresses across the dielectrics under constant current. The stress was approximately 0.5 coulombs/cm^2 per step.

DISCUSSION

ROHATGI: I can see that nitrided oxides are very good for VLSI, but from the point of your solar cells, they may not work because most of the nitrided oxides have been fabricated at temperatures of around 1100°C to 1200°C.

LAI: Well, I can tell you that for our purposes, for our work, we look at nitration conditions, which is consistent with VLSI processing. The conditions that I have shown you, up until now, in detail, there is no inconsistency at all with VLSI processing.

ROHATGI: That is what I am trying to point out, it is very good for VLSI because it takes care of radiation problems.

LAI: By VLSI, I mean that we are going away from high-temperature processes altogether. I don't see the nitration condition we have used is much lighter, compared with everything that is reported in the literature.

ROHATGI: I have made some nitrated oxide for passivating solar cells. Our solar-cell junctions have to be very thin, also, so I stayed at temperatures around 850°C. So I grew 100 Å oxide nitrided in ammonia at 850, and there was no real difference in the passivating properties of the oxide I had and the nitrided oxide. Then I went to a thermal nitride without any oxide, trying to make an MIS contact, and that was even worse. So it looks like if you are going to use this nitrided approach you have to figure out a way of doing it at low temperatures, because you don't see all these beneficial effects.

LAI: Well, I guess the important thing is, what properties you look at for passivation. I will have to calibrate it to the point of data I have here. Have you looked at interface properties, CV curves, at bonded or impurity diffusion, those kinds of conditions?

ROHATGI: I think interface properties is the key here, because that is what determines the surface recombination velocity, and like you said, unless you do the nitridation at temperatures 900 or above, you don't see all the good effects that have been reported in literature.

LAI: That is what I said earlier, though. I don't think my experience has been that it does not really improve the surface. But all I have stated here is more for long-term reliability, and it is a much more stable system, which I think is a very important thing, at least for our process.

GRUNTHANER: I think the dielectric material that you are looking at with the nitrided oxide shows a lot of really exciting possibilities, particularly in terms of generation mechanisms of more excited states. But there is one piece of information that you may or may not be aware of that has come out of the Hewlett-Packard studies, which I think may have some severe impact on the solar cell situation here. That is, the experiments looking at the lattice imaging of the silicon surface, comparing thin SiO_2 films with these nitrided oxides. The interesting thing about

those results is that the surface of the silicon itself at the very abrupt determination, the last three or four atomic layers of the silicon, has significantly relaxed. There is much less strain at that surface situation, as you can see from the lattice-imaging TEM micrographs, and I think there are some very serious implications for some of these recombination losses and so on in that. I don't know what they will turn out to be but I think --

LAI: Well, is that good or bad, though?

GRUNTHANER: That's right. I don't know which way it is going to go, but there clearly is a difference, and I think the first difference that has really been seen is in these dielectric films that have been grown. A variety of other approaches have been taken, but always very similar reconstruction strains, and so on, on the surface of the silicon. Yet only in this nitrided oxide are they seeing an actual relaxation of the top surface there for such sharp and coherent planes.

RAO: In those annealing experiments -- this is just a takeoff on his question -- what happens when you use, say, an inert gas like argon at the same temperature instead of nitrogen? Have you had any results on that?

LAI: No. I have not done the experiment.

N85-31628

SURFACE PASSIVATION AND JUNCTION FORMATION USING LOW ENERGY HYDROGEN IMPLANTS

S. J. Fonash
Engineering Science Program
The Pennsylvania State University
University Park, PA 16802

I. Introduction

The use of high current, low energy ion beams in device fabrication is a relatively recent development. Outstanding examples of this new, emerging use of low energy ions are the passivation of grain boundaries in polycrystalline silicon with low energy, hydrogen ion implantation [1] and the solar cell performance improvement resulting from low energy hydrogen ion implantation into Mobil Solar ribbon [2]. Recently we have demonstrated that there are additional, innovative applications for low energy hydrogen ion implants which can be very useful for crystalline silicon. We discuss these new applications for high current, low energy hydrogen ion implants in this paper.

The paper is arranged as follows: first, the effects of low energy hydrogen ion beams on crystalline Si surfaces are considered; next, the effect of these beams on bulk defects in crystalline Si is addressed; and, finally, specific applications of H^+ implants to crystalline Si processing are discussed. In all of the situations reported on here, the hydrogen beams were produced using a high current Kaufman ion source.

II. Hydrogen Beams: A Cause and Cure for Surface Defects

When a low energy hydrogen ion beam impinges on a single crystal silicon surface, the surface is sputter etched, hydrogen is implanted, and the silicon lattice is damaged. That low energy hydrogen ion beams damage Si surfaces may seem surprising in view of the ability of such beams to passivate grain boundaries in polycrystalline Si. However, the presence of this damage is demonstrated in Fig. 1. The figure shows Rutherford backscattering (RBS) data for two silicon samples: one which was subjected to a 0.4 keV H^+ beam and another which was subjected to a 1.0 keV H^+ beam. The two traces for these cases are RBS channeling data; the third trace is the random backscattering yield from a silicon sample.

As may be seen from the figure the lattice damage from to 1.0 keV H^+ beam exists deeper down into the Si than does the lattice damage from the 0.4 keV H^+ beam. Converting the energy scale into a measure of the field of energy dissipation for the H^+ ions gives a 200 Å deep layer of lattice damage for 0.4 keV H^+ and a 400 Å deep layer for 1.0 keV H^+ ions. This measure of the lattice damage is based on the full width in energy of the RBS channeling peak at half maximum of the yield. By noting that the channeling peak yields for both 0.4 H^+ and 1.0 H^+ beam exposures coincide with the random yield, it can be deduced that this layer of lattice damage, resulting from exposure to the hydrogen beams (dosage $\sim 10^{18}$ cm^{-2} in both cases), is amorphized.

A further demonstration of the fact that low energy hydrogen ion beams themselves damage Si is provided by Table I. This table gives peak to peak heights for the electron spin resonance (ESR) signature of silicon dangling bonds [3]. The table shows how this ESR measure of lattice damage varies as the H^+ ion beam energy is varied from 0.2 keV to 1.0 keV. The data indicate that lattice damage increases up to ∿0.8 keV and then appears to saturate. This saturation effect may be due to sputtering which reduces the volume of damaged material or to an annealing effect. Again all the dosages were of the order of $\sim 10^{18}$ cm^{-2}.

TABLE I

Peak-to-Peak ESR Signal Heights

Ion Beam Species & Energy		ESR Signal Heights Minimum Power Microwave	Medium Power Microwave	Maximum Power Microwave
Control Sample		<1	<1	--
H^+	0.2 keV	<1	∿1	∿2
	0.4 keV	<1	∿2	∿3
	0.6 keV	<1	∿2	∿3.5
	0.8 keV	∿2	∿4.5	∿8.5
	1.0 keV	∿1.5	∿4	∿7
Ar^+	0.2 keV	<1	·2	∿4
	0.4 keV	<1	∿2.5	∿7.5
	1.0 keV	∿5.5	∿15	∿40

An electrical assessment of the damage caused at crystalline Si surfaces by low energy hydrogen ion beams is presented in Fig. 2. Here current-voltage (I-V) data are given for Au dots deposited on p-Si. As expected Au contacts to chemically prepared p-Si (the control) show a low barrier height. However, Au contacts to chemically prepared p-Si, which was subsequently subjected to various H^+ beam exposures, yield I-V characteristics which indicate the presence of positive charge. That is, positive charge is created in a layer near the Si surface due to the H^+ beam exposure and this causes the increased barrier height seen in Fig. 2 [3-6].

Thus the RBS data of Fig. 1, the ESR data of Table I, and the I-V data of Fig. 2 establish that low energy H^+ ion beams damage single crystal Si surfaces. All measures of this damage agree that it is worse at the higher energies (for the range used) and least at the lower energies. However, these measures do not all yield data that vary with energy in exactly the same manner. For example, the amount of positive charge present, as judged from the I-V data, is not found to be simply proportional to the strength of the ESR signal.

Other low energy ion beams also damage single crystal silicon surfaces. In fact, as we will see, they inflict more damage (holding dosage and beam energy constant) than does hydrogen. We begin this consideration of the damage

effects of other ion beams by turning to Fig. 3. This figure establishes that low energy Ar^+ beams (again a total of $\sim 10^{18}$ ions/cm^2 impinged on these samples) damage the silicon lattice at and below the surface. In this case the RBS data indicate that the field over which energy is dissipated by 0.4 keV Ar^+ ions extends $\sim$100 Å below the surface whereas the field over which energy is dissipated by 1.0 keV Ar^+ ions extends $\sim$200 Å. These RBS data point out that the Ar^+ beams, unlike the hydrogen, have not been able to amorphise the Si surface layer.

Table I also contains the ESR assessment of the damage caused by Ar^+ ion beams. As may be noted from the table, the damage increases with beam energy and the damage signal is higher for Ar^+, for the same dosage and energy, than it is for H^+. Fig. 4 shows the I-V data for a Au dot on p-Si which was chemically prepared and subsequently subjected to a 1.0 keV Ar^+ beam. The positively charged surface layer (i.e., the surface layer containing damage-induced donors) is clearly present as a result of the Ar^+ exposure as is apparent from the I-V characteristic.

Hydrogen ion beams cause surface damage and other ion beams such as would be present in plasma deposition, sputtering, or dry etching (we took Ar^+ as an example), also cause surface damage. This observation immediately causes several questions to present themselves: (1) how does the damage caused by H^+ compare with that caused by Ar^+, (2) how can H^+ implants passivate poly Si and Mobil Solar ribbon Si without causing surface damage, and (3) can H^+ implants passivate the damage caused by Ar^+ implants. We begin addressing these questions by comparing H^+ and Ar^+ ion beam damage in single crystal Si.

As may be seen from Fig. 1 and 3, the RBS channeling data indicate that the field of damage (Si atoms knocked out of their lattice positions) is more extensive, for a given dosage and energy, for hydrogen than it is for argon. Also the hydrogen amorphises the Si surface layer; the argon does not. However, the ESR data of Table I indicate that there are more dangling bonds in the damage layers caused by Ar^+ -- even though Figs. 1 and 3 show these Ar^+ - caused layers are thinner -- than there are in the corresponding (same energy and dosage) layers caused by H^+. This is our first indication that, although the H^+ beam is very effective in tearing up the Si lattice, it also passivates its own damage as seen by the reduced ESR signal. The I-V data of Figs. 2 and 4 support this contention; i.e., there is less positive charge present after a 1.0 H^+ ion beam exposure than there is after a 1.0 Ar^+ ion beam exposure (both situations had a total of $\sim 10^{18}$ ions/cm^2 impinging on the Si).

This brings us to the question of how can H^+ implants passivate poly Si and Mobil Solar ribbon Si without causing surface damage. We believe the answer must be that these H^+ implants do cause damage to the surfaces of these materials. The picture that emerges is as follows: As the H^+ is implanted, if the self-caused damage is not too severe, some H can escape the implant region and diffuse to bulk defects or grain boundaries for passivation. The implant induced surface damage is partially (or completely) passivated by remaining hydrogen. This layer can then remain, be etched off, or be annealed out. We speculate that, if it remains in a completed n^+/p solar cell structure, any residual positive charge in the layer would only perform the beneficial service of forming a front surface field which would aid short wave length spectral response. However, if dangling bonds also remain these could increase surface recombination in the emitter lead-

ing to a degradation in V_{oc} (if it is controlled by the emitter) and to a degradation in the short wavelength spectral response. Put another way, if V_{oc} degrades after H^+ implantation, it suggests that V_{oc} is being controlled by the emitter and emitter recombination is being enhanced by exposure to the H^+ beam.

The pertinent question of whether or not H^+ implants can passivate surface lattice damage now needs to be considered. To do that we turn to Fig. 4. Here we see the I-V characteristic for an Au dot evaporated onto Si that has been subjected to 1.0 keV Ar^+ and then subjected to 0.4 keV H^+ beams. The Ar^+ damage seen in Fig. 4 (1.0 keV Ar^+ I-V curve) is clearly passivated by the H^+ implant. In fact, the damage (as judged by the presence of positive charge) is seen from Figs. 2 and 4 to be less after the Ar^+ plus H^+ beam exposures than it is after a simple 0.4 keV H^+ beam exposure.

Comparing Figures 2 and 4 indicates that there is a synergism involved in the 1.0 Ar^+ exposure/0.4 H^+ exposure. One can speculate that the damage caused by the 1.0 keV Ar^+ beam retards the penetration of the subsequent 0.4 keV H^+ beam trapping the hydrogen in a smaller volume. This allows it to be more effective in passivating the donor levels (positive charge) caused by the Ar^+ ion beam lattice damage. However, this retardation of the hydrogen by the Ar^+ damage has yet to be established by RBS. It also must be determined if the remaining damage (after 1.0 Ar^+/0.4 H^+) is electrically inactive but detectable by ESR measurements.

It is clear that hydrogen implants can be the cause as well as the cure for surface damage in crystalline silicon. The manner in which the hydrogen acts (i.e., whether it results in a net cure or cause of damage) depends on the previous history of the surface. It remains to be determined if implanting through thin oxide or nitride layers can modify this behavior and if hydrogen implants can improve the quality of thin oxide/Si or thin nitride/Si interfaces.

III. Hydrogen Beams: A Cure for Bulk Defects

From the results of Section II, from references [1] and [2], and from the wealth of data from amorphous Si work, it seems clear that hydrogen implants can passivate dangling bonds in silicon. Hence, if hydrogen can reach bonding defects in bulk Si, it will passivate them. Recently, it has also been suggested that hydrogen can passivate deep levels resulting from impurities in silicon [7,8]. However, this latter point remains somewhat in doubt since surface damage, incurred in the act of introducing the hydrogen, can getter fast diffusing impurities. Hence it remains to establish if hydrogen is passivating deep impurity levels or, if hydrogen-caused damage, is gettering the impurities.

IV. Applications of H^+ Implants to Crystalline Silicon

A. Surface Property Modification

As was discussed in Section II, if Si is exposed to a low energy hydrogen ion beam, there is a surface layer produced which contains lattice damage. This lattice damage gives rise to donor levels which cause the barrier seen in Fig. 2. As noted in Fig. 2, there is also an insulating Si:H or Si:H:O layer produced by the lower energy H^+ ion beam exposures [4]. Its presence is not

detected in Fig. 2 (it would appear as a large series resistance in the I-V) since these samples were all given an HF etch and DI water rinse.

The presence of this apparently wide gap, insulating Si:H or Si:H:O layer, produced by the lower energy H^+ beam exposures, is seen in Fig. 5. This figure presents capacitance-voltage (C-V) data for a p-type Si sample that was subjected to a 0.4 keV H^+ ion beam. In this case the Au front contact was deposited on the H^+ implanted surface without the HF etch to allow the insulating surface film to remain. These C-V data show that the wide gap Si:H or Si:H:O layer is capable of supporting both accumulation and inversion; i.e., the layer is a good insulator. We note that the conducting, lattice-damaged layer, containing the donor levels giving rise to the barrier seen in Fig. 2, lies below this insulating layer. This same type of insulating layer appears for the lower energy H^+ implants on n-type single crystal Si samples also.

This wide gap insulating surface layer created by the lower energy H^+ implants appears attractive for surface passivation of solar cells. The H^+ implants which produce this layer seem especially attractive for n^+ emitter structures since the wide-gap layer could passivate the emitter surface while the donor layer, produced by the H^+ implant, would create a front surface field. Such H^+ implants, when done through thin oxides or nitrides, may produce optimum emitter structures. However, this all remains speculation at this point since the effect of this processing on emitter recombination has not been determined nor has there been any attempt at optimization, or at studying, the effects of the presence of thin oxide or nitride layers.

B. Low Temperature Junction Formation

From the preceeding sections and from the literature there is extensive evidence pointing towards the virtues of hydrogen in the passivation of electrically active bonding defects in silicon. Hence, it seems only natural to determine if H^+ implants can improve the quality of implanted, shallow n^+/p and p^+/n junctions. The objective is to obtain high quality, low leakage implanted shallow junctions without recourse to the high temperature processing currently employed.

In our study, n^+/p diode structures were fabricated by implanting 75-keV As^+ ions into (100) p-type Si which had channel stops present. The dosage used was 5×10^{15} As atoms/cm^2 and the implant area was 3.7×10^{-2} cm^2. Using a Kaufman-type ion source, we subsequently implanted low-energy hydrogen ions into the damaged silicon. The hydrogen ion beam had an accelerating voltage of 0.4 keV, an extractor voltage of 0.3 keV, and an accelerator current of 200 mA. These silicon samples were then annealed at 500 or 600°C for 1 hr. in nitrogen or argon ambients. Spreading resistance measurements were subsequently made to examine the dopant profile and the degree of dopant activation. Current-voltage-temperature (I-V-T) measurements were made to examine the diode characteristics and transport mechanisms. Experimental details may be obtained from ref. [9].

We found that the low-temperature anneal, following the H^+ implant, is a very necessary part of this processing. The characteristics of our diodes, immediately after the H^+ implantation but before the low-temperature anneal, are extremely poor. The high series resistance and very large leakage currents (of the order of hundreds of μA/cm^2) indicate that the damage has not been fully passivated and that the dopant is not activated by the hydrogen implant alone. The inactivity of the dopant is borne out by the spreading resistance measure-

ments. (See Fig. 6). The lack of dopant activation after the H^+ implant is not surprising as the temperature of the silicon sample during the H^+ implant rises to temperatures less than 150°C. The results of our spreading resistance measurements (Fig. 6) indicate that junction depth after a 600°C 1-hr. anneal shows very little dopant redistribution. The dopant concentration as measured from spreading resistance shows that most of the implanted As has been activated by this 600°C anneal following the H^+ implantation.

Turning specifically to the diode I-V behavior resulting from this HILT processing (from hydrogen ion-assisted, low temperature anneal), it is seen in Fig. 7 that excellent diode characteristics result even though processing temperatures have never exceeded 600°C. Leakage currents of the order of 5 nA/cm^2 at 1.5 volt reverse bias are attained for ∿5-10Ω-cm p-Si base material. The forward bias n-factors in this case are n = 1.03 over ∿5 decades. We have obtained similare results for p^+/n implanted junctions.

In summary, we assert that this novel, genuinely low-temperature process offers an alternative to the numerous other processes being investigated to anneal out implantation damage and to activate dopants in implanted Si. Our preliminary studies, with very little optimization, show that this low-energy hydrogen-ion implantation/low-temperature anneal processing for damage passivation and dopant activation gives results comparable to the other annealing processes (we have looked at p^+/n junctions also). In addition it allows for passivation of any residual defects and thereby provides an advantage not offered by other techniques. Although at present we use furnace anneals to activate the dopants, we are by no means limited to them and can use low-energy H^+ implants in conjunction with lower-temperature RTA approaches. This will reduce the processing time involved. With the development of broad-beam ion sources, this process can very easily be adapted to the fabrication of the extremely shallow junctions needed for solar cells.

At this time the mechanism by which hydrogen implants improve device characteristics is not clear. Indeed several groups (including us) have found that H begins to evolve from silicon at a temperature of ∿350°C and is completely lost by 600°C. Thus the simple explanation of hydrogen bonding itself to the silicon "dangling bonds" does not seem to be adequate. Further work to identify the mechanisms of annealing and dopant activation is under way.

C. Enhancement of Web Solar Cell Performance

As we first pointed out at the 1983 European Photovoltaics Conference Meeting [10], low energy hydrogen ion implants can improve the performance of solar cells fabricated on Westinghouse web material. Subsequently [11] we have shown that these low energy implants reduce the J_o for the recombination-diffusion current controlling V_{oc} and, thereby, enhance V_{oc} in these cells. Also the long wavelength spectral response is improved by the implants [11] implying the diffusion length is increased in the base. This latter fact suggests that J_o is controlled by the base; consequently, V_{oc} and the spectral response improve due to an improved base diffusion length. From this picture one is led to the deduction that the H^+ implant is passivating bulk defects in the web Si.

There is an alternative explanation: the H^+ implants may be reducing recombination in the emitter; i.e., J_o may be controlled by the emitter. The enhanced long wavelength spectral response would not be due to enhance base properties in

this picture; but, rather, it would be due to a widened band gap in the emitter which allows long wavelength photons to penetrate into the base. That is, before the H^+ implant the band gap in the emitter is narrowed due to the high doping levels used in the Westinghouse cells. This narrow band gap causes enhanced long wavelength photon absorption in the emitter. After the H^+ implant, the band gap is widened and, as noted, these photons can now penetrate into the base giving an apparent increase in the base diffusion length.

Whether base material properties are actually being improved by these H^+ implants into web material or whether all the changes (reduced recombination and widened band gap) are taking place in the emitter remains to be determined. Given the fact that sample history affects the way hydrogen interacts with Si - as we established in Section II - it follows that the interaction of H^+ implants with web Si can be a complicated phenomenon which needs additional study.

V. Conclusions

As a result of our examination to date of the effects of hydrogen ion beam exposure on crystalline silicon, the following conclusions may be drawn:

1. Hydrogen ion exposure can cause, as well as cure, surface defects. These defects include damage-caused donor states and dangling bonds. Whether a hydrogen implant results in increased damaged or passivation depends on the energy of the implant and on the past processing history of the silicon surface.

2. Very low energy hydrogen ions can produce a wide-gap insulating film at the surface of silicon. It may be possible to use this layer, perhaps by implanting through thin oxide or nitride films, to passivate surfaces.

3. Hydrogen ion exposure can passivate bulk bonding defects.

4. Hydrogen implants can be used to give high quality, shallow implanted junctions. The use of the hydrogen implant allow this to be accomplished with processing temperatures of only 600°C.

5. Low energy hydrogen implants can improve solar cell performance. It appears that there are two possible scenarios that can explain this:

   One assumes that the hydrogen implants do not affect the emitter or, in the other extreme, damage the emitter. It is assumed that the implants passivate bulk defects. In this case, cells where V_{oc} is controlled by the base would show enhancement of the V_{oc} after the hydrogen implant and cells where V_{oc} is controlled by the emitter would show no change in V_{oc} or degradation. In both situations the long wavelength spectral response should improve.

   The other scenario assumes that the hydrogen implants reduce recombination in the emitter and also may widen the band gap

in the emitter, depending on emitter doping level. In this case, cells where V_{OC} is controlled by the base would show no change in V_{OC} after an implant; however, cells where V_{OC} is controlled by the emitter would show improvement. In both situations the long wavelength spectral response may improve due to band gap widening.

Acknowledgements

We wish to thank P. Rai-Choudhury and A. Rohatgi of the Westinghouse R & D Center for providing the impurity doped Si as well as the web Si. We also wish to thank E. Poindexter and P. Caplan of the U. S. Army Electronics Technology and Devices Laboratory for the ESR measurements and E. Wolf of Cornell's National Research and Resource Facility for Submicron Structures for the broad technical support of that facility.

Portions of this work were supported by the National Science Foundation under Grant #ECS-8305646.

References

1. C. H. Seager, D. J. Sharp, J. K. G. Panitz, and R. V. D'Aiello, J. Vac. Sci. and Technol., 20 (3), 430, 1982.

2. J. Hanoka, C. Seager, D. Sharp, and J. Panitz, Appl. Phys. Lett. 42, 618 (1983).

3. R. Singh, S. Fonash, P. Caplan, and E. Poindexter, Appl. Phys. Lett., 43, 502 (1983).

4. R. Singh, S. Fonash, S. Ashok, P. Caplan, J. Shappirio, M. Hage-Ali, and J. Ponpon, J. Vac. Sci. Technol. A1, 334 (1983).

5. J.-S. Wang, S. Fonash, and S. Ashok, IEEE Electron Device Lett., EDL-4 433 (1983).

6. A. Climent and S. J. Fonash, J. Appl. Phys., July 1984.

7. S. Pearton and A. Tavendale, Phys. Rev. B26, 7105 (1982).

8. S. Pearton, J. Kahn, W. Hansen, and E. Haller, J. Appl. Phys. 55, 1464 (1984).

9. R. Singh, S. J. Fonash, A. Rohatgi, P. Rai-Choudhury, and J. Giganti, J. Appl. Phys. 55, 867 (1984).

10. R. Singh, S. Fonash, A. Rohatgi, and P. Rai-Choudhury, Proc. European Photovoltaic Conference, Athens, Greece (1983).

11. D. Meier, A. Rohatgi, R. Campbell, P. Alexander, S. Fonash, and R. Singh, Photovoltaic Specialists Conference, Orlando, Florida, May, 1984.

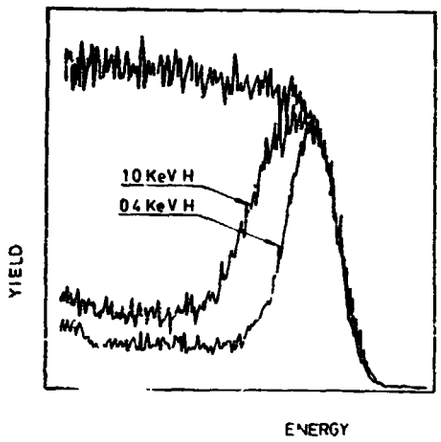

Figure 1. Rutherford backscattering channeling data for 0.4 keV and 1.0 keV H^+ beam exposures. Also shown is the random yield.

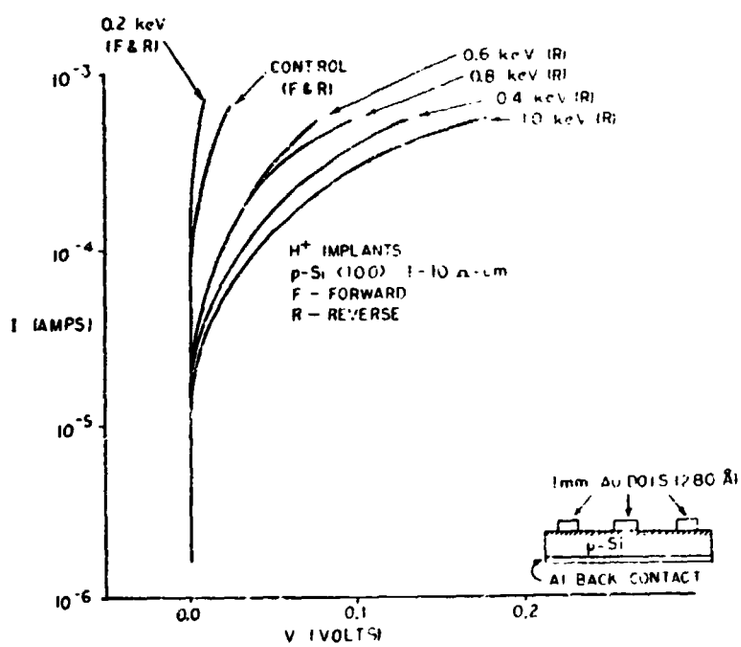

Figure 2. Current-voltage (I-V) data for Au dots evaporated onto p-Si surfaces subjected to various hydrogen ion beam exposures. The Au dots were deposited after the H^+ exposures and after an HF etch and DI water rinse. This etch and rinse is used to remove a high resistance Si:H or S:H:O layer that forms for the lower energy beams. See Figure 6.

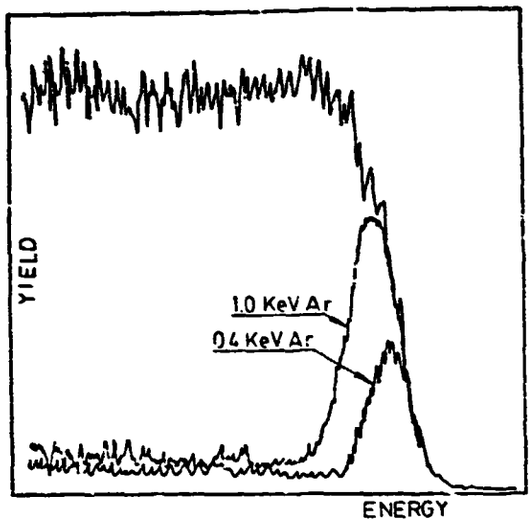

Figure 3. Rutherford backscattering channeling data for 0.4 keV and 1.0 keV Ar^+ beam exposures. Also shown is the random yield.

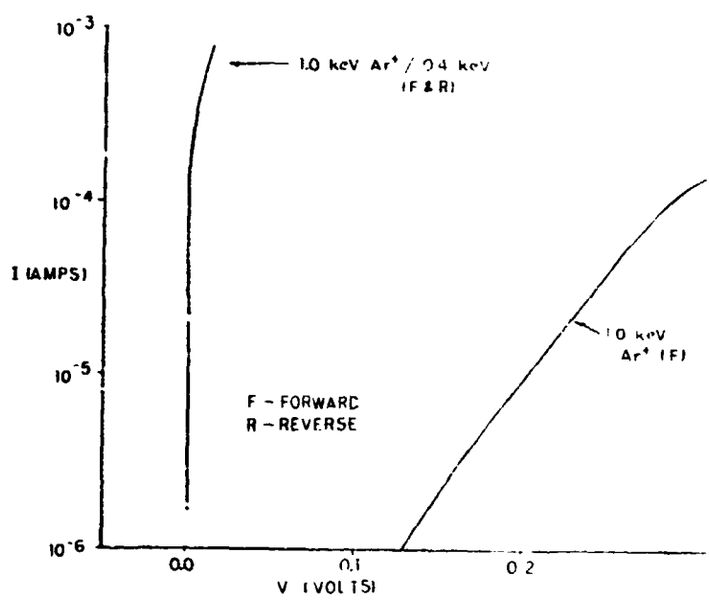

Figure 4. Current-voltage (I-V) data for Au dots evaporated onto p-Si surfaces subjected to 1.0 Ar^+ exposure. In one case the Ar^+ exposure was followed by an H^+ exposure. In each case the Au dots were deposited after the ion exposures and after an HF etch and DI water rinse.

ORIGINAL PAGE IS
OF POOR QUALITY

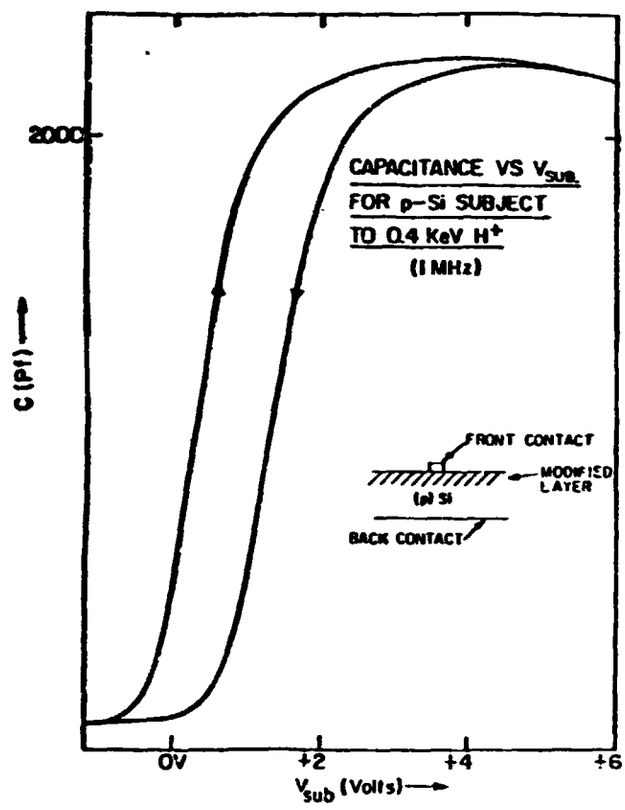

Figure 5. Capacitance-voltage data for p-Si which was implanted with H^+ (0.4 keV beam energy) but which was not given the subsequent HF etch and DI rinse used for the samples of Fig. 2. Accumulation and inversion are clearly occurring due to the presence of an insulating surface film.

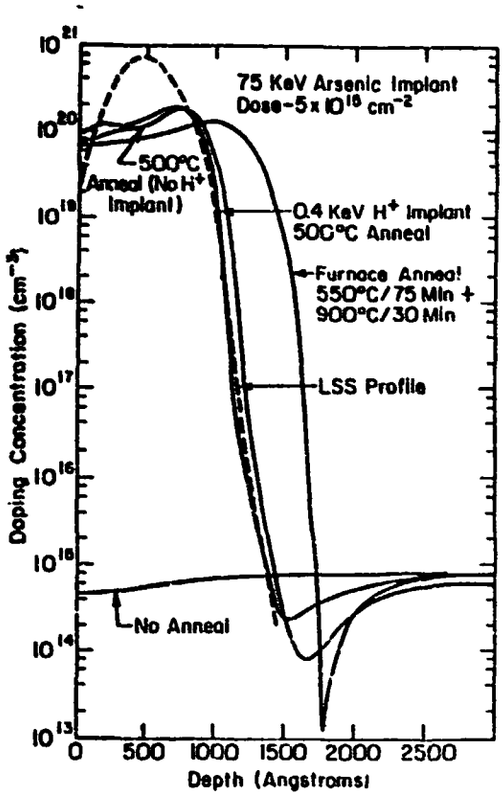

Figure 6. Spreading resistance plots for 75 keV As^+ implanted Si. Treatments following the As^+ implants are shown on the figure as is the theoretical LSS profile.

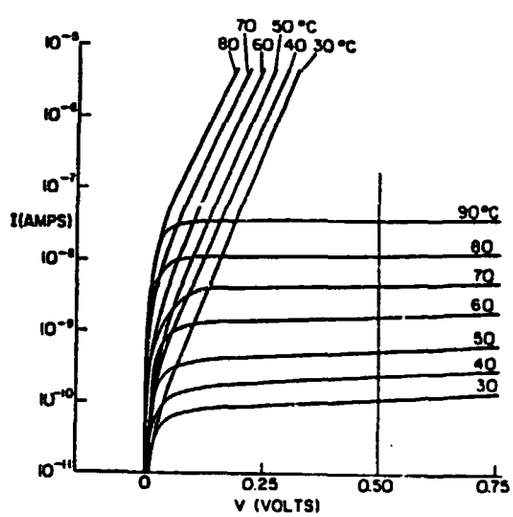

Figure 7. Current-voltage-temperature data for As^+ implanted Si. This n^+/p diode structure has had a 0.4 keV H^+ implant for 1 minute followed by a 600°C 1 hour furnace anneal in N_2. The diode area is 3.7×10^{-2} cm^{-2}

DISCUSSION

TURNER: I would propose an experiment by which you might be able to differentiate between those two models. That is, to shine blue light and red light -- as long as it is not infrared -- on the back of the cell, cut a window through the back metallization and shine light on that, and that will be sensitive to the diffusion length through the base of the material. The emitter won't make any difference, except for minor reflectivity.

FONASH: That is a good suggestion.

KAZMERSKI: Or you could try implanting through the rear.

FONASH: We haven't tried the former suggestion, the latter suggestion is being tried right now. We are trying implanting through the rear.

LESK: In your one-minute implantations, with your system, what dose are you getting?

FONASH: The dosages are on the order of $10^{18}/cm^2$.

LESK: And that is your general dose you are using for all this work?

In the last work you talked about, the emitter band-gap widening, were your measurements taken before the AR coat or after, and if after, did the temperature involved in the AR coat deposition have any effect on the annealing?

FONASH: The measurements that I just showed for the web material -- all the data that I showed was before AR coating. There was no temperature processing involved at all in that. Now Westinghouse has subsequently taken these cells and put on AR coatings to see what would happen and the performance continues to be enhanced to the degree that one would expect from an AR coating. They have also done -- and again, I think Ajeet (Rohatgi) will probably discuss this -- Westinghouse has also taken these cells that we have implanted and they have done some temperature stability studies on them, and what have you, and the answer to your general question is that they don't find any destabilization on the cells with moderate temperature cycling.

SCHRODER: Have you done any DLTS measurements on the damage layers themselves?

FONASH: Yes we have.

SCHRODER: The data you showed was after it was removed, on the gold sample?

FONASH: Yes it was.

SCHRODER: On the previous samples?

FONASH: We have done DLTS, and we see a broad damage signal around the middle

of the gap, a little bit above the middle of gap. We have also implanted silicon into silicon and done DLTS to compare the damage signals, and they compare. But that is work that we have just been into for about a month or so. I would not really like to comment on that too much, other than to say that we are doing precisely what you have suggested.

SCHRODER: OK. Another question is, do you think your hydrogen implant conditions are similar to what I assume you referred to -- proton work, plasma, or even recently, I think, they use an electron technique?

FONASH: That is right.

SCHRODER: Are the conditions similar, you think?

FONASH: In a plasma, as you know, the governing quantity that one needs to look at is the voltage across the sheet, because that is the energy that the ions would impact the surface with. So I really don't know; given the power, there is no way to convert that directly into what the energy of the ions is, so I can't comment on whether the situation is the same. I don't know the energy of their ions when they impact the surface. They are also talking about a process where they do the hydrogen treatment at 300°C, as I remember. It is done for something like two hours. To summarize my answer, I don't know the energy of their ions. Theirs is a process done at elevated temperature, and it is a process that is done for some two hours. Ours is a process that is done at essentially room temperature, at one minute, for very carefully controlled ion energy.

LOFERSKI: I was going to suggest perhaps a third mechanism that would account for the increase of diffusion length in the Westinghouse web samples. Perhaps, also, for what is going on in that gold-doped cell. You know, for one thing, the implantation certainly produces a lot of vacancies in the silicon, at interstitials and vacancies. You know the work by George Watkins -- and the ESR studies in silicon -- and of other people, that shows that vacancies form complexes and these complexes are what result in the deep levels that control lifetime. Now vacancies can also -- some of the complexes can be in a direction where they wipe out something that was a lifetime killer, and, you know, just neutralize it, so that it is possible that what is happening in both cases is that you have generated vacancies in excess of what you would have had at that temperature and they go down into the complexes; the vacancies are very mobile. Watkins showed that you don't see any free vacancies, and if you produce them at temperatures higher than, I think something at 1K, they move rapid· even down there at 20K, and so forth.

FONASH: I realize that.

LOFERSKI: So, anyway, that is another possibility.

FONASH: I think it is a possibility. That is one of the reasons why we are going to the implant from the back. But there is always a possibility that that experiment, implant from the back, could be clouded by the vacancies coming all the way up to the emitter. One could always argue that that is not the definitive experiment. I am aware of the high

mobility of vacancies, and it does indeed further cloud the issue. Getting back to the gold, I don't think it is the explanation there, because I think we have pretty well established that the gold is captured in that damaged layer and we remove it when we etch off the damaged layer.

LOFERSKI: I was wondering about the gold, whether anybody has studied gold and vacancies, complexes; whether Watkins has done that or not?

FONASH: I don't know.

MILSTEIN: As you may be aware -- I am sure aware -- we also looked at hydrogen implants at 300 eV in web materials and our RBS data and some other things differ a little bit from yours. At 400 eV for 1000 minutes of passivation, just to make sure we saw the damage if it was going to be there. We saw no amorphous material, and that is consistent with the fact that we saw no change in the reflectance under those implant conditions. However, when we went to 900 eV or 1500 eV, we saw several hundred Å of amorphous material, and in fact we saw a very dramatic change in the absorption, which is consistent with the appearance of amorphous material. In that sense, I would question whether at 400 eV, which is a mere 100 eV above where we were, you are seeing the kinds of things you are seeing.

FONASH: Well, I don't question it, because we have reproduced it several times, so I know it's real. And I think these other data -- there is a group at IBM for example, that has used Rutherford back-scattering to study damage incurred in reactive ion etching, and they have found that for comparable energies, 300 eV, 400 eV, the RBS does indeed detect a substantially damaged layer. So I don't doubt the data, that there is a damaged layer that is produced there at 400 eV.

MILSTEIN: Well, we saw latticed damage, ~600 Å of lattice damage, we did not see amorphous at 400 eV.

FONASH: Oh, you mean the RBS yield was not up to the amorphous level?

MILSTEIN: That is correct.

FONASH: Well, I don't know the explanation for that other than to suggest that perhaps you did some thermal treatment. It could be that your energies are not the same.

MILSTEIN: No.

FONASH: Well, we find this reproducible.

SAH: I would like to ask you if you have tried it on an encapsulated silicon?

FONASH: Yes.

SAH: What happens?

FONASH: Well, what do you want to discuss?

SAH: For instance, you called this level a donor level.

FONASH: That is right, it is symmetric. It lowers the barrier in n-type silicon. We have published that in a number of places.

SAH: It is still donor, or is it not donor?

FONASH: It is still donor. It lowers the barrier in n-type silicon. In other words, you get an n^+n type of layer on n-type silicon. You see, it's one of the first things we did to see if the effect is symmetric between p and n silicon, and indeed it is. It is not a special case of a donor that shows up for p material and mysteriously disappears for n type material.

HANOKA: The stuff we've done leaves no doubt that the first of your two explanations is the right one. The second one is not, because we have done a lot of diffusion-length measurements using, let's say, a liquid-junction technique, which does not change the sample at all. It is totally nondestructive. It doesn't heat it or anything. We take a sample with no junction, just measure diffusion length for an implanted sample. Diffusion length definitely goes up, and it's definitely a bulk effect. We etch off samples and measure it again. The same sort of thing. Etch off some of the material and measure again.

FONASH: What energies are you using now?

HANOKA: These are higher energies. I think 1500 to 1700 eV.

FONASH: I think we have to keep that in mind -- that you are talking about energies that are 1500 eV.

HANOKA: But I don't see where that makes a difference here.

FONASH: Well, just last week we did some implants for Westinghouse. We took a sample -- Westinghouse had measured the diffusion length by surface photovoltage -- we did the implant and gave them the samples back. They measured the diffusion length by surface photovoltage and it didn't change. But we are down around 400 eV.

HANOKA: We do find the diffusion length changes from sample to sample. It is a function of the kind of defects you have in the sample.

FONASH: Well, I think an important point is, you are looking at your material, are you not?

HANOKA: This is only on EFG now.

FONASH: Right. And we are looking at web material, and the nature of the defects is quite different, is it not? In your material don't you have a lot of defects that intersect the surface, and so one could think of conduits that could carry the hydrogen down into the bulk.

HANOKA: That's right.

FONASH: We have a different kind of material, so I think we have to watch an apples-and-oranges kind of comparison.

HANOKA: Well, I still think it is apples, but I think it is McIntosh and Delicious.

LOFERSKI: I just wonder if the difference between your results and his could relate to temperature control.

FONASH: That's what I think.

LOFERSKI: Dose up to 10^{17} cm^{-3} in one minute at 400 eV. That is a big jolt of energy, and the temperature may be fluctuating.

FONASH: Well, of course it works the other way though, doesn't it? You would think that we might get some regrowth if we are dumping all that hydrogen in in such a short time, but yet he is claiming that perhaps he's got some regrowth. So I think it is going in the opposite direction.

LOFERSKI: If he has the same dose as you have for that long he is going to explode the surface.

FONASH: I think he is using the same dose.

HANOKA: A factor of three lower.

FONASH: Oh, is it a factor of three lower?

LOFERSKI: A lot less.

FONASH: I think temperature is the key to that difficulty. I don't think there is anything fundamentally significant in that.

N85-31629

Frank J. Grunthaner's abstract is presented here. His paper and visual material were not presented for publications.

CHEMICAL STRUCTURE OF INTERFACES

Frank J. Grunthaner

Jet Propulsion Laboratory
California Institute of Technology
Pasadena, California

The interfacial structure of silicon/dielectric and silicon/metal systems is particularly amenable to analysis using a combination of surface spectroscopies together with a variety of chemical structures of Si/SiO_2, $Si/SiO_2Si_3N_4$, Si/Si_2N_2O, $Si/SiO_2/Al$, and Si/Native Oxide interfaces using high resolution (0.350 eV FWHM) X-ray photoelectron spectroscopy. The general structure of these dielectric interfaces entails a monolayer chemical transition layer at the Si/dielectric boundary, which consists of specific distributions of the intermediate oxidation states of silicon (Si^{+1}, Si^{+2}, and Si^{+3}), which appear to be related to local morphology of the silicon substrate. Amorphous Si substrates show a wide variety of hydrogenated Si and $Si(OH)_x$ states that are not observed in thermal oxidation of single crystal material. Extended SiO_2 layers greater than 8 Å in thickness are shown to be stoichiometric SiO_2, but to exhibit a wide variety of local network structures. In the nitrogen-containing systems, we see an approach to stoichiometric oxynitride compounds with interesting impurity- and electron-trapping properties. In native oxides, we find substantial topographical non-uniformity in oxide thickness and composition (e.g., a nominal 25Å oxide can be shown to have 4 different areal distributions of SiO_2 ranging in thickness from 12 to 165 Å). Analysis of metal/oxide interfacial layers is accomplished by analytical removal of the Si substrate by UHV XeF_2 dry etching methods. The general question of the importance of the chemical state of the starting silicon surface to the final dielectric/silicon interface composition will be addressed in a series of experiments using covalent silicon surface substitution. Finally, the modification of silicon surface bonding and hybridization in the presence of sub-monolayer levels of transition metals will be examined from the perspective of a modification in interfacial reactivity.

PRECEDING PAGE BLANK NOT FILMED

DISCUSSION
(GRUNTHANER)

No discussion.

SESSION IV

BULK EFFECTS

E. Sirtl, Chairman

N85-31630

Erhard Sirtl's abstract is presented here. His paper and visual material were not presented for publication.

STRUCTURAL DEFECTS IN CRYSTALLINE SILICON

Erhard Sirtl

Heliotronic GmbH
Burghausen, Federal Republic of Germany

The basic photovoltaic properties of a given crystalline silicon specimen seem to be governed by density and nature of two- to three-dimensional lattice defects. These are mainly generated by primary growth conditions as grain boundaries of more or less intrinsic character or second-phase precipitates from supersaturated solutions of carbon or oxygen. Considerably high values of both solubility and diffusivity in connection with their abundance in common refractory material systems account for the predominance of the two particular elements. Unsaturated dislocations of different types very often can be seen as a consequence of the existence of more-dimensional defects as described initially.

The final performance of a solar cell, however, is dependent of the concentration and distribution of recombination-active centers in the different regions of this device. Typical representatives are fast-diffusing transition metals in form of either single atoms or simple complexes.

Their avoidance, annihilation, or removal has been of great concern in different fields of electronic materials development for years. Presently we are still in a very early stage of thorough comprehension in terms of interaction of metal atoms with the one- to three-dimensional crystal defects discussed.

DISCUSSION

RAI-CHOUDHURY: What needs to be improved in polycrystalline silicon, without paying a price for solar performance?

SIRTL: (First part of answer not recorded) . . .wouldn't it be better to take a single crystal? It was not the alternative for us in this case, because we didn't work on that, and we didn't even plan to work on that because we wanted to create something that has to be much more economical in the future. But we were pleased to see that grain boundaries in general must not mean, from the beginning, a terrible situation. If we optimize that over the years, in a certain way, we may well end up with something that will just please us to be there. We have seen that people have managed rather well, or very well, in the meantime, to overcome the problem of a grain boundary running through a p-n junction. That is one subject I would say I missed, that has not been brought up explicitly around here, but it may be a subject for some further meeting because, I think we would learn a lot of interesting things.

SCHWUTTKE: May I answer the previous question, if you don't mind? I think that you should not confuse the electrical capture cross section of a defect as its capability to getter impurities. These are two totally different situations. I think it is possible that you can getter impurities, maybe by some mechanism that I don't want to go into right now, but that the electrical capture cross section for electrons of that particular defect is totally different. You may be just fortunate in this respect.

SIRTL: Your point is well taken.

N85-31631

Oxygen and Carbon Impurities and Related Defects in Silicon

Charles W. Pearce
AT&T Technology Systems
Allentown, Pa.

Oxygen and carbon are the predominant impurities in Czochralski-grown silicon. Their concentrations usually exceeding those of any intentional dopants. The behavior of these impurities during the heat treatments characteristic of device processing generally determines the defect morphology of the processed wafer. As a result this topic has been considerably researched. This paper will review the topic starting with the incorporation of oxygen and carbon during crystal growth and proceed to a discussion of device effects.

Specifically, methods for controlling oxygen and carbon incorporation during crystal growth will be discussed and results supporting a segregation coefficient of k=0.5 for oxygen will be presented. The nucleation and precipitation behavior of oxygen is complex. This paper will focus on temperature and doping level effects which add insight into the role of point defects in the nucleation process. In general precipitation is found to be retarded in N+ and P+ silicon. The types and quantities of defects resulting from the oxygen precipitates is of interest as they are technologically useful in the process called "intrinsic gettering". A comparison will be made between the available defect sites and the quantities of metallic impurities present in a typical wafer which need to be "gettered". Finally, a discussion of the denuded-zone, intrinsic-gettered (DZ-IG) structure on device properties will be presented.

Introduction

Oxygen and carbon are important impurities in Czochralski-grown silicon as the defect morphology of a processed wafer often depends on the behavior of these impurities during the heat treatments used in device fabrication. In particular, denuded zone (DZ), intrinsic gettering (IG) techniques (1) are used to improve the yield and performance of bipolar and MOS devices. These DZ-IG techniques transform oxygen into a beneficial impurity. Because of this technological importance the subject of oxygen in silicon has been considerably researched and periodically reviewed (1, 2, 3). The present state of the art includes the following observations. Oxygen is now considered a controllable impurity in Czochralski (CZ) silicon. Most supplies of silicon wafers will supply material to a specification. Secondly, there is an assort-

ment of published heat treatments which can be used on wafers to develop a "denuded zone", i.e., a near surface region free of oxygen-related defects, and an interior "intrinsically gettered zone" where the precipitation of oxygen and related defects is promoted. These treatments involve heat treatments at different temperatures to outdiffuse oxygen for a denuded zone, nucleate and precipitate oxygen, and promote the growth of defects resulting from the precipitation process. Figure 1 illustrates a typical cycle. Although such methods allow for the control of oxygen during processing, questions still remain as to the fundamental aspects of nucleation and precipitation. This is evident in the behavior of crystals grown to the same apparent oxygen content, but exhibiting markedly different precipitation behavior during device processes. To use a practical example we have observed situations where given the same level of oxygen content wafers from one supplier will readily precipitate during processing, whereas another vendor's material remains precipitate-free. Such observations have led to an interest in the role of point defects (i.e., vacancies and interstitials) in the nucleation process. Differences in precipitation behavior are thought to be related to the effect of the thermal cycles, a crystal receives in-situ in the grower, on the point defect populations (4). The role of carbon as a precipitation promoter is also being studied (5).

Another recent area of interest is the behavior of oxygen in N+ and P+ silicon. The use of N/N+ and P/P+ epitaxial silicon wafers for NMOS and CMOS devices (6, 7) has stimulated research into this area. Beyond the immediate technological importance studies of N+ and P+ silicon provide another avenue to evaluate the role of point defects in the nucleation process.

This paper will review the topic starting with oxygen incorporation and proceed to device effects with an emphasis on newer results.

Oxygen Incorporation

The quantity of oxygen incorporated into a growing crystal is at any point in time a function of the segregation coefficient and the oxygen content in the molten silicon (melt). The melt concentration depends on the erosion rate of the quartz crucible and the evaporation of SiO from the melt-ambient interface (8). Although the erosion rate is temperature dependent it is significantly increased by the presence of convection currents in the melt. In large crucibles characteristic of industrial-scale growers thermal convection effects are usually larger than those from forced convection. Given the Grashof number as an index of thermal convection (9). The melt turbulence tends to be reduced as the level of the melt decreases in the crucible during growth. Also, the surface area which is eroding simultaneously decreases. The net result is a decrease in the oxygen content of the melt. However, methods to alter the erosion rate or otherwise control the melt oxygen content have been found. These include the use of magnetic fields to suppress convection currents in the melt (10), double crucible techniques (11) which provide a constant erosion rate and surface area of an inner crucible, and reduced ambient pressure growth (12). In short, techniques exist which improve the uniformity of oxygen in an as-grown CZ crystal by 10X compared to unrefined CZ growth processes.

Beyond melt dynamics the influence of impurities on crucible erosion needs to be considered. The carbon reduction of SiO_2 into CO and SiO has already been shown to be a favorable reaction (8). Thus, higher levels of carbon in the melt increase the erosion rate. Note that since carbon has a low segregation coefficient (k=.07) it tends to enrich in the melt as growth proceeds thus increasing the crucible erosion rate. We have noticed a similar effect for boron. As seen in Table I crystals grown with high levels of boron tend to exhibit a higher oxygen content when grown under otherwise identical conditions. This is attributed to the glass forming properties of boron because similar melt levels of antimony a non-glass former do not increase the level of oxygen. This fact needs to be considered when comparing the behavior of P-, P+ and N+ crystals. It cannot be tacitly assumed identical growth conditions result in identical oxygen levels.

Fundamental to understanding dopant incorporation is an accurate value for the segregation coefficient. For many years the value for oxygen was generally accepted as k=1.25. Such a value was extracted from the axial distribution of oxygen in an as-grown crystal. However, in hindsight the substantial variation in melt oxygen content due to the convection effects just discussed render such an approach invalid. Recent experimental work by Lin (13) suggests a value of k=0.25. We have calculated k from first principles and re-evaluated existing solubility data for the liquid and solid phases and similarly conclude k=0.5 $\pm$ .25 (14).

A related issue to the incorporation of oxygen is the method by which it is measured. The most common method is infrared (IR) absorption measurements at 1106 cm^{-1}. However, the measurement is sensitive only to oxygen in interstitial lattice sites and needs to be calibrated with another analytical method. In fact, five calibration constants have been reported (15, 16, 17, 18, 19). Secondary Ion Mass Spectrometry (SIMS) and Charged Particle Activation Analysis (CPAA) have also been used for oxygen determinations. In our experience the CPAA does seem to indicate more oxygen than the IR method by about 50% (Table I). However, due to uncertainties in the calibration of each technique and the oxygen inhomogeneity within a sample it is unclear whether a real difference is present. Evidence of a real difference comes from Jastrzebski (20) who has heated wafers at high temperatures (1200-1300°C) and observed increases in the IR oxygen content of up to 2X. This indicates a substantial amount of oxygen in non-interstitial sites in the as-grown crystal. However, we have not observed a similar increase upon heating in our crystals. This leaves open the question of whether precipitation differences in material are due to nucleation effects or simply a difference in oxygen content. If the latter is true it means any calibration constant for IR measurements is good only for the material on which it was produced.

Nucleation and Precipitation

The particulars of the nucleation process have been a source of controversy for some time. Discussions have centered on whether the nucleation is homogeneous or heterogeneous and if heterogeneous the nature of the nuclei. Specifically, the role of interstitials and vacancies.

Insight into these questions can be gained from a study of N+ and P+ silicon.

We have observed (6) as has De Kock and van de Wijgert (7) that precipitation is suppressed in N+ silicon above a doping level $1x10^{18}$ atoms/cm^3 when heated at high temperatures (T=1000°C). However, given a suitable heat treatment (24 hr-700°C, 24 hr-900°C, ref 6) precipitates can be formed. At still higher N+ doping levels ($5x10^{19}$ atoms/cm^3) no precipitates are observed even given the heat treatment just described. Furthermore, the lack of precipitation in N+ silicon is not due to a lower oxygen content as discussed in the prior section. Additionally, we have found that precipitation is retarded, but not totally suppressed, at doping levels of $5x10^{19}$ atoms/cm^3) for boron-doped silicon. Doping levels of $9x10^{19}$ atoms/cm^3 still exhibit precipitation, but at densities up to 10^2 less than densities in P- samples given the same heat treatment (Figure 2). These results are consistent within a framework of a vacancy model. Vacancies in silicon exist in three charge states and a neutral configuration (21). The levels are shown in Figure 3. For n-silicon a movement of the Fermi level towards the conduction band means negatively charged vacancies become the dominant point defect. If these negative vacancies pair with oppositely-charged dopant atoms then they are unavailable for nucleation as proposed by De Kock (7). In p silicon a similar movement of the Fermi level will not produce a dominance of positively-charged vacancies as the energy level for the V+ lies much closer to the valence band edge. So even at high p doping levels some neutral vacancies still exist so some precipitation does occur. The available data does not conclusively prove the role of vacancies, but does indicate the role of point defects having asymmetric energy levels within the band gap.

Device Issues

DZ-IG treatments produce bulk stacking fault (BSF) densities in the 10^9-10^{10} BSF/cm^3 range. Typical metallic impurity contents of processed wafers are in the 10^{12}-10^{15} atoms/cm^3 (22). At either extreme complete capture (gettering) of impurities by defects requires 10^2-10^4 atoms/BSF. Given a typical BSF circumference of 10 microns a fault need only capture 10^{-4}-10^{-2} atoms/Å. Thus, the fault need only retain a relatively few atoms along its perimeter. This does not appear to be the limiting feature of intrinsic gettering. The limitations of IG probably stem from other sources. First, although BSF do exhibit a net capture of impurities it is not known how efficient this process is compared to other capture processes such as ion pairing in phosphorous gettering. Secondly, the capture of a metallic impurity at a BSF does not neutralize it electrically. Rather removal of a metallic impurity from the depletion region of a device to a BSF in the interior of the wafer results in the impurity being changed from a factor in diffusion rather than generation current. As such a net improvement in junction leakage will result, but the leakage current will now be a function of DZ width. Increasing the DZ width can only be accomplished up to half the thickness of the wafer at the expense of the number of gettering sites. The IG region remains a region of high recombination for photoexcited carriers.

Conclusion

In spite of considerable research into this topic full and final answers to some questions are still not obtainable, but there exists a sufficient body of data and information to successfully control the behavior of oxygen in CZ silicon. In particular, the study of heavily-doped silicon offers new insights into nucleation and precipitation processes.

Comparison of Oxygen Contents of Silicon
as a Function of Doping Level and Type

Table I

	IR	CPAA
n+ (.02 ohm-cm.)	-	1.5×10^{18}
n+ (.02 ohm-cm.)	-	1.9×10^{18}
p- (5 ohm-cm.)	1.1×10^{18}	1.5×10^{18}
p- (5 ohm-cm.)	0.8×10^{18}	2.1×10^{18}
p- (5 ohm-cm.)	1.0×10^{18}	1.1×10^{18}
p+ (.01 ohm-cm.)	-	1.3×10^{18}
p++ (.001 ohm-cm.)	-	2.7×10^{18}
p++ (.001 ohm-cm.)	-	2.5×10^{18}

References

1. C. W. Pearce, L. E. Katz and T. E. Seidel, "Semiconductor Silicon 1981", edited by H. R. Huff and R. J. Kriegler, The Electrochemical Society, Pennington, N.J., p. 705.

2. J. R. Patel, ibid, p. 189.

3. W. M. Bullis and L. C. Kimmerling eds., "Defects in Silicon", The Electrochemical Society, Pennington, N.J., 1983.

4. H. Nakanishi, Jpn. J. Appl. Phys., 19, 561 (1980).

5. J. Leroueille, Phys. Stat. Sol. (a) 67, 177 (1981).

6. A. J. R. De Kock and W. M. van de Wijgert, J. Crystal Growth, 49, 718 (1980).

7. C. W. Pearce and G. A. Rozgonyi, "VLSI Science and Technology - 1982", edited by C. J. Dell'Oca and W. M. Bullis, The Electrochemical Society, Pennington, N.J., p. 53.

8. S. M. Sze, editor, "VLSI Technology", McGraw Hill, N.Y., 1983, p. 26.

9. J. R. Carruthers et al, "Semiconductor Silicon 1977", H. R. Huff and E. Sirtl eds., The Electrochemical Society, Pennington, N.J., p. 61.

10. T. Suzuki et al, "Semiconductor Silicon 1981", H. R. Huff and R. J. Kriegler eds., The Electrochemical Society, Pennington, N.J., 1981, p. 90.

11. W. Lin and C. W. Pearce, J. Appl. Phys., 51 (10), 5540 (1980).

12. W. Lin and D. W. Hill, "Silicon Processing", D. C. Gupta ed., The American Society for Testing and Materials, Phila., Pa., 1983, p. 24.

13. W. Lin and D. W. Hill, J. Appl. Phys., 54, 1085 (1983).

14. C. W. Pearce and R. J. Jaccodine, "Defects in Silicon", W. M. Bullis and L. C. Kimmerling eds., The Electrochemical Society, Pennington, N.J., 1983, p. 115.

15. Y. Yatsurugi et al, J. Electrochem. Soc., 120, 975 (1973).

16. W. Kaiser and P. H. Keck, J. Appl. Phys., 28, 822 (1957).

17. K. Graff et al, Sol. State Elec., 16 887 (1973).

18. J. A. Baker, ibid, 16, 1431 (1970).

19. T. Sizuka et al, "Defects in Silicon", W. M. Bullis and L. C. Kimmerling eds., The Electrochemical Society, Pennington, N.J., 1983, p. 265.

20. L. Jastrzebski et al, J. Electrochemical Soc., 124 1638 (1982).

21. J. A. Van Vechten and C. D. Thurmond, Phy. Rev. B, 14, 3551 (1976).

22. P. F. Schmidt and C. W. Pearce, J. Electrochem. Soc., 128, 630 (1981).

ORIGINAL PAGE IS
OF POOR QUALITY

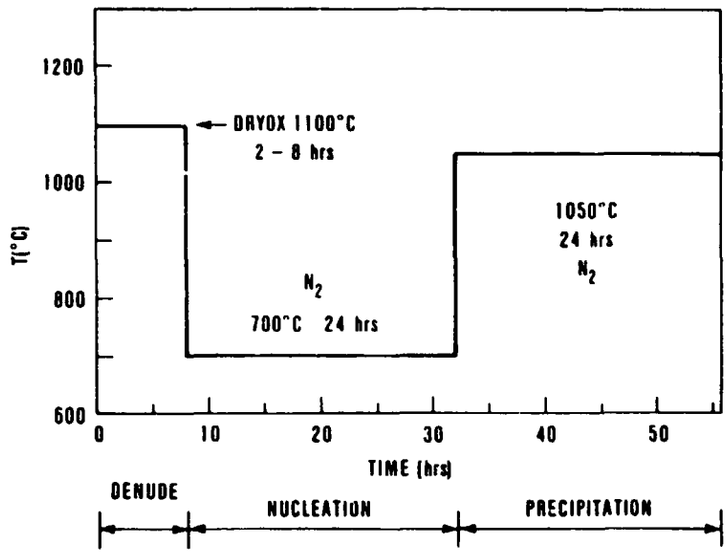

Figure 1. Hi-Lo-Hi Thermal Cycle for Intrinsic Gette ng

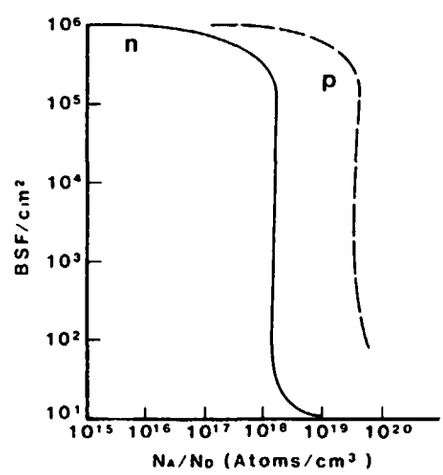

Figure 2. Doping Density Effect on Defect Density

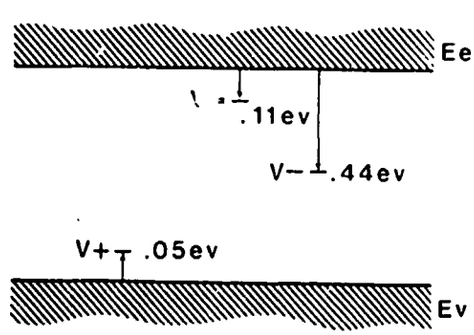

Figure 3. Estimated Vacancy Energy Levels in Silicon

DISCUSSION

SAH: The denuded zone gettering -- can you have a heavily doped region there that also could be used as the region for intrinsic gettering, like the region you are talking about where eventually you have a large concentration of metallic impurities?

PEARCE: Are you asking if you can have a denuded zone in something very heavily doped?

SAH: Yes. Denuded zone in front of a very heavily doped region; that heavily doped region is the region that would getter.

PEARCE: The structure that I mentioned earlier, the pp^+. One of the reasons that it works so well is that we form a denuded zone in the p^+ substrate, and then the heavy doping plus the precipitation there captures all the impurities. That turns out to be a very efficient structure for impurity capture. The heavy doping then reduces minority carrier concentrations so there are very few electrons available using the doping level for diffusion current. This is why we get these fantastic lifetimes.

LESK: Could you not measure the distribution coefficient of oxygen in silicon directly by using one of the melt refreeze techniques, where within a matter of five or 10 seconds you have melted and refrozen, and just look at the difference in oxygen content on either side of the interface?

PEARCE: Yes. I guess you could. We were looking for a fast answer and did some of the things we had done and when elected to do the variation of pull rate -- it's just amazing that we had the wrong number for so many years.

SWANSON: Some one, years ago -- I think it was Rohatgi -- reported that he was able to lower the oxygen concentration with HCl oxidations below the solid solubility at 1250°C where the oxidations were being done. We took some Cz wafers, 100 micrometers thick, and repeated his treatment, which according to the report would have depleted the oxygen almost completely from the wafer, and also gave a float-zone wafer the same treatment. The float-zone wafer had a high lifetime after this and the Cz wafer did not. Do you have any feeling maybe why that would be the case, or what we did wrong?

PEARCE: The work with the HCl -- I was involved in that with George Rozgonyi -- and we had done some stuff each way. We did it with and without HCl and at that time it looked like the HCl did give a pronounced improvement. We even had some charged-particle data that seemed to support that. I think, in retrospect, we were just seeing some samples of sample fluctuation. Maybe the role of the HCl wasn't as large as we had originally expected. There is a recent paper out of Penn State, and some others, which shows that in the presence of chlorine, at high temperatures, the diffusivity of oxygen is increased, and they have an interstitial vacancy model, so I guess it does have an effect. I guess it is an effect mostly on the diffusivity rather than on anything else.

SWANSON: Then you really see no strong evidence that the oxygen concentration is below solid solubility at the processing temperature?

PEARCE: It is probably not below the solid solubility.

RAI-CHOUDHURY: There is some evidence that this oxygen precipitates, although these precipitates behave as recombination sites or generation sites. Especially if you put in diodes, looking at the diode characteristics. Do you have any data to show what kind of electrical activity these precipitates have? Can you comment on that?

PEARCE: We don't have any direct evidence on the precipitates. There was some early EBIC work by Kimmerling at Murray Hill that showed decoration or impurities around the circumference of the fault, so that has been more or less proved. There was also some work by -- I think it was Varker, out of Motorola -- doing some diode measurements on things that were precipitated with no extended defects and it did show a degradation in lifetime. I personally have not done anything, but there are some data that support that the precipitates apparently attract metallic impurities as well as gettering centers and show the same effect.

LANDSBERG: Do you have any views about the incorporation of defects as you lower the temperature? After you have had a high solubility at a higher temperature, some of these oxygen -- or defects of some kind -- will get incorporated? I am looking for people who know how to describe this or whether there are some rules or some laws on that.

PEARCE: One of the things we felt, at least with metallic impurities, is that -- we call them saucer pits, fog, haze, things like this -- you go through an oxidation, do an etch, you find a small density of pits. One of the things we have found is that metallic impurities will precipitate very rapidly, so that if you cool the material fairly slowly, starting at some high temperature down to some low temperature, you can precipitate the metallics, or so-called saucer pits. But now, since they are not in solution, the lifetime tends to go up in many cases. On the other hand, if you quench the material -- very rapid cooling keeps all the metallics in solution -- the lifetime is low. So a lot of the effects people see with leakage currents and lifetime in silicon deal with how they cool the material out of the furnace, and the particulars of the metallics that they have present. But even very small changes in pull rate will dramatically affect the amount of precipitates that form.

LANDSBERG: Right. Are there any sort of systematic studies with this?

PEARCE: There is some good work in some of the semiconductor silicon series, like 1981 Electrochem Society, on defects in silicon -- out of the San Francisco meeting, I guess, last year. Yes, there are some papers I can give you the references on.

LANDSBERG: But there is no single law that kind of transpires as a result of all this, like in my talk I used -- a number of times -- E to some energy divided by some temperature?

PEARCE: Well, there is some work by Graff and co-workers who look at how these things precipitate as a function of solubility and diffusivities. You can start with that kind of information and see how something like a titanium would precipitate relative to an iron, and he has been able to predict that some of the metallics will be haze formers, etc. That is pretty good work. That is published in a 1981 volume.

CHENG: I just heard you mention that the wafer can be denuded up to 100 micrometers. This seems to ring a bell for solar-cell people, since people can make a four-mil cell thickness. Could you say some more how that is processed?

PEARCE: Yes. It basically is a time-temperature thing. We did a lot of denuding up at 1250°C, and at that temperature, if you go for something 20 hours, or whatever, one can denude into some very high thicknesses. On this graph here, Curve No. 1, is the work we did at 1250°C and at several hundreds of minutes you can get up over 100 micrometers denuding. There is a book out, VLSI Technology, edited by S.M. Sze, and the first chapter has the experimental data at 1250°C versus time.

SAH: I have just one more question: p-p process gave very good results, so how about nn^+ or pn^+ or np^+? Is there any indication that you would expect the same or different results?

PEARCE: The problem [illegible] n on n^+ is that it doesn't precipitate, of course, and we had a pa[illegible] that we published, "VLSI," it was in the Electrochem Detroit meeting, the first VLSI Symposium, in 1982. The problem with n on n^+ is that there are no intrinsic getter sites, so all the impurities tend to go to the surface and you get a lot of precipitates at the surface, and it is very poor material. To get the so-called intrinsic gettering to work in nn^+ you have to go up to something above 5×10^{19}. There has been some work published on phosphorus gettering as to what concentration level you need. It is around 5×10^{19}, so you have to get a substrate level up to there. There was some work at RCA where they did that. They grew some layers on some n^{++} material and the lifetimes were quite high. It is just difficult to routinely grow epitaxial layers and grow background doping at those high levels of arsenic or phosphorus. Furthermore, the crystal growers don't like to grow crystals like that because of the hazards. But, yes, it does work if you get up to that level.

SIRTL: You mentioned this distribution coefficient of oxygen. I would have some mixed feelings if you would call it theoretical distribution coefficient. If it is the effective distribution coefficient for Czochralski pulling, that would certainly be all right.

PEARCE: I would agree with that.

SIRTL: The work of a Japanese scientist was an outstanding contribution to this particular point. What exactly he did was, he avoided escape of oxygen during zoning so that he got the ideal conditions in terms of oxygen incorporation. And if you'll just remember the diagram I showed during my t[illegible] in this case, ingot solidification in a mold is a nearly

ideal condition in this respect. You may have seen that we indeed have found a distribution coefficient higher than 1, and that was not just once. so I think that from the ideal standpoint, the Japanese work is really the true theoretical value.

PEARCE: Yes. I think one of the things that make people accept that is that if you take the slope of that one plot that we presented with the unrefined Czochralski growth, seed versus tail, and then use classic solidification theory to extract a k from that, you usually do get something greater than one. So that tended to reinforce that, even though what is called the effective value in Czochralski is probably something lower and was clouded by all the variation of oxygen within the melt. So I would agree with your comments.

N85-31632

CURRENT UNDERSTANDING OF POINT DEFECTS AND DIFFUSION PROCESSES IN SILICON

T. Y. Tan
IBM T. J. Watson Research Center, Yorktown Heights, NY 10598

U. Gösele
Max-Planck Institut Für Metallforschung, Stuttgart, FRG

ABSTRACT

In this paper we first discuss the effects of oxidation of Si which established that vacancies (V) and Si self-interstitials (I) coexist in Si at high temperatures under thermal equilibrium and oxidizing conditions. Some essential points associated with Au diffusion in Si are then discussed. Analysis of Au diffusion results allowed a determination of the I-component and an estimate of the V-component of the Si self-diffusion coefficient. A discussion of theories on high concentration P diffusion into Si is then presented. Although presently there still is no thoery that is completely satisfactory, significant progresses are recently made in treating some essential aspects of this subject.

1. INTRODUCTION

Atomic diffusion in Si can proceed via both direct and indirect mechanisms. Impurity atoms having no strong bonding interactions with Si atoms, and are hence located exclusively in interstices, can jump directly between the interstices. Species such as H, He (and presumably other noble gases), and Cu^+ and Au^+ (presumably the Cu and Au interstitials, respectively) are supposed to diffuse in this manner. Oxygen atoms, though possess strong bonding interactions with Si atoms, are also believed to diffuse directly by jumping between the bond-centered interstitial positions. By contrast, substitutional impurity and self-diffusion in Si need intrinsic point defects as diffusion vehicles. The vacancy (V-) mechanism is known to control self-diffusion in metals and in Ge, and, as will be discussed, in Si below about 1000°C. Above 1000°C, however, the interstitialcy (I-) mechanism plays a prominent role in Si self-diffusion as well as in the diffusion of substitutional dopants P, B, Al and Ga.

The nature of the dominant point defect species in Si at high temperatures has been a long controversial subject, though it is clear that there can only be three possibilities: V only, I only, and I and V coexist. The controversy arises for two reasons: (i) Presumably because of the small point defect concentrations in Si, direct experimental methods have not been helpful. There is no reported absolute measurement (1) results, and there is only one very recently reported quenching result (2) which indicated the presence of V (in the opinion of the present authors, however, this does not imply that I do not exist); (ii) Theoretical calculations, which are more suitable for low temperature cases, have not yielded the needed ≈5eV activation enthalpy and the ≈10k (k: Boltzmann constant)

PRECEDING PAGE BLANK NOT FILMED

activation entropy commonly observed for Si self-diffusion. There were several early discussions associated with some aspects of the possibility of I and V coexisting in Si: Seeger and Chik (3) considered that I and V may be contributing equally to Si self-diffusion at 800°C; Prussin (4) considered that I and V should reach a local dynamical equilibrium under oxidizing conditions; Hu (5) considered that B should be diffusing in Si via an I-mechanism while As via a V-mechanism at high temperatures. In the last few years progesses in two areas helped to clarify our understanding of the nature of point defects and diffusion processes in Si considerably. Analyses of oxidation effects on stacking fault (SF) growth kinetics (6,7) and on dopant diffusion (8-10) showed beyond reasonable doubt that I and V coexist in Si at high temperatures under thermal equilibrium as well as oxidizing conditions. Analyses of Au diffusion in Si showed that I must exist (11,12) and that the features are totally consistent with the idea that I and V coexist (13). Studies of Au diffusion into dislocation-free Si allowed to determine the I-component (14) and to estimate the V-component (15) of the Si self-diffusion coefficient. In this paper the essential points associated with these two areas are first discussed. We then examine theories on high concentration P diffusion into Si. For various reasons, we believe that there is still no satisfactory theory. However, progresses have been made in treating some essential aspects of this subject.

2. OXIDATION EFFECTS

Oxidation of Si surfaces leads to the so called oxidation-enhanced and -retarded diffusion (OED and ORD) of the substitutional dopants and to the generation of the oxidation-induced stacking faults (OSF). These phenomena need to be considered together and are due to the fact that oxidation injects I into Si (5,16). It has been shown that a consistent interpretation of the data on OED/ORD phenomena is not obtained if either I or V alone were assumed to be present under thermal equilibrium conditions (10). Therefore for our present purpose, we consider that I and V are both present in Si at high temperatures under thermal equilibrium conditions. This requires that we consider I and V have attained a local dynamical equilibrium condition (4,17), which was actually fulfilled for long time experiments (8-14,18,19). The condition is given by (17)

$$C_I C_V = C_I^{eq} C_V^{eq}, \tag{1}$$

where C_I and C_V denote the I and V concentrations respectively and the superscript eq denotes thermal equilibrium values. Eq. (1) is arrived at via the reaction

$$I + V \rightleftarrows 0 \tag{2}$$

(where 0 denotes the ideal lattice) under steady state conditions. Using some of the more reliable OSF size data (20-22), phenomenological but satisfactory analyses of the OSF growth/shrinkage kinetics have been carried out (6,7). Define the I and V supersaturation ratios respectively as $S_I = C_I/C_I^{eq} - 1$ and $S_V = C_V/C_V^{eq} - 1$ during the oxidation, we obtain (7)

$$\frac{\Omega}{A\alpha_{eff}}\left(\frac{dR_{SF}}{dt}\right) = -(D_I C_I^{eq} + D_V C_V^{eq})\frac{\gamma}{kT} + D_I C_I^{eq} S_I - D_V C_V^{eq} S_V \tag{3}$$

for the OSF with a radius R_{SF}. Here A is the area per atom in the fault (6.38×10^{-16} cm^2), Ω the atomic volume (2×10^{-23} cm^3) and γ the stacking fault energy (0.026eV/atom). The dimensionless quantity α_{eff} has a numerical value of ≈2 and contains all factors related to interaction potentials between I and the Frank partial dislocation binding the OSF. Emperically, for (100) Si wafers oxidized in dry O_2, the OSF sizes are fitted satisfactorily by (6,7)

$$R_{SF} = 1640\exp(-\frac{2.5eV}{kT})t^{3/4} - \frac{4.8\times10^{9}}{kT}\exp(-\frac{5.02eV}{kT})t \quad cm. \tag{4}$$

We use Eq. (1) to relate S_I and S_V by $S_V=-S_I/(1+S_I)$. A comparison of Eqs. (3) and (4) then yields (8,9),

$$S_I^{o2} = 6.6\times10^{-9}\ \exp(2.52eV/kT)\ t^{-1/4}, \tag{5}$$

where the superscript o2 denotes the fact that this quantity is only suitable for (100) wafers oxidized in dry O_2. Eq. (5) is a most important piece of information obtained from OSF studies: it is used to obtain quantitative fittings of OED/ORD data. S_I is an instantaneous value, the time averaged value $\bar{S}_I$ used in the actual OED/ORD data fitting is obtained by replacing the pre-exponential value in Eq. (5) by 8.8×10^{-9} and by noting that t then denotes the oxidation duration.

In the presence of both I and V, the substitutional dopant diffusivity is given by

$$D^s = D_I^s + D_V^s, \tag{6}$$

where D_I^s and D_V^s are respectively the I- and V-component of the dopant diffusivity. Under an oxidation which perturbs the thermal equilibrium I and V concentrations, the dopant diffusivity changes to

$$D^s = D_I^s(C_I/C_I^{eq}) + D_V^s(C_V/C_V^{eq}). \tag{7}$$

In terms of the normalized diffusivity enhancement defined as $\Delta_{ox}^s=D_{ox}^s/D^s-1$, the use of Eqs. (1) and (7) yields (8,10)

$$\Delta_{ox}^s = (2G_I+G_IS_I-1)/(1+S_I), \tag{8}$$

where G_I is the fractional I-component of the dopant diffusity under thermal equilibrium conditions defined as $G_I=D_I^s/D^s$. Eq. (8) applies to an instantaneous diffusion enhancement. In experiments the time averaged value $\bar{\Delta}_{ox}^s$ is measured, but Eq. (8) still holds to a good approximation by having $\bar{S}_I$ used together with $\bar{\Delta}_{ox}^s$. A plot of Eq. (8) is shown in Fig. 1 for three G_I values. The value of $\bar{\Delta}_{ox}^s$ is either positive or negative (OED or ORD) depending on the value of G_I and S_I. In Fig. 2 we show a fitting of available Sb ORD data to Eq. (8). It is seen that the fitting is quite satisfactory on a quantitive basis with G_I=0.02. This kind of good fitting indicates that the model of I and V coexisting and attained local dynamical equilibrium is correct, particularly in light of the fact that no other reasonably thought of model can be equally satisfactory (10). The use of Eq. (8) allows to determine G_I for a dopant at a given temperature. Some such values have been given elsewhere (15,23,24). To briefly summarize, it is found that the I-mechanism plays a prominent role in the diffusion of B, Ga, P and Al

at high temperatures, i.e., $G_I \gtrsim 0.5$ for these dopants at a temperature above 1100^oC.

The above discussion applies for experiments with sufficiently long oxidation times. For short oxidation times, a transient exists for I and V to reach the local dynamical equilibrium. This is due to the presence of an energy barrier against I and V recombinations. The existence of such an energy barrier was suggested by Wertheim (25) to explain the fact that the rate of A-center (E_c-0.16eV) production by high energy electron irradiation is strongly dependent upon the irradiation temperature (below room temperature). For high temperature cases, Hu (26) suggested that such a barrier of a few to several eV may exists, so that to a large extent I and V may behave indenpendently. The experiments on ORD of Sb (18,19) shown in Fig. 2 demonstrated that for oxidation times longer than a few hours local dynamical equilibrium according to Eq. (1) is reached. By performing similar experiments for shorter times (5 to 60 min.) Antoniadis and Moskowitz (9) showed that Eq. (1) is not readily satisfied when oxidation first started. At 1100^oC they found a small OED for a 5 min. oxidation which gives way to ORD for an oxidation longer than 10 min., and, the diffusion retardation approaches the value expected for local dynamical equilibrium at about 60 min. Their findings may be rationalized as follows: during oxidation I are injected into Si by the SiO_2-Si interface but it takes about 1 hr at 1100^oC for I-V recombination to proceed to such an extent that local dynamical equilibrium is reached. As a consequence, at the begining there is no V undersaturation so that the oxidation induced I supersaturation enhances Sb diffusion via the small I-component of its diffusivity ($G_I \simeq 0.02$).

We use Waite's theory of diffusion controlled reaction (27) to obtain from

$$\tau_{dif} \leq \Omega/4\pi D^{SD} r_{IV} \qquad (9)$$

an estimate of the time τ_{dif} required to establish the local dynamical equilibrium in the Antoniadis-Moskowitz experiment if no recombination barrier were present. With $D^{SD} \simeq 10^{-15}$ $cm^2 sec^{-1}$ and the recombination radius $r_{IV} \simeq 5x10^{-8}$ cm, Eq. (9) yields $\tau_{dif} \lesssim 0.05$sec which is about 10^5 shorter than observed. We therefore conclude that I-V recombination is controlled by the overcoming of a recombination barrier that exceeds the Gibbs free energy of diffusion (of I and V) by ΔG. In this picture the factor of 10^5 by which the experimental τ value differs from that estimated from Eq. (9) arises from the Boltzmann factor $\exp(\Delta G/kT)$. Antoniadis and Moskowitz interpreted their observation in terms of an enthalpy barrier corresponding to $\Delta H \simeq 1.4$eV assuming that in the expression

$$\Delta G = \Delta H - T\Delta S \qquad (10)$$

the entropy contribution is negligibly small. By contrast, Gösele et al. (28) proposed that the main part of ΔG originates from the term $T\Delta S$ where ΔS is negative, i.e., from an entropy barrier, which is due to a consideration of the large pre-exponential factor associated with D^{SD}.

Irrespective of the detailed origin of the barrier. with $\Delta G \simeq 1.4$eV, the barrier limited reaction time, τ_{bar}, for establishing the local dynamical equilibrium between I and V is given by

$$\tau_{bar} \simeq (\Omega/4\pi D^{SD} r_{IV})\exp(1.4eV/kT). \quad (11)$$

Eq. (11) is plotted in Fig. 3 using $D^{SD}=0.5(D_I C_I^{eq}+D_V C_V^{eq})$ with the quantities $D_I C_I^{eq}$ and $D_V C_V^{eq}$ taken from Eq. (21) which will be discussed. It is seen that τ_{bar} increases rapidly with a decrease of the temperature and attained values of 2, 17 and 170 days at 1000, 950 and 900°C respectively. Even if it is assumed that these results are over-estimated by a factor of 10, τ_{bar} values are still 5hrs, 1.7days and 17days at 1000, 950 and 900°C respectively. One significance of this finding is that in the expression

$$D^s_{per} = D^s_I(C_I/C_I^{eq}) + D^s_V(C_V/C_V^{eq}), \quad (12)$$

the quantities C_I and C_V, arising from experimental perturbation of the respective thermal equilibrium values, are not related by Eq. (1) in an experiment performed in such low temperature range and having time durations much less than the appropriate τ_{bar} values. For device processing in the temperature range of 850 to 950°C for a few hrs, should there be any reason that the point defect thermal equilibrium values are perturbed, the change only applies to the perturbed species independently, i.e., I and V need to be considered as not having attained the local equilibrium condition.

The fact that I-V dynamical equilibrium is attained extremely slowly at lower temperatures offers the possiblity of measuring the quantities D_I and D_V independent of each other and independent of the I and V concentrations. There already exist some OSF and OED/ORD experiments conducted with the intention of measuring D_I at 1100°C or above (29-31). However, because of the temperatures and oxidation times involved, I-V local dynamical equilibrium should have been reached in these experiments and we have shown that such experiments yield an effective diffusivity given as (15,24,32)

$$D^{eff}_{IV} \simeq (D_I C_I^{eq}+D_V C_V^{eq})/(C_I^{eq}+C_V^{eq}), \quad (13)$$

instead of D_I. Depending upon the relative magnitude of C_I^{eq} and C_V^{eq}, which are unknown quantities themselves, Eq. (13) may yield an approximate value for either D_I or D_V. We have argued that the diffusivity values obtained from these experiments (29-31) should be interpreted as D_V (24,32). However, for the lower temperature range, e.g., 850 to 950°C, the I-V local dynamical equilibrium will not be reached for an experiment involves less than a day's time. For such cases, effects associated with dopant diffusion or stacking fault growth would be solely due to the point defect species whose thermal equilibrium concentration has been perturbed by the experimental condition. This means the other species does not contribute to the experimental deviations observed if its thermal equilibrium concentration has not been also directly perturbed by the experimental condition. We can now suggest an experiment to directly determine D_I: High concentration P diffusion into Si proceeds efficiently in the temperature range noted above and the diffusion causes a quite high I supersaturation in the Si interior. Thus, experiments similar to those performed for OED/ORD and OSF (29-31) can be carried out at the low temperature range (850 to 950°C) with surface P diffusion replacing oxidation to obtain D_I. Similarly, D_V can be determined upon finding an interface reaction which injects V into Si. Presently we do not know with

certainty of such a reaction.

3. DIFFUSION OF GOLD INTO DISLOCATION-FREE SILICON

Gold atoms, which under thermal equilibrium conditions may be incorporated in Si either as substitutional (Au_s:Au^{3-}) or interstitial (Au_i:Au^+) atoms, may diffuse via either the kick-out mechanism (11) or the Frank-Turnbull mechanism (33). The two mechanisms have in common that long range transport of Au atoms occur via migration of Au_i atoms which may either jump from interstice to interstice to remain as Au_i atoms or from interstice to lattice positions to become Au_s atoms. This is true because though the thermal equilibrium concentration of Au_s is much larger than that of Au_i, the mobility of Au_i is much much larger than that of Au_s and hence long range transport of Au_s may be ignored. However, the two mechanisms differ in the ways Au_i and Au_s atoms interchange. In the kick-out mechanism the interchange involves I according to (11)

$$Au_i \rightleftarrows Au_s + I. \tag{14}$$

This mechanism creates an I supersaturation in the crystal which is balanced by I out-diffusion. This means if the mechanism is operative than I are involved in Si self-diffusion but it does not a priori mean that V are not contributing to Si self-diffusion. In the Frank-Turnbull mechanism the interchange process involves V according to (33)

$$Au_i + V \rightleftarrows Au_s. \tag{15}$$

This mechanism creates a V undersaturation in the crystal interior which is balanced by V in-diffusion. If operative, it means that V are involved in Si self-diffusion but it does not mean I are not contributing to Si self-diffusion. We now assume that local dynamical equilibrium betweem I, V, Au_i and Au_s is established. The necessary and sufficient condition for this assumption to be true is that the three reactions (2,14,15) have reached their equilibrium state. This requires that two out of the three reactions to be sufficiently fast. It is not required that the third reaction be equally fast, since if equilibrium conditions are satisfied by two of the reactions, then the third is automatically under equilibrium conditions. Under this assumption the normalized Au_s concentration $C=C_s/C_s^{eq}$ to be measured in an experiment on Au diffusion into dislocation-free Si may be approximately described by

$$\frac{\partial C}{\partial t} = \frac{\partial}{\partial x}\left(D_{eff}\frac{\partial C}{\partial x}\right) \tag{16}$$

with the effective diffusion coefficient given by (13)

$$D_{eff} = (C^{-2}+D_V C_V^{eq}/D_I C_I^{eq})D_I C_I^{eq}/C_s^{eq}. \tag{17}$$

In Eq. (17) contributions to the Au_i-Au_s interchange process due to both kick-out and Frank-Turnbull mechanisms are accounted for. In deriving Eq. (17) the

following approximations are used

$$C_i = C_i^{eq}, \qquad (C_i\text{: } Au_i \text{ concentration}) \tag{18a}$$

$$C_s^{eq} \geq C_V^{eq}, \tag{18b}$$

$$C_s >> (C_s^{eq} C_I^{eq})^{1/2}. \tag{18c}$$

If only V and no I are present Eq. (17) yields a constant effective Au_s diffusity (11,33)

$$D_{eff}^V = D_V C_V^{eq} / C_s^{eq}. \tag{19}$$

The same result holds if $D_I C_I^{eq}$ is not zero but among the reactions (2,14,15) only (15) operates sufficiently fast. If only I and no V are present Eq. (17) yields a strong concentration dependent diffusivity

$$D_{eff}^I = C^{-2} D_I C_I^{eq} / C_s^{eq}. \tag{20}$$

The same result holds if $D_V C_V^{eq}$ is not zero but among the reactions (2,14,15) only (14) operates sufficiently fast. As observed by Stolwijk et al. (14), Au concentration profile after diffusion into dislocation-free Si at and above 800°C can not be described by the constant diffusity given by Eq. (19) but are satisfactorily fitted by the use of Eq. (20). Fig. 4 shows a typical experimental profile due to Stolwijk et al. It can be seen that an erfc-function type profile as expected for D_{eff}^V failed to fit the data while the use of D_{eff}^I is quite satisfactory. This shows that I are contributing to Si self-diffusion but it does not mean that V are not contributing for the reasons that: (i) It can not be certain that this is not only due to the fact that of the reactions (2,14,15) only (14) operates sufficiently fast; and (ii) The strong dependence of D_{eff}^I on C^{-2} reduces the effect of $D_V C_V^{eq}$ by this factor for most part of the experiment for which C<1 and C^{-2}<<1 hold. Indeed Morehead et al. (13) found that while almost perfect fitting were obtained for short time diffusion profiles small but observable deviations occured if Eq. (20) were used but a much better fitting is obtained by the use of Eq. (17). This not only shows that V are contributing to Si self-diffusion but also allowed to estimate that $D_V C_V^{eq} \approx D_I C_I^{eq}$ at 1000°C. The quantity $D_I C_I^{eq}$ has been determined by Stolwijk et al. (14) as

$$D_I C_I^{eq} = 914 \exp(-4.84 eV/kT) \quad cm^2 sec^{-1}. \tag{21a}$$

We have already shown that at T≤900°C reaction (2) is expected to become ineffective. At still lower temperatures, as will be discussed, reaction (14) is also expected to become ineffective. In that case only reaction (15) will be operating and an erfc-function type profile should show up. Willcox et al. (34) found such a case at 700°C. With their data we obtained that $D_V C_V^{eq} \approx 8.8 \times 10^{-22}$ $cm^2 sec^{-1}$ at 700°C (15). This together with the data of Morehead et al. (13) yields the rough estimate

$$D_V C_V^{eq} = 0.6\exp(-4.03eV/kT) \quad cm^2 sec^{-1}. \tag{21b}$$

Eq. (21) is plotted in Fig. 5 in which a data point on $D_V C_V^{eq}$ obtained by analysing the Ni precipitation behavior (15) of Kitagawa et al. (35) is also shown. An important point is, as rough estimates, the sum of the formation and migration entropies are now obtained from Eq. (21) as 3k for V and 10k for I. That is, while I are quite extended (3), V are fairly point-like. Experimentally observed D^{SD} values from relatively higher temperature measurements are usually of 10^3 exp(-5eV/kT) while those from relatively lower temperature experiments are of lexp(-4eV/kT) (36-40). These values are quite compatible with Eq. (21).

We now make an estimate to show that at very low temperatures the kick-out mechanism, reaction (14), can become ineffective, while the Frank-Turnbull mechanism, reaction (15), still operates. It is important to note that if this can not be true then it can not be explained why Au diffuses into dislocation-free Si apparently via the kick-out mechanism at higher temperatures but the Frank-Turnbull mechanism at a very low temperature. Eqs. (19) and (20) show that Au diffusion would appear as dominated by the kick-out mechanism in so long as $C^{-2} D_I C_I^{eq}/D_V C_V^{eq} > 1$ holds. Because for a large part of the experiment $C^{-2} >> 1$ holds, the kick-out mechanism may still appear as dominating the diffusion process even for a case for which the frequency of the kick-out events is less than that of the Frank-Turnbull events. On the other hand, the frequency of the kick-out events should decrease more rapidly than that of the Frank-Tuenbull events with a decrease in temperature because the former involves the creation of I which is charaterized by an activation enthalpy (the I formation enthalpy) while for the latter there is not yet a good reason for assuming that a high enough energy barrier exists to prevent an Au_i atom drops in a V. In the following we show that under thermal equilibrium conditions a quantitative estimate can be made which indicates that the above discussed situation can be true.

For the Frank-Turnbull mechanism, if an Au_i atom and a V meet, there is a definete probability $\Gamma \leq 1$ that reaction (15) will go forward to produce an Au_s atom. Under thermal equilibrium conditions, we obtain the rate of increase in C_s via this mechanism as

$$(dC_s/dt)_{FT} = \Gamma(4\pi r_{iV}/\Omega) D_i C_i^{eq} C_V^{eq}. \tag{22}$$

For the kick-out mechanism, reaction (14), the Au_i atom has a certain frequency ν_i by which it produces Au_s and I. We do not know this frequency but if Au_s and I meet there is a definite probability $\Theta \leq 1$ for reaction to produce Au_i and under thermal equilibrium conditions this reaction balances that due to ν_i. Therefore we have,

$$(dC_s/dt)_{ko} = \Theta(4\pi r_{Is}/\Omega) D_I C_I^{eq} C_s^{eq}. \tag{23}$$

From Wilcox et al. (34) we have

$$D_i C_i^{eq} = 1.8\text{x}10^{-2}\exp(-1.13eV/kT) C_s^{eq} \quad cm^2 sec^{-1}. \tag{24}$$

Eqs. (21a) and (22) to (24) yield for the rate of converting Au_i into Au_s via

the kick-out mechanism to that via the Frank-Turnbull mechanism as

$$r \approx (dC_s/dt)_{ko}/(dC_s/dt)_{FT} = \alpha \exp(-3.71eV/kT)/C_V^{eq}, \qquad (25)$$

where α is a constant of the order of 10^5. We do not know the quantity C_V^{eq} but it can be seen from Eq. (25) that r decreases with a decrease of temperature unless the V formation enthalpy ΔH_V^f is equal to or larger than 3.71eV, which, judging from Eq. (21b), is unlikely. In Fig. 6 we show the calculated values of r(T)/r(1000°C) assuming ΔH_V^f is in the reasonable range of 1.5 to 3eV. It is seen that the effectiveness of the kick-out mechanism decreases much more rapidly with a decrease in temperature than that of the Frank-Turnbull mechanism.

With this discussion, it becomes understandable why Au diffusion can appear as dominated by the kick-out mechanism (related to I) at higher temperatures, while by the Frank-Turnbull mechanism (related to V) at lower temperatures. It is expected that other metals may also exhibit a similar kinetical behavior in Si for experiments involving their diffusion: in- and out-diffusion experiments, precipitation and precipitate dissolution experiments. We suggest that by now the following rule should be kept in mind: in an experiment if it is found that I in Si appears as dominating the diffusion process of an impurity, it means that I exist as a species of Si point defect under thermal equilibrium conditions and the experimental conditions are suitable for I to appear as dominating, it does not mean that V do not also exist as a species of Si point defects under thermal equilibrium conditions; the reverse is also true. The diffusion experiments of Kitagawa et al. (41) on Ni (dominated by V) and of Mantovani et al. (42) on Pt (dominated by I) are good examples.

4. ON THEORIES OF HIGH CONCENTRATION PHOSPHORUS DIFFUSION INTO SILICON

Diffusion of group-III and -V dopants shows several anomalous features that are quite thoroughly discussed in the literature (43-47). To summarize, Willoughby (45) and Gösele and Strunk (47) mentioned that the most prominent features are: (i) The emitter push effect, which is the extremely rapid diffusion of base dopant (B or Ga) of the doubly diffused npn transistor structure which results in an enhanced movement of the base-collector junction; (ii) The kink-tail structure of the in-diffusion P profile, which is resulted from the use of high concentration surface sources. This is shown in Fig. 7a with conveniently designated surface and tail regions. In the tail region the P diffusion rate is much higher than expected for isoconcentration studies or OED studies; (iii) Movement of burried dopant layers can be extremely rapid if the surface P concentration is high. There exist ample evidences that P rich precipitates form during P in-diffusion (48-55), we therefore add to the above list by (iv) During P in-diffusion, the P concentration in the Si surface region exceeds its normal solubility limit. We consider that the following facts have been established: (i) The dopant diffusivity enhancement are caused by supersaturation of intrinsic point defects. The enhancement are much larger than that due to oxidations; (ii) The point defect supersaturations are related to high surface concentration of P, and, in some cases, of B or As (56-58); and (iii) Mechanisms involve dislocations in an essential manner, e.g., dislocation climb, are not the origin of the point defect supersaturations.

Since untill recently it was widely believed that V are the dominant thermal equilibrium point defect species in Si, earlier models (59-61) put forth to explain the P anomalous diffusion have been based on calculating the V supersaturations. Among these models, that of Fair and Tsai (61) gave a most complete treatment and was apparently able to calculate quantitatively the kink-tail structure in the P diffusion profile. Even if V were the only point defect species present in Si at high temperatures, the model still can not be regarded as satisfactory because of: (i) As pointed out by Kroger (62), the analytical development is questionable with respect to the relation between the total P concentration and the total carrier concentration on the one hand, and with respect to the derivation of the electrical field on the other; and (ii) As pointed out by Mathiot and Pfister (63), the V supersaturation was accounted for by a multiplication factor for deriving the fast diffusing tail region P diffusivity instead of solving the V diffusion equation. By correcting these problems Mathiot and Pfister (64) found that the model of Fair and Tsai can not give a good qualitative description of the P diffusion profile. Here we mention two fundamental objections generally applicable to these models: (i) Formation of P-rich precipitates (48-55) is not accounted for; and (ii) By now there also exist ample evidences that during P indiffusion an I and not V supersaturation is present in the Si interior (55,64-67) but the V based models can only predict a V supersaturation.

Recently, two new models have been proposed. One is a vacancy percolation (modified E-center) model due to Mathiot and Pfister (68), which has also been extended to include an I-component in the diffusivities of both dopant diffusion and Si self-diffusion (69). The other is a model due to Hu et al. (70) who proposed that a substantial part of P occupies interstitial positions which we shall call interstitial P model. Unfortunately, these two models seems are also not satisfactory. In the following (Sections 4.1 and 4.2) we discuss some essential points of these two models and give some detailed reasons for arriving at this conclusion. In section 4.3 we discuss a possible reason for P diffusing into Si in a supersaturated concentration.

4.1. The V Percolation Model

By correcting the problems of the model of Fair and Tsai and by incorporating the idea of V percolation (71), Mathiot and Pfister were able to quantitatively fit some P diffusion profiles (68). Later on they were also able to exted the model to include an I-component in the dopant and Si self-diffusion coefficients with an apparently even better success (69). Their earlier model (68) can be straight forwardly regarded as unsatisfactory since it is purely V based. The incorporation of an I-conponent in the dopant and Si self-diffusion coefficients (69) is a good step forward, but the model is not satisfactory because:

(i) Formation of P-rich precipitates is not accounted for;

(ii) They concluded that $G_I \sim 0.1$ to 0.3 for the dopants B, As and P from 900 to 1200°C for low and high concentration diffusions. For the cases of higher temperature experiments, we expect that local dynamical equilibrium between I and V to be reached, this can only result in a net V supersaturation in the Si interior. This is in contradiction with experimental results (55,64-67) that can only be explained by a net I supersaturation;

(iii) The finding that $G_I < 0.5$ for P, which requires that the observed ORD of P for (111) Si wafers oxidized for long times be explained without assuming a

net V supersaturation (as Francis and Dobson (72) and the present authors (8) have assumed), is in contradiction with the Sb OED result (10,19) which was observed under an almost identical experimental condition for observing the P ORD. A qualitatively consistent interpretation of these results is not obtained unless $G_I>0.5$ for P and $G_I<0.5$ for Sb and under the experimental conditions a net V supersaturation exists.

(iv) The observation of ORD of B at 1200°C by Hill (73) can not be explained by their finding $G_I<0.5$ for B, since in that experiment a 6% HCl was used. By analysing the OSF data of Shiraki (21) the present authors have shown that for this experimental condition a net V should have been injected (7,10). If $G_I<0.5$ for B, then it should have resulted in an OED instead of the observed ORD.

The present authors believe that the V percolation idea is a very important point for which the full significance seems have not yet been realized. This subject is certainly a nice contribution of Mathiot and Pfister is well worthy of some discussions. To invoke the V-mechanism for the diffusion of a substitutional impurity species which exhibit a higher diffusivity than that of self-diffusion of the host crystal atoms, it is necessary to assume that the diffusion proceeds in the form of i-V pairs (i denotes a substitutional impurity atom), and a pair has to partially dissociate during its migration process. In Si the saddle point for the i-V pair dissociation process corresponds to having a V on the third nearest neighbour position of i. The remaining binding energy between i and V determines the cohesion of the pair. For the case of having a very high impurity concentration, the impurity atoms effectively form a network or cluster in the crystal lattice in the sense that now each impurity atom would have some other impurity atoms situated at its fifth or even closer neighbour positions. The i-V pair diffusion process changes now since upon reaching the saddle position of the pair partial dissociation process, the V can also be at a third neighbour position of another i. Now V can migrate to the other i atom with a potential barrier smaller than that needed for the isolated i-V pair case. This means with a sufficiently high impurity concentration, V can freely diffuse through the i network or cluster, which does not only enhance the V diffusion but also the i diffusion. This is the idea used by Mathiot and Pfister in their models (68,69). We now mention a few points associated with the percolation idea that have not yet been explicitly considered:

(i) We believe that the percolation idea is equally applicable to an I-mechanism;

(ii) In the presence of a high impurity concentration, and hence the percolation network, we believe it is sensible to also suggest that the point defect formation energy is also lowered. This means the thermal equilibrium point defect concentrations are increased because of the presence of a high impurity concentration (not to be confused with that due to electrical charge effect);

(iii) The presence of the percolation network necessarily changes the i-I and i-V pairing potentials and hence G_I for low and high impurity concentration cases are in principle of different values.

4.2. The Interstitial Phosphorus Model

Hu et al. (70) have recently criticized most of the V models (59-61) and proposed a new model to remedy the situation. An important contribution of their work is that formation of P-rich precipitate during P in-diffusion is very much emphasized and therfore in the model this is accounted for and hence removing one major shortcomings common to all other models. They have written down the basic equations but not yet performed the needed calculations and it is therefore not possible to see whether a net I supersaturation in the Si interior can result from the model or not. An examination of the basic assumptions involved in this model has led the present authors to believe that the model in its present form is probably also not satisfactory. Their major assumptions are: (i) A portion of the P atoms in Si occupies the substitutional sites (P_s) while the rest occupies interstitial sites (P_i); (ii) Mutual conversion between P_s and P_i is very slow; and (iii) Both P_s and P_i are shallow donors. Assumption (i) is needed since they invoked a two stream diffusion mechanism as the a priori reason for obtaining the kink-tail diffusion profile. The best way to see what is a two stream diffusion is to imaging that there are two distinct chemical species A and B diffusing into Si simultaneously but otherwise independently and we are looking for $C_{A+B}=C_A+C_B$, see Fig. 7b. Now there is only one P species chemically but in Si they can occupy different sites, e.g., P_s and P_i. In so far as diffusion is concerned, P_s and P_i can behave independently. Assumption (ii) is needed since if P_s and P_i are converting into each other rapidly enough then their individual identity will be lost and a kink-tail structure in the P concentration profile can not be obtained. Assumption (iii) is needed since atomically dissolved P atoms in Si is known to be electrically active. The assumption that a substantial portion of the P atoms occupies interstial sites is very different from that invoked conventionally: P atoms occupy substitutional sites only. By definition, P_i diffuses primarily via an I-mechanism. Thus, there will always be a substantial number of P atoms on interstitial sites whether they are migrating or not. In the converntional picture, P atoms can diffuse via an I-mechanism and hence those migrating P atoms are on interstitial sites temporarily but there will only be a negligibly small fraction of P atoms that are migrating at any instant in time and hence for practical purposes all P atoms are occupying substitutional sites.

In the following we present four arguments which jointly constitute as a strong indication that the above mentioned assumptions involved in the model of Hu et al. do not form a realistic enough basis for regarding the model as satisfactory (admittedly, though, each argument individually may be only constituting as a weak indication):

(i) The fact that there is but one shallow donor level associated with P doping is generally accepted. While it is legitimate to postulate that P_i is also a donor, it is difficult to believe that the donor is also a shallow one, and, in particular, its energy level needs to be almost identical to that due to P_s;

(ii) High concentration P diffusion into Si can induce the formation of a dislocation network to accomodate the Si lattice parameter change in the diffused layer due to the incorporation of P atoms to a large concentration. Analyses of such dislocation networks indicated that the P diffused layer has a smaller lattice parameter (74) which is consistent with the knowledge that P atoms are all on the substitutional sites (the ratio of the covalent radii

C - 4

of P atoms to Si atoms is 0.94). In order to explain the P diffusion profiles by the two stream mechanism, it needs to be assumed in some cases C_{Pi} can be almost equal to C_{Ps}. If this is so, it seems that by now there should be some indication that the opposite, i.e., the P diffused layer has a lattice parameter larger than that of the undiffused Si, is true;

(iii) The requirement that P_i and P_s are converting into each other very slowly is an extremely stringent condition. Considering the diffusion times involved in a typical experiment, a simple estimate would show that the energy barrier against the P_i-P_s conversion needs to be higher than 3eV and quite likely in the neighbourhood of 4 to 5eV. This is the same energy barrier prevent the interstitialcy pair from dissociation, and hence the pair needs to be regarded as very stable. If so, it is not easy to understand why P_i can diffuse so fast, which is also required in the model;

(iv) In an Au gettering experiment, Lecrosnier et al. (75) found that the Au concentration in the P diffused layer developed a kink-tail profile similar to the P profile. This phenomenon is consistent with the interpretation that all P atoms occupy substitutional sites but not equally consistent with the interpretation that a substantial portion of P atoms occupies interstitial sites.* The interstitial P model requires that the surface region P atoms be mostly P_s (diffusion slow) while the tail region P atoms be mostly P_i (diffusion fast). We first mention that in the Au gettering experiment all the gettered Au atoms should be Au_s since normally $C_s^{eq} >> C_i^{eq}$ holds and since if they were Au_i then we expect the P and Au concentration profiles follow a complementary rather than a similar distribution pattern since the charge states of the P and Au atoms should result in a repelling force (P is a donor in spite of whether in substitutional or interstitial positions, and, Au_i is also suppose to be a donor, i.e., Au^+). Assuming that Au atoms are indeed Au_s atoms, then the best interpretation is that P atoms are all P_s atoms since now charge compensation occurs between P^+ and Au^{3-} (presumably Au_s) atoms and atomic size compensation also occurs (covalent radius of Si atom is larger than that of P_s but smaller than that of Au_s). If the P atoms are P_i then we expect a large compressive stress to develop in the Si which tends to result in a complementary distribution pattern between the P_i and Au_s concentrations. The worst case is that both P and Au atoms occupy interstitial sites since then it will result in a compressive strain as well as a charge repelling situation.

4.3. Physical Reasons for P Diffusing into Si in Supersaturation

While the kink-tail diffusion profile of P has been recognized as an outstanding feature for a long time, it is only recently that the equally outstanding (and undoubtly related) feature of P diffusion into Si in supersaturation is also recognized. Why is it so? Hu et al. (70) provided one possible reason which is dynamical in nature: P diffusion (using a P-rich oxide source) is usually carried out in a partial oxygen ambient and hence oxidation, i.e., a chemical reaction, occurs. They suggested that the excess chemical potential responsible for P entering Si exceeding its solubility limit derives from this chemical reaction (oxidation). However, this may not be the primary reason because

*This problem was brought to the attention of one of the present authors (TYT) by Dr. T. E. Seidel.

of: (i) The I supersaturation associated with high concentration P diffusion far exceeds that due to an oxidation of Si, and, in particular, this seems to be true at very low temperatures, e.g., 750°C, for which an oxidation of Si ceases to function; (ii) There are some indications that P can diffuse into Si in a supersaturated amount for cases that the annealing ambient is inert. Nobili et al. (54) concluded that the electrically active P concentration limit (presumably the solubility limit) is about $4x10^{20}$ cm^{-3} at 1100°C, but at the same temperature P can enter Si to a concentration of about $1x10^{21}$ cm^{-3} in an N_2 drive-in annealing using a P-rich oxide source (76).

As an alternative possibility, we suggest a mechanism due to phase-equilibrium requirements to explain the phenomenon of P diffusing into Si in supersaturation. This mechanism is readily understandable if the materials involved constitute as a binary alloy system. Therefore, for our present purpose we discuss the case that the source of diffusion is gaseous P (P_g) at the standard presure instead of the more commonly used P rich oxide. In Fig. 8 we show the phase diagram of the Si-P system and an appropriate free energy diagram in the temperature range of our interest. The significance of Fig. 8 is that, under phase-equilibrium conditions: (i) the two primary phases, α (Si containing atomically dissolved P) and γ (P_g), and the binary intermediate phase SiP, can each exists alone; (ii) The α phase and SiP can coexist; (iii) SiP and P_g can coexist. This means for a diffusion experiment using P_g as source, to start with, the materials (Si and P_g) do not exist in a phase equilibrium state. Hence, the materials will proceed to reach the appropriate phase-equilibrium states by creating coexisting phases permitted by the phase-equilibrium conditions, i.e., the above discussed possiblities (ii) and (iii). We coined the term that, before the phase-equilibrium state is reached, the materials are in a diffusion-transient state. A primary phenomenon associated with this transient state is that P will diffuse into Si in excess of its normal solubility limit which is defined per coexistence of the α and SiP phases. Refer to Fig. 8b, the normal P solubility in Si is represented by concentration A. The material near the Si surface is now, however, not coexisting with SiP but with P_g which gives a P solubility in Si represented by concentration B. Since B>A has to hold, we see P enters Si at a concentration exceeding its solubility limit A. That is, by the very fact that now P_g and Si coexist, the material P_g directly exerts a chemical potential on Si to maintain a P concentration in excess of the P solubility deverived per coexistence of Si and SiP. If kinetical conditions permit, SiP precipitates can now form inside the Si crystal or alternatively a continuous layer of SiP can form at the Si surface. Before a sufficiently thick continuous SiP layer forms, the supersaturation phenomenon will persist.

Per this discussion, we see that there is a thermodynamic reason for P to diffuse into Si in supersaturation. For experiments for which a P rich oxide layer is used as source, the argument is also applicable. The analysis leading to this conclusion is, however, considerably more complicated than the binary example just discussed. This complexity arises because a Si-O-P ternary situation is involved. We have carried out the analysis for this ternary situation and the details will be given elsewhere (77). In that analysis we have also shown that the O solubility limit is also changed. There exists one experimental result (76) indicating that this seems to be the case.

5. CONCLUDING REMARK

In this paper some essential points associated with oxidation effects and Au diffusion in Si are discussed. Progresses in these areas in the last few years seems to have established beyond reasonable doubts that I and V coexist in Si under thermal equilibrium conditions. Within the frame work of coexisting I and V species, some new understanding is now emerging. We look forward for more progresses in our understanding of the nature of point defects and their roles in the materials transport properties in Si in the near future.

REFERENCES

1. R. Simmons and R. W. Balluffi, Phys. Rev. 129, 1532 (1963).
2. A. Chantre, M. Kechouane and D. Bois, Physica 116B, 547 (1983).
3. A. Seeger and K. P. Chik, Phys. Stat. Solidi 29, 455 (1968).
4. S. Prussin, J. Appl. Phys. 43, 2850 (1972).
5. S. M. Hu, J. Appl. Phys. 45, 1567 (1974).
6. B. Leroy, J. Appl. Phys. 50, 7996 (1979).
7. T. Y. Tan and U. Gösele, J. Appl. Phys. 53, 4767 (1982).
8. T. Y. Tan and U. Gösele, Appl. Phys. Lett. 40, 616 (1982).
9. D. A. Antoniadis and I. Moskowitz, J. Appl. Phys. 53, 9214 (1982).
10. T. Y. Tan, U. Gösele and F. Morehead, Appl. Phys. A31, 97 (1983).
11. U. Gösele, W. Frank and A. Seeger, Appl. Phys. 23, 361 (1980).
12. U. Gösele, F. Morehead, W. Frank and A. Seeger, Appl. Phys. Lett. 38, 157 (1981).
13. F. Morehead, N. Stolwijk, W. Frank, W. Meyberg and U. Gösele, Appl. Phys. Lett. 42, 690 (1983).
14. N. Stolwijk, B. Schuster, J. Hölzl, H. Meher and W. Frank, Physica 116B, 335 (1983).
15. U. Gösele and T. Y. Tan, in 'Defects in Semiconductors II' S. Mahajan and J. W. Corbett eds. (North-Holland, NY 1983) p45.
16. P. S. Dobson, Phil. Mag. 24, 567 (1971); 26,1301 (1972).
17. E. Sirtl, in 'Semiconductor Silicon 1977', H. R. Huff and E. Sirtl eds. (The Electrochem. Soc., Princeton, 1977) p4.
18. S. Mizuo and H. Higuchi, Jpn. J. Appl. Phys. 20, 739 (1981).
19. T. Y. Tan and B. J. Ginsgerg, Appl. Phys. Lett. 42, 448 (1983).
20. S. M. Hu, Appl. Phys. Lett. 27, 165 (1975).
21. H. Shiraki, Jpn. J. Appl. Phys. 15, 1 (1976).
22. S. P. Muraka, J. Appl. Phys. 48,5020 (1977).
23. S. Matsumoto, Y. Ishikawa and T. Niimi, J. Appl. Phys. 54, 5049 (1983).
24. T. Y. Tan, in 'Electron Microscopy of Materials', W. Krakow, D. A. Smith and L. W. Hobbs eds. (North-Holland, NY, 1984) in press.
25. G. K. Wertheim, Phys. Rev. 115, 568 (1959).
26. S. M. Hu, J. Vac. Sci. Technol. 14, 17 (1977).
27. T. R. Waite, Phys. Rev. 107, 463 (1957).
28. U. Gosele, W. Frank and A. Seeger, Sol. State Commun. 45, 31 (1982).
29. S. Matsumoto, Y. Ishikawa and T. Niimi, J. Appl. Phys. 54, 5049 (1983).
30. K. Taniguchi, D. A. Antoniadis and Y. Matsushita, Appl. Phys. Lett. 42, 961 (1983).
31. S. Mizuo and H. Higuchi, Jpn. J. Appl. Phys. 21, 272 (1982); 22, 12 (1983); J. Electrochem. Soc. 129, 2292 (1982).

32. T. Y. Tan, F. Morehead and U. Gösele, in 'Defects in Silicon' W. M. Bullis and L. C. Kimerlin eds. (The Electrochem. Soc., Pennington, 1983) p325.
33. F. C. Frank and D. Turnbull, Phys. Rev. 104, 617 (1956).
34. W. R. Wilcox, T. J. LaChapelle and D. H. Forbes, J. Electrochem. Soc. 111, 1377 (1964).
35. H. Kitagawa, K. hashimoto and M. Yoshida, Jpn. J. Appl. Phys. 21, 276 (1982).
36. J. M. Fairfield and B. J. Masters, J. Appl. Phys. 38, 3148 (1967).
37. H. J. Mayer, H. Mahrer and K. Maier, in 'Lattice Defects in Semiconductors 1976' (Inst. Phys. Conf. series 31, London, 1977) p186.
38. L. Kalingnowski and R. Seqin, Appl. Phys. Lett. 35, 211 (1979); 36, 141 (1980).
39. I. R. Sanders and P. S. Dobson, J. Mat. Sci. 9, 1987 (1974).
40. A. Hirvonen and J. Anttila, Appl. Phys. Lett. 35, 703 (1979).
41. H. Kitagawa, K. Hasimoto and Y. Yoshida, Jpn. J. Appl. Phys. 21, 276 (1982).
42. S. Mantovani, F. Nava, C. Nobili, M. Conti and G. Pignatel, Appl. Phys. Lett. 44, 328 (1984).
43. S. M. Hu, in ' Atomic Diffusion in Semiconductors', D. Shaw ed. (Plenum, NY, (1973) p217.
44. A. F. W. Willoughby, J. Phys. D10, 455 (1977); Rep. Prog. Phys. 41, 1665 (1978).
45. A. F. W. Willoughby, in 'Impurity Doping Process in Silicon' F. F. Y. Wang ed. (North-Holland, NY, 1981).
46. A. Seeger, W. Frank and U. Gösele, in 'Defects and Radiation Effects in semiconductors 1978' (Inst. Phys. Conf. Series 46, London, 1979) p148.
47. U. Gösele and H. Strunk, Appl. Phys. 20, 265 (1979).
48. M. C. Duffy, F. Barson, J. M. Fairfield and G. H. Schwuttke, J. Electrochem. Soc. 115, 84 (1968).
49. P. F. Schmidt and R. Stickler, J. Electrochem. Soc. 111, 1188 (1964).
50. T. W. O'Keefe, P. F. Schmidt and R. Stickler, J. Electrochem. Soc. 112, 878 (1965).
51. E. Kooi, J. Electrochem. Soc. 111, 1383 (1964).
52. R. J. Jaccodine, J. Appl. Phys. 39, 3105 (1968).
53. A. Armigliato, D. Nobili, M.Servidori and S. Solmi, J. Appl. Phys. 47, 5489 (1976).
54. D. Nobili, A Armigliato, M. Finnetti and S.Solmi, J. Appl. Phys. 53, 1484 (1982).
55. R. J. Jaccodine, in 'Defects in Semiconductors II' S. Mahajan and J. W. Corbett eds. (North-Holland, NY, 1983) p101.
56. J. E. Lawrence, J. Appl. Phys. 37, 4106 (1966).
57. C. L. Claeys, G. J. Declerck and R. J. Van Overstraeten, Revue de Physsique Appliquee 13, 797 (1978).
58. H. Shibayama, H. Masaki, H. Ishikawa and H. Hashimoto, J. Electrochem. Soc. 123, 743 (1976).
59. F. N. Schwettmann and D. L. Kendall, Appl. Phys. Lett. 19, 218 (1971); Appl. Phys. Lett. 20, 2 (1972).
60. M. Yoshida, Jpn. J. Appl. Phys. 19, 2427 (1980).
61. R. B. Fair and J. C. C. Tsai, J. Electrochem. Soc. 124, 1107 (1977).
62. F. A. Kroger, J. Electrochem. Soc. 125, 995 (1978).
63. D. Mathiot and J. C. Pfister, J. Appl. Phys. 53, 3053 (1982).
64. C. L. Claeys, G. J. Declerck and R. J. Van Overstraeten, in 'Semiconductor Characterization Technique' P. A. Barnes and G. A. Rozgonyi eds. (The Electrochem. Soc., Princeton, 1978) p336.
65. H. Strunk, U. Gosele and B. O Kolbesen, Appl. Phys. Lett. 34, 530 (1979).

66. R. M. Harris and D. A. Antoniadis, J. Appl. Phys. to be published.
67. P. Fahey, R. W. Dutton and S, M. Hu, Appl. Phys. Lett. 44, 777 (1984).
68. D. Mathiot and J. C. Pfister, Physica 116B, 95 (1983).
69. D. Mathiot and J. C. Pfister, J. Appl. Phys. 55, 3518 (1984).
70. S. M. Hu, P. Fahey and R. W. Dutton, J. Appl. Phys. 54, 6912 (1983).
71. D. Stauffer, Phys. Reports 54, 1 (1979).
72. R. Francis and P. S. Dobson, J. Appl. Phys. 50, 280 (1979).
73. C. Hill, in 'Semiconductor Silicon 1981' H. R. Huff, R. J. Kreigler and T. Takeishi eds. (The Electrochem. Soc., Princeton, 1981). p988.
74. W. F. Tseng, S. S. Lau and J. W. Mayer, Phys. Lett. 68A, 93 (1978).
75. D. Lecrosnier, J. Pangan, F. Richou, G. Pelous, F. Beniere, J. Appl . Phys. 51, 1036 (1981).
76. D. Heck, R.E. Tressler and J. Monkowski, J. Appl. Phys. 54, 5739 (1983).
77. T. Y. Tan and U. Gosele, Appl. Phys. A, to be puablished.

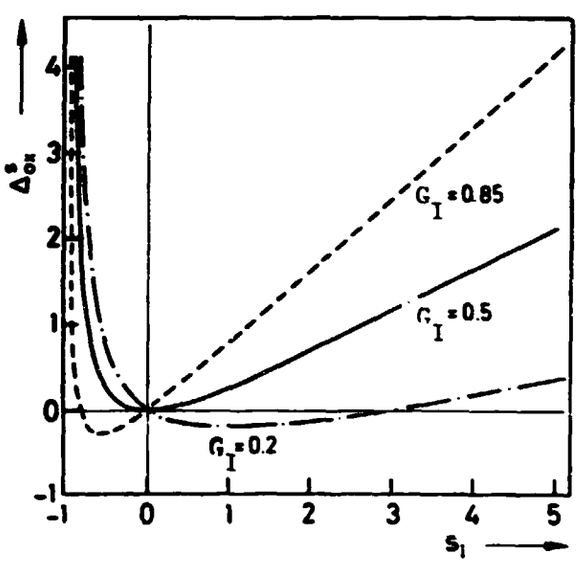

Fig. 1. Prediction of dopant diffusivity changes due to an oxidation. The model assumes that I and V coexist in Si in thermal equilibrium and in oxidation at high temperatures and that during the oxidation I and V attained local equilibrium.

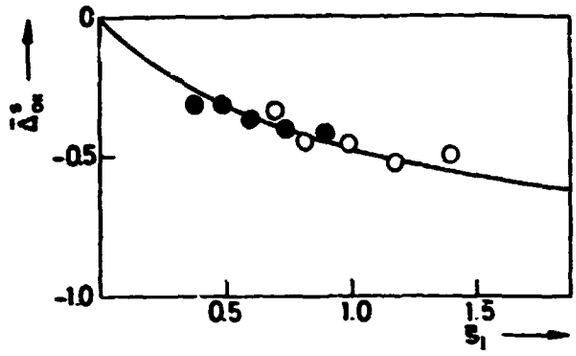

Fig. 2. Quantitative fitting of available Sb ORD data from (100) wafers to the calculated G_I=0.02 curve per Eq. (8). Unfilled circle: Mizuo and Higuchi [18]; filled circle: Tan and Ginsberg [19].

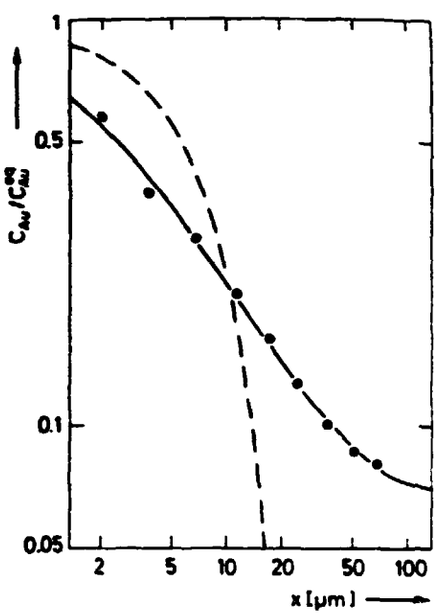

Fig. 4. Gold concentration profile after a 1hr diffusion into dislocation-free Si at 900°C [14]. Dash line: an erfc-function fitting per Eq. (19); solid line: fitting per Eq. (20).

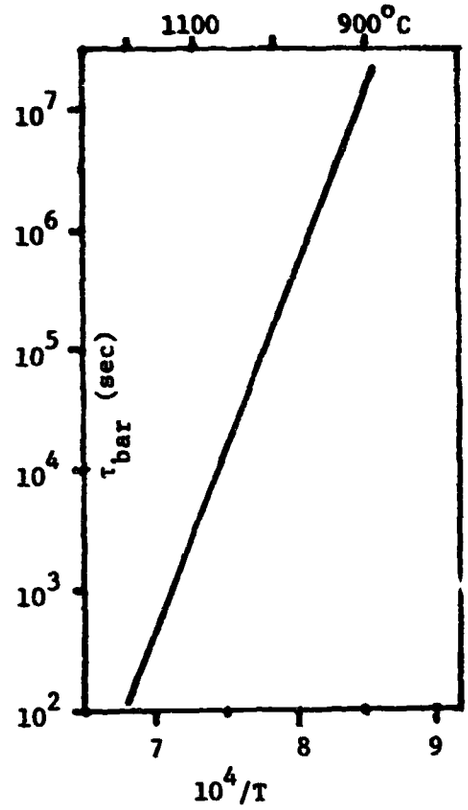

Fig. 3. The recombination barrier limited time constant, τ_{bar}, for I and V to reach dynamical equilibrium as a function of reciprocal temperature calculated per Eq. (11).

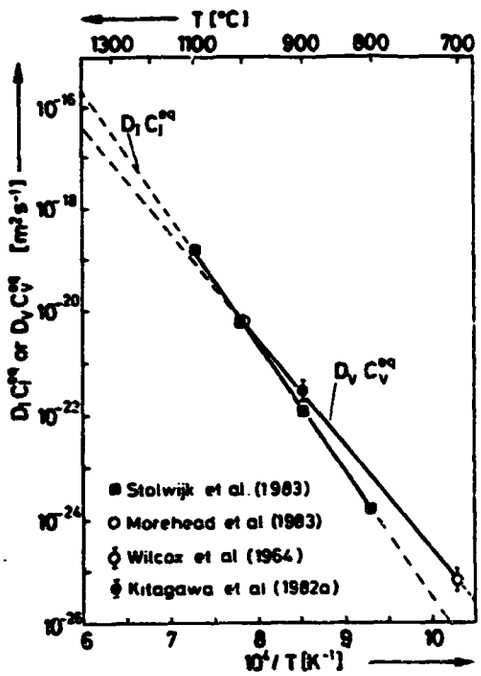

Fig. 5. $D_I C_I^{eq}$ and $D_V C_V^{eq}$ vs. reciprocal temperature.

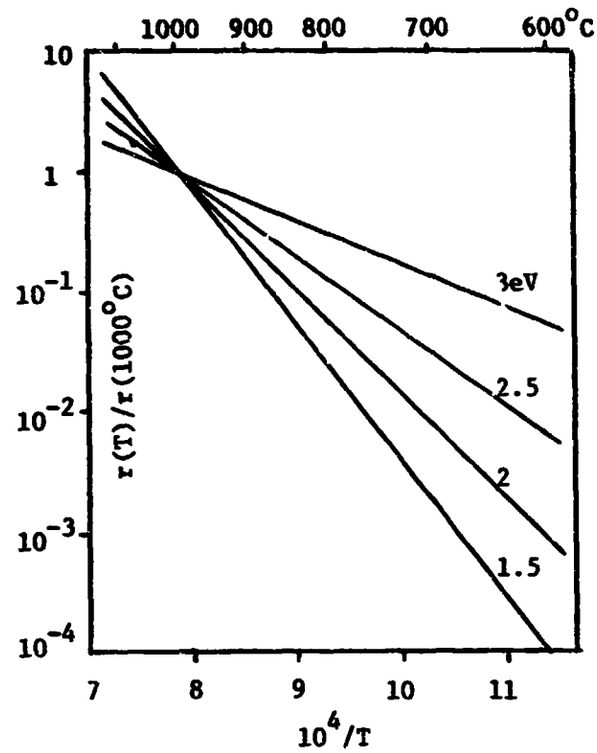

Fig. 6. The function r(T)/r(1000°C) vs. reciprocal temperature, r is the ratio of the efficiency of converting Au_i into Au_s due to the kick-out mechanism to that due to the Frank-Turnbull mechanism. Numbers above each curve are the possible ΔH_V^f values.

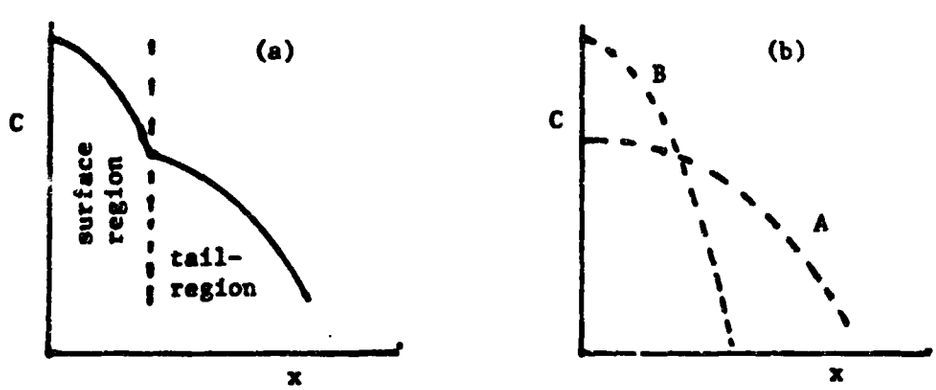

Fig. 7. (a) Schematic dra 'ng of the kink-tail structure of P profile, which, hypothetically, may be obtained by adding (b) profiles of physically distinguishable A and B atoms diffusing independently.

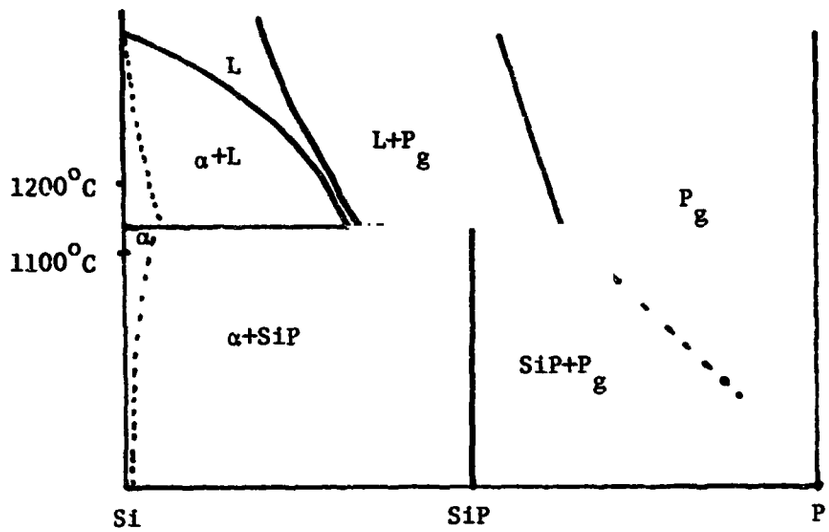

(a)

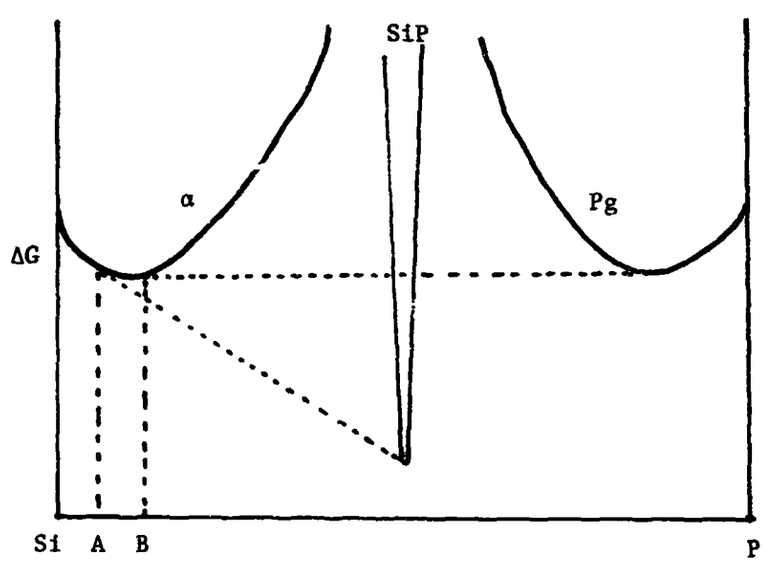

(b)

Fig. 5. The Si-P binary system phase diagram (a) and an appropriate free energy diagram (b) showing the thermodynamic origin for P to diffuse into Si in excess of its normal solubility limit. The solubility limits A and B are obtained from the usual common tangent constructions per coexistence of the α phase with the SiP and P_g phases respectively.

DISCUSSION

ROSE: On one of your viewgraphs you showed during the phosphorus diffusion, something like 40% of it is electrically active. I wonder if you might comment further on what physical form does it take?

TAN: It takes precipitated form. A small part of it, about 15%, is identified as SiP structure. About 85% of them are only observed in terms of no more than 15-Å-sized precipitates. They are too small to be identified by transmission electron microscope. Therefore they are only inferred to be SiP precipitate, but not proven.

N85-31633

Electrical and Structural Characterization of Web Dendrite Crystals

G. H. Schwuttke
Arizona State University
Tempe, AZ 85287

K. Koliwad and K. A. Dumas
Jet Propulsion Laboratory
California Institute of Technology
Pasadena, CA 91109

Abstract

Minority carrier lifetime distributions in silicon web dendrites are measured. Emphasis is placed on measuring areal homogeneity of lifetime, show its dependency on structural defects, and its unique change during hot processing. The internal gettering action of defect layers present in web crystals and their relation to minority carrier lifetime distributions is discussed. Minority carrier lifetime maps of web dendrites obtained before and after high temperature heat treatment are compared to similar maps obtained from 100 mm diameter Czochralski silicon wafers. Such maps indicate similar or superior areal homogeneity of minority carrier lifetime in webs.

Introduction

Recently, calculations have been made which show that the presence of [illegible]al inhomogeneity of minority carrier lifetime in silicon wafers can devast[illegible]lar cell efficiency (1). For instance, it was shown that for no more than 5[illegible] the solar cell area being inferior compared to the rest of the cell area, solar cell efficiency can be as poor as it would be if the entire area would be of inferior quality (1). Thus areal homogeneity of minority carrier lifetime is an important requirement for high efficiency solar cells.

This paper reports measurements of minority carrier lifetime "distributions" made on silicon web dendrite sections. Such measu[illegible] are compared to similar data obtained from 100 mm diameter Czochralski silicon wafers.

Structural Aspects of Silicon Web

A brief description of the as-grown web geometry and dislocation structure is needed to describe our electrical measurements clearly. For detailed results we refer to the original papers on web growth (2) and dislocation structures (3-5).

The web surface is parallel to the (111) plane, and the web pulling direction is $[2\bar{1}\bar{1}]$. A cross-section of web shows its most prominent structural feature: multiple twin lamellae in the center of the web covered by two thick (100 μm) surface layers which are also in twin relation. An example is shown in Figs. 1a,b.

PRECEDING PAGE BLANK NOT FILMED

Dislocations in web are generated through "melt entrapment" caused by "wing" growth along the dendrites (Fig. 2). Propagation of such dislocations depends on the curvature of the solid-liquid interface of the web during growth. An interface curvature of concave downward concentrates the dislocations in the center of the web (Fig. 3). Webs grown with a straight interface concentrate the dislocations in the fillet region. Thus the web grows free of any dislocations (4), Fig. 4. Most webs of today contain bundles of very long dislocation lines parallel to the [2$\bar{1}\bar{1}$] direction (Fig. 5). They are piled up against the twin planes. In addition, annealed web contains large area stacking faults. The electrical activity and the influence of these faults on solar cell efficiency has not yet been investigated. Such an influence is assumed to be relatively small but it may be of importance for high efficiency solar cells. These defects are described in more detail in References 3 and 5, examples are shown in the x-ray topographs of Figs. 6.

If excessive stresses are present during web growth (buckling) large numbers of slip dislocations and small angle grain boundaries may occur. Such defects degrade minority carrier lifetime. An example is shown in the x-ray topographs of Figs. 7.

Minority Carrier Lifetime Measurement In Web

Silicon web dendrite sections of various quality (Figs. 5, 6, 7) were evaluated through minority carrier lifetime "mapping" using 1.5 mm diameter MOS capacitors. The total number of MOS capacitors per web section was 300. The MOS dots were arranged into 15 rows. The dendrites were included into the evaluation. The dimensions of the web sections were 2 inches long and 32 mm wide. The webs were evaluated after each oxidation cycle (15 min wet-110 min dry-15 min wet at 1000°C. Three or four consecutive oxidation cycles were used. Minority carrier lifetime maps of the total web section were obtained after each oxidation cycle by measuring the lifetime under each capacitor as described by Fahrner & Schneider). Subsequently, the lifetime was computer plotted versus its position on the web surface. Local lifetime degrading defects revealed by such lifetime maps were analysed by advanced characterization techniques. A result typical for web sections of quality as shown in Figs. 5 and 6 is given in Fig. 8. This figure summarizes the influence of high temperature heat cycles on minority carrier lifetime. The lifetime data are displayed in 6 maps. Each map represents a matrix of 300 capacitor dots. The maps on the left side of the figure carry the label oxidation 1 to 3 and represent the lifetime data obtained after the first, second, and third oxidation cycle. The devices were obviously stripped before every successive oxidation step. The z-scale represents the measured lifetime values in microseconds. The range of lifetime data present on the web section is also included in the label. For instance, the minimum lifetime obtained at a specific location (capacitor) after the first oxidation was 0.274 microseconds. The maximum lifetime is 207 microseconds. The lifetime map shows a relatively smooth plateau. Noteworthy is, that this plateau extends over the total web section surveyed. Accordingly, this web is of excellent crystal quality and compares well with the best Czochralski silicon as available today. Interesting is a comparison of the maps obtained after the first, second and third oxidation. The lifetime plateau obtained after the second oxidation is well above the one obtained after the first oxidation and the same is true for the third oxidation. The third plateau is a little bit lower than the second one. Using Czochralski wafer quality as a standard, the

material obtained after the third oxidation shows very uniform lifetime distribution data.

The maps on the right side of Fig. 8 are labeled DECREASE or INCREASE. The DECREASE map shows the degradation of lifetime as a result of the second or third oxidation cycle. The INCREASE map shows the area where the lifetime increased after the third oxidation relative to the first oxidation. These maps show clearly the improvement of lifetime as a result of oxidation. This improvement is fairly uniform and covers practically the total web area. Decreases in lifetime occur only along the dendrites, the fillet region or along the edges where the web section was cut by the dicing saw. This result is unique and relates to the special crystal structure of the "perfect" web. The defect planes, sandwiched between the perfect web surface layers, provide for "internal" gettering during high temperature heat cycles. Thus a substantial improvement of minority carrier lifetime can result.

Web material of the quality as displayed in the topographs of Figs. 7 do not give comparable results. It was found that the "slip" dislocations - which result from buckling stresses - degrade minority carries lifetime substantially. These dislocations are of the same type as the "process" induced slip dislocation encountered during IC processing. It is known that the electrical activity of these dislocations is high. The lifetime map shown in Fig. 9 corresponds to the sample shown in Fig. 7b. Note the good correlation between low lifetime and defect area in the center of this sample.

Minority Carrier Lifetime Measurements in Czochralski Silicon

Recently, we conducted an evaluation of 100 mm diameter Czochralski silicon wafers as available from major vendors throughout the world. The evaluation concentrated on minority carrier lifetime mapping as described for the web crystal. Four consecutive oxidation cycles were used. The MOS dot matrix consisted of 25 times 25 MOS capacitors of 1.5 mm diameter. A result typical for the evaluated Czochralski wafers is shown in Fig. 10. The lifetime data shown in Fig. 10 are displayed in 4 maps. The maps on the left carry again the oxidation number. The data obtained after the first oxidation indicate excellent wafer quality. The map has a plateau at approx. 250 to 300 microseconds and extends practically across the total wafer area. This wafer represents silicon of the best quality. Nevertheless, successive oxidation results in steady degradation of lifetime. This is seen by comparing the maps obtained after the first and fourth oxidation.

Interesting are the DECREASE and INCREASE maps shown on the right of Fig. 10. The decrease map confirms that degradation occurs uniformly across the total wafer area. After the fourth oxidation cycle small lifetime increases are observed only at 9 locations. In all other areas lifetime degraded substantially.

Discussion and Summary

The data given in Figs. 8 and 10 are representative of "perfect" web and Czochralski silicon wafers. We note a basic difference between these two materials. Oxidation increases generation lifetime in Web but decreases the

same lifetime in Czochralski material. The decrease in lifetime in Czochralski wafers correlates with the precipitation phenomena of oxygen in silicon (7).

The large extent to which areal inhomogeneities exist in todays silicon and influence device performance (1) is not well known. However, uniform minority carrier lifetime distributions are a pre-requisite to high performance solar cell technology. Solar cell efficiency in excess of 15% for large area single crystal silicon cells (10 cm x 10 cm) will be very difficult to achieve without proper control of minority carrier lifetime distributions during large scale manufacturing.

References

1. F. A. Lindholm et al., Solid State Electronics, 23, 967, (1980).

2. S. O'Hara and A. I. Bennett, J. Appl. Phys., 35, 409, (1964).

3. S. O'Hara and G. H. Schwuttke, J. Appl. Phys., 36, 2475, (1965).

4. T. N. Tucker and G. H. Schwuttke, Appl. Phys. Letter, 9, 219, (1966).

5. E. S. Meieran and I. Blech, J. Appl. Phys., 38, 3495, (1967).

6. W. Fahrner and C. P. Schneider, J. Electrochem. Soc., 123, 100, (1976).

7. G. H. Schwuttke, Semiconductor Industry Association (SIA) Lecture, Stanford Univ., Sept. 1981, Palo Alto, CA.

Figure Captions

Fig. 1 a. Web Crystal Geometry
b. SEM-micrograph of cleaved web cross-section after preferential etching. Note twin lamellae in center.

Fig. 2 SOT X-ray topograph of cm wide web dendrite. Note wing growth (arrows) at dendrites due w web loading to liquid entrapment and dislocation generation during growth.

Fig. 3 SOT X-ray topograph of 3 cm wide web dendrite. Note dislocation generation at stress centers and propagation of dislocations during growth toward center.

Fig. 4 SOT X-ray topograph of perfect 1.5 cm wide web. Dislocations are trapped in fillet region.

Fig. 5 SOT X-ray topograph of high performance web 220-reflection. Note long dislocations, 73 degree type; Burgers vectors [101], [110]. Low electrical activity.

Fig. 6 SOT X-ray topographs of high performance web. Width 3.2 cm.
a. $(\underline{111})$ reflection: Surface twin lamellae
b. $(\overline{111})$ reflection: Bottom twin lamellae
Note difference in crystal perfection: Bottom lamellae contains large area stacking faults. Topographs recorded after third oxidation. Electrical activity of defects low. Electrical data in Fig. 8.

Fig. 7 a. SOT X-ray topograph of low quality web. Note slip dislocations. Electrical activity high. Lifetime range: 0.01 - 1 μsec.
b. SOT X-ray topograph of medium quality web. Electrical data in Fig. 9.

Fig. 8 Minority carrier lifetime maps of high performance web. Lifetime range: 0.2 - 207 μsec.

Fig. 9 Minority carrier lifetime map of low performance web. Corresponding SOT topograph is shown in Fig. 7b. Note correlation between dislocation density and low lifetime. Lifetime range: 0.1 - 50 μsec.

Fig. 10 Minority carrier lifetime map of Czochralski wafer for comparison. Lifetime range: 4 - 478 μsec.

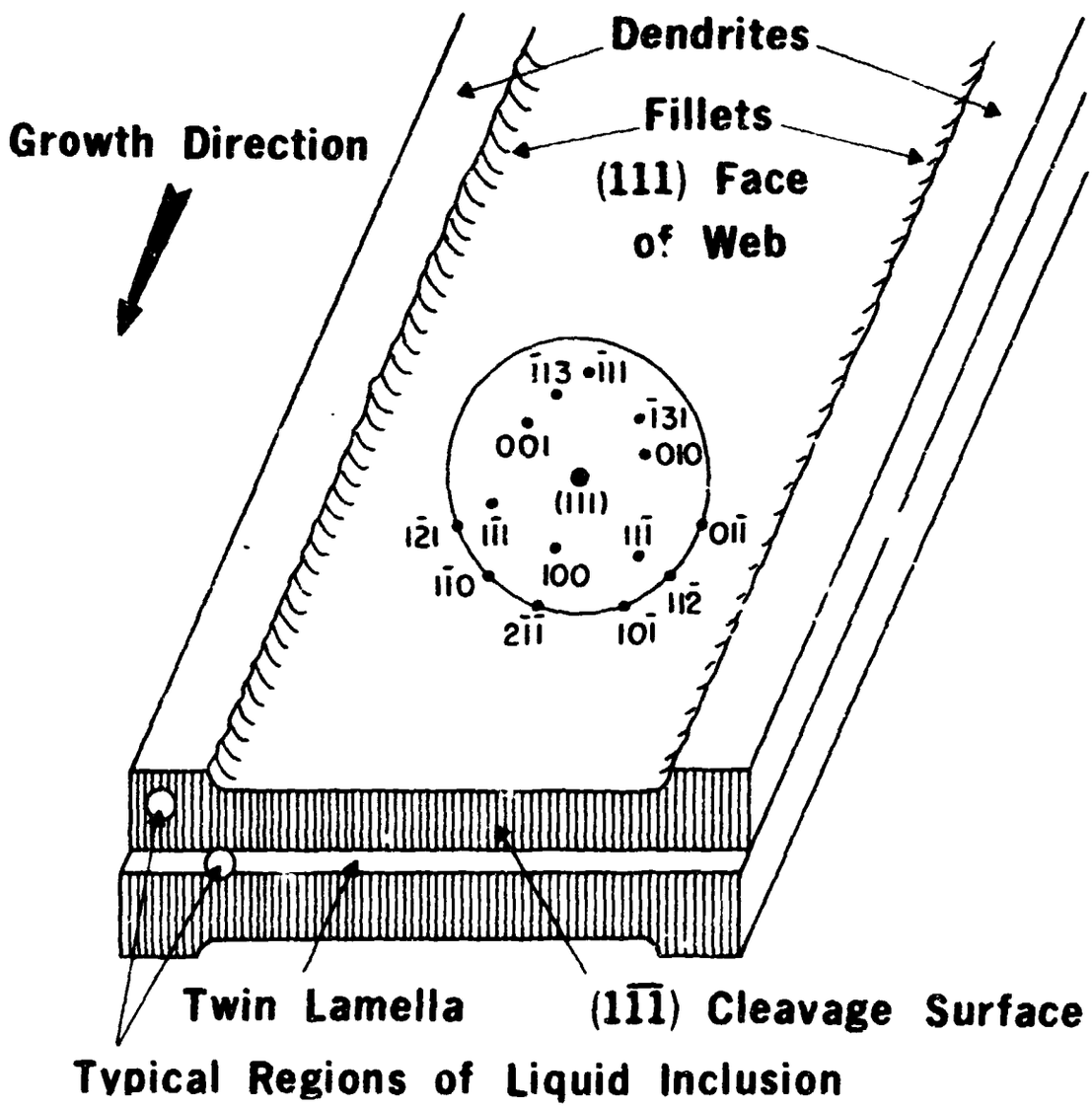

Fig. 1a Web Crystal Geometry

ORIGINAL PAGE IS
OF POOR QUALITY

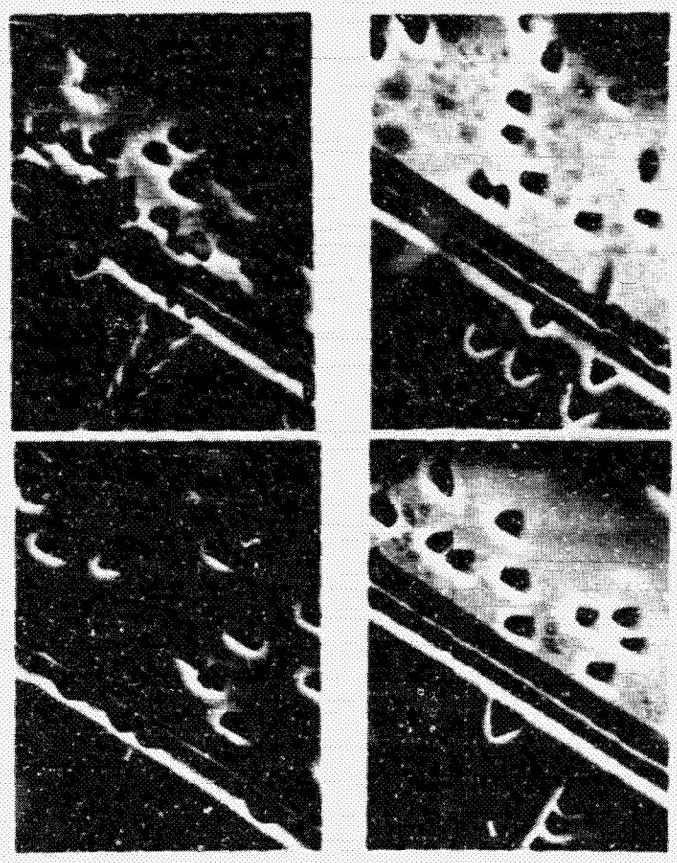

Fig. 1b SEM-micrograph of cleaved web cross-section after preferential etching. Note twin lamellae in center.

Fig. 2 SOT X-ray topograph of 2 cm wide web dendrite. Note wing growth (arrows) at dendrites below web leading to liquid entrapment and dislocation generation during growth.

ORIGINAL PAGE IS
OF POOR QUALITY

ORIGINAL PAGE IS
OF POOR QUALITY

Fig. 3 SOT X-ray topograph of 3 cm wide web dendrite. Note dislocation generation at stress centers and propagation of dislocations during growth toward center.

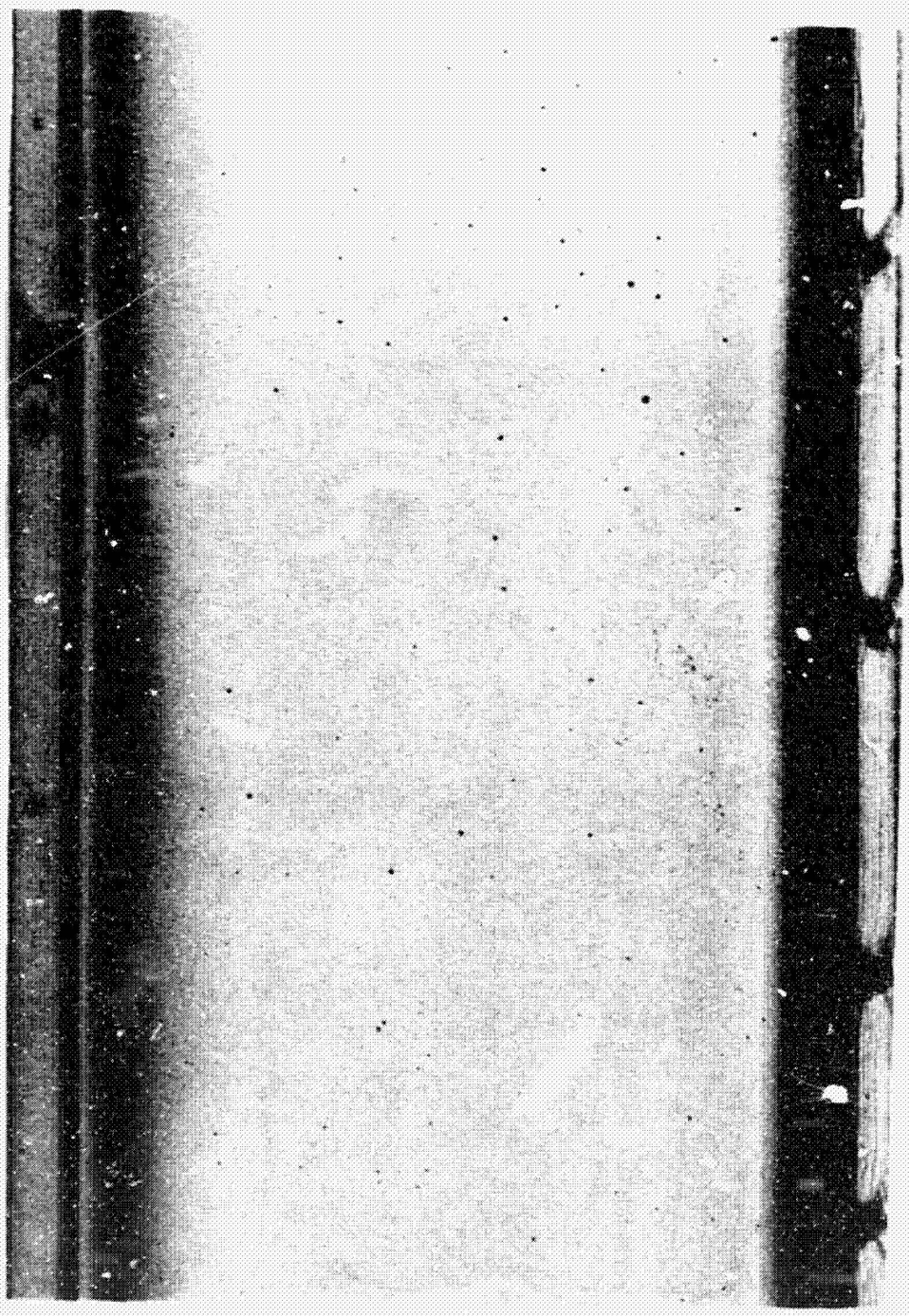

Fig. 4 SOT X-ray topograph of perfect 1.5 cm wide web. Dislocations are trapped in fillet region.

ORIGINAL PAGE IS
OF POOR QUALITY

Fig. 5 SOT X-ray topograph of high performance web, 220-reflection. Note long dislocations, 73 degree type; Burgers vectors [101], [110]. Low electrical activity.

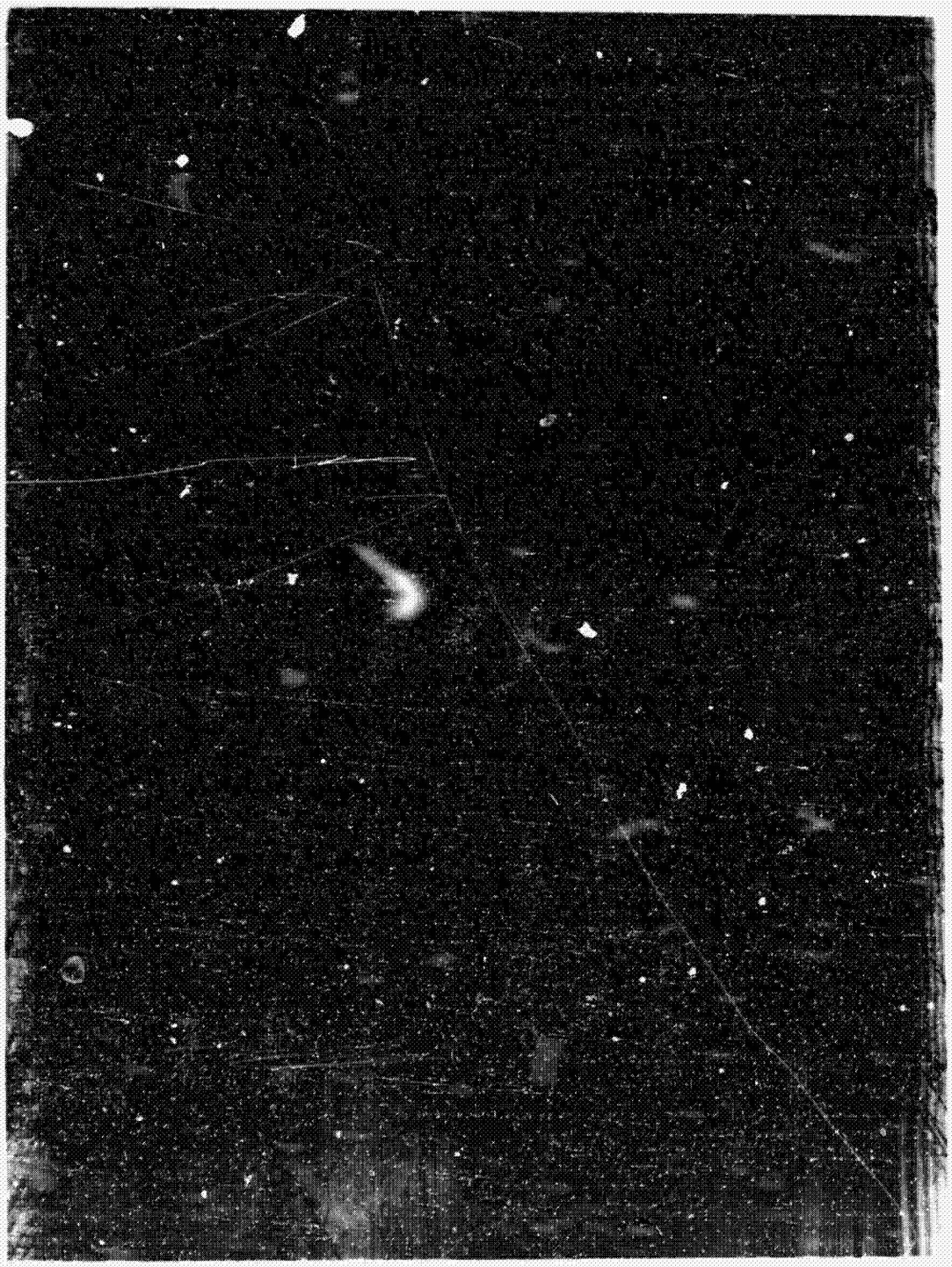

Fig. 6a SOT X-ray topographs of high performance web. Width 3.2 cm.
(111) reflection: Surface twin lamellae.
Electrical data in Fig. 8.

ORIGINAL PAGE IS
OF POOR QUALITY

Fig. 6b SOT X-ray topographs of high performance web. Width 3.2 cm. $(\bar{1}\bar{1}\bar{1})$ reflection: Bottom twin lamellae
Note difference in crystal perfection: Bottom lamellae contains large area stacking faults. Topographs recorded after third oxidation. Electrical activity of defects low.

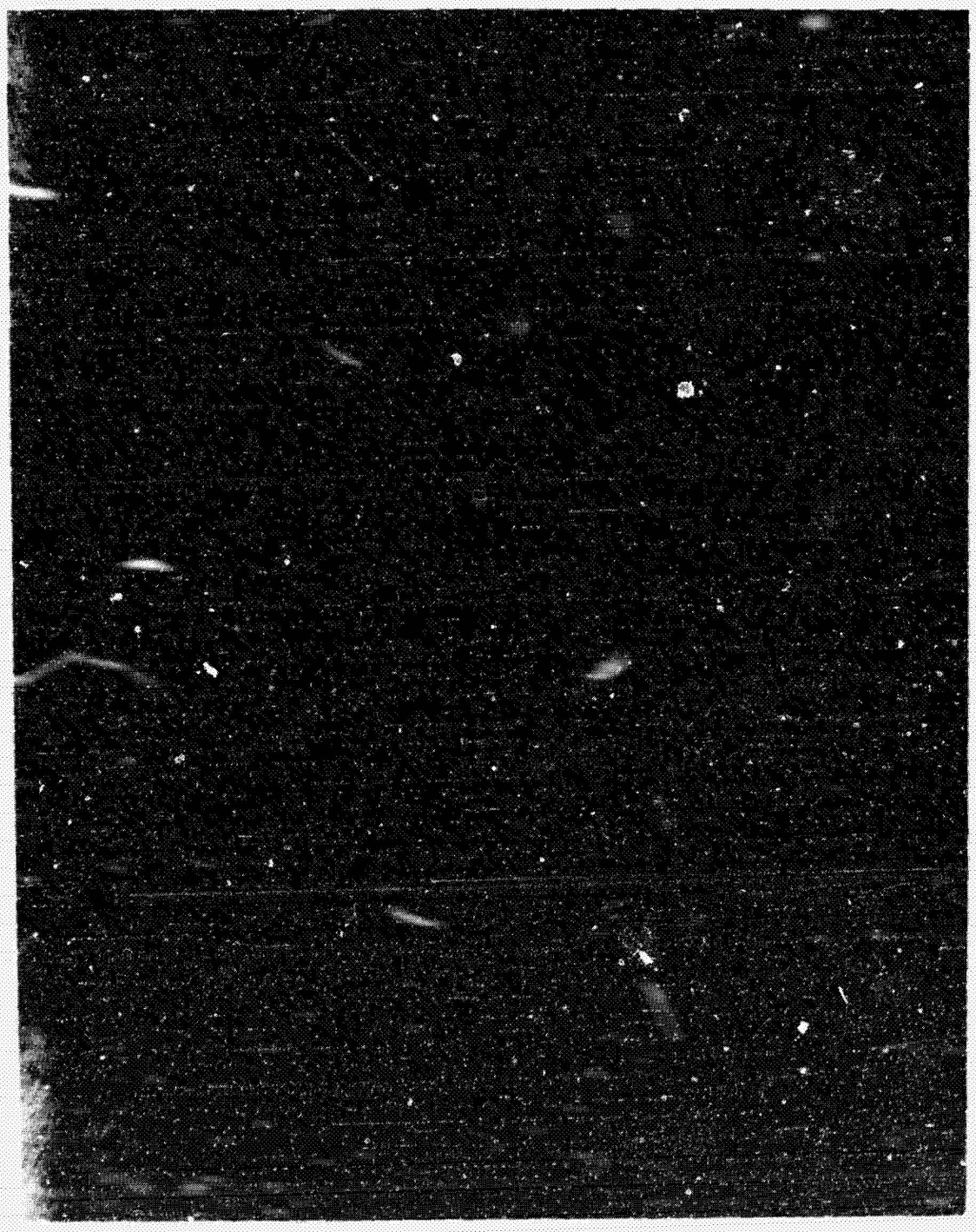

Fig 7a SOT X-ray topograph of low quality web. Note slip dislocations. Electrical activity high. Lifetime range: 0.01 - 1 μsec.

ORIGINAL PAGE IS
OF POOR QUALITY

Fig 7b SOT X-ray topograph of medium quality web. Electrical data in Fig. 9.

ORIGINAL PAGE IS
OF POOR QUALITY

Web Dendrite Silicon Lifetime Distribution Data

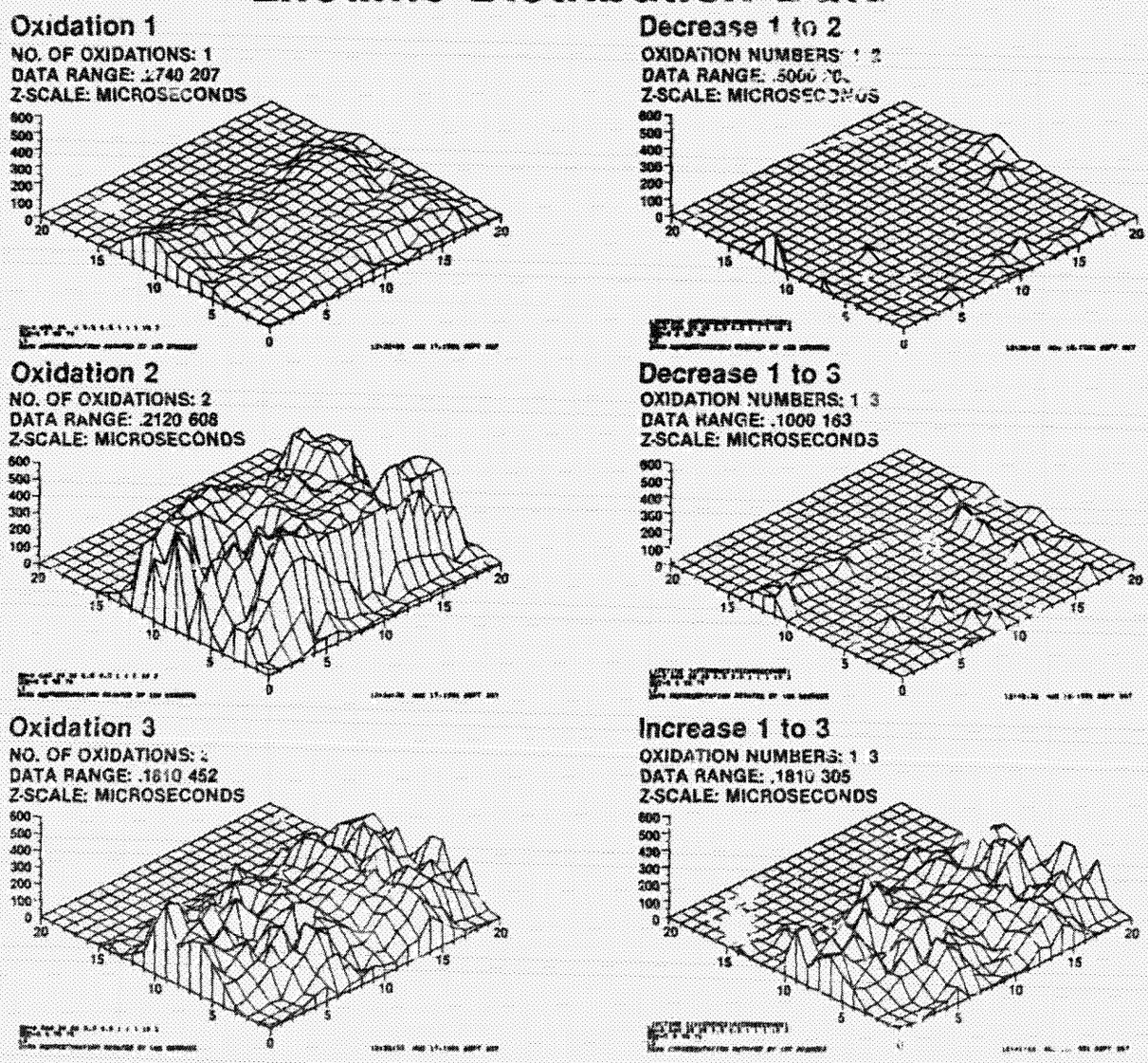

Fig. 8 Minority carrier lifetime maps of high performance web. Lifetime range: 0.2 - 207 μsec.

ORIGINAL PAGE IS
OF POOR QUALITY

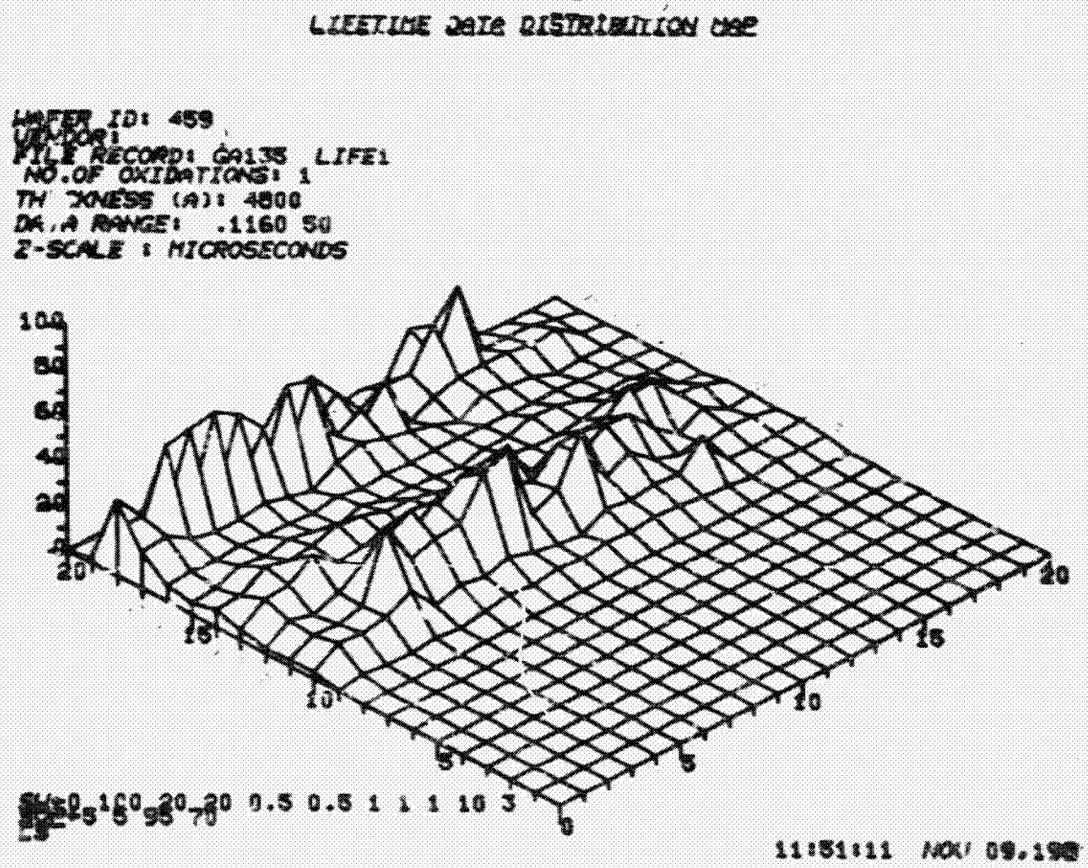

Fig. 9 Minority carrier lifetime map of low performance web. Corresponding SOT topograph is shown in Fig. 7b. Note correlation between dislocation density and low lifetime. Lifetime range: 0.1 - 50 μsec.

Lifetime Data Distribution Map
Vendor B

Oxidation 1

NO. OF OXIDATIONS: 1
DATA RANGE: 4.0000 478
Z-SCALE: MICROSECONDS

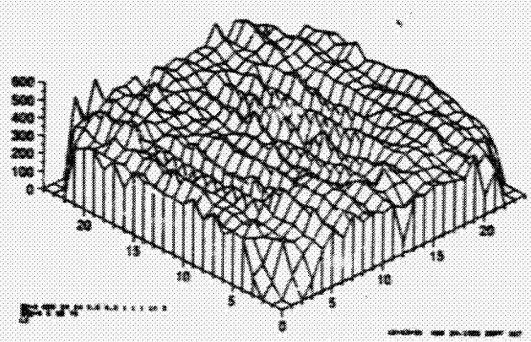

Decrease

OXIDATION NUMBERS: 1 4
DATA RANGE: 7.0000 442
Z-SCALE: MICROSECONDS

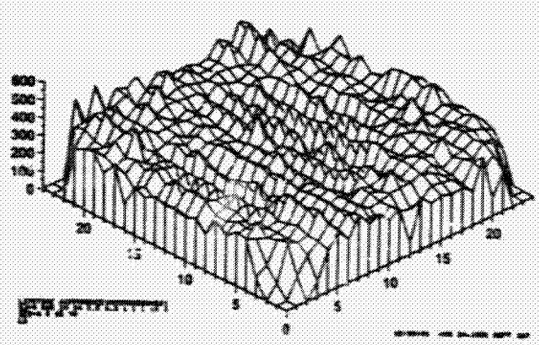

Oxidation 4

NO. OF OXIDATIONS: 4
DATA RANGE: .5300 129
Z-SCALE: MICROSECONDS

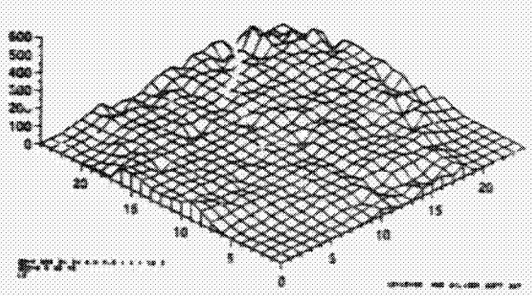

Increase

OXIDATION NUMBERS: 1 4
DATA RANGE: 2.0000 48
Z-SCALE: MICROSECONDS

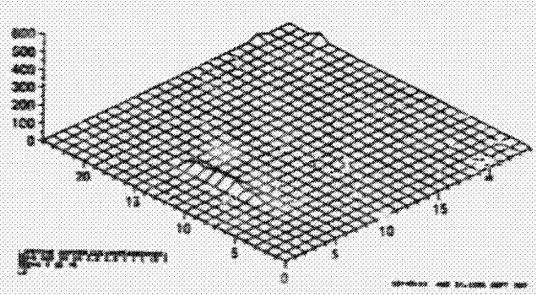

Fig. 10 Minority carrier lifetime map of Czochralski wafer for comparison. Lifetime range: 4/8 μsec.

DISCUSSION

HAMOKA: Do you have any idea why the grown dislocations seem to be not electrically bothersome, whereas the stress-induced ones are?

SCHWUTKE: First of all, the core structure of this grown dislocation is very benign. It makes an angle of 73°, and this type of dislocation has been described in the literature. This structure is very benign, while a 60° dislocation, which is a slip dislocation, is very active due to its core structure.

N85-31634

EBIC Characterization and Hydrogen Passivation in Silicon Sheet

Jack I. Hanoka
Mobil Solar Energy Corporation
Waltham, Massachusetts 02254

ABSTRACT

As a general qualitative tool, the electron beam induced current (EBIC) method can be very useful in imaging recombination in silicon sheet used for solar cells [1,2]. In this paper, work using EBIC on EFG silicon ribbon will be described. In particular, some efforts at making the technique more quantitative and hence more useful, some limitations of the method, and finally specific application to hydrogen passivation will be treated. As an introduction, some brief remarks will be made regarding the technique itself.

The EBIC Technique

Figure 1 shows a schematic of the EBIC process. An electron beam impinges on a semiconductor sample containing a junction of some sort. The energy of the electrons in the beam typically ranges from 1 to 50 keV while the minimum energy to create hole-electron pairs in a semiconductor is the band gap, which is on the order of 1 eV. As a result, a single high energy electron incident on the semiconductor produces many hole-electron pairs, on the order of 10^3 to 10^4 per incident electron. The electron-hole pairs are created within the material in a volume termed the generation volume. The important carriers here are the minority carriers -- electrons in the p-type layer and holes in the n-type layer. If the diffusion length of the generated minority carriers is long enough, they will diffuse to the p-n junction and be swept across it by the strong field present, thus producing a current that can be measured externally. This is the electron-beam-induced current. This current can then be amplified even further and the amplified signal used to drive the CRT display of the SEM, while it is scanned synchronously with the electron beam. The result is a mapping of the current collected at every scanned point. If a defect such as a grain boundary or a dislocation is present, the resulting recombination at such a defect will produce less collected current and a darker image (corresponding to less current collection) in the CRT display. Examples of EBIC images of recombination at grain boundaries and at dislocations will be shown in later figures in this paper.

The description above indicates that EBIC is an electron-beam analog of the photovoltaic effect. The images one obtains using light beam induced current (LBIC) are, in fact, similar to those seen from EBIC. LBIC generally has poorer resolution than EBIC but offers the ability to generate carriers at varying distances according to the wavelength of the light chosen.

With EBIC, the depth of penetration or the range R, of the electron beam is a function of the electron beam energy, E, with this form for silicon:

PRECEDING PAGE BLANK NOT FILMED

$$R = (0.032)\ E^{1.67} \qquad (1)$$

where R is in microns and E is in keV. The range-energy relation depends on the model chosen, another commonly used model gives R ~ 7 μm at 30 keV [1].

A reasonable and useful approximation for silicon is to consider the electron-hole pair generation volume to be a sphere tangent to the sample surface. R is then the diameter of this sphere. For a 30 keV beam, R ~ 9 μm. R is also a measure of the resolution obtainable. It is important to note that the resolution is only weakly dependent on the minority carrier diffusion length and is mainly determined by the value of R.

There is a considerable body of literature now available on quantifying EBIC, but we will concern ourselves with two or three techniques in particular which we have found useful in studying solar cells.

Low Temperature EBIC

As mentioned above, an EBIC image provides a recombination map. In addition to simply knowing the spatial location of recombination sites, it is important, particularly from the point of view of making higher efficiency silicon ribbon solar cells, to further understand what is taking place at these recombination sites.

Accordingly, we have investigated the use of EBIC at low temperatures [3]. In general, a considerable amount of recombination contrast enhancement is seen in EFG ribbon silicon when going from room temperature to, say, 200°K. Through the use of a trapping model, it was shown that the experimental results obtained could be interpreted as due to shallow energy states located below the conduction band and that the activation energy of these levels could be calculated from the low temperature EBIC data.

Furthermore, the behavior of these traps as a function of thermal processing and $[O_i]$ has been studied and will be discussed below.

The ribbon samples studied here were p-type, with ρ ~ 1 Ω-cm. Both Al Schottky barriers and PH_3 diffused junctions were used as collecting junctions for the EBIC work. The low temperature EBIC was done using a liquid nitrogen-cooled specimen mount which was fitted to a Cambridge S4-10 SEM. The ribbon sample and a single crystal CZ reference sample were mounted on a thick copper block with a thermocouple between the two samples. With this arrangement, the electron beam induced current at a particular defect could be measured by adjusting the condenser lenses on the SEM to give a pre-selected value of the EBIC for the CZ reference cell. No significant defects were observed in the CZ reference cell at 300°K or down to 200°K. An assumption used in making the measurements is that the EBIC of the reference cell is independent of temperature.

The general result observed is shown in Fig. 2 where the enhanced recombination along and between the linear boundaries at low temperature can readily be seen. In the room temperature photograph in Fig. 2 (top photograph), the prototypical defects seen by EBIC on EFG ribbon are evident. These are linear boundaries parallel to the growth direction and arrays of dislocations

within bands bordered by linear boundaries.

Quantifying the above is done by measuring the EBIC signal at a particular defect as a function of temperature. Using the single crystal reference cell and the value of the EBIC signal at the defect, a diffusion length L, could be assigned to the region enclosing the defect [3,4].

A model was developed in which the enhanced recombination seen at lower temperatures was viewed as due to trapping of electrons at shallow levels below the conduction band [3]. Figure 3 shows the scheme used for the model. If such a level is at an energy ΔE below the conduction band, then it was possible to show that

$$L^2 T^{1/2} \propto e^{-\Delta E/kT} \qquad (2)$$

Thus, measuring the value of L at a particular defect as a function of temperature would permit the calculation of the trap activation energy, ΔE. In this way, three shallow traps were found, $E_c - 0.04$ eV, $E_c - 0.10$ eV, and $E_c - 0.13$ eV.

The behavior of these traps indicates considerable sensitivity to both the particular growth conditions (quartz or graphite crucibles), addition or non-addition of CO_2 to the growth ambient used, and also to the temperature employed for the n-type diffusion.

A feature common to all the above cases is the spatial anchoring of these traps at dislocations or at linear boundaries. The location of these traps is not affected by diffusion temperatures up to 1050°C, at least within the EBIC spatial resolution limit of ~9 μm for a 30 keV electron beam. Figures 4 and 5 illustrate some differences in EBIC temperature behavior (increasing recombination with decreasing temperature) for the as-grown quartz crucible and as-grown graphite crucible silicon ribbon. The graphite material (Fig. 5) shows a saturation at temperatures below 153°K indicating that below this temperature electrons do not detrap back into the conduction band but undergo a transition to a deeper level at which recombination takes place. This latter process takes place with relatively little temperature sensitivity as opposed to the exponential behavior of the detrapping process. The quartz-grown material (Fig. 4), on the other hand, shows either no saturation down to 140°K or the trap distribution changes at ~188°K from the 0.04 level to a dominance of either the 0.10 level or the 0.13 level.

Trap behavior in solar cells made from the graphite crucible material in which the $[O_i]$ was varied by changing the CO_2 partial pressure in the growth ambient showed a transition from the 0.04 eV level to the 0.10 eV level only when $[O_i] > 10^{16}$ cm^{-3}. Also, in cases at higher diffusion temperatures (1040°C, instead of 900°C), all shallow trap levels could be suppressed. These results are summarized in the four cases shown in Fig. 6. Figure 6 also indicates that we believe that these shallow states communicate in some way with deeper mid-gap states, but little can be said about this at this time.

The results suggest that some sort of oxygen-related complex is formed at these electrically active dislocations. The complex then dissolves or breaks up when T > 1040°C. For $[O_i] > 10^{16}$ cm^{-3}, there is an interaction with the

shallowest trap at $E_c - 0.04$ and traps at $E_c - 0.10$ and $E_c - 0.13$ eV then manifest themselves. The effect of carbon in all this remains to be uncovered, but since carbon is present in concentrations of the order of 10^{18} cm^{-3}, it probably has a major role to play.

Recently, we have begun using low temperature EBIC to study dislocations which are formed under known stress and temperature conditions. In order to establish a reference, initial work has been done on single crystal material. The utility of low temperature EBIC in enhancing recombination at the dislocations formed in this case by plastic deformation can be seen in Fig. 7. Shallow trap levels have not yet been measured here but the highly enhanced low temperature EBIC contrast of these dislocations is quite evident from Fig. 7.

Diffusion Length and Surface Recombination Velocity Measurements

The inhomogeneous distribution of the two types of defects which are easily imaged by EBIC, namely dislocations and grain boundaries, means that the diffusion length, L, also varies spatially in material which contains these defects.

In analyzing the current collection in EBIC when defects or regions of diminished values of L are present, several approaches are possible. One approach is to treat the defect as a perturbation such that L changes abruptly when a defect is encountered. With this approach to the problem, an analysis built up using point defects can be done so that line defects and planar defects can be studied. Donolato [5] has used this method extensively in his papers and we will show how it can be utilized further on in this section.

An approach which represents an opposite extreme can also be taken [4] where one assumes (1) that the defects are distributed over a finite volume and in fact fill the generation sphere, and (2) that L varies in a smoother and less abrupt fashion in moving from a defect to a defect-free region.

Both of these approaches will be illustrated with experimental examples which will also show the advantages and disadvantages of each approach.

The shallow trapping level model utilized in the interpretation of the low temperature EBIC data implicitly used the second approach where the defect is visualized as filling the generation sphere. This, of course, is a simplistic assumption but it allows us to assign a number or diffusion length at any particular point along an EBIC line scan. Figure 8 shows EBIC micrographs of the same region of a sample of EFG silicon ribbon before and after thermal processing. In Fig. 9 are shown line scans through the same region before and after thermal processing along with the decrease in diffusion length values at various points following the thermal processing. The recombination seen after the thermal processing occurs at the same sites which exhibit enhanced recombination at low temperatures. This type of data as well as the low temperature EBIC data leads to a picture of the intragranular dislocation arrays as being the sites at which recombination changes take place, including changes in the shallow electron traps.

The first approach to measuring L, that used by Donolato [5], allows one to measure a surface recombination velocity, S, at a given boundary as well as

the diffusion length for intragranular regions on either side of this boundary. One takes a line scan through the grain boundary and by measuring simple geometric properties of the line scan related to the half width, these parameters can be extracted. This method is more accurate than the one described above, but requires a relatively "clean" boundary without extremely dense dislocation arrays adjacent to it, a situation which is often found in silicon ribbon. In the following section on hydrogen passivation, an application of this method will be described.

Hydrogen Passivation

In the early work on hydrogen passivation of grain boundaries, it was demonstrated that the electrical properties of grain boundaries could be dramatically altered after hydrogen passivation [6]. This was a perfect application for EBIC, and, in fact, dramatic before and after EBIC photos of hydrogen passivation of grain boundaries were obtained [7], along with impressive improvements in solar cell efficiency.

An example is shown in Fig. 10. EBIC photos such as these indicated that in some cases hydrogen passivation could virtually eliminate any EBIC contrast due to grain boundary recombination. These EBIC photos were made at 30 keV, where R ~ 9 μm. Thus, passivation proceeded down to this depth, but did it proceed any further?

To answer this question, a technique was developed to measure the depth of penetration of hydrogen passivation down grain boundaries [8]. Figure 11 is an illustration of the configuration used. The sample is cleaved and the cleaved surface is exposed to hydrogen ions. A blocking layer of PH_3 diffusion-produced glass subsequently covered with a thin layer of evaporated Ti is used to confine the hydrogen penetration to be normal to the cleaved surface. After passivation, the sample is turned 90° and EBIC is done on the side with the blocking layer. The Ti layer is thin enough to permit penetration of the electron beam. A typical result obtained with this technique is shown in Fig. 12. In this way, passivation depths of anywhere from ~5 μm to ~200 μm were found. This variation was due to great differences in the recombination properties of different boundaries. Using the method of Donolato, referred to above, to measure S, a roughly linear relationship for ln S vs. the passivation depth, x, was found for $x \lesssim 35$ μm and $S \gtrsim 2 \times 10^4$ cm²/sec. This is shown in Fig. 13.

Exploiting this technique even further, it was found that diffusivities of hydrogen down grain boundaries could be measured at 400°C and ranged from 10^{-8} to 10^{-10} cm²/sec. These values were the first direct diffusivity measurements of hydrogen diffusion down grain boundaries and show the power of EBIC in better understanding hydrogen passivation.

Summary

The utility of EBIC in studying recombination in silicon ribbon has been described. Efforts at quantifying the technique have begun to yield some fruit. The behavior of shallow electron trapping levels associated with dislocations in the material has been monitored. The situation, while undoubtedly complex, does show that there are three basic traps and that they are especially sensitive to

[O_i] and thermal processing. Thus, the method could be of use in better understanding the role of oxygen and thermal processing in this material. The use of low temperature EBIC in studying these traps, and, in general, in studying the electrical behavior of dislocations has been discussed.

Hydrogen passivation of defects in silicon ribbon is a particularly apt application of EBIC analysis. EBIC work has already shown that passivation depths can vary from 5 to 200 μm along grain boundaries and that hydrogen diffusivities along such boundaries can vary from 10^{-8} to 10^{-10} cm^2/sec.

References

1. J.I. Hanoka and R.O. Bell, Ann. Rev. Mater. Sci., 11, 353 (1981).

2. J.I. Hanoka, Solar Cells, 1, 123 (1979/80).

3. J.I. Hanoka, R.O. Bell and B. Bathey, in: Proc. of Symposia on Electronic and Optical Properties in Polycrystalline or Impure Semiconductors and Novel Silicon Growth Techniques, ed. by K.V. Ravi and B. O'Mara, The Electrochem. Soc., Princeton, 1980.

4. R.O. Bell and J.I. Hanoka, J. Appl. Phys., 53, 1741 (1982).

5. C. Donolato Appl. Phys. Lett., 34, 80 (1979), and C. Donolato, Scanning Electron Microsc., Part I (1979), p. 257; also, C. Donolato and R.O. Bell, Rev. Sci. Instrum., 54(8), 1005 (1983).

6. C.H. Seager and D.S. Ginley, Appl. Phys. Lett., 34, 5 (1979).

7. J.I. Hanoka, C.H. Seager, D.J. Sharp, and J.K.G. Panitz, Appl. Phys. Lett., 42(7), 618 (1983).

8. C. Dubé, J.I. Hanoka, and D.B. Sandstrom, Appl. Phys. Lett., 44(4), 425 (1984).

ORIGINAL PAGE IS
OF POOR QUALITY

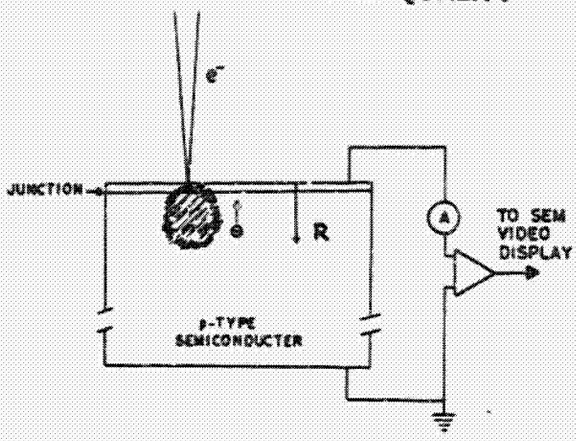

Fig. 1. Schematic of the EBIC process. Electron-hole pairs are generated within the shaded region. In the p-type region, electrons diffuse to the junction, are collected, and then form the beam-induced current.

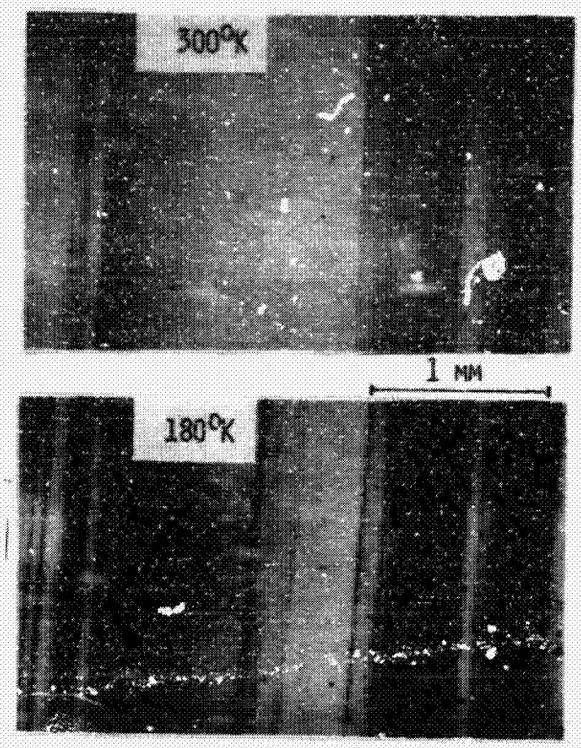

Fig. 2. Room temperature (top) and low temperature EBIC (lower photo) of the same region. Direction of growth of the ribbon is vertical.

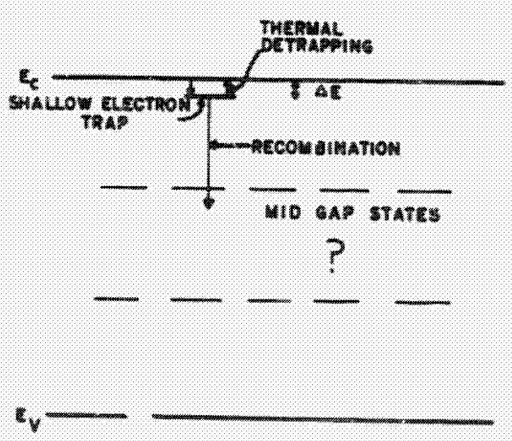

SCHEME FOR SHALLOW TRAPPING MODEL

Fig. 3.

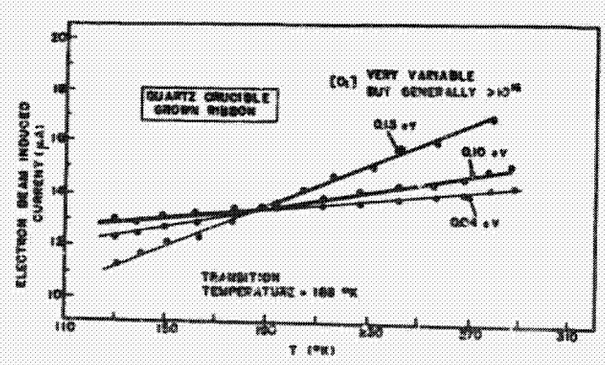

Fig. 4. EBIC temperature behavior for quartz crucible-grown ribbon.

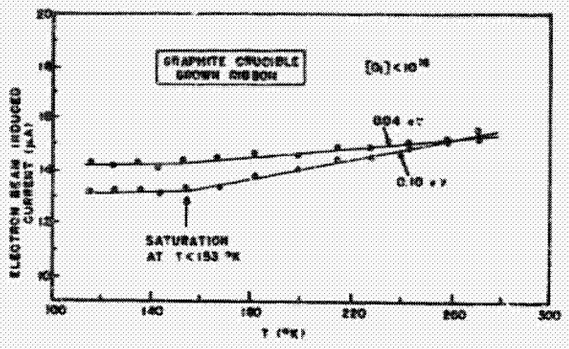

Fig. 5. EBIC temperature behavior for graphite crucible-grown ribbon.

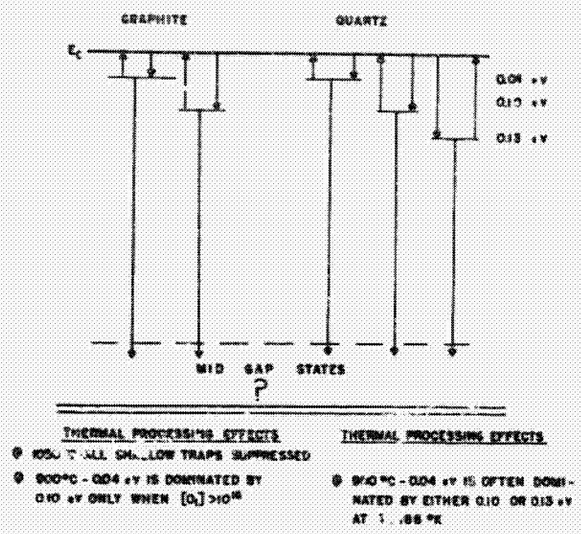

Fig. 6. Summary of shallow trap behavior.

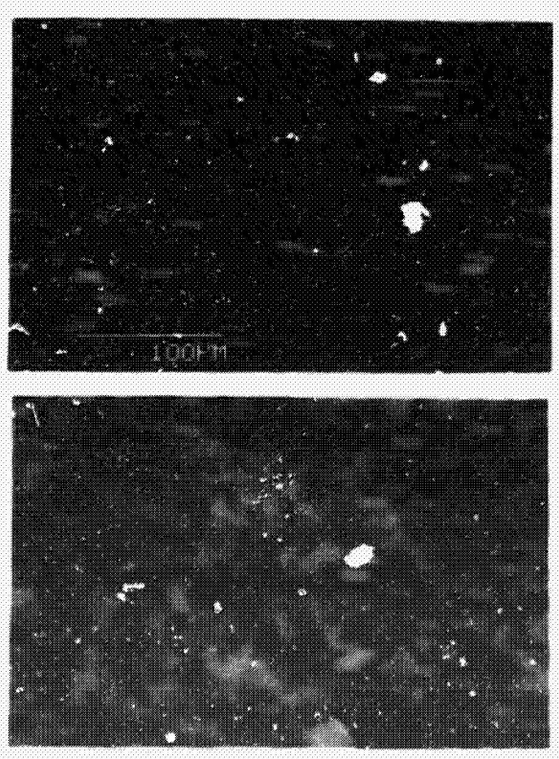

Fig. 7. Dislocations in CZ single crystal sample stressed at 1300°C using four-point bending. Top: room temperature; bottom: 150°K.

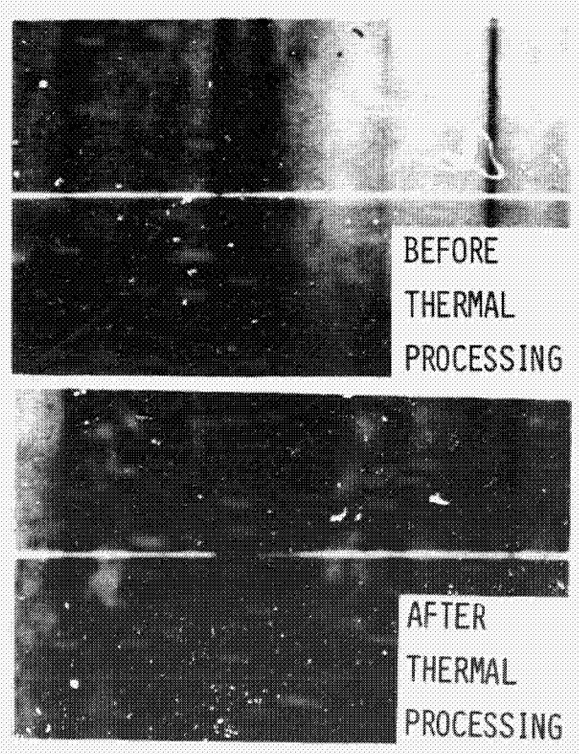

Fig. 8. EBIC micrographs of the same region before and after thermal processing.

ORIGINAL PAGE IS
OF POOR QUALITY

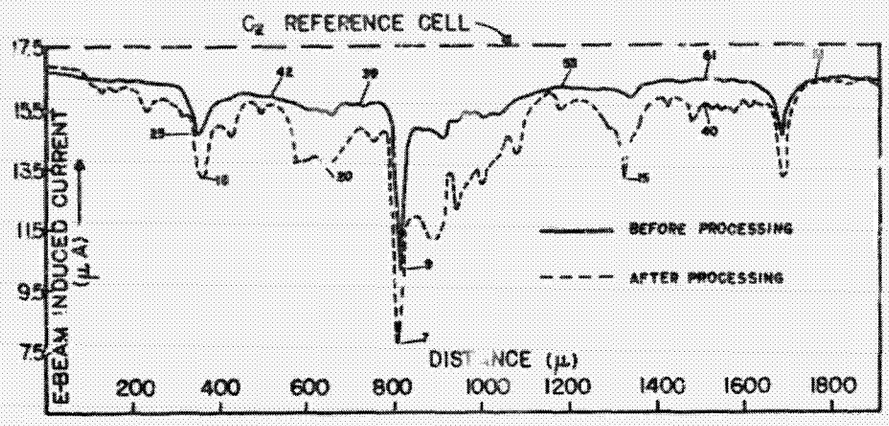

Fig. 9. Line scans for the two cases in Fig. 8.

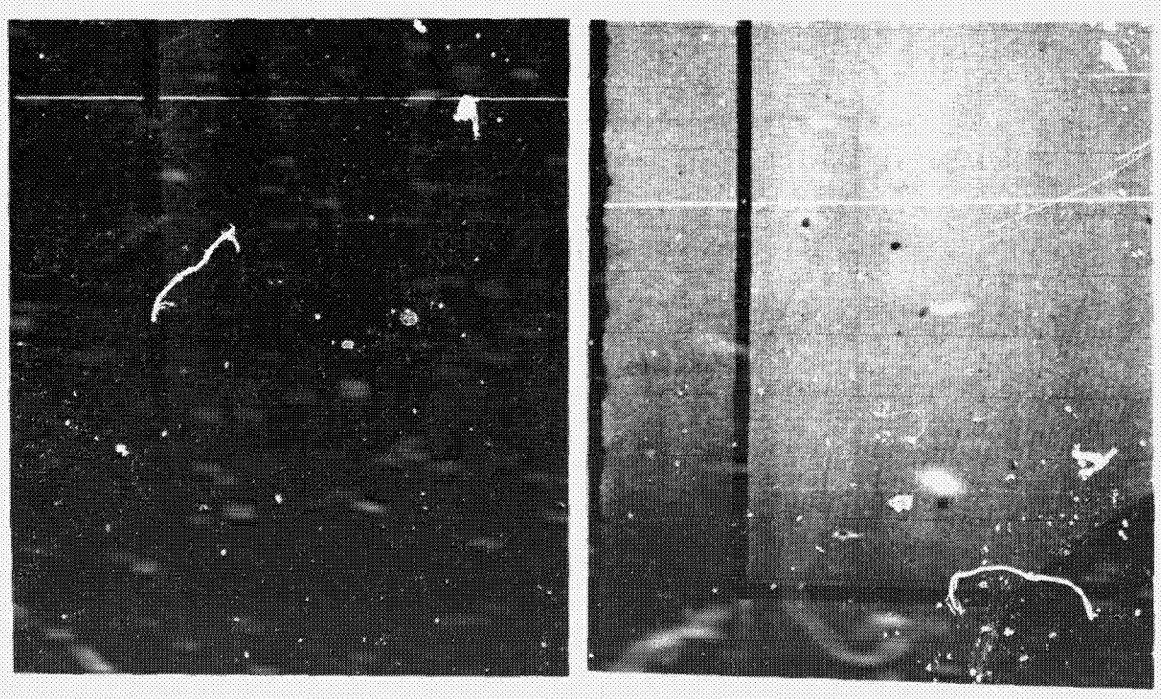

Fig. 10. EBIC photos of a ribbon solar cell before and after passivation.

ORIGINAL PAGE IS
OF POOR QUALITY

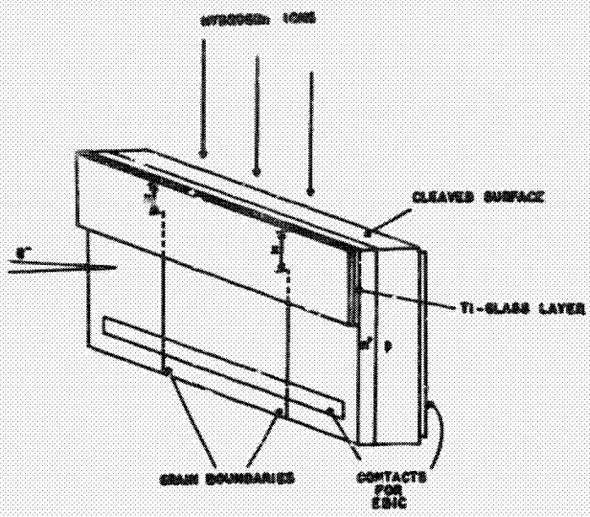

Fig. 11. Scheme used for passivation depth measurements.

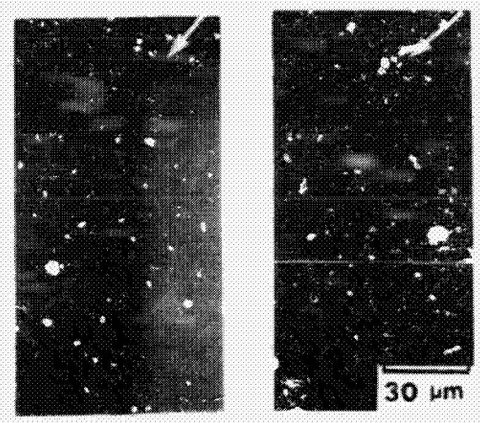

Fig. 12. Passivation depths using the technique of Fig. 11.

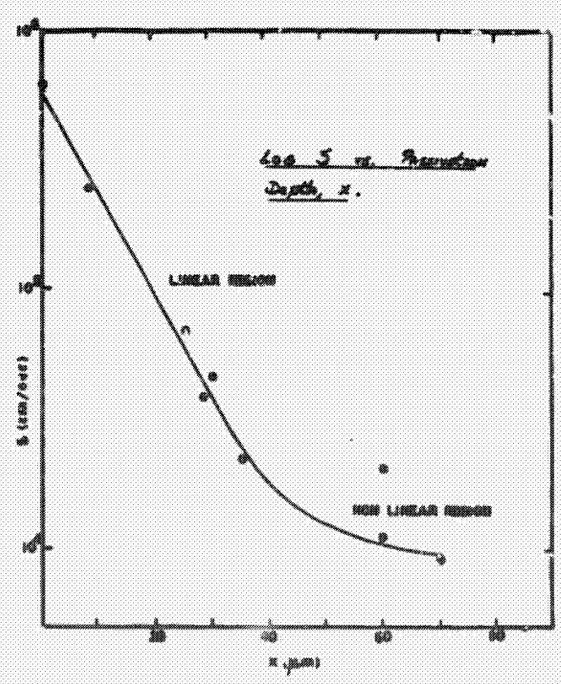

Fig. 13. Relation between surface recombination velocity S and passivation depth, x.

DISCUSSION

ROHATGI: When you showed the diffusivities of 10^{-8} to 10^{-10}, I take it you are saying that this is the diffusivity in the grain boundaries, but not necessarily in the bulk silicon.

HANOKA: That is right.

ROHATGI: You also indicated that you think that hydrogen went in the bulk, also through one of your measurements. Did I read you right?

HANOKA: That is right.

ROHATGI: How deep was the detection of the hydrogen?

HANOKA: In fact, it is not something I am discussing here, but we have a considerable amount of evidence to indicate that the hydrogen goes down in the bulk rather deeply also. We will be publishing some data on that very soon.

ROHATGI: This is in contrast to what Larry (Kazmerski) said in his talk this morning, that hydrogen doesn't go through the bulk silicon.

HANOKA: It is not a simple bulk diffusion. Through ordinary good non-defect-free silicon, because there isn't much data on the diffusion of hydrogen down bulk silicon, but data indicate that the diffusivities are something like 10^{-14}, so you don't expect -- it's only Angstroms that you would expect the hydrogen to be going that way. So it has to be a defect-assisted diffusion down the bulk region.

ROHATGI: Then I take it this range of 10^{-8} to 10^{-10} that you had was based on this range of passivation that you saw all the way from 5 to 100 micrometers.

HANOKA: Yes, that is right.

ROHATGI: That is the reason for this big range?

HANOKA: Yes. Generally, the boundaries that show the shallowest passivation are the one that have the highest surface recombination velocity.

LESK: Can you please mention your beam current densities and whether or not you had attempted to control the temperature during the implant?

HANOKA: The current densities were about 2 milliamps/cm^2 and the temperature -- it is hard to measure the temperature and there is some controversy about this -- but I think the temperatures of our samples are fairly high, something on the order of 400°C to 500°C when we passivate.

DALD: Could you comment about your numbers for the diffusion length? If the distance between the grain boundaries is less than the diffusion length in this area, is your measurement correct?

HAMOKA: You are probably right but generally what you find is the distance between the electrically active boundaries on the order of several hundred micrometers on average, and our diffusion lengths unfortunately are not several hundred micrometers. So I don't think that is a problem in most cases.

SIRTL: You mentioned these trap levels, and particularly the one correlated with oxygen. Is this something that has been reported the first time by you?

HAMOKA: Actually, I gave it at the ECS meeting in Minneapolis about two or three years ago, but I have not published it. It was just an oral presentation, but I am planning to publish it soon.

SIRTL: So far nobody else has.

HAMOKA: Not that I am aware of.

N85-31635

MEASUREMENT OF ELECTRICAL PARAMETERS AND CURRENT COMPONENTS IN THE BULK OF SILICON SOLAR CELLS

Arnost Neugroschel
Department of Electrical Engineering
University of Florida
Gainesville, FL 32611

ABSTRACT

A review and illustration of electrical measurements for determination of the bulk parameters in silicon solar cells is given. The presentation concentrates on transient and small-signal admittance measurements. These measurements yield accurate and reliable values of the base lifetime and the surface recombination velocity at the back contract without inaccuracies that normally results from electrons and holes in the p/n junction space-charge region. This then allows the determination of the recombination current in each region of the cell. As an example, current components in the emitter, low-doped base, high-doped base and junction space-charge region of the back-surface field cell are obtained. Such analysis is essential in determining the relative importance of the base and the emitter and, thus, the region that limits the cell efficiency.

I. INTRODUCTION

The efficiency of state-of-the-art solar cells is determined primarily by the minority-carrier diffusion length in the base of the cell and for some cells also by the surface recombination velocity at the back contact. It is, thus, very important to have measurement methods for fast and reliable determination of these two parameters.

Various methods are available at the present, some of which were reviewed by others [1]. In this presentation we concentrate on two methods only: (1) the short-circuit-current decay method [2], and (2) the small-signal-admittance methods [3-5]. It will be demonstrated that these two approaches yield reliable results directly from the data without any adjustable parameters which are usually taken from the literature when using some other techniques. The methods also allow the determination of the relative importance of the base and the emitter regions of the cells.

II. SHORT-CIRCUIT CURRENT DECAY (SCCD)

This is a relatively new method described in detail in [2]. We will describe it here only briefly. A solar cell is forward-biased with voltage V causing forward current I_f. At time t=0, the cell is short-circuited through a fast and very low resistance MOS transistor, by applying a voltage pulse to the

gate, see Fig. 1(a). The current transient measured across a small resistor R is displayed on an oscilloscope. The current transient can be expressed as an infinite series of exponential decays

$$i(t) = \sum_{i=1}^{\infty} i_i(0)\, e^{-t/\tau_{di}} \equiv i(0)e^{-t/\tau_d} + \sum_{i=2}^{\infty} i_i(0)\, e^{-t/\tau_{di}} \qquad (1)$$

where τ_{di} is the decay time constant of the i-th mode and $i_i(0)$ is the corresponding initial value at t=0. As shown in [2] the first mode is dominant and the higher decay modes can be neglected. The value of the first-mode τ_d is obtained simply from the $\log_e i(t)$ vs t plot, and the corresponding i(0) is obtained by extrapolating the straight portion of the plot to t=0. This extrapolation is necessary partly because the delay time constant of the measurement circuit prevents accurate measurement immediately after the closing of the switch. The resulting plot is schematically illustrated in Fig. 1(b). Figure 1(c) shows the measured current decay for a $n^+/p/p^+$ back-surface-field (BSF) solar cell with τ_d = 6.4 μsec yielding L_n = 180 μm, $S_{eff} = 1.3 \times 10^3$ cm/sec.

The two measured quantities, i(0) and τ_d, are both functions of the minority-carrier base lifetime τ and the effective surface recombination velocity S_{eff} at the back contact. Simultaneous solution of these two dependencies (see Appendix A) yields the desired parameters: τ and S_{eff}.

The discharging of the excess electrons and holes in the junction space-charge-region (SCR) occurs within a time of the order of $\sim 10^{-11}$ sec. The discharging of the excess carriers in the emitter occurs within a time about equal to the emitter lifetime or emitter transit time, both of which are much smaller than the first-mode τ_d. As a result, the SCR and the emitter do not affect the transient observed on a time scale about equal to τ_d.

This fact is one of the main advantages of this method of measurement of the base properties in comparison with more conventional transient methods, such as the open-circuit voltage decay (OCVD) and the reverse-step recovery (RSR). As discussed in detail in [2], both the OCVD and the RSR methods suffer from distortions caused by the recombination within the SCR and the emitter that persist throughout the entire decay.

The sensitivity of the SCCD method to the bulk lifetime and to the surface recombination velocity is illustrated in Figs. 2(a) and 2(b). These figures show that for thin cells with W << L, the SCCD method is very sensitive to S_{eff} but rather insensitive to τ. For cells with W >> L, the method is very sensitive to τ but insensitive to S_{eff}. This behaviour can be explained by realizing that if W << L, then most of the minority carriers recombine at the back surface. However, if W >> L, then most of the recombination occurs in the bulk.

In the two limiting cases above, the SCCD technique will yield only one of the desired parameters, either L or S. In order to determine the other parameter for these two cases, the SCCD measurement has to be supplemented by

some other external charcteristic of the cell dependent on both S and L. For example, one can use the dark saturation current I_D or the open-circuit voltage V_{oc} for this purpose. Both I_D and V_{oc}, however, may be affected by the emitter region and the combination of SCCD - I_D or SCCD - V_{oc} may give misleading results for the base parameters.

In the next section we explore small signal admittance techniques that are sensitive primarily to the base properties. The combination of the SCCD and the admittance techniques gives the base parameters (S, L) for any cell regardless of the W/L ratio.

III. SMALL-SIGNAL ADMITTANCE MEASUREMENTS [3-5]

Small-signal admittance measurements can be used to analyze a variety of semiconductor devices. We discuss here specifically the applications for analyzing the solar cells, namely measurement of the base L and S_{eff} and the separation of the emitter and the base current components. The small-signal measurements can be performed either at low-frequencies ($\omega\tau \ll 1$) or high frequencies ($\omega\tau \gg 1$). The choice of a particular frequency range will depend on the W/L ratio.

A. Low-frequency method (LF) [3,4]

Consider a $n^+/p/p^+$ BSF solar cell shown in Fig. 3(a). For a low-frequency signal with $\omega\tau_n \ll 1$, where τ_n is the minority-carrier electron lifetime in the p-type base, we derive the expressions for the small-signal quasi-neutral base capacitance C^{LF}_{QNB} and conductance G^{LF}_{QNB}, respectively (see equations (B1) and (B2) in Appendix B). Equations (B1) and (B2) contain four unknowns: C^{LF}_{QNB}, G^{LF}_{QNB}, L_n, and S_{eff}. The parameters C^{LF}_{QNB} and G^{LF}_{QNB} are measured and the combination of (B1) and (B2) yields L_n and S_{eff}.

It is worthwhile to discuss in more detail a few special cases:

A.1 Long diode: W > L

For this case, (B1) and (B2) yield a simple expression for C^{LF}_{QNB} and τ_n

$$C^{LF}_{QNB} = \frac{q}{kT}\frac{Aqn_i^2L_n}{2N_{AA}}\left[\exp\left(\frac{qV}{kT}\right) - 1\right] \tag{2}$$

and

$$\tau_n = \frac{2C^{LF}_{QNB}}{G^{LF}_{QNB}} \quad . \tag{3}$$

The base diffusion length is obtained either from (2) or from (3). The details concerning the deduction of C^{LF}_{QNB} and G^{LF}_{QNB} from the data are discussed in [3]. As an illustrative example, we show in Fig. 4 the measured $C^{LF}_{QNB}(V)$ and

$G^{LF}_{QNB}(V)$ plots for the p^+/n device with $N_{DD} = 1.25 \times 10^{15} cm^{-3}$. The analysis using (3) or (3) gives $L_p = 80$ μm.

A.2 BSF solar cell: $W_p \leq L_n$, $W_p D_n/L_n^2 < S_{eff} < (D_n W_p)$

In this case, (B1) and (B2) are solved to yield L_n and S_{eff}. Figure 5 shows the measured C(V) and G(V) dependencies for a $p^+/n/n^+$ BSF solar cell from which we derive $L_p \approx 500$ μm and $S_{eff} \approx 80$ cm/sec.

The method fails, however, for $S_{eff} << D_n W/L_n^2$; in this case $G^{LF}_{QNB} \approx KW_p/\tau_n$ yields τ_n, but S_{eff} cannot be found. Another limitation exists for high values of $S_{eff} >> D_n/W_p$; in this case both (B1) and (B2) are independent of L_n and S_{eff}.

The above difficulties with the LF method can be largely eliminated by the high-frequency approach.

B. High-frequency method (HF) [5]

We treat the high frequency method for two special cases.

B.1 $\omega\tau_n > 10$ and $0.1 \lesssim W_p/L_n \lesssim 1$

The small-signal admittance then is

$$Y^{HF}_{QNB} \approx \frac{KD_n}{L_n}\left[\left(\frac{\omega\tau_n}{2}\right)^{1/2} + j\omega\left(\frac{\tau_n}{2\omega}\right)^{1/2}\right] = G^{HF}_{QHB} + j\omega\, C^{HF}_{QNB} \quad . \tag{4}$$

The important conclusion from (4) is that the $\omega^{1/2}$ dependence gives the range of $0.1 \lesssim W_p/L_n \lesssim 1$ regardless of the value of S_{eff}. To obtain the desirable parameters, we measure G^{HF}_{QNB} vs ω for $\omega\tau \gtrsim 10$ and extrapolate to lower frequencies to obtain an intercept ω_I with G^{LF}_{QNB} given by (B2). This gives

$$L_n^2 = \left(\frac{2\, W_p^2\, D_n}{\omega_I}\right)^{1/2} \left(\frac{D_n}{W_p}\right) \frac{1 + (S_{eff} L_n^2/D_n W_p)}{(D_n/W_p) + S_{eff}} \tag{5}$$

Equation (5) cannot be be solved for L_n and S_{eff} except for the following cases:

a) $S_{eff} < D_n W_p/L_n^2 < D_n/W_p$

$$L_n \approx (2W_p^2 2D_n/\omega_I)^{1/4} \tag{6}$$

b) $D_n W/L_n^2 < S_{eff} < D_n/W_p$

$$S_{eff} \approx (\omega_I D_n/2)^{1/2} \quad . \tag{7}$$

The method is illustrated in Fig. 6 for the $p^+/n/n^+$ solar cell of Fig. 5. G^{HF}_{QN} follows the $\omega^{1/2}$ dependence for $f \gtrsim 10^4$ Hz with the intercept at ω_I =

$(2\pi)10^3$ 1/sec. Using (5) and combining with $S_{eff} \approx 80$ cm/sec obtained by the LF method, we have $L_p \approx 503$ μm, which is in excellent agreement with $L_p \approx 500$ μm using the LF method alone.

Even though the general solution (5) cannot give L and S_{eff} exactly, and only one of the parameters is obtained either from (6) or from (7), the method is very useful because: (i) the G_{QN}^{HF} vs $\omega^{1/2}$ dependence shows that L > W; (ii) the G_{QN}^{HF} vs $\omega^{1/2}$ dependence indicates that the emitter contribution to the conductance (and dark current) is negligible (this point is discussed further below); (iii) the SSCD for L > W yields an accurate value of S_{eff} only and using this value in (5) we obtain an accurate value for L. The combination of these two methods gives L and S_{eff} for practically any cell.

The sensitivity of the HF method to the emitter component G_{QNE}^{HF} of the total measured quasi-neutral conductance $G_{QN}^{HF} = G_{QNB}^{HF} + G_{QNE}^{HF}$ is explored in Fig. 7. The time constant τ_E of G_{QNE}^{HF} is given by either the Auger lifetime τ_A in the heavily doped emitter, or by the combination of τ_A and the transit time [6]. The emitter time constant is much shorter than the base lifetime, thus G_{QNE}^{HF} is frequency independent up to $f \approx 1/\tau_E \gg 1/\tau_B$. Figure 7 shows $G_{QN}^{HF} = G_{QNB}^{HF} + G_{QNE}^{HF}$ for an arbitrary choice of $G_{QNE}^{HF}/G_{QNB}^{HF}$. The region far away from the knee can be fitted to a straight line with $G \propto \omega^{1/m}$, where m > 2. Notice, however, that ω_I for $G_{QNE}^{HF} > 0$ is close to the intercept value ω_I for $G_{QNE}^{HF} = 0$. Furthermore, since $L \propto \omega_I^{1/4}$, a small error in ω_I gives only a negligible error in L. For example, for $G_{QNE}^{HF} = G_{QNB}^{HF}$, $\omega_I \approx 1.5\ \omega_I$ ($G_{QNE}^{HF} = 0$), this gives an error in L of only about 10%.

B.2 $\omega\tau_n > 10$, $W_p/L_n \leq 0.1$

The condition $W_p/L_n \leq 0.1$ may apply for the thin cells (50 - 100 μm) with a very long lifetime. For this case we have

$$G_{QN}^{HF} \approx KD_n \frac{(\omega^2 W_p^3/3) + S_{eff}(D_n + S_{eff}W_p)}{(D_n + S_{eff}W_p)^2} \quad . \tag{8}$$

For BSF cells, $S_{eff} < D_n/W_p$ and (8) yields

$$G_{QN}^{HF} \approx K[\omega^2(W^3/3D_n) + S_{eff}] \quad . \tag{9}$$

Figure 8 shows the G_{QN}^{HF} vs ω dependence for a 8 μm thick epitaxial n-type layer with doping density $N_{DD} = 5 \times 10^{15}$ cm^{-3}. The ω^2 dependence for f > 1.5 MHz immediately gives $L_p > 10W > 80$ μm and also $S_{eff} \ll \omega^2 W^3/3D_n \ll 1.2 \times 10^3$ cm/sec. More accurate analysis of the knee region below the ω^2 dependence gives $S_{eff} \approx 120$ cm/sec and using this value in (B1) gives more accurate $L_p \approx 90$ μm.

Note, that the HF method for L > 10 W gives only the lower limit of L and the upper limit of S_{eff}. A combination of this technique with either the LF method or the SCCD can give more accurate results.

B.3 $\omega\tau_n \sim 10$, $W_p/L_n \sim 0.1$

For the previous two special cases we have obtained $G_{QNB}^{HF} \propto \omega^{1/2}$ for $W_p/L_n \lesssim 0.1$ and $G_{QNB}^{HF} \propto \omega^2$ for $W_p/L_n \lesssim 0.1$. Obviously, there has to be an intermediate range for $W_p/L_n \sim 0.1$ where $G_{QNB}^{HF} \propto \omega^m$ ($< m \lesssim 2$). One possible approach here is to obtain S_{eff} from the SCCD method and then fit the theoretical $G_{QN}^{HF}(S_{eff}, L_n)$ with the experiment. A very reasonable approximation of τ_n can be made, however, by realizing that the G_{QN} vs ω dependence begins to increase from its low-frequency value for $\omega = \omega_I \approx 10/\tau_n$ [5]. Thus, $\tau_n \approx 10/\omega_I$, where ω_I can be approximated as the intercept of the G_{QN}^{LF} line with the extrapolated $G_{QN}^{HF} \propto \omega^m$ dependence.

IV. REGIONAL ANALYSIS OF SOLAR CELLS

It is important to analyze the contributions of each region of the cell to the total dark current (or V_{oc}). Such an analysis is demonstrated here for a $n^+/p/p^+$ BSF solar cell shown in Fig. 3(b). The analysis is based on the determination of the base parameters τ_n and S_{eff} by one of the methods discussed in Section II and III. This is sufficient to calculate the profile of the minority electrons in the base. The recombination losses in the base are given by (B2) and the recombination losses in the p^+-BSF portion of the base are

$$I_n(W_p) \approx I_B^+ = AqS_{eff}N(W_p) \quad . \tag{10}$$

The SCR recombination current I_{SCR} can be determined graphically [7] and the emitter contribution I_E is obtained by realizing that the total dark current is

$$I_D = I_E + I_{SCR} + I_B + I_B^+ \quad . \tag{11}$$

For example, such analysis of the $p^+/n/n^+$ BSF cell of Fig. 5 gave [4]: $L_p \approx 500$ μm, $S_{eff} \approx 80$ cm/sec, $I_B \approx 0.8\ I_D$, $I_{SCR} \approx 0.2\ I_D$, $I_E \ll I_D$, $I_B^+ \ll I_D$.

V. SUMMARY

Table I gives a summary of results for a number of different cells. A comparison of results obtained by different methods, shown for some cells, demonstrates very good agreement. Notice, in particular, the last cell in Table I, which is a thin cell (W_{base} - 92 μm) with $L_n > W_B$. For this cell, the SCCD method gives $S_{eff} \approx 180$ cm/sec, but the method is insensitive to L_n (see Fig. 2(a)). We have to combine the SCCD method with the high-frequency small-signal admittance method and then use (5) with S_{eff} obtained from the SCCD method to determine L_n.

The main conclusion of this study is that the SCCD method and the small-signal admittance methods yield a rapid and reliable determination of the base

parameters. They also allow the determintion of the relative importance of the base and the emitter regions with regard to cell efficiency. Identification of the region limiting the efficiency is a key to an informed cell design.

Acknowledgement: This work was supported in part by NSF Grant No. ECS-8203091.

APPENDIX A

To obtain the base diffusion length L and effective surface recombination velocity S_{eff} at the back contact we have to solve the following two equations for the first-mode decay [2]:

$$1 + (D_p K_1/L_p S_{eff})\cot(W_{QNB} K_1/L_p) = 0 \tag{A1}$$

$$i(0) = -\frac{qD_p P(0,0^-)K_1}{S_1 L_p} \frac{\cot(K_1 W_{QNB}/L_p) - (D_p K_1/L_p S_{eff})}{(\tau_p/2K_1^2) + (W_{QNB}/2S_{eff})[\mathrm{cosec}^2(K_1 W_{QNB}/L_p)]} . \tag{A2}$$

Here $K_1 = (-1 - S_1\tau_p)^{1/2}$, $S_1 = -1/\tau_{D1}$, W_{QNB} is the width of the quasi-neutral base, and $P(0, 0^-) = (n_i^2/N_{DD})[\exp(qV/kT) - 1]$ where V is the steady forward voltage applied for $t < 0$.

APPENDIX B

The small-signal quasi-neutral base capacitance and conductance are given by [4]:

$$C_{QNB}^{LF} = \frac{KD_n}{2L_n}\left[\frac{\frac{W_p D_n}{L_n} - \frac{L_n W_p^2 S_{eff}}{D_n} - S_{eff} L_n}{(\sinh^2\frac{W_p}{L_n})(\frac{D_n}{L_n}\coth\frac{W_p}{L_n} + S_{eff})^2} + \tau_n \frac{\frac{D_n}{L_n} + S_{eff}\coth\frac{W_p}{L_n}}{\frac{D_n}{L_n}\coth\frac{W_p}{L_n} + S_{eff}}\right] \tag{B1}$$

$$G_{QNB}^{LF} = \frac{KD_n}{L_n} \frac{\frac{D_n}{L_n} + S_{eff}\coth\frac{W_p}{L_n}}{\frac{D_n}{L_n}\coth\frac{W_p}{L_n} + S_{eff}} \tag{B2}$$

where $K = Aq(q/kT)(n_i^2/N_{AA})\exp[(qV/kT) - 1]$.

Table I: Summary of results for some typical solar cells. The values for L_{base} and S_{eff} were obtained using the SSCD method, unless marked otherwise

CELL	ρ_{base} (Ωcm)	W_{base} (μm)	L_{base} (μm)	S_{eff} (cm/sec)
$n^+/p/p^+$ BSF	10	227	454 450*	105
$n^+/p/p^+$ BSF	10	103	250	2.9×10^3
$n^+/p/p^+$	10	360	512	2×10^5
$n^+/p/p^+$	0.15	295	100	---
$p^+/n/n^+$ BSF	10	320	303* 500†	80†
$n^+/p/p^+$ BSF	10	92	~600*	~180

* obtained from G_{QN}^{HF}

† obtained from G_{QN}^{LF}

REFERENCES

1. J. H. Reynolds and A. Meulenberg, Jr., J. Appl. Phys., 45, 2582 (1974); A. Azim Khan, J. A. Woolam, and A. M. Hermann, Appl. Phys. Commun., 2, 17(1982).

2. T. W. Jung, F. A. Lindholm, and A. Neugroschel, IEEE Trans. Electron Devices, ED-31, 588(1984).

3. A. Neugroschel, P. J. Chen, S. C. Pao, and F. A. Lindholm, IEEE Trans. Electron Devices, ED-25, 485(1978).

4. A. Neugroschel, IEEE Trans. Electron Devices, ED-28, 108(1981).

5. F. N. Gonzalez, A. Neugroschel, IEEE Trans. Electron Devices, ED-31, 413(1984).

6. M. A. Shibib, F. A. Lindholm, and F. Therez, IEEE Trans. Electron Devices, ED-26, 959(1979).

7. A. Neugroschel, F. A. Lindholm, and C. T. Sah, IEEE Trans. Electron Devices, ED-24, 662(1977).

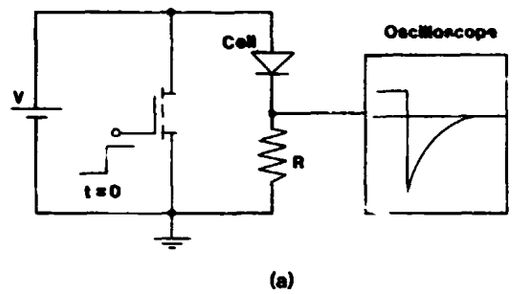

Fig. 1. (a) Electronic circuit used in the SCCD method. The switching time of a power MOST is less than 100 nsec.

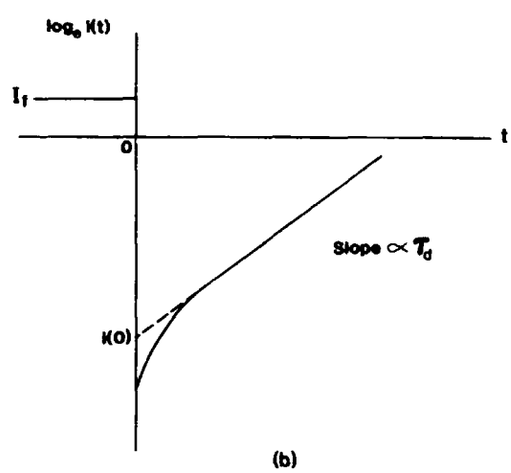

(b) Schematic illustration of the current decay displayed on a log scale.

ORIGINAL PAGE IS
OF POOR QUALITY

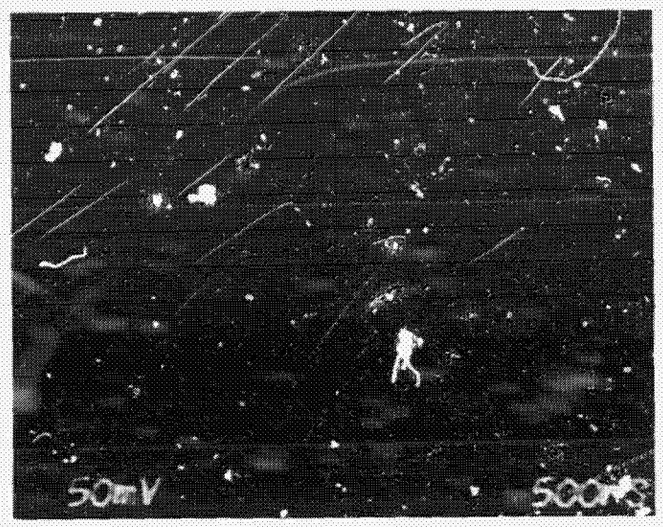

(c) Experimental current decay for a $n^+/p/p^+$ BSF solar cell ($\rho_{base} \simeq 0.3$ Ωcm, $W_{base} \simeq 367$ μm, $\tau_d \simeq 6.4$ μsec, $L_n \simeq 180$ μm, $S_{eff} \simeq 1.$ x 10^3 cm/sec). The vertical scale is 100 mA/division.

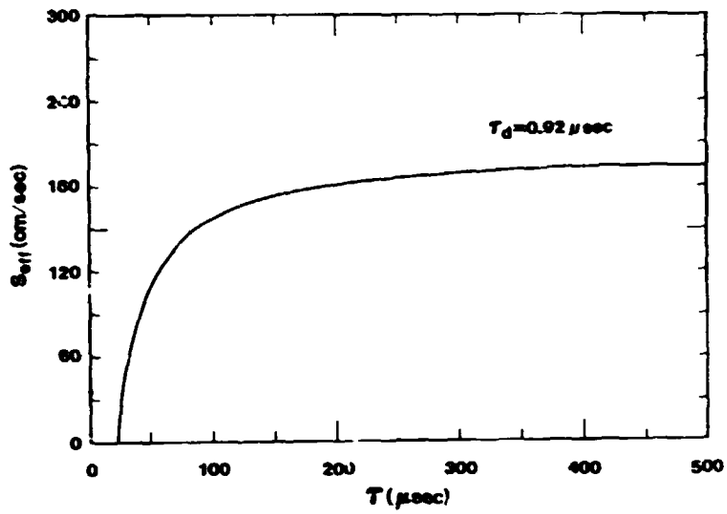

(a)

Fig. 2. (a) Plot of S_{eff} vs τ for a thin $n^+/p/p^+$ BSF solar cell (ρ_{base} = 10 Ωcm, W_{base} = 92 μm).

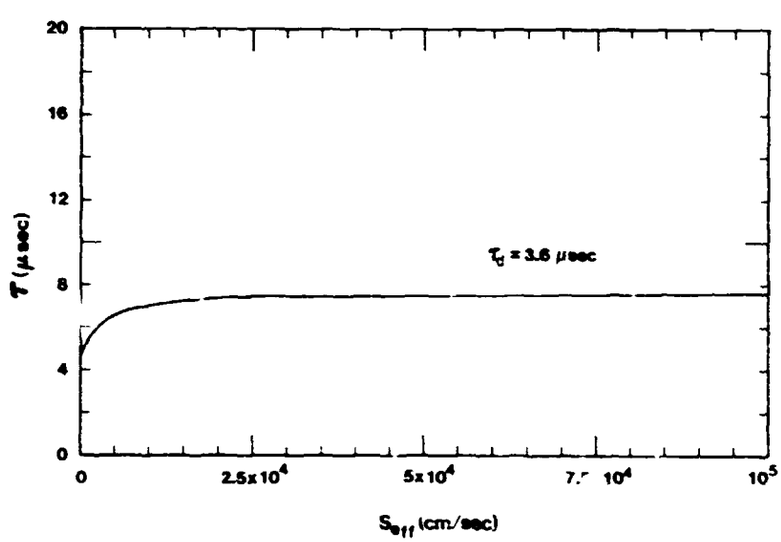

(b)

(b) Plot of τ vs S_{eff} for a thick $n^+/p/p^+$ BSF solar cell (ρ_{base} = 0.15 Ωcm, W_{base} = 295 μm).

ORIGINAL PAGE IS
OF POOR QUALITY

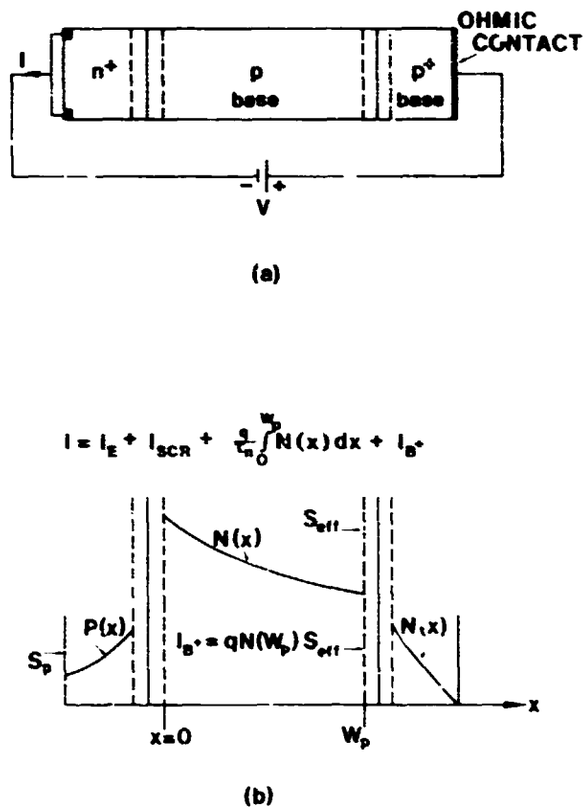

Fig. 3 (a) Schematic diagram of an $n^+/p/p^+$ BSF solar cell.
(b) Qualitative sketches of minority-carrier distributions in the dark.

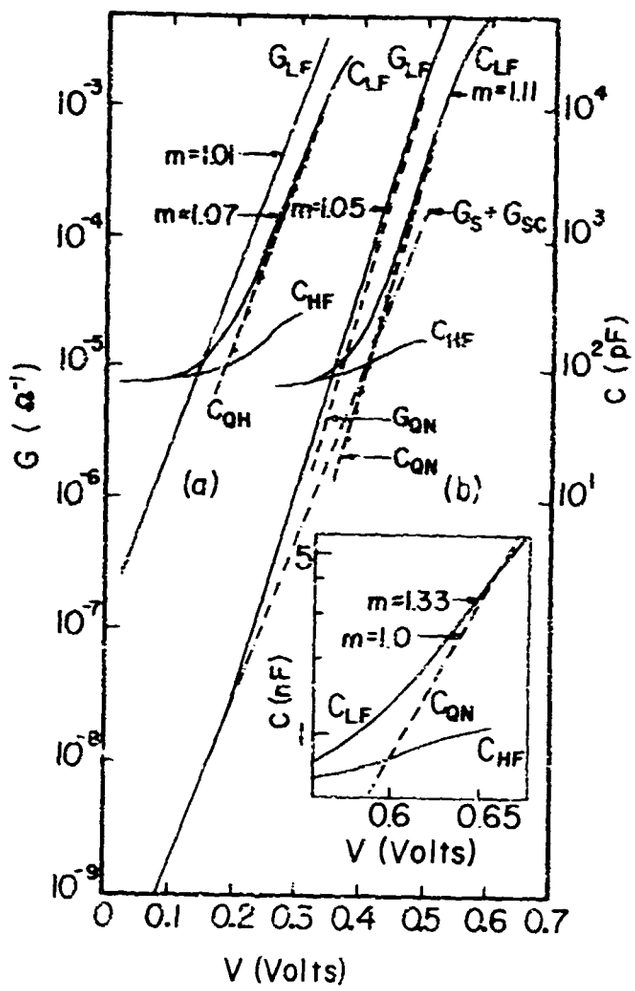

Fig. 4 Measured conductance and capacitance vs forward-bias V for a long p^+/n diode with $N_{DD} = 1.25 \times 10^{15}$ cm^{-3} and $W_{base} \approx 250$ μm (from Ref. [3]).

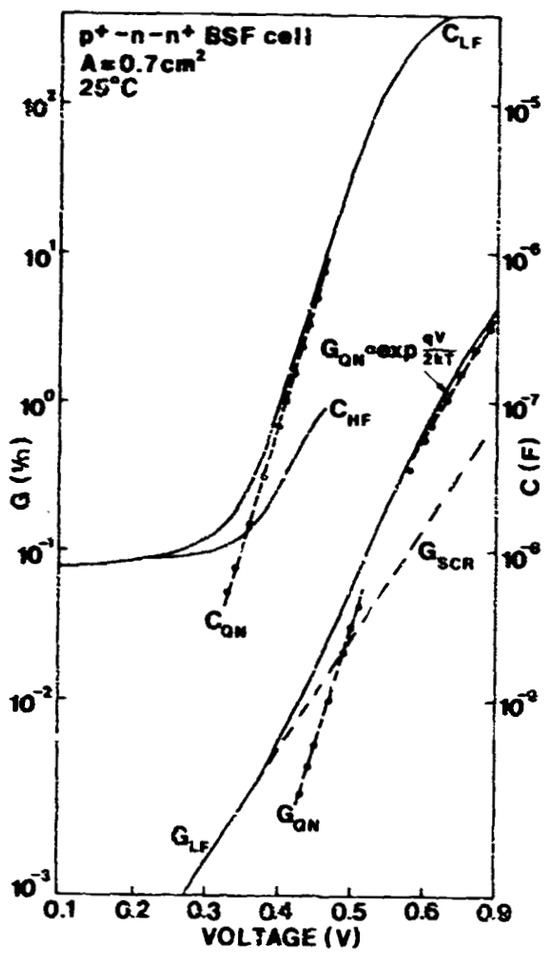

Fig. 5 Measured capacitance and conductance vs forward bias for a $p^+/n/n^+$ BSF solar cell (from Ref. [4]). Here, $N_{DD} = 6 \times 10^{14}$ cm^{-3}, $W_{base} = 320$ μm.

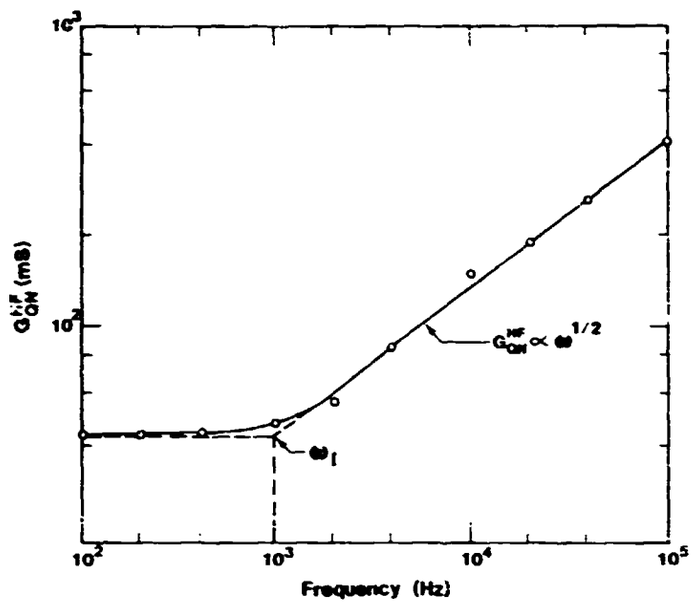

Fig. 6. Measured high frequency conductance G_{QN}^{HF} vs freqency for the $p^+/n/n^+$ solar cell of Fig. 5. The conductance was measured at forward bias V = 0.5 V and shows $\omega^{1/2}$ dependence.

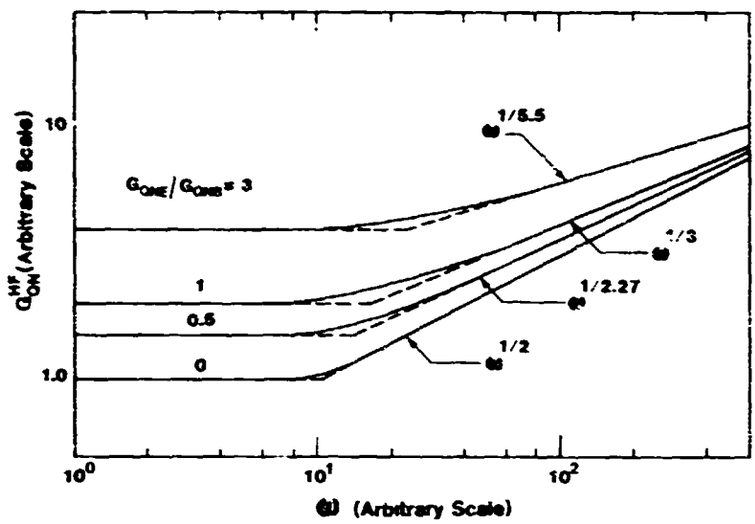

Fig. 7. Plot of a $G_{QN}^{HF} = G_{QNB}^{HF} + G_{QNE}^{HF}$ for different ratios of $G_{QNE}^{HF}/G_{QNB}^{HF}$ = 0, 0.5, 1, 3.

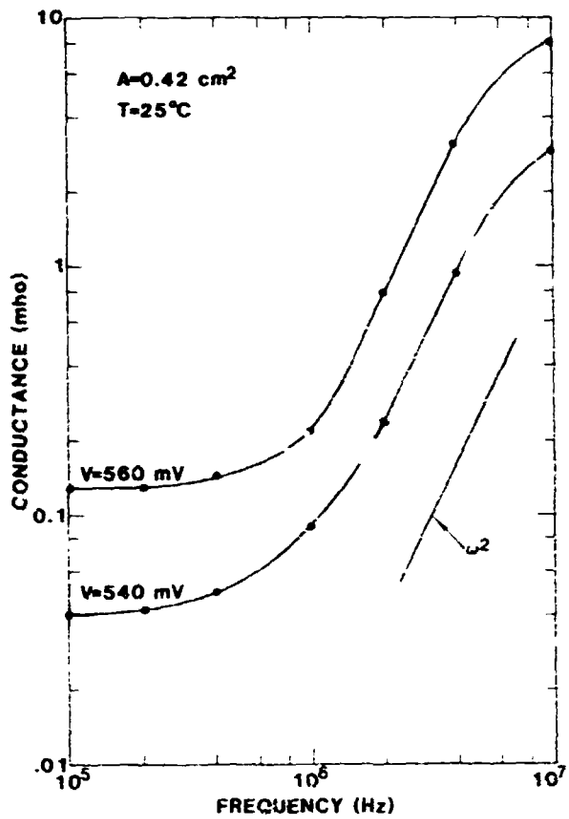

Fig. 8 Frequency dependence of high-frequency conductance for a thin (8 μm) n-type epitaxial layer (from Ref. [5]). The conductance follows ω^2 dependence.

DISCUSSION

VON ROOS: You made one comment I would to talk about, and that was the diffusion length -- if it is much larger then the width of the cell, it cannot be measured by any other means. Now, that is not quite correct. There is another means to do that, and that is with the EBIC or amplitude-modulated electron beam; measuring the phase shift will indeed give you the lifetime, and therefore the diffusion length -- also in the case where the ratio of width over diffusion length is very small.

SESSION V

MODELING

R. Schwartz, Chairman

N85-31636

Current Status of One and Two-Dimensional Numerical Models: Successes and Limitations

by R. J. Schwartz, J. L. Gray, and M. S. Lundstrom
Purdue University
School of Electrical Engineering
West Lafayette, IN 47907

Abstract

The capabilities of one and two-dimensional numerical solar cell modeling programs (SCAP1D and SCAP2D) are described. The occasions when a two-dimensional model is required are discussed. The application of the models to design, analysis, and prediction are presented along with a discussion of problem areas for solar cell modeling.

Introduction

Accurate numerical models for single crystal silicon solar cells have proven to be very reliable in the simulation of the performance of these cells. These models have proven to be extremely useful in: the interpretation of experimental measurements; the identification of processes which limit cell performance; the prediction of benefits which will result from design and materials changes; the comparison of various cell designs; and the prediction of efficiencies which may eventually be obtained in silicon solar cells as various technological barriers are overcome.

The capabilities of a one-dimensional (SCAP1D) and a two-dimensional model (SCAP2D) are described and examples of their use for each of the above purposes are given.[1-3] It will be shown that there are circumstances under which cells which appear to be one-dimensional require a two-dimensional model to properly simulate their behavior.

As cells become more efficient the requirements on the accuracy of the physics used in the model become more stringent. Effects which are of little significance in poor or moderately good cells can take on major significance in high efficiency cells. A number of problem areas which are of concern in the modeling of high efficiency cells are discussed. These include heavy doping effects, metal-semiconductor boundary conditions, minority carrier mobilities, high injection lifetimes, and carrier-carrier scattering. Each of these may have a major impact on the performance of the cell under certain operating conditions.

The Model

Physical Effects of Importance

One of the major advantages of a numerical model is that it affords one the opportunity to include the very large number of physical effects which may be acting simultaneously within a solar cell. The complexity of the phenomena and their interactions with each other preclude analytic solutions in anything except highly idealized situations, which are not indicative of actual cells or operating conditions. An attempt has been made in the formulation of SCAP1D and SCAP2D to include as many of the physical effects which are known to influence cell performance as possible and to do this in a manner which represents our

present knowledge of these effects. One of the goals in writing these codes was to have them be sufficiently accurate in their representations so that they could be used in a predictive mode. This is possible only if all of the pertinent physical effects are included.

In those cases where the physics is questionable, we have attempted to include options which allow one to choose between various models. For example, in the case of heavy doping effects, one is able to choose between the models of Slotboom, Lanyon-Tuft, and Mahan, or to supply a subroutine of one's own choosing.

We have attempted to choose materials parameters which in our estimation are the most reliable. These materials parameters are used as default values. The user can easily change these parameters to values that he views as more reasonable.

The following physical effects are included in the codes: hole and electron mobilities, including their doping and temperature dependencies; heavy doping effects, using the formulation of Lundstrom, Schwartz, and Gray; absorption coefficients, including their temperature dependence; recombination, including Auger, Hall-Shockley-Read, and surface recombination. Surface recombination is handled through the specification of the surface recombination velocity. In the case of SCAP2D, the effects of surface potentials are also included.

Semiconductor Equations

The programs perform a full simultaneous numerical solution of the two continuity equations and Poisson's equation subject to the boundary conditions appropriate to one and two-dimensional cells. The equations are formulated as shown in equations 1-3.

$$\nabla^2 v = -\frac{q}{\epsilon}(p-n+N_D-N_A), \tag{1}$$

$$\nabla \cdot \mathbf{J}_p = q(G-R), \tag{2}$$

$$\nabla \cdot \mathbf{J}_n = q(R-G). \tag{3}$$

The generation term in equations 2 and 3 are given by

$$G(x) = \int_0^\infty \Phi \alpha e^{-\alpha x} d\lambda \tag{4}$$

and the recombination term is given by equations 5, 6 and 7.

$$R = (pn-n_{ie}^2)\left[A_n n + A_p p + \frac{1}{\tau_n(p+p_1) + \tau_p(n+n_1)}\right] \tag{5}$$

$$\tau_p = \frac{\tau_{po}}{1 + \frac{(N_D+N_A)}{N_c}} \tag{6}$$

$$\tau_n = \frac{\tau_{no}}{1 + \frac{(N_D+N_A)}{N_c}} \tag{7}$$

The hole and electron current densities which appear in equations 2 and 3 are given by

$$J_p = -q\mu_p p \nabla v_p - kT\mu_p \nabla p \tag{8}$$

$$J_n = -q\mu_n n \nabla v_n + kT\mu_n \nabla n \tag{9}$$

$$v_p = v - (1-\gamma)\frac{\Delta_G}{q} \tag{10}$$

$$v_n = v + \gamma\frac{\Delta_G}{q} . \tag{11}$$

where v_p and v_n are the effective potentials defined in equations 10 and 11 and Δ_G and γ are parameters which account for variations in the band structure, such as density of states and band gap, and account for Fermi-Dirac statistics.

No low injection assumptions are made. The equations are solved from contact to contact with appropriate boundary conditions so that the solutions are valid for all ranges of operation and include minority and majority carrier flow. The latter places some restrictions on the CPU word size required for solution.

These codes have been extensively tested for accuracy by comparing the results of their predictions with experimental results obtained on very carefully and extensively characterized cells for a wide range of cell designs and operating conditions. The agreement has been such that a high degree of confidence has been developed in results computed using these codes.

Code Description

Figure 1 is a block diagram of the structure of SCAP1D and SCAP2D. The operator must supply information about the materials parameters, a description of the device to be analyzed, the type of analysis which he wishes to perform, and the spectrum, if appropriate. He also can, if he wishes, control some of the details of the numerical solution; the amount of information supplied while the program is converging to an answer and how the output information will be stored or displayed.

The results of the computation are presented in printed summary form and the detailed results of the calculation are stored on magnetic tape. A separate plotting routine is used to access the information on tape and to display the appropriate parameters. The plotting capability is one of the most valuable features of the code, in that it allows one to effectively have a microscopic view of most of the parameters of interest in the interior of the cell under operating conditions. We will show some of the available graphical output as we discuss the capabilities of the code. Table I shows the input control offered to the operator. In every case default parameters are specified if the operator chooses not to supply a parameter.

Table II contains a listing of plots which are available through the plotting program. In this case the operator specifies the type of plot which is required and the region of the cell for which he desires that plot. Most of the figures which follow were obtained directly from this plotting routine.

In addition to the reliability of the output, the utility of codes of this type will depend on their ease of use and efficiency of computation. For example, in a design mode, it is

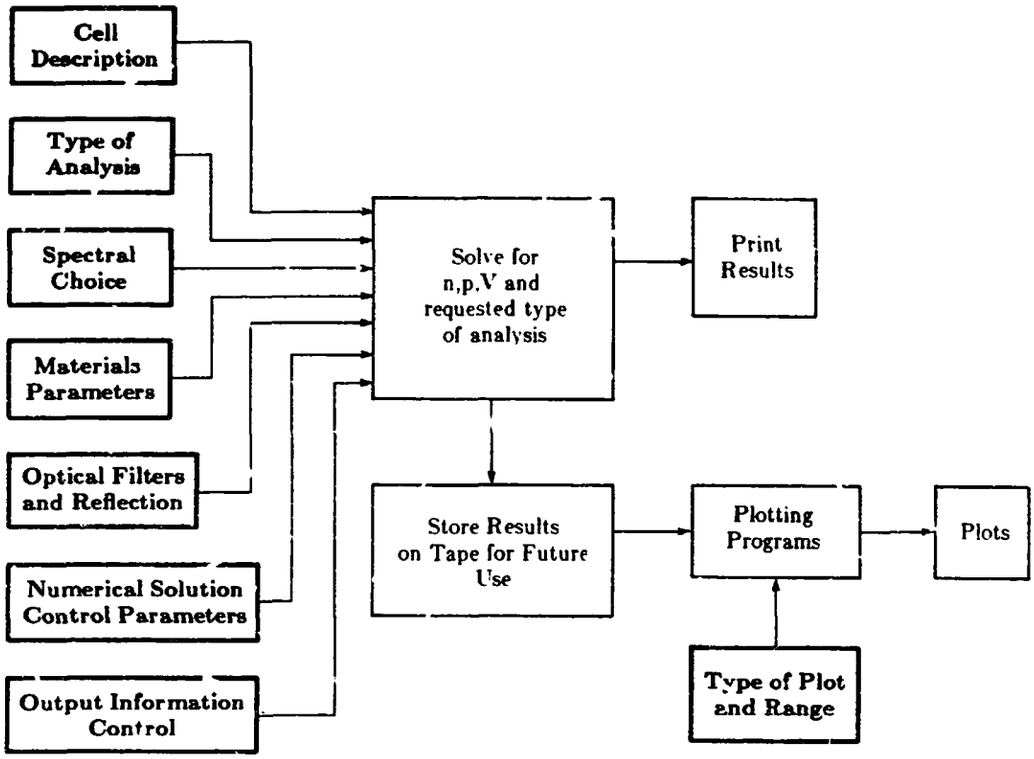

Figure 1 Block Diagram of the Structure of SCAP1D and SCAP2D

Table I - Input Parameters

Device Description
- Doping Profiles
  - Step junction
  - Erfc (N_s,x_j)
  - Experimental Profile
  - SUPREM II
- Dimensions

Materials Parameters
- Lifetime (τ and energy)
- Surface Recombination
- Auger
- Bandgap narrowing
  - Slotboom
  - Mahan
  - Lanyon-Tuft
  - User supplied

Spectral Choices
- AM 0
- AM 1.0
- AM 1.5 direct & global
- Monochromatic
- Uniform generation
- User supplied

Optical Filters & Reflection
- Filter (Ge, Si, SiO_2, GaAs)
- Back surface reflector

Types of Analysis
- Dark I-V
- Illuminated I-V
- Solar Cell
- Spectral Response

Table II - Plotting Options

Carrier concentration	Hole current density and components
Hole and electron current densities	Electron current density and components
Change in potential (from equilibrium)	Mobility
Doping density	Lifetime
Energy band diagram	Ratio of n_{ie}/n_{io}
Electric field	Potential
Hole and electron quasi-electric fields	Recombination rate
Effective fields (electric plus quasi-electric) for holes and electrons	Charge density
	Excess carrier concentration
Optical generation	

advantageous to be able to make multiple runs in a reasonable length of time and at reasonable cost. While SCAP1D can be run effectively on nearly any mainframe computer (a typical run on a CDC 6600 requires 100-300 CPU seconds), SCAP2D requires a very fast machine with a large amount of actual or virtual memory. On a Cyber 205, 300 CPU seconds are required for a typical run.

Situations Requiring Two-Dimensional Analysis

In many situations a one-dimensional simulation is quite adequate and there is no need to use the more complex and expensive two-dimensional simulation. On the other hand, there are a number of situations which only a two-dimensional simulation will suffice.

Some of the situations which require two-dimensional analysis are quite obvious, while others appear to be one-dimensional in nature, but, in fact, require a two-dimensional solution for proper description of the cell performance. Most of the cell structures which have been proposed as high efficiency silicon cells fall into the obviously two-dimensional analysis category. Among these structures are the Interdigitated Back Contact cell, the Vertical Multi-Junction cell, the Etched Multiple Vertical Junction cell, the Polka Dot cell, and the Grating cell. As an example of the use of SCAP2D in the analysis of these two-dimensional cells, we show figures 2 through 4 for an IBC cell. In Figure 2 we show the total short circuit current flow under one sun-conditions. In Figures 3 and 4 we show the majority and minority carrier flows for this same cell operating under the same condition.

Less obvious applications of the two-dimensional code are shown in Figures 5 through 6 in which a conventional solar cell has been analyzed. In Figure 5 we show the potential distribution along the emitter from a point half way between the grid lines up to the grid lines under open circuit conditions. This figure illustrates that there is a lateral voltage drop along the emitter, even under open circuit conditions, as a result of the current which is injected in the vicinity of the grid line. Figure 6 shows the circulating currents which exists in the vicinity of the grid line.

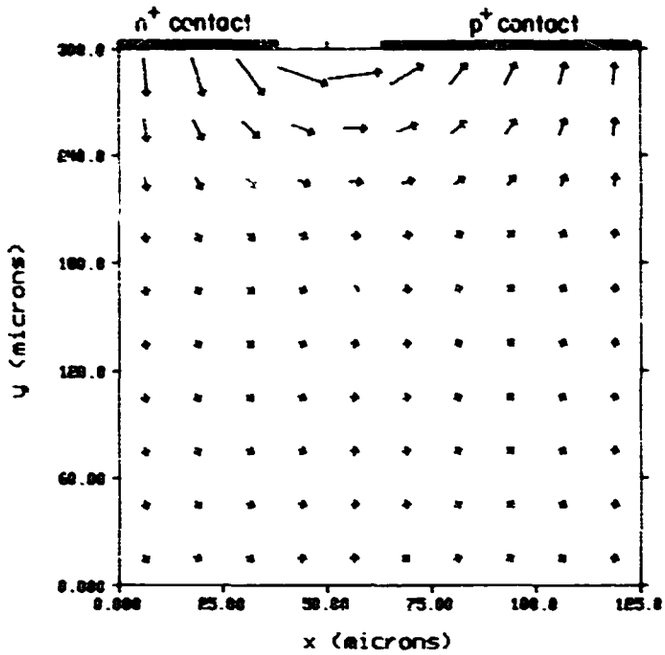

Figure 2 Total Short Circuit Current for an IBC Cell 1 Sun AM1.0

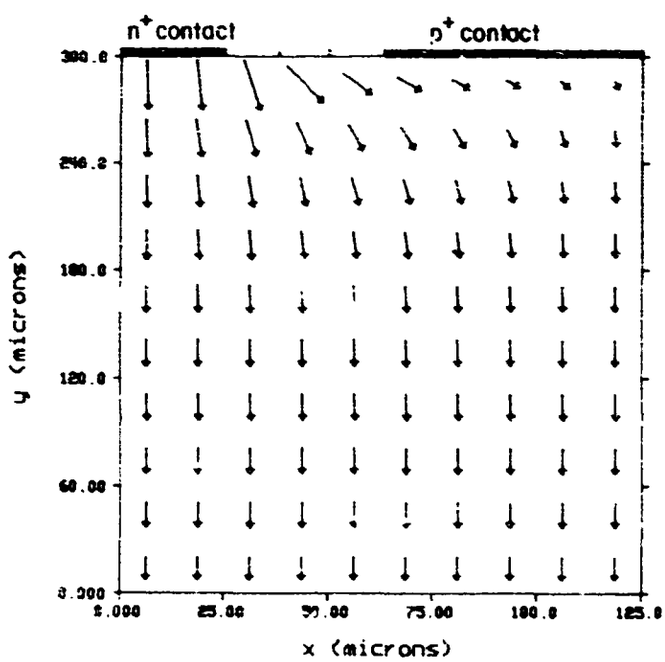

Figure 3 Majority Carrier Current Flow for the Cell of Figure 2

ORIGINAL PAGE IS
OF POOR QUALITY

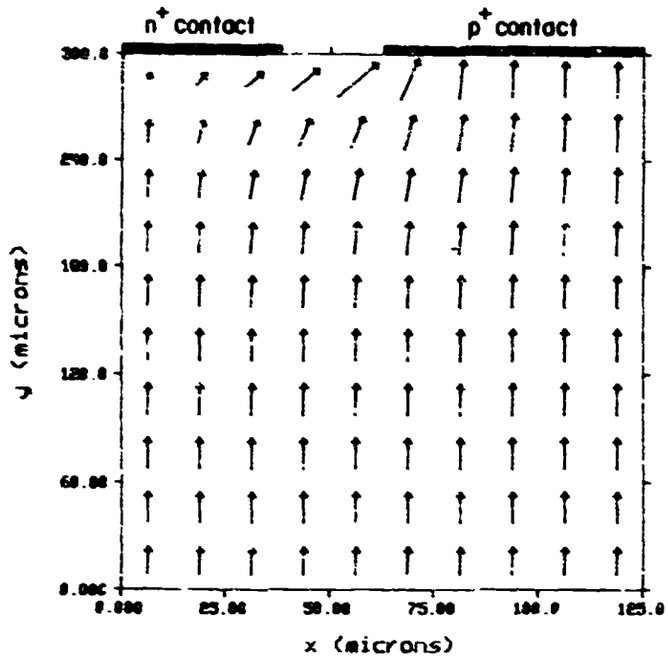

Figure 4 Minority Carrier Current Flow for the Cell of Figure 2

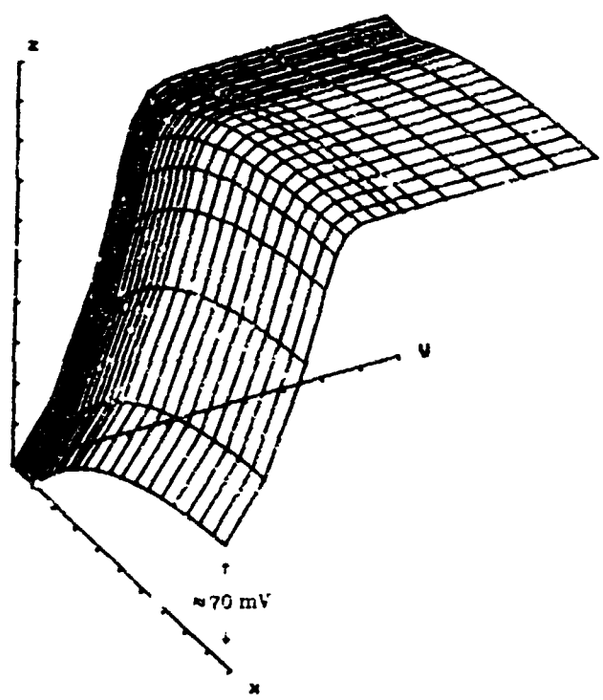

Figure 5 Potential Distribution in the Emitter of a Conventional Solar Cell Operating at 400 suns.

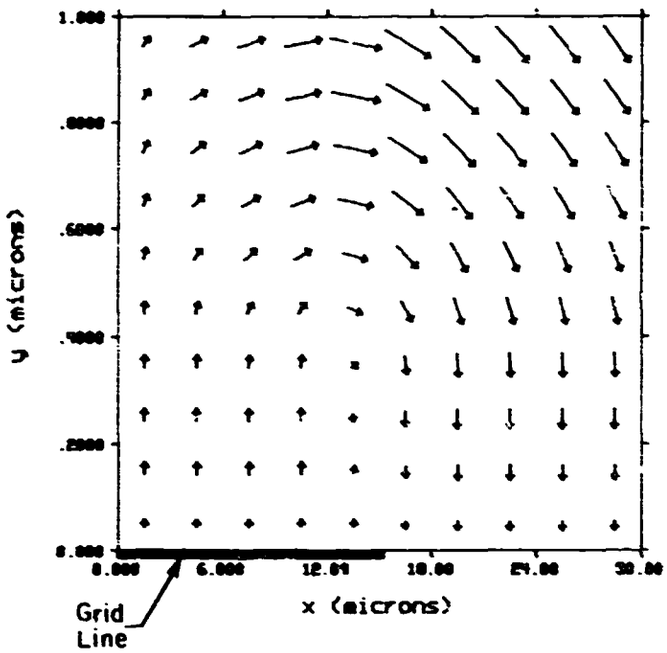

Figure 6 Circulating Current in the Vicinity of a Grid Line for a Conventional Solar Cell

An even less obvious problem with one-dimensional simulation occurs when one tries to properly model the front surface of a conventional cell. This surface is composed of a SiO_2-Si interface and a metal-semiconductor contact. In a one-dimensional simulation, one is forced to aggregate the two effects with some equivalent front surface recombination velocity, S_F. Figure 7 illustrates the difficulty with this approach. Under short-circuit conditions the proper value of S_F is equal to the surface recombination velocity of the SiO_2-Si interface. However, near open circuit conditions, the proper value of S_F may be 3 to 4 orders of magnitude larger. This is a result of the fact that the metal semiconductor contact may be a very effective recombination site for minority carriers. This is particularly important as the operating voltage of the cell increases. For proper operation of a one-dimensional code, the front surface recombination velocity should be a function of operating condition. The two-dimensional code does not have this problem, since the surface recombination velocity at the SiO_2-Si interface and the metal semiconductor interface are specified separately, and the recombination along the entire surface is properly accounted for under all operating conditions.

At high operating conditions, such as are found in concentrator solar cells, even the conventional cell behaves in a two-dimensional fashion and must be modeled using the two-dimensional code. Minority carrier current flow for a conventional cell operating at 800 suns is shown in Figure 8. If this cell is modeled using the one-dimensional code under these operating conditions, serious errors are encountered in the computation of the fill factor which can not be compensated for by including an external series resistance in the model, as the effect is nonlinear.

ORIGINAL PAGE IS
OF POOR QUALITY

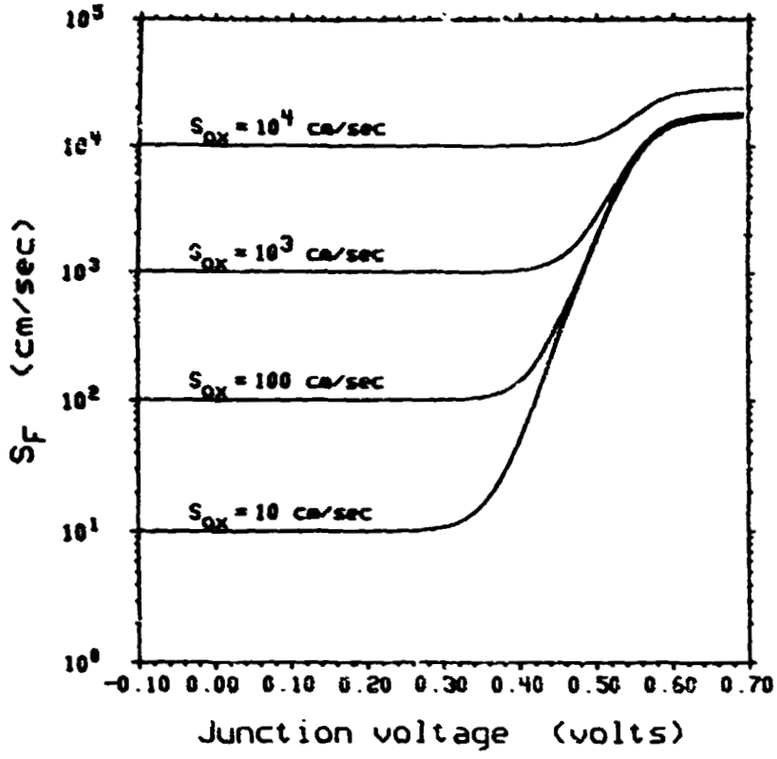

Figure 7 Effective Surface Recombination Velocity as a Function of Operating Voltage and the SiO_2-Si Surface Recombination Velocity

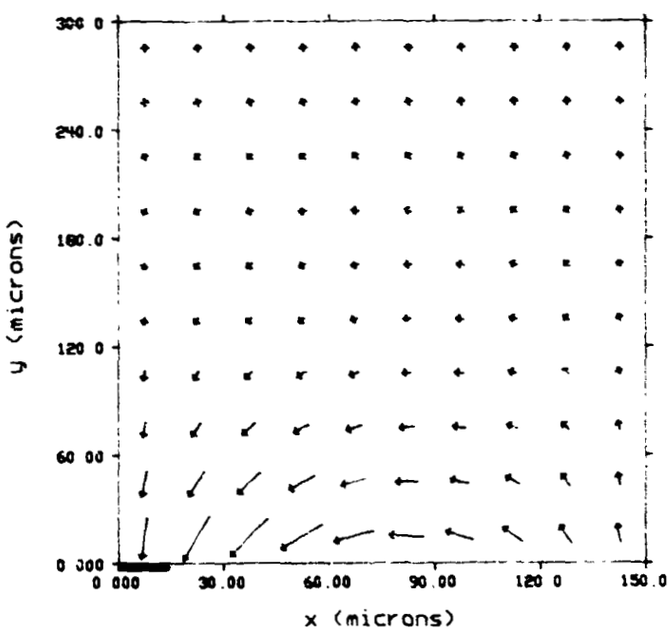

Figure 8 Minority Carrier Current Flow for a Conventional Solar Cell Operating at 800 Suns (V=.600 volts J=21.6 amp/cm^2)

Modes of Utilization

As we mentioned previously, a carefully prepared solar cell model is useful in a number of modes. In this section we will discuss the use of SCAP1D and SCAP2D as a design tool, a sensitivity analysis tool, an aid in the analysis of experimental data, an aid in the provision of insight into the operation of the cell, and, finally, as a predictive tool for the comparison of proposed cell designs and as a means of projecting performance as various technological barriers are removed. For the sake of continuity, we have chosen to use the Sandia high concentration cell operating at 1 sun as a base line design. This is a cell which has exhibited 18% conversion efficiency at one sun, and 20% conversion efficiency in the 50-100 sun range for an AM 1.0 spectrum.

Design

As a simple example we show, in Table III, the effects of variations in the base doping about the present design doping of 2.29×10^{16}, on the performance of this cell. We see that the present base doping is nearly optimum for the design parameters used in the other parts of the cell.

Table III

Solar Cell Performance Dependence on Base Doping
AM 1.0 (one sun)

Base Doping cm^{-3}	V_{oc} volts	J_{sc} ma/cm^2	F.F.	Efficiency %
5×10^{15}	.634	35.1	.828	18.35
1×10^{16}	.640	34.8	.833	18.46
2.29×10^{16}	.649	34.4	.836	18.55
1×10^{17}	.656	33.3	.838	18.21
5×10^{17}	.650	30.2	.836	16.37

Sensitivity Analysis

By utilizing a computer code such as SUPREM to simulate fabrication conditions one can model the sensitivity of device performance to fabrication parameters. Here, as an extreme case, we examine the effects of changes in the emitter doping profile on cell performance. The Sandia cell was simulated using the two emitter profiles shown in Figure 9. In Table IV, a comparison of these simulations is shown. Note that the erfc emitter profile simulation predicts a higher V_{oc}. This is due to the lower net recombination in the emitter as compared to the SUPREM II emitter profile simulation, as shown in Figure 10. Recombination is higher in the SUPREM II emitter because the doping is higher over most of the emitter volume, and therefore Auger recombination is correspondingly higher also.

If the results of a process simulation program such as SUPREM are coupled with SCAP1D or SCAP2D as shown above the sensitivity of the cell to process variations can be readily established.

ORIGINAL PAGE IS
OF POOR QUALITY

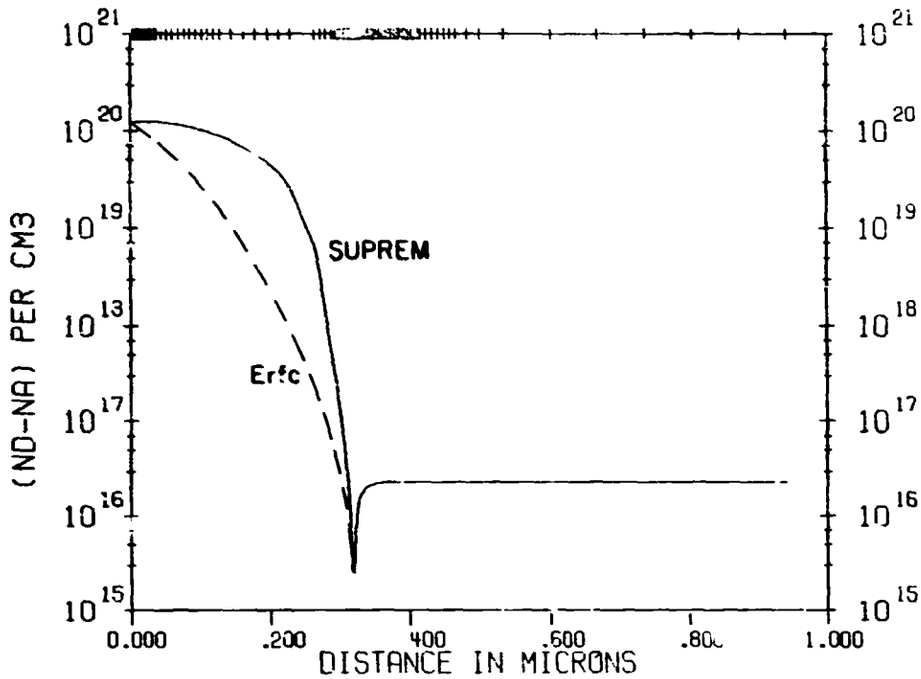

Figure 9 Emitter Doping Profiles as Determined by SUPREM II and Complimentary Error Function

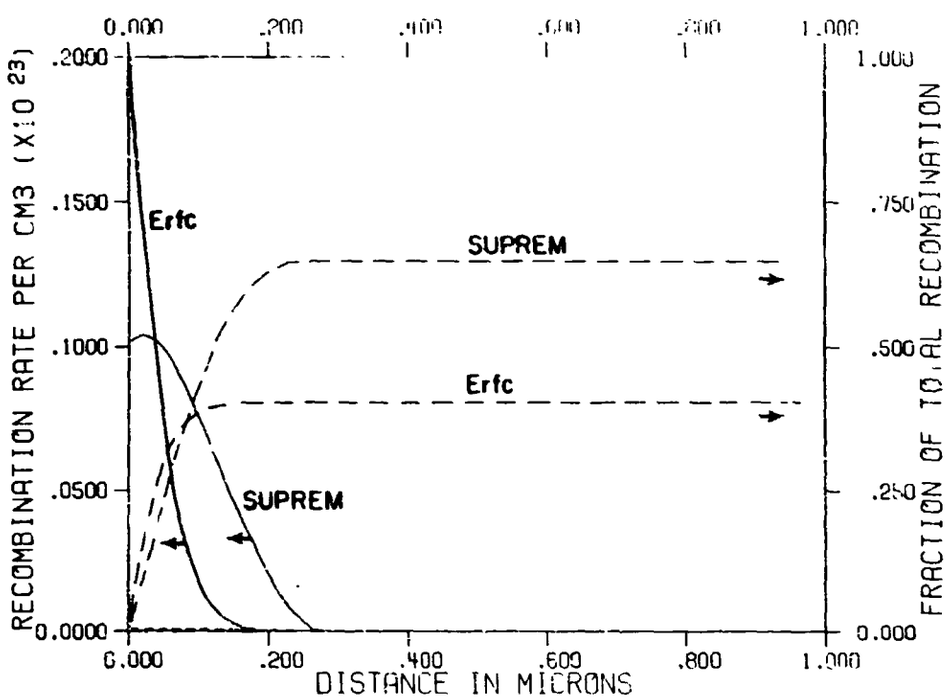

Figure 10 Emitter Recombination for the Two Doping Profiles Shown in Figure 9

Table IV

Dependence of cell performance on emitter doping profile
AM 1.0 (one sun)

Type of Profile	V_{oc} volts	J_{sc} ma/cm^2	FF	Efficiency %
Erfc	.648	34.3	.836	18.6
SUPREM II	.632	33.9	.833	17.75

Analysis

It is possible, by adjusting the parameters entered into the code, to obtain a fit between the model generated results and experimental dark I-V, solar cell, and spectral response curves. If this fit can be obtained for a single set of parameters, then one has a reasonable expectation that these are the correct parameters describing this device.

Insight

With the ability to observe most of the parameters of interest as a function of position and operating conditions anywhere within the cell, it is possible to achieve a great deal of insight into the limiting factors on any cell design. Examination of the model for the 20% Sandia cell very quickly establishes that the cell appears to be emitter limited, and, in fact, that further efforts in improving the performance of the cell should be devoted to reduction of the metal-semiconductor contact recombination and in reducing the volume of the heavily doped emitter.

Prediction

Potentially one of the most valuable, and also one of the most risky, uses of the numerical models is as a predictive tool. The models have already been shown to be quite reliable in comparing the relative merits of different cell designs. One particularly attractive way to utilize the code is to use it to identify limiting phenomenon in a particular cell design and then to remove that limitation and observe the effect on cell performance. In this fashion, one can predict benefits which will accrue through various advances in technology, and, in fact, can make some reasonable estimates of the ultimate performance of silicon single crystal solar cells. This latter use of the code is particularly risky since as the performance of the cell improves, physical effects which may have been insignificant in their effect on cell performance before, may suddenly become the dominant limitation.

Problem Areas

There are a number of areas in which there is concern about existing solar cell models either because the physics is not well understood, available data is thought to be unreliable, or because the effect has not been include in the model. These areas of concern are discussed below.

Heavy Doping Effects

There is a controversy over the origins and magnitude of heavy doping effects. There is a great deal of scatter in the measured effective band gap narrowing, particularly in the very heavily doped samples where we have our major concern. In order to alleviate this situation somewhat, we have provided the operator with the option to choose between most of the popular band gap narrowing models. This remains an area of major concern and is probably the least reliable area in the modeling of silicon solar cells.

Auger Recombination

Some uncertainty exists about the reliability of published Auger coefficients. At least two groups (Sandia and General Electric) have indicated that published Auger coefficients may be too large.

Minority Carrier Mobility

Reliable measurements of minority carrier mobility do not exist. Various authors have proposed that the minority carrier mobility is larger, smaller, and the same as the majority carrier mobilities of the same type carrier. As a consequence, SCAP1D and SCAP2D assume that the minority carrier mobilities for electrons are the same as they would be if electrons were majority carriers. A similar assumption is made for holes.

Metal-Semiconductor Contacts

In well designed high efficiency solar cells, the metal semiconductor contact limits the open-circuit voltage. The removal of this high dark current source, through the use of tunneling contacts or through the reduction of the metal-semiconductor contact area, has already demonstrated a significant improvement in open-circuit voltage. Further advances in this area may well employ heterojunction structures in addition to the present tunneling structures. SCAP1D and SCAP2D allow for specification of a finite minority carrier surface recombination velocity to model this effect.

Doping Profiles

We have already seen that device performance can be a strong function of the shape of the emitter doping profile. SCAP1D and SCAP2D allow for the use of a complimentary error function, a computed profile based on the Fair diffusion model for phosphorus, doping profiles obtained from a process simulation program such as SUPREM, or experimental data. The use of data from SIMS measurements has the problem that it includes the total impurity concentration not just the electrically active dopants. If any precipitation is present in the highly doped region, SIMS will overestimate the amount of active dopant. Spreading resistance measurements are a measure of the free carrier concentration. Near the depletion region this can lead to significant errors in the doping profile if the spreading resistance profile is interpretated as being the same as the doping profile.

Spectral Response

Spectral response measurements are particularly useful for obtaining information about the base lifetime and the surface recombination velocity. However, some difficulty is experienced in matching long wavelength response with computed response. This difficulty has been traced to the fact that small changes in device temperature can lead to large changes in the long wavelength response as a result of changes in the absorption coefficients due to a shift in the band edge.

In order the determine the surface recombination velocity of the SiO_2–Si interface, it is also highly desirable to have spectral response measurements in the very high absorption regime of .35 - .4 μm. Accurate measurements of the internal quantum efficiencies are difficult to obtain at these wavelengths.

Effects of Band Gap Narrowing on Long Wave Length Absorption Coefficients

At the present time no corrections for the effect of band gap narrowing are made to the absorption coefficients.

Carrier-Carrier Scattering

Carrier-carrier scattering can be a significant effect in high concentration solar cells, and will become a significant effect in one sun solar cells as the efficiency is increased.

High Injection Lifetime

At the present time very little data is available on majority carrier lifetime. A typical modeling approach is to assume that the majority carrier lifetime is the same as minority carrier lifetime. This seems to give reasonably good agreement with cell performance under high injection conditions, but direct measurement of the high injection lifetime would be highly desirable.

Conclusions

One and two-dimensional device models have been quite successfully employed as an aid to design, interpretation, sensitivity analysis, and prediction. However, the predictive capability of any device code is only as good as the physics which is modeled and the data which is supplied. If further improvements are to be made in the performance of single crystal silicon solar cells, careful attention will have to be paid to both of these areas and a great deal of effort will have to be devoted to measurement techniques which will allow the independent determination of the parameters which must be supplied to the device code.

Acknowledgment

SCAP1D and SCAP2D were developed under the sponsorship of Sandia National Laboratories on contract number 52-5675.

References

1. M. S. Lundstrom, R. J. Schwartz, "Annual Report on Interdigitated Back Contact Solar Cells," TR-EE 80-14, School of Electrical Engineering, Purdue University, West Lafayette, IN.
2. R. J. Schwartz, M. S. Lundstrom, J. L. Gray, "Annual Report on High Intensity Solar Cells, TR-EE 82-5, School of Electrical Engineering, Purdue University, West Lafayette, IN.
3. R. J. Schwartz, J. L. Gray, M. S. Lundstrom, "Report on High Intensity Solar Cells," TR-EE 83-21, School of Electrical Engineering, Purdue University, West Lafayette, IN.

DISCUSSION

SAH: I would like to ask you about that particular example you gave, the complementary error function, also the SUPREM. There is quite a difference in the results. What is the basic mechanism? What are the recombination mechanisms that give you the difference?

SCHWARTZ: What's included in the code is Hall-Shockley-Read and Auger using Schmidt Auger coefficients, and for that particular run -- thank you for asking -- I should have mentioned at the time: for that particular run we used the Slot-Boom band-gap narrowing model, so there is a significant amount of band-gap narrowing occurring, and recombination mechanisms. For that particular run, Auger and Hall-Shockley-Read, and I didn't bring the plot along. The plot shows the split between them. I don't recall what the split was.

SAH: For the particular profile, was it the Auger that causes the one to be better than the other one?

SCHWARTZ: Yes, I believe that it was Auger, but I don't have the plot with me.

NEUGROSCHEL: You said that the published Auger coefficients don't agree with the experiment. In order to get agreement, do you need larger lifetimes or shorter lifetimes?

SCHWARTZ: The recombination wants to be reduced. I should qualify that a little bit. I was repeating what is said in a couple of publications by Posene at GE and Weaver at Sandia. It is possible that the problem lies in the band-gap narrowing model and not in Auger, so one wants to be a little careful. There is a problem in the emitter, and that's clear, and people have tended to blame Auger. I guess I'm not completely convinced that it is Auger -- it may well be related more to the band-gap narrowing.

DAUL: I would like to follow up on Sah's question. You have the same carrier density at the surface for the SUPREM and for error function. So, normally you have much larger field right at the surface in case of complementary function, and I would expect less recombination there. Would you give some reason why?

SCHWARTZ: Yes. There are a number of reasons. One is that the recombination r only depends on the Auger coefficients and lifetime, but also on the excess minority carrier concentration, and if I had shown the plot, what you would have seen is that many of the carriers are recombining in the case of SUPREM as they moved, and the axis cure was lower at the surface. The other difference is in the way that the band-gap narrowing effective field is distributed. The minority carriers in the emitter don't see just an electrostatic driving force due to the gradient. There is another component, which is associated with band-gap narrowing itself, and it tends to reduce the effect of pulling minority carriers away from that surface or keeping them out of the emitter. Both are operating and they are distributed differently.

DAUD: The second question has to do with actually running this program. We find that one of the items that one has to put in is the τ_{p0} and τ_{n0}. Normally when we measure, we either measure the lifetime or diffusion length where the doping is already there. How does one reconcile with this? What kind of numbers one should put for τ_{p0} τ_{n0}?

SCHWARTZ: I'm sorry. You say you normally measure what?

DAUD: Say we have a cell where we measure the diffusion length or the lifetime. We cannot directly put that in your model because your model corrects it for the doping.

SCHWARTZ: Yes. There were a lot of features that were not talked about here, and since we have sent a copy of the code out to JPL, he is asking. You have the option of turning on what amounts to a Kandel fit to doping. If in fact you have that turned on and if the base doping is above the transition doping for the the Kandel fit, then you have to correct that. If you have measured the lifetime at that particular doping level, you either have to correct it or just turn Kandel fit off and enter the value you measure. It's your choice. It is under your control on the input deck.

LINDHOLM: I have three questions. They are all, I think, fairly quick. Just to remind the audience: you recast some of the -- what you might say, equations which were truer to the physics -- into a form that one is more used to seeing in a conventional treatment of semiconductor device physics. In so doing, you introduce the parameter that you called small gamma, lower case gamma, and I think that that parameter was supposed to have taken care of various things that were being violated by the density of states. You made a big point, which is an extremely valid point -- that the parameters that go into the model have to be measurable. So with that preparation for the audience, I could have just asked you what success have you had in measuring gamma, and how do you do it? How don't you do it, if you can't do it?

SCHWARTZ: I tried to stay away from the equations, Fred, and I apologize for the poor quality here. The gamma that Fred is talking about entered into the effective potential that we showed. Here is the electrostatic potential, and here is the term which I said was an effective asymmetry factor, and that term is not normally known. As one gets measurement of the effective band-gap narrowing, which in fact looks like this -- the band gap plus all the degeneracy and band structure effects. Gamma, in fact, has electron affinity divided by the delta G minus terms for degeneracy. The answer to your question is, you don't know. But before I let that go, it turns out that for solar cells you seldom care, and the reason for that is the following: GE observed this first, the range on that numbers from 0 to 1 and one can run the full range and see almost no detectable change in the device characteristics. On the other hand, if you look inside the device, there are radical differences in the electric field distribution in the emitter, in that region. There are huge differences. But it turns out, and you can do this in closed form, that if you are dealing with a region which is quasi-neutral and low injection, as the

emitter is under anything except extreme conditions, you can show in analytic form that, in fact, terminal characteristic is independent of that parameter. There are places where it makes a difference. It does make a difference in junction capacitance: you can show that fairly readily. It makes a difference in the electric field. And a dramatic one if, for instance, you are concerned with avalanche, not in a solar cell, but calculations of avalanche, and you are in a heavily doped condition. Then possibly one should be worried about present-day avalanche coefficients if they are based on classically calculated electric fields. But the answer is that it doesn't affect the terminal characteristics.

LINDHOLM: The reason I asked that is twofold. First of all it would seem to me that for diagnostic purposes it would be desirable to know what you call gamma, or what I would rather just call the electro. finity, and I know about the comment you made about the quasi-neutral region. But as you start entering a little bit into the junction transition region, then I think it becomes more important. And the reason I asked that is, if I correctly read your earlier paper with Mark Lundstrom, that you indicated a method for measuring gamma. And so I come back to my original question: what degree of success have you had in measuring gamma?

SCHWARTZ: Very little. We're still working on it.

LINDHOLM: I think it is a good thing to work on, actually. The reason is that it's very easy, even though you did not intend to do this -- in fact, your wording was very careful -- but people will take sort of special cases and say it doesn't matter, but it does matter from a diagnostic point of view in finding out what's going on with the profiles,how you can improve the device, that kind of thing. I'm very glad you used such careful wording, so congratulations on that.

SCHWARTZ: I'm glad you read the paper, very few people have.

LINDHOLM: Its a very interesting and very good paper. I was extremely interested in your measurement of gamma.

SCHWARTZ: I have a Ph.D. student who is extremely interested too.

LINDHOLM: The other thing that I noted that you said, and since you word things so carefully, I was noticing that you said that most of the people who made electrical measurements in effect were measuring the p-n product. Now, I think that that's probably true of the Slot-Boom graph you use, the transistor structure; I think it's not true of EBIC people. Would you agree with that? A good portion of the data now coming out is EBIC data and the guys from GE who aren't here are talking about p-n product and I think that they can't do that. The fundamental reason is that Fermi levels have to remain sensibly, spatially invariant over a significant region of the device in order for that measurement to yield the p-n product.

SCHWARTZ: That's absolutely right, and from a physics point of view is very pleasing. And from a modeling point of view it's difficult, because now

in the intermediate region, where one worries about what happens to the band shape, you've got a problem in using it.

LINDHOLM: One last one. You keep mentioning two-dimensional programs, and I would like to know about three-dimensional programs, and why you can get away with two-dimensional.

SCHWARTZ: It's not so much getting away with two-dimensional, it's really a level of difficulty. In our case -- one thing I didn't mention, and I neglected it inadvertently -- I told you that it cost about $5.00 and takes 100 to 300 seconds on a 6500 CDC if you run the 1-D code. It takes about 300 CPU/second on our CYBER 205 Supercomputer to run the 2-D code. Now, what I mean by that is to run a full analysis, something like 10 points, and do all the associated stuff. That uses about 2,000 mesh points. So right now it's about what we are capable of tackling. If Purdue will put another two million words into the main memory of that computer then we will look at the three-dimensional.

LINDHOLM: If the next speaker is successful in cutting the computer time significantly by his technique, as he suggests, would you then strongly advocate three-dimensional steady-state modeling as a highly useful, moderately useful or rarely useful vehicle for solar cell design optimization and for monitoring manufacturing processes?

SCHWARTZ: I think that's a very good question, whether it's asked about one, two or three-dimensional, and the answer lies in how easy it is to use, whether it's fast, are the turn-arounds quick, and what is reasonably cheap. Because you do have to make a lot of runs, and if it's very expensive or very time-consuming, the utility becomes a lot less.

LINDHOLM: Suppose it doesn't cost anything?

SCHWARTZ: Then its very useful to do even for one sun. Is that what you think?

LINDHOLM: I haven't thought enough about it.

SCHWARTZ. If you want to do a cell like Dick Swanson's.

LINDHOLM: A more conventional cell is very useful there? Or is it moderately useful?

SCHWARTZ: I doubt it, I can't see the benefit to a conventional cell with three dimensions.

QUESTION: Dick, a quick question. Did you decide that radiative recombination and trap Auger effect could be neglected safely?

SCHWARTZ: No, we didn't. I told you the status of the code as it was. It is a fairly straightforward matter to add those components to it, we just haven't driven things, we haven't made any runs where the other lifetime-limiting mechanisms were low enough to do that. But clearly, if you do, that's a limiting mechanism that is not present and needs to be added.

QUESTION: And on the surface recombination you might also have trap Auger effects, or do you wrap it all up in a surface recombination velocity?

SCHWARTZ: Well in the one-dimensional code it's wrapped up in the surface recombination velocity. I didn't talk about how it's handled in two dimensions. In two dimensions you could either do it by integrating through the trap states and capture cross-sections, or you could do it by a lumped parameter, which is probably not as good -- and you do have to control surface potential, which we do by setting the charge in the oxide.

QUESTION: Now, a last question: capacitance. Do you work it out or do you do current-voltage, capacitance voltage?

SCHWARTZ: No, JPL doesn't know if their version of the code does have capacitance in it, we just didn't tell them. It is the equivalent of very low-frequency capacitance I'll tell you what it is and you can name it. It is the integral of either the electrons or holes with the appropriate voltage term put in, and you are quite right.

QUESTION: It can miss by a factor of three or four?

SCHWARTZ: Yes. We don't use it that way.

N85-31637

APPLICATION OF CLOSED-FORM SOLUTIONS TO A MESH POINT FIELD IN SILICON SOLAR CELLS

M. F. Lamorte
Research Triangle Institute
Research Triangle Park, NC 27709

Abstract

A computer simulation method will be discussed that provides for equivalent simulation accuracy, but that exhibits significantly lower CPU running time per bias point compared to other techniques. This new method is applied to a mesh point field as is customary in numerical integration (NI) techniques. The assumption of a linear approximation for the dependent variable, which is typically used in the finite difference and finite element NI methods, is not required. Instead, the set of device transport equations is applied to, and the closed-form solutions obtained for, each mesh point. The mesh point field is generated so that the coefficients in the set of transport equations exhibit small changes between adjacent mesh points. In contrast to the NI linear approximation, the closed-form solutions more accurately represent the physical system and the device physics incorporated in the transport equations.

Application of this method to high-efficiency silicon solar cells is described; and the method by which Auger recombination, ambipolar considerations, built-in and induced electric fields, bandgap narrowing, carrier confinement, and carrier diffusivities are treated. Bandgap narrowing has been investigated using Fermi-Dirac statistics, and these results show that bandgap narrowing is more pronounced and that it is temperature-dependent in contrast to the results based on Boltzmann statistics. It is also suggested that carrier diffusivity relationships that apply to degenerate materials in thermal equilibrium may also be applicable to regions in which high injection exists even in nondegenerate material.

Imposing the appropriate boundary conditions on the closed-form solutions results in a set of equations which require simultaneous solution. This results in obtaining the solution of all constants of integration, from which, in principle, all cell characteristics may be derived. It has been demonstrated that recursion relationships exist between the constants of integration. Trial or "guess" solutions are not required in this new method for devices operating at any injection level, because the closed-form solutions obtained at each mesh point, in fact, fulfill this role. This carries over to those devices operating at high injection levels, but the inclusion of Auger recombination introduces nonlinear terms in the continuity equations, and special attention must be devoted to satisfying Poisson's equation. Under these conditions, an initial estimate must be made of the value of the independent variable for inclusion in the continuity equations at the initial mesh point. An iterative procedure is then used to obtain a consistent solution.

INTRODUCTION

Computer modeling simulations have been shown to be very useful in the development of semiconductor devices in those cases where the simulation is an accurate representation of the physical device. However, to be an effective aid to the experimentalist and to become an equal partner in the technologies used in device development, it may be required to operate the computer program frequently each day in an active developmental program. For frequent use, as required in solar cell development, CPU costs must be low. Moreover, low CPU cost allows for engaging in computer experiments, which can be made to be a very useful and powerful technique.

Computer modeling using numerical integration (NI) methods in Si device technology have usually shown fair-to-good agreement with experimental data. However, CPU costs for the execution of computer programs that are based on numerical integration methods are prohibitively high for their use as a laboratory or manufacturing tool [1]. The number of bias points that are required to study optimized device designs usually exceeds 5,000 runs. Similarly, a comprehensive study involving device structures or new types of devices may exceed 10,000 runs. Increased CPU cost results if convergent problems arise. In most cases, the cost of such studies, for the benefits gained, may not be attractive.

Simulation accuracy is determined by both the accuracy of the algorithm/analytical method representing the device transport equations, and the accuracy of the phenomena submodels in representing the corresponding experimental data related to material properties. For most efficient use of the CPU, the accuracy of the algorithm/analytical method and of the phenomena submodels should be commensurate. For example, even if the algorithm/analytical method accurately represents the device, simulation results may not agree with experimental data if the phenomena submodels are accurately represente The reverse is also true. In solar cells, the phenomena submodels that produce first-order effects in terminal characteristics are: absorption curve, built-in and induced electric fields, bandgap, lifetime, mobilities, diffusivities, photoexcited carrier concentrations, surface recombination velocities, junction transport, etc. The representation of the phenomena submodels must take on an importance equal to the analytical method used to represent the system.

Under some operating conditions and for a number of solar cell structures, two-dimensional modeling may be required to obtain improved agreement between simulation results and experimental data. Although the results presented above apply generally to one- and two-dimensional modeling, the CPU execution time is significantly greater for two-dimensional simulations.

In this paper, a new method is described which has been used to simulate semiconductor device characteristics. Although this method shares similarities with some aspects of NI methods, it differs markedly in other aspects. Abbreviated forms of analytical relationships representing the solution of solar cell transport equations that are obtained using this new method are presented and discussed. The similarities and differences between the methods are also discussed.

SIMULATION METHODS

In this section, the transport equations are discussed as they relate to the simplifications and approximations that are required to be made in order to use NI methods and the new method, which is the application of closed-form solutions applied to a mesh point field. The finite difference (FD) and finite element (FE) methods, which are considered NI methods, are briefly discussed because they are most similar to this new method. An outline of these methods is presented and the procedures are developed to apply them.

Numerical Integration Methods

The most commonly used transport model in semiconductor devices is due to Van Roosbroeck and is represented by the set of equations:

$$\frac{\partial n}{\partial t} = \frac{1}{q} \nabla \cdot \vec{J}_n + (G-R) \quad , \tag{1}$$

$$\frac{\partial p}{\partial t} = -\frac{1}{q} \nabla \cdot \vec{J}_p + (G-R) \quad , \tag{2}$$

$$\vec{J}_n = q\mu_n n\vec{E} + qD_n \nabla n \quad , \tag{3}$$

$$\vec{J}_p = q\mu_p p\vec{E} - qD_p \nabla p \quad , \tag{4}$$

$$\nabla \cdot \vec{E} = \frac{q}{\varepsilon} (p-n + N_D - N_A) \tag{5}$$

The above set of relationships is applicable to nondegenerate and degenerate materials, low and high injection levels, dc and ac operation, and to most semiconductor device structures.

The Van Roosbroeck transport equations comprise a system of coupled partial differential equations that describe a semiconductor carrier concentration and current density in position and time. The net balance of generation sources and recombination sinks of electrons and holes are described by the respective continuity equations, and the Poisson equation describes the electric field distribution that is produced by the charge distribution within the semiconductor. For solar cells, the steady-state condition is assumed, which greatly simplifies the transport set because $\partial n/\partial t$ and $\partial p/\partial t$ vanish. Device phenomena submodels may be added to the transport equations to accurately describe a variety of carrier dynamical and other internal physical processes.

However, the Van Roosbroeck equations must be significantly modified in order to describe the effects arising from velocity overshoot, ballistic transport, and very thin surface layers [3]. In solar cells, only the latter may need consideration. The phenomenon in thin n-type surface layers, where an oxide charge insulator (OCI) produces an electron accumulation, may introduce sidebands within the conduction band, where each sideband corresponds to a quantized level for electron transport in a direction normal to the surface.

Solution of the transport equations is more difficult for higher order models; i.e., time-dependent requirements, and two- and three-dimensional geometries [2-11]. Moreover, this difficulty is brought into sharp focus in two-dimensional modeling when comprehensive phenomena submodels are considered [2,12].

In comprehensive representations, the complexity of the Van Roosbroeck transport equations does not allow for closed-form solutions which accurately simulate semiconductor devices. Accurate solution of the transport equations requires a method that simplifies these equations. The most popular approach is to divide the device structure into small parts [2-15]. In one-, two-, and three-dimensional solutions, these small parts are defined as infinite slabs, areas, and volumes, respectively. Each of these small parts is assigned a mesh point, which is identified by one, two, or three indices corresponding to a one-, two-, or three-dimensional representation of the device. These small parts must be made sufficiently small so that all dependent variables in the transport equations exhibit small changes in value between adjacent mesh points [2,4,5,8, 15]. In addition, the coefficients in the transport equations also exhibit small or negligible changes between adjacent mesh points [15]. If either of these conditions is not met, a solution is not obtained because convergence does not occur. NI methods and the closed-form solutions may be applied to mesh point fields.

In applying the FD method, all derivatives are replaced by finite differences between discrete points in an active domain in the interior of the structure. The residue of the newly established difference equation is set to zero at each mesh point. Thus, the differential equations are transformed into difference operator equations. The value of the dependent variable is determined at each mesh point from the set of equations obtained [2,4].

For example, the differential equation to determine the temperature distribution is given by [4]

$$\frac{d^2T}{dx^2} = 0 \quad . \tag{6}$$

The difference operation is represented by

$$\frac{d^2T}{dx^2} \approx \frac{\dfrac{T_{i+2} - T_{i+1}}{\Delta x} - \dfrac{T_{i+1} - T_i}{\Delta x}}{x} \quad , \tag{7}$$

where T_i, T_{i+1}, and T_{i+2} are the values of the dependent variable, T, at the mesh points i, i+1, and i+2, and Δx is the independent variable representing the separation of the mesh points i and i+1, and i+1 and i+2, assumed to be equal. A corresponding equation is constructed at each mesh point. The resultant set of equations requires the simultaneous solution for T_1, T_2, --, T_i, --. Thus, the value of the dependent variable, T, is obtained <u>only</u> at the mesh points 1, 2, --. The value for T in the region between the mesh points is not

obtained explicitly and may only be approximated by one of the established methods. Typically, a linear approximation is used.

In the FE method, a typical assumption made is that the dependent variable is a linear function, where, for the system discussed above involving temperature [4],

$$T = T_i + \frac{T_{i+1} - T_i}{x_{i+1} - x_i} (x - x_i) \quad . \tag{8}$$

This relationship is substituted into an equation, called the "functional," that describes the system to obtain a set of equations. Simultaneous solution of this set results in discrete values of the dependent variable at each of the mesh points. Between the mesh points, the dependent variable is governed by a linear relationship similar to that represented in Eq. (8).

The full numerical solution of partial differential equations as described above, which is applied to a physical system and which describes all regions of this system in a unified manner, was first suggested by Gummel [5]. In this work, Gummel applied his method to a one-dimensional bipolar transistor. Subsequently, the method was further developed by DeMari [6,7] who applied it to p-n junctions, and by Scharfetter and Gummel [8] to IMPATT diodes. Although this initial work was confined to one-dimensional structures, the Gummel approach has also been adapted to two-dimensional modeling [3,9-12]. However, the two-dimensional algorithm requires excessive CPU execution time [3,12].

Phenomena submodels may be imposed on the coupled nonlinear partial differential equations which may result in nonlinear transport equations; i.e., band-to-band Auger recombination introduces a term involving n^2 or p^2, and the electric field in the quasi-neutral region depends on the injection level. In NI numerical methods, the transport relationships are linearized. Two schemes have been used and both require initial "guess" solutions. The decoupled method proposed by Gummel [5] is to assume the coupling is weak so that the equations are solved serially. While the method is not difficult to implement, it fails to give accurate results for highly nonlinear systems. The coupled method, proposed by Hachtel et al. [14], solves the transport equations simultaneously. However, this is more difficult to implement. The implementation of the algorithm becomes complex when recombination-generation and electric field drif terms are included [4]. In addition, this results in significantly higher CPU execution time and increased main memory requirements.

As discussed above, using NI methods results in values for the dependent variables, such as the carrier concentrations and electric field, at discrete points in the semiconductor; i.e., at the mesh points. Thus, the continuum of the dependent variables, described by the transport equations, is transformed into a discontinuous or discrete set of values representing these variables at each of the mesh points. In contrast, the method that is proposed in this paper does not resort to this transformation.

Closed-form Solutions Applied to a Mesh Point Field

The major point of departure between the algorithms of the new method and NI methods is that the new method uses a closed-form solution which is applied to a mesh point field that defines the system in space and in time [15]. This requires the application of the transport equations to each mesh point. In order to obtain a closed-form solution to the transport equations, the mesh point field is generated so that the equations accurately represent each mesh point. The closed-form relationships represent analytical solutions and result in a continuum of values for the dependent variables in the region between adjacent mesh points. Analytical solutions of adjacent mesh points also provide a continuum of values for the dependent variables in their corresponding regions. Analytical solutions of neighboring mesh points satisfy the usual boundary conditions that are demanded in semiconductor devices in accordance with the electronic/optical model under consideration. The analytical solutions representing the dependent variables at each mesh point contain constants of integration, which are determined by imposing the boundary conditions on each of the solutions.

A procedure has been established in applying the closed-form solutions to a mesh point field. The procedure is as follows [15]: (1) establish the electronic/optical model of the solar cell within the generic transport equations; (2) impose the phenomena submodels, represented in analytical or tabular form, on the transport equations; (3) develop mesh point field distribution of order f which reduces the complexity of, and makes the coefficients that are present in, the continuity equations constant or nearly constant, so that a closed-form solution is obtained at each mesh point with minimum restrictions; (4) establish 2f-boundary conditions on the mesh point field; (5) apply the 2f-boundary conditions on the f-closed-form solutions; and (6) solve the resultant 2f-equations simultaneously to obtain the 2f-constants of integration through recursion relationships. In principle, the transport equations are uniquely and completely solved after the relationships for the 2f-constants of integration are obtained. Electron current is calculated at the depletion region edge; the hole current is determined by a similar relationship. Adding the electron and hole currents results in the J-V relationship from which most of the terminal characteristics are recovered.

The well-established solar cell electronic/optical model is imposed on the transport equations; i.e., optical pair generation of carriers, and minority carrier collection and transport across a p-n junction. This is followed by imposing the phenomena submodels which are subsequently discussed. A mesh point distribution is established so that the electric field, lifetime, mobility, diffusivity, absorption coefficient, and bandgap exhibit small changes between adjacent mesh points. Figure 1 shows the subdivision of a one-dimensional solar cell structure. The n-region $(0, X_2)$ and the p-region (X_3, X_5) are subdivided into f_n- and f_p-mesh points, respectively. To illustrate the method, the p-region transport solution is discussed below. The electron continuity equation is represented by

$$\int_0^{\lambda_c} \alpha N_0 \exp\left(-\int_0^x \alpha dx'\right) d\lambda + D_n \frac{d^2 n_{pe}(x)}{dx^2} + \mu_n E_p \frac{dn_{pe}(x)}{dx} - \frac{n_p(x) - n_{p0}}{\tau_n} = 0 \ , \quad (9)$$

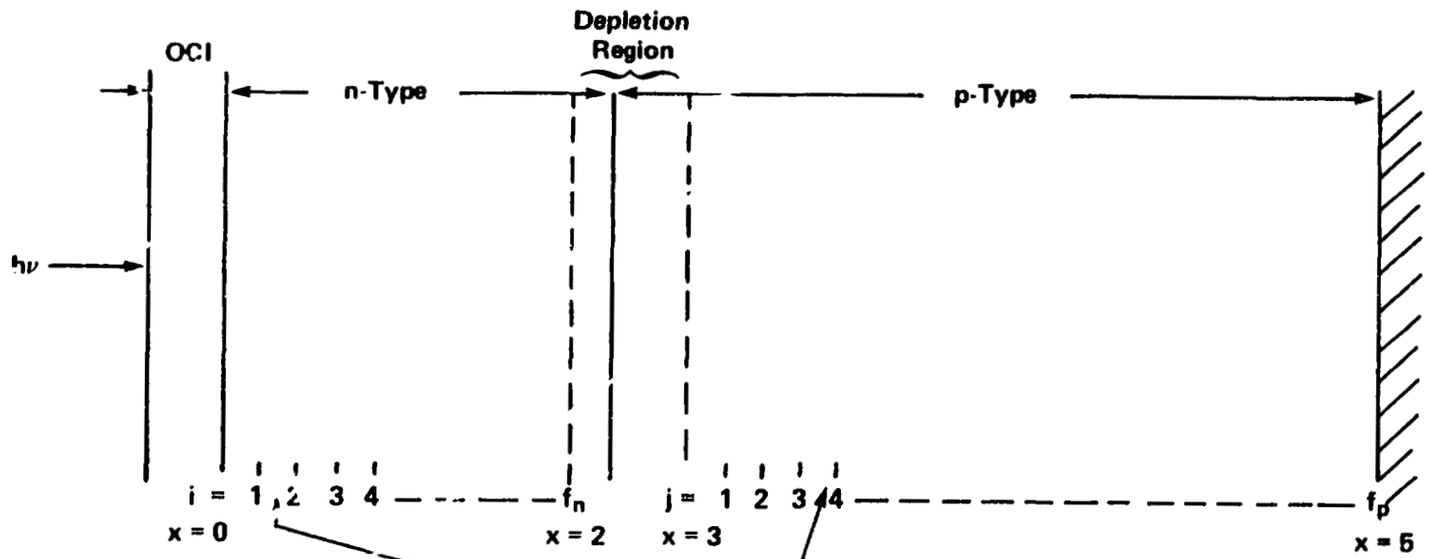

$$J_{p2} = q\mu_{p2}p_{n2}E_{n2} - q\,D_{p2}\frac{dp_{n2}}{dx}$$

$$p_{n2} = A_{12}e^{\omega 12x} + A_{22}e^{\omega 22x} + A_{32}(x)$$

$$J_{n4} = q\mu_{n4}n_{p4}E_{p4} + q\,D_{n4}\frac{dn_{p4}}{dx}$$

$$n_{p4} = B_{14}e^{\omega 14x} + B_{24}e^{\omega 24x} + B_{34}(x)$$

Figure 1. Discretization of 1-dimensional solar cell structure.

where the Poisson equation takes its usual form. The symbols have their usual definitions, where n_p and n_{pe} represent the total and photoexcited electron concentrations, respectively. Implicit in Eq. (9) is that the subdivision results in a condition in which the slope of the electric field, dE_p/dx, is small and may be neglected in a region between adjacent mesh points. Although the electric field slope is assumed to be negligible, the electric field itself, in general, is allowed to vary from mesh point to mesh point. Moreover, under these conditions the remaining material properties also exhibit small changes between neighboring mesh points for low injection levels. These changes become large under high injection levels, in which case a more dense mesh point field may be required to maintain comparable changes. As a result, a near-exact closed-form solution is obtained at each mesh point for the photoexcited electron concentration, which is an exact solution of Eq. (9) and is represented by

$$n_{pej}(x) = B_{1j}\exp(\omega_{1j}x) + B_{2j}\exp(\omega_{2j}x) + B_{3j}(x) \quad , \qquad (10)$$

where the terms comprising Eq. (10) are given in Table 1.

The subscripts, j, in Eqs. (10)-(30) represent the jth mesh point in the p-region as indicated in Figure 1. Correspondingly, in Eq. (10), B_{1j} and B_{2j} represent the constants of integration, and B_{3j} in Eq. (11) represents the photoexcited electron concentration, produced by photon absorption in the region of the jth mesh point. In the context of the conditions imposed on the continuity equations at each mesh point, ω_{1j} and ω_{2j} in Eq. (14) are constants. Photoexcited electron concentration, Eq. (10), is governed by the exponential terms and B_{3j} which are all functions of position; in addition, B_{3j} is also a function of wavelength through Eqs. (12) and (13). Eq. (10) provides for continuous values of n_{pe} through the assignment of values to x, where the range of x is restricted to the region between the (j-1) and j mesh points. In contrast to numerical integration methods, the continuum of values describing the behavior of n_{pe} is preserved in the closed-form scheme as was the original intent proposed by the Van Roosbroeck concept related to the use and the interpretation of the transport equations.

It is clear that the relationship used in the closed-form method, to represent the photoexcited electron concentration, Eq. (10), is an analytical solution that is demanded by, and has its support in, the transport equations. Moreover, this relationship may also incorporate a comprehensive set of phenomena submodels as dictated by the transport equations, imposed boundary conditions, and the representations of the material properties coupled with the mesh point field. The phenomena submodels that influence Eq. (10) are represented in the relationships for the parameters, Eq. (11)-(30), that describe their behavior in the region bounded by the (j-1) and j planes in Figure 1. Eqs. (11)-(13) describe the photon absorption generation rate and the redistribution of the photoexcited electron-hole pairs, while Eq. (14) governs the electron effective diffusion length in the presence of an electric field. Drift and diffusion components of the electron current are represented in Eq. (15), and the electric field used in

Table 1. List of relationships of terms appearing in the solution of the electron concentration, Equation (10).

$$B_{3j}(x) = \frac{1}{\omega_{2j} - \omega_{1j}} [G_{1j}(x)\exp(\omega_{1j}x) + G_{2j}(x)\exp(\omega_{2j}x)] \tag{11}$$

$$G_{1j}(x) = \frac{1}{D_{nj}} \int_o^x \exp(-\omega_{1j}x') \int_o^{\lambda_c(x')} \alpha_j N_{0j} \exp(-\int_o^{x'} \alpha_j dx'')d\lambda dx' \tag{12}$$

$$G_{2j}(x) = -\frac{1}{D_{nj}} \int_o^x \exp(-\omega_{2j}x') \int_o^{\lambda_c(x')} \alpha_j N_{0j} \exp(-\int_o^{x'} \alpha_j dx'')d\lambda dx' \tag{13}$$

$$\left.\begin{matrix}\omega_{1j} \\ \\ \omega_{2j}\end{matrix}\right\} = -\frac{\mu_{nj}E_{pj}}{2D_{nj}} \pm \sqrt{\left(\frac{\mu_{nj}E_{pj}}{2D_{nj}}\right)^2 + L_{nj}^{-2}} \tag{14}$$

$$J_{nj} = q\mu_{nj}E_{pj} + qD_{nj}\frac{dn_{pj}}{dx} \tag{15}$$

$$E_{pj} = E_{p\Omega j} + E_{pBNj} + E_{plPj} + E_{pPEj} \quad , \tag{16}$$

where

$$E_{p\Omega j} = \frac{b_{pj}J_1}{q\mu_{nj}\Gamma_{pj}} \quad , \tag{17}$$

$$E_{pBNj} = (b_{pj} - \xi_p)\frac{n_{poj}}{\Gamma_{pj}} E_{pBNoj} \quad , \tag{18}$$

$$E_{pBNoj} = -\frac{kT}{q}\frac{2}{n_{iej}}\frac{dn_{iej}}{dx} \quad , \tag{19}$$

Table 1 (continued).

$$E_{pIPj} = \left[(b_{pj} - \xi_p) \frac{n_{poj}}{\Gamma_{pj}} + \xi_p \frac{N_{Aj}}{\Gamma_{pj}} \right] E_{pIPoj} \quad , \tag{20}$$

$$E_{pIPoj} = \frac{kT}{q} \frac{1}{N_{Aj}} \frac{dN_{Aj}}{dx} \quad , \tag{21}$$

$$E_{pPEj} = - \frac{kT}{q} \frac{b_{pj} - \xi_p}{\Gamma_{pj}} \frac{dn_{pej}}{dx} \quad , \tag{22}$$

$$\Gamma_{pj} \equiv (b_{\mu j} + \xi_p) n_{pj} + \xi_p N_{Aj} \quad , \tag{23}$$

$$b_{nj} = \frac{F_{1/2}(\eta_j)}{F_{-1/2}(\eta_j)} \tag{24}$$

$$b_{pj} \equiv \frac{F_{1/2}(-\varepsilon_{Gj} - \eta_j)}{F_{-1/2}(-\varepsilon_{Gj} - \eta_j)} \tag{25}$$

$$b_{\mu j} \equiv \frac{\mu_{nj}}{\mu_{pj}} \tag{26}$$

$$D_{nj} = \frac{kT}{q} \mu_{nj} b_{nj} \tag{27}$$

$$J_1 = J_n(x) + J_p(x) \tag{28}$$

$$n_{iej}^2(T, N_A) = n_{io}^2(T) e^{\Delta E_G/kT} \tag{29}$$

$$n_{pj} = n_{poj} + n_{pej} \tag{30}$$

the drift term is given by Eq. (16). The electric field components are defined in Eqs. (17)-(27), arising under equilibrium and nonequilibrium conditions, and include effects produced by ohmic voltage drops in the quasi-neutral regions, bandgap narrowing, impurity concentration profile, and photoexcited electron concentration distribution. Eq. (29) describes the intrinsic concentration with respect to temperature and bandgap narrowing.

In contrast, the relationship that is used in NI methods, corresponding to Eq. (10), is typically linear and is of the form given by

$$n_{pe}(x) = n_{pe}(x_{j-1}) + \frac{n_{pe}(x_j) - n_{pe}(x_{j-1})}{x_j - x_{(j-1)}} (x - x_{(j-1)}) \quad , \qquad (31)$$

where x is the independent variable in the region bounded by the (j-1) and j planes. The photoexcited carrier concentrations, n_{pej} and $n_{pe(j+1)}$, do not normally represent algebraic expressions, but represent discrete values and require initial estimates of the concentrations at their designated positions. The richness of Eq. (10) and its associated parameters, defined in Eqs. (11)-(30), in representing device physics is clearly evident in contrast to the representation in Eq. (31). This relationship, Eq. (31), is used in NI methods because it simplifies the matrix equation that requires solution, but it is artifical in its representation of the photoexcited electron concentration because it has been constructed independent of the transport equations.

The difference in the results obtained by applying Eqs. (10) and (31) to the same mesh point distribution, which defines the solar cell structure, is significant. Applying Eq. (10) results in the determination of the constants of integration, B_{1j} and B_{2j}, assigned to the carrier analytical relationship at each mesh point. Substituting B_{1j} and B_{2j} in Eq. (10) provides for an analytical relationship at each mesh point, describing the behavior of n_{pej} for a continuum of values of x in the range $x_{(j-1)}$ and x_j. In contrast, the results of applying Eq. (31) is a set of discrete values for n_{pej} at each mesh point.

In the work reported in this paper, the general case is treated as it relates to injection level. The information of injection level is contained in the electric field and its components, Eqs. (16)-(30), lifetime through the diffusion length, L_n, and boundary conditions at the depletion edges bounding the p-n junction, and in the carrier mobilities and diffusivities. Application of Eq. (10) requires negligibly small changes in electric field between adjacent mesh points. Under these conditions, Eq. (10) is an excellent approximation to the exact solution at the assigned mesh point region. The measure for which Eq. (10) approaches the exact solution is the self-consistency obtained from the solution of the Poisson equation using the analytical relationships for n_{pej} and the number of iterations required to obtain values of B_{1j} and B_{2j}.

The f_p-mesh point distribution in the p-type region of the solar cell comprises (f_p-1) internal boundaries, and external boundaries at x_3 and x_5. At the external boundaries, the usual p-n junction boundary condition on minority

carrier concentration applies. At each of the (f_p-1) internal boundaries, the electron concentration and electron current, separately, are continuous and are represented by

$$n_{pej}(y_{oj}) = n_{pe(j+1)}(0)k_j \tag{32}$$

where

$$k_j = e^{\Delta Ecj/kT} \tag{33}$$

and

$$J_{nj}(y_{oj}) = J_{n(j+1)}(0) \quad , \tag{34}$$

where y_{oj} is the separation between the $(j-1)^{th}$ and j^{th} mesh points. A surface recombination velocity boundary condition is imposed at the x_5 boundary. This results in $2f_p$-boundary conditions, from which $2f_p$-equations are obtained that must be solved simultaneously to obtain the solution of the $2f_p$-constants of integration.

Applying the boundary conditions using Eqs. (10) and (15) results in $2f_p$-equations which are represented in matrix form by

$$\begin{bmatrix} 1 & 1 & 0 & 0 & 0 & & & & & & & \\ \sigma_1 k_1 & \tau_1 k_1 & -1 & -1 & 0 & & & & & & & \\ \delta_1\sigma_1 & \epsilon_1\tau_1 & -\delta_2 & -\epsilon_2 & 0 & & & & & & & \\ 0 & 0 & \sigma_2 k_2 & \tau_2 k_2 & -1 & -1 & & & & & & \\ 0 & 0 & \delta_2\sigma_2 & \epsilon_2\tau_2 & -\delta_3 & -\epsilon_3 & & & & & & \\ & & & & & & & & & & & \\ & & & & & & \sigma_i k_i & \tau_i k_i & -1 & -1 & & \\ & & & & & & \delta_i\sigma_i & \epsilon_i\tau_i & -\delta_{i+1} & -\epsilon_{i+1} & & \\ & & & & & & & & & & & \\ & & & & & & & & & & \sigma_{f_p}[h_{f_p}+S_n] & \tau_{f_p}[\epsilon_{f_p}+S_n] \end{bmatrix} \begin{bmatrix} B_{11} \\ B_{21} \\ B_{12} \\ B_{22} \\ B_{13} \\ B_{23} \\ \vdots \\ B_{2i} \\ B_{i(i+1)} \\ \vdots \\ B_{2f_p} \end{bmatrix} = \begin{bmatrix} n_{pe}(x_3) \\ F_{01} \\ F_{02} \\ F_{03} \\ F_{04} \\ F_{05} \\ \vdots \\ F_{0(2i-1)} \\ F_{0(2i)} \\ \vdots \\ F_{2f_p} \end{bmatrix} \tag{35}$$

The constants of integration are denoted B_{11}, B_{12}, ---, B_{1f_p}, B_{2f_p}, and the relationships for the other factors contained in Eq. (35) are the material and structure properties at corresponding mesh points. The Fletcher boundary condition [16] is used at x_3, because it represents the boundary for the complete range of conditions that may exist: from equilibrium (i.e., the photovoltage $V_{Jph} = 0$) through increasing positive values of V_{Jph} up to and including high injection levels where $V_{Jph} \sim V_{bi}$.

In Eq. (33), ΔE_{cj} represents the band edge discontinuity located at the j mesh point. If ΔE_{cj} is positive, the boundary condition describes minority carrier confinement (i.e., electrons confined to the junction region).

The factors ω_{1j} and ω_{2j}, Eq. (14), are the reciprocals of the effective electron diffusion length in the p-type region, and describes the recombination of electrons in the presence of an electric field in the region bounded between the (j-1) and j mesh point. It describes the recombination related to those electrons entering this region across the planes defined by the (j-1) and j mesh points as well as those photoexcited carriers produced by photon absorption within that region. If the electric field, $E_{pj} = 0$, then $\omega_{1j} = -\omega_{2j}$ and are equal in magnitude to the reciprocal of the diffusion length, $L_n = \sqrt{D_n \tau_n}$. Similarly, for degenerate material or for high injection levels, low values of the electric field are obtained, and $\omega_{1j} \approx -\omega_{2j}$. In both cases, electron drift toward the junction occurs by means of diffusion rather than a combination of diffusion and field-assisted drift. Eq. (10) reduces to the more familiar form to represent photoexcited carriers.

The constants of integration are obtained by solving Eq. (35). While the matrix in Eq. (35) may be inverted to obtain the solution, a recursion relationship exists between the constants of integration. As a result, there is a significant reduction in CPU execution time to obtain the values of these constants through the recursion relationships. For example, in certain iteration procedures, some of the terms in these relationships that depend on geometry and materials properties may not change and need not be calculated for every iteration. There are probably other benefits, which will be revealed as more experience is gained in using this type of modeling program.

The recursion relationships for the constants of integration are given by the following equations:

$$B_{2f_p} \equiv \frac{F_{(2f_p)} - S_n B_{3f_p}(y_{0f_p}) - \sigma_{f_p}\theta_{nf_p}(\delta_{f_p}+S_n)}{\tau_{f_p}(\varepsilon_{f_p}+S_n) - \gamma_{nf_p}\sigma_{f_p}(\delta_{f_p}+S_n)} , \qquad (36)$$

$$B_{1f_p} \equiv \frac{\tau_{f_p}\theta_{nf_p}(\varepsilon_{f_p}+S_n) - \gamma_{nf_p}[F_{(2f_p)}-S_nB_{3f_p}(y_{0f_p})]}{\tau_{f_p}(\varepsilon_{f_p}+S_n) - \gamma_{nf_p}\sigma_{f_p}(\varepsilon_{f_p}+S_n)} \quad , \tag{37}$$

$$\vdots$$

$$B_{2j} \equiv -\frac{B_{2(j+1)}[\delta_{(j+1)}-\varepsilon_{(j+1)}]+F_{2(j-1)}\delta_{(j+1)}-F_{(2j)}-\sigma_j\theta_{nj}[\delta_{(j+1)}k_{nj}-\delta_j]}{\tau_j[\varepsilon_j-\delta_{(j+1)}k_{nj}]-\gamma_{nj}\sigma_j[\delta_j-\delta_{(j+1)}k_{nj}]} \quad , \tag{38}$$

$$B_{1j} \equiv \theta_{nj}-\gamma_{nj}B_{2j} \quad , \tag{39}$$

$$\vdots$$

$$B_{21} \equiv -\frac{B_{22}(\delta_2-\varepsilon_2)+F_{01}\delta_2-F_{02}-\sigma_1\theta_{n1}(\delta_2k_{n1}-\delta_1)}{\tau_1(\varepsilon_1-\delta_2k_{n1})-\gamma_{n1}\sigma_1(\delta_1-\delta_2k_{n1})} \quad , \tag{40}$$

and

$$B_{11} \equiv \theta_{n1}-\gamma_{n1}B_{21} \quad , \tag{41}$$

There also exists recursion relationships for the θ_{nj}'s and the γ_{nj}'s which are functions of material properties at their assigned mesh points.

Having obtained the constants of integration and substituting them into the relationship representing the appropriate mesh point, there results f_p-relationships which fully describe the behavior of n_{pe} in the p-region. In principle, all device properties may be recovered through the manipulation of n_{pej}s. Using Eqs. (10) and (15) and the corresponding relationships for holes in the n-region, the hole current J_1, Eq. (28), is obtained. Eq. (28) represents a relationship relating photocurrent versus photovoltage. The photovoltaic J-V_{Jph} curve may be obtained from which maximum power and efficiency is calculated. Moreover, the effects on the J-V_{Jph} curve of the phenomena submodels, and material and structure parameters may be investigated through B_{1j}, B_{2j}, and B_{3j}.

SUMMARY

A new computer modeling method is described and is applied to silicon solar cells. The method is similar to numerical integration (NI) methods in that

both require the use of a mesh point field. The set of transport equations is applied to each mesh point, and through a judicious selection of the mesh point distribution, an accurate closed-form analytical function is obtained at the assigned mesh point. Application of the boundary conditions, to an f-mesh point field, results in 2f-equations that require simultaneous solution. This solution is manifested through the determination of the 2f-constants of integration, where each closed-form solution, representing a mesh point, contains two constants of integration. Solar cell transport solution is represented by the complete set of constants of integration obtained in the n- and p-regions. Substituting the constants of integration into the corresponding closed-form analytical function, representing an assigned mesh point, results in a set of analytical functions that is applicable only to its assigned region in the mesh point field. As a result, the complete set of closed-form functions describes the behavior of the photoexcited carrier concentration for a continuum of x-values in the n- and p-regions. The photoexcited carrier relationship is used to obtain the current-voltage relationship, from which the maximum power point and conversion efficiency are determined. Effects of temperature, solar concentration, submodel parameters, and structure parameters may be studied through changes at each mesh point in ω_{1j}, ω_{2j}, B_{1j}, B_{2j}, and B_{3j}.

REFERENCES

1. T. Wada and J. Frey, IEEE Trans. Electron Devices, ED-26, 476-90, 1976.

2. P. Antognetti, Editor: Process and Device Simulation for MOS-VLSI Circuits, S. Selberherr, A. Schiitz, and H. Pötzl, 490, Martinus Nijhoff Publishers, Boston, 1983.

3. T. Wada and J. Frey, "Physical Basis of Short-Channel MESFET Operation," IEEE Trans. Electron Devices, ED-26, 476-90, 1979.

4. J. J. H. Miller, Editor: An Introduction to the Numerical Analysis of Semiconductor Devices and Integrated Circuits, E. M. Buturla, 9-15, Boole Press, Dublin.

5. H. K. Gummel, "A Self-Consistent Iterative Scheme for One-Dimensional Steady-State Transistor Calculations," IEEE Trans. Electron Devices, ED-11, 455-465, 1964.

6. A. DeMari, "An Accurate Numerical Steady-State One-Dimensional Solution of the P-N Junction," Solid-State Electron., 11, 33-58, 1968.

7. A. DeMari, "An Accurate Numerical One-Dimensional Solution of the P-N Junction Under Arbitrary Transient Conditions," Solid-State Electron., 11, 1021-1053, 1968.

8. D. L. Scharfetter and H. K. Gummel, "Large-Signal Analysis of a Silicon Read Diode Oscillator," IEEE Trans. Electron Devices, ED-16, 64-77, 1969.

9. D. P. Kennedy and R. R. O'Brien, "Computer Aided Two-Dimensional Analysis of the Junction Field Effect Transistor," IBM J. Res. Dev., 14, 95-116, 1970.

10. M. Reiser, "A Two-Dimensional Numerical FET Model for DC, AC and Large-Signal Analysis," IEEE Trans. Electron Devices, ED-20, 35-45, 1973.

11. K. Yamaguchi and H. Kodera, "Drain Conductance of Junction Gate FETs in the Hot Electron Range," IEEE Trans. Electron Devices, ED-23, 545-53, 1976.

12. J. L. Gray, "Two-Dimensional Modeling of Silicon Solar Cells," Ph.D. Dissertation, Purdue University, August 1982.

13. D. P. Kennedy and R. R. O'Brien, "Two-Dimensional Mathematical Analysis of a Planar Type Junction Field-Effect Transistor," IBM J. Res. Dev., 13, 662-74, 1969.

14. G. D. Hachtel, M. Mack, and R. R. O'Brien, "Semiconductor Device Analysis via Finite Elements," Eighth Asilomar Conference on Circuits and Systems, Pacific Grove, Calif., 1974.

15. M. F. Lamorte and D. H. Abbott, Final Report No. AFWAL-TR-81-1016: "III-V Detector Modeling," March 1981, WPAFB Contract No. F33615-79-C-1828.

16. N. H. Fletcher, "General Semiconductor Junction Relations," J. Electronics, 2, 609-610, 1957.

DISCUSSION
(LAMORTE)

LINDHOLM: I have a number of small questions. You put your attention on the dependent variables, which you treat as the hole and electron densities. I'm wondering how you enter the external boundary conditions since you are not feeding in hole and electron densities at the ends of the device.

LAMORTE: At the junction side of the end region, for example, meaning the emitter, the boundary condition becomes the Fletcher boundary condition for the photo-excited holes, because we are treating the general case of high injection level. At the surface region we are calculating the recombination velocity, by means of a Δx divided by the lifetime at the center of the first mesh point. And we have gotten some interesting results there, in that it appears that even for calculating the surface recombination velocity in that manner, it may not be consistent with the slope of the photo-excited holes at the surface. If you don't recalculate the surface recombination velocity, the solution will oscillate. We're just putting a fix in that, and the fix is that you want to update the surface recombination velocity at the surface by the exact relationship. Meaning the product of the surface recombination velocity times the photo-excited hole concentration at the surface, and that is equal to the surface recombination current, which includes a drift field component and a diffusion component. So that becomes the left-hand boundary.

LINDHOLM: I have a related question. If you are going to do a non-illuminated analysis where you apply a voltage, then how do you get into the external boundary conditions? I'm not now concerned with the edge of what you call the depletion region but rather the contacts of the device.

LAMORTE: I don't know whether it will work for that, but we can probably make it work. We have not given that any consideration.

LINDHOLM: Would you integrate the electric field? Would that be the way of doing it? Getting integrated, the electric field through the material, and setting that equal to zero, and then you would have to iterate, I suppose.

LAMORTE: Yes, we have that in the model because under high injection level you want to determine what the voltage drop is across the quasi-neutral region.

LINDHOLM: When you say the Fletcher boundary condition, you mean the Fletcher Masawa boundary condition as modified by Houser?

LAMORTE: No, the Fletcher and Masawa conditions are separate. They account for the same thing, but they require different information. The Fletcher boundary condition applies to the edges of the depletion region and thats what we are using. The Masawa uses the right-hand edge of the depletion region and the left-hand contact.

LINDHOLM: How do you define the edge of the depletion region in your numerical analysis?

LAMORTE: We calculate the depletion region for either a graded case or the abrupt case.

LINDHOLM: You calculate it how? Depletion approximation?

LAMORTE: Yes.

LINDHOLM: That won't work, I'm afraid, because you probably need to make a correction because of the free electrons and holes in that region. We could discuss that privately. That is probably an updating of the physics that goes into the model.

LAMORTE: Well, that is updated.

LINDHOLM: Oh, I see. You don't use the depletion approximation to calculate the depletion thickness?

LAMORTE: We use it to get it started.

LINDHOLM: Oh, I see, then you update. Okay. Then how do you define the edge of the depletion region once you get it updated? Somehow you have to use some criterion to define the edge of the depletion region.

LAMORTE: Then we use the depletion approximation.

LINDHOLM: Okay, I don't understand the answer to that, but maybe we could discuss that privately, unless you want to elaborate on it now. What I thought you said was, as your starting point to get the edge of what you call the depletion region, you would use the depletion approximation and then you would iterate up in, including the electron hole densities, in order to redefine the depletion approximation. Then I asked you what the criterion was after you did the updating.

QUESTION: Maybe that's something the two of you could discuss.

LINDHOLM: I have one last question. This is a very interesting idea to me. I have been sounding very negative; I'm sorry to sound negative. I just was looking at some small points. I don't do numerical analysis, but I'm somewhat familiar with what Mike did, and Gummel, and all these other people, and the only place I have ever seen this done previously, similar to this, is in a book by some Russians. I wonder if this is the first time this method has been used?

LAMORTE: I have not seen it anywhere else, and I have spoken to about a dozen people who have done computer modeling in other areas, other than semiconductors, as well, and they claim that they have not seen it. And I have not seen it elsewhere.

LINDHOLM: This Russian book is not quite numerical analysis, so I guess I haven't seen it either, but that's as close as I have come to seeing it.

It's very interesting.

LAMORTE: One of the things that this does for you, and what we showed in the avalanche photo diode -- because you're reflecting a lot of the physics in the closed form solution -- when you look at the convergence of the solution as a function of mesh points, you find that you do not need as many mesh points, for example, in the avalanche photo diode. We didn't need to go above 15 to 20 mesh points when we had a half-micrometer depletion width, and we went all the way up to 80 mesh points, and at 15 to 20 we were within 1% of the asymptotic solution with 80 mesh points. I'm fully convinced that since you have a closed-form solution, which is a good approximation, the physical system, that it's forgiving in terms of using a lesser number of mesh points. And so, therefore, that combined with the recursion formulas, the CPU time is reduced greatly.

LINDHOLM: I was wondering if you could describe the output that you got from your model and do you have it set up to give you graphs of carrier distributions and so forth?

LAMORTE: No, we haven't done that yet. We almost have the model working, meaning that with one of your cells we got something like 38 milliamperes, and it's about 20% too high, so we have gotten it that far and we are still trying to debug and determine where that is. And it may be just a simple matter that the lifetime we are using is too high.

LINDHOLM: So the code doesn't give you plots of carrier distributions and things that help one see what's going on in the physics of the device.

LAMORTE: We get discrete points, for example, of carrier concentration, okay, at the mesh points, and we get it at two points actually, we get it at each of the mesh points and in between. But if you wanted to, by taking the relationship that applies to that particular region of the cell in combination with the appropriate constants of integration, you could plot the entire thing on the continuum if you wished.

N85-31638

PHENOMENA SIMULATION FOR HEAVY DOPING AND SURFACE RECOMBINATION VELOCITY

Fred A. Lindholm
Department of Electrical Engineering
University of Florida
Gainesville, FL 32611

CONTENTS

LIST OF SYMBOLS
1. Introduction
2. Basics
   2.1 Quantum
   2.2 Statistics
3. High Concentrations
   3.1 Fermi Level
   3.2 Einstein Relation for Majority Carriers
   3.3 NP Product if There is No Energy Gap Narrowing
   3.4 Slope of Mobility Edge for Minority Carriers
   3.5 Energy Gap
   3.6 Minority Carrier Diffusivity and Mobility
   3.7 Trapping Model
   3.8 Other Parameters
4. Moderate Concentrations
   4.1 Fermi Level Saturation and Consequences
   4.2 Einstein Relation for the Majority Carriers
   4.3 Einstein Relation for the Minority Carriers
   4.4 Past Treatments
   4.5 Unsolved Problems and Consequences for Computer Simulation
5. Basic Equations for Simulation
   5.1 Importance of Time Variations
   5.2 Conventional
      5.2.1 Counting
      5.2.2 Remark on Quasi-Fermi Potentials or Levels
   5.3 Modified Basic Equations
      5.3.1 Modifications for Computer Solution
   5.4 Modifications Needed But Not Available
6. Areal Inhomogeneity and Multi-Dimensional Flow
7. Recommendations and Conclusions
8. References
9. Figure Captions
10. Figures

PRECEDING PAGE BLANK NOT FILMED

LIST OF SYMBOLS
NOT DEFINED IN TEXT

a	cutoff distance in derivation of energy-gap model
div	divergence operator
D	diffusivity or displacement flux density (context determines)
e	magnitude of electron charge
E	energy of electrons or electric field (context determines)
E'	kinetic energy of free carriers normalized by kT
E_G	energy gap
F	Fermi level
g	generation rate from external source (does not include thermal generation rate)
grad	gradient operator
kT	thermal energy
kT/e	thermal voltage
I	Fermi integral of order one half
j	convection current density, augmented by subscript N or P means electron or hole current density
m	rest mass of electron
m*	effective (or crystal) mass
N_{AA}	ionized acceptor atom concentration
N_C	effective density of states of conduction band
N_{DD}	ionized donor concentrations
n_i	intrinsic carrier concentration
n	electron concentration (also used as subscript)
p	hole concentration (also used as subscript)
T	absolute temperature
QDS(E)	quantum density of states
QFL	quasi-Fermi level
V	applied potential or internal potential (content determines)
v	total time-varying applied or internal potential
v_N	quasi-Fermi potential for free electrons, equals quasi-Fermi level for free electrons when multiplied by -e, prime denotes normalized with respect to thermal voltage, N subscript replaced by P subscript means hole quasi-Fermi potential
W	energy of bound electron in derivation of model for energy-gap narrowing
α	optical absorption coefficient
γ	kinetic energy of free electrons, normalized by kT
ΔE_G	energy-gap narrowing
ε	dielectric permittivity
λ	optical wavelength or screening length (context determines)
χ	electron affinity
ρ	space charge density
τ	recombination lifetime or relaxation time (when symbol is augmented)

1. INTRODUCTION

We survey the theoretical models now available that characterize heavily doped (highly conducting) regions in silicon and analytical and numerical approaches that try to determine the influence of such regions on the conversion efficiency of solar cells. Heavily doped regions are bounded by adjoining regions. As one example, a physical surface bounds the front surface. This physical surface may consist of a mixture of ohmic-contact metal with either an anti-relection coating or with a thermal or deposited oxide. As another example the adjoining surface may define a transition between heavily doped and more lightly doped silicon. The interplay between the heavily doped and adjoining regions constitutes a key to designs for improved performance. This will receive attention, as will the multi-dimensionality of variables such as current and mobile-carrier density.

Although dilutely doped silicon is well characterized except for some disagreement about optical absorption coefficients, what exists now for heavily doped silicon and its interplay with adjoining regions is an incomplete theory in which not all contributers to transport, recombination, generation, and trapping are defined. Further the parameters relating to these mechanisms and their values as determined by experiment are subject to various interpretations. The presentation will bear in mind these uncertainties and will treat the characterization of heavily doped silicon not as a theory but rather as an imperfectly articulated and incompletely formalized body of experience. This view is intended to help point the way toward the attainment of a more complete theory of heavily doped silicon and thereby toward more informed designs of solar cells. Because computer programs constitute tools both for design and for estimating performance limits, the review will include some remarks pertinent to existing and developing programs.

2. BASICS

Highly doped silicon differs fundamentally from silicon of dilute doping in several main respects.

2.1 Quantum

As the concentration of shallow impurity atoms increases, their ground-state orbitals begin to overlap (Fig. 1), resulting in a distorted quantum density of states which includes an impurity band (Fig. 2). From an experimental viewpoint, one sees the resulting metal-insulator (or Mott) transition occuring for common dopant species at about 10^{18} cm^{-3} (Fig. 3). The theoretical interpretation of Mott and Davies (1967) involves the warped quantum density of states shown in Fig. 4.

At concentrations above about 10^{19} cm^{-3}, the abundance of majority free carriers and the associated screening yields a quantum density of states that more closely approximates the standard dependence, QDS(E) $\propto \sqrt{\ }$(kinetic

energy), which applies for dilute concentrations of the impurity atoms. Experimental evidence supporting this conclusion comes from electronic specific heat and other observations (Keyes 1979) and (Shibib and Lindholm 1980).

The random component of the atomic potential introduced by the approximate random positions assumed by the impurity atoms in the host lattice results in band tails, as Lifshitz (1942) first notes. A portion of these band tails comprises bound quantum states where trapping of majority and minority carriers can occur.

Macroscopic lattice strain introduced by a high concentration of impurity atoms, and the accompanying structural imperfections, in principle can also influence the quantum density of states, mainly through changes in the energy gap.

Thus we conclude: (a) the warped quantum density of states at the lower end of the range of high doping concentrations may decidedly affect device performance, particularly near the edge of the p/n junction transition region and particularly if the device design emphasizes avoidance of high impurity concentrations, as in recent cell designs advanced by Green and Blakers, by Wolf, by Spitzer and co-workers, by Rohatgi and by others [1]; (b) the prevalence of a near standard quantum density of states for concentrations > 10^{19} cm^{-3} admits treatment of the majority carriers as a Fermi gas and associated simple screening models enter; (c) the existence of bound states near the minority-carrier band edge may introduce trapping as an important mechanism if many such states exist.

These conclusions receive attention in the sections that follow.

2.2 Statistics

Electrons (and holes) are fermions. Thus their distribution in energy is described by Fermi statistics. At low enough carrier concentrations, the Fermi function tends toward a Maxwell-Boltzmann function (Boltzmann statistics). Fermi statistics contain Boltzmann statistics. Thus there is no fundamental reason to argue the issue whether Botlzmann or Fermi statistics apply, as many workers have done. The answer is that Fermi statistics always apply. From a practical viewpoint, however, some need exists for further consideration. As one example, if past work has used Boltzmann statistics, correctly or incorrectly, as a vehicle for framing such experimental results as energy-gap narrowing ΔE_G, then one must take care in the introduction of Fermi statistics when using these results. If raw data exist, however, then one can use Fermi statistics to reframe the parameters of interest. Such a parameter is energy-gap narrowing and its dependence on impurity concentration. As

---

1) See the special issue of the IEEE Transactions Electron Devices, May 1984.

another example, one may wish to avoid Fermi statistics to obtain expressions that yield more easily to analytical or numerical treatment. For numerical solution of the finite-difference or finite-element counterparts of the basic differential equations, however, the availability of a variety of accurate approximations to the related Fermi integrals (Blakemore 1982) apparently makes this unnecessary.

As a fundamental point, one may remember that Fermi statistics always describe electrons or holes. This is not true for Boltzmann statistics which introduce considerable error if the majority-carrier density > 10^{18} cm^{-3}. Incorrect temperature dependence of variables may be one result of misuse of Boltzmann statistics. We would not belabor this issue if it had been discussed less in the literature.

Fermi statistics also describe the occupancy in equilibrium of bound states, such as those in band tails. But a difficulty enters here because the Fermi statistics must be altered to contain the degeneracy of the bound state. This degeneracy apparently is unknown for band tails. The same difficulty prevails, of course, if one uses Boltzmann statistics.

Finally we define explicitly the term, Fermi gas, used in Sec. 2.1. The concentration of such a gas is determined by the integral of the product of the standard Fermi function for delocalized states and the standard quantum density of state, $QDS \propto \sqrt{(\text{kinetic energy})}$. This integral, the Fermi integral to order one-half, will enter later into models for ΔE_G through the screening length of a Fermi gas.

3. HIGH CONCENTRATIONS

By high concentrations of shallow acceptor or donor states we mean > $10^{19}/cm^3$, approximately. For such concentrations, as suggested above, the quantum density of delocalized states of both conduction and valence bands obey,

$$QDS(E') \propto \sqrt{(E')}dE' \qquad (3.1)$$

where E' is the kinetic energy measured from the mobility edge of the band. For developments that follow, note that an electron, or hole, at this band edge has only potential energy, according to quantum theory. Thus the band edge corresponds to the energy reference for kinetic energy.

Thus the hole or electron concentration in thermal equilibrium is the integral, from the band edge to infinity, of the product of (3.1) and the standard Fermi-Dirac function. For the majority carriers this integral, the Fermi integral of order one-half, describes a Fermi gas. Because the Fermi function goes into a Boltzmann distribution for low particle concentrations, the Fermi gas becomes a Boltzmann gas for the minority carriers.

3.1 Fermi Level

The Fermi level F or Fermi potential of a Fermi gas follows from standard expansions (Kubo, 1966, p. 231); the Fermi level shows only a slight temperature dependence, which for terms up to the order T^4 is

$$F(T)/F(T = 0K) = 1 - (\pi^2/12)[kT/F(0)]^2 - (\pi^4/80)[kT/F(0)]^4 + \ldots \quad (3.1.1).$$

The weakness of this temperature dependence will prove useful in the discussion below concerning the energy gap, measured electrically.

3.2 Einstein Relation for Majority Carriers

For a position-dependent doping concentration, the principles of detailed balance requires oppositely directed majority-carrier drift and diffusion currents, equal in magnitude, for thermal equilibrium. This requirement, together with the position independence of F and with the association of a band edge with potential energy (discussed in regard to Eq. 3.1), establishes the slope of the majority-carrier band edge and hence the drift field acting on the majority carriers. The energy-gap narrowing $\Delta E_G(x)$ then determines the drift field (or quasi-field) acting on the minority carriers (Fig. 5). In general, the majority-carrier and minority-carrier fields differ in magnitude and may be opposite in sign. This has central importance in the analysis of the performance of devices.

Because of the balance, and for other reasons, the ratio of diffusivity D to mobility μ is significant. For the Boltzmann gas of the minority carriers,

$$D/\mu = kT/e \quad (3.2.1)$$

which is the standard Einstein relation of 1905. If trapping influences the transport of minority carriers, as later we shall suggest, the Einstein relation remains valid because trapping is spontaneous and random.

For majority carriers, the Einstein relation of the Fermi gas shows that D has a stronger dependence on particle density than does μ. Lindholm (1984) has suggested that this behavior originates in the kinetic pressure dependence of a Fermi gas, the gradient of which is related to the gradient of the chemical potential and hence to diffusion. For T = 300K, the dependence is shown in Fig. 6, first plotted by Lindholm and Ayers (1968). Landsberg (1952) first derived the D/μ relation for a Fermi gas as a ratio of Fermi integrals, a simple yet accurate approximation of which is due to Kroemer (1978).

3.3 NP Product if there is no Energy Gap Narrowing

The hole concentration product with the electron concentration for thermal equilibrium enters semiconductor device physics because excitations may often be assumed to provoke a small perturbation (quasi-equilibrium) of the equilibrium condition. Thus use of the PN product in equilibrium often yields a pre-exponential constant multiplying a term of the form, $\exp[V/(kT/e)] - 1$.

For a Boltzmann gas,

$$PN = n_i^2(T), \quad \text{(equilibrium)} \tag{3.3.1}$$

which is often called the law of mass action. For a Fermi gas, the PN product falls with increasing majority carrier density. Kleppinger (1970) first plotted this dependence (Fig. 7). Because

$$n_i^2 \propto \exp[-(E_G/kT)] \quad , \tag{3.3.2}$$

one might think that Fig. 7 implied an increase in energy gap as the majority carrier concentration increases. But the construction of Fig. 7 assumed independence of the energy gap on majority carrier concentration. Thus the result shown derives only from use of Fermi rather than the more familiar Boltzmann statistics.

Many previous workers have interpreted experimental results using Boltzmann statistics to deduce the carrier concentration dependence of the energy gap. Because of the dependence shown in Fig. 7, when a Fermi gas is used to describe majority carriers, larger energy-gap narrowing is inferred from experimental data. This partly explains the discrepancy between the results of Neugroschel, Pao, and Lindholm (1982) and those of many other workers. A related elaboration appears below.

3.4 Slope of Mobility Edge for Minority Carriers

We have discussed this issue above in Sec. 3.2, relating to the inequality between the drift fields acting on the majority and the minority carriers. For a diffused junction, for example, a huge drift field acts on the majority carriers. If this same field were to act on the minority carriers, those injected over the p/n junction barrier into the quasineutral emitter, or front layer, would be so significantly drifted back toward the junction transition region that the probability of reaching the surface would be low (Lindholm, Li and Sah, 1975). Experimental evidence indicates that such minority carriers reach the surface in great abundance where they vanish, if the front surface recombination velocity is high, without contributing to current in the external circuit (Iles and Sockloff, 1975), (Fossum, Lindholm and Shibib, 1979). The inequality of the majority-carrier and minority-carrier quasi fields helps explain this result.

3.5 Energy Gap

If we restrict consideration to donor or acceptor impurity atom concentrations high enough (Sec. 2.1) that a Fermi gas description becomes adequate, then an approximate model for the energy-gap narrowing ΔE_G as a function of majority-carrier concentration (n or p) emerges. The central parameter entering this model is the Debye or Thomas-Fermi screening length λ, as first suggested by Sah and collaborators (1981) and discussed systematically by Landsberg, Neugroschel, Lindholm and Sah (1984).

The model starts from the view that the highly doped semiconductor is, to some extent, a neutral dielectric continuum in which positive and negative particles are smeared out over macroscopic volume. This model continuum consists implicitly of particles in complicated and correlated motions, the correlation coming from the forces among the particles. The correlated motions of the actual many body problems incorporate the long-range part of the Coulomb forces between the electrons (assuming for concreteness n^+ silicon) and between them and other charges, both those fixed in the lattice (ions) and those that are mobile. The most significant forces are short-range which one can view as forces altered by screening of the many electrons. These forces one can characterize, with no additional approximation involved, as a screened potential, the relation being the equality between the gradient of the scalar potential and the vector force field. The introduction of the screened potential simplifies discussion, as will be seen.

We treat the screening length for this potential as a constant, which is an approximation (Landsberg, et. al., 1984). Then we consider the creation of an electron-hole pair, which at the first instant are in a bound state at $r = 0$, to fix the reference position. Then we imagine the hole to remain trapped and the electron to be removed to infinity against the screened Coulomb attraction. The total energy to create the pair, and to separate it, is (Fig. 9)

$$\text{ENERGY} \equiv W + (e^2/\varepsilon a)\exp(-\lambda a) \qquad (3.5.1)$$

where W is the energy required to create the pair in the bound state and the second term on the right side is the energy required to separate the pair. The sum of these two energies then yields a created **free** electron and **free** hole. Thus this sum is the energy gap,which depends on n and p through the screening length λ. The consequent energy gap narrowing, ENERGY(0,0) - ENERGY(n,p), illustrated in Fig. 9, depends only on $\lambda(n,p)$ because subtraction cancels W and the cut-off distance a (Landsberg et. al., 1984), which are regarded as concentration independent. The energy W is concentration independent because the model employed attributes energy-gap narrowing only to carrier screening.

The question remains as to the choice of λ, a parameter that enters many part of physics (Landsberg, 1981). Using Debye or Thomas-Fermi screening gives the same result in the limit of extreme degeneracy. The result, which in cgs units is

$$\Delta E_G = e^2\lambda/\varepsilon \quad , \qquad (3.5.2)$$

is a function of the effective mass of the majority carriers, ε, and n for n^+ silicon. If one assumes equality between the effective mass and the rest mass, $\varepsilon = 11.7$, one obtains

$$\Delta E_G = 215\ (10^{20}/n)^6\ \text{meV} \quad . \qquad (3.5.3)$$

This energy-gap narrowing exceeds that of Lanyon and Tuft (1979) who adopted a different screening model and used a different physical picture following the suggestion of Hauser (1969). The difference is a factor of 1.33.

We note the prediction of an energy-gap narrowing of 215 eV for a carrier concentration of $10^{20}/cm^3$.

For a general value of n, and for a parabolic band (Sec. 2.1), the energy gap becomes

$$\Delta E_G = (e^2/\varepsilon)\{[4\pi e^2/\varepsilon kT]\ N_C\ I(\gamma)\}^{1/2} \qquad (3.5.4)$$

where I is the Fermi integral of order one-half and γ is the kinetic energy of the electrons normalized by kT. If both holes and electrons are numerous, one need only add a similar Fermi integral for the holes multiplied by the effective density of states for the valence band.

This last formula we shall adopt for comparison with experiment. Though it applies for all levels of concentrations, we shall recall our previous discussions (particularly that of Sec. 2.2) emphasizing the inappropriateness of the assumed parabolic bands that underlie the origin of the Fermi integrals of order one half. Moreover, because of physics related to the cutoff distance a in (5.3.1), the expression holds with good accuracy only for concentrations up to $5 \times 10^{20}/cm^3$ (Landsberg, et al., 1984).

If we now compare with experiment (Fig. 10) obtained by electrical measurements, we note the excellent fit of this theory with the values obtained for Si:As by Neugroschel, Pao, and Lindholm (1982), (full circles), and for Si:B by Landsberg, Neugroschel, Pao, Lindholm and Sah (1984) (full triangles) by the same method. We note that the agreement is good only for majority carrier concentration $> 5 \times 10^{19}/cm^3$, as expected from the discussions of Sec. 2.1 and elsewhere above. In constructing Fig. 10, we have assumed for the experimental results in full circles and triangles an effective mass of electrons and holes that is a factor of 1.1 larger than the electron rest mass. The effective masses have uncertain values for highly doped silicon, though the assumption just stated agrees with the values usually advanced for the effective electron mass of dilutely doped silicon. In regard to most of the rest of the measurements of energy-gap narrowing in the literature, some of which are shown in Fig. 10 without explicit identification, Boltzmann statistics were used. We have recalculated these data so as to allow a fair comparison.

The agreement between the model above and the various experiments approaches the agreement between different experiments. The agreement tends to be better for larger concentrations, as expected (Sec. 2.1).

The experimental results of workers other than those mentioned are smaller than ours cited above. Apparently several reasons exist for this disagreement. In some of the work of others, the impurity concentration was or

may have been markedly dependent on position. Thus enters the effect of the quasi-field on the minority carriers (Sec. 3.4); moreover these workers used some spatial average of the impurity concentration. Another significant difference between the work referenced above and that of others involves assumptions about the minority carrier mobility μ. The energy-gap narrowing from electrical measurements pictured in Fig. 10 comes from the minority-carrier current, which depends on the product $\mu\exp(\Delta E_G/kT)$. Other workers have assumed an equality between the minority carrier and majority carrier mobility, which has the convenience that the majority carrier mobility is perhaps adequately known from conventional measurements. In contrast, in the work cited above, we assumed only a near temperature independence of μ and ΔE_G in a small range of temperatures near 300 K. This leads to evidence that μ is about one order of magnitude smaller than the majority carrier mobility for concentrations of about $10^{20}/cm^3$ in Si:As (Neugroschel and Lindholm, 1983). This contributes to the differences noted. Controversy about these issues exists, as evidenced by the communications exchanged between del Alamo and Swanson (1984) and Neugroschel and Lindholm (1984).

Figure 11 compares our model predictions (Eq. 5.3.4) with the recent 5 K photoluminescence and photoluminescence excitation data of Wagner (1984). At 5 K and for these doping concentrations, the effective masses for holes and electrons are unknown. Thus we introduce the noncommital symbol m^*/m for the effective mass ratio with the electron rest mass. For intrinsic silicon at 5 K, the ratio is about 1.06 (electrons) and 0.59 (holes). Using the temperature dependence implicit in our model above, we find that best agreement with Wagner's data occurs for $m^*/m = 0.45$ (Fig. 11).

3.6 Minority-Carrier Diffusivity and Mobility

Exploiting temperature dependencies, Neugroschel and Lindholm (1983) have presented evidence, as noted above, for a much lower minority-carrier mobility and diffusivity than that assumed previously. They obtained these results for Si:As having a doping concentration of about $10^{20}/cm^3$, for which a customary Fermi integral of order one-half was assumed to describe the majority electrons. This fixes the electron quasi-Fermi level approximately 100 meV in the conduction band above the band edge. In a simple physical picture advanced to explain these results, Neugroschel and Lindholm supposed the trapping of minority carriers at the bound states of band tails (or at acceptor states in the compensated n^+ silicon). Holes while trapped do not contribute to current of the hole Boltzmann gas. Thus for this mechanism to enter significantly, the characteristic time for thermal emission of a hole from a shallow bound state must be of the same order as the scattering time of holes within the valence band. Although band tails appear near both conduction and valence-band edges, trapping of the majority electrons is a negligible mechanism because the electrons contributing to curent lie near the Fermi level, about 100 meV away from the nearest band tail state. An illustration of the pertinent hole trapping appears in Fig. 12.

3.7 Trapping Model

To explore this mechanism from a theoretical viewpoint, it is useful to generalize the Boltzmann equation to include band-bound transitions. This generalization, discussed, for example, by Smith, Janak, and Adler (1967) and worked out in detail by Sah and Lindholm (1973), involves approximating the collision integral, for small departures from equilibrium, by the sum of two terms of the form, $(f - f_0)/\tau(\text{relaxation})$. This first term is the customary relaxation time approximation for the nonequilibrium distribution function f in which $\tau(\text{scattering}) = \tau(\text{relaxation})$ is the scattering time that characterizes intraband transitions. In the second term, $\tau(\text{trapping})$ instead appears, which characterizes the mean trapping time of holes for localized states near the valence-band edge. Thus $\tau(\text{trapping})$ enters into the description of the hole current and of $\mu(\text{holes})$, as described by Sah and Lindholm (1973). In principle, this enables detailed investigations of the trapping model and of the bound states of the minority-carrier band tails.

3.7 Other Parameters

Besides the functional dependencies of the energy-gap narrowing and the minority-carrier mobilities and diffusivities, emphasized in the preceding discussions, other parameters important for solar-cell analysis and design remain uncertain for silicon having donor or acceptor atom concentrations in the moderately high and high ranges. We point to the absorption coefficient $\alpha(\lambda)$, which has importance not only for the obvious reason of detailed calculation of photogeneration in the emitter or front layer. It also has importance in schemes for measuring other parameters. We have not touched on the lifetime in the volume of the heavily doped emitter and have referred only tangentially to the front surface recombination velocity. This is intentional, based on the assumption that other authors in the JPL Research Forum will focus on parameters relating to these mechanisms. In an extensive recent review of electrical current and carrier density in degenerate semiconductors, Marshak and van Vliet (1984) have emphasized the need for better knowledge of such parameters as the effective masses, dielectric permittivity ε, and electron affinity χ. We agree with their assessment, and refer the reader to their paper for details.

4. MODERATE CONCENTRATIONS

For impurity concentrations approximately $\sim 10^{18}/\text{cm}^3$, the metal-insulator transition implies that the majority-carrier quantum density of states will differ sharply from the standard dependence. This occurs partly because of the existence of impurity bands, according to the theory that interprets this transition.

Thus many aspects of the physical electronics become more difficult and less precise.

4.1 Fermi Level Saturation and Consequences

The severe warping of the quantum density of states from the rigid-band model (parabolic band) results in far less penetration of the Fermi level into the majority carrier band as the doping concentration increases. Indeed for a range of doping concentrations one may anticipate that the Fermi level nearly saturates. This leads to (a) a smaller energy-gap narrowing than interpretation of data on emitter recombination current by the rigid-band model would imply, and (b) a stronger quasi-field on the holes (minority carriers) that drifts holes toward the surface. This in turn yields a stronger dependence of emitter recombination current (and open-circuit voltage if emitter recombination current (and open-circuit voltage if emitter recombination current is important in a cell design on the front surface recombination velocity.

Figure 13 illustrates result (b) for a concentration of free electrons decreases in the n^+ silicon with x from its value at the surface (x=0).

4.2 Einstein Relation for the Majority Carriers

In its simplest derivation, the Einstein relation for D/μ derives from detailed balance between drift and diffusion tendencies in thermal equilibrium. Diffusion depends on the gradient of chemical potential, which is related to the kinetic pressure. The kinetic pressure of a Fermi gas having a non-standard band differs considerably from that for a standard band. Thus so also does the Einstein relation differ from that pictured in Sec. 3.2.

4.3 Einstein Relation for the Minority Carriers

The minority carriers are a Boltzmann gas, and the Einstein ratio is standard: $D/\mu = kT/e$.

4.4 Unsolved Problems and Consequences for Computer Simulation

These issues are treated in Sec. 5.3.

5. BASIC EQUATIONS FOR SIMULATION

The basic equations for analysis or for computer simulation follow from the foregoing discussion of the physics for high concentrations of impurities (Fermi gas for majority carriers). As the discussion has indicated, these equations involve approximations, especially for such parameters as energy-gap narrowing and the minority-carrier diffusivity and mobility. The approximation becomes more severe for the moderate range of dopings, between approximately 10^{18} to 10^{19} per cm^3, where impurity banding warps the quantum density of states for majority carriers from its standard dependence on energy. Thus the position of the Fermi level and consequently the quasi field for the majority carriers and the temperature dependence of these variables become more

uncertain than they are for the higher range of doping concentration. The Einstein ratio for the majority carriers, the energy-gap narrowing, and other quantum and transport paraemters also becomes less accurately known.

5.1 Importance of Time Variations

Although when delivering power a solar cell operates in the steady-state, time variations of the carrier concentrations, quasi-Fermi levels, potential, and particle current still have significance for several reasons. First, for example, many methods of measuring parameters such as lifetime τ involve either a transient or an $\exp(i\omega t)$ variation. As a second example, trapping of minority carriers at bound states in the band tails or at impurity states in compensated silicon may play a role in determining the minority-carrier diffusivity D and mobility μ. As a third example, inclusion of the full set of the Maxwell equations among the basic equations, when combined with phenomenological parameters such as ε, in principle yields reflection and transmission at the heavily doped surface.

5.2 Conventional Equations

In the absence of the effects indicated in the preceding sections that make the physical electronics of heavily doped silicon differ from the physical electronics of dilute silicon, the conventional equations are:

$$\partial n/\partial t = \mathrm{div}(j_N/-e) - R_n + g(\mathrm{external}) \tag{5.2.1}$$

$$\partial p/\partial t = \mathrm{div}(j_p/e) - R_p + g(\mathrm{external}) \tag{5.2.2}$$

$$j_N = e\mu_n E + eD_n \mathrm{grad}(n) \tag{5.2.3}$$

$$= -e\mu_N n \ \mathrm{grad}(v_N) \tag{5.2.3a}$$

$$j_p = e\mu_p E - eD_p \ \mathrm{grad}(p) \tag{5.2.4}$$

$$= -e\mu_p p \ \mathrm{grad}(v_p) \tag{5.2.4a}$$

$$\mathrm{div}(D) = \rho \tag{5.2.5}$$

$$= e(p - n + N_{DD} - N_{AA}) \tag{5.2.5a}$$

$$j = j_N + j_p + \partial D/\partial t \quad . \tag{5.2.6}$$

If recombination dominates, the removal rates, R_n and R_p become equal. For electrons and holes from quasineutral regions, this equality defines the lifetime τ: $(R \rightarrow \Delta n/\tau)$.

A seventh equation will describe, for the steady state, some assumed model for the recombination rate and hence the lifetime τ. Sah (1977) has expressed this equation in its most general form to unify impact-Auger, Shockley-Read-

Hall and other mechanisms. For greater generality, the kinetic rate equation for the time variation of particle density on traps (Sah 1971) supplements the equation of the steady state recombination rate. This then provides a quantitative characterization of the minority carrier diffusivity D and mobility μ when the trapping rate at bound states becomes comparable to the scattering rate within the minority carrier band (Sah and Lindholm, 1973), as discussed earlier. This equation, or equations, not given explicitly here, is numbered (5.2.7).

To these seven equations are added auxiliary relations to enable or aid solution.

$$\mathrm{div}(j + \partial D/\partial t) = 0 \qquad (5.2.8)$$

$$E = -\mathrm{grad}(V) \qquad (5.2.9)$$

$$E = D/\varepsilon \qquad (5.2.10)$$

$$n/n_i = \exp(v' - v'_N) \qquad (5.2.11)$$

$$p/n_i = \exp(v'_p - v') \qquad (5.2.12)$$

$$\text{diffusivity/mobility} = kT/e \quad . \qquad (5.2.13)$$

Here the primes denote normalization by the thermal voltage kT/e to yield a dimensionless variable. Eq. (5.2.8) assures the position independence of the total current, which becomes the position independence of convection current j for the steady state and $j \neq f(x)$ in a one-dimensional model. This relation simplifies analysis. Maxwell's other three equations are added, but not shown, for reasons given directly above.

We omit detailed discussion of the lifetime τ for heavily doped silicon, assuming that other authors in this Research Forum will provide this.

5.2.1 Counting

To assess the possibility of solution, we now count unknowns and equations. The first two equations, (5.2.1) and (5.2.2), the continuity equations for holes and electrons, introduce four unknowns: the electron and hole densities and current densities. The optical excitation determines the generation rate through a relation of the form,

$$g(\text{external}) \propto \int \exp[-\alpha(\lambda)x]d\lambda \quad , \qquad (5.2.14)$$

where the constant of proportionality depends on the fraction of the sunlight transmitted past the surface into the volume of the solar cell. For a given solar-cell design, g(external) is assumed known.

If we deal with the current densities as expressed in terms of drift and diffusion components, we introduce one more unknown: the electric field $E(x) = -\text{grad}[v(x)]$. Assuming ε is known in (5.2.10), (5.2.5a) then becomes Poisson's equation for $v(x)$, the fifth equation in five unknowns.

If we deal with the electron and hole currents expressed in terms of the gradient of their quasi-Fermi potentials, we have as unknowns, in the two current density and two continuity equations, the following: the hole and electron densities, and the hole and electron quasi-Fermi potentials, and the hole and electron current densities. This gives six unknowns in four equations. But (5.2.11) and (5.2.12) introduce only a single additional unknown, $v(x)$, the electric potential. Thus adding Poisson's equation, from combining (5.2.5a), (5.2.9) and (5.2.10), yields in principle a solvable set of equations.

The equations are nonlinear. To illustrate this, note that the product of n and $\text{grad}(-v(x))$ appears in the equation for the electron current density. But n and v are related through (5.2.5) when put in the form of Poisson's equation. Assuming analytic functions, one can express this relation by a Taylor series. Thus the equation for electron density involves a sum in which n, n^2, n^3, n^4, n^5 ... appear.

Because of nonlinearity, solution of the basic equations requires either approximations for special cases that yield analytic solutions or numerical solutions of the finite-difference or finite-element counterparts of the basic equations.

5.2.2 Remark on Quasi-Fermi Potentials or Levels

Solar cells must contain ohmic contacts to enable power delivery. An ohmic contact is a union between metal and semiconductor that allows electrons and holes to flow freely between the metal and the semiconductor. Hence, at the contact, electrons and holes can neither accumulate or become depleted, their densities stay at equilibrium values (assumed known), and the hole and electron quasi-Fermi levels converge to the Fermi level F. This implies that at an ohmic contact the merged quasi-Fermi levels in the semiconductor join the Fermi level in the metal without discontinuity. But the Fermi level at any point in a metal is the electric potential at that point. Thus the potential difference between two ohmic contacts in a solar cell or any semiconductor device equals the difference between the merged quasi-Fermi levels in the semiconductor at the two contacts.

As a result, a potential difference in an external circuit causes an equal potential difference in the quasi-Fermi levels at the two contacts. Hence use of the quasi-Fermi level description of hole and electron currents allows a simple introduction of the boundary conditions on electric potential. The alternate description in terms of drift and diffusion components requires satisfaction of the boundary conditions on potential by setting a line integral of the electric field through the semiconductor equal to the potential difference appearing at the terminals.

Advantages thus apparently result for numerical simulation. Moreover a preference for description in terms of quasi-Fermi levels enables a straightforward introduction of trapped particles at bound states in the forbidden gap. This is done by use of quasi-Fermi levels (or occupancy probabilities) for each of the bound states. If then one restricts attention first to variations in the potentials at the terminals and hence to variations in the quasi-Fermi potentials within the volume of the semiconductor device that are much smaller than the thermal voltage kT/e, the set of basic equations become linear. To these linear equations corresponds a electric circuit representation. That circuit representation often can be simplified by using the theory of electric circuits; for example, Y to Δ transformations can yield simplifications. Thus numerical solution of the finite difference equations becomes easier. To obtain solutions to the nonlinear equations, one simply adds the consequences of successive small-signal responses to potentials small relative to kT/e.

Sah has advanced and utilized computer algorithms related to those just described; for example, see Sah (1971) and Sah, et al. (1981).

5.3 Modified Basic Equations

We now consider the modifications needed to include the phenomena occuring in highly doped silicon treated in the foregoing sections. The reader may refer to Sec. 5.2 on the conventional basic equations, which we now modify.

The continuity equations remain intact; they serve the bookkeeping purpose of summing all contributors to changes in particle density with time.

Because carriers at the mobility edge have only potential energy, we see that the electric field E governing the drift component of the majority-carrier current becomes grad[mobility edge/-e]. This is the same relation prevailing in the conventioanl equations except that the mobility edge has replaced the band edge. If we take n^+ material for concreteness of discussion

$$E \rightarrow -\mathrm{grad}[E_C/-e] \quad , \tag{5.3.1}$$

where

$$\mathrm{grad}[E_C/-e] = \mathrm{grad}(v) + \mathrm{grad}(\chi/-e) \tag{5.3.2}$$

as in Sah and Lindholm (1977) and Marshak and van Vliet (1984).

Typically majority carrier concentrations will be perturbed only slightly in nonequilibrium; that is, the low-injection condition will prevail. Thus we anticipate a near position independence of the majority-carrier quasi-Fermi level, and we anticipate that the energy separating this quasi-Fermi level from the mobility edge for the majority-carrier band will remain as in equilibrium, to a good approximation. Thus the left side of (5.3.2) will be determined; the right side will become unimportant to the majority-carrier drift component.

For a Fermi gas (parabolic band), the diffusion component of the majority carriers remains intact; the D/μ ratio reflects the Fermi statistics, as discussed in Sec. 3.2. For a moderately doped region, we have emphasized the warping of the quantum density of states, in accord with the metal-insulator transition. The diffusion current then depends on the random force (Prigogine, 1980) or kinetic pressure appropriate to this quantum density of states. To account for this the diffusion component of the majority carrier current, a term involving a gradient in addition to the gradient of n appears (Marshak and van Vliet, 1984).

We note that these complications concerning the majority-carrier diffusion current vanish if one deals with (5.2.3a) in which this current is simply the electron conductivity times the gradient of the electron quasi-Fermi potential (electrochemical potential). The electrochemical potential is a basic thermodynamic variable whose gradient is linear in the particle current except for large deviations from equilibrium. The vanishing of the complications referred to is only apparent, however, because they will reappear in the relation between the quasi-Fermi levels and the particle densities, as we shall soon see.

Equation (5.3.1), for the majority carriers, relates to the drift component of hole current (minority current) through

$$\mathrm{grad}[E_V/-e] = \mathrm{grad}[E_G'/-e] - \mathrm{grad}[E_C/-e] \quad . \qquad (5.3.3)$$

The product of this gradient (left side) times the hole conductivity determines the hole drift current (minority-carrier drift current) in terms of the gradient of the majority-carrier mobility edge (known through Eq. (5.3.1)) and the energy gap dependence, assumed known through the model of Sec. 3.5 or through experimental determination.

If we assume that the band tails of the minority-carrier band are mainly bound states, the hole (minority-carrier) current is the conventional sum of drift and diffusion components, with $D/\mu = kT/e$, for a Boltzmann gas.

Thus the conventional description for the minority-carrier current survives except that the gradient of the quasi-field, influenced by the gradient of the energy gap, replaces the conventional electric field. This replacement has key importance, as we have emphasized earlier. But the survival of a simple description of the minority-carrier current permits, for the quasi-neutral emitter, many approximations that give simple relations for the quasineutral emitter recombination current. Examples include the transparent-emitter model of Shibib, Lindholm, and Therez (1979) extended by del Alamo and Swanson (1984), the field-free model introduced by Fossum, Lindholm, and Shibib (1979), etc.

5.3.1 Modifications for Computer Solution

Having just discussed anlaytic solutions for the qusineutral regions, we now turn attention again to contact-to-contact computer solution by finite-difference or equivalent formulations of the basic equations.

Consider Poisson's equation, resulting from combining (5.2.5a) with (5.2.9) and (5.2.10). The key issue becomes the relation of potential v(x) to n(x)and p(x) in view of (5 3.2). Consideration that p and n are proportional to integrals of the form, $\int$[QDS(E)](probability(E,QFL)]dE, will show an asymmetry in the expressions for n and p not present in the standard relations (5.2.11) and (5.2.12). This occurs because the probability function in the integral will be Fermi-Dirac form for electrons (majority carriers) and Boltzmann form for holes, and because the QDS may contain the effects of impurity banding for the electrons but not for the holes. In principle, knowledge of the QDS for both bands will permit replacing the standard relation by

$$n = A\ f[(E_C/-e) - v_N] \qquad (5.3.1.1)$$

$$p = B\ f^*[v_p - (E_V/-e)] \quad . \qquad (5.3.1.2)$$

These are the most general relations. If we assume that the bandtail states of the minority band are localized, f* becomes an expontial function and B becomes the standard density of states for the valence band. If, for highly doped semiconductors, we assume impurity-banding effects are negligible, f becomes the Fermi integral of order one-half and A becomes the standard density of states for the conduction band (we allow for a deviation of the effective mass from its standard value). Otherwise f, f*, A, and B become determined by the integral indicated above, and are known only if QDS is known.

To these two equations, we add seven more to yield ten equations in ten unknowns, suitable for finite-difference, contact-to-contact computer solution:

$$\partial n/\partial t = -\mathrm{div}(j_N/-e) - R(n,p) + g(\mathrm{external}) \qquad (5.3.1.3)$$

$$\partial p/\partial t = -\mathrm{div}(j_p/e) - R(n,p) + g(\mathrm{external}) \qquad (5.3.1.4)$$

$$j_N = -e\mu_n n\ \mathrm{grad}(v_N) \qquad (5.3.1.5)$$

$$j_p = -e\mu_p\ p\ \mathrm{grad}(v_p) \qquad (5.3.1.6)$$

$$\nabla^2 v = -(e/\varepsilon)[p - n + N_{DD} - N_{AA} \pm \Sigma\ \mathrm{trapped\ particles}] \qquad (5.3.1.7)$$

$$E_c - E_v = E_G \quad , \quad \mathrm{grad}(E_c) - \mathrm{grad}(E_v) = \mathrm{grad}(E_G) \qquad (5.3.1.8)$$

$$\mathrm{grad}(E_c/-e) = \mathrm{grad}v + \mathrm{grad}(\chi/-e) \qquad (5.3.1.9)$$

$$j = j_N + j_p + \partial D/\partial t \quad , \quad D = \varepsilon E \quad , \quad E = -\mathrm{grad}(v) \quad . \qquad (5.3.1.10)$$

These equations are basic for exact computer simulation. Apparently they have not appeared as the identified basic set before, though Marshak and van Vliet (1984) discuss many relevant issues.

The equations require knowledge of many parameters such as energy-gap narrowing, minority-carrier mobility, and charged bound states. The last of these will be most important near the metallurgical junction for low forward voltage. They require also knowledge of the position dependence of the electron affinity $\chi(x)$, which apparently has received little attention, and of the quantum density of states of the majority-carrier band for moderately high concentrations (roughly $\sim 10^{18}/cm^3$) which has received most attention for the metal-insulator transition at approximately 4K.

Approximations simplify the basic equations for the quasi-neutral emitter. Just below (5.3.2) we noted that the gradient of the majority-carrier mobility edge is known, partly because of the position independence of the majority-carrier quasi-Fermi level. In the quasi-neutral emitter, low injection implies that the dependence of electric potential $v(x)$ will remain to a good approximation as it was in equalibrium. Thus Poisson's equation and the resulting entry of $\chi(v)$ can be ignored for the quasineutral emitter. This simplified computer solution. This adds emphasis, however, to a need for precise determination of the edge of the quasineutral emitter.

6. AREAL INHOMOGENEITY AND MULTIDIMENSIONAL FLOW

Apparently all detailed analyses of the highly doped emitter of silicon solar cells are based on a one-dimensional model. But the emitter surface in the best solar cells will be a mixture of ohmic-contact metal ($S \sim 10^7$ cm/s) and of a surface passivated over perhaps 95% of the area by thermal oxides or other methods that reduce the surface recombination velocity S there to orders of magnitude below 10^7 cm/s.

At least two cases of relevance exist. If the emitter is doped in the moderately high doped range ($\sim 10^{18}/cm^3$) to avoid the so-called degrading heavy-doping effects, then the relatively long diffusion lengths in this region will lead to three-dimensional minority-carrier flow. The ohmic contact metal will so reduce the minority carrier density that large minority-carrier concentration gradients will exist. Even if the design includes an n//metal contact system, partly with the motive of providing an n/n^+ low/high junction to ward minority carriers away from the ohmic contact while permitting the majority carriers to pass by the usual dielectric relaxation mechanism, this will likely not work. Because of energy gap narrowing on the n^+ side, no significant barrier in the energy band can exist at the n/n^+ junction when the doping concentration of the n side is of the order of $10^{18}/cm^3$. Thus three dimensional flow enters, and the open-circuit voltage decreases as a consequence.

In the other case, the design includes n^+ silicon over the great majority of the emitter volume. Then the diffusion length of minority carriers in the emitter will be short enough to admit estimates by neglecting three- or two-dimensional flow. In the resulting model, one-dimensional flow prevails. But over the 5% of the area covered by the ohmic contact the diode there will have a high reverse saturation current, resulting from vanishing of minority carriers at the surface. Over the remaining 95% of the area, the reverse saturation current will be much smaller because of the low S over that area. Thus, in good designs in which the recombination current of the quasineutral base is small enough that the emitter enters significantly into determining the open-circuit voltage and the efficiency, the importance of a relatively bad diode over 5% of the area becomes potentially important.

Lindholm, Mazer, Davis and Arreola (1980) have considered this issue quantitatively. The result, for their type 1 areal inhomogeneity pertinent to this discussion, is that 5% of ohmic contact metal gives performances that nearly approaches that of a solar cell for which no thermal oxide is present to passivate the front surface. This is not seen experimentally. Perhaps the reaons for this lies in the quasi-fields and in the low D and μ treated in earlier sections. Thus the work of Lindholm, et al. (1980) needs updating to help toward informed design. This updating will help decide whether decreasing ohmic contact area can lead to high efficiencies in already highly efficient silicon solar cells.

Note that the issue here is not metal shading of the incident light. Rather it is the fraction of the surface area that is covered by ohmic contact.

7. CONCLUSIONS AND RECOMMENDATIONS

The main findings discussed here are:

(a) The quantum density of states for moderately doped silicon (approximately in the range 5×10^{17} to $10^{19}/cm^3$, deviates sharply from the standard quadratic dependence on kinetic energy. This can lead to pinning of the majority-carrier quasi-Fermi level and produce thereby, for a position-dependent impurity concentration, a quasi field on the minority carriers that drifts them toward the surface. The modeling of many pertinent variables in this moderate concentration range is incomplete, although other workers, particularly Slotboom and deGraaf (1975), have emphasized this doping range. The incompleteness results from the model they and others have used, which combined Boltzmann statistics with an implicit quadratic relation between the quantum density of band states and the free-carrier kinetic energy. The metal-insulator transition dramatically illustrates the inadequacy of this quantum density of states for moderate doping concentrations. As a potential benefit, note that the long and continuing interest in the metal-insulator transition, both experimental and theoretical, provides clues for the modeling of this range of moderate doping concentrations.

(b) For higher doping concentration, experimental evidence suggests the adequacy of describing the majority carriers by a Fermi gas, that is, by a Fermi integral of order one-half. This admits use of a majority-carrier screening model, which, though much less ambitious than the many-particle computations that have and are emerging, gives simple theoretical dependencies of energy-gap narrowing on impurity concentration and temperature. These dependencies agree favorably with the experimental results on energy-gap narrowing of several different groups of workers. Compared with the many-particle model, the carrier-screening model has the virtues of simplicity and of yielding an analytic expression. This carrier-screening model in its earliest form ((Sah, Chan, Wang, Sah, Yamakawa, and Lutwak) 1981) and in its more detailed form (Landsberg, Neugroschel, Lindholm, and Sah, 1984) differs substantively from earlier carrier-screening models (Hauser, 1969), (Lanyon and Tuft, 1979).

(c) The randomness of the atomic potential contributed by the assumed random positioning of the impurity atoms leads to the formation of tails on both the conduction and valence bands. The characteristic time associated with trapping at localized states in the tail adjoining the minority-carrier band may involve a mechanism that contributes to low minority-carrier diffusivity and mobility of the Boltzmann gas describing the minority carriers. Experimental evidence exists to support this conclusion (Neugroschel and Lindholm, 1983), although contrary suggestions appear in the literature. Computer simulation of solar-cell performance requires detailed knowledge of minority-carrier diffusivity and mobility just as much as it requires such knowledge of the energy-gap narrowing. Moreover, experimental interpretation involving electrical response also requires such knowledge.

(d) The optical absorption coefficient $\alpha(\lambda)$ in moderately and highly doped silicon is highly uncertain; apparently it is also uncertain for silicon having dilute doping concentrations. Because the absorption coeffient provides suggestions about the energy-momentum relation of heavily doped silicon, it has fundamental importance to the unravelling of the detailed transport and optical properties of the material. This use we view as more significant than is the moderate need for knowing $\alpha(\lambda)$ for detailed computer simulation of solar-cell performance parameters.

(e) The results of simple models for a heavily doped region containing ohmic contacts mixed with thermal oxide suggests that the one-dimensional model conventionally used may not accurately predict the performance parameters of the emitter region, particularly the open-circuit voltage. Other sources of areal inhomogeneity also exist, such as impurity clustering (.... 1984).

(f) The basic equations for computer simulation of solar cells containing heavily doped silicon require inclusion of all of the effects described above. Present computer programs are based on equations that fall short of the status aimed for by this recommendation. Continual updating is needed as experiment and theory reveal more about the dependence of transport and quantum parameters on doping concentration, chemical species, temperature, etc. The

most severe need exists at the moderately high doping concentrations defined above. There the conventional treatment as a Fermi or Boltzmann gas fails.

(g) In their greatest generality, the basic equations for the simulation of solar-performance must include time variations. This need arises particularly because time variations of response exist in many measurements used to determine parameters. For greatest generality, one may add the Maxwell's equations to the customary continuity and current equations. Maxwell's equations admit the view of light as a wave phenomenon; when combined with the phenomenological material paramaters normally introduced, reflection and transmission results. (Absorption and the optical generation rate in the continuity equations involve, at least fundamentally, the particle model of light as incident photons that produce quantum transitions between the bands or to bound states in the forbidden bands.)

(h) The basic equations include a kinetic equation of the time-rate change of occupancy at a bound state resulting from transitions from band states. This kinetic equation, emphasized by Sah (1971), is absent in most formulations of the basic equations for computer simulation. It enters markedly into such issues as the detailed modeling of minority-carrier mobility and diffusivity, discussed above. For the steady state inclusion of trap occupancy in the Poisson equation is highly important near the metallurgical p/n junction, where the donor and acceptor dopant concentrations nearly cancel (Lindholm and Sah, 1977). It is important also for work aiming toward high conversion efficiency using relatively thin and inexpensive silicon, such as that deriving from the WEB process. Most computer programs neglect the trapping mechnaism, even in the steady state. The notable exception appears to be the computer simulations of Sah and co-workers (1981).

(i) The recent work of Neugroschel and Lindholm (1983) on low mobility and diffusivity of minority carriers in Si:As of doping concentration about $10^{20}/cm^3$ suggests a novel method of protection from surface recombination at both the front and back surfaces. These arise from the possibility of significant gradients in minority-carrier D and μ provoked by very highly doped silicon ($\sim 10^{21}/cm^3$ or above) in thin layers (~500 Å or less) near the surfaces. The work now evolving in non-equilibrium growth following eximer laser radiation (and melting) may provide a method of sealing the surfaces against minority-carrier loss. This sealing might occur despite the large impact Auger recombination rates in such n^{++} or p^{++} silicon. Experiment will decide this. The issue is the inhibiting of flow by the gradients of D and μ versus the opposing effects of energy-gap narrowing and Auger recombination. As one aspect of the issue, we may expect that the Auger recombination, if band-band, will have a rate that is proportional to n^2 (for n-type material) whereas the gradients in minority-carrier D and μ may have sufficient strength to offset this n^2 dependence by warding minority carriers away from the volume of the n^{++} region. We note that nothing is known of the physical electronics of n^{++} or p^{++} silicon, as defined above. Essentially no detailed experimental data are available about the physical electronics, and the model for energy-gap narrowing of Sec. 3.5 does not apply for concentrations greater than about 5 x $10^{20}/cm^3$, according to Landsberg, et al. (1984).

(j) From the discussion in Sec. 5.3.1, it follows that apparently the formulation of the basic equations for finite-differenct computer solutions from contact to contact remains far from complete. By this we mean to suggest that apparently computer programs now developed cannot accomodate important aspects of heavily doped silicon that physical theory and experimental studies have identified and in the future may yield values of relevant parameters.

8. REFERENCES

Blakemore, J. S., 1982, Solid-State Electronics, 25, 1067.

del Alamo, J. A., and R. M. Swanson, 1984, IEEE Trans. Electron Devices, 31, 123; Reply by A. Neugroschel and F. A. Lindholm. ibid, p. 124.

del Alamo, J. and R. M. Swanson, 1984, Proc. 18th Photovoltaic Conf., Orlando, FL.

Fritzsche, H., 1979, The Metal-Nonmetal Transitions in Disordered Systems, Proc. 19th Scottish Summer School in Physics.

Fossum, J. G., F. A. Lindholm, and M. A. Shibib, 1979, IEEE Trans. Electron Devices, 26,165.

Hauser, J. R., 1969, NSF Final Report.

Iles, P. and I. Sockloff, 1976, NASA Final Report.

Keyes, R. W., 1979, Solid-State Communications, 32, 179.

Keyes, R. W., 1981, Comments Solid State Phys., 10,23.

Kleppinger, D. D., 1970, An extension of the engineering theory of semiconductors,with applications, Ph.D. dissertation, University of Florida, Ch. 2.

Kubo, R., 1971, Statistical Mechanics: An Advanced Course with Problems and Solutions (North-Holland, Amsterdam, London).

Landsberg, P. T., 1952, Proc. R. Soc. London, Ser. A, 213, 226.

Landsberg, P. T., 1981, Europ. J. Phys., 2, 213.

Landsberg, P. T., A. Neugroschel, F. A. Lindholm, and C. T. Sah, 1984, Proc. 18th Photovoltaic Specialists Conf., Orlando, FL, IEEE, New York.

Lanyon, H. P. D. and R. A. Tuft, 1979, IEEE Trans. Electron Devices, 26, 1014.

Lifshitz, I. M., 1941, J. Exp. Theor. Phys., 2, 117, 137, 156.

Lindholm, F. A. and R. W. Ayers, 1968, Proc. IEEE, 56, 371.

Lindholm, F. A., S. S. Li, and C. T. Sah, 1975, Proc. 11th Photovoltaic Specialists' Conf., Phoenix, AZ, 32, IEEE, New York.

Lindholm, F. A. and C. T. Sah, 1977, IEEE Trans. Electron Devices.

Lindholm, F. A., J. A. Mazer, J. R. Davis, and J. I. Arreolla, 1980, Solid-State Electron., 23, 967.

Lindholm, F. A., 1984, Solar Cells, 12, 131.

Marshak, A. H., and C. M. van Vliet, 1984, Proc. IEEE, 72, 148.

Mott, N. F., 1949, Proc. Phys. Soc. (London), 62, 416.

Mott, N. F. and W. D. Twose, 1961, Adv. Phys., 10, 107.

Mott, N. F. and E. A. Davis, 1971, Electronic Processes in Non-Crystalline Solids (Clarendon,Oxford).

Neugroschel, A. and F. A. Lindholm, 1983, Appl. Phys. Lett., 42, 176.

Prigogine, I., 1980, From Being to Becoming: Time and Complexity in the Physical Sciences (Freeman, San Francisco).

Sah, C. T., 1971, Physica Status Solidi (a), 7, 541.

Sah, C. T. and F. A. Lindholm, 1973, Solid-State Electron., 16, 1447.

Sah, C. T., 1977, IEEE Trans. Electron Devices, 24, 410.

Sah, C. T., 1977, IEEE Trans. Electron Devices, 24, 358.

Sah. C. T., P. C. Chan, A. C. Wang, R. L. Y. Sah, K. A. Yamakawa and R. Lutwak, 1981, IEEE Trans. Electron Devices, 28, 304; also see references therein.

Shibib, M. A., F. A. Lindholm, and F. Therez, 1979, IEEE Trans. Electron Devices, 26, 959.

Shibib, M. A. and F. A. Lindholm, 1980, IEEE Trans. Electron Devices, 27, 1304.

Slotboom, J. and H. de Graaf, 1975, Int. Electron Devices Meeting; also Solid-State Electron., 29, 857.

9. FIGURE CAPTIONS

Fig. 1 Overlapping impurity states give rise to

Fig. 2 impurity band in the energy gap.

Fig. 3 The resistivity ρ in Ω cm at 4·2K of Si:P plotted as a function of donor concentration (Alexander and Holcomb, 1968).

Fig. 4 Density of states for an electron in an n-type semiconductor showing the splitting of the impurity band into the ε_3 band (a), and the ε_2 band (b). (c) is the conduction band.

Fig. 5 Illustrating that grad(E_v $\neq$ grad(E_c) in the n^+ emitter. The conduction- and valence-band edges, $E_C(x)$ and $E_V(x)$, are mobility edges, the boundaries between localized and delocalized states; $E_G(x)$ is the mobility gap where disorder exists.

Fig. 6 The Einstein diffusivity-to-mobility ratio for majority carriers, under the assumption of a square root dependence of the quantum density of states on the majority carrier kinetic energy.

Fig. 7 The equilibrium product of the hole concentration P and the electron concentration N normalized by the standard square of the intrinsic concentration as a function of the reduced Fermi level, under the constraints of no energy gap narrowing and a square root dependence of the quantum density of states on the majority carrier kinetic energy. The increasing values on the abscissa correspond to increasing dopant concentration.

Fig. 8 Not present in manuscript (because of oversight).

Fig. 9 Schematic diagram showing the decomposition of the band-gap energy into W and the work done against attraction. More carriers are assumed present for curve 1 than for curve 2.

Fig. 10 Gap shrinkage ΔE_G as inferred from transport measurements for n-type layers from various sources at a mean temperature of ~ 340 K. The upper curve is for m^*/m = 1.45, the lower curve is for m^*/m = 1.10, and ε = 11.7 (Si) has also been used. The horizontal axis is the majority carrier concentration.

Fig. 11 Comparision with recent optical data at 5 K.

Fig. 12 Qualitative illustration of the band edges of heavily doped n^+-silicon. The broken lines show the unperturbed parabolic bands. The positions of both the electron and hole quasi-Fermi levels is also indicated. The arrows near E_V indicate hole capture and emission by

the tail states and by the acceptor level from the p-type substrates. The penegration of the tail states into the forbidden gap is assumed to be very small in comparison with the bandgap $E_G = E_C - E_V$.

Fig. 13 The band edges for the n^+ silicon in which the donor dopant concentration decreases sharply with x (x = 0 is the surface). - - -, band edges corresponding to the rigid band model (these illustrate a deep penetration of the Fermi level and a modest force field (nearly zero) acting on the holes); ———, band edges corresponding to a majority carrier quantum density of states warped relative to that of the rigid band model (these illustrate Fermi level saturation and a consequent strong force field drifting holes toward the surface).

ORIGINAL PAGE IS
OF POOR QUALITY

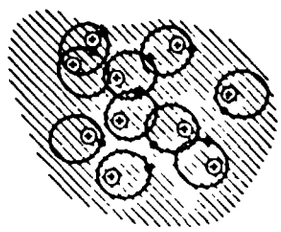

Fig. 1

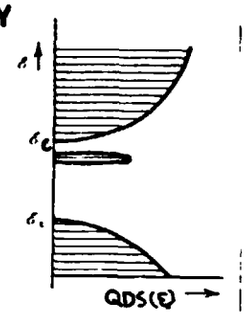

Fig. 2

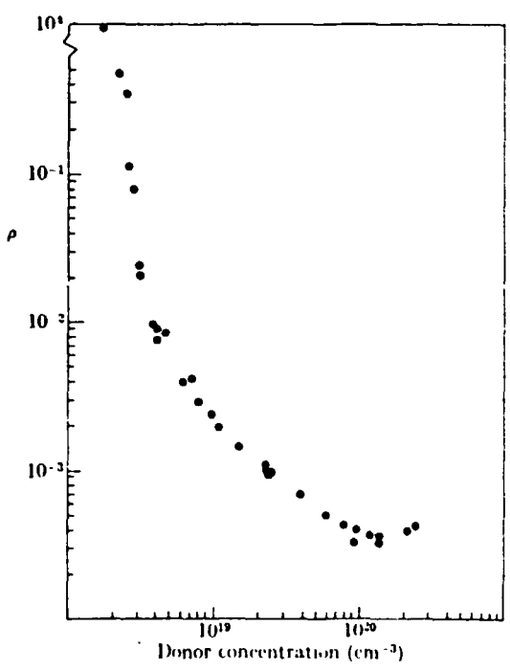

Fig. 3

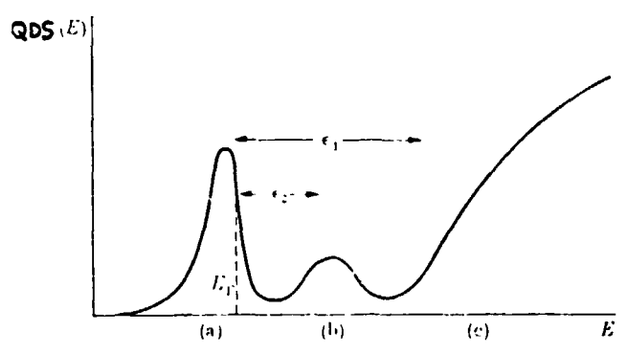

Fig. 4

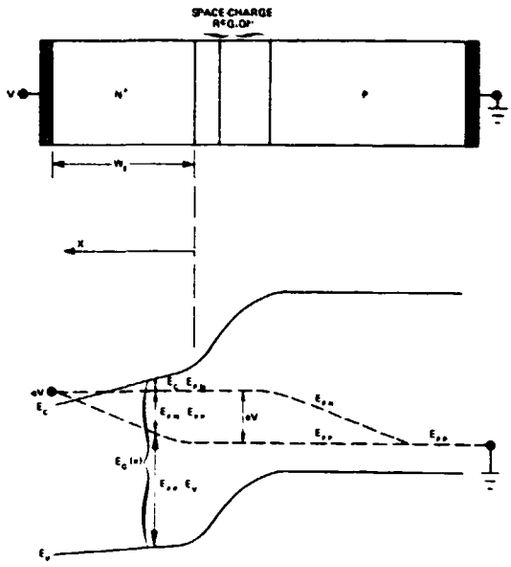
SPACE CHARGE
V
N+
P
x
eV

Fig. 5

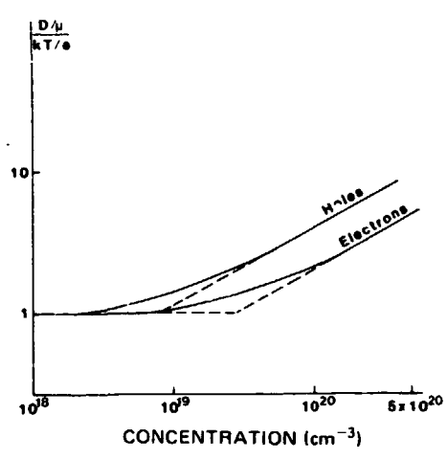
D/μ
kT/e
10
1
Holes
Electrons
10^18
10^19
10^20
5x10^20
CONCENTRATION (cm^-3)

Fig. 6

ORIGINAL PAGE IS
OF POOR QUALITY

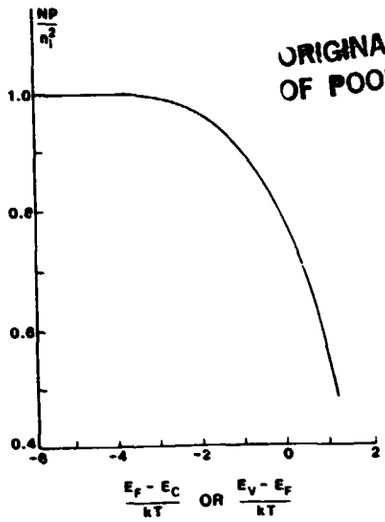

Fig. 7

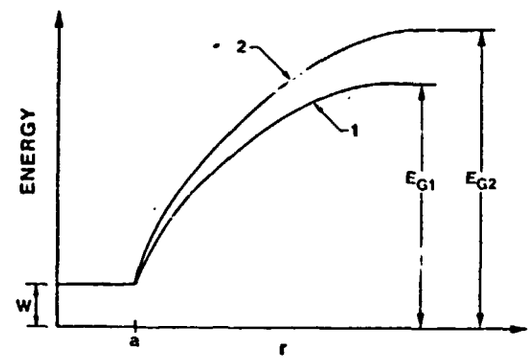

Fig. 9

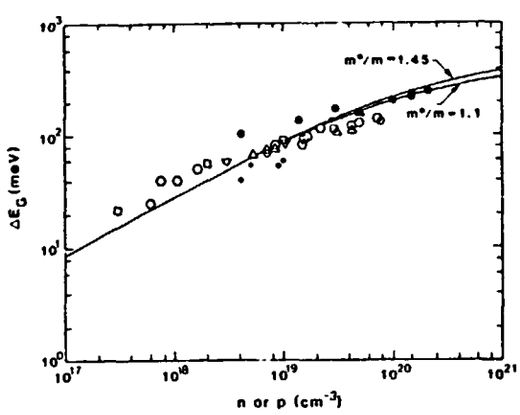

Fig. 10

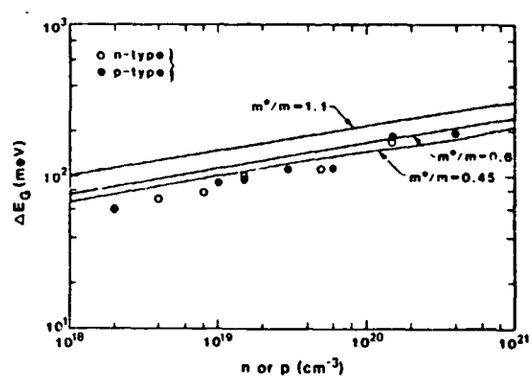

Fig. 11

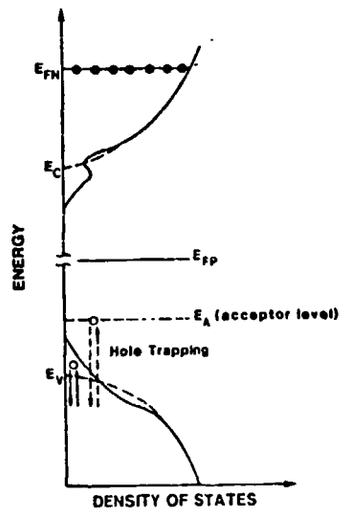
E_{FN}
E_C
ENERGY
E_{FP}
E_A (acceptor level)
Hole Trapping
E_V
DENSITY OF STATES

Fig. 12

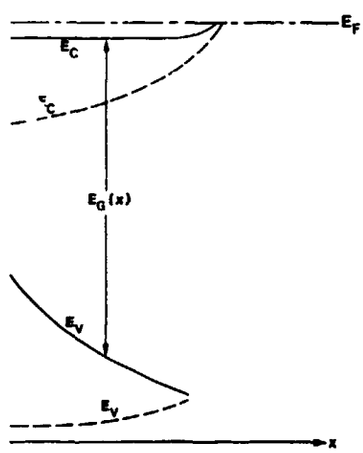
E_F
E_C
E_C
$E_G(x)$
E_V
E_V
x

Fig. 13

DISCUSSION

QUESTION: Fred, I just have a couple of simple questions. You talk about the definition of the ohmic contact. Have we seen any such ohmic contacts?

LINDHOLM: Yes, I think in Martin Green's cell contact, the tunneling junction has a hetrojunction such that there is a blocking barrier for the holes in the end-type material, yet the electrons tunnel freely into the conduction band of the metal. That would be one example. Another place -- I might just mention a very good book on contacts, which is called Photoconductivity and Allied Problems, by Albert Rose, is very good, because it is so thin. I think we should think a lot about contacts.

QUESTION: Some 30 years ago, when the effort was solving the junction equations, I worked with a mathematical physicist named Paul Wise. His opinion, unshakably, was that the quasi-Fermi level was a mathematical artifact. In other words, if your carrier concentrations were constant then you could say, yes, quasi-Fermi level was constant; if they weren't, they weren't. Rather than give a physical significance and work from there, he insisted that you just can't use it. I haven't followed the literature since then. I'm wondering if he is wrong?

LINDHOLM: Yes, he is completely wrong. The electrochemical potentials are basic thermodynamic variables. This question was asked of Peter Landsberg in a heavy-doping workshop some time ago, and I remember his answer. The electric potential we all know about; if you look in any book on the theory of heat or thermodynamics you'll find the chemical potential. And it's the algebraic sum of the two. So there's no problem, except with your friend. Oldwig (von Roos) said only in local thermal equilibrium, and it is true that the linearity between the current and the gradient and the quasi-Fermi level will not work if you have extraordinary variations in the quasi-Fermi level, but that's not surprising, because linearity -- as we know -- only applies for small perturbations, anyway. On the other hand, small perturbations can be very large currents of the sort we get with 1,000 suns with no problem at all.

SCHMIDT: You still believe in the rigid band approximation?

LINDHOLM: No, I don't. Only for doping concentrations above, say, 5×10^{19} to 10^{20} it is pretty good. Except the band edges on the minority carrier bands would be important there, even for the high doping concentrations.

SCHMIDT: You mentioned a variable electron affinity and if it affects the forces acting on carriers. Now the electron affinity is very little known, so that's a problem. However, I found some time ago that if you have low-level injection conditions and you have a variable chemical composition or doping or other facts, then the force on minority carrier is strictly the gradient of the band gap. Plus, of course, the potential force.

LINDHOLM: That is absolutely correct.

SCHMIDT: So there is no influence of the electron affinity?

LINDHOLM: This is absolutely true in low injection, and other workers have found that also and have published it. However, the low injection implies that you have a minority carrier, and that implies that you are in a quasi-neutral region. So when you get out of a quasi-neutral region and get into what people call a depletion region -- which I don't like to call it, I like to call it junction-transition region or space-charge region -- then if the gradient in the electron affinity is present, then it will introduce an effect. I can discuss that with you with this very simple picture. You probably know that anyway.

SCHMIDT: With this background, I like the way you deduced your points and you came to some conclusions. And just to make a test of it, my question is: do you question the present ideas about the Auger recombination correlated with the concentrations of certain dopants? Because, for a practical person, this is an extremely important thing. We had not been sure up to now: the correlations that you often had seen, up to the present time, of carrier concentrations or doping concentrations and the boundary of Auger recombination seem to be, let's call it, rigid. Do you think, from your point of view now, that that can be questioned?

LINDHOLM: Yes. I'm heavily opinionated on this issue also. My opinion is that the Auger coefficients are open to question. Since there has been a single experiment done at rather high doping concentration, and some of these other things I have talked about could influence these things. I would say on a theoretical level that the primary person who has worked on the theory of those Auger combinations is Peter Landsberg. And his physics is impeccable, but it involves many, many approximations. So he can only give us an estimate. So we will have to find the results from experiment, and I think it's an open question. Mainly when people talk about Auger recombination, they think about band-to-band Auger recombination but, as you know -- you have pointed out in your talks -- there are many recombination states in a diffused junction and, therefore, the Auger process may be extremely important, and that should not be overlooked. And that is only estimated, as far as I know, from a theoretical viewpoint, and by Peter Landsberg and Robbins first. You bring attention to a very important point.

SCHMIDT: I think you may have sensed why I asked you that question. For somebody who is responsible to prepare semiconductors, it is extremely important to know what kind of doping level could be tolerated and still make good solar cells.

LINDHOLM: That's an excellent point. The band-to-band Auger process gives you an ultimate upper bound. For higher doping concentrations, certainly the band-to-band Auger recombination gives you an upper bound. That needs to be looked at carefully, and experimentally, again.

SCHMIDT: Do you think that the situation may be changing again in case you have a highly counter-doped material?

LINDHOLM: Could be.

SESSION VI

HIGH-EFFICIENCY DEVICE PROCESSING

P. Rai-Choudhury,
Chairman

N85-31639

HIGH EFFICIENCY LARGE AREA POLYSILICON SOLAR CELLS†

S.M. Johnson and C. Winter*

Solarex Corporation, Rockville, Maryland 20850

ABSTRACT

Large area ($100cm^2$) polysilicon solar cells having efficiencies of up to 14.1% ($100mW/cm^2$, 25°C) were fabricated and a detailed analysis was performed to identify the efficiency loss mechanisms. The I-V characteristics of the best cell were dominated by recombination in the quasi-neutral base due to the combination of minority carrier diffusion length and base resistivity. An analysis of the microstructural defects present in the material and their effect on the electrical properties is presented.

INTRODUCTION

Developments in the fabrication of $4cm^2$ single crystal solar cells have yielded efficiencies exceeding 18% under standard terrestrial test conditions [1,2]. More recently, single crystal cell efficiencies exceeding 19% have been reported [3]. In comparison, $4cm^2$ polysilicon solar cells have been fabricated having terrestrial efficiencies up to 17% [4]. Based on these successful results an effort was made to determine the maximum efficiency achievable on large area cast polysilicon material.

MATERIAL AND DEVICE CONSIDERATIONS

Short-Circuit Current

Earlier analyses of short-circuit current limitations in polysilicon solar cells have indicated that for an effective grain diameter (based on electrically active grain and subgrain boundaries) exceeding 1-2 mm, the short-circuit current is essentially determined by the minority carrier diffusion length within the grain volumes [5,6]. Recently it was shown that polysilicon material can be modelled using the concept of an effective minority carrier diffusion length, which depends on the grain diameter and grain boundary surface recombination velocity, incorporated together with single crystal device models [7].

†Work supported by DOE, Cooperative Agreement No. DE-FC01-80ET23197 and by Solarex Corporation

*Current Address: Maryland National Capital Park and Planning Commission

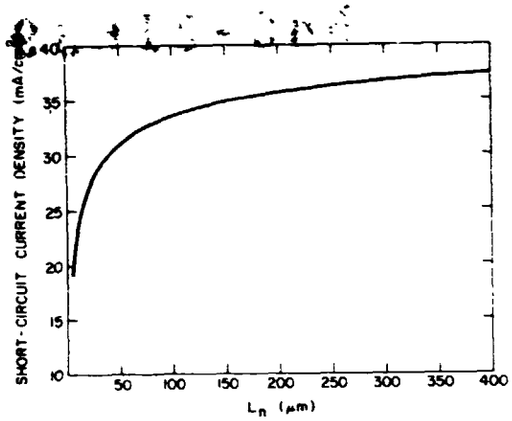

Figure 1. Theoretical Maximum Short-Circuit Current Density Versus Minority Carrier Diffusion Length For a Long-Base Solar Cell ($W >> L_n$), AM1.5, 100mW/cm^2, 400-1100 nm

Figure 1 is a graph of the theoretical maximum obtainable short-circuit current density, in the wavelength range 400 - 1100 nm, versus the minority carrier diffusion length, L_n, in a long-base solar cell (cell thickness W, where $W >> L_n$), calculated using a recently published AM1.5 global spectral irradiance curve (97mW/cm^2) [8]. The calculated values were then increased by 3% to approximate 100mW/cm^2 conditions. Figure 1 shows that for diffusion lengths exceeding approximately 100 μm, in a long-base solar cell, the short-circuit current increases asymptotically with increases in diffusion length. For an effective grain size of 1-2 mm, intragrain diffusion length of 250 μm, and an infinite grain boundary surface recombination velocity, the effective diffusion length in polysilicon material would be approximately 120 - 170 μm and grain boundary effects on short-circuit current are minimal [7].

The material used in this study has average grain diameters of 2 - 10 mm, however the presence of dislocation subgrain boundaries within some of the large grains locally reduces the effective grain size and the effective minority carrier diffusion length. A detailed study of the origins and electrical properties of subgrain boundaries in cast polysilicon material has been performed [9]. For typical subgrain diameters in the range 0.1 - 0.3 mm the effective diffusion length can be reduced to 40 - 90 μm, using the previous values of intragrain diffusion length and surface recombination velocity, and reduce the short-circuit current [7]. A decreased effective lifetime in regions containing subgrain boundaries, revealed using a Secco etch, has been reported earlier [10]. Thus it is important to obtain polysilicon material which has a long intragrain diffusion length and has a minimum density of subgrains.

Open-Circuit Voltage and Fill Factor

Neglecting series resistance and shunt conductance the dark I-V characteristics of a solar cell can be written as

$$J_d = J_{sco}[\exp(qV/nkT)-1] + J_{qno}[\exp(qV/kT)-1] \qquad (1)$$

where the first term is the current component arising from recombination in the space-charge region (with a diode ideality factor, n) and the second term is the current component due to recombination in both the quasi-neutral emitter and quasi-neutral base of the solar cell [11]. With the use of single crystal base material and high quality, careful, cell processing, the space-charge component is usually negligible.

In order to maximize the open-circuit voltage most workers have first minimized the quasi-neutral base recombination component by using boron-doped, high lifetime, low resistivity (0.1-0.3 Ω-cm) float-zoned single crystal silicon as a base material and then minimized the quasi-neutral emitter recombination by a combination of tailoring the emitter doping profile and/or passivating the surface with a thermally grown oxide [12-17,2]. The most successful work to date is the MINP solar cell design [18-19].

Empirically it has been found in the past that the minority carrier diffusion length in cast polysilicon material decreases rapidly for base resistivities below approximately 1 Ω-cm and that good quality material can be grown in the 1-2 Ω-cm resistivity range. Thus in order to apply these results the recombination current in the quasi-neutral base must first be estimated for this range of base resistivity. The quasi-neutral base recombination current, J_{qno}, can be calculated for two different conditions [14], (1) the long-base solar cell ($W \gg L_n$):

Long-base $$J_{qno} = \frac{q n_i^2 D_n}{N_A L_n} \quad (2)$$

and (2) the perfect back surface field (BSF) condition (back surface recombination velocity is zero):

BSF $$J_{qno} = \left(\frac{q n_i^2 D_n}{N_A L_n}\right) \tanh(W/L_n) \quad (3)$$

where q is the electronic charge, n_i is the intrinsic carrier concentration, D_n is the minority carrier diffusivity, N_A is the base doping concentration, L_n is the minority carrier diffusion length and W is the base thickness. Using Figure 1, and equations (2) and (3) the maximum, base-limited, open-circuit voltage under 100mW/cm^2, 25°C conditions was calculated as a function of minority carrier diffusion length for $\rho = 1$ Ω-cm, W = 150 μm and $\rho = 1.7$Ω-cm, W = 225 μm, and is shown in Figure 2. These resistivity/thickness combinations correspond to base parameters for a high efficiency 4cm^2 and the 100cm^2 polysilicon solar cells respectively discussed later.

Figure 2 shows that for a 1 Ω-cm, 150 μm thick cell the minority carrier diffusion length must be, for a base-limited open-circuit voltage to exceed 600mV, greater than 170 μm for a BSF cell and greater than 240 μm for a long-base cell. For a 1.7 Ω-cm, 225 μm thick base the minority carrier diffusion length must be greater than 300 μm for a BSF cell and greater than 400 μm for a long-base cell. Thus, the use of high base resistivity material puts a large lower limit on the range of the minority carrier diffusion length necessary to reach a base-limited open-circuit voltage of 600 mV and places further emphasis on obtaining material with a minimal lifetime inhomogenity. It was recently demonstrated experimentally that reduced open-circuit voltages in large-grained polysilicon solar cells were due to a lower minority carrier diffusion length in the base substrate material [20]. As discussed previously, the effective minority carrier diffusion length in regions containing subgrain boundaries can be as low as 40-90 μm. In these localized regions, using Figure 2, the open-circuit voltage can range from 550 - 575 mV for 1 Ω-cm material and from 530 - 550 mV for 1.7 Ω-cm material. Open-circuit voltage degradation due to increased quasi-neutral base recombination associated with

subgrain boundaries was recently reported [21]. In order to estimate areal inhomogenity effects the I-V characteristics of a large area cell can be obtained by summing the short-circuit and dark current components from the different regions of the cell in parallel.

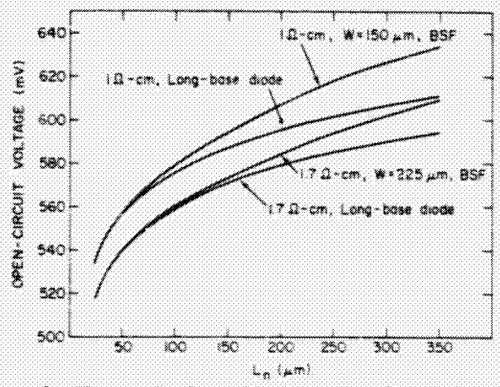

Figure 2. Theoretical Maximum, Base-Limited, Open-Circuit Voltage Versus Minority Carrier Diffusion Length for Various Base Parameters, 100mW/cm^2, 25°C

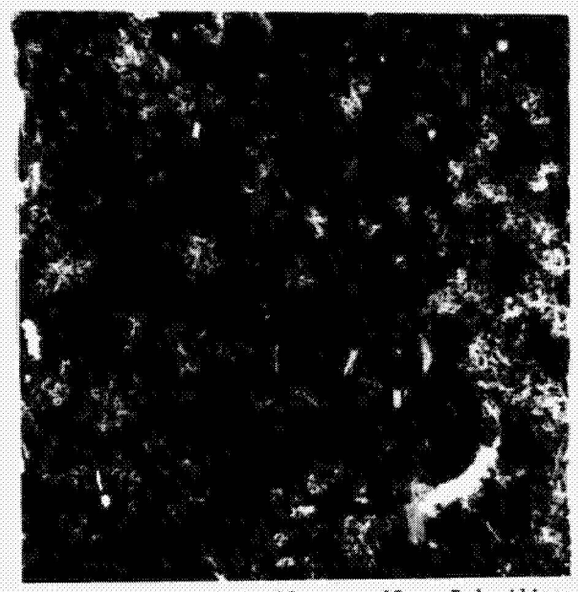

Figure 3. Secco-Etched 10cm x 10cm Polysilicon Wafer Serial Section

In order to minimize recombination in the base material, wafers were selected on a basis of having a reasonably long decay time, proportional to the free-carrier lifetime, measured with a contactless modulated microwave reflectance technique [10] and having a minimal number of subgrain boundaries. Figure 3 shows a photograph of a Secco-etched 100cm^2 polysilicon serial section used in this effort and Figure 4 is a micrograph of a typical region containing subgrain boundaries with spacings of 0.1 - 0.5 mm. Subgrain boundaries have always been found to cause minority carrier recombination as seen in both fine light spot scanning [10] and EBIC [9] measurements. It was estimated by inspection of the Secco-etched 100cm^2 wafer that approximately 8% of the total wafer surface is comprised of regions similar to Figure 4.

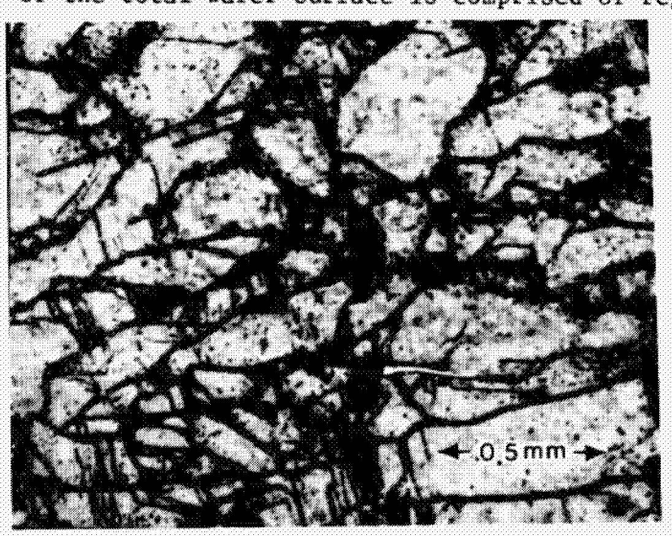

Figure 4.
Micrograph Showing A Dense Array of Subgrain Boundaries

ORIGINAL PAGE IS
OF POOR QUALITY

Figure 5. 100cm^2 Cell Showing Grid Design

ORIGINAL PAGE IS
OF POOR QUALITY

CELL AREA (cm^2)	NO. CELLS	STATISTIC	J_{sc} (mA/cm^2)	V_{oc} (mV)	F.F.	EFFICIENCY (%)
100	50	MEAN	30.5	574	0.761	13.4
		σ	0.66	5.9	0.011	0.31
100	1	-	31.3	589	0.771	14.1
4.05	1	-	34.6	601	0.779	16.2

Table 1. Polysilicon Solar Cell Illuminated I-V Characteristics (100mW/cm^2, 25°C)

Although recombination in the space-charge region is normally negligible in single crystal silicon solar cells, it can, if present, seriously reduce the fill factor and open-circuit voltage. Increased space-charge recombination is associated with subgrain boundaries in polysilicon solar cells and has the largest influence on fill factor rather than open-circuit voltage [21]. Thus there was a further reason to minimize the area of such regions in a large area polysilicon solar cell.

CELL FABRICATION AND RESULTS

A total of fifty 100cm^2 cells were fabricated using space-quality cell processing technology. The p-type wafers were thinned to a nominal thickness of 225 μm using a CP etch and then given a short etch in NaOH to yield a slightly textured surface. (Although a further reduction in thickness would allow for a more beneficial BSF effect, the difficulty in processing a 100cm^2 wafer thinner than approximately 225 μm was too great for the scope of the experiment.) The wafers were then phosphorus diffused to a sheet resistance of approximately 100 Ω/□; aluminum paste was screen printed, alloyed, and the residual paste was removed with HCl. Contacts were photolithographically defined and the metallization consisted of evaporated/ electroplated Ti/Pd/Ag. Figure 5 is a photograph of a 100cm^2 cell showing the grid metallization design. Four buss conductors were used to help minimize the metallization shadowing. A two-layer evaporated antireflection coating was applied, consisting of Ta_2O_5 as the first layer and MgF as the second layer, followed by a brief sintering step.

The short-circuit current was measured outdoors at 100mW/cm^2 illumination, referenced to a global pyranometer measurement (Eppley PSP), and the I-V curves were then completed on a filtered xenon simulator at 25°C. The average and standard deviation of the illuminated I-V characteristics of the fifty cells is given in Table 1. These cells had an average efficiency of 13.5% and

the best cell had an efficiency of 14.1%. Table 1 also summarizes the illuminated I-V characteristics of the best large area cell together with the characteristics of a small area ($4.03cm^2$) 16.2% efficient polysilicon solar cell fabricated during an earlier study [4]. The efficiency of the small area polysilicon solar cell was independently confirmed at the Solar Energy Research Institute [22].

ANALYSIS

Short-Circuit Current

In order to quantify the efficiency loss mechanisms, a detailed loss analysis of the best large area cell together with a high efficiency small area cell was performed. Figures 6 and 7 show the internal and external quantum efficiencies of the 16.2%, $4.03cm^2$ cell and the 14.1%, $100cm^2$ cell respectively in the wavelength region 400 - 1100 nm. Of particular note is that both cells exhibited a spectral response which varied with light intensity [23]. The observation of a minority carrier diffusion length which is dependent on injection level has been studied previously in other silicon materials [24,25]. The quantum efficiency of the 16.2% cell was measured with a chopped monochromatic beam and a steady white light bias of approximately 1 sun intensity [23]. The large area cell was measured with a white light bias of approximately 0.1 sun bias intensity due to measurement limitations. Thus, although it is possible that the near infrared quantum efficiency measured for this cell is inaccurate, no significant variation was found in the range of 0.05 - 0.1 sun bias indicating that the traps dominating the low injection lifetime were saturated.

Figure 8 shows the internal quantum efficiency measured, at approximately 1 sun bias, in a region containing subgrain boundaries and an adjacent region free of subgrain boundaries (both regions are in the 14.1%, $100cm^2$ cell). The effective minority carrier diffusion length in the subgrain region was calculated from the linear plot of inverse quantum efficiency versus inverse absorption coefficient [26] to be 80 μm. This value is approximately one-third of the base thickness so that ignoring BSF effects in the diffusion length calculation is justified. In contrast, a calculation of the diffusion length in the subgrain-free region, or for the curves in Figure 6 and 7 using this method yields diffusion length values close to or exceeding the base thickness. Thus the analysis assumptions are violated and these values are inaccurate.

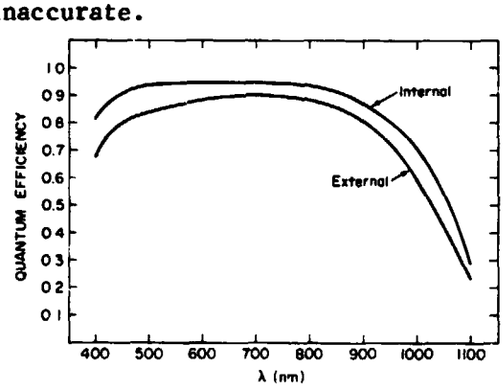

Figure 6. Internal and External Quantum Efficiency Versus Wavelength For the 16.2%, $4.03cm^2$ Polysilicon Solar Cell (∿ 1 sun bias condition)

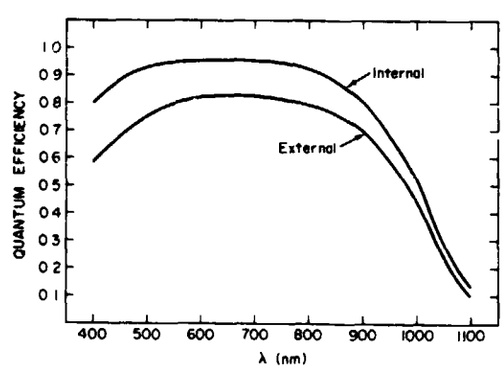

Figure 7. Internal and External Quantum Efficiency Versus Wavelength For the 14.1%, $100cm^2$ Polysilicon Solar Cell (∿ 0.1 sun bias condition)

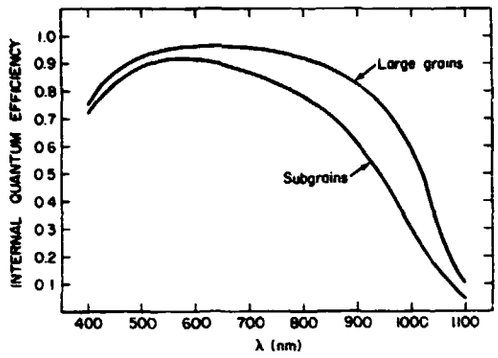

Figure 8. Internal Quantum Efficiency in Large-Grain and Subgrain Regions of the Large Area Polysilicon Solar Cell (∿ 1 sun bias condition)

	16.2% (4.03cm²)		14.1% (100cm²)	
LOSS MECHANISM	FRACTION AVAILABLE AFTER LOSS	J_{sc}(mA/cm²) AVAILABLE AFTER LOSS	FRACTION AVAILABLE AFTER LOSS	J_{sc}(mA/cm²) AVAILABLE AFTER LOSS
THEORETICAL MAXIMUM	1.0	43.2	1.0	43.2
INTERNAL QUANTUM EFFICIENCY LOSS	0.87	37.6	0.85	36.7
ANTIREFLECTION COATING LOSS	0.97	36.5	0.97	35.6
GRID SHADOWING LOSS	0.95	34.6	0.88	31.3
NET	0.80	34.6	0.73	31.3

Table 2. Short-Circuit Current Losses for the Small and Large Area Polysilicon Cells in the Region 400 - 1100 nm

By separately integrating the product of each quantum efficiency curve with the AM1.5 solar spectral irradiance curve [8] over the wavelength range 400 - 1100 nm, and by measuring the percentage grid shadowing, the percent losses in short-circuit current due to internal quantum efficiency, antireflection coating, and grid shadowing were calculated. This short-circuit current loss analysis is summarized in Table 2. The short-circuit current associated with the internal quantum efficiency of the small area cell is approximately 2% greater than the large area cell partly due to a reduced cell thickness (150 μm versus 225 μm), which enhances BSF effects, and the addition of a back-surface reflector (BSR) which was not used for the large area cells. From an analysis of Figure 8 a total internal quantum efficiency loss in short-circuit current of only approximately 1% can be attributed to the 8% area of the cell containing subgrain boundaries. Antireflection coating losses were identical. The major difference between the two cells was the percentage of grid shadowing, representing approximately 5% for the small area cell and 12% for the large area cell. The grid shadowing is approximately twice the design value for the large area cell and was due to excessive grid line broadening during the photolithography and metallization processes.

Open-Circuit Voltage and Fill Factor

The dark I-V characteristics of both cells were generated by measuring I_{sc}-V_{oc} at different illumination levels to eliminate the effect of series resistance and then subtracting the shunt conductance contribution (determined from reverse-bias measurements). This data was then fitted to equation (1) using a computer program designed to minimize the differences between the measured data and the I-V characteristics calculated from equation (1) [27]. The series resistance was calculated from the difference in the I_{sc}-V_{oc} and dark forward-bias I-V characteristics. The base resistivity was calculated from junction capacitance measurements. These results are summarized in Table 3.

Using the shifting approximation, the illuminated I-V characteristics were calculated from the short-circuit current and dark I-V characteristics in Table 3. This calculation was done by starting with the quasi-neutral component alone, calculating the illuminated I-V characteristics, and then sequentially adding the space-charge component, shunt conductance, and series

PARAMETER	16.2% (4.03cm²)	14.1% (100cm²)
SHUNT CONDUCTANCE G(mW/cm²)	0.18	0.90
SERIES RESISTANCE R_s(Ω-cm²)	0.38	0.32
SPACE-CHARGE DIODE QUALITY FACTOR, N	3.5	2.0
SPACE-CHARGE CURRENT J_{sco}(mA/cm²)	4.6×10^{-3}	6.3×10^{-4}
QUASI-NEUTRAL CURRENT J_{ono}(mA/cm²)	2.3×10^{-9}	3.6×10^{-9}
EQUIVALENT VOLTAGE V_E(mV)	522	496
BASE RESISTIVITY (Ω-cm)	1.0	1.7

Table 3. Dark I-V Characteristics for the Small and Large Area Polysilicon Solar Cells

INCLUDED DARK I-V COMPONENTS	I-V CHARACTERISTICS CALCULATED FROM INCLUDED DARK I-V COMPONENTS			
	V_{oc} (mV)	F.F.	η (%)	Δη (%)
QUASI-NEUTRAL RECOMBINATION	602	0.829	17.2	-
QUASI-NEUTRAL & SPACE-CHARGE RECOMBINATION	599	0.796	16.4	0.8
QUASI-NEUTRAL, SPACE-CHARGE & SHUNT CONDUCTANCE	599	0.793	16.4	0
QUASI-NEUTRAL, SPACE-CHARGE, SHUNT CONDUCTANCE & SERIES RESISTANCE	599	0.775	16.1	0.3
MEASURED CHARACTERISTICS	601	0.779	16.2	-

TABLE 4A

INCLUDED DARK I-V COMPONENTS	I-V CHARACTERISTICS CALCULATED FROM INCLUDED DARK I-V COMPONENTS			
	V_{oc} (mV)	F.F.	η (%)	Δη (%)
QUASI-NEUTRAL RECOMBINATION	588	0.826	15.2	-
QUASI-NEUTRAL & SPACE-CHARGE RECOMBINATION	584	0.803	14.7	0.5
QUASI-NEUTRAL, SPACE-CHARGE & SHUNT CONDUCTANCE	583	0.791	14.4	0.3
QUASI-NEUTRAL, SPACE-CHARGE, SHUNT CONDUCTANCE & SERIES RESISTANCE	583	0.777	14.2	0.2
MEASURED CHARACTERISTICS	584	0.779	14.1	-

TABLE 4B

Table 4. Illuminated I-V Losses Calculated Using the Shifting Approximation and the Dark I-V Characteristics in Table 3 for the Small Area (Table 4A) and Large Area (Table 4B) Polysilicon Solar Cells

resistance, and repeating the calculation after each addition. Table 4A summarizes the results of this calculation for the 16.2% small area cell. Space-charge recombination reduced the open-circuit voltage minimally (∿3 mV), however it caused a 0.8% reduction in cell efficiency (17.2 to 16.4%) due to a decreased fill factor. The cause of this increased space-charge component was not identified. The shunt conductance was sufficiently low to not affect the cell efficiency, however series resistance decreased the fill factor and caused a 0.3% reduction in cell efficiency. The uppermost curve in Figure 2 shows that, theoretically, the open-circuit voltage of a perfect BSF cell of this thickness and base resistivity must have a base minority carrier diffusion length exceeding approximately 180 μm, which may be possible, in order to achieve a base-limited open-circuit voltage larger than experimentally obtained. The base diffusion length and back surface recombination velocity are difficult parameters to measure in a BSF cell and were not measured in this study. (Techniques to separately determine the base and emitter dark current components have been recently reported [28,29]). However, based on the above analysis of the dark current and Figure 2, the open-circuit voltage of the 16.2% cell is approaching the level where recombination in the quasi-neutral emitter begins to dominate.

Table 4B summarizes the calculated I-V characteristics of the 14.1% large area cell. Space-charge recombination again reduced the open-circuit voltage minimally (∿4 mV) however it caused a 0.5% reduction in cell efficiency due to a reduced fill factor. It is reasonable to assume that part of the increased space-charge recombination is due to the presence of subgrain boundaries. Shunt conductance and series resistance accounted for efficiency losses of 0.3% and 0.2% respectively due to a decrease in fill-factor. The next to lowest curve in Figure 2 shows that, theoretically, the base minority carrier

diffusion length of a perfect BSF cell of this thickness and base resistivity must exceed approximately 200 μm in order to achieve a base-limited open-circuit voltage larger than experimentally observed for the large cell. The diffusion length must exceed 300 μm, which is not likely, in order to achieve a base-limited open-circuit voltage of 600 mV. Thus it is concluded that the open-circuit voltage of this cell is limited by recombination in the quasi-neutral base due to both base resistivity and minority carrier diffusion length limitations. This conclusion is consistent with results in 2 Ω-cm single crystal silicon solar cells [15].

The extent of this base recombination due to an approximately 8% area containing subgrain boundaries was calculated from the measured effective diffusion length of 80 μm in this region and equations (2) or (3). The interesting result is that approximately 40% of the total quasi-neutral current results from an region comprising approximately 8% of the cell area. This emphasizes the need to eliminate these defects by modification of the crystal growth process or possibly by passivation of these defects using, for example, atomic hydrogen [30].

SUMMARY AND CONCLUSIONS

Large area ($100cm^2$) polysilicon solar cells having efficiencies up to 14.1% ($100mW/cm^2$, 25°C) were fabricated and a detailed analysis was performed to identify the efficiency loss mechanisms. The I-V characteristics of the best cell were dominated by recombination in the quasi-neutral base due to the combination of minority carrier diffusion length and base resistivity (1.7 Ω-cm). Approximately 40% of the total quasi-neutral recombination current was attributed to regions comprising approximately 8% of the total cell area containing subgrain boundaries. These subgrain boundaries substantially reduced the local effective minority carrier diffusion length which locally increases the base recombination current. By comparison, an analysis of a 16.2% small area polysilicon solar cell ($4.03cm^2$) indicated that the open-circuit voltage of this cell was approaching the level where recombination in the quasi-neutral emitter begins to dominate.

Further efficiency increases in large area polysilicon solar cells can be realized by an improvement in the crystal growth, and/or post-solidification processes, to reproducibly yield low resistivity material having a long, spatially uniform, minority carrier diffusion length. After a suitable reduction in the base recombination is accomplished, a further development and application of the surface passivation and emitter formation techniques, successfully demonstrated with single crystal material, should allow efficiency advances to be made.

ACKNOWLEDGEMENTS

The authors wish to express their appreciation to L. Brickman, E. Coccia, J. Culik, D. Fardig, T. Migliorini, C. Osterwald and G. Storti for their contributions to this effort and to P. Fazio for preparing this manuscript.

REFERENCES

1. A.W. Blakers, M.A. Green, S. Jiquin, E.M. Keller, S.R. Wenham, R.B. Godfrey, T. Szpitalak and M.R. Willison, IEEE Electron Device Letters, Vol. EDL-5, No. 1, 1984.

2. M.B. Spitzer, S.P. Tobin, and C.J. Keavney, IEEE Trans. Electron Devices, Vol. ED-31, No. 5, May 1984, in print.

3. M.A. Green, A.W. Blakers, Jiqun Shi, E.M. Keller and S.R. Wenham, Appl. Phys. Lett. 44 (12), June 1984.

4. G.M. Storti, Conf. Rec., 15th IEEE Photovoltaic Specialists Conf., 442, (1981).

5. G.M. Storti, S.M. Johnson, H.C. Lin, and C.D. Wang, Conf. Rec., 14th IEEE Photovoltaic Specialists Conf., p. 191, (1980).

6. S.M. Johnson, R.G. Rosemeier, C.D. Wang, R.W. Armstrong, H.C. Lin, G.M. Storti, Proc. Int. Electron Devices Meeting, p. 202 (1980).

7. S.M. Johnson, to be published.

8. R.J. Matson, K.A. Emery, and R.E. Bird. Solar Cells, Vol. 11, No. 2 (1984).

9. K.C. Yoo, S.M. Johnson, W.F. Regnault, to be published.

10. S.M. Johnson, J.C. Culik, Conf. Rec., 16th IEEE Photovoltaic Spec. Conf., 548, (1982).

11. F.A. Lindholm, J.G. Fossum and E.L. Burgess, IEEE Trans. Electron Devices, Vol. ED-26, No. 3, March 1979.

12. J.A. Minnucci, K.W. Matthu, A.R. Kirkpatrik, and A. McCrosky, in ref. [5], p. 93.

13. M.P. Godlewski, T.M. Kluche., G.A. Mazaris, and V.G. Weizer, in ref. [5], p. 166.

14. R.A. Arndt, A. Meulenberg, and J.F. Allison, in ref. [4], p. 92.

15. E.S. Rittner, A. Meulenberg, and J.F. Allison, J. Energy, Vol. 5, No. 1, 1981.

16. A. Meulenberg and R.A. Arndt, ref. [9], 348.

17. H.T. Weaver and R.D. Nasby in ref. [9], 361.

18. M.A. Green, et.al., in ref. [4], p. 1405.

19. M.A. Green, et.al., in ref. [9], p. 1219.

20. J. Culik, P. Alexander, K.A. Dumas, and J.W. Wohlgemuth, Fifth E.C. Photovoltaic Solar Energy Conference, Athens, p. 1090-1094, (1983).

21. J. Culik, K. Grimes, 17th IEEE Photovoltaic Specialists Conf., in print (1984).

22. C. Osterwald, Report No. 296, Solar Energy Research Institute, September 20, 1983.

23. L.A. Brickman, unpublished research.

24. E. Fabre, M. Mautref, and A. Mircea, Appl. Phys. Lett., Vol. 27, pp. 239-241, (1975).

25. R. Shimokawa and Y. Hayashi, IEEE Trans. Electron Devices, Vol. ED-30, No. 12, (1983).

26. E.D. Stokes and T.L. Chu, Appl. Phys. Lett., Vol. 30, No. 8, (1977).

27. J.C. Culik, unpublished research.

28. B.H. Rose, H.T. Weaver in ref. [21].

29. V.G. Weizer, C.K. Swartz, R.E. Hart, M.P. Godlewski in ref. [21].

30. C.H. Seager, D.J. Sharp, J.K.G. Panitz, and R.V. D'Aiello, J. Vac. Sci. Technol. 20, 430, 1982.

DISCUSSION

RAI-CHOUDHURY: I notice your internal quantum efficiencies around 0.4 micrometer were in excess of 80%. Would you comment on why you had such high internal quantum efficiency without the surface passivation?

JOHNSON: I think it's strictly due to our thinner junction. We have a fairly high sheet resistance of 100 ohms per square -- maybe slightly larger than that.

RAI-CHOUDHURY: What is your surface dopant concentration?

JOHNSON: I don't know. We haven't measured that.

RAI-CHOUDHURY: It's not clear why you had such high collection efficiencies. There has got to be either low emitter surface dopant concentration or somehow your surface has got to be very well passivated, because usually even if you take a single crystal material at 0.4 micrometer you see internal quantum efficiencies of about 50% to 60% at the most, and you had 80% there.

JOHNSON: All that I can say is that it may be just from the particular way we do our diffusions.

LESK: I was just wondering, there was a paper in your organization on hydrogen passivation of defects, and I was wondering if you see any passivation of the sub-grain boundary regions with hydrogen, or can you look at it closely?

JOHNSON: We haven't done that yet. Jerry Culick, who is here, will be doing that, and there is a lot of promise for passivation of those regions, because the region where you are going to get the passivation is probably at the dislocations, where you are going to get diffusion down the boundaries due to the presence of dislocation.

SIRTL: I have two questions. One is, could you briefly describe or show the crystalline features of the two top cells you were discussing? The second question is, did you -- with the same cell technique -- make solar cells from standard monocrystal like Czochralski, just to show the differences in terms of this sophisticated cell technology?

JOHNSON: Yes. For Czochralski material, for 2 x 2 cells we can get 16 1/2% - 17% without too much difficulty. For large areas, we did process a few five-inch wafers, where we cut off the edges. We started about four of them; we got two of them finally to the end. One of the cells had an open-circuit voltage of about 600 millivolts and the other one was somewhat less than that, maybe 590 or so. This is due more to processing limitations, I think. Efficiencies run in the order of 15 1/2% for the large area cells.

SIRTL: Could you describe the two samples? Was the 2 x 2 16.2% cell largely monocrystalline, or how did it look?

JOHNSON: No, the grain size was larger, and I don't have a picture of that particular cell. The grain size in that cell was probably closer to half centimeter to a centimeter or so in size. I'd say closer to about half centimeter in size. The large-area cells, optically visible grain size is still in the range of 3 to 5 millimeters. Again, it's not the optically visible size that is important to us, it's the size under a defect. That's where we see these small-grain regions and sub-grain regions.

QUESTION: I'd like to follow up on that. Your 4 cm^2 cell had very good characteristics; do you have any feeling what is the percentage of grain boundaries? What kind of grain boundaries? Earlier you called it 8%.

JOHNSON: Oh, subgrains in that particular cell. We did not want to destroy it, naturally, but I would estimate subgrain boundaries in that particular cell were very minimal. I would say very few are in that region. For small-area cells you have the luxury of choosing good areas out of a large area. For large-area cells you have to take what the material gives you.

RAO: It's interesting that you have this 8% of the material having sub-grain boundaries, and you showed some nice pictures of that. Is there any way that can relate this to location and the sample where you have high density sub-grain boundaries, and do you know what happens at the subgrain boundaries? Why they are forming? Are they forming because of impurity segregation there, perhaps?

JOHNSON: Impurity segregation would be difficult for us to measure. Someone like Larry Kazmerski could probably measure it relatively easily. What we have found is that the electrical activity of grain boundaries is associated with dislocations at the interface. First-order twins, which do not need dislocations to make up the orientation difference, are rarely electrically active. Second-order twin boundaries can have regions that fit together coherently; there's no dislocations needed. They are all relatively active electrically. Small-angle boundaries that are totally compressed at this location are always found to be electrically active. We have always seen that to be so. Whether it's impurities, atmosphere being formed around these dislocations causing their recombination, is not very clear, but as we have seen, a lot of the people have talked about low-temperature work. It's not very straightforward why dislocations are electrically active. People have looked at this but whether it's impurities or the poor structure of the dislocation -- but again, we believe that the recombination at the grain boundary is associated with dislocation, whether it's impurities there or the natural structure of the dislocation itself.

DYER: Mine is mainly a comment, and it is in response to Rai-Choudhury's remark earlier, on how come you have this higher quantum efficiency and so forth? It just recalls to me a chemical monkey wrench that I want to throw into this whole business: that is, the chemical processing of the early slice is very important. If you thin the slice with hydroxides and then if you texture it with dilute hydroxides there are some things that will plate out of solution. For example, iron plates out of solution. If you don't do anything to remove that before you diffuse, then you

would drive iron into the emitter, and so forth, and I don't think that would be very good for the device. So, I just want to remind people of this, and of course if you are using acid cleanups, acids plate gold and copper out of solutions; you have to guard against the buildup of these materials and then replating them out. They are also bad. Just to mention this as possible effect on the V_{oc} that earlier in the meeting someone pointed out was slightly lower from texturing.

BICKLER: I'd like to comment on the origin of some of these stresses at the corners of the grain boundaries. I think it would be valuable if you did a thorough study on grain orientation from the freezing point of silicon. I'm sure the stresses you mentioned from the crucible are probably minor by the time you get in a few grains and it may submit itself to an analysis. Since you get a dimension change and different directions it may focus that force, that strain at those stress points.

DYER: It may be this, the changes in thermal gradient in the ingot, which are not nearly as well controlled as material like Czochralski, that we are getting. Now, Yoo at Texas Instruments has done a lot of looking at the origin of these stresses and what the effect is on different grain orientations. The approach that he has taken is that if you assume a particular stress direction due to thermal stresses, just based on how the ingot is going to cool, what is the resolved shear stress on the grains of different orientation? So if you have a grain in the right orientation you are going to get a very large shear stress on that particular grain and you are going to get a slip.

BICKLER: The analysis that I am talking about would be isothermal cooling, if such a thing, theoretically, exists. There still would be a differential expansion as a function of grain orientation. You could analyze that after the fact. You could look at these samples that you show pictures of and see if, in fact, there is any stress or strain.

HANOKA: I just want to follow up and try get it clear. What you are saying, in effect, is that the dislocations that are electrically active and giving you a problem are due to thermal stress. And if that's so, it's basically the same distinction then that Schwuttke made yesterday also with web, with only the stress locations that seem to be electrically troublesome. Is that right?

DYER: No, what I was saying was that the sub-grain boundaries themselves seem to be indications that they are formed from stress in the ingot. In other words, the collation of the dislocations there. When they are in a particular boundary, then their nature is very difficult to determine. We have always seen the boundaries to be electrically active. Some of the dislocations in the material, however, we only saw at low temperature. Whether they are formed from stress or they have grown into dislocations I really can't say. So we see some dislocations electrically active, some are not. I have not made a clear distinction.

QUESTION: A lack of clear contrast at room temperature does not mean that they are not adversely affecting you, though. We have seen crystal samples that have we have stressed in the JPL program. Those two pictures that I

showed yesterday: you have difficulty sometimes seeing these dislocations that you formed by stressing at room temperature. But they do affect the diffusion length, so just looking for contrast can be a little deceptive. You have to be careful without having any absolute measure of what the real lifetime or diffusion length is.

QUESTION: If you don't see a contrast at a particular defect, I would say that at room temperature it's not strongly electrically active, unless you have such a high density of defects that you can't tell the difference between the various contrasts. The contrast you see for dislocation depends on the recombination efficiency at the particular dislocation and also on the diffusion length in the surrounding material. The surrounding material is limited by impurities or point defects or some other defect; you may see a very low contrast. It may not be indicative of what's happening at dislocations. It may be the bulk material around it.

QUESTION: I generally would agree with that. But I still think one has to be careful, though. If you don't see contrast, you can't state absolutely that you don't have dislocations and that it's not affecting your lifetime.

JOHNSON: Well, I agree. I wouldn't want to say anything absolutely about it. I made a statement that if we don't see that they are not a dominating factor as far as efficiency is concerned, I wouldn't argue that they are not a factor at all.

MILSTEIN: I would comment on the two previous discussions. It is all well and good to understand how the stress interacts in causing dislocations and things of that nature; however, I think the problem that really needs to be addressed is what does one do about controlling it. In that sense, that's really the crux of what you are addressing.

JOHNSON: That is the crux of why we are spending a lot of time figuring out what forms these particular defects. We would like to tailor our particular thermal environment so as not to produce these in the as-grown crystal rather than have to try to passivate them later.

ILES: You are saying you are working on a polycrystalline material, so by definition you have, I take it, grain boundaries and sub-grain boundaries. What I would like you to comment on is what you were planning to do in the near future to improve the lifetime or the diffusion length, and some feel for what kind of a number you expect in some given time frame. Would you like to comment on that?

JOHNSON: I certainly cannot give you a number of what I would expect. What we would like to look at in more and more detail is why our lifetime does drop off as a function of dopant density, to try to determine where the actual limitations are, and it's very important to try to overcome the technological limitation of the material. Try to get to lower resistivity. So we are looking at that particular area right now. I don't have a feel for what I could say if we cast silicon sheet having resistivity of 0.5-ohm centimeters -- that we would still expect our diffusion length to be 150 micrometers. I have no basis to make a judgment.

ILES: The reason I asked that question is you have now 3.2 ohm centimeters between your float zones. Everybody's working on it and getting the diffusion length hit and miss; some crystals have it, most of them don't. What kind of ultimate limits can we gain in efficiency? If somebody has that number, and would like to comment on it?

QUESTION: I'd like to make a comment on that. It is that we know relatively well that our efficiency losses are due to the structural defects, such as grain and sub grain boundaries. We can minimize the sub-grain boundary density; that can be controlled. Independent of that, there is a problem with inter-grain minority carrier diffusion, which is related to the doping density. It's seen in Czochralski material, not seen in float-zone, in that particular area that we are looking at, and it's something that's independent of the fact that there are grain and sub-grain boundaries around. You can separate the two, but it may not be separate from the actual method that we grow the crystal. It may be, or it looks to be, inherent in Czochralski, and I hope there are some improvements down the line. I really can't say what they would be at this time.

N85-31640

HIGH EFFICIENCY SOLAR CELL PROCESSING

F.Ho and P.A.Iles
Applied Solar Energy Corporation
City of Industry, California, 91749

INTRODUCTION

At the time of writing, cells made by several groups are approaching 19% efficiency (AM1) (already achieved by the UNSW group). To help focus the forum objectives, we have chosen to discuss some more general aspects of the processing required for such cells, rather than presenting detailed cell results.

Most processing used for high efficiency cells is derived from space-cell or concentrator cell technology, and recent advances have been obtained from improved techniques rather than from better understanding of the limiting mechanisms.

Theory and modeling are fairly well developed, and adequate to guide further asymptotic increases in performance of "near-conventional" cells. There are several competitive cell designs with promise of higher performance (> 20%) but for these designs further improvements are required.

The main trend recently has been the increased number of groups which can combine the available technology to fabricate high efficiency cells, and later we will discuss this trend in relation to the goals of the forum.

HIGH TECHNOLOGY PROCESSING

The available cell processing technology which has been exploited can be listed as follows:

- Choice and use of high quality silicon (mostly highly doped, mostly float-zone refined).
- Processing to preserve the high quality of the silicon.
- Formation of polished or textured front surface with low damage, accompanied later by the formation of a well designed (and carefully deposited) AR coating.
- Formation of shallow, lightly doped, good quality PN junction (usually by diffusion, in some cases by ion-implantation).
- Use of contacts with low contact resistance, perhaps with tunnel oxide layers to reduce recombination.
- Use of grid patterns with low shading (3-4%) and reduced series resistance (few %), giving fill factors above 0.80.
- Use of front surface passivation.
- In some cases, use of fields, reflectors or passivation at the back surface.

In addition, when required, space cell groups have demonstrated the fabrication of thousands of thin (50-100um) cells with high efficiency.

Tables 1 and 2 show the intrinsic and extrinsic properties required for high efficiency cells, along with the process steps which mainly determine these properties. We have also indicated the cell parameters most affected.

TABLE 1

INTRINSIC CELL PROPERTIES AND PROCESS STEPS WHICH INFLUENCE THESE PROPERTIES

INTRINSIC PROPERTY	PROCESS STEPS	AFFECT
HIGH BULK DIFFUSION LENGTH	STARTING SILICON, CLEANING, PROCESSING	Jsc
GOOD JUNCTION QUALITY	SURFACE PREPARATION, CLEAN DIFFUSION	Voc (CFF)
LOW BULK LEAKAGE CURRENT	JUNCTION, PURE SILICON, DOPING OF SILICON.	Voc
LOW SURFACE RECOMBINATION	SURFACE PASSIVATION (BSF, FSF, OXIDES, ETC.) MIN. METAL (AREA, PASSIVATION)	Voc (Jsc)
SHALLOW JUNCTION	DIFFUSION CONTROL	Jsc

TABLE 2

EXTRINSIC CELL PROPERTIES AND INFLUENCING PROCESS STEPS

EXTRINSIC PROPERTY	PROCESS STEPS	AFFECT
LOW REFLECTANCE	AR COATING, (TEXTURED)	Jsc (Voc)
LOW SHADING	GRID DESIGN	Jsc
LOW RESISTANCE LOSS	GRID DESIGN, LOW CONTACT RESISTANCE	CFF

INTERACTIONS

SILICON QUALITY/PROCESSING

JUNCTION QUALITY/SHALLOW JUNC./PASSIVATION/GRIDDING

SURFACE PREPARATION/AR/PASSIVATION

If can be seen that there is considerable interaction of the process steps. This emphasizes the fact that to equal (or exceed) the best state-of-the-art cell performance, most of the processes listed must be acquired and combined successfully. In fact the main requirement is to minimize the unwanted interactions as far as possible. Often the key requirements eg. texturing and passivation, are in conflict.

In some cases, the effect of a different (hopefully improved) process can only be evaluated by including it in a cell fabrication sequence with most of the other necessary steps. Experience shows that to achieve the best cell performance, all the process steps must be applied well.

In other cases, involving severe conflict of process steps, relief is sought by moving to alternate structures. For example, use of mostly back surface structures, can ease the shading and passivation requirements, but may lead to the need for higher carrier diffusion lengths, and for effective back surface passivation, as well as requiring a more complex (interdigitated) contact design.

In a few cases, the conflicts are resolved by using more complex steps eg. the use of "dot" contacts to reduce metal Si contact area, and to reduce the need for contact passivation. Figure 1 shows pictorially the high technology processes which have been combined to give ~19% and it can be seen that a fairly good level of optimization is needed for almost all the steps.

FIGURE 1

EFFICIENCY ACHIEVABLE WHEN VARIOUS PROCESSES OPTIMIZED

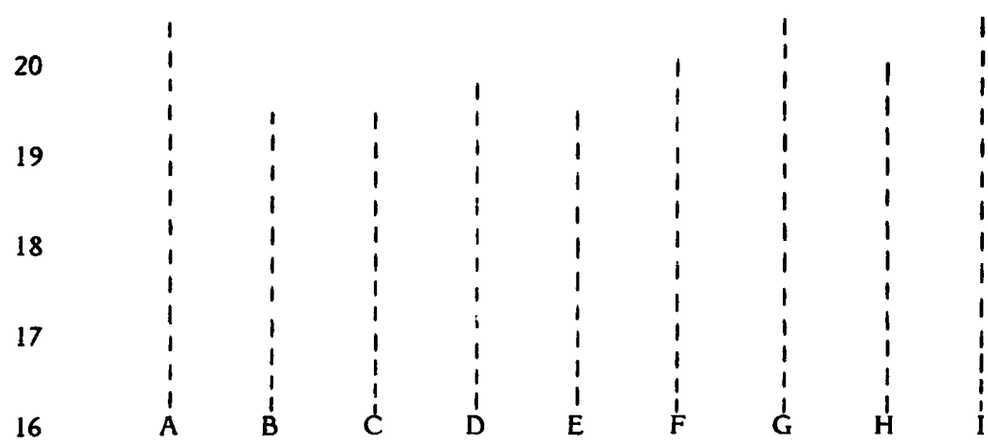

EFF (AM1.5) (%) — PROCESS FUNCTION

LEGEND:

A	GOOD QUALITY SILICON
B	SURFACE PREPARATION
C	QUALITY JUNCTION
D	SHALLOW, LIGHTLY DOPED SURF. LAYER.
E	REFLECTANCE LOW.
F	LOW SERIES RESISTANCE
G	REDUCED SURFACE RECOMBINATION.
H	LOW SHADING AREA.
I	CONTACT PASSIVATION

If some of the steps (e.g. G or I) are omitted, 17-18% is still achievable (this is the level often seen on production runs of space or concentrator cells).

To exceed 18%, most of the processes shown must be well controlled and combined. To reach 19-20%, it is important to make improvements in steps A, G and I.

Silicon Quality

Most of the present high efficiency designs, and most of the projections for further increase to ~20%, involve the use of very high quality silicon.

Almost all high efficiency cells have used float zone refined silicon, often with multiple zone passes. Such high quality silicon in the high doping ranges required,is not readily available (high efficiency solar cells represent a very limited market), and the quality is not easily specified or guaranteed. In fact, there is danger that the highest efficiencies claimed world-wide could all have been obtained using very few (perhaps one or two) ingots. This is of academic interest to show the feasibility of the combined processes to meet the design goals, but additional action is required if these cell designs are to be useful for meeting long term flat plate efficiency goals (array efficiencies in excess of 15%, at a price of $90 per square meter, and with 20-30 years projected lifetime).

We have had much experience with Czochralski-grown silicon, but limited experience with highly doped Cz-Si. Generally for equivalent doping concentrations, cell efficiencies are lower by 1-2% in conversion efficiency (5-10% lower in power), when Cz-Si replaced Fz-Si. However, lightly doped Cz-Si has shown very good quality, and very little work has been done to check if the problems at high doping levels are derived from the doping pellets used, or from crucible interactions. Although the latter would appear to be the cause when comparing to the zone-passing improvements, it is hard to explain why lightly doped Cz ingots are so good. Microelectronic technology has made significant improvements in the quality of surface devices, by use of internal gettering. It appears that more work should be done to identify the causes for reduced performance of highly doped Cz-Si. For production purposes Cz-Si has proved capable of high throughput and high quality, and although not yet satisfactorily inexpensive, it still is competitive with most other types of silicon.

DISCUSSION

We have indicated above that:

a) Continued optimization of cell technology (mostly already used at low "production: levels) can provide cells ~20% efficient; also most of the same technology can be deployed to test new cell designs.

b) The feasibility of cells which can meet the efficiency requirements for future flat plate arrays, has been demonstrated.

c) At present, in order to demonstrate small improvements, it is necessary for each group involved to master most of the processes required to make a cell.

d) Most designs rely on use of very special quality silicon.

However, there are some important areas which require assessment, especially for this forum:

i) More work is required, to widen the choice of silicon which has the chance of meeting the long term goals.

ii) Although it is necessary at present to show successful combination of all the process steps, in the long run it is inefficient to expect various cell development groups to acquire all these processes. In some cases, the time spent in such acquisition detracts from effort in areas where their real technical strengths can be used, whether it is in cell modeling, or in development of new processes.

The only solution to this appears to be the formationof "teams", wherein the basic processing skills are used to complement some of those groups.

Consideration of this option, leads to the realization that there are several different motives which drive cell development, including basic interest in theory and practice, commercial interest in the flat-plate array goals, the need to obtain financial gain or prestige for establishments or self, or even patriotism. These motives must be reconciled to make best use of all available talents.

iii) Now that the cell technical requirements have reached a competitive efficiency plateau (19-20% cells should meet 15% array goals) it is not too early to begin assessment of the cost and production limitations, and also to demonstrate adequate environmental stability. Here again, as in (i) a different set of skills may be needed, and it is important that some of the groups developing cells should be attuned to interaction with production groups.

iv) A minor consideration is offered - that perhaps a cell design should be selected which can be used in both flat plate and concentrator arrays (with slight known modifications for the latter) as the best compromise for short term production evaluation.

v) In parallel with (iii), work should continue to extend the demonstrated feasibility (towards 23-25%) either by routes which do not demand utilization of many precise technology process steps, and which overcome some physical limitations (eg. high doping effects), or perhaps by effective team efforts.

Some of the areas discussed above can be explored by decisions reached after the forum, by suitable direction from JPL or other agencies.

SUMMARY

Using near-conventional cell structures, present cell process technologies, when suitably combined can give cell efficiency ~19%, and with slight improvements, mostly in Si quality, 20% seems feasible.

The successful designs to-date are derived from space and concentrator cell technologies which have demonstrated medium scale production levels (100KW flat-plate output per year), although without meeting the flat-plate array cost goals.

We feel that already manufacturing assessment should be made for cells operating in the 19-20% plateau.

Some theoretical designs offer the possiblity of exceeding 20%, and should be pursued without constraints of costs, etc.

One non-technical purpose of the forum maybe to combine the various motivations involved, to provide an effective program; one area of promise is the deliberate formation of balanced teams which include a wide range of skills (and motives).

DISCUSSION
(ILES)

CISZEK: Peter, I'm intrigued by these older space cells that were worked out at AMO and a lot of people say they would have done real well under terrestrial conditions. Isn't it possible to dig some of those out from the old Spectrolab or OCLI cells that are textured?

ILES: Yes, they are still being made. The strange thing is that textured cells have only been made for a limited run and a different reason. The textured cells run 10°C to 15°C hotter in space, and most people in the terrestrial areas don't understand that, that we can get a higher efficiency on the block but we don't get a higher efficiency when we interface with a real system. Space cells are a little more sophisticated, and the customer puts his specifications in there very early on and he knows very well what he is going to gain. I'm sure you are right. Matter of fact, I think Daud wanted some decent cells, back-surface fields so that he and Fred Lindholm and some other people could find out whether there was a voltage drop at the back surface. They came and got some Class 2 mechanical reject cells -- we don't make that many back-surface fields. He took them back and phoned us the next day and said do you know these are 17 something percent, and we said yes, you never asked us what, you just wanted some Class 2 cells.

CISZEK: It would be interesting to hear more of the results on some of those space cells and sees how they really stack up terrestrially.

ILES: I think the bottom line is they look very like these other cells; these are mainly 10 ohm-centimeter with a good back-surface field. It's hard to compare the 0.1, 0.2 ohm-centimeter concentrator-type cells. They are not very different in diffusion, gridding -- all those things are very similarly done. We can get you some of them if you want to analyze them.

RALPH: Here I'd like to pin you down, I guess, as you have heard, we all have put in bells and whistles and that type of thing to make our cells and we all can agree that we could make like 17% with the bells and whistles we put in daily. What would you do different to get the 19% jump? In other words, there has to be something additional. Is it just resistivity change, or is it plus the passivation, or is it the material that's limiting it? What would you do different, what additional bells and whistles would you add?

ILES: At the moment, the material is the driving factor. To look very carefully, you want to get 19% with high yield -- we are not talking about the best of the week or the best of the month. I think you have to divide the maximum diffusion length on the material and a reasonably high doping level. I don't think at the moment -- the trade-off to having lighter doping and a back surface field is not quite competitive, but very close when you get to that level. It's not easy in production but quite feasible to make shaded areas at one sun less than 3%. I think that would be no big deal. It would be a little tricky for a while but not unfeasible. The coatings and everything else are fairly straightforward. That's why I get so frustrated -- now we are talking about

production levels in a solar cell that is largely still hand production, but these processes are being automated for very large scales and, in different areas like the coatings, as you know, automated by different industries. The diffusion and the slicing and the polishing, all that stuff is well taken care of. So I think that the answer is that it's just a matter of putting them together. It depends on the material. I think it's sort of a weaselly answer, but my feeling is it's nice to use these nice materials, but if you are going to set up a production line, you look at the best material you can buy in production quantities and then that sets your target as to what your line efficiency would be.

RALPH: Basically, is it a Green cell design or something different?

ILES: It's shallow-diffused, probably textured, if you are going to do some external cooling of some sort. Probably textured with a multilayered coating and presence of contacts. And, I'll point out, without surface passivation, and without contact passivation I believe you cannot go over 17% anyway.

RALPH: To get to 19% or so are you still going to have to surface passivate?

ILES: At 19% you are going to have to do surface passivation to get the voltage up and if you want to agree there consistently, you have to keep the contacts out of it.

SCHRODER: In the quest for the high-efficiency cell, in your view, what would be the three most important problems that you face today, or perhaps the most unknowns today? Not 10 or 12, but the top three.

ILES: I think the most important thing would be to find a process sequence. Well, first of all, choose the material, you have to choose the material, because that fixes your design, and there are several competitive designs. The second is quite important -- that you pick a process sequence that can really take you up all the way and not sort of falter as you go. You don't need super-processing at each stage, but you need each stage to be done very well, and I think you choose a sequence maybe where these trade-offs are made. There are certain trade-offs, as there are in any semiconductor device, and it's how you fit into the trade-off that matters. Now in the past, some of those trade-offs have been internal technology that -- like a guy has only a shadow mask, so he says I can't get very good shading areas so I'll make up for it, I'll do something else that's very clever, and I'll stress that I've got some advantage, even though I don't have a good process. I think when you are getting up to 19% or 20% you have to have everything working very well -- the whole sequence has to work very well.

SIRTL: Peter, you made a fairly strong point on the material, of course, and the worst thing that could happen after the meeting is a strong inflow of orders to get the super-material, or something that would come near to it. I think I should comment a little more on that. On the one hand, when you get some extraordinarily good material on the float-zone side, it has to be a byproduct of a much larger portion on a production scale. That's where the money has to come from. So in every case, such a kind

of material would always be very limited. Of course, it could be supported in terms of a project being made out of a long-range task to create, under any circumstances, such a super-material. But, on the other hand, if you remember, I made a strong point yesterday on the subject of gettering. I think the science of gettering still is in its infancy. My expectations, at least, go stronger in this direction -- that we would learn, over the years to come, a lot more about gettering and to handle material that can be produced under reasonable cost conditions and give it the final touch by the most appropriate gettering system. And that, of course, has to vary from one type of cell, or type of processing, to another.

ILES: I think that's a good point. It takes us away from the route of having to have clean rooms at every stage and building a whole extensive processing sequence. That's philosophically a nice approach. Do you think there's no chance of scaling-up for float-zone? There is obviously not a large enough market now, but supposing somebody said there was a quarter of a gigawatt market.

SIRTL: I have my serious doubts with it, economically, that this would ever be able to work.

LOFERSKI: Peter, you made a rather strong point, and I think I agree with it, that the significance of what one has to do is to make it happen in the real world, on real-world materials. I think my understanding of how the process might go is that on the one hand you have to understand all the bits and pieces of how -- perhaps in the laboratory -- you would reach a 20% level, which might translate in the real world to an 18% level. In that regard, perhaps the Cz material in its finest form might be capable of that kind of quality. The point about understanding what is required to get to the very highest level you can is also important, and in that sense -- having determined that -- now you attempt to apply that with the things that are available. I believe that is the next step that should, and perhaps will, take place. The float-zone material -- you are putting all the load on the guy producing the material -- and the Czochralski, I think we are implying some sort of in-line gettering or updating or whatever. I think that's important. If you tell a manufacturing man "Here is what we want you to make -- oh, by the way, you are not going to get that material, you are going to have to somehow or other in that sequence put a gettering thing in there," that's not fair to him. I think you have to present him with the two options and see which he can produce. I think in a sense you are right, but I think the conception that was held at the time when the high-efficiency work that I am supporting was put in place was simply: let us, in terms of understanding the details, remove as many of the roadblocks as we can. Let's work on the best material available to see what comes out. If you know you have a number of defects in the materials that are going to be limiting features, no matter how well you do the job, and no matter how good your understanding, you will be hindered by that. Perhaps after you understand what's required you then work your way around this one point, and knowing you might get the answer is better than saying "We think we can get the answer. Let us try to find the way without knowing where the pitfalls might possibly be." We are a little sensitive, because we are like the guy who can jump 7'9"

but we can't tell anyone else how to jump 7'9". I'd hate to see a sprinter trying to jump 7'9".

ILES: When you are talking about a 20% cell, you cannot put all the burden on material; I think your earlier comment was well taken. So it's very important that we know how to make this 20% cell in the laboratory so that eventually one can optimize a cost or simplify later.

SWANSON: Peter, we have seen in selected Czochralski wafers, 10 to 20 ohm-centimeter resistivity range, as high a lifetime as we have seen in float-zone, and that was about four years ago. It was very sporadic, and averaged more like 20 microseconds to 50 microseconds. I think today, perhaps, with much more understanding on controlling oxygen concentration, that a serious effort to go back and try to learn how to get the lifetime up in Czochralski would be successful, in light of the better material today. What we found is that the gettering procedures that have been optimized around generation lifetime considerations are simply not appropriate, and generally do not work when you are concerned with recombination lifetime in the bulk of the material.

ILES: If you want to make fast-switching solar cells in good shape.

PROCESS AND DESIGN CONSIDERATIONS FOR HIGH-EFFICIENCY SOLAR CELLS

N85-31641

A. Rohatgi and P. Rai-Choudhury
Westinghouse R&D Center
Pittsburgh, PA 15235

ABSTRACT

This paper shows that oxide surface passivation coupled with optimum multilayer anti-reflective coating can provide ~ 3% (absolute) improvement in solar cell efficiency. Use of single-layer AR coating, without passivation, gives cell efficiencies in the range of 15-15.5% on high-quality, 4 ohm-cm as well as 0.1-0.2 ohm-cm float-zone silicon. Oxide surface passivation alone raises the cell efficiency to > 17%. An optimum double-layer AR coating on oxide-passivated cells provides an additional ~ 5-10% improvement over a single-layer AR-coated cell, resulting in cell efficiencies in excess of 18%. Experimentally observed improvements are supported by model calculations and an approach to > 20% efficient cells is discussed.

1. INTRODUCTION

The idealized efficiency[1] of a silicon solar cell is about 25%, assuming the best material and surface parameters achievable to date, although present day cells fall considerably short of this limiting value. This is largely a consequence of heavy doping effects, bandgap narrowing, and high recombination at and near the cell surfaces. The major problems of efficiency improvement fall in the above categories; however, there are additional design requirements for efficient contacts and antireflective coating. Although these areas are well understood, they are not trivial and must be optimized consistent with the device structure. In this paper we will discuss the design, fabrication, and analysis of 18% efficient surface-passivated solar cells on high-quality, 0.1-0.2 ohm-cm float-zone silicon. Results on 4 ohm-cm silicon cells are also shown. Various electrical measurements, along with a simple theoretical model which uses internal recombination velocity to assess minority carrier losses in various regions of the solar cell, are used to analyze the cell data and address the requirements for surface-passivated 20% efficient cells on low-resisitivity silicon.

2. CONSIDERATIONS FOR HIGH-EFFICIENCY SOLAR CELLS

It is clear that high efficiency is a major attribute that will en ce the large-scale applicability of solar photovoltaic systems. Assuming 5% reflector absorption losses, 1% mismatch losses, and 96% packing factor for rectangular cells, 20% efficient cells will be required for 18% efficient

modules. Current module efficiencies are about 12-13% in production. In the last two to three years, solar cell efficiencies have been in the range of 14-17%, even at the research level; however, recent breakthroughs have occurred in single-crystal cell efficiency at the research level. Cell efficiencies in the range of 17-19.1% have been reported by several investigators (Table 1). To achieve 20% or greater efficiency cells, a considerable amount of further research will be required in the areas of:

- Material and carrier lifetime improvements
- Process development
- Design improvements such as surface passivation, reduced heavy doping, and multilayer AR coating
- Tandem cells

Module efficiencies can be further enhanced by:

- Improved packing factor
- Reduced reflection losses from the glass
- Reduced interconnect losses
- Reduced mismatch losses by near-uniform cells

2.1 Material and Carrier Lifetime Considerations

High carrier lifetime is desirable because it improves both J_{sc} and V_{oc}. The best measured lifetime values in silicon to date are on the order of 1 msec, well below the ultimate value based on the radiative band to band recombination. Fossum et al.[11] have hypothesized a vacancy-related fundamental defect in silicon crystals which limits the lifetime in nondegenerate silicon. Based on our experience, it is difficult to detect any deep-level defect in good-quality silicon even with the help of the most sensitive techniques, such as deep-level transient spectroscopy, that are available today. There is some concern about the accuracy of true lifetime or diffusion length measurements, especially when diffusion length becomes greater than the base width.

In Table 1, use of very high-quality low-resistivity (0.1-0.3 ohm-cm) float-zone silicon was a key factor in 17-19.1% efficient cells fabricated by Westinghouse, Spire Corp., and the University of New South Wales. It is not clear why these crystals are much better or less sensitive to process-induced lifetime degradation compared to the majority of low resistivity Czochralski or float-zone crystals. Therefore, there is a need to identify, understand, and minimize the lifetime-limiting centers and develop more reliable techniques for measuring true base diffusion length and surface recombination velocities.

2.2 Process Considerations

High carrier lifetime in the starting silicon becomes academic if processing introduces new defects and unwanted impurities. Special care must be taken during substrate cleaning, and favorable gettering ambients consisting of $POCl_3$ and HCl gas should be utilized whenever possible. Slow

Table 1

Some Recent High-Efficiency Silicon Solar Cells
Tested Under One Sun AM1 Illumination

J_{sc} mA/cm^2	V_{oc} mV	FF	η %	Substrate Resistivity ohm-cm	Source
36.0	625	.805	18.1	0.15	Applied Solar Energy
36.5	610	.775	17.2	10.0	Corporaton
36.2	600	.793	17.2	4.0	Westinghouse
36.0	627	.800	18.1	0.2	Westinghouse
35.9	627	.800	18.1	0.3	Spire Corporation
34.9	643	.813	18.1	0.2	University of New South Wales, Australia
33.0	653	.810	17.5	0.3 Concentrator Cell	Sandia National Laboratories
34.0	624	.820	17.6	0.3 Concentrator Cell	Applied Solar Energy Corporation
35.1	623	.780	17.1	0.3	Catholic University of Leuven, Belgium
36.0	653	.811	19.1	0.1-0.3	University of New South Wales, Australia

cooling and gradual wafer withdrawals from the furnace could also be important in preserving the lifetime of the starting material.

2.3 Design Considerations

If a very high carrier lifetime cannot be obtained in the finished cell, then a clever cell design can still give high-efficiency cells. As suggested by recent model calculations of Sah,[12] 20% efficient p^+-n-n^+ cells can be realized with a base lifetime of 20 μsecs provided that cell thickness is reduced to 50 μm and the back-surface field is 20 μm deep with N_D of 5×10^{18} cm^{-3}. Wolf's[1] design criteria for very high-efficiency cells include equal impurity concentration in the base and emitter up to the onset of heavy doping effects, coupled with reduced surface recombination velocities on the order of 10 cm/sec.

In this paper our own model calculations show that a combination of design features such as surface passivation, reduced heavy doping, and

Table 2

A Comparison of Measured and Calculated Open-Circuit Voltage for High- and Low-Resistivity Solar Cells With and Without Surface Passivation Designs

ID and Cell Design	S_{ejb} cm/sec	S_{eje} cm/sec	J_{ob} pA/cm^2	J_{oe} pA/cm^2	$J_{ob} + J_{oe}$ pA/cm^2	Measured J_{sc} mA/cm^2	Calculated V_{oc} mV	Measured V_{oc} mV	Cell η %
	$N_A = 3.5 \times 10^{15}$, L = 400 μs, W = 250 μm								
No Passivation Cell #2	883	4826	7.9	1.5	9.4	33.4	569	582	15.2
Front and Back Surface Passivation Cell # HIEFY 4-5	517	3340	4.6	1.0	5.6	36.2	584	600	17.2
Passivation and Reduced Heavy Doping	456	117	4.1	0.04	4.14	36.2*	592	-	18. Δ
	$N_A = 2 \times 10^{17}$, L = 168 μs, W = 375 μm								
No Passivation Cell #C-2	956	12129	0.15	1.3	1.45	31.7	616	612	15.6
Front and Back Surface Passivation Cell #C-8	953	9301	0.15	0.97	1.12	33.2	625	628	17.0
Surface Passivation and Double-Layer AR Cell #C-12	953	9301	0.15	0.97	1.12	36.0	625	627	18.0
Surface Passivation Reduced Heavy Doping, Double-Layer AR	925	332	0.14	0.03	0.17	36.0*	675	-	20.0Δ

*Assumed
ΔExpected

multilayer AR coating can give ~ 20% efficient cells on 0.1-0.3 ohm-cm float-zone silicon with base diffusion lengths in the range of 150 to 200 microns.

3. MODEL CALCULATIONS

We have developed a simplified analytical model to provide guidelines for maximizing V_{oc} and cell efficiency. This model, which is described elsewhere in detail,[2,3] includes the effect of bandgap narrowing, Auger recombination, and recombination at the cell surfaces, but it neglects the electric field effects resulting from the gradient of doping concentrations.[4,5] With the help of this model we can calculate internal recombination velocity (S_e) in any region of the cell using surface recombination velocity (S_o), diffusion length, cell width, and doping density as input parameters. The solar cell is divided into several small elements and S is calculated iteratively from the surfaces toward the junction using the following equation:

$$S_2 = \frac{N_2}{N_1} \frac{D}{L} \exp\left(\Delta V_{G2} - \Delta V_{G1}\right) \frac{S_1 \frac{L}{D} + \tanh\left(\frac{W}{L}\right)}{1 + S_1 \frac{L}{D} \tanh\left(\frac{W}{L}\right)} \qquad (1)$$

where W is the width of the element; (S_1, N_1, ΔV_{G1}) and (S_2, N_2, ΔV_{G2}) are the recombination velocity, doping density, and the bandgap narrowing at the two boundaries of the element; and D and L are the diffusivity and diffusion length of the minority carriers within the element. The model uses empirical equations to calculate diffusivity, diffusion length, and bandgap narrowing primarily from the doping density.[2,3]

Examples of internal recombination velocity plots are shown in Figures 1 and 2. Figure 1 shows the calculations for 4 ohm-cm cells with a base diffusion length of 400 μm, and Figure 2 is for 0.1-0.2 ohm-cm cells with a base diffusion length of 168 μm. Each figure includes the calculation for three different back-surface field (BSF) and emitter designs, namely: a) no surface passivation, b) surface passivation where S_o is reduced to 500 cm/sec, and c) surface passivation plus reduced heavy doping where the surface dopant concentration has been lowered from 2×10^{20} cm^{-3} to 10^{19} cm^{-3}. S_o at the metal and bare silicon surface is assumed to be 10^6 cm/sec and 10^4 cm/sec, respectively. A junction depth of 0.3 μm and a BSF width of 0.5 μm were determined by spreading resistance measurements on the actual cells. Exponential doping profiles are assumed in the diffused regions, and the doping density at the emitter depletion boundary in Figures 1 and 2 has been estimated to be 1×10^{17} cm^{-3} and 3×10^{17} cm^{-3}, respectively.

Using the values of the internal recombination velocities at the depletion region boundaries in Figures 1 and 2, total reverse saturation current (J_o) for any case can be calculated according to:

$$J_o = J_{ob} + J_{oe} = q\, n_i^2 \left(\frac{S_{ejb}}{N_A} + \frac{S_{eje}}{N_D}\right) \qquad (2)$$

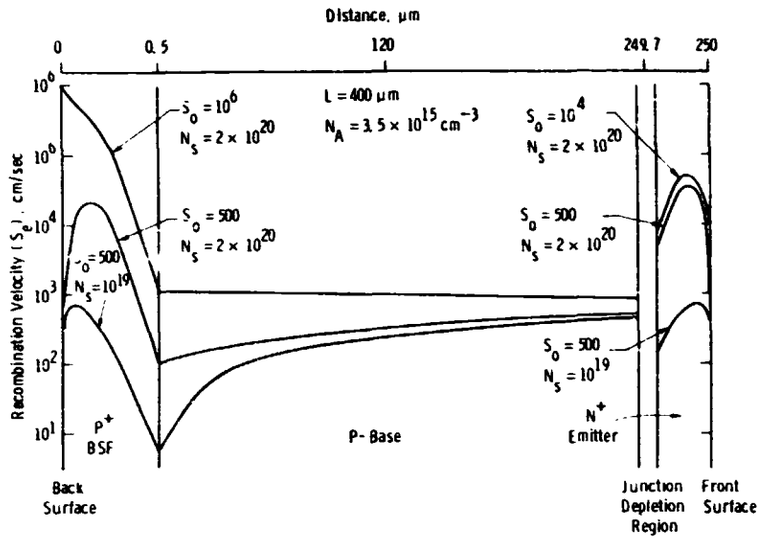

Figure 1. Model calculations and internal recombination velocity plots for 4 ohm-cm base cells with a base diffusion length of 400 microns.

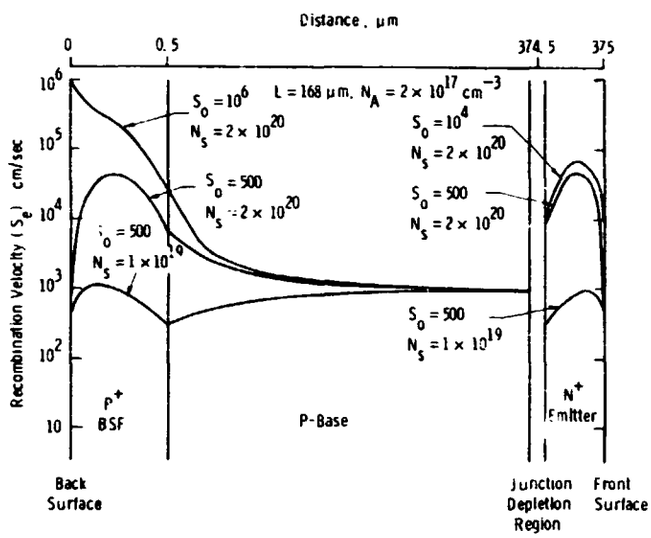

Figure 2. Model calculations and internal recombination velocity plots for 0.1-0.2 ohm-cm base cells with a base diffusion length of 168 microns.

where J_{ob} and J_{oe} represent the base and emitter contribution of J_o and (S_{ejb}, N_A) and (S_{eje}, N_D) are the recombination velocity and the doping density at the depletion region boundary in the base and emitter, respectively. Finally, V_{oc} is calculated from

$$V_{oc} = \frac{KT}{q} \ln \left(\frac{J_{sc}}{J_o}\right)$$

where J_{sc} is either estimated or measured short-circuit current density. Table 2 shows the calculated J_o and V_{oc} for various cell designs in Figures 1 and 2.

4. EXPERIMENTAL WORK

Following the guidelines of our model calculations, we fabricated oxide-passivated cells on high-quality a) 0.1-0.2 ohm-cm, boron-doped, (100), 15 mils thick float-zone silicon and b) 4 ohm-cm, boron-doped, (111) float-zone and dendritic web silicon. The baseline cell structure was n^+-p-p^+, where the n^+ emitter was formed by a 850°C $POCl_3$ diffusion which resulted in a junction depth of 0.3 μm and a sheet resistance of 60-80 ohm/square. The p^+ back-surface field was fabricated by a 950°C boron diffusion. Thermal oxide for passivation was grown at 800°C, which resulted in an oxide thickness of ~ 100 Å on top of the n^+ region and ~ 50 Å on the p^+ surface. About 600 Å thick single-layer AR coating was applied by a spin-on process on the passivated cells. AR coating thickness on the unpassivated cells was ~ 750 Å. In selected instances a double-layer AR coating was applied on the oxide-passivated cells by a spin-on process. The double-layer AR coating consists of 475 Å TiO_2 and 980 Å SiO_2 layers on top of 100 Å passivating oxide. Ti-Pd-Ag contacts were made on front and back, and the front grid design had an area coverage of 2%.

Both reflectivity and spectral response measurements were performed over a wavelength range of 0.4 to 1.1 μm to obtain the internal quantum efficiency. In selected instances, minority carrier lifetime in the cells was measured by the open-circuit voltage decay (OCVD) technique, where the injection current was made equal to the short-circuit current.

5. RESULTS

Table 3 shows the data for the 4 ohm-cm float-zone silicon cells, with and without oxide surface passivation. Without passivation, J_{sc} is ~ 33 mA/cm^2, V_{oc} is ~580 mV, and cell efficiency is ~ 15%. With both surfaces passviated, the cell efficiencies are in excess of 17%, with V_{oc} ~ 600 mV and J_{sc} ~ 36 mA/cm^2. Dark I-V measurements showed that oxide passivation reduces J_o by about a factor of two.[3] Quantum efficiency plots in Figure 3 clearly show that front- and back-surface passivation enhances the short- and long-wavelength responses of the cell. OCVD lifetime in the 17.2% cells was 50 μsecs, corresponding to a diffusion length of ~ 400 μm, which was used in the model calculations in Figure 1.

Table 4 shows the data for the passivated and unpassivated 0.1-0.2 ohm-cm base cells. Unpassivated cell efficiencies are ~ 15.5%, with J_{sc} of 31.5 mA/cm^2 and V_{oc} of 612 mV. After oxide passivation, cell efficiencies approach 17% with J_{sc} = 33 mA/cm^2 and V_{oc} = 627 mV. Dark I-V data showed a decrease in J_o from 7.1 x 10^{-13} A/cm^2 to 5.0 x 10^{-13} A/cm^2. Quantum efficiency plots in Figure 4 show that oxide passivation on this low-resistivity silicon increases only the short-wavelength response, but has negligible effect on the long-wavelength response. OCVD lifetime on these

Table 3

Solar Cell Data on 4 ohm-cm Float-Zone
Silicon With and Without Oxide Passivation
With Single-Layer AR Coating

Cell ID	J_{sc} mA/cm^2	V_{oc} Volts	Fill Factor	Efficiency %
		WITHOUT PASSIVATION		
1	33.3	0.582	0.767	14.8
2	33.4	0.582	0.780	15.2
		WITH PASSIVATION		
HIEFY 4-4	36.1	0.599	0.794	17.1
-5	36.2	0.600	0.793	17.2

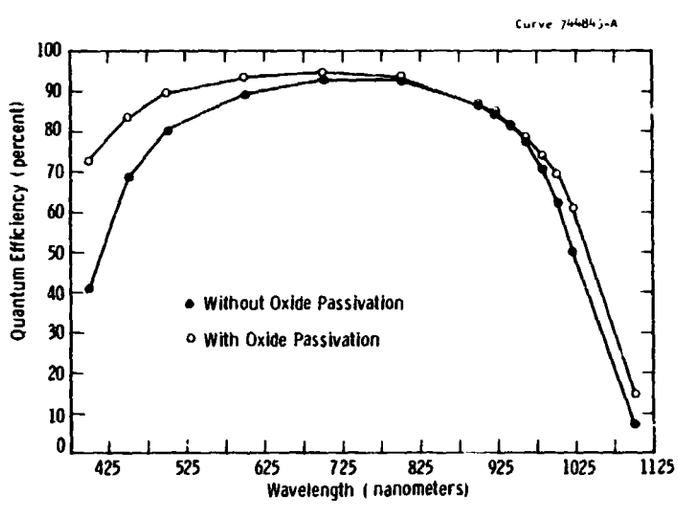

Figure 3. Internal quantum efficiency plots for a 15.2% unpassivated cell and a 17.2% efficient oxide-passivated cell on 4 ohm-cm float-zone silicon.

cells was ~ 168 μm, which was used in the model calculations in Figure 2. Table 4 also shows that double-layer AR coating increased J_{sc} from 33 mA/cm^2 to ~ 36 mA/cm^2 and gave > 18% efficient cells. Figure 5 shows the measured spectral reflectivities on single-layer AR-coated 17% efficient cells and double-layer AR-coated 18% efficient cells.

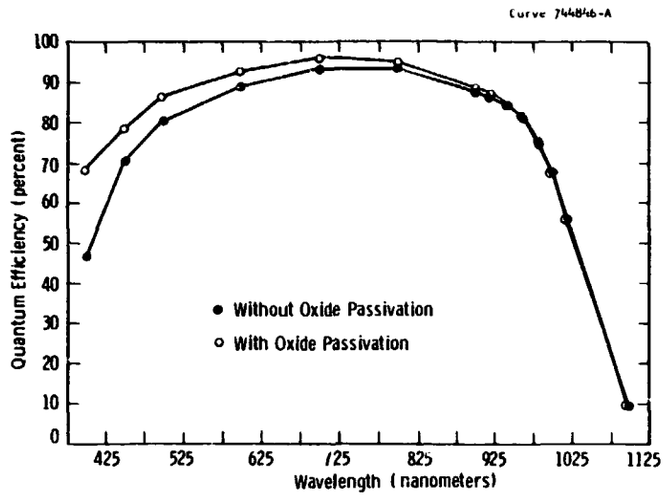

ORIGINAL PAGE IS
OF POOR QUALITY

Figure 4. Internal quantum efficiency plots for a 15.6% efficient unpassivated cell and a 16.9% efficient oxide-passivated cell on 0.1-0.2 ohm-cm float-zone silicon.

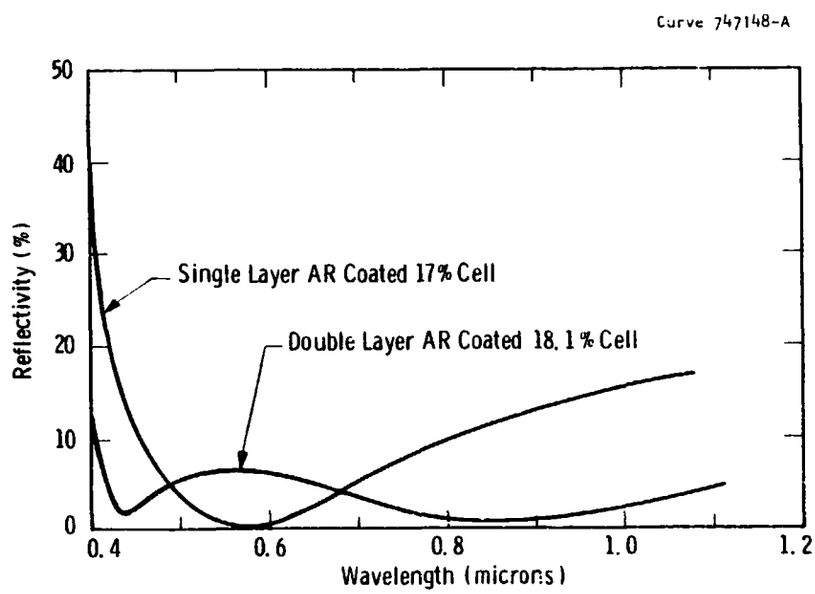

Figure 5. Measured reflectivities of single-layer AR-coated 17% efficient cell and double-layer AR-coated cell.

Oxide-passivated cells were also fabricated on 4 ohm-cm dendritic web silicon crystals. Table 5 shows that without oxide passivation, good-quality web crystals give average efficiency of ~ 14.5%, but with oxide passivation the cell efficiencies are ~ 16%. As in the case of 4 ohm-cm float-zone silicon cells, an oxide passivation-induced 1 to 2% increase in web cell efficiency was associated with an increase in J_{sc} and V_{oc} and a reduction in J_o.

Table 4

Solar Cell Data on 0.1-0.2 ohm-cm Float-Zone Silicon With and Without Oxide Passivation

Cell ID	J_{sc} mA/cm^2	V_{oc} Volts	Fill Factor	Efficiency %
		WITHOUT OXIDE PASSIVATION		
C-2	31.8	0.613	0.802	15.6
C-5	31.7	0.612	0.797	15.5
		WITH OXIDE PASSIVATION		
C-7	33.0	0.627	0.815	16.9
C-8	33.2	0.628	0.815	17.0
		PASSIVATION AND DOUBLE-LAYER AR		
C-9	34.7	0.626	0.810	17.6
C-10	35.1	0.624	0.803	17.6
C-11	36.0	0.620	0.808	18.0
C-12	36.0	0.627	0.800	18.1

Table 5

Solar Cell Data on 4 ohm-cm Dendritic Web Silicon With and Without Oxide Passivation

Cell ID	J_{sc} mA/cm^2	V_{oc} Volts	Fill Factor	Efficiency %
		WITHOUT PASSIVATION		
W6	32.7	0.575	0.782	14.7
W7	33.1	0.577	0.784	15.0
		WITH OXIDE PASSIVATION		
W1	34.6	0.584	0.784	15.9
W2	34.5	0.586	0.794	15.8

6. DISCUSSION

Table 2 shows that oxide passivation coupled with careful cell processing can produce cell efficiencies greater than 17% (AM1) on high-quality 4 ohm-cm float-zone silicon, with $V_{oc} \sim 600$ mV and $J_{sc} \sim 36$ mA/cm^2. This corresponds to a ~ 18 mV increase in V_{oc}, 3 mA/cm^2 increase in J_{sc}, and 2% improvement in absolute cell efficiency compared to the unpassivated cells. Model calculations in Figure 1 and Table 2 for the 4 ohm-cm base cells indicate that without any surface passivation, J_{ob} and J_{oe} contribute appre-

ciably to the total J_o; therefore, both front- and back-surface passivation become important in reducing J_o or improving V_{oc}. For example, Table 2 shows that: a) without any passivation, J_o = 9.4 pA/cm^2 and the calculated V_{oc} is 569 mV; b) with front-surface passivation alone, J_o = 7.9 + 1.0 = 8.9 pA; c) with only back-surface passivation, J_o = 4.6 + 1.5 = 6.1 pA; and d) with both surfaces passivated, J_o = 5.6 pA, resulting in a calculated V_{oc} of 584 mV. Thus, model calculations predict an increase of 15 mV in V_{oc} if both surfaces of a 4 ohm-cm cell are passivated and its base diffusion length is 400 μm. This is in very good agreement with the experimentally observed increase of 18 mV in V_{oc}. However, it should be noted in Table 2 that the absolute values of calculated V_{oc} are about 15 mV smaller than the measured values. This difference can be attributed to a number of assumptions and estimated inputs that went into the model calculations, e.g., surface recombination velocities, exponential doping profiles, diffusion length obtained by OCVD lifetime, and estimated doping density at the depletion region boundary in the emitter. More accurate values of the above parameters are needed for precise modeling; nevertheless, such model calculations provide very useful guidelines as to what should be done to which region of the solar cell in order to obtain high V_{oc}.

Figure 2 and Table 2 show a similar calculation for a 375 μm thick cell on 0.1-0.2 ohm-cm silicon with a base diffusion length of 168 μm. Unlike the 4 ohm-cm cells, here J_{oe} dominates J_o,[9] with or without surface passivation. In addition, J_{ob} remained unchanged (0.15 pA/cm^2) after back-surface passivation, because the minority carrier diffusion length in the base is much smaller than the thickness of the base. Therefore, back-surface passivation in these low-resistivity cells becomes unimportant, and only the front-surface passivation contributes to the increase in V_{oc}. A calculated increase of 9 mV in V_{oc} is in good agreement with the observed increase of 13 mV, considering the number of model assumptions. Notice in Table 2 that the calculated values of V_{oc} are in much better agreement (± 4 mV) with the measured values for the low-resistivity cells. This is probably the result of the better estimates for the model inputs for this case.

In the 4 ohm-cm base cells, we measured a 3 mA/cm^2 improvement in J_{sc} compared to 1.5 mA/cm^2 in the low-resistivity cells as a result of oxide passivation. This can also be explained in terms of the difference in the effectiveness of back-surface passivation in the two cells. In the low-resistivity cells, diffusion length to cell thickness ratio (L/W) is much less than one; therefore, reduced recombination at the back surface does not improve the collection or quantum efficiency of the carriers generated by the long-wavelength photons near the back surface (Figure 4). The improved J_{sc} in the low-resistivity cells only results from front-surface passivation, which enhances the quantum efficiency of the short wavelengths (Figure 4). In the 4 ohm-cm base cells, (L/W) is much greater than one; therefore, we observe an improvement in short- as well as long-wavelength response (Figure 3).

Table 4 shows that the use of double-layer AR coating raises the low-resistivity cell efficiencies from 17% to 18.1%. Single-layer AR-coated 17% efficient cells and double-layer AR-coated 18.1% cells on 0.1-0.2 ohm-cm float-zone silicon were analyzed in detail by spectral response and reflectivity measurements. Figure 5 shows a comparison of the measured reflectivity of the two cells as a function of wavelength. The double-layer AR-coated cell has smaller integral reflectivity compared to the single-layer

AR-coated cell. However, as shown in Figure 6, their internal quantum efficiency as a function of wavelength is virtually similar. It is important to remember that in the calculation of internal quantum efficiency, the effects of reflectivity are removed; therefore, identical internal quantum efficiencies imply that the interior quality of the two cells is nearly the same. Thus, the difference in the cell efficiency is primarily due to the difference in the reflectivity of the AR coatings. This is consistent with the cell data in Table 4, which show that the ~ 2 to 3 mA/cm^2 increase in short-circuit current is the main reason for increased cell efficiency from 17 to 18.1%.

Table 2 also shows model calculations for a cell design with reduced heavy doping in the emitter and the BSF regions. In this case dopant concentration at the surfaces has been reduced from 2 x 10^{20} cm^{-3} to 10^{19} cm^{-3}. It is interesting to note that reduced heavy doping in a 4 ohm-cm base cell gives additional improvement of only 8 mV (592-584) in V_{oc}, but in the low-resistivity case the calculated improvement is 48 mV (673-625), neglecting the drift field effects. This is because reduced heavy doping in the BSF region does not change J_{ob} very much, but reduced doping in the emitter lowers J_{oe} by more than an order of magnitude (Table 2). Since the V_{oc} of the oxide-passivated 4 ohm-cm cells is controlled by J_{ob}, reduced heavy

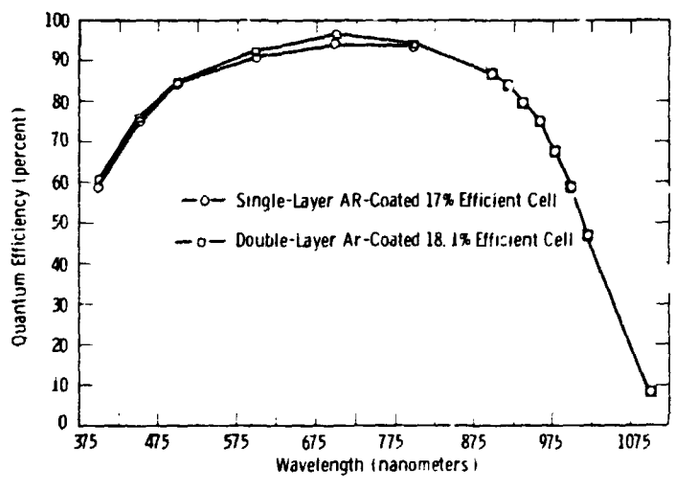

Figure 6. Internal quantum efficiency versus wavelength plots for a 17% efficient single-layer AR-coated cell and an 18.1% efficient double-layer AR-coated cell.

doping has little effect on V_{oc}. The V_{oc} of oxide-passivated 0.1-0.2 ohm-cm cells is controlled by J_{oe}; therefore, reduced heavy doping in the emitter increases V_{oc} very significantly. Therefore, use of multilayer AR coating and reduced heavy doping can make these low-resistivity surface-passivated cells (Table 4) 20% efficient with V_{oc} of 675 mV, J_{sc} of 36 mA/cm^2, and fill factor of 0.82. Calculations in Table 2 point out that at 20% efficiency, V_{oc} of these low-resistivity cells will become base-limited ($J_{ob} >> J_{oe}$). Therefore, in order to obtain greater than 20% efficient cells, either base thickness will have to be reduced or higher base diffusion lengths will be required. Some experiments are being conducted to verify this model design.

CONCLUSIONS

Consistent with our model calculations, we were able to improve open-circuit voltage and short-circuit current by oxide passivation of the cell surfaces. Oxide-passivated cell efficiencies on 4 ohm-cm as well as 0.1-0.2 ohm-cm float-zone silicon were 17% compared to 15 to 15.5% without surface passivation. Use of double-layer AR coating raised the low-resistivity cell efficiencies from 17% to 18.1%. In 4 ohm-cm cells, both front- and back-surface passivation was important, and their combined influence increased V_{oc} by 18 mV and J_{sc} by 3 mA/cm^2. In 0.1-0.2 ohm-cm cells, where diffusion length was much smaller than the cell thickness, back-surface passivation did not help significantly. In these cells, V_{oc} went up by 13 mV and J_{sc} increased by 1.5 mA/cm^2. Our model calculations indicate that in low-resistivity cells, J_{oe} dominates J_o; therefore, back-surface passivation does not improve V_{oc}. However, front-surface passivation reduces J_o and improves the short-wavelength response quite significantly. Model calculations indicate that oxide passivation coupled with reduced heavy doping in the emitter can give a very substantial increase in V_{oc} in the low-resistivity cells with efficiencies of 20%.

REFERENCES

1. M. Wolf, Proc. of 14th IEEE Photovoltaic Specialists Conf., p. 674 (1980).

2. J. R. Davis and A. Rohatgi, Proc. of 14th IEEE Photovoltaic Specialists Conf., p. 569 (1980).

3. A Rohatgi and P. Rai-Choudhury, IEEE Trans. on Electron Devices, ED-31, No. 5, p. 596 (1984).

4. M. Wolf, Proc. of 14th IEEE Photovoltaic Specialists Conf., p. 563 (1980).

5. M. P. Godlewski, C. R. Barona, and H. W. Brandhorst, Proc. 10th IEEE Photovoltaic Specialists Conf., p. 40 (1973).

6. A. Rohatgi, J. R. Davis, R. H. Hopkins, P. Rai-Choudhury, P. G. McMullin nad J. R. McCormick, J. Solid State Electronics, Vol. 22, p. 415 (1980).

7. A. Neugroschel, F. Lindholm and C. T. Sah, IEEE Trans. on Electron Device, Vol. ED-21, p. 662 (1974).

8. H. J. Hovel, "Semiconductor and Semimetals," Solar Cells, Vol. II, Academic Press (1975).

9. J. G. Fossum, F. A. Lindholm and M. S. Shibib, IEEE Trans. on Electron Devices, Vol. ED-26, p. 1294 (1979).

10. A. Rohatgi et al., Second Monthly Report on "Research on the Basic Understanding of High Efficiency in Silicon Solar Cells," SERI Contract No. XB-3-02090-4.

11. J. G. Fossum and D. S. Lee, Solid State Electronics, Vol. 25 (8), p. 741 (1982).

12. C. T. Sah, "Study of Relationships of Material Properties and High-Efficiency Solar Cell Performance on Material Composition," First Technical Report, DOE/JPL Contract No. 956289-83/1, July 1983.

ACKNOWLEDGEMENTS

The authors would like to acknowledge the invaluable contribution of the late J. R. Davis for device modelling and guidance. They would also like to thank T. W. O'Keeffe, D. L. Meier, and D. N. Schmidt for special response measurements; T. W. O'Keeffe, B. Yoldas, and N. J. Rooney for double-layer AR coating J. B. McNally, F. S. Youngk, and G. Machiko for cell processing; S. Karakoro help in cell testing, computer programming, and model calculations; and G. S. Law for reading and preparing the manuscript. This work was supported by SERI Contract No. XB-3-02090-4 and by the U.S. Department of Energy under prime Contract No. DE-AC02-83CH10093.

DISCUSSION

CISZEK: Ajeet, could you comment whether there is any influence on the process or the temperature of the oxidation that you use to create your passivation -- on the effectiveness of it?

ROHATGI: Yes, that's a very good question. That passivating oxide is not so easy to grow, because first of all you are growing it on a highly doped surface. It is not like growing an oxide on a silicon wedge, as you do in MOS. So the quality is very critical and the thickness control becomes difficult, especially when you are making such types of cells, because the oxidation rates on n^+ and p^+ are very different. On n^+ the oxidation rate is about three times faster than on the p^+. So it is very critical that you process your device under well-controlled conditions for the oxidation step. You almost have to tailor the oxidation in-house, because it is very sensitive to the processing condition. The thickness there is very critical. If you are off by 30 to 40 seconds you find out that you have exceeded the oxide thickness that is optimum for the passivation and the advantage that you are going to get from anti-reflection coating. But if it is very thick you are going to get hurt in reflection losses.

MILSTEIN: Basically, what I want to do is to confirm some of the hydrogen passivation work that Steve and Ajeet have talked about. We also have passivated a string of cells. These were provided by Bob Campbell; they are made on web. I presented most of this at the IEEE meeting, but we have some further data. The point that Ajeet made on improving efficiency, I think is very important. All of this is published, and will be out in the IEEE Proceedings. But basically, if you look at some of the not-even-so-good cells, you see a 1.5 efficiency. The numbers are hard to read. You will see full one point efficiency improvements on some of the others, again, on cells that were not all AR-coated. We have also looked at the spectral-response data. When Ajeet mentioned his results we took a look at some of ours, and I'll show you two unpassivated cells that we did. Here is cell 10, which was passivated, and here is cell 3, which was not passivated, and if I can line them up we find that for one of the cells the response, in fact, improved; for the other, it did not change very much from virgin cells that had not been passivated in any way. The upper curve is cell 5 and the lower curve is again cell 10, passivated, and you can see that there has been virtually no change there. So the hydrogen passivation clearly is doing things and it is not a one-shot result, it's been seen by more groups than one. The question is, what's going on, and are we going to work on that problem? I might point out that we have an experiment in progress too. We took two pieces of web, one as-received, and after about a 30-minute implant, pumping as much hydrogen as we could, we sent it off to NBS to have them look at it with neutron activation to try to locate hydrogen in the sample.

QUESTION: Just to follow up on what you said, we also have attempted to find out where the hydrogen is located by neutron resonance reaction technique, where we come with nitrogen 15, which reacts very strongly with hydrogen gas. This measurement was done at the University of Western Ontario, by

Professor Tong, and what we found was that 5 ppm hydrogen is present right at the surface, and this concentration goes down to about 1 ppm when you are 1,000 Å deep. Unfortunately, the detection limit is only 1 ppm, so we were not sure whether we had hydrogen beyond 1,000 Å, which is well within the emitter depth that we have. So we have been able to detect hydrogen at least as deep as 1,000 Å, and it could be beyond that.

RAO: Ajeet, in all of your data on that material with the hydrogen passivation and all the other data that other people have presented, I think you have one piece of data where you show the efficiency before AR coating and then after AR coating. I think, if I'm not wrong, the rest of the data including the one Joe presented just now don't show what happens after the AR coating. Looking at your data, the AR coating only improves by about 36% in your hydrogen-passivated cell, which is much lower than the 43% that you are talking about.

ROHATGI: There is a very good reason for that, because this AR coating was applied after the cell was finished, and when you try to spin the AR coating with the grid lines you never get the kind of improvement that you get when you put on the AR coating without the grids -- because when you are spinning it, you don't get the same thickness of AR coating near the grid lines.

RAO: So you anticipate that you will be able to get the 40% to 43% improvement with AR coating on the hydrogenated cells?

ROHATGI: No, this experiment was not done for that. I think we will have to modify our process sequence a little bit. We will have to do hydrogen-ion implantation at a different stage; we will not do it at this stage. It may be even more interesting to find out that hydrogen-ion implantation really works from the back, and this is another reason for looking into that. That way we don't have to do anything to the front. You finish the whole cell and before you put on the back metal you hit the cell with hydrogen-ion implantation and then put on the back metal. So you have to play some clever games with cell processing when you get to this stage.

TURNER: Your optical optimization calculation implied that you were using an oxide layer that was only 100 Å thick. Was that really what you used?

ROHATGI: For the oxide passivation, that's the lowest layer, which is the passivating oxide. Then on top of that we put 475 Å of TiO_2 and then on top of that we have 986 Å of SiO_2.

TURNER: But you got good passivation out of 100 Å of oxide, and that's very good.

ROHATGI: You don't want to go thicker than that -- otherwise it's going to hurt you in the reflection losses.

SAKIOTIS: I don't know if I missed it or not: did you mention the area of these cells you discussed?

ROHATGI: Most of the cells are 1 x 1 cm; we are now making cells that are 4 cm square.

SAKIOTIS: Do you have any results on the larger ones?

ROHATGI: Yes, larger ones are not quite as good. The 18.1% cell that you saw is 1 x 1 but the larger one is about 17.8. So we have some difficulty. But they are not more than 4 cm square in any case.

LESK: The nuclear people at Westinghouse have reported that above a few times of 10^{19} hydrogen, there is loss of hydrogen at the surface, and you are doping at 10^{18} I'm wondering if anybody has looked at the possibility that hydrogen implant at these levels may be removing something from the surface area that may have been hurting us in improving the characteristics.

ROHATGI: Okay, if we did the reflectivity measurement to see if we have modified the surface in any sense and -- in at least reflective measurement within what we have -- done anything drastic to the surface, the reflectivity we did before and after the implantation was identical. But we are not sure if we are removing anything, and that's a very good point. We should really do the spreading with this measurement to see if we have actually taken something off and our surface dopant concentration has changed.

QUESTION: May I make just a short comment? I have worked with hydrogen implantation years ago using high energy and pumped in at 10^{18}. It is my experience if you go that high that hydrogen forms bubbles in silicon, so if you go to lower energy then it's most likely that you remove some from the surface.

ROHATGI: That's a good comment. I don't think we know the answer to what we have inside our cell at this point. We don't know where the hydrogen is located or if it has formed any bubbles. We are just trying to do more measurements to find out more about it.

YOO: What is your oxide passivation temperature and time, roughly?

ROHATGI: It's a low-temperature oxide, it's about 800°C, and the time you have to set depending on what kind of dopant surface concentration you have, because oxidation rate, as I mentioned, is a function of how heavy doping you have. So there is no real fixed time. If you are working with low surface doping concentration, you have to go to longer times.

N85-31642

PROCESSING TECHNOLOGY FOR HIGH EFFICIENCY SILICON SOLAR CELLS

M. B. Spitzer and C. J. Keavney
Spire Corporation
Bedford, Massachusetts 01730

ABSTRACT

Recent advances in silicon solar cell processing have led to attainment of conversion efficiency approaching 20%. In this paper we review the basic cell design investigated at Spire and indicate features of greatest importance to achievement of 20% efficiency. We discuss in detail experiments to separately optimize high efficiency design features in test structures and discuss the integration of these features in a high efficiency cell. In this work, ion implantation has been used to achieve optimal concentrations of emitter dopant and junction depth. The optimization reflects the trade-off between high sheet conductivity, necessary for high fill factor, and heavy doping effects, which must be minimized for high open circuit voltage. A second important aspect of our design experiments is the development of a passivation process to minimize front surface recombination velocity. We indicate the manner in which a thin SiO_2 layer may be used for this purpose, without increasing reflection losses, if the antireflection coating is properly designed. We also present details of processing intended to reduce recombination at the contact/Si interface. Data on cell performance (including CZ and ribbon) and analysis of loss mechanisms are presented. We conclude with a discussion of the ultimate performance that may be achievable with this type of processing.

INTRODUCTION

The attainment of 20% conversion efficiency in flat-plate Si solar cells is presently the goal of the National Photovoltaics Program (1). To this end, we have been conducting research on the ion implanted Si cell. This work recently led to the achievement of conversion efficiency of 18%, and efficiency approaching 20% appears possible in the near future (2,3). In this paper, we review the results to date with emphasis on cell processing aspects, and we indicate the device design and cell processing techniques that appear necessary for achievement of the national goal.

The high efficiency cell process to be discussed is based on the use of high lifetime float zone Si. This material was selected owing to superior minority carrier lifetime over a broad resistivity range. One promising alternative is the use of Czochralski silicon, which will be feasible if modest diffusion length (~200μm) can be achieved in low resistivity wafers. Many aspects of the techniques to be presented are applicable to polycrystalline material as well, with conversion efficiency commensurate with the diffusion length in such material. We will report in this paper on the application of some of our processing techniques to sheet materials.

PRECEDING PAGE BLANK NOT FILMED

The junction formation technique to be discussed is based on ion implantation and thermal annealing. As was shown in a recent paper, the ion implantation process allows one to reproducibily adjust the emitter dopant concentration to near optimal values (4). In addition, the thermal anneal process can provide a passivating surface oxide if oxygen is admitted to the gas stream. The versatility of this junction formation technique has made possible rapid progress in emitter design.

In order to gain a better understanding of the loss mechanisms operating in our developmental cells, we have used a solar cell modelling code developed at Brown University by one of the authors (5). The results of the modelling will be provided where appropriate throughout this discussion. The one-dimensional model is described in detail in reference 5, and will only briefly be described here.

The modelling code evaluates the analytic solution of the inhomogeneous diffusion equation which we assume governs minority carrier transport in the quasi-neutral emitter and base of the solar cell. The quasi-neutral regions are assumed to terminate at the space-charge region on one side, and at a minority carrier mirror (characterized by a surface recombination velocity) at the other side. The analytic solution for the sum of the diffusion current and a space-charge region light-generated current is integrated over the solar spectrum to obtain short circuit current (J_{SC}), open circuit voltage (V_{OC}) and efficiency. In addition, provisions have been made for front surface reflection loss, shadow loss, reflection from a back surface mirror, and light-trapping (6).

The equilibrium minority carrier concentrations are calculated using Fermi statistics. The rigid band approximation is used to calculate the effects of band gap narrowing. Position dependence of doping, mobility, and lifetime are not included in this model and this limits the agreement between calculated and measured spectral response for short wavelengths. Nevertheless, we are able to achieve reasonable agreement with most other measurement data.

In the next section, we discuss the selection and characterization of the silicon used in our work. We follow this with a discussion of emitter design and fabrication, including the importance of surface passivation and ohmic contact design. The results of this work indicate the significance of high base minority carrier lifetime, and we report on new results from an investigation of the effects of cell processing on diffusion length. We conclude with a description of the cell design that we are pursuing for attainment of 20% conversion efficiency.

SELECTION OF SILICON

It is well known that fabrication of superior silicon cells based on conventional p/n junction designs requires silicon of the highest minority carrier lifetime (7). Development of a particular design and process sequence requires knowledge of the post-process lifetime; such data are of particular importance to the selection of base resistivity. For this reason, we investigated post-process lifetime of a variety of float zone slices.

Back surface field (BSF) cells were fabricated using a simple baseline process (8) from float zone slices obtained from Wacker and elsewhere. No antireflection (AR) coatings were used. Figure 1 replicates diffusion length data obtained by the method of Stokes and Chu (9) from quantum efficiency (QE) measurements of completed cells. The triangular data points indicate Wacker WASO-S slices. The square data points are Czochralski slices. Cell data is indicated in Table 1. It can be seen that AM1 conversion efficiency is about 10-11% for the WASO-S material of each resistivity. In order to determine how efficiency might be improved, we examined loss mechanisms in detail. In this way we were able to make significant improvements to the baseline process.

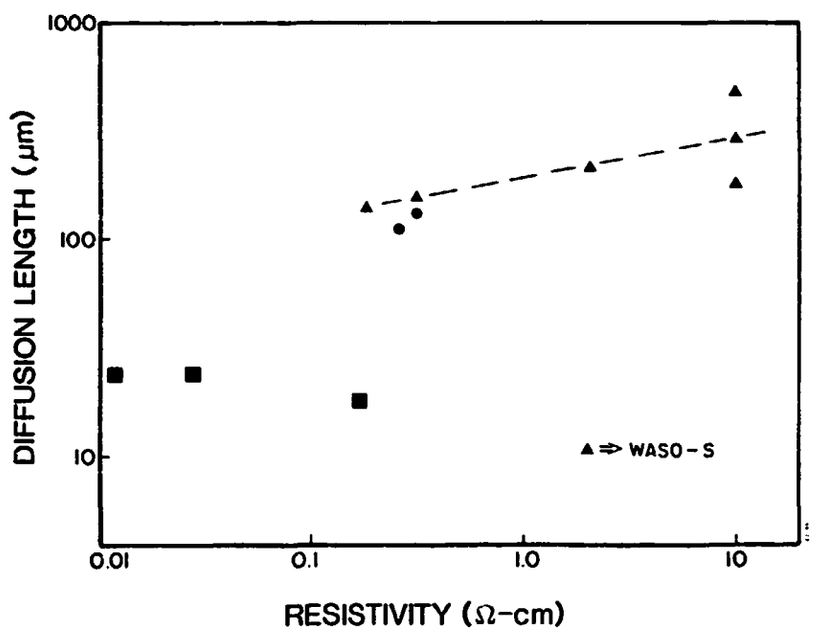

FIGURE 1. DIFFUSION LENGTH AS A FUNCTION OF RESISTIVITY. The dotted line indicates the functional dependence of L_D upon N_A that is assumed in our theoretical calculations.

TABLE I. CELL PERFORMANCE DATA FOR Si EVALUATION EXPERIMENT

GROUP	GRADE	RES. (Ωcm)	L_D (μm)	V_{OC} (mV)	J_{SC} (mA/cm^2)	FF (%)	EFF (%)
A	CZ	0.17	18	585 (003)	18.5 (0.6)	77.7 (2.7)	8.4 (0.5)
B	FZ	0.26	109	598 (001)	22.3 (0.1)	79.0 (0.7)	10.5 (0.1)
C	WASO-S (FZ)	0.18	139	597 (002)	22.3 (0.1)	77.3 (1.4)	10.4 (0.2)
D	WASO-S (FZ)	0.33	154	599 (001)	22.8 (0.1)	78.2 (1.0)	10.7 (0.1)
E	WASO-S (FZ)	2.1	212	583 (001)	23.4 (0.1)	78.9 (0.3)	10.8 (0.1)
F	WASO-S (FZ)	10	462	571 (001)	24.4 (0.1)	77.4 (0.3)	10.8 (0.1)
G	WASO-S (FZ)	10	227	563 (004)	24.1 (0.2)	77.1 (0.4)	10.5 (0.2)
H	FZ	0.32	129	597 (001)	22.8 (0.1)	78.9 (0.5)	10.7 (0.1)
I	CZ	0.027	—	530 (036)	12.0 (0.1)	54.6 (16.8)	3.8 (0.7)
J	CZ	0.012	—	364 (079)	7.6 (.02)	53.2 (1.8)	1.5 (0.4)

NOTES: Area = 4 cm^2, T = 28°C, L_D derived from quantum efficiency curves (9). Standard deviation shown in parenthesis.

Careful inspection of Table 1 indicates a large variation in fill factor (FF) for lower resistivities; this variation increases with decreasing resistivity. An examination of the dark I-V curves for representative cells, shown in Figure 2, indicates that leakage current increases as resistivity decreases. Through experimentation, we determined that this leakage current arises at the edges of the solar cells, which in our process are cut from the original wafers with a diamond wheel dicing saw. Etching of the edges to remove the saw damage removes this leakage path but also removes some active junction area. The deleterious effects on J_{SC} that edge etching causes can be minimized by either use of mesa etching defined by photolithography, or by using an ion implantation mask similarly defined so as to restrict the junction from kerf areas. Both methods were found to reduce the leakage current to negligible levels. For large-area cells in which edge leakage current is small compared to the diode forward current, this type of processing will probably be unnecessary.

ORIGINAL PAGE IS
OF POOR QUALITY

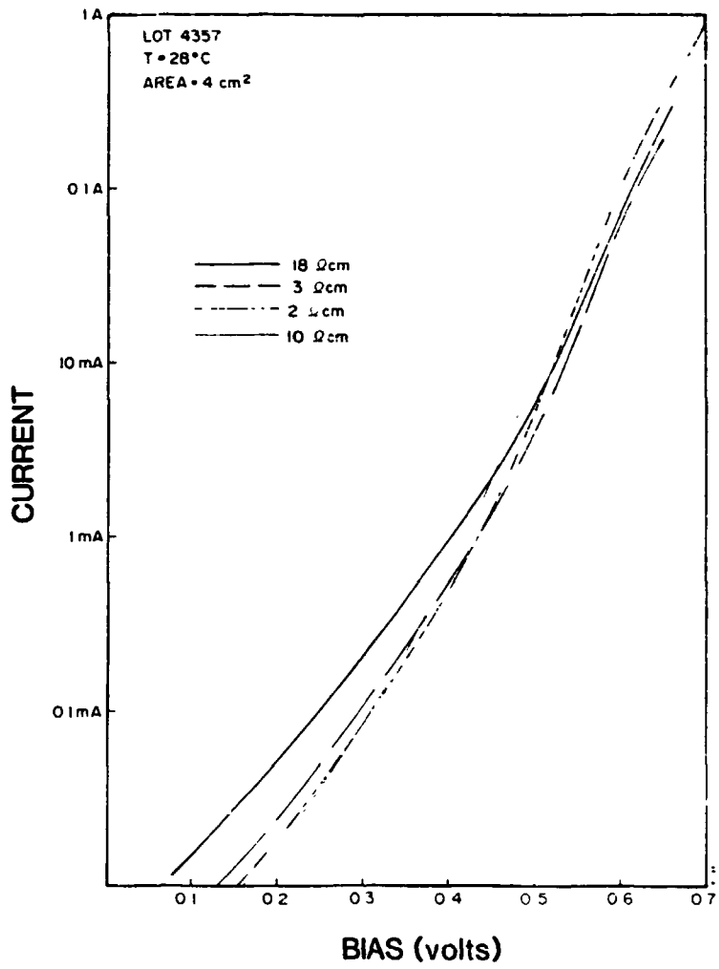

FIGURE 2. DARK I-V FOR REPRESENTATIVE CELLS OF VARIOUS RESISTIVITIES.

Figure 3 illustrates a comparison of measured external quantum efficiency (QE) data to the results of cell modelling, for a representative cell from group G in Table 1. Good qualitative agreement is obtained. Exact fitting was not attempted for two reasons: first, the absolute error in the QE data is not precisely known and second, the code cannot model position dependent parameters that are believed to be important in the emitter. Integration of the model QE data, however, yields good agreement with measured J_{SC}, and this is shown as a function of resistivity in Figure 4 with front surface recombination velocity as a parameter. In Figure 5 we present a comparison of the measured V_{OC} data to the calculated values, with band gap narrowing (ΔEg) as a parameter. The modelling suggests that for low resistivity Si, band gap narrowing and surface recombination velocity dominate V_{OC}.

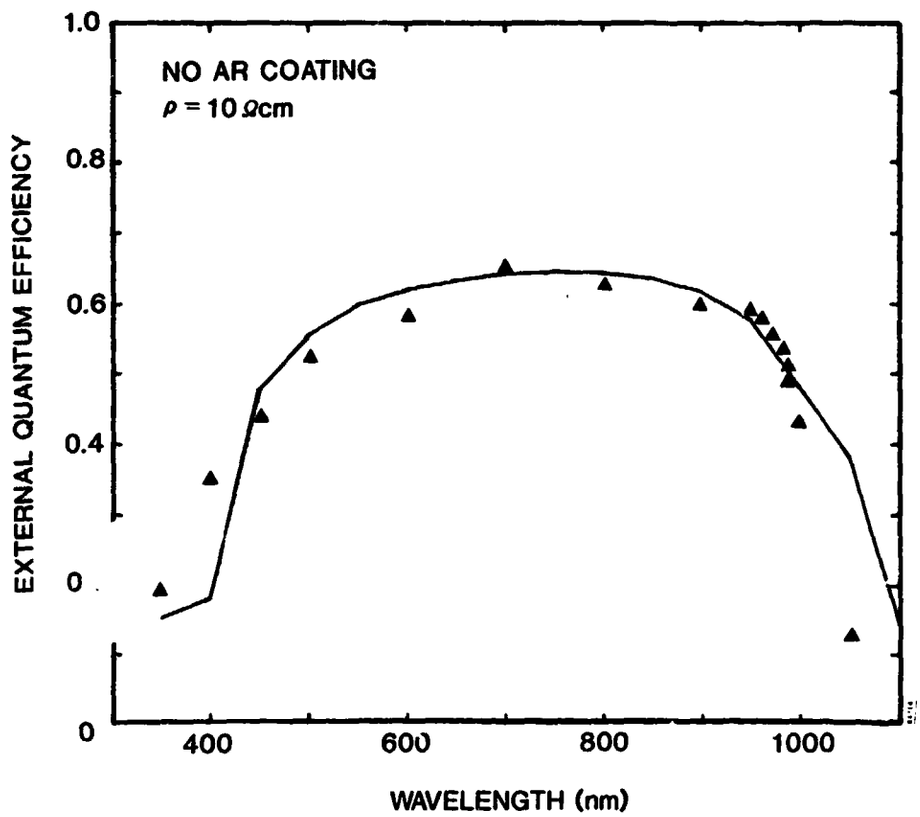

FIGURE 3. COMPARISON OF QUANTUM EFFICIENCY DATA TO MODEL CALCULATIONS FOR A CELL FROM GROUP G, TABLE 1.

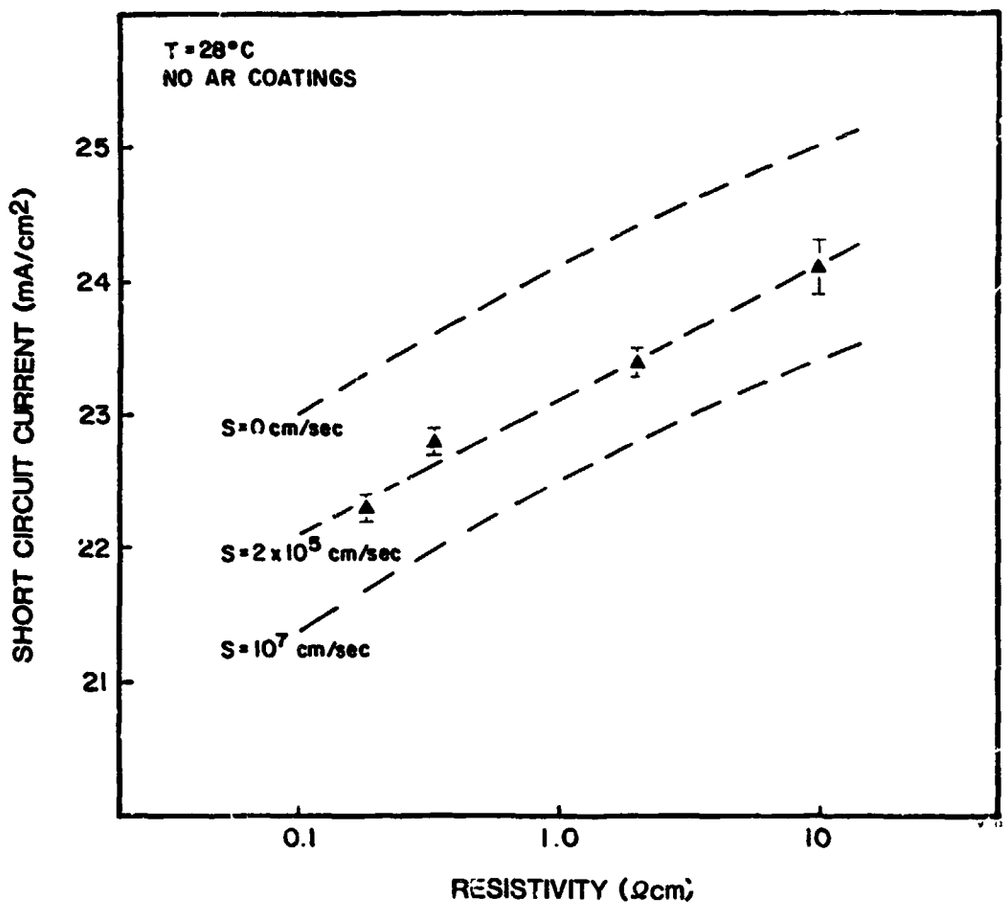

FIGURE 4. COMPARISON OF MEASURED AND CALCULATED J_{SC} AS A FUNCTION OF BASE ACCEPTOR CONCENTRATON.

We elected to work with cells of conventional thickness, even though calculations have shown that thin cells have theoretical advantages if minority carrier mirrors and light-trapping can be achieved (10). Our choice avoided the extraordinary care that handling thin (~50μm) cells requires. The modelling of cells with conventional thickness (~400μm) indicated that best efficiency would be obtained from low resistivity Si, provided that the emitter saturation current could be reduced, thus indicating the importance of pursuing research on emitter design.

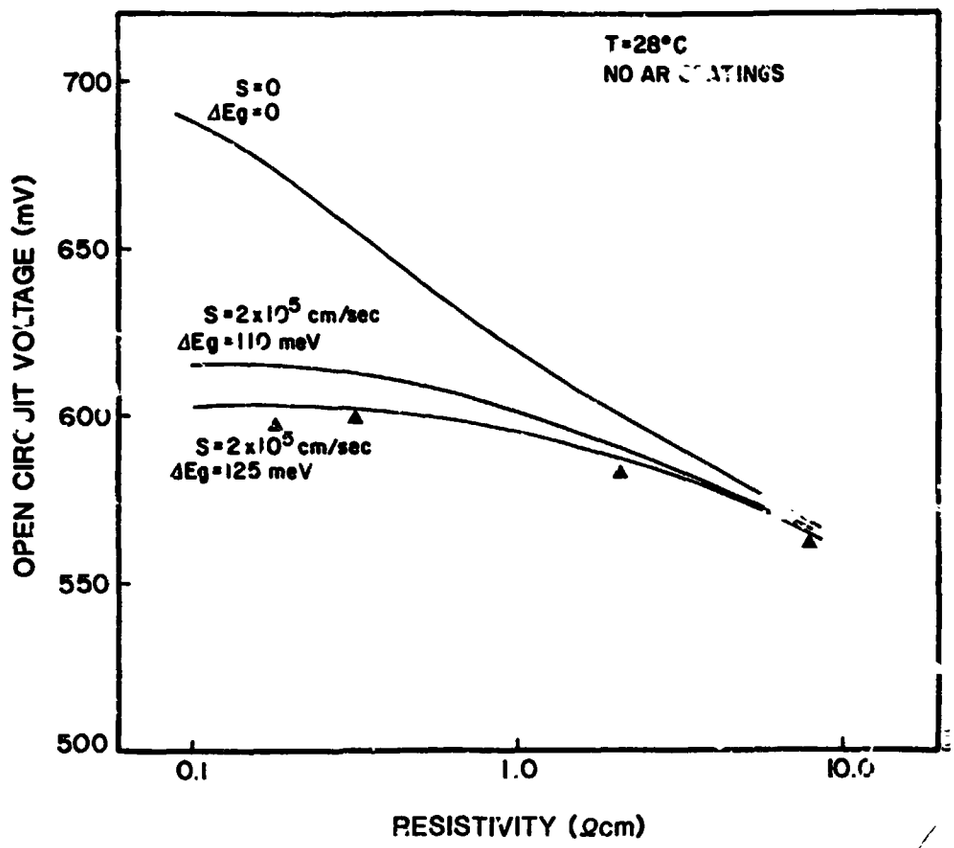

FIGURE 5. COMPARISON OF MEASURED V_{OC} DATA TO MODEL CALCULATIONS.

EMITTER EFFECTS

In a recent paper, we analyzed the importance of reduction of peak emitter dopant concentration, and it was shown that a very wide range of doping concentrations can be achieved with ion implantation (4). In Figure 6, we reproduce data that indicate that optimal QE at 350 nm is obtained for either arsenic or phosphorus emitter dopant concentrations of about 2×10^{19} cm^{-3}. V_{OC} appears to have a peak in this range as well, as shown in Figure 7. Unfortunately, the actual emitter concentration for which the maximum V_{OC} is obtained is obscured by low base diffusion length; i.e. in the neighborhood of the optimal donor concentration, the V_{OC} is base-limited. We will return to this point in a later section.

Figures 6 and 7 indicate that there is an advantage to passivating the front surface when shallow (~0.2μm) junctions are employed. Our experience indicates that as the junction is made deeper, the beneficial effects of passivation diminish; however, we have not conducted controlled experiments on this aspect.

ORIGINAL PAGE IS
OF POOR QUALITY

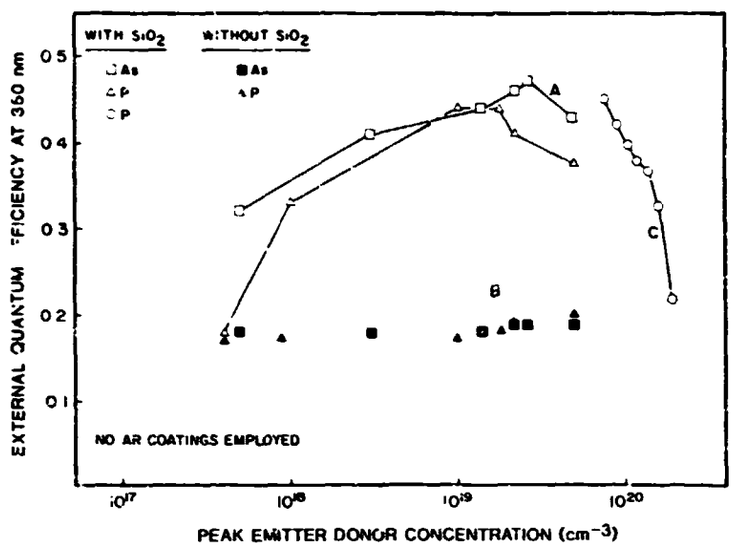

FIGURE 6. QUANTUM EFFICIENCY AT 350 nm. (A) Passivated As and P implanted emitters in 0.2 ohm-cm Si, (b) Non-passivated As and P implanted emitters in 0.2 ohm-cm Si, and (C) Passivated P implanted emitters in 0.3 ohm-cm Si.

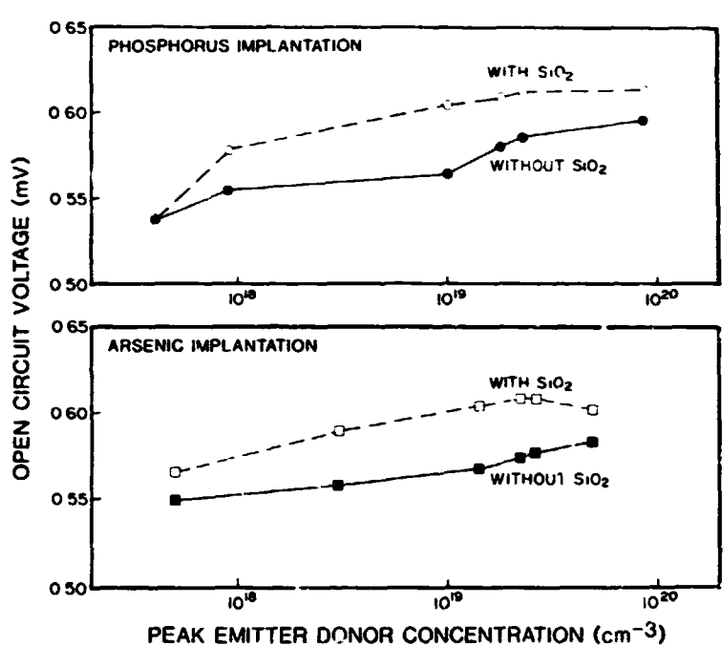

FIGURE 7. V_{OC} AS A FUNCTION OF N_D, WITH AND WITHOUT SiO_2 PASSIVATION.

Surface preparation can often affect the attributes of the ion-implanted emitter. In a later section, we describe the use of texture-etching to reduce reflectivity and enhance absorption. This etching, however, increases the front surface area, which necessitates a change in the ion implantation dose. To identify the optimal ion implantation dose for such an etched surface, we fabricated texture-etched solar cells with a range of doses. Details of this experiment are reported in reference 2. Figure 8 replicates the V_{oc} data for cells having SiO_2 passivation and for the same cells with SiO_2 removed. It can be seen from Figure 8 that the removal of the SiO_2 has a strong effect on V_{oc}.

There would seem to be three factors that control minority-carrier transport in the emitters of both the textured and polished devices: deleterious surface recombination, deleterious recombination and/or energy gap narrowing resulting from heavy doping effects, and advantageous minority-carrier reflection by the field resulting from the gradient of the doping. When SiO_2 surface passivation is present, the optimal ion implantation dose is approximately 5×10^{15} ions/cm^2 for a textured surface. Use of higher doses would seem to introduce deleterious heavy doping effects in the emitter which cause an increase in the saturation current. The existence of enhanced recombination in the near surface region is suggested by spectral response measurements that show that blue response decreases as the doping is increased (Figure 6). For lighter implantation doses, a loss in minority-carrier reflection occurs, owing to the reduction in the gradient of the doping near the surface. This reduction in doping perhaps allows an increase in carrier recombination at the front contact, and so V_{oc} decreases as the concentration is decreased. For the case in which the SiO_2 passivation is removed, the recombination at the surface exerts a strong influence on V_{oc}. In such a case, an increase in the peak dopant concentration that results from increase of dose increases the reflection of minority carriers, but the improvement is limited.

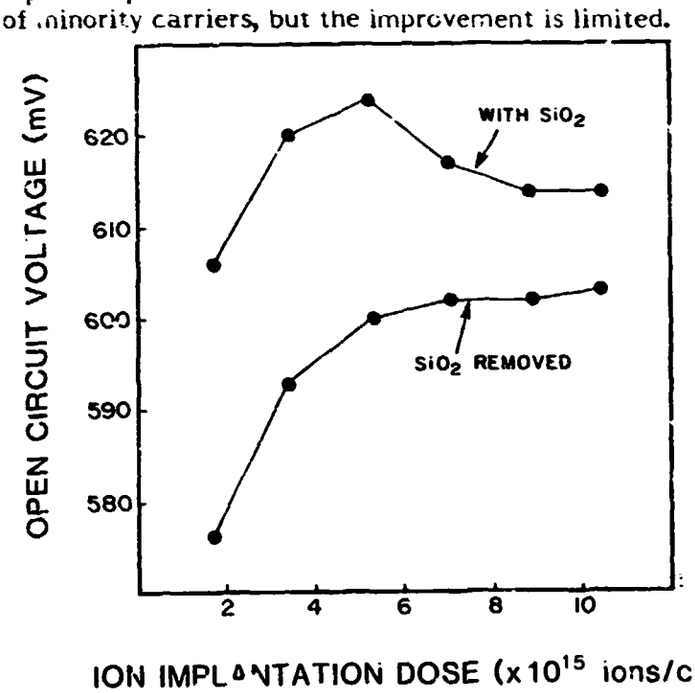

FIGURE 8. OPEN-CIRCUIT VOLTAGE AS A FUNCTION OF ION-IMPLANTATION DOSE FOR TEXTURE-ETCHED CELLS. The dose shown is the total dose measured by the implanter and is not corrected for the texture present on the target.

The optimization and theoretical analysis of our junction formation process applied to a textured surface requires knowledge of the resultant doping profile formed by the above implantation parameters on the {111} surfaces of the pyramids. For diffused junctions, one may perhaps assume that the junction profile replicates that which is formed on a standard {111} surface. It is not clear, however, that the depth distribution of implanted ions is equivalent to that obtained in an ordinary polished wafer, owing to scattering effects that may differ in the two cases. A further difference between diffusion and ion implantation is the increase in surface area mentioned above that obtains when texture is present. This increase requires a corresponding increase in ion dose.

For the above reasons, measurement of the dopant profile would be desirable. Unfortunately, the textured surface is not easily profiled using conventional techniques such as secondary ion mass spectroscopy, owing to obvious difficulties with depth calibration. For this reason, we conducted an experiment based upon ion implantation of a polished (111) wafer, suitably oriented with respect to the ion beam, to simulate the implantation of the {111} facets of the pyramids. This experiment is described in greater detail in reference 12.

A polished control (100) wafer was first implanted with $^{31}P^+$ using the conventional geometry. The implantation energy was 5 keV and the dose was 2.5×10^{15} ions/cm^2. An experimental (111) wafer was then implanted with $^{31}P^+$ at 5 keV to a dose of 5.2×10^{15} ions/cm^2, with the (111) surface oriented at an angle of 54.7° with respect to the ion beam to replicate the orientation of the facets of the textured surface. The specific dose, which includes an area correction related to the implantation angle, was 3×10^{15} ions/cm^2. Both wafers were then annealed in flowing dry N_2 using a three step process: 550°C-2hr., 850°C-15 min., 550°C-2hr. with ramping between steps. Dry oxygen was admitted to the gas stream during the 850°C step to grow the thin oxide necessary for passivation.

Spreading resistance analysis was obtained for both wafers, and is shown in Figure 9. The analysis indicates that the profiles are without detectable difference. This is not surprising, since the implantation parameters for polished and textured wafers were separately optimized for high cell performance. The value of the peak dopant concentration obtained in this experiment has been used in the modelling which follows in the next section.

To further refine our solar cell emitters, we have been investigating the role of recombination at the front ohmic contact. To this end, we have been experimenting with the reduction of ohmic contact area, while keeping the shadow loss constant, as has been done elsewhere (13). Figure 10 illustrates two methods of implementing this technique. In method A, the opening in the passivating oxide through which contact is made is reduced in width so that the opening is more narrow than the grid line. In method B, the openings are small separate squares. Both techniques require photolithography and alignment; however, one method of producing type A contacts would be to make the grid lines as narrow as the desired openings in the oxide. The width of the lines might then be increased to the desired width by electroplating, thus obviating alignment.

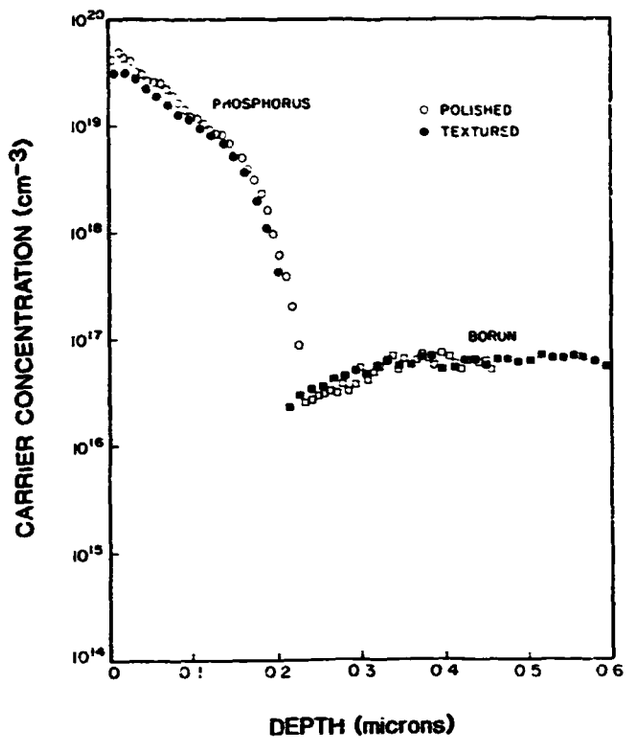

FIGURE 9. SPREADING RESISTANCE ANALYSIS OF A SIMULATED TEXTURED (111) WAFER AND A (100) CONTROL.

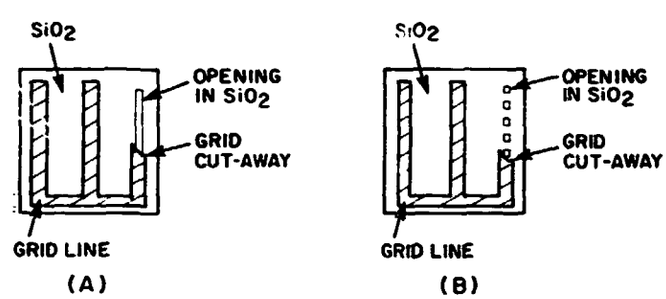

FIGURE 10. TWO METHODS OF REDUCING OHMIC CONTACT AREA.

Results with this type of processing are thus far inconclusive. In Figure 11 we replicate data from an experiment in which the ohmic contact area was varied as described above (4). Best results were achieved for reduced area, but the saturation current in these devices may arise mainly in the base, and so the optimal value of ohmic contact area may be obscurred. Further experiments are in progress and will be reported at a later time.

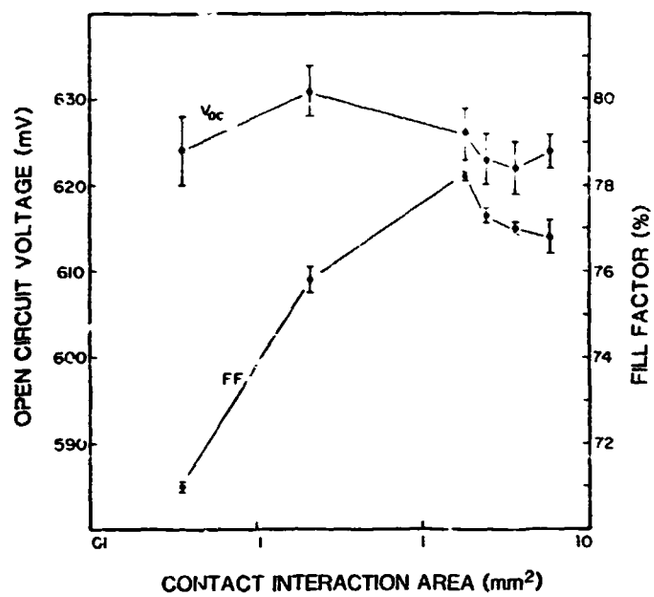

FIGURE 11. V_{OC} AND FF AS A FUNCTION OF OHMIC CONTACT AREA. (Base resistivity is 0.3 ohm-cm.)

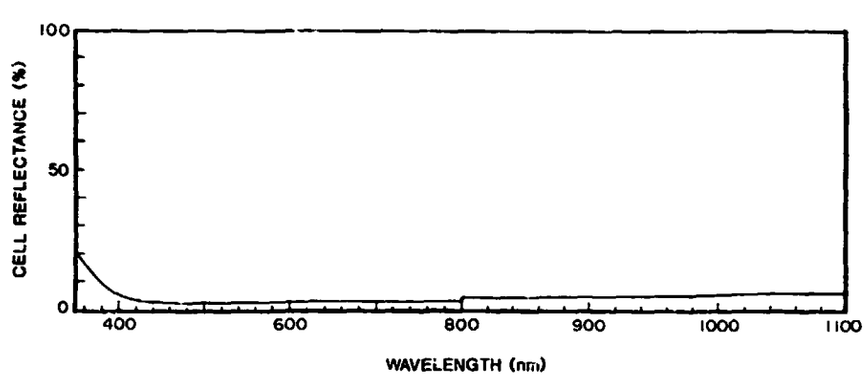

FIGURE 12. REFLECTION LOSS FOR A TEXTURED PASSIVATED SOLAR CELL.

Our results thus far on emitter design indicate the importance of both reduction of emitter dopant concentration and use of passivating oxide. This passivating oxide exerts a negligible influence on the reflection loss. To emphasize this point, we show in Figure 12 the measured reflectivity (courtesy of Dr. D. Arvizu, Sandia) from a textured solar cell. It can be seen that the reflection loss is indeed very small. The passivation can also be applied to sheet materials without severely affecting the AR coating. Recently we applied our emitter formation process to nonagon EFG ribbon. AM1 efficiency prior to AR coating was 9.7%. After evaporation of a single TiO_2 layer, efficiency increased to 13.2%, indicating a gain of 36%; higher gain would be possible with a more suitable AR coating (such as Ta_2O_5).

HIGH EFFICIENCY CELL DESIGN

Figure 13 illustrates the details of the solar cell structure yielding the highest efficiency to date. The texture-etched front surface is ion-implanted to form the emitter, as discussed in the previous section. The surface is provided with a thin layer of SiO_2 to reduce the front surface recombination velocity. An AR coating of Ta_2O_5 is applied on top of the SiO_2; the thickness of this layer is optimized to minimize the reflection resulting from the presence of the SiO_2. We have not reduced the ohmic contact area in this design.

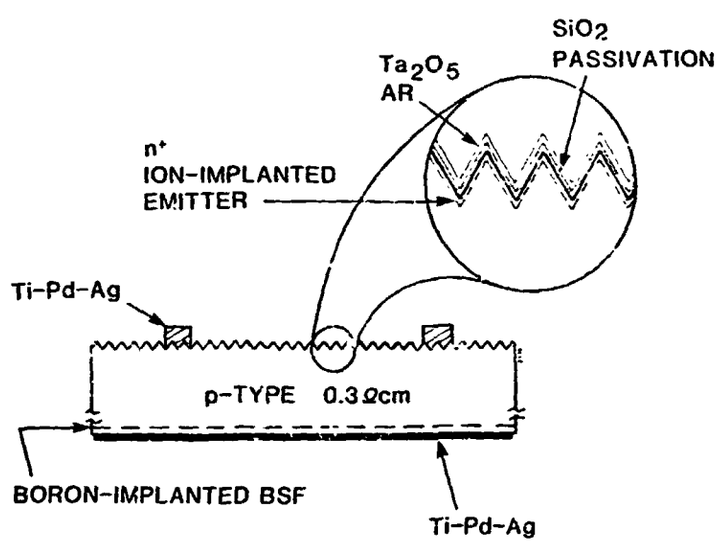

FIGURE 13. ILLUSTRATION OF THE SOLAR CELL STRUCTURE INVESTIGATED IN THIS WORK (not to scale).

Table 2 indicates the fabrication process for this cell design. The back surface is first implanted with $^{11}B^+$ and annealed to form a p^+ region. During the anneal, a thick surface oxide is grown to be used later for masking purposes. The resulting p^+ layer is about 1 m deep and has a peak concentration of 10^{20} cm^{-3}(14). Because the diffusion length is much less than the cell thickness, the p-p^+ junction is probably not effective as a back surface field (15); however, the p^+ region does aid the formation of a low resistance back contact.

TABLE 2. CELL FABRICATION PROCESS

Implant back	$^{11}B^+$ 50 keV, x 10^{15} ions/cm^2
Anneal/oxide	550°C -- 2 hrs. dry N_2 950°C -- 2 hrs. wet O_2
Pattern oxide	Acid etch
Texture	Hydroxide etch
Implant front	$^{31}P^+$ 5 keV, dose-variable
Anneal/oxidize	550°C -- 2 hrs. 850°C -- 15 min. 550°C -- 2 hrs.
Apply contacts	Evaporated Ti-Pd-Ag
Saw to size	2 cm x 2 cm
Plate contacts	Ag
Apply AR coating	Evaporated Ta_2O_5
Test	AM1, 100 mW/cm^2, 28°C

As discussed earlier, the surface oxide on the front was patterned to form an emitter ion implantation mask. The oxide mask defined the edges of the front phosphorus implant and so formed a planar emitter structure on each solar cell.

After patterning of the front oxide, the fronts of the wafers were texture-etched in a potassium hydroxide solution. Oxide on the back protected the boron implant from the etch. The fronts were then implanted with $^{31}P^+$ and annealed as described in the previous section. Evaporated Ti-Pd-Ag contacts were applied to both sides of the wafers and were patterned on the fronts using the photolithographic lift-off process. Electroplating was used to decrease the contact line resistance. The final step consisted of electron-beam evaporation of a Ta_2O_5 AR coating.

The resulting cells have been described in several recent publications (2, 16). Efficiency of up to 18% has been obtained, and the devices have been well characterized. We report here that an abbreviated form of the above process has been applied to Czochralski wafers supplied by Arco Solar Crystal Production. Efficiency of 16.8% was achieved (AM1, 28°C) and higher efficiency may be possible if the complete process is applied.

In Table 3, we summarize calculations of theoretical efficiency that indicate aspects of cell design that limit efficiency in the 18%-efficient FZ cells. The first entry in the table indicates the limit efficiency for a cell with width of 381 μm, made from 0.3 ohm-cm silicon. The only loss mechanism included in this calculation is Auger recombination (17); perfect light trapping and minority carrier mirrors are assumed (10). It is interesting that the upper limit to J_{SC} is 43.8 mA/cm^2, considerably higher than has been obtained in actual cells. Thus, considerable improvement is possible in J_{SC}. If neither light-trapping nor a back surface reflector (BSR) is present, the limit to J_{SC} is 42.2 mA/cm^2. Incorporation of actual reflection loss measured on a high efficiency cell (see Figure 12) indicates that J_{SC} can be as high as 40.6 mA/cm^2.

The diffusion length measured on our best cells is about 150 μm. Replacement of the Auger-limited diffusion length (~900μm) with the actual value reduces the J_{SC} to 36.9 mA/cm^2. Thus, a considerable amount of current is lost in our cells owing to bulk recombination. This loss can be overcome by increasing the diffusion length through more careful processing or by gettering. An alternative would comprise thinning the cell and adding a BSR.

The V_{OC} indicated for a 150μm diffusion length is 649 mV. The calculation of V_{OC} is extremely sensitive to the value of the effective masses, or in another formalism, to the value of the intrinsic concentration assumed. In our calculation, we used Fermi statistics with an effective density of states given by the average effective masses for electrons and holes (18). Owing to uncertainties in the effective masses, the effective density of states, and to heavy-doping effects in general, this calculation can be considered only as a rough estimate of the V_{OC}.

Inclusion of front surface recombination and bandgap narrowing reduces V_{OC} to values as low as 618 mV, if the data from reference 11 is used. By using a value for ΔEg of 70 meV, we find good agreement with experiment. This may reflect the fact that our model assumes uniform doping, so 70 meV is perhaps an average value characterizing the heavily doped region near the surface and the lightly doped region beneath it. The shadow loss in our cells is approximately 3.5%; however, the reflection loss (already subtracted) includes reflection from the contact. Therefore, we only include a shadow loss of 2% in our calculation. Inclusion of the measured series resistance of 0.32 ohm-cm^2 (2) drops the FF to 81.6%. It can be seen that reasonable agreement with an experimental cell is attained.

The results in Table 3 reveal that a large amount of carriers are lost to bulk recombination. To quantify the effects of L_D on J_{SC}, we modelled the cell described above with L_D as a parameter. The result is shown in Figure 14. It can be seen that for the case of no BSR, increase in L_D to 200μm yields nearly 1mA/cm^2 gain. The addition of a BSR with reflectivity of 90% would increase J_{SC} to 36.6 mA/cm^2; increasing L_D to 200μm in that case would yield J_{SC} of over 37 mA/cm^2. In the next section we will describe experiments intended to raise L_D to over 200 μm.

TABLE 3. ANALYSIS OF LOSS MECHANISMS OF SPIRE'S HIGH EFFICIENCY SOLAR CELLS

	V_{oc} (mV)	J_{sc} (mA/cm^2)	FF (%)	EFF (%)
Limit Efficiency of 0.3 Ωcm cell (Auger recomb. only)	713	43.8	84.7	26.5
No Light-Trapping	713	43.0	84.7	26.0
No BSR	712	42.2	84.7	25.5
Finite Reflection Loss	711	40.6	84.7	24.5
SRH Recombination (L_D=150μm)	649	36.9	83.6	20.0
Front Surface Recombination (S=2x10^4 cm/sec)	646	36.3	83.6	19.6
Bandgap Narrowing ΔEg				
(100 meV	618	36.3	83.0	18.6)
(80 meV	629	36.3	83.2	19.0)
70 meV	633	36.3	83.3	19.2
J_{oe} Penalty for Front Texture	625	36.3	83.3	18.9
Shadow Loss (2%)	624	35.6	83.3	18.5
Series R (0.32 ohm-cm^2)	624	35.6	81.6	18.1
Actual Data, Cell 22B	627	35.9	80.0	18.0

Notes: Calculations assume base width is 381 μm, T=28°C, Intensity = 100mW/cm^2, AM1.

In the event that efforts to raise L_D beyond 200 μm fail, one can consider thinning the base of the cell. A calculation of J_{sc} as a function of base width is shown in Figure 15, for the case of back surface reflectivity of 90%. For a cell with base width of 200μm, an increase in J_{sc} of about 0.5 mA/cm^2 is gained. If the cell is thinned and L_D is raised to 200 μm, J_{sc} of greater than 37 mA/cm^2 will be attained.

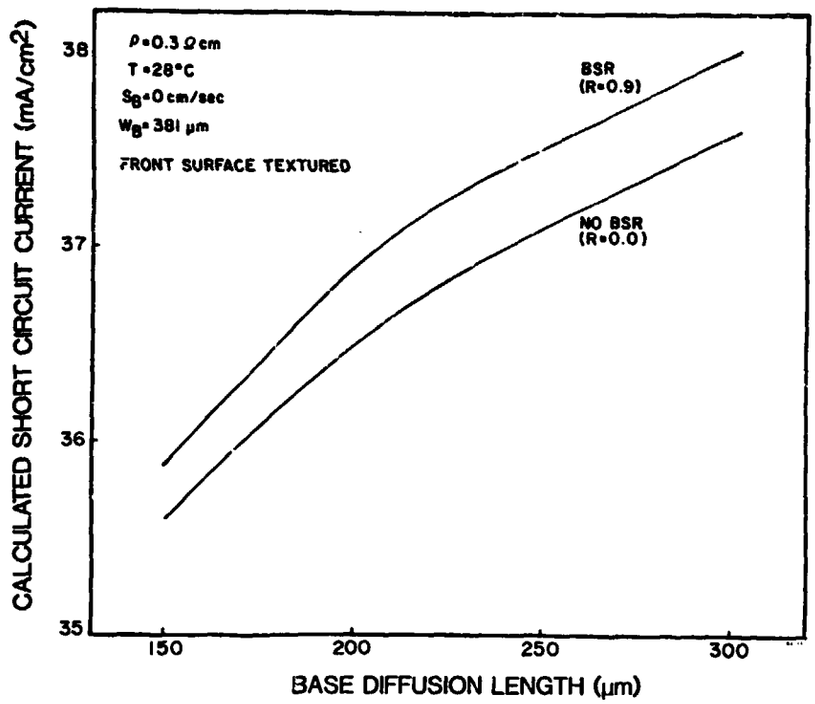

FIGURE 14. SHORT CIRCUIT CURRENT AS A FUNCTION OF DIFFUSION LENGTH.

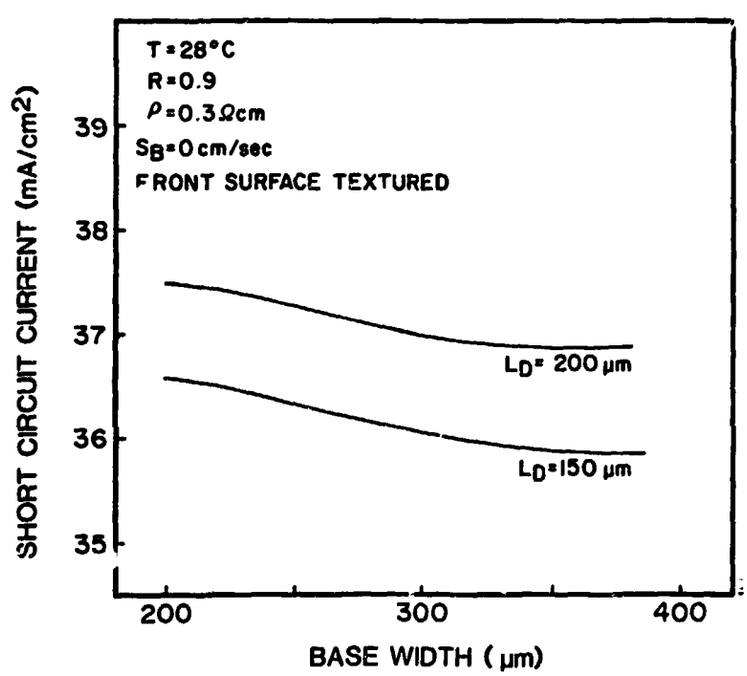

FIGURE 15. SHORT CIRCUIT CURRENT AS A FUNCTION OF CELL THICKNESS.

Improvements to L_D will also affect V_{OC}, although the gain is harder to quantify, owing to the large number of assumptions needed for calculation of V_{OC}. Nevertheless, V_{OC} as high as 660 mV is consistent with base resistivity of 0.3 ohm-cm and diffusion length of 200 μm, and experiments to reduce the ohmic contact area may reduce the emitter saturation current to negligible levels, thus enabling us to realize the base-limited V_{OC}. Similar results have already been demonstrated elsewhere (3).

EXPERIMENTS TO INCREASE J_{SC}

The preceding discussion has assumed that a BSR with reflectivity of 90% can be achieved. In fact we have developed such a BSR and in Figure 16 replicate experimental reflectance data from a polished AR-coated sample with Al evaporated on the back. The reflectivity of photons having energy less than the band gap, for which silicon is largely transparent, is greater than 90%. It is our assumption that the reflectivity of the BSR is as high for shorter wavelengths but the reflectance of photons with energy greater than the band gap has not been measured. However, the wavelengths that penetrate to the BSR are in general near the band edge, so the assumption is probably a good one.

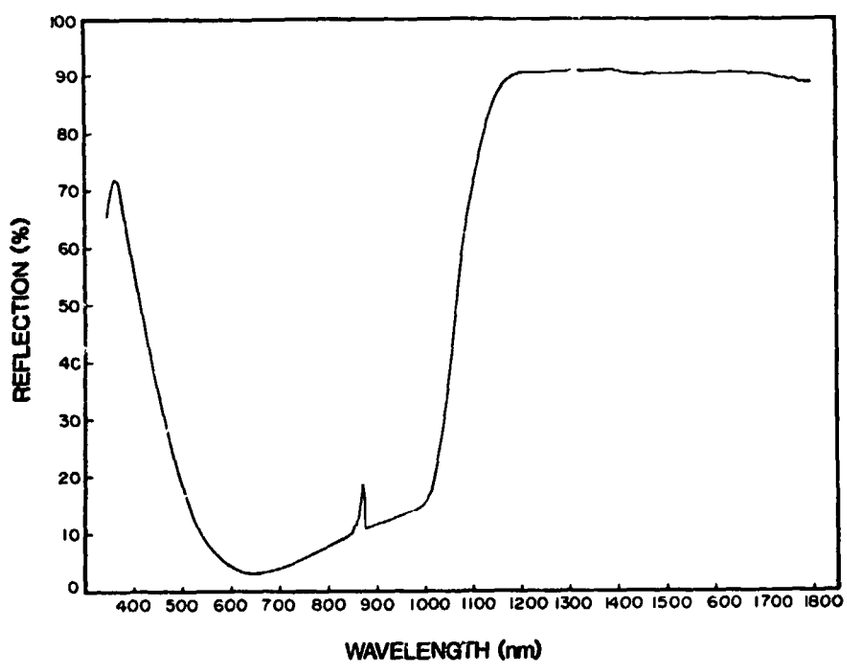

FIGURE 16. BSR REFLECTIVITY FOR AN AR-COATED CELL.

We have also examined the effect of our processing on cell lifetime. This was motivated by the anomalously low values of L_D that were obtained in a number of experiments, such as those reported in reference 4 and in earlier sections of this paper. In many of our emitter experiments, it was found that the base diffusion length had been degraded by the processing. We therefore devoted most of our attention to this problem. After a detailed examination of our furnace and gas lines, cleaning processes, annealing gases, and ramping, we identified our wet oxidation process to be a step that degrades lifetime. We have now eliminated wet oxidation from our sequence.

Recently we began experiments to increase diffusion length by gettering. The exact gettering processes that we are pursuing were taken from the literature and will be reported upon in a later publication. Owing to reservations about conducting an unusual process in our annealing tube, we used a sintering tube for the first gettering experiment. Since this tube is used for sintering solar cell contacts, it might be contaminated by Ti, Pd, or Ag. After a high temperature procedure in the sintering tube the wafers were fabricated into cells. It was found that L_D in control cells had degraded to about 100 μm, but L_D in the gettered cells increased to 170 μm. It is our conjecture that annealing in a clean tube may yield much higher values of L_D, and this is presently being tested.

CONCLUSIONS

Processing experiments have shown the importance of surface passivation, not only to V_{oc}, but also to J_{sc}. Analysis of loss mechanisms indicates that considerable improvement to J_{sc} may be obtained if diffusion length is increased. Improvement to V_{oc} is also possible by reducing emitter recombination. Many of these techniques can be applied with advantage to sheet materials. Certainly all of the above processing can be applied to CZ, with efficiency approaching that of FZ if gettering is successful in improving L_D. High efficiency can also be achieved with other sheet materials such as ribbon by using our junction formation and passivation techniques.

This work has indicated the manner in which the goal of 20% conversion efficiency may be achieved. Through process improvements such as gettering, thinning of the base, and addition of a BSR, J_{sc} of FZ cells may be increased to 38 mA/cm^2. Improvements to the emitter, including reduction of ohmic contact area, may increase V_{oc} to 660 mV. We have already achieved FF of greater than 0.8. If these features can be integrated in one cell, efficiency of 20% will be achieved. The application of this processing to present-day sheet Si will be an important step toward the DOE goal of 10% efficiency at \$90/m^2.

ACKNOWLEDGMENTS

The authors are grateful to a number of contributors at Spire Corporation, and in particular acknowledge the assistance of H. Drake and L. Geoffroy with cell fabrication. The authors also wish to thank Dr. J. Milstein of SERI for help throughout this work. The authors thank Arco Solar Crystal Production and Mobil Solar Energy Corporation for supplying some of the materials used in this work. This research was supported by the U.S. Department of Energy through contracts with SERI, JPL and the DOE Small Business Innovative Research Office.

REFERENCES

1. "Five Year Research Plan 1984-1988" of the U.S. Department of Energy National Photovoltaics Program Photovoltaic Energy Technology Division, Office of Solar Electric Technologies, U.S. DOE, (May 1983).

2. M.B. Spitzer, S.P. Tobin and C.J. Keavney, "High Efficiency Ion-Implanted Silicon Solar Cells," IEEE Trans. Electron Devices ED-31, No. 4 (1984).

3. M.A. Green, A.W. Blakers, J. Shi, E.M. Keller, and S.R. Wenham, "19.1% Efficient Silicon Solar Cell," Appl. Phys. Lett. 44, 1163 (1984).

4. M.B. Spitzer, C.J. Keavney, S.P. Tobin, F.A. Lindholm, and A. Neugroschel, "Mechanisms Limiting Open Circuit Voltage in Silicon Solar Cells," Record of the 17th IEEE Photovoltaic Specialists Conference, Orlando (1984).

5. M.B. Spitzer, "The Upper Limit to the Theoretical Efficiency of P-N Homojunction and Interfacial Layer Heterojunction Solar Cells," Ph.D. Thesis, Brown University (1981).

6. D. Redfield, "Multiple-pass thin-film silicon solar cell," Appl. Phys. Lett. 25, 647 (1974).

7. M. Wolf, "Updating the Limit Efficiency of Silicon Solar Cells," IEEE Trans. Electron Devices ED-27, 751 (1980); see also; D.L. Bowler and M. Wolf "Interactions of Efficiency and Material Requirements for Terrestrial Silicon Solar Cells," IEEE Trans. Components, Hybrids, and Manufacturing Technology, CHMT-3, 464 (1980).

8. M.B. Spitzer, "Basic Understanding of High Efficiency in Silicon Solar Cells," Annual Report for SERI Contract 2B-3-02090-3 (1984).

9. E.D. Stokes and T.L. Chu, "Diffusion Length in Silicon Solar Cells from Short-Circuit Current Measurements," Appl. Phys. Lett. 30, 425 (1977).

10. M. Spitzer, J. Shewchum, E.S. Vera and J.J. Loferski, "Ultra High Efficiency Thin Silicon P.N. Junction Solar Cells Using Reflecting Surfaces," Rec. of the 14th IEEE Photovoltaic Specialists Conference, San Diego, 1980, p. 375.

11. W. Slotboom and H.C. de Graaff, "Measurements of Bandgap Narrowing in Si Bipolar Transistors," Solid-State Electronics 19, 857 (1976).

12. C.J. Keavney and M.B. Spitzer, "Solar Cell Junction Profiles in Ion-Implanted Texture-etched Surfaces," accepted for publication in J. Appl. Phys. (1984).

13. A Meulenberg and R.A. Arndt, "Surface Effects in High Voltage Silicon Solar Cells," Rec of the 16th IEEE Photovoltaics Specialists Conference (1982) p. 348.

14. M.B. Spitzer, M.M. Sanfacon, and R. J. Wolfson, "Ion Implanted Junctions for Silicon Space Solar Cells," Rec. of the 18th Intersociety Energy Conversion Engineering Conference, Orlando, 1983, p. 1213.

15. H.T. Weaver, "Ineffectiveness of Low-High Junctions in Optimized Solar Cell Designs," Solar Cells, 5, 275 (1982).

16. M.B. Spitzer, C.J. Keavney, S.P. Tobin, and J.B. Milstein, "Ion Implanted Cells with 18% Conversion Efficiency," Record of the 17th IEEE Photovoltaic Specialists Conference, Orlando (1984).

17. J. Dziewior and W. Schmid, "Auger coefficients for highly doped and highly excited silicon," Appl. Phys. Lett. 31, 346 (1977).

18. S.M. Sze, Physics of Semiconductor Devices, John Wiley & Sons, 1981.

DISCUSSION

CISZEK: Mark, do you have any thoughts on how you might be able to get reduced area contact to a wafer through an oxide?

SPITZER: I'll have to draw a slide of that. What's the Green secret? I don't have to draw that, I can explain it. What you do is you make a very fine-line grid. It would not be suitable for carrying the currents that you want, but it has the area of the opening in the oxide that I showed. And then you overplay it, you let the electroplating balloon the grid lines in their proper proportions; then you are left with grid lines that just touch a very small area along the surface. There is no alignment involved. The problem with that, I think, is the grid lines fall off; you have to be careful. I don't like it.

QUESTION: You can cross the lines, you make your slot and then cross your grid lines, you'll get a dot contact.

SPITZER: I was worried in doing that technique. I was worried about depositing the AR and having stripes on the wafer.

QUESTION: Mark, in your 18% efficient cell the surface dopant concentration was 3×10^{18}, or what?

SPITZER: In the 18% cell we think it was 3×10^{19}. So we used the same implant parameters for that experiment, where we measured the profile, as had been used on the 18% cells.

OLSON: Both in your work and Ajeet's you applied some of the things you learned to sheet materials, and I really think with some neat results. I think one interesting point to make is that your work on the good float-zone material is really a leading edge, and I think it is really important to have the high-efficiency work on this high-quality material lead the way. And it's clear that now you are beginning to apply it to work on low-cost sheet material.

SPITZER: I agree with that. And there is one other thing that we are working on, and that is to scale up the area of the cell. I think it also has to be applied to a fairly large-area device.

OLSON: It's there we are going to really learn what's really limiting the performance, and ultimately that might pay off.

SPITZER: I agree. I think we should stay with float-zone for a while.

JOHNSON: Mark, what was the sheet resistance of your emitter?

SPITZER: The baseline emitter that we started out was about 80 ohms per square and the one that is 3×10^{19} is about 200 ohms per square.

DAUD: Mark, could you tell me what the resistivity of the Czochralski silicon was that you got from ARCO?

SPITZER: Actually, I know what it is, but I don't have permission to disclose anything about the material, so you can ask one of the ARCO guys. But there is nothing crazy about it, its just ordinary stuff.

TEXTURE ETCHING OF (100) SILICON FOR SOLAR CELLS

Lawrence D. Dyer
Texas Instruments, Incorporated
Sherman, Texas 75090

N85-31649

INTRODUCTION

In a solar cell it is desirable for the light-absorbing surface to consist of facets such that incident rays must undergo at least two reflections prior to escape. This can be accomplished by mechanical means (1) or by photolithographic protection of lines or arrays, but the former results in deeply damaged material and the latter requires polished surfaces and expensive processing. In 1974 Haynos, et al (2), reported an unspecified chemical means of creating the proper kind of light-collection texture on (100) silicon slices. This procedure converted the (100) silicon surfaces to random arrays of microscopic pyramids. Only 50 days later, Baraona and Brandhorst (3) reported nearly identical texturing with aqueous solutions of hydrazine hydrate, and showed that such behavior could be deduced from device fabrication etching experiments and observations of Lee (4). Soon thereafter similar texturing was accomplished by safer and less expensive sodium and potassium hydroxide solutions (5-7). In the meantime other benefits of this texturing had been realized: improved collection from lateral refraction (2) and internal reflection in the case of thin cells (3).

Various workers have reported studies, optimizations, and improvements of texturing using basic solutions (3-13). In 1977 Fissore, et al (7) proposed that the pyramid texture was generated in the case of KOH etching by nucleation sites covered by silicate salts precipitated at random. In 1977 Scott-Monck, et al, (9) proposed a similar situation for 2% NaOH etching with and without isopropyl alcohol (IPA). In 1978 Dyer (10, 11) proposed a similar model except that most protective sites were thought to be growths, not precipitates. An attempt was made to quantify the various promotional effects. The purpose of the present paper is first to explain in detail the attempt at understanding and quantifying texturing; second, to give an experimental description with observations on the proximity effect (8) and the effect of additions of water glass that were discovered during this work; and third, to show that the precipitate or growth models account for almost all of the known promotional effects.

PROCEDURE

QUALITATIVE.--Qualitative test runs were made in which concentration, temperature, pretreatments, ultrasonics, alcohol additions, containers, etc. were varied. Since similar procedures have been described in many texturing reports to date, they will not be repeated here.

QUANTITATIVE.--In order to quantify texturing it was first tried to measure the fraction of light reflected back from the textured surface. A simple apparatus consisting of a light source, a stereomicroscope, and an exposure meter was constructed and used to get relative numbers of merit for various treatments. This approach was abandoned when it was realized that the measurement lacked sensitivity in the final stages of texturing, as well as in the early stages where specular reflection swamps the readings. In addition this approach reveals nothing about the microscopic details of texturing.

The approach taken to quantify texturing was to measure the fraction of area covered by pyramids, as seen under the microscope, realizing that, for all practical purposes on (100) silicon, texturing is the degree to which the surface is converted to pyramids. Exceptions are 1) anomalous reflection when the pyramids have sizes comparable with the wavelength of light, 2) extra reflection when the large pyramids formed have lost their protective tops and begin dissolving from the apexes of the pyramids. The measurement of fractional area coverage has several advantages: it is versatile over a wide range of pyramid-producing capabilities because the etching time selected can be varied to produce convenient densities of pyramids, and the measurement is independent of pyramid size or magnification.

DETAILS OF QUANTITATIVE TESTS.--Texturing was done at 90 deg. C. at two concentrations, 1 and 4 wt. % NaOH. Isopropyl alcohol (IPA) was semiconductor grade, and water glass ($Na_2SiO_3.xH_2O$) was reagent grade 40-42 deg. Be'. The proximity of the test surface to another surface was established by either of two methods. In the first, simple jigs were constructed, each consisting of a stainless paddle and Teflon® or Delrin® screws. The screws protruded through the paddles at three positions around the slice and were located radially such that slices with flats could be wedged into place by rotating the slice until the flat was out of alignment with the screw. Proximities were controlled by choice of screw thread for a given thickness of slice. In the second method the slices were placed between glass slides with suitable spacers. Ordinary rubber bands were used to hold each pack together, and the angle of the slice from the horizontal was measured. Three-inch silicon wafers, p-type, 1 ohm-cm, (100) were used. Polished wafers were used for the fractional coverage studies to eliminate the enhancement of pyramid formation by rough surfaces (3, 10). Pyrex and stainless steel containers were used and each wafer was etched 3 min. in 30% aqueous NaOH at 100 deg.C. prior to texture etching.

MEASUREMENT METHOD.-- A compound incident-light microscope with 10x10 counting reticle was used. A convenient method of assessing the area covered by pyramids was to count the pyramids in each row of the grid in size groups: 0.1-0.2, 0.2-0.3, etc. (Fractional sizes of a unit square on the grid.) This assessment of pyramid size can be done surprisingly rapidly and accurately. The numbers

for the ten rows in the grid were totaled in each size group and converted to relative areas by the appropriate size factors. The fractional coverages were summed to obtain the total pyramid coverage. These values were measured at two or more places on the slice and averaged.

RESULTS

QUALITATIVE OBSERVATIONS.--Results of previous workers will be listed as well as those of the present study.

POSITIVE INFLUENCES.--The following chemical additions to KOH or NaOH solutions enhance texturing of (100) silicon:

- o Alcohols (5-9)
- o Methyl ethyl ketone (MEK) (9)
- o Films of long-chain carboxylic acids (9)
- o Fingerprints (11)
- o Water Glass (10)

The following physical conditions promote texturing:

- o As-cut or lapped surfaces (3)
- o Terraces in NaOH-etched as-cut surfaces (10)
- o Proximity to another surface (8). This effect was discovered by noticing that the places where the slices were wedged into holders were often textured better than the remainder of the slices. Optimum proximity for developing pyramids was found to be 0.4-1.0 mm. The controlling factor appears to be the entrapment of hydrogen bubbles between the two surfaces, and thus viscosity, flow, and angle of the surfaces from the horizontal are all factors. The observation of the beneficial effect of the bubbles is in contrast to previously-reported ideas about the effect of bubbles (9,13).
- o Repeated use of texturing solution (11)
- o Adherent growths or particles left after NaOH or KOH pretreatment. In fact, some growths or precipitates remain attached to the tops of the pyramids after texturing, even after rinsing with D.I. water. Figure 1 shows such a growth as seen by the scanning electron microscope (11).

NEGATIVE INFLUENCES.--In the present work it was noted that texturing was inhibited by polyvinyl chloride cement and by cer-

tain plastic slice holders. In addition, the following observation was made by Baraona and Brandhorst (3):

> "For a given etch composition and temperature, there appears to be an optimum etch time to achieve maximum structural perfection and uniformity. If etching continues beyond this time the pyramids begin to disappear, and flat, shiny regions_____begin to emerge."

NEUTRAL FACTORS.--If a texturing bath was used repeatedly, visible precipitates accumulated in it, but had no apparent effect on texturing.

RESULTS OF QUANTITATIVE TESTS.--Figure 2 compares the results of various treatments in 1% NaOH on percentage of surface coverage by pyramids. The result was that each additive or promoting condition (proximate surface) caused a 2 to 20-fold increase in pyramid coverage. Also a threshold concentration exists for $Na_2SiO_3.xH_2O$. Figure 3 compares the results of various treatments in 4% NaOH. Similar results to those at 1% were seen. The proximity effect exerted a strong influence at both concentrations.

INTERPRETATION OF RESULTS

Several authors have reached the conclusion that texturing of (100) silicon occurs by the formation of protected spots on the surface (7,9). This conclusion could, in fact, be reached from the knowledge in device fabrication on (100) silicon that any masking material will generate pyramidal mesas. The following is a line of reasoning from the atomic model that allows the same conclusion. After that, the protective mechanism will be discussed.

ATOMIC MODEL.--In order to more clearly appreciate the surface orientation aspect of the texturing problem, atomic models are shown. Figure 4 shows a Fisher- Hirschfelder-Taylor model or "sphere" model of a perfect (100) surface of silicon. The surface consists of an array of pyramid tips having <111> sides. Each surface atom has an equal chance to become the tip of a pyramid. Therefore, some external influence selects the preferred sites of pyramid formation. Figure 5 shows a model of a pyramid on the (100) face. The selectivity of etchants, including sodium and potassium hydroxides, can be explained by considering the two ways in which atoms are held into the illustrated surfaces: One type is bonded only twice and is typified by the perfect (100) surface and by the tip of a pyramid, the other kind is bonded three times and is typified by the perfect (111) surface and by the sides and edges of the pyramids. The perfect (111) surface etches very slowly compared with the (100) surface in preferential etchants (14). Clearly, if a means can be found to protect small areas of the (100) surface, each area will become the tip of a pyramid as the (100) surface is progressively dissolved.

MECHANISM OF FORMING PROTECTED SITES ON (100) SILICON IN SODIUM OR POTASSIUM HYDROXIDES.

The chemical reaction for texturing in NaOH or KOH solutions is as follows:

$$2MOH + Si + H_2O \rightarrow M_2SiO_3 + H_2 \uparrow,$$

where M represents sodium or potassium. Since pyramid formation is enhanced in dilute (1/2-4%) and not in concentrated (30-40%) aqueous NaOH solutions, the protective factor is related either to product insolubility in the etchant or to its low dissolution rate. Third, since addition of small amounts of $Na_2SiO_3.xH_2O$ to NaOH solutions enhances pyramid formation; and the Na_2SiO_3 produced in the reaction has limited solubility in aqueous NaOH and even lower solubility in NaOH-H_2O-IPA mixtures, some reaction product like M_2SiO_3 must be the protective factor and it must be grown or precipitated at random sites. Figure 6 shows a schematic diagram of the stages in the process for texturing with NaOH, with and without enhancement effects.

The reasons for favoring the idea that the protective products are growths rather than precipitates are: first, it is difficult to see why precipitates would occur preferentially on the terraces of pitted surfaces. Second, precipitates have only a slight tendency to bond to the silicon under a liquid, particularly one under agitation from gas development. Third, the neutral effect of the precipitates that accumulate from extended use of the texturing bath favors the growth hypothesis.

The positive influences can now be explained as follows: Alcohols and MEK decrease the solubility of the reaction product. Water glass suppresses dissolution of growths of reaction products by the mass-action principle. Fingerprints and films of long-chain carboxylic acids slow the vertical diffusion of reaction product; proximity (intermittent bubble-entrapment) acts the same way by providing a gas barrier to product diffusion. As-cut or rough surfaces texture better because they are already closer to the textured state. Repeated use of the texturing solution works progressively better because of build-up of reaction product.

The negative influences are explained as follows: PVC cement stops the reaction instead of slowing it. Too long texturing eventually removes the protective growths from tops of the pyramids, which leaves them free to dissolve down to base level.

PRACTICAL USES OF RESULTS.--The variety of agents that promote texturing make it possible to select a wide variety of texturing solutions. The synergistic effect of combined additives or physical conditions broadens the possibilities further. By more rapid pyramidization, a smaller range of sizes for pyramids is possible. If a texturing process has stopped producing adequate absorption of light, one can look for inhibiting agents such as PVC cement

residues, or examine the pyramid tops to see if they are dissolving away either from some contaminant like a fluoride, or from over-etching.

CONCLUSIONS

o Texturing of (100) silicon surfaces in sodium or potassium hydroxides occurs by the growth of a reaction product in a random array of surface sites, which leads to pyramids remaining at the sites after other parts of the surface dissolve away.

o Various additives and conditions promote texturing by increasing the probability of localized growth of reaction product.

o A new texture-promoting influence--a proximity effect--was discovered in this work. This effect was found to further enhance texturing in the presence of promotional additives.

o A method of quantifying the pyramid-producing capabilities of each texturing solution was developed.

o Combined effects of additives or physical conditions are synergistic with respect to pyramid density.

ACKNOWLEDGMENTS

The support of this work by JPL contracts 954405 and 954881 is gratefully acknowledged. Discussions with R. Roques, D. Coldwell, and B. Carbajal are greatly appreciated.

REFERENCES

1. B. Dale and H. G. Rudenberg, "Photovoltaic Conversion, 1. High Efficiency Silicon Solar Cells", Proceedings of the 14th annual Power Sources Conference, U.S. Army Signal Research and Development Lab. Ft. Monmouth, N.J., May(1960)22.

2. J. Haynos, J. Allison, R. Arndtt and A. Meulenberg," Proc. Int. Conf. Photovoltaic Power Generation", Hamburg, Germany, COMSAT Report 74-35-CLR,(1974)487.

3. C. R. Baraona and H. W. Brandhorst, NASA Technical Memorandum TMX 3326, Record of Meeting at Lewis Res. Center, 14-15 Nov 1974.

4. D. B. Lee, J. Appl. Phys. 40(1969)4569.

5. W. E. Taylor and F. M. Schwartz, "Demonstration of the Feasibility of Automated Silicon Solar Cell Fabrication", NASA Lewis Contract NAS3- 18566, Rept. TR3, Oct. 1975.

6. P. Stella and J. Scott-Monck, JPL Contract 954600, First Quarterly Rept., Dec. 1976.

7. A. Fissore, B. Waldman, and G. M. Oleszek, J. Electrochem. Soc. 124(1977)216C.

8. L. D. Dyer, see B. G. Carbajal, JPL Contract 954405, Second Quarterly Rept., Apr. 1977.

9. J. Scott-Monck, C. Gay, P. Stella and F. Uno, Tech. Rept., AFAPL-TR77-36(1977).

10. L. D. Dyer, see B. G. Carbajal, JPL Contract 954881, Second Quarterly Rept., Apr. 1978.

11. L. D. Dyer, J. Electrochem. Soc. 125(1978)256C.

12. G. T. Jones, S. Chitre and S. S. Rhee, ERDA/JPL-954605-78/5; Final Rept.; Apr. 1978.

13. S. R. Chitre, Conference Record of the Thirteenth IEEE Photovoltaic Specialists Conference, IEEE Press, (1978)152.

14. D. L. Kendall, Appl. Phys. Lett. 26(1975)195.

15. A. I. Stoller, RCA Rev., Jun(1970)271.

16. A. D. Morrison, private communication, (1984).

APPENDIX

VERTICAL METALIZATION IN SOLAR CELLS AND OTHER SEMICONDUCTOR DEVICES

One of the factors that reduces solar cell efficiency (and device packing density) is that a fraction of the active area (about 10%) must be metalized to collect current from the remainder of the device area. This metalization is in the form of "fingers" and "bus bars" that are much thinner than their breadth, and is placed parallel to the slice surface. The metal is at least 2 microns thick so that light is prevented from entering and generating carriers in the underlying volume beneath the metal. The present proposal is to place the metallization vertically so that much of the area formerly beneath metal can generate carriers. A gain in efficiency of almost all that lost to metallized area can be expected, i.e. perhaps 9.5% if 10% was metal.

The proposed method consists essentially of metalizing deep, narrow grooves in silicon that have been introduced by the orien-

tation-dependent etching of (110) surfaces (15). In a solar cell, the collection junction would be formed after the grooves were installed, and metalization would then be carried out.

The metalization could be accomplished by various techniques: ion plating, electroless deposition, low temperature chemical vapor deposition, or sputtering. It would preferably coat both sides of a groove; filling up the groove might give problems with mismatched thermal expansion coefficients. Connection of the several collection fingers could either be accomplished by metalization of the solar cell edges or by introducing a second set of groove directions that lie 70.53 deg. from the first set. Contacts could be made to the edges or to small horizontal patches of metalization. The foregoing idea may also be used in device manufacture in which the goal is to conserve area that is presently used in horizontal metalization.

If this method is successful, the benefit to earth-based solar cells will be offset by the inability to texture-etch the required (110) silicon surfaces; on the other hand, space-based solar cells may still benefit because of difficulties with the textured cells in this application (16).

ORIGINAL PAGE IS
OF POOR QUALITY

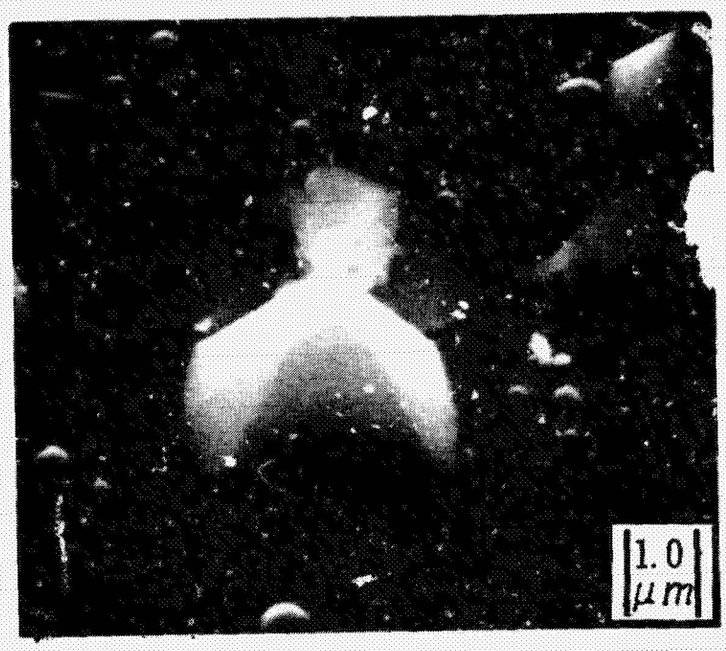

Figure 1. Reaction Product Growth at Top of Texturing Pyramid on (100) Silicon

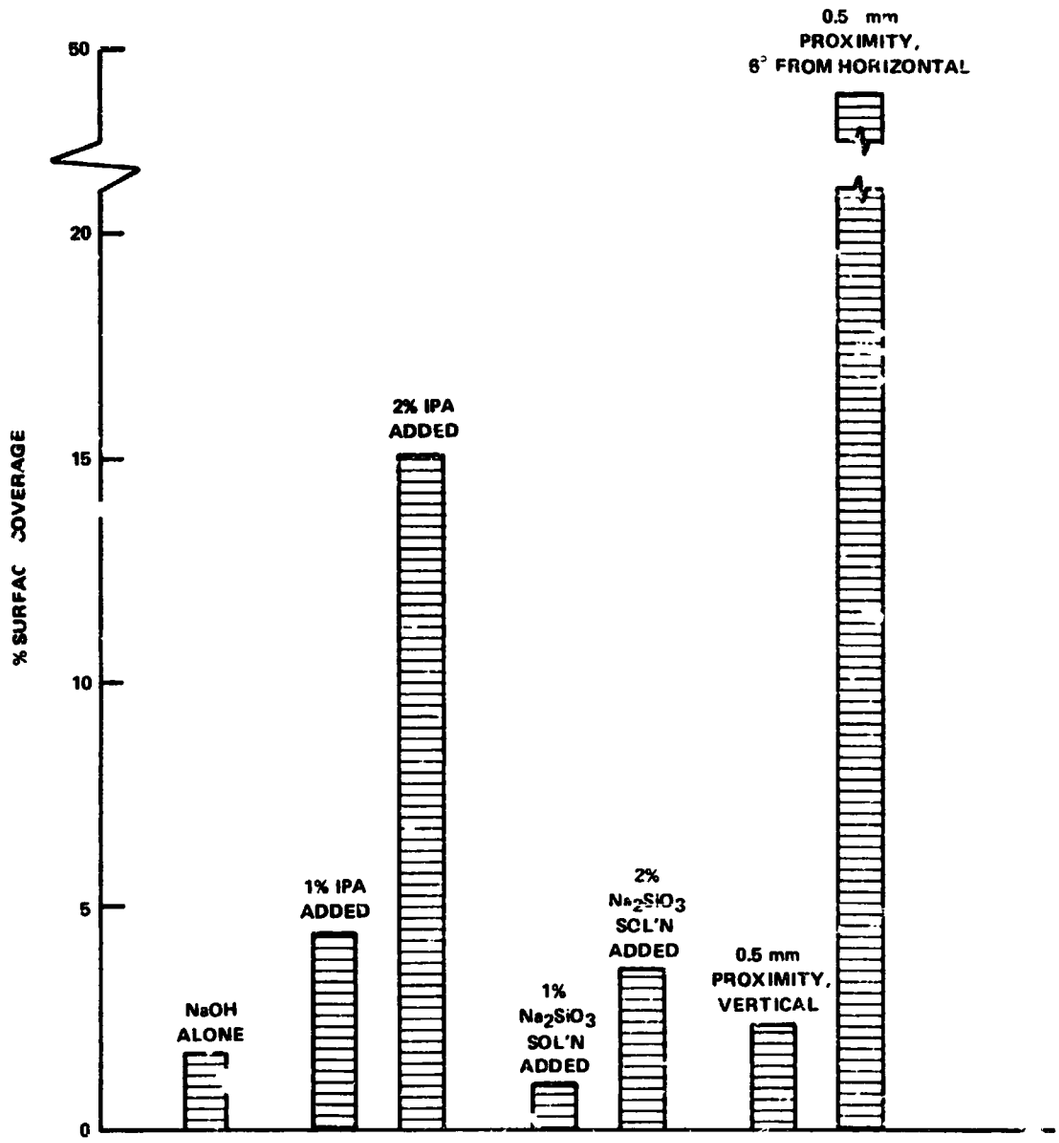

Figure 2. Effects of Various Enhancement Conditions on % Coverage by Pyramids After Texturing in 1% NaOH for 5 min. at 90 deg. C.

ORIGINAL PAGE IS
OF POOR QUALITY

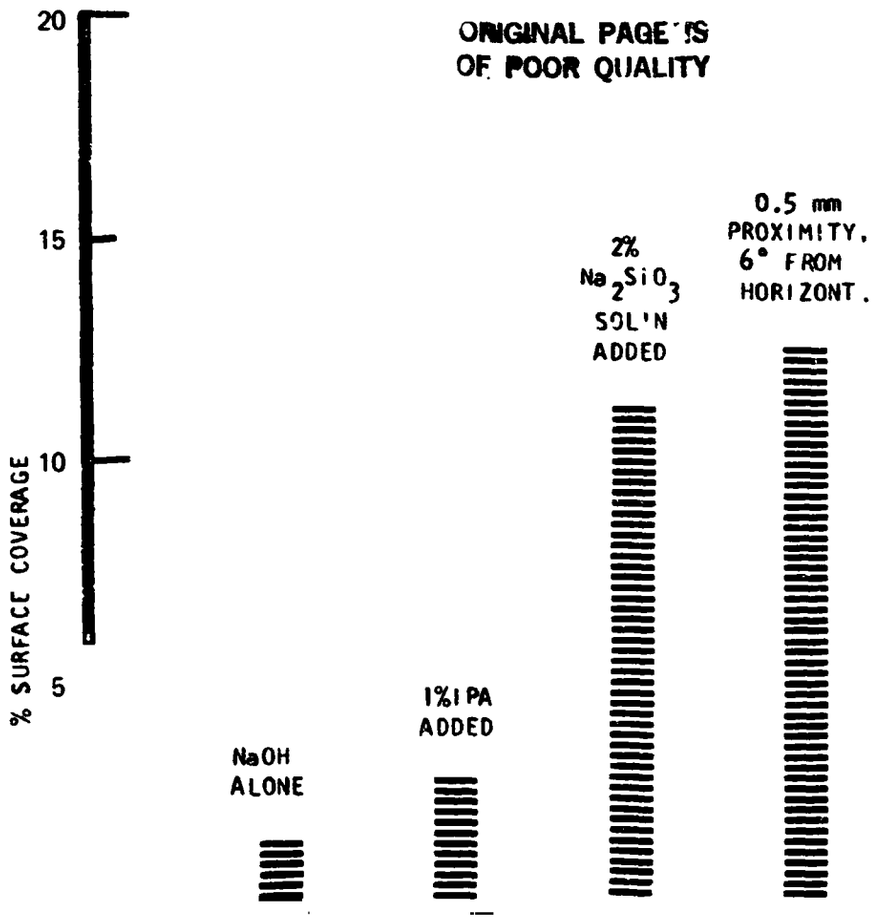

Figure 3. Effects of Various Enhancement Conditions on % Coverage by Pyramids After Texturing in 4% NaOH for 10 min. at 90 deg. C.

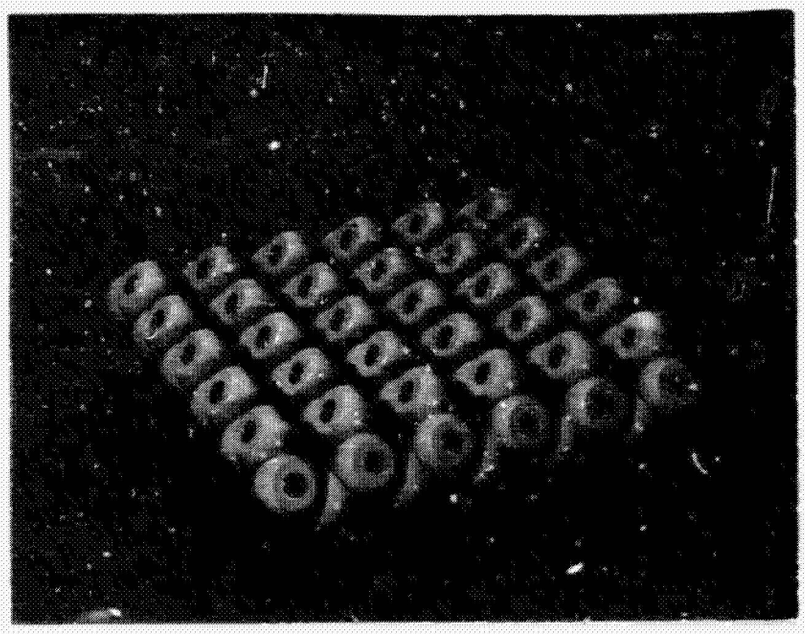

Figure 4. Atomic Model of (100) Face of Silicon

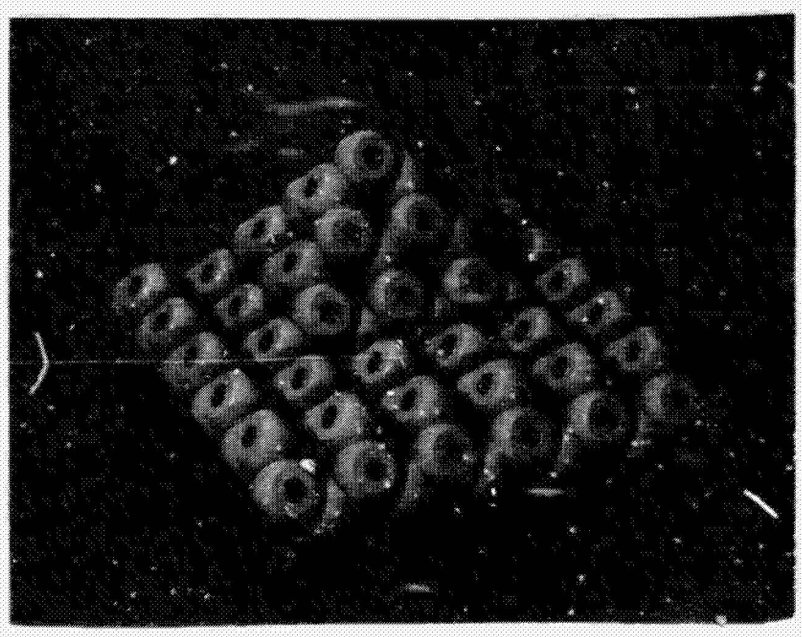

Figure 5. Atomic Model of Texturing Pyramid on (100) Face of Silicon

ORIGINAL PAGE IS
OF POOR QUALITY

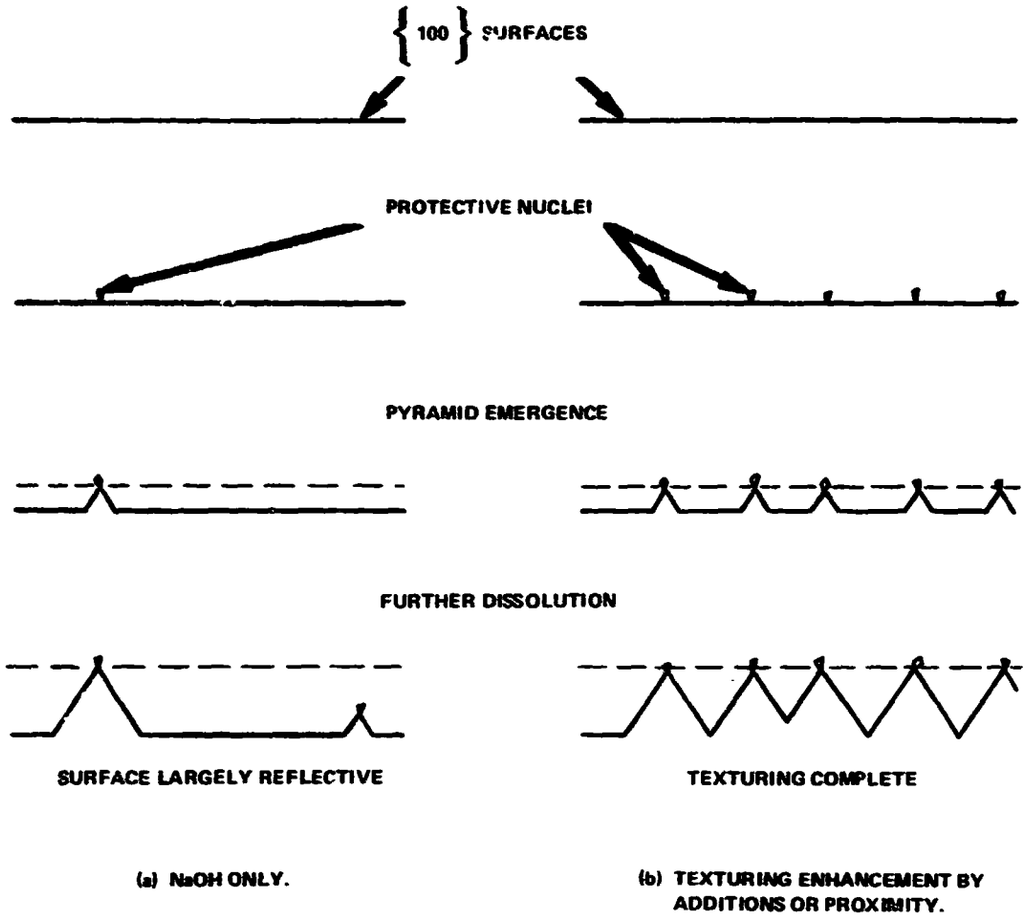

Figure 6. Schematic Diagram of Stages in Texturing Process with and without Enhancement Effects

DISCUSSION

QUESTION: Is there any difference between that structure and the DMVJ cell? With Sandia's support, the development of that kind of metallization, we are probably six or seven years . . .

DYER: I was on one of the DMVJ contracts so I know something about the structure. The making of the grooves is the same idea, you have to do masking, and you have to use a substrate with [110] orientation. It has disadvantages: you can't texture it then if it's [110] unless someone discover some new way of texturing a non-[110] orientation. That may be, then, only an advantage for space, where you can't use the texturing.

ROSE: We supported it from a concentrator point of view, because you can etch those grooves deep, and the way you extract the current out of it at very high concentrations is no different from dragging out through a thin layer. The reason we gave it up -- it's still a good operating cell, even up in 800-sun concentration -- the reason we gave it up, is it is a large-emitter-area cell and there's limitations on V_{oc} involved in it. All I do is bring it up because it doesn't seem to me like it is a new idea, it's something we have supported and given up.

DYER: Except that here you are putting the metallization down here. In other words, there's no metal contact on the top; there is no shadowing.

ROSE: That's right. That is the DMVJ cell.

DYER: Well, you still had to have bus-bars come across and collect from that.

ROSE: No, you run them out the ends.

DYER: Well, I was involved with the VMJ concept, and it had this idea in about 1976 after a contract like that and there are some differences, which I guess we can talk about. Of course you don't have shadowing and shingling.

RAI-CHOUDHURY: If this texturizing takes place by these reaction products, masking the reaction, why does it not work on [111]? Can you comment? People always have difficulty texturizing.

DYER: We already have the low-energy face there; you are stuck.

MARTIN WOLF: I have been requested to prepare a summary of this meeting, not here, at some later time, and I would like to ask the presenters of all the sessions, not just this one here, to be so good as to supply me with perhaps four to six of their slides or viewgraphs, namely those that they think are either the most instructive or the most impressive-looking, which might help me then to perhaps select one or two from among them to use in the summary. So it doesn't have to be here that you get me the slides or viewgraphs, but if you could send them to me, the address is in the attendees list. I would appreciate this very much. Thank you.

SUMMARY AND DISCUSSION SESSION

R. Kachare, Moderator

SUMMARY AND DISCUSSION SESSION

PRINCE: Anything you want to say? The major problem we have in the Department of Energy, as I mentioned the other day, is that we are being squeezed again. We will not have as much money to spend on each of the areas as we originally thought we were going to have. So the question is, what should we be doing in the Department of Energy to improve the efficiency of solar cells? We have heard all sorts of different approaches to things: modeling of various types, general theoretical analyses, some experimental work that has resulted in moderately high-efficiency cells, and so on. We heard also about measurements of various types that will enable us to evaluate what we are getting out of these devices. So, I thought we would just start off by -- well, actually, I don't know where to start off. Perhaps by explaining what I think I heard during the session that I headed. I think that's what we all were asked to do, but I think I'm going to forego that. I'll tell you one thing that did bother me: I heard several comments about the importance of the emitter region -- and in one talk, that the emitter region has very little effect on the efficiency of solar cells. On the other hand, I heard in other talks that unless you have very low surface recombination velocity on the emitter surface, you're never going to get 20% cells. That's inconsistent. I've heard a lot of other inconsistencies during the last three days. I'd like to clarify these inconsistencies.

QUESTION: May I comment on that? That's not inconsistent at all. I think what you're seeing is, it depends on what the limiting mechanism is in the cell that you're looking at, and it's clear that if you're base limited, it really doesn't make any difference whether you passivate the surface. If you are emitter-limited, and Auger isn't large, and band-gap narrowing isn't killing, you then emitter is very important. I thought it was very healthy, this conference, because I think that realization is now getting to a lot of people that simply running an experiment -- passivation, not passivation -- and observing that it did not make any difference, doesn't tell you anything. As a number of people have said, you really have to optimize the entire cell and that is what really is important. I don't think any of those things are inconsistent.

SCHWUTTKE: I'm challenging. I'd like to see if I can say something without getting into trouble. I think the question, as I see it, is: where do we go from here? In that sense, I think the problem has a couple of different facets. From my point of view, certainly; I think I have already expressed the idea that we need to have a complete understanding of what it takes to get to a specified level of efficiency in terms of the best-first-principles kinds of things we can do. I think there are people who are working on that problem, and I think they are going to give us some pretty impressive results in the near future. I think the other thing that really matters is the industrial participants in the program doing those things that allow their product to be a better product. Because that's really what this entire program is all about. From that point of view, I have tried to make available to DOE participants, and to people who are not participating in DOE programs at this stage of the game, that information that we have. I would hope that kind of thing would continue; I would hope that the information that we are finding will be

used. In terms of the critical issues, I would totally agree that the material issue is one that needs to be resolved: how do you get a real-world material that is good enough to be able to make cells consistently that are worthy of the processing we are finding out about? If there has to be something done in that area, then maybe it behooves us to think about that kind of a question. I think materials questions in general, in all photovoltaics, are a major issue.

SIRTL: Do you expect me to say something as a part of the wrapup of we have been listening to for several days? It may be a kind of egotistical wish. I already mentioned that to make gettering or gettering systems a science, he situation now, and the situation in other areas that have nothing to do with solar technology, is that so many different companies have their "black boxes" of what they call gettering processes. They never would like to disclose anything on that. On the other hand, we need to make it a more consistent technology in later years. We need a kind of well-understood buffering system that prevents the outbreak of blaming each other for being the culprit. The manufacturer of the material, or the device maker; if we would have reached some kind of gettering science, we would be much better off, and that of course includes a better knowledge of what direct combinations that predominate what recombination centers may look like. We really are at the very beginning of any understanding, and my feeling is, that is included in the science of gettering.

KOLIWAD: I have three observations. One is in the same line that you talked about, emitter importance. I have this concern about the work in the process-related area, process research area, as an example: do we have optimum emitter profile? It concerns me especially because of the heavy doping effects, and the field, as a result of the band gap or the band-gap tailing. Dick commented this morning that in a static field they distribute in ways that are complementary to each other, so we are not doing any research at all in tailoring the profiles. The second observation I have, I would again emphasize what Fred mentioned this morning, on the contacts -- the importance of contacts for high efficiency. There are a couple of areas that I think are in the area of process research, if you will, or process technology research, and I think some emphasis should be given to those areas.

LOFERSKI: I guess the thing that struck me particularly was Peter's discussion. I have heard him say this before, that the space cells may have been 18%, the stuff that they normally make, and of course by changing resistivity they would probably have been there. That's a question of many different steps and high-quality processing all along the road, I guess. Like the gap between what's possible in cells and what exists in commercial cells for space, I think, is rather small -- the things that are found in the laboratory and up in those space cells. But that is not so for terrestrial cells; there is a gap, and I guess what Peter is saying is that it's pretty much the same cell, that it's a space-quality cell that you are asking for, different resistivity and the higher quality material to get beyond the 18%. Like Mark Spitzer was saying: just give us better material, and pretty much the same processing that we are using to make the 18% cell will get us to 20%. But the big problem is that gap between what's demonstrated as possible and what comes out of the manu-

facturers. That is an economic problem. Like Martin says, we'll make a good cell and then learn how to make it cheap. I have heard someone else in the course of the talks say that's not the way to go, but that's basically it. For space the price is not what people are worrying about when they are manufacturing the cells, but for terrestrial application it's price -- economics -- that finally get in there. Now you said we shouldn't talk economics here, it's high efficiency that we are talking about, but there is that gap somehow in communication, perhaps not communication so much as the feeling of the terrestrial people that you cannot make these high-quality cells cheaply. I don't know how you change that.

QUESTION: I don't feel that way at all, Joe. I think many of us have been in the semiconductor industry for many years and we have learned from experience that you do the best you can. And when you learn how to do those things well, you push your yields up and you get your cost way down, now that we have gotten up to this 15%, 16%, 17% range.

LOFERSKI: I think we have gone through this cycle of "Well, it can't be that it's that space cell that will be the terrestrial cell." There was the business about solar-grade silicon that was going to be a lower-grade silicon and not the best silicon there is, and now we have come around to "It's got to be this solar-grade silicon for high-quality cells, it's the best kind of silicon there is, and it's the best for processing all along the way." It's a question of doing all those things inexpensively or at an acceptable price.

QUESTION: Just a comment. I think everything is going in the right direction, and what we are learning in high efficiency is being applied to making the cells for the commercial market today. Their cost is important, as it always will be. You have to compete at $6 a watt or whatever it happens to be at the present time. These things are applicable; we are not going to be selling that kind of cell right away. think there is one thing perhaps where DOE is a little off, in my opinion, of dead center, and that's in specifying efficiency on a module-sized basis. In other words, a 15% module requires 18% cells. What is important is the efficiency of the cell under glass. You could make 30% cells and fill up half a module and you have a 15% module. But that's not going to do it. It is not very important to a first approximation whether the module is 20% bigger or smaller than the average size. It may be for central-power systems, where everything has to be squeezed together. We are not going to be in that business for many years in this country because there are many other technologies that may dominate that market. What is important is the world-wide market for small systems. I think that's the real market that we are facing today. For that it's not so important, now; whether DOE's objective is that or not, perhaps, does not make any difference to the world market, but for American industry it may have some effect. I think we should be realistic and say what's important. We need efficient cells. We want to get the most we can. But what is more important is the cell efficiency under glass, cell efficiency in the module. We can worry about whether 10% is more crowded or not but thats not important, in my opinion, to the world market today.

DYER: I want to make a comment on something that someone else brought up in this conference about Czochralski vs float-zone. I want to expand on that. Czochralski growth is not optimized for solar cells at all and the economic question does come into it. Because whoever makes the silicon -- and in our case, we make it for our own divisions, our own front ends -- has to make it as cheaply as they can, and right now they are asked by front ends to make it optimized in several ways. They, of course, want to have a very constant resistivity over the whole thing. The segregation laws make it so that you have to, I mean the resistivity changes from one end to the other, so they are going to lose something there. It would be very nice if you could have one front end want the top part of the crystal and another one want another part and so on down to the tail. But when one device engineer decides that so-and-so ohm-centimeters is right, they all do. So you are putting the manufacturers in that bind. Then, in recent years, it has been realized that to have oxygen in the crystal is a good thing, and they don't want the oxygen to be measured just in one place, but both radially and axially along the crystal. So there is another restraint put on again, not by the solar-cell industry but by the device industry. No one has ever asked "make us some material for solar cells." It seems to me that in addition to all of these other requests someone has to sit down with people in the growth and selling of Czochralski silicon to see if they can't also do something else and provide a material that is good for solar cells. And that could be done, but the economic question has to be brought up and addressed. I rest my case there, I don't think they have gone as far as they can on it, because that isn't the one who is paying the bills.

QUESTION: I want to take up on Kris Koliwad's comment. Correct me, somebody, if I'm wrong. Most of the solar cells that we make, with the exception of float-zone silicon, seem to be base-limited. Hence, again the emphasis on bulk material is so much more urgent than the process. Tailoring of the emitter, if you leave the process in the hands of those who have good experience in semiconductor processing, not just solar-cell. Ion implantation diffusion from solid source, liquid dopant, you name it, more than one way. More than one way to tailor the emitter profile and I don't think we have run out of steam there yet. I think there are problems still: in the high-efficiency area is one, of the starting material -- Czochralski, of course, we talked about it; the recombination center in Czochralski, especially as a result of heat treatment. One has to address it; it is really a materials issue. Hence, how do you get around it so that you can apply the knowledge to a cheaper sheet growth process?

QUESTION: Maybe I should comment a little bit on the same question. It seems to me that there are two basic reasons why we live today with this emitter profile. The one is that we have not learned really to bring the surface recombination velocity to very low values, so that we need what I called, in my talk yesterday, the potential step, or in other words a large drift field that the profile gives us. It helps to reduce the effect of the high surface recombination velocity. The second is just strictly process historical. We have learned how to control diffusions, we have learned how to do ion implantations. Both leave us with a steep impurity gradient in the layer that we generate by this process, so we automatically end up with this type of profile just because of the process we use. Okay,

what's the other alternative? Really, it could be alloying, a liquid face regrowth; we don't have those very well under control. We have gas-phase CVD epitaxy. We seem to have problems with that. That would give us different profiles, then we could live with something else. We haven't learned as well to use these processes for solar-cell fabrication. So to some degree it is historical. Again, if you could make one of these other processes work, we would not necessarily -- probably we wouldn't at all -- want such a high surface concentration, and we probably would have other means available to control the surface recombination velocity better, if you don't have such a high surface concentration of impurity. So we could move into a quite different technology here, but we don't quite know how to do it. So that's my response to Kris's question.

I have two other things I wanted to mention. I think this meeting has shown us very clearly that we really have moved to a new technology level. People have made use of modeling, of the the available analytical measurements, to understand exactly what the devices they are making are like, where their limitation are. They have analyzed where the next step for improvement has to be. They have moved along and made improvements in understanding of device physics, modeling, and the analysis of devices through measurements, and they have reached this new level of 18% to 19% efficiency. And we see that it can be done by quite a few people. It's not that just one individual that has this capability, and we also see that each one has put emphasis a little bit differently in how he got to this 18% to 19% level and through the modeling and analysis has seen what else, with today's technology, he can do to design this device better, to process it a little bit better, so that he probably can get to 20%. So we have heard a number of people who felt that 20% is essentially just around the corner. That seems to be the level of today's technology, and I think it's a good move ahead from where we were a couple of years ago. The question then becomes, what's the next thing? How do we get significantly beyond that point? It looks like, from everything that we have been hearing here, that that's not exactly accomplishable with today's technology. Again and again we heard that really to get significantly beyond, we need better material, and it seems to me, with that, we come pretty much to the talks we heard yesterday about what do you do with surfaces, what's happening with surfaces. We saw some very impressive pictures of what we have learned about how surfaces are reconstructed, for instance, and so on. What are the defects in materials, where do defects come from in the material? The question then comes, okay, since we start to understand what the surfaces are like, we start to understand how they reconstruct themselves, how can we foster it, how can we develop processes that will give us this desirable type of surface practically all the time? It seems to me we have made considerable research progress in understanding but we haven't yet learned really how to apply it. I don't know whether my understanding is right or not, but that's the impression I got. So I think this might be perhaps a subject we might want to discuss a little further here.

I have an answer for Erhard Sirtl. I didn't like his comments so much; let me tell you why. To me, it looks like gettering is something to repair what you didn't do well enough before. So, shouldn't we learn

first to do the things as well as we can or better than we do it now? And maybe then still do some gettering, but maybe the first emphasis should be to reduce the defects in the material rather than afterwards try to repair it; make it right the first time out on the production line, and don't send it to the repair shop before you sell it. Those are my comments. Let's see whether we can get some good discussion from those.

QUESTION: I always used to say gettering is an act born out of desperation but at some time it is necessary, but on the other side, it spoils manufacturing to be sloppy. I would really like to pick up on the comment made by Larry Dyer and also by Marty. Not too long ago the solar-cell industry used silicon that the IC industry was throwing away. Maybe, just over the last couple of years, they have become more conscious, and they buy Czochralski silicon; and then they heard about float-zone silicon, so they all rush out and want the float-zone silicon, because somebody told them that it's a lot better. Shortly before that everybody was hot on sheet silicon because you didn't have to slice it; now we cast for the kilo silicon and nobody asks about slicing any more. So there are a lot of contradictions in that particular field. What I believe we have to do now is come out aggressively and specify the material we would like to have and then go after the vendor to develop it. So far, we just take what we get. I would like to say we really don't know what your process can do, we don't know what float zone can do and we don't know what sheet technology can do for us. We have never taken the time to sit down, and we have done a lot of modeling, but the hell with it, I'd like to sit down with you guys and draw up the specs of the material for a high-efficiency cell. You tell me what you want and then we go and find somebody who is going to make it.

QUESTION: Let me now give the answer to Martin Wolf and maybe dwell on some inconsistencies in thinking. Let's comment briefly on Schwuttke's comment. Presently we have to live in microelectronics exclusively with gettering. Whether it's oxide gettering, whether it's internal or intrinsic gettering, whatever you may call it, we have to live with it until somebody comes up with a better understanding to make good and cheap Czochralski materials that don't need all that, including the device processing. Let's talk about solar cells now. What has been the reason I so strongly would like to see gettering becoming a science? What is the situation we are in right now? On the one hand we are striving for the highest-efficiency cells possible. That's something else, that's special research, and we want to give it all the support possible . . . we may learn a lot more about the mechanism of a solar cell in general, the mechanism of different device concepts and the like. But we must never forget that this type of solar cell nearly exclusively is made from a material that I would call exotic. Exotic means that I don't see, in the near future, ways to realize a production of some sizeable quantity. That means it's good to have found out how we can make high-efficiency cells, but later on we have to learn to live with a material that's economically available, and that we can scale up, and it's done best in connection with the device maker in a way where I think we need gettering. But that may not be the only solution. And by gettering, I mean it in all senses; it means that could include hydrogen

passivation, that may even include some kind of intentional complexing in the original material. When we now talk about something that has not gotten the share of attention in this meeting that it should have, about all the terrestrial approaches to make real cheap solar cells and real cheap material, I think we haven't come to a point yet where we can talk about the standard final quality of material that may have come out from any kind of process. Developing some special additional treatment to improve things here means just a temporary situation, because we have not reached maturity in whatever the process may look like. In my feeling, gettering can be an early solution to improve things at least to a point where the efficiency that can be seen as possible by the device maker has reached a certain attractiveness already. But we still have this gap between high efficiency of space types of solar-cell technology and the technology we mostly are talking about, namely for terrestrial application. That's where we need help to get into shape early to make solar cells attractive and efficient -- but it cannot be the maximum efficiency that we may reach during the next five years.

QUESTION: The question about gettering. I think that your comparison is not a better comparison with microelectronics, where all the action is on the surface. One-dimensional, two dimensional-device. Better compared with power devices, where current flows through the thickness of the material. A solar cell is essentially such a device. When you have a device such as that, you can getter but you have to have a material that does not have bulk precipitation, something going on in the bulk as a result of gettering, because in my experience, or that of all the people I know in the processing area, we never even dream of starting with a bad material and getter it and then make a device. The only purpose of gettering is to prevent contamination during processing. It's not really an answer. Can one take a material that is not so good, and getter-improve it, and make solar cells? I think the whole area needs to be examined.

QUESTION: I would like to just follow on what Ajeet made a point about. I think it's an excellent point, because if you try to getter something within the bulk, it's going to kill you . . . Now, the other choice is to go to the surface, which is like back-surface damaging, and that is going to kill you again because now you are going to raise your surface recombination velocity. So it becomes very difficult. And the third point is that generally the best gettering is achieved at high temperatures. All those things stand to hurt solar cells, so how you are going to do it and apply it to solar cells is going to be a slightly difficult question.

SCHWARTZ: I'd like to switch topics for a moment and talk about modeling. I think Martin Wolf probably said it best, near the end of his session: he stood up and said this sounds like a modeling session that we have. The one thing that struck me was that there were very few device papers presented that didn't either use as a guide, or rely upon as an interpretive tool, some sort of a model. There are all levels of sophistication. But almost everyone had some sort of a model that they were using, and I was very pleased to see this because I think that the device is deceptively simple-looking and still very sophisticated. The realization that the model is a design tool, an interpretive tool, seems to be widespread, and

I was very pleased to see that. The current status, I think, of the device codes is that they really are very good in spite of all the time I spent last night talking about the things that need to be done. In fact, one can show large numbers of plots of all kinds over wide ranges of operating conditions and over wide design ranges for which the predictions fall dead on the measurements, within the experimental accuracy of the measurements. The codes are designed to do it, really do an outstanding job of fitting what's there. In fact, they really do a very good job of predicting of what will happen under changes before the experiments are made. The status is really very good. So what does it need? There were needs: maybe three dimensions, time -- actually, time is very easy to do, that's a very small extension from where we really are. There are some needs, and they were not very well expressed directly, but it was implied by a number of questions, and that was the codes are only good, useful and easy to use. Therefore, the output is very important, and good graphical output, where you can sit down and look at things very quickly and understand what is going on, is very important to the use of modeling. I have one other comment: it seems to me that there should be larger, wider access to some of the more sophisticated codes. At the present time they really aren't widely available for people to use, and that's probably something JPL has been looking into. That in fact would help a great deal if there were wide access to some of the existing codes.

QUESTION: Perhaps we could resolve the controversy between Martin Wolf and Sirtl if we made the gettering part of the wafer manufacturing process. You know your material the best of anybody. If you feel it can profit from gettering, you can make a better wafer, include it in the production process and maybe get more money for it.

QUESTION: I think I have to give a better definition of what I understood about gettering. It finally, very clearly, should be a help for the device maker to get the best quality of his specific device after having done, at a fairly late stage of his process, some kind of gettering. I'm just speaking for the material supplier because in general, the device maker has not had as good an understanding of materials problems as the materials maker in general. So we have to live with a situation that there are many device production areas that just have to have a very simple recipe available that, of course, needs a lot of exploration before we get to that point in terms of gettering science, as I call it. Later on it should be particularly a help for the device maker to get the best device possible.

SIRTL: If you want to getter wafers downstream in the process it has to be at low temperature, unless you know some miraculous way of making the atoms move faster at low temperature. The problem then is to make a junction device. How do you getter downstream without disturbing the device?

WOLF: One thing bothered me a little on Schwuttke's comment, which is basically a very desirable one, but it's somewhat a chicken-and-the-egg problem. The solar-cell industry is a very small industry in comparison with the integrated-circuit industry, and probably even the power-devices industry. So can we even move the material manufacturers at this point.

QUESTION: I don't think you have to move it at the present point, but what does prevent you from sitting down and drawing up the specs you would like to see? That's the first step, and if we do we will move the guy who is going to make it. If you have the specs, maybe you'll find the guy who wants to do it.

SCHMIDT: I would like to agree, and perhaps elaborate a little bit on Schwartz's comments. I think it is very encouraging that we have computer codes that are in agreement in many cases with the performance from the terminals of existing devices. That's a real plus, and the codes have been very useful for a number of years, in lending the kind of understanding that has helped more people drive the efficiency up. On the other hand, I recall that in 1978 Paul Stella gave a paper at the Photovoltaics Conference in which he reported a 16+% AMO cell, which I'm fairly sure was an 18% AM1 cell. That was a very expensive cell. The point that I am going to make is that we have also heard some talks, particularly earlier in this Research Forum, concerning 25% cells, which is sort of No Man's Land. They are pretty easily designed on paper and with computer codes. The problem is that the physical parameters are probably not available to enable those designs to be achieved in the laboratory. Assuming some good lifetime in the base, there is probably something that will creep in when you do some heavy doping things. Secondly, I would guess there are probably a large number of ways of getting high-efficiency cells. I'm now going to say maybe 20% in a year or two and I think we have to pay a lot of attention to the multitude of different ways, because not all of those will be easily manufacturable. There the device codes are going to come in very handy as we explore different ways, for example, of emitter profiling, of contacting, and other things that will lend themselves to cells of high efficiency that can be manufactured in large volume as economically as possible. Which also brings up the utilization of computer codes for the purposes of monitoring the manufacturing process by enabling a very sophisticated and detailed interpretation of experiments that are going on in fabrication processing, as well as those after the cell has been made. At the same time I would agree with Dick that the codes are working very well and that we have some physics in there that will predict existing 18% cells, I think that there is an awful lot more work that needs to be done in fundamental understanding, particularly at the physics end of the spectrum. I'm not speaking as a software person, but I think Dick's comment last night was that if we can get the physics understood, then the software will probably take care of itself, because there are some capable people around doing the software. I'm interested in trying to work on some of these fundamental problems, but I think that it's very urgent that we think of not just achieving a 20% cell but of achieving a 20+% cell in a multitude of different ways so that we can evolve one or two or three different ways of manufacturing such cells in large volume and fairly inexpensively, and keeping the production line up with appropriate monitoring. So this is a much larger view of the computer codes than many people think of them.

DAUD: I guess Fred touched a little bit on what I was going to say of going beyond 20%, and I wanted to ask a question: if one wanted to go beyond 20%, what does the panel or audience think is the prime issue? Like do

we have to go for different design of contacts or different design of the cell itself, go to plasma on cell or whatever? What would be the comments of the chairmen, as well as anyone from the audience?

QUESTION: While everybody is thinking of a good answer, I would like to make one remark. Of course, I don't actually make any of these cells, so I am just an outsider and therefore don't know quite what's going on. But I would like to concentrate on the notion of a defect because that really seems to be badly understood. First of all you start with the original material. What are the defects in there? You then have processing; thermal defects are produced, and then the materials cool down and some of these defects are annihilated and others survive and get frozen into the material. This whole area seems to be where metallurgists and engineers and physicists could really usefully work together. But it is an area of considerable ignorance. In one of the talks somebody put up energy levels, and how they changed with time . . . . It seems to me that if you want to improve these solar cells and get long lifetimes and get rid of these defects, one really has to be very scientific and extremely careful about each of these steps that introduce new defects or get rid of others. I am now including in my remarks what Sirtl said about gettering, because that's also got defects, and how to get rid of them. So it seems to me that there we have an area where I feel we are at a very early stage and really surprisingly ignorant. All these defects contribute to recombination, and so to understand that, the defect really comes first. Then we have to understand the recombination mechanisms. There is a lot of work to be done.

QUESTION: You know that for so-called good cells, that make say 18%, or for that matter 15%, 16% cells, we really don't have any technique of determining what defects are in them. Nothing we have on hand is sensitive enough, absolutely nothing electrically. You can detect only 17%, 18% cells. Clean as anything, no deep levels of any kind. With the kind of techniques we have on hand, we have to find some methods that can determine defects in those good cells we are producing now. If anybody has any ideas or anything they are working on, I would like to hear about it.

SCHWETTKE: Obviously I agree 100% what was said about the tremendous need of such detailed characterization before and after processing, and its final correlation with device performance. And I'm in this field now for 20 years, and all I have learned is that it is tremendously complex and extremely expensive. And that the instrumentation that has been developed over the last 20 years is so extremely sophisticated that it is very difficult for a smaller laboratory to have access to such instrumentation. And then, the major problem is to get people interested in working in this field, because you cannot get very famous by doing this type of work. There is no fast reward, only a lot of sweat and long hours, and these guys are tough to find. Nevertheless, I think there are dedicated people who are working exactly along these lines and there may not be enough around, so maybe we can motivate some more to assist us in solving these extremely complex problems. You know, material science has always had the short end of the stick, compared with device science. The money is made on the device side, not on the material side.

QUESTION: I think I would say talking about good-quality silicon, float-zone and that sort of thing, you cannot specify anything but electrical stuff, you can specify oxygen, carbon, and then what do you specify is the diffusion length, the lifetime, the resistivity uniformity, things that we can measure. Now, how come this thing has a 100 microsecond lifetime? I want a millisecond lifetime. There is no good way of measuring what's the cause of it, so a crystal grower does not know what to do.

QUESTION: Let me respond to that. Usually the crystal grower is not expert in those ways to have the ability to guess, out of the periodic table, these things that will be likely to be in my puller and would be affecting his material that way. Usually he doesn't know that. Do we know what we are gettering? If we knew what we were gettering we could watch out for it in the reactors, in the pullers, it seems to me somebody ought to pin down what element or elements it is we are gettering.

PRINCE: I'm going to let our chairman close out our session.

KACHARE: One thing for sure, all of us agree that in the last two and half days, we learned a lot. I believe that with this High-Efficiency Research Forum we are really entering into a new technology. I think most of us also accept the fact that basic material requirements need to be defined. When we say that, I believe that gettering became a major issue also, and some element of research is needed there. But if I can summarize that in one sentence, basically we need to understand the loss mechanisms -- not only in the bulk; we also should know what are the defects, what are the chemical impurities, what are the dislocations, and also the loss mechanisms between silicon surface and metal, silicon surface-passivant interfaces. To understand these loss mechanisms, I believe that we have to have reliable measurement techniques. I think Lindholm said "let us use the effective parameters," but I have a lot of reservation about them because effective parameters may mislead us. So, basically, I am saying that to understand these loss mechanisms we have to have reliable measurement techniques. Cell fabrication research also needs additional efforts, whether we should use ion implantation, whether we should use diffusion, or whether we should have shallow junctions, whether we have this kind of emitter, whether we should have high or low junction -- all these issues are again for research. Furthermore, I think modeling is very useful and I feel that we just started using it. We have a tool now, I believe. It's not yet a perfect tool, but at least gives some kind of information. We can use it to refine our processing, refine our device design. As of today, float-zone material is a research material and not final material for our 15% module, $90/m^2$ kind of requirement for DOE goals. But that material is still useful because by using it, it is at least possible to make a 20% cell, so we are at least establishing some upper limit or a proof-of-concept. Can we bring low-cost sheet materials or any other cast material by gettering or by some other techniques to the level of float-zone? I have serious doubts about that, but at least we know that if you have some kind of material of excellent quality, it is possible to make 20% cells. I believe that measurement techniques are needed to enhance our basic understanding of, for example, heavy doping effects and Auger recombination coefficients. I had a lengthy discussion with Swanson from Stanford about the Auger recombination coefficients measurement that

has been made in Germany. We are using those particular numbers as if they are reliable numbers. Many people are now questioning those numbers. So to understand the heavy doping effects, to understand device performance, to understand loss mechanisms, we need to have reliable measurement techniques. In short, I have tried my best to summarize two areas for obtaining high-efficiency cells: one is from the material end, and one from the design and device processing end -- and then bringing the material end and the device end together to achieve the 20% solar cell, at least in the lab. I think it is possible.

On behalf of DOE, SERI, FSA and the organizing committee, I want to thank all of you. I hope the conference was useful for all of us.